10th Hull Performance & Insight Conference

HullPIC'25

Edited by Volker Bertram

Sponsored by

www.jotun.com

tutech.de

albis-mp.com

www.ascenzmarorka.com

https://cloudtowingtank.com/

https://www.cmp-chugoku.com

www.coach-solutions.dk

www.enamor.pl

www.hasytec.com

www.hempel.com

www.hoppe-marine.com

www.idealship.de

www.ppg.com

toqua.ai

Veinland.net

www.vpsolutions.dk

Media Partners

https://hansa-online.de/

https://home.rina.org.uk/

Index

Preface

Geir Axel Oftedahl, Breakthrough Factory, Norway gao@breakthroughfactory.no

It is with a mix of pride and regret that I write this preface for the 10th Hull Performance & Insight Conference (HullPIC). Pride, because HullPIC has grown into the leading forum for advancing data-driven decision-making in field of hull and propeller performance. Regret, because I am unable to attend this milestone edition in person and take part in the discussions that continue to shape our industry.

Looking back, it is remarkable to see how far we have come. What started as an idea born out of the ISO 19030 working group discussions has flourished into an annual gathering of experts, ship operators, solution providers, and researchers – all dedicated to improving ship performance through better data and deeper insights. At the heart of this success is the commitment of the HullPIC community to openly share knowledge and challenge conventional thinking. This willingness to collaborate across industry boundaries is what sets HullPIC apart and ensures that it remains a driving force for innovation.

Of course, HullPIC would never have gotten out-of-dock without Volker Bertram. It was his (admittedly somewhat quirky) leadership and reluctant agreement to organize the first conference that made it all possible. His ability to wrangle diverse stakeholders (a true superpower), combined with his tireless work behind the scenes, has been instrumental in shaping HullPIC into what it is today. The ongoing contributions from speakers, attendees, and supporting organizations have sustained this momentum, turning HullPIC into a unique and invaluable event for the maritime community.

Now, more than ever, we need data-driven decision-making. HullPIC's mission has always been to contribute to this goal – not just by showcasing the latest technologies and methodologies, but by fostering discussions that lead to real-world improvements in ship efficiency and environmental impact.

As the tenth edition unfolds, I have no doubt that the presentations and conversations will continue to push the industry forward. To all those participating, I want to express my gratitude. Your work in advancing ship performance monitoring is essential, and HullPIC would not be what it is without your engagement and expertise.

I look forward to following the conference outcomes and hope to join you again in the future. Until then, I wish you productive discussions, insightful debates, and continued success in shaping the next decade of performance monitoring.

Geir Axel Oftedahl

February 2025

10 Years of HullPIC - Progressing in Hull Performance Monitoring

Volker Bertram, DNV, Hamburg/Germany, volker.bertram@dnv.com

Abstract

This paper describes a personal walk down memory lane for the series of HullPIC conferences, giving background on the conferences, but also on how the state of the art in ship performance monitoring has evolved in 10 years. HullPIC is, after all, a technical conference and I should stick to the rules, even if taking liberty in stretching them.

1. Introduction

The 10th edition of HullPIC is a milestone that nobody foresaw when we planned the first HullPIC conference. A decade later, it is a good time to look back to see HullPIC in perspective, as a conference mirroring the evolution in performance monitoring in the industry.

Fortunately, 10 years later, we are by no means reduced to worshipping the ashes, but the flame (of performance monitoring developments) is still burning strongly as we share it and pass it on to new generations of HullPIC participants. The time is right to look at where we have come from and see where we are now.

2. Before HullPIC – The ISO 19030 working group years

The roots of HullPIC lie in the development of the ISO 19030, *ISO (2016)*, standard. The working group, although changing in composition over the years and meetings, set a tone that focused on sharing expertise rather than pushing the own company products. Svend Søyland of Bellona Foundation was the Convener of the working group ("the elder statesman"), Geir Axel Oftedahl from Jotun (at that time) the Project Leader ("the captain", doing most of the work to drive the ship forward, avoiding collisions and grounding on the rocks of resistance), Fig.1.

Fig.1: Svend Søyland (left) and Geir Axel Oftedahl (right)

The following summary of the period of the working group for ISO 19030 is taken from *Søyland and Oftedahl (2016)*: "The process towards developing the ISO19030 started when the Environmental NGO Bellona Foundation and Jotun A/S had informal discussions on how to improve energy efficiency within the maritime sector. Bellona Foundation looked for a robust and verifiable way to reduce CO2

emissions, whereas Jotun A/S saw the need for a more transparent approach to verify a myriad of performance claims on hull and propeller maintenance.

A series of workshops held in accordance with Chatham House Rules involved a steadily increasing number of stakeholders and paved the way for a common understanding among performance monitoring companies, measurement manufacturers, ship maintenance system providers, classification societies, shipbuilders and ship-owners and their associations. Bellona Foundation and Jotun subsequently held a side-event at IMO-MEPC meetings and presented the embryo for a reliable and transparent hull and performance standard at several maritime conferences.

Work on the ISO-Standard was initiated in June 2013 when Working Group 7 under SC2 TC8 was formed. Svend Søyland from Nordic Energy Research serves as the Convener of the working group and Geir Axel Oftedahl from Jotun has the role as Project Manager. A series of Working Group meetings were held: Oslo (June 2013), Tokyo (November 2013), Hamburg (July 2014), Pusan (November 2014), San Ramon (February 2015) and Copenhagen (September 2015). More than 50 experts and observers, representing ship owners, shipping associations, new build yards, coatings manufacturers, performance monitoring companies, academic institutions, class societies and NGOs participated in the ISO working group that reached consensus on ISO 19030 standard. Additional industry stakeholders have been consulted and involved as a part of this extensive process. Worldclass experts shared their deep expertise in a truly collaborative effort and put aside their professional ties. A determination to find workable compromises was the hallmark of the drafting process. Representatives that in other contexts would be fierce competitors share expertise, policies and performance data etc. This was a larger than usual Working Group under the ISO-system and the by far largest with the Ship Technology section. The drafting process uncovered a need to address both the most rigorous methods available and the most commonly used approaches used. This led to the division into three parts.

A Committee Draft of part 1 and 2 (CD) was submitted in March 2015. A Ballot among P-members was concluded in May 2015 with sound support. The target date for submitting a Draft International Standard (DIS) of all three parts was December 2015. An ISO-Ballot was concluded in March 2016 and it is expected the Standard will achieve final approval and official publication by June 2016. The Working Group (WG7) will remain operational in order to prepare future revisions and refining the standard."

3. Build it and they will come

3.1. When a no means yes

It must have been in early 2015 that I received an email from Geir Axel Oftedahl. He would be coming to Hamburg to visit our offices, and would I have time to meet him on that occasion? Sure, I had time. A few days later, Geir Axel walked into my office and surprised me with the idea of continuing the healthy spirit of exchange of the working group in a post-ISO 19030 conference. And he asked me if I would organize it, while Jotun would give flanking support as the main sponsor.

I said no. I had enough on my platter with my full-time job and three other conferences to organize each year. Geir Axel understood and asked for some advice. Somehow, 30 minutes later I had outlined the concept, suggested a venue (a castle in Italy) and drafted a flyer. And reluctantly agreed to organize the event. I shall be eternally grateful for Geir Axel's powers of persuasion…

A key parameter in any conference is the number of participants as it determines the required size of the lecture hall. I estimated that maybe 25 participants would come, based on the number of participants in the last meeting of the ISO 19030 working group. Geir Axel was much more optimistic with his estimate of 50 participants. In the end, we were 82, Table I.

Table I: HullPIC key statistics

Year	2016	2017	2018	2019	2020*	2021*	2022	2023	2024
Venue	Pavone	Ulrichshusen	Redworth	Gubbio	Hamburg	Pontignano	Tullamore	Pontignano	Tullamore
Participants	82	99	103	95	17	58+	100	117+	95
Papers	33	31	36	31	21	19	27	19	23

* COVID years
+ HullPIC and PortPIC combined

Key cornerstones of the concept of HullPIC were quickly hammered out:

1. No parallel sessions
2. Free proceedings available on website http://hullpic.info
3. "No presentation without a paper" rules (as a means to filter out marketing and political presentations)
4. Jotun sponsored dinner on last day to avoid that presenters face an almost empty lecture hall
5. In a nice environment, typically in a venue with history, with most participants staying in same hotel to facilitate networking
6. Provide a list of participants with contact details to all attendees to avoid any tedious hunt for business cards, as a flanking measure for continued networking
7. Limit number of participants to maximum 100; the idea was again that at the end everybody should know everybody else and have good interaction within the group of participants
8. Aim to attract all types of stakeholders, particularly ship owners and operators

3.2. HullPIC 2016

The first HullPIC was held 13-15 April 2016, in the Castello di Pavone, https://www.castello-dipavone.com/, in northern Italy. Unbeknownst at the time, it started another tradition: HullPIC is generally held in historic places that are difficult to reach. But that was more by accident than intention. It is perhaps telling that the first flyer only said HullPIC conference, and not 1st HullPIC conference. At the outset, we did not foresee a long series of yearly HullPIC conferences. However, by the time of the conference, the response of the community had largely surpassed our expectations, and we were already preparing a 2nd HullPIC conference to be announced for the following year.

Despite all controversial discussions on ISO 19030 and the best approach to performance monitoring, there was general support for the HullPIC conference itself. Both developers and users of performance monitoring systems welcomed the aggregation and exchange of knowledge during the event leading to better understanding of ISO 19030, limits and possibilities of data acquisition and correction methods.

Fig.2: Group photo with key ISO 19030 working group members on castle grounds

Fig.3: Lecture hall inside the castle

3.3. 2nd to 9th HullPIC

The popularity of the 1st HullPIC and the growing reputation of the conference led to a rapid increase in participation numbers. The upper threshold of 100 participants that Geir Axel Oftedahl and I had agreed upon was almost reached by the 2nd HullPIC, Fig.4, and surpassed with the 3rd HullPIC, Fig.5, Table I.

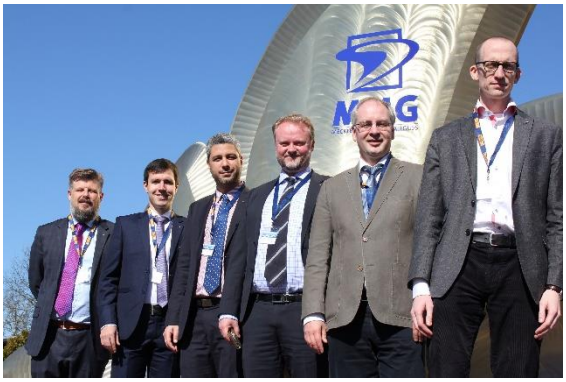

Fig.4: Jotun representatives and myself (2017)

Fig.5: Full house at 3rd HullPIC in 2018

Fig.6: Pontignano 2023, joint HullPIC and PortPIC, with record number of participants

The 2nd HullPIC saw the introduction of another tradition, the "Forum", where two representatives from solution vendors and two representatives from ship operators sat up front to answer questions from moderators and audience. The late Michael vom Baur moderated the first forum, kicking off with a heretic question: Isn't ISO 19030 fairly useless, seeing the many flaws that have been pointed out during the conference? To his and my surprise, the two ship operator representatives were strongly supportive of the standard. "A few years ago, we were not even aware that our performance monitoring was basically non-existent. What we have now is not perfect, but we have progressed from being blind to being one-eyed." Generally, the Forum session has allowed flexible discussion on themes of current interest in the field.

HullPIC was on the up and up, until the COVID pandemic disrupted our lives in 2020. We were lucky to continue with the conferences, even if on-site participation dropped sharply, Fig.8. Many presentations had to be given via video conferencing; the proceedings were still good, but it was a stopgap solution in exceptional times. Due to the low numbers, both in papers and participants, we merged the newly introduced PortPIC and HullPIC conferences in 2021. Born out of necessity, this merger of themes and people proved to be very popular. Post-COVID, participation numbers bounced back rapidly, Fig.9, with the 8th HullPIC (again merged with PortPIC, following popular demand) reaching demand levels where 25% of the requests for participation had to be turned down, as they exceeded the capacity limit of the venue lecture hall.

Fig.8: HullPIC 2020 – 17 participants

Fig.9: HullPIC 2022 – 100 participants

In response, we narrowed down the list of acceptable topics for presentations, excluding robotic in-water inspection and cleaning, as well as descriptions of measures to improve energy efficiency, such as wind assisted propulsion, propulsion improving devices, antifouling technologies, etc. These excluded topics were then exclusively covered by the HIPER conference and the PortPIC conference (see below).

Over the years, new features of HullPIC have strengthened the feeling of community, most notably:

- Richard Marioth (Idealship) introduced a participants' questionnaire and tombola (first time at the 4th HullPIC in Gubbio), Fig.9. Besides multiple-choice questions on performance monitoring for ships, there is also a free-form question on what participants like particularly about the HullPIC conference, Fig.12.
- The 8th HullPIC conference saw a "Hull Management Hero" award given to a member of the community with special merits in advancing the state of the art in hull management. The first laureate was Geir Axel Oftedahl, Fig.10. In 2024, the second laureate was Beom Jin Park (KRISO).

Fig.9: Gifts at Richard Marioth's tombola (at 8th HullPIC in 2024)

Fig.10: Geir Axel Oftedahl receives first Hull Management Hero award (2023)

3.4. HIPER and PortPIC

HullPIC grew too big for our self-imposed capacity limits. At the same time, there was demand for more time to discuss in-water inspection and cleaning, with new guidelines and standards evolving, notably:

- Jotun's Guideline for Proactive Cleaning of Hull Areas in Port & at Anchorage, *Oftedahl and Enström (2020)*
- BIMCO industry standard for in-water cleaning with capture, *Sørensen (2020)*
- New ISO standard on proactive hull cleaning and the associated Clean Hull Initiative, *Oftedahl and Skarbø (2021)*

In response, Geir Axel Oftedahl approached me to organize a "sister conference", which in time was named PortPIC, short for Port In-Water Cleaning Conference. The name similarity between HullPIC and PortPIC was chosen on purpose.

Geir Axel predicted that PortPIC would be [in due time] become bigger than HullPIC. It was a nice plan, but between the first announcement and the first conference, COVID struck. PortPIC started with a handicap, and we were lucky to get it started at all, in Hamburg. The day after the first PortPIC, the city of Hamburg closed down all conference venues and all restaurants. (We had the conference dinner with maybe 15 persons in an otherwise empty restaurant in Hamburg which has 1000+ capacity.) PortPIC has been held twice in conjunction with HullPIC, but has established itself by now as a stand-alone conference with 50-60 participants and a set of sponsoring companies in the field of in-water inspection and cleaning. Proceedings are hosted on the HullPIC conference website.

The HIPER (High-Performance Marine Vehicles) conference, www.hiper-conf.info, has a different history. It started out in 1999 as conference on high-speed and unconventional craft, but the theme has evolved over the years towards "technologies for future ships and shipping", which means these days a strong focus on innovations supporting the decarbonization process in our industry. HullPIC has the focus measuring, HIPER the focus on measures (in design and operation). The conference enjoys increasing popularity with ship owners and operators.

4. Mirroring the state of the art in the industry

Not surprisingly, many papers in the first HullPIC conferences addressed ISO 19030. The newly published standard was in the position of a future son-in-law being presented for the first time: inspected with polite interest, but not yet adopted wholeheartedly except by its own parents. Some working group members presented first practical experience with implementing the standard. Other conference paper came from people who had not participated in the development standard and were now faced with a fait accompli. There was no shortage of suggestions for what should be changed in ISO 19030, coming from both groups, but many had yet to realize that "one does not simply change ISO 19030", Fig.11.

Fig.11: Many had yet to realize that changing an ISO standard was not so simple

The process to implement changes required approval of formal submissions from accredited norming organizations, and a basic prerequisite for that was wide consensus on what exactly should be changed, i.e. getting a large number of stakeholders to support that sentence "ABC" should be changed to "DEF".

Initially, papers and discussions at HullPIC focused on the core topics of ISO 19030:

- Sensors and proxies: issues with speed log accuracy, using speed over ground instead, estimating current speed, propeller thrust measurements, wave measurements with on-board radar or using hindcast meteo data as proxies in performance monitoring models
- Filtering: ISO 19030 recommendations for filtering (perceived as too strict) vs high data frequency (seen as cure it all by some), with some suggestions for filter threshold adapted to estimated errors rather than rigid filter thresholds
- Normalization: baseline models based on CFD (of varying sophistication and accuracy), based on machine learning (still largely 'terra incognita' for most in the community in 2016), or "naval architectural" models (of questionable applicability to off-design drafts and speeds)

Everybody claimed to be ISO 19030 compliant, but only Jotun seemed to follow the default method (ISO 19030 Part 2). And compliance with ISO 19030 is until today by self-proclamation; nobody seems to certify compliance with the ISO 19030, and nobody seems to see a need for that.

Adoption and application in practice of ISO 19030 has developed differently from what its founding fathers probably intended or imagined. But such is life. Children often grow and develop in their own ways and the founding fathers can be proud of what ISO 19030 achieved:

- better documentation with more transparency on techniques employed for data acquisition, filtering and normalization;
- better awareness of data uncertainties and model uncertainties;
- better awareness that various approaches may lead to similarly good performance monitoring results.

Over time, the community, both ship operators and solution providers, got smarter in best business practices for data acquisition and processing. Market and methods have seen consolidation, with mergers and acquisitions of smaller companies, but also fusion of technologies in the performance monitoring process. There have also been more and more papers being presented at HullPIC with joint authoring from solution providers and ship operators.

In the early years, associated topics joined in the conference, mainly related to managing and improving ship performance (as opposed to just monitoring as covered by ISO 19030):

- Developments in coatings and alternative fouling protection techniques (such as ultrasonic hull protection)
- Robotic cleaning of ship hulls
- Energy saving measures (propulsion improving devices, wind assisted propulsion systems, etc.)

These are now redirected towards HIPER and PortPIC, striving for a clearer focus on performance monitoring and measuring technologies. The gaps left by these restrictions have been filled quickly by new developments:

- New monitoring issues related to IMO's CII (Carbon Intensity Indicator) and EU fuel and emission regulations coming in
- Looking beyond the scope of ship operation considered in ISO 19030, e.g. for propulsion (twin-screw, CPP (controllable-pitch propeller), diesel-electric, or wind-assisted propulsion) and ambient conditions (shallow water, ice-infested water)
- Development of methods yielding faster insight, deviating from ISO 19030's traditional view of averaging performance indicators over one year

Predictions are always risky, just remember how far off target Geir Axel Oftedahl and I were in our initial estimates on the popularity of HullPIC. But let's look into the crystal ball.

5. Looking forward

"It is very hard to predict, especially the future", said Niels Bohr, a Nobel prize winner. But the future is generally more interesting than the past. Another appropriate quote is: "Build it and they will come". Jotun and I have every intention to keep building "it" (HullPIC), and it is likely that the community will continue to come – as long as we don't degenerate into an old-boys club reminiscing about the past and presenting the same stuff under new titles.

9. What do you like most about HullPIC/PortPIC?

(Collection of free text answers by participants)

Nice atmosphere // stakeholders get together // the people // friendly and honest attitude // the great atmosphere and time to meet // the venue // community // gathering of people interest in measuring and monitoring performance. Utterly needed. // the people // good combination of presenting vs. time vs. breaks // everything // the tempo, tone and context of presentations // presentations & networking // the local coffee // 6 year mix of academic and market approach // good mix of expertise present and nice organization // Irish Coffee // weather // the jokes // the people // meeting knowledgeable people // the group of participants // location // presentations // whiskey // the expertise // exchange ideas // Volker // exchange & experiencing // making global network among various fields of shipping // the diverse range of topics & view points // conviviality, focused conference // the Spa // high scientific value/standard // good for networking and knowledge sharing/net experience // food, whiskey, people // location // audience, participation & networking // yet to find out // see friendly faces again // let me discover // close to our // great colleagues // information sharing // the interesting discussions with attendees // can tell you on Wednesday // the people // people // discussions with colleagues // Tullamore dew // the good atmosphere // I like to comment, that I would like more shipowners/operators should share more experience // everything // thought provoking discussions with industry professionals // good broad program. Good networking. // conference // presentations and network // good presentations, friendly people, good community // the organizer!

Fig.12: 2024 feedback in Richard Marioth's questionnaire

So far, the conference has managed to stay young and interesting, not least to the influx of new participants and new entries to the performance monitoring market. The continuing and self-enforcing success is largely due to two factors that make the winning formula for HullPIC, Fig.12:

- Quality of presented papers – Papers come from experts in the field, not the silver-tongued me-too salespersons and top managers. The HullPIC proceedings have contributed to the reputation of the conference, and have become a standard reference reflecting the state of the art in ship performance monitoring.
- The networking – HullPIC differs from other conferences. It is hard to put into words how exactly, but there is a special atmosphere of collaboration rather than competition. And over the years, the HullPIC participants have formed a community. The mix of ship operators and solution providers is healthy and productive: "Part of the charm of HullPIC is that it attracts a hearty

mix of ship owners and operators matched with an equal number of technology and service providers," *Austin (2022).*

Both are needed. HullPIC is not a journal where you just add to your publication list, nor is it a cocktail conference.

Vincent Joly (Bureau Veritas), participating for the first time in 2024, described the unique character of HullPIC perhaps best: "This [conference] is truly special, I have never experienced such a sincerity and collaborative spirit in Maritime. I [have now] the conviction that peer-to-peer knowledge sharing for a common interest is not just a good idea, it happens."

Acknowledgements

Failure is an orphan; success has many fathers. First and foremost, I am indebted and grateful to Geir Axel Oftedahl (then Jotun, now Semcon), who had the visionary idea and persistence to twist my arm into organizing HullPIC in the first place. I am very grateful to my partner in crime Jotun, now with Morten Sten Johansen in the lead. Thanks to all the other sponsors, many of which have committed to HullPIC for many years, year after year. I thank specifically Richard Marioth, for his questionnaire and his reviews in the Hansa journal. Finaly, my thanks go to the authors of the 240 papers in total until 2024 inclusive, and the many participants who have contributed to the unique atmosphere.

References

AUSTIN, C. (2022), *CII takes centre stage at the 2022 Hull Performance and Insight Conference (HullPIC)*, Internet article, Selektope, https://selektope.com/cii-takes-centre-stage-at-the-2022-hull-performance-and-insight-conference-hullpic/

ISO (2016), *Measurement of changes in hull and propeller performance*, Int. Standard Org., Geneva

OFTEDAHL, G.A.; ENSTRÖM, A. (2020), *Proactive Cleaning and the Jotun Hull Skating Solution,* 1st PortPIC Conf., Hamburg, pp.66-71, http://data.hullpic.info/PortPIC2020_Hamburg.pdf

OFTEDAHL, G.A.; SKARBØ, R.A. (2021), *The Need for an International Standard for Proactive Hull Cleaning and the Clean Hull Initiative (CHI)*, 2nd PortPIC Conf., Pontignano, pp.66-71, http://data.hullpic.info/PortPIC2021_Pontignano.pdf

SØRENSEN, A.F. (2020), *Industry Standard for In-water Cleaning with Capture*, 1st PortPIC Conf., Hamburg, pp.79-81, http://data.hullpic.info/PortPIC2020_Hamburg.pdf

SØYLAND, S.; OFTEDAHL, G.A. (2016), *ISO 19030 – Motivation, Scope and Development*, 1st HullPIC Conf., Castello di Pavone, pp.292-297, http://data.hullpic.info/HullPIC2016.pdf

Bunker Parcel Data Collection: Enhancing Emissions Reporting

Matteo Barsotti, Oceanly, Genova/Italy, matteo.barsotti@theoceanly.com

Abstract

Accurate emissions reporting is a critical component of modern maritime operations, driven by the need for compliance with regulations such as the EU Emissions Trading System (ETS) and FuelEU, as well as the goal of optimizing operational costs. Achieving this accuracy requires a robust and configurable system for recording fuel consumption onboard ships, which must also be intuitive and user-friendly to ensure effective implementation. A method for bunker parcel reporting has been developed to address these needs. This approach involves recording detailed technical specifications for each fuel parcel received onboard, including quantity, category, viscosity, sulphur content, density, and lower calorific value (LCV). Additionally, it allows for tracking the use of each parcel, enabling precise calculations of emissions directly linked to actual fuel consumption. This enhancement to emissions reporting systems ensures a higher level of precision in data collection and calculations. By incorporating detailed fuel parcel data and usage timelines, the methodology significantly improves the reliability of emissions data, benefiting all stakeholders involved in regulatory compliance and operational monitoring. This presentation will explore the technical aspects and implementation of the bunker parcel reporting approach, demonstrating how it contributes to precise and transparent emissions reporting while aligning with industry requirements for accuracy and efficiency.

1. Introduction

An accurate reporting is what customers are seeking nowadays; it is maybe forced by emission regulations but more and more the very first question when presenting a data collection system is about validation and data accuracy. The emission regulations of course have driven the improvement of the software in terms of validation and accuracy but until very recently the system should be also flexible and allow adjustment from the ship or from the onshore users. Usually for emission reporting were reported just the Remains of board (R.O.B.) of the different fuel type available on board. This kind of reporting satisfy the majority of the monitoring method of the emission regulations. The game changer here is the biofuel but in general the FUEL EU MARITIME, the new regulations entered into force on January 1st 2025.

Before diving deeply into the regulation in the next chapters, it is necessary to clarify what is meant by Fuel Product, Fuel Category, Fuel Category Group and Parcel:

- Fuel Product is the name of the fuel bunkered, and it usually tells something about its characteristics but it does not tell much about all the emissions related characteristics, usually it is also the commercial name of the bunkered fuel.
- Fuel Category is the emissions related categorization as per ISO8217 standard IMO and MRV regulations
- Fuel Category Group refers to the type of category, if it is fossil (oil, gas, alcohol) , biofuel, or RFNBO (Renewable fuel from non-biological origins)
- Fuel Parcel is the specific bunkered fuel onboard (maybe known as batch)

It will be shown also that not only the regulations drive this kind of fuel reporting but also the needs to keep track of the fuel, maintain segregated and in case of commingling to know exactly what is to be commingled.

2. Fuel EU and Biofuel

The Fuel EU Maritime regulation entered into force this year, use the general principle of the well-known EU MRV in terms of the voyage leg and port stay definition but did take in consideration the

energy associated to each part of the voyage or port; this energy comes from the fuel burned on board, from the electrical power used in the shore power connection but the real news is the fact that now it is taken into account the energy associated with the production of the fuel. Afterwords, the result is compared to a target energy and if not met there is a fuel penalty in Euro to be paid to be compliant.

As the formula did use the real consumption associated with the specific characteristics of the fuel an excellent accurate reporting is vital and not only for the fossil fuel that have static characteristics but especially for the biofuels.

	GHG intensity $\left[\frac{gCO2eq}{MJ}\right] = f_{wind} \times (WtT + TtW)$ Equation (1)
WtT	$\frac{\sum_i^{n\ fuel} M_i \times CO_{2eq\ WtT,\ i} \times LCV_i + \sum_k^c E_k \times CO_{2eq\ electricity,k}}{\sum_i^{n\ fuel} M_i \times LCV_i \times RWD_i + \sum_k^c E_k}$
TtW	$\frac{\sum_i^{n\ fuel} \sum_j^{m\ engine} M_{i,j} \times \left[\left(1 - \frac{1}{100} C_{slip\ j}\right) \times (CO_{2eq,\ TtW,i,\ j}) + \left(\frac{1}{100} C_{slip\ j} \times CO_{2eq\ TtW,\ slip,\ i,j}\right)\right]}{\sum_i^{n\ fuel} M_i \times LCV_i \times RWD_i + \sum_k^c E_k}$
f_{wind}	Reward factor for wind-assisted propulsion

Here are highlighted where the parcel management intervene, as the specific fuel characteristics shall be used for the calculation.

The biofuels are quite unique in terms of emission related characteristics, two biofuels of the same category with similar viscosity can have different emission related characteristics. In other words, the parcel reporting is extremely important when reporting biofuels. Biofuels can also be blend so a mixture of fossil fuels and a biological component and again here a parcel solution is required in order to not mix the fuel in the reporting, so blends can be treated separately.

3. Bunker Parcel solution

The bunker parcel solution allows recording each batch of fuel using a unique identifier, this identifier can be ship specific and also customized by the customer. The system checks of course that this identifier is not used on the same ship and also in the fleet.

The parcel can be then referenced to the consumption related to a specific activity and equipment; by doing this, the resulting calculation will be taking into account the exact characteristics of the fuel in use. Practically will be not applied any FIFO or LIFO logic.

- FIFO means First In First Out and it is usually the logic applied onboard where the first fuel available in the tank is also the first to be used because of the fact that usually the fuel exit from the bottom of the tank.
- LIFO means Last In First Out and it is the common behaviour of the emission reporting software where adding a fuel in the same fuel type will immediately updates the characteristics of the fuel itself.

From emission regulation point of view, there was no difference between LIFO and FIFO but there was a difference from other two point of view:

- Sulphur
- Engine performance

The sulphur content is managed but the IMO 2020 regulation and by ECA areas regulation, but such

regulations are just limits of the sulphur content, therefore if the sulphur content is 0.33 or 0.37 nothing change for the regulation but it did change when it is necessary to calculate the sulphur emissions.

The engine performance is affected by the fuel that is in use and in a monitoring system either is using high frequency or manual input data, it is important to have recorded the correct information. i.e. not having an updated Heat of Combustion will result in having a wrong Specific Fuel Oil Consumption.

These are other two reason why a bunker parcel solution is much more realistic and accurate.

Let us now have a look at the new feature of the system, the bunker parcel solution can be applied in the system to all fuels (fossil, biofuels and RFNBO) or just to biofuels according to the specific needs of the customer. The proper process is distinguished into 2 parts, the fuel bunkering form and the consumption recording.

3.1. Bunkering Form

The fuel bunkering form allows recording all the important and required information:

- Unique identifier
- Quantity
- Category
- Viscosity
- Density
- LCV
- Water content
- Sulphur content

In case of biofuel, it is also possible to record:

- Type of raw material
- Emission intensity E
- POS Proof of Sustainability number
- EU RED compliant

As those last values are available from the POS document, it may require several weeks to receive such information so the mentioned fields are not mandatory during the insertion of the fuel bunkering form but they become required whenever the fuel will be used and then the vessel report will remains in status draft until the information will be added.

3.2. Consumption recording

As already explained, the emission related information became important or better mandatory when the fuel is actually used. So whenever the fuel is used the first time it will be asked to record the missing information (if any). Then the fact that there is a consumption of course will reduce the quantity of fuel of the specific parcel and then there is a validation on the maximum consumable amount (it cannot be consumed more than what is available).

The user will be then able to select for each equipment the fuel type used, the exact parcel of the fuel type selected and in case add the emission characteristics.

This simple recording will generate the correct recording for the Fuel EU maritime, all the other emission regulations and, as said, all the engine parameters.

3.3. Next Possible Steps

The procedure explained here has one limitation, no commingling is allowed, unless a de-bunkering and a new bunkering is created but of course calculations of the emission parameters should be done externally. The next possible step is to create a specific commingling operation to allow mixes of the fuel already on board, but it has to be seen what really happens in this and next years, maybe other modification to the software will be needed.

4. Conclusions

As Latins said “Scripta manent, verba volant” let’s write it down what means have a reliable reporting using the bunker parcel solution. Let’s imagine having on board 100 tons of biofuel from waste cooking oil with an emission intensity of 7.5 and loading a new batch of 50 tons of biofuel same from waste cooking oil but with an emission intensity of 13.2. Now with a system without parcel management, the total biofuel is 150 tons with an emission intensity of 13.2; if we then imagine having 10 MT consumption of the first batch and 10 MT of the second batch, we have the following results:

Assuming fwind =1, C, K and TtW are same in both case

- Case no parcel: GHG intensity = 1 * [(10 * 13.2 * C + 10 * 13.2 * C) / K] + TtW
- Case with parcel: GHG intensity =1 * [(10 *7,5 * C + 10 * 13,2 * C) / K] + TtW

This illustrates that a small difference of 5.2 gCO2eq/MJ with just 20 MT can cause over a ship’s yearly consumption.

As very well underlined it is of utmost importance have a robust and accurate reporting for emissions but also in general for performance monitoring. The new feature presented here goes in that direction allowing to have a strict and precise control of the bunker onboard allowing the operator on shore to have a clear situation of the bunkers on board, the emission regulation calculation, the reliable engine performance calculations and of course cost savings.

On the Speed and Loading Condition Dependency of the Most Common Performance Values

Andrea Farkas, Hempel, Zagreb/Croatia, afar@hempel.com
Ditte Gundermann, Hempel, Lyngby/Denmark, digu@hempel.com
Saeed Mehri, Hempel, Lyngby/Denmark, smeh@hempel.com

Abstract

The calculation of key performance indicators (KPI) in ship performance monitoring relies on adequate performance values (PV). In ISO 19030 two performance values are defined: percentage speed loss and percentage power increase which basically represent speed and power deviations. These performance values serve as the most common performance values used in nowadays ship performance monitoring. However, their drawbacks related their speed-dependency have been already discussed. In addition to this, it is important to notice that these performance values are subjected to loading condition dependency as well. The ISO 19030 method addresses this issue with the averaging of performance values in reference and evaluation period for the calculation of key performance indicators. This could be the case if the operational profile of the ship does not change significantly through dry-docking period, which is unfortunately quite rare. In this paper, the simple numerical approach, based on a new method for the assessment of frictional resistance coefficient, for the assessment of fouling effects on ship hydrodynamic characteristics is proposed. The proposed method has been validated by comparison of the obtained results for fouling effects and results of CFD simulations published in the literature for one containership, bulk carrier and tanker ship and fouling with barnacles. Thereafter, a case study is prepared for which speed-dependency and loading condition dependency of the most common performance values are demonstrated. Finally, the challenges in finding suitable performance values for ship performance monitoring are discussed.

1. Introduction

Ship performance monitoring secures safe and environmentally friendly operation with minimal costs. It also helps in optimization of maintenance scheduling, raises awareness about equipment availability and monitors its rate of deterioration. The global standard of ship performance monitoring was published in ISO 19030, *ISO (2016)*. It has been developed to be widely acceptable by shipbuilders, ship owners, engine manufacturers, coating companies, classification societies, the IMO etc. The goal of the standard it to enable ship owners and operators a comparison of hull and propeller solutions with simple and transparent method and data, that they can select the most efficient options for their vessels. Back in 2016, the standard was developed based on input from a wide range of representatives in the marine industry including academia and should as such represent the state of the art within performance monitoring. However, it soon became evident that the applicability of the standard was not as wide as intended, mainly because of the extensive filtering required by the method, which in many cases results in data scarcity and poor foundation for decision making. The introduction of various environmental regulations in the shipping industry has emphasized the importance of reliably documenting achieved energy savings and the evaluation of various energy saving measures. Namely, with numerous mitigation measures suggested by academia and industry which enable potential energy savings and also represent valuable investment, ship owners and operators are confronted with important need for making educated decisions, *Sfiris et al. (2023)*. This strongly incentivized the development of various methods in ship performance monitoring and since the release of ISO 19030, lot of studies in the literature have been carried out in order to improve standard analysis, *Gupta et al. (2024), Esmalian et al. (2023), Dalheim and Steen (2020), Taskar and Andersen (2023), Gundermann and McLaughlin (2019), Berthelsen and Nielsen (2021)*.

Regardless of the applied model or method, every ship performance monitoring method relies on the calculation of PV (performance value) which are later on used in the determination of KPIs. PVs are calculated for every datapoint and then Performance Indicators (PI) are calculated by averaging PV in

reference and evaluation period. Obviously, if ISO 19030 standard is applied, the number of analyzed data points will be limited because only loading conditions which refer to sea trial conditions can be analyzed. In a case where ship performance model is used as reference model, more datapoints can be analyzed after certain filtering and corrections depending on model.

Most studies in the literature refer to the advancements of ship performance models, filters and corrections and do not investigate much PVs and issues related to them. Few studies discussed drawbacks of the most common PVs: speed and power deviations, related their speed-dependency, *Bertram (2017)*, *Schmode et al. (2018)*. *Bertram* (*2017*) outlined two main problems related to PVs: fouling mostly causes changes in frictional resistance, which has more importance at lower speeds; and added resistance in waves depends strongly on speed, while the most common method for wave correction does not depend on speed. Additional effort to solve speed-dependency of these PVs is presented in *Oliveira et al. (2018)*, introducing new PV and PI which can be used in performance monitoring – equivalent sand grain roughness (k_S). However, due to the inability of estimating k_S for negative power differences, the proposed algorithm still relies on finding median of power deviations in three months period and then finding k_S for this value. The authors concluded that although their approach enables more reliable comparison between the vessels and against the vessel itself, the final result is still speed-dependent, *Oliveira et al. (2020)*. *Schmode et al. (2018)* introduced a new hull performance index from the viscous components only. Using the assumption that the fouling will only affect viscous resistance, the authors have derived a performance value which is less speed dependent, however it requires accurate decomposition of ship total resistance and relies on certain additional assumptions.

Except for speed-dependency of the most common PVs, these PVs are subjected to loading condition dependency as well. The ISO 19030 method addresses this issue with the averaging of PVs in reference and evaluation period for the calculation of PIs. This could be valid if the operational profile of the ship does not change significantly through dry-docking period, which is unfortunately quite rare.

2. Method

In order to demonstrate speed and loading condition dependency of speed and power deviations a relatively simple numerical approach is used. This approach relies on hypothesis that propulsive efficiency will not change dramatically due to the presence of fouling on the ship hull because of opposite effects of increasing hull efficiency and decreasing open water efficiency, *Svensen (1983)*. Same hypothesis is applied in *Oliveira et al. (2020)* and confirmed in *Song et al. (2020a)*, where the authors demonstrated that propulsive efficiency varies less than 2 % with increasing hull roughness if the propeller is clean using CFD simulations. With the application of this hypothesis the delivered power for fouled ship can be expressed as:

$$P_{DR} = \frac{R_{TR} v}{\eta_{PR}} = \frac{\rho v^3 S C_{TR}}{2\eta_{PS}} \tag{1}$$

R_{TR} is the total resistance of a fouled ship, v is the ship speed, η_{PR} is the propulsive efficiency for fouled ship which is the same as the propulsive efficiency for smooth ship η_{PS}, ρ is the density of the water, S is the wetted surface area, C_{TR} is the total resistance coefficient of a fouled ship.

To adequately account for the effect of increased hull roughness on ship hydrodynamic performance, first the increase in frictional resistance coefficient (ΔC_F) has to be determined, which can be done with the Granville similarity law scaling method, *Granville (1958)*. However, this method has been criticized lately in the literature, as it accounts for only a single value of friction velocity (u_τ), and consequently a single roughness function value (ΔU^+) across the entire flat plate. This approach is simplification, because it is well established that u_τ can vary even on a flat plate, *Demirel et al. (2017a)*. A novel method for predicting frictional resistance coefficient of a flat plate is presented in *Farkas et al. (2021)*, where the authors presented the method which can account for varying u_τ across the flat plate and in that way overcome this important disadvantage of Granville method. What is more, the method is

capable of taking into account the effect of heterogeneous roughness on frictional resistance.

This method relies on Granville's proposal for the determination of ΔU^+ values with the local method without displacement thickness, *Granville (1987)*:

$$\Delta U^+ = \left(\sqrt{\frac{2}{C_f}}\right)_S - \left(\sqrt{\frac{2}{C_f}}\right)_R - 19.7\left[\left(\sqrt{\frac{C_f}{2}}\right)_S - \left(\sqrt{\frac{C_f}{2}}\right)_R\right] \quad (2)$$

at the same value of $Re_x C_f$, where Re_x represents the local Reynolds number and C_f is the local frictional resistance coefficient, and the application of certain roughness function model for a given surface condition. The roughness function model applied in this study is Grigson type which is proven to be adequate for barnacle fouling in *Demirel et al. (2017b)*:

$$\Delta U^+ = \frac{1}{\kappa} ln(1 + k^+) \quad (3)$$

where κ is the von Karman constant and k^+ is the roughness Reynolds number.

Firstly, the flat plate has to be longitudinally discretized, and Re_{xS} and C_{fS} have to be determined for every discretized point. Then $u_{\tau R}$ is iteratively calculated by equating Eqs. (2) and (3). After that, C_{fR} and corresponding Re_{xR} is calculated using the following equation:

$$Re_{xR} = \frac{Re_{xS} C_{fS}}{C_{fR}} \quad (4)$$

The procedure continues as long as x_R is lower than the length of the analyzed flat plate.

This method allows the investigation of the effect of heterogeneous fouling on frictional resistance coefficient by simply having $\Delta U^+=0$ in the areas where fouling is not present. More details about this iterative algorithm can be found in *Farkas et al. (2021)*.

While the method for the prediction of frictional resistance coefficient of a flat plate has been thoroughly verified and validated in *Farkas et al. (2021)*, a numerical approach for the prediction of fouling effects on delivered power still has to be validated. This is done by calculating ΔC_F using the method presented in *Farkas et al. (2021)* for fouling with barnacles and then evaluating the increase in total resistance and delivered power for one containership - KCS. The obtained results are thereafter compared to CFD results available in *Song et al. (2020a)* for KCS fouled with barnacles with the smooth propeller. The analyzed surface conditions, Table I, match the ones presented in *Song et al. (2020a)*.

Table I: Investigated surface conditions, *Song et al. (2020a)*

Surface condition	Barnacle height, mm	Surface coverage, %	Roughness length scale – *k*, μm
S10%	1.25	10	24
S20%	1.25	20	63
S40%	1.25	40	149
S50%	1.25	50	194
M10%	2.5	10	84
M20%	2.5	20	165
M40%	2.5	40	388
M50%	2.5	50	460
B10%	5	10	174
B20%	5	20	489

In this method, the obtained increase in total resistance will be the same as the obtained increase in delivered power as propulsive efficiency is assumed to be the same for fouled and smooth ship:

$$\Delta P_D = \frac{P_{DR}-P_{DS}}{P_{DS}} = \frac{\frac{R_{TR}v}{\eta_{PR}} - \frac{R_{TS}v}{\eta_{PS}}}{\frac{R_{TS}v}{\eta_{PS}}} = \frac{R_{TR}-R_{TS}}{R_{TS}} \quad (5)$$

Therefore, even though propulsive efficiency will change with speed, this will not make any difference on the final power deviations.

Since the analyzed conditions represents uniformly distributed roughness, i.e. barnacle fouling which is uniformly distributed, using the relationship proposed in *Demirel et al. (2017b)* roughness length scale – *k*, which goes into equation for deriving k^+ can be determined:

$$k^+ = \frac{ku_\tau}{\nu} \quad (6)$$

where ν is the kinematic viscosity coefficient.

Consequently, real uniform barnacle fouling with various height and surface coverage can be replaced with uniformly rough surface having roughness height equal to *k* and described with Grigson roughness function model, *Demirel et al. (2017b).*

An additional important disadvantage of Granville similarity law scaling method is that only increase in frictional resistance coefficient of equivalent flat plat can be studied and the influence on the remaining ship resistance characteristics cannot be performed *Song et al. (2019)*. This disadvantage is also present in the method presented in *Farkas et al. (2021)*, since this method is developed for the assessment of ΔC_F for flat plate. Several studies in the literature demonstrate that roughness causes changes in the remaining ship resistance characteristics and not only in frictional resistance. Thus *Farkas et al. (2020)* demonstrated that roughness causes slight decrease in ratio between frictional resistance coefficients of a ship and equivalent flat plate (k_f). *Song et al. (2019), Farkas et al. (2020a,b)* demonstrated that roughness causes decrease in form factor, while *Song et al. (2019), Farkas et al. (2020a,b)* demonstrated that the presence of roughness causes the decrease in wave resistance coefficient. Even though the presence of roughness causes the decrease in form factor value, the viscous pressure coefficient - C_{VP} will increase due to the presence of roughness, just not with the same "pace" as C_F and that is why form factor for rough ship will be lower in comparison to the smooth ship. However, roughness decreases the wave resistance coefficient - C_W. While all before-mentioned studies represent CFD studies, the validation of such CFD approach for the prediction of biofouling influence on total resistance is presented in *Song et al. (2020b)*, where also it was experimentally demonstrated that the presence of roughness causes the decrease in wave resistance coefficient.

All those studies demonstrate the capability of CFD to adequately capture the impact of roughness on individual resistance components. Within these studies total resistance coefficient for rough ship is decomposed using following equation:

$$C_{TR} = (1 + k_R)C_{FR} + C_{WR} \quad (7)$$

k_R is the form factor coefficient for rough ship obtained using double body simulations, C_{FR} the frictional resistance coefficient for rough ship obtained using double body simulations and C_{WR} the wave resistance coefficient obtained using a combination of free surface and double-body simulations.

In order to obtain more reliable power deviations due to presence of roughness and compensate for inability to capture the effects of fouling on the remaining resistance components additional cases are also checked: KCS fouled with hard fouling, *Farkas et al. (2020a)*, KVLCC2 fouled with hard fouling at 15.5 kn, *Farkas et al. (2020a),* and one handymax bulk carrier (BC) fouled with hard fouling at 16.32 kn, *Farkas (2021)*. The hard fouling was described using the same roughness function as for barnacles, just with different roughness length scales, Table II.

As discussed in *Farkas et al. (2020c)*, even though form factor will slightly decrease due to the presence of roughness, it can be considered that 1+*k* value will not significantly change, meaning that the relative increase in C_{VP} due to the presence of roughness will be quite similar to relative increase in C_F. What is more, since only increase in frictional resistance for flat plate is available, which is slightly lower than increase in frictional resistance for ship, this will additionally compensate for slight reduction in form factor for fouled ship. During the analysis of results presented in papers dealing with impact of biofouling on ship hydrodynamic performance it was noticed that relative change in C_W is usually equal to 1/3 of relative change in C_{VP}. Therefore, the equation for calculation C_{TR} used in this study is:

$$C_{TR} = C_{TS} + \left[1 + k_S - \frac{C_{WS}}{3C_{VPS}} k_S\right] \Delta C_F \tag{8}$$

where C_{TS} is the total resistance coefficient of smooth ship, k_S is the form factor of smooth ship, C_{WS} is the wave resistance coefficient of smooth ship, C_{VPS} is the viscous pressure coefficient of smooth ship and ΔC_F is the increase in frictional resistance coefficient for equivalent flat plate obtained using the method presented in *Farkas et al. (2021)*.

The support for making such hypothesis lies in the fact that C_{VP} will increase due to the presence of roughness, while C_W will decrease due to the presence of roughness. Also, both Granville similarity law scaling method and method presented in *Farkas et al. (2021)* predict ΔC_F for flat plate due to the presence of roughness. Even though, it was demonstrated that roughness will cause slight decrease in k_f, k_f will still be above 1, meaning that ΔC_F for ship will be slightly higher than for flat plate. Therefore, with such decomposition ΔC_F for flat plate can be used to represent change in total resistance coefficient: ΔC_T for a ship.

Longitudinal discretization of flat plate representing investigated ships were made using very fine mesh (points were placed every 1 cm), since computational cost of this numerical calculation is quite low, i.e. typical simulation runs around 20 s.

The results for the impact of hard fouling on total resistance coefficients are presented in Table II. Quite accurate results are obtained, with the highest relative deviation around 2.5 %, but for most of cases it is below 2 %. The obtained increases in ΔC_T for a fouled ships are captured with adequate trends, Fig.1.

Table II: The validation study for hard fouling

k, μm	$10^3 C_T$, KCS CFD	$10^3 C_T$, KVLCC2 CFD	$10^3 C_T$, BC CFD	$10^3 C_T$, KCS equation (8)	$10^3 C_T$, KVLCC2 equation (8)	$10^3 C_T$, BC equation (8)
0	2.083	1.796	2.198	2.083	1.796	2.198
2065	4.079	3.977	4.717	4.153 (1.83 %)	4.038 (1.54 %)	4.607 (-2.32 %)
1475	3.886	3.755	4.425	3.954 (1.75 %)	3.817 (1.65 %)	4.367 (-1.32 %)
923.5	3.623	3.478	4.112	3.703 (2.21 %)	3.539 (1.74 %)	4.065 (-1.16 %)
659.64	3.458	3.299	3.915	3.540 (2.38 %)	3.368 (1.77 %)	3.869 (-1.19 %)
413	3.254	3.096	3.665	3.334 (2.48 %)	3.137 (1.02%)	3.622 (-1.16 %)
295	3.122	2.947	3.507	3.200 (2.51 %)	2.978 (1.06 %)	3.461 (-1.30 %)

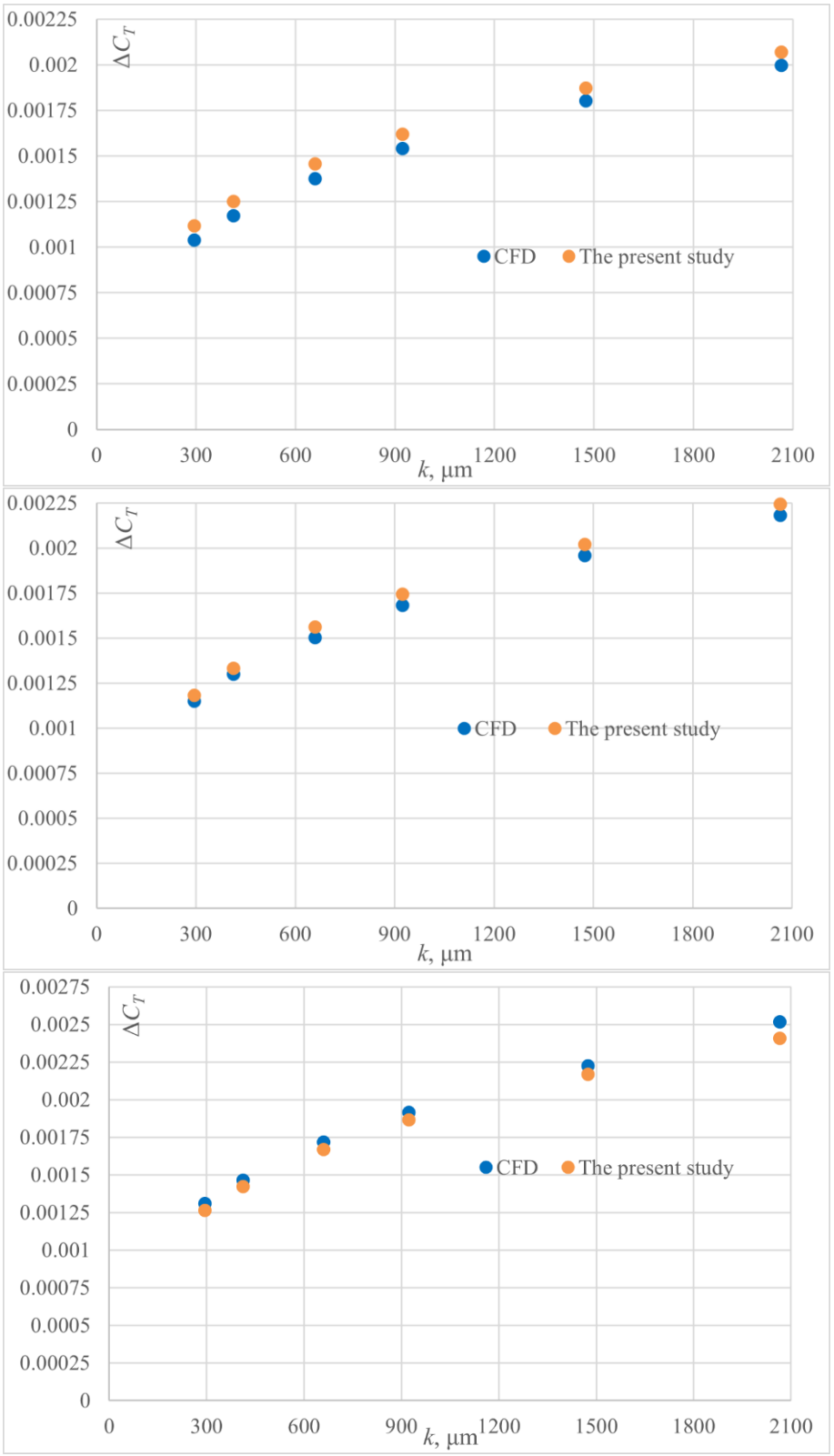

Fig.1: The validation study for hard fouling: KCS (upper), KVLCC2 (middle) and BC (lower)

After the validation study for hard fouling, where the obtained total resistance coefficient for fouled ships is compared with the results from CFD studies, we decided to also compare the results obtained delivered power for ship fouled with barnacles using the proposed method and CFD study available in the literature, *Song et al. (2020a)*, Table III. The proposed numerical approach is capable of adequately capturing the effects of fouling on the ship delivered power and total resistance. The highest relative

deviation (*RD*) from the CFD results in the prediction of R_T is lower than 1 %, while for the prediction of P_D these values are lower than 2.6 %. Fig.2 shows the obtained ΔC_T. The proposed method adequately captures the trend of ΔC_T. Considering two hypothesis used in the this method, i.e. Eq.(8) and $\eta_{PR} = \eta_{PS}$, the achieved level of accuracy in comparison to current state of the art – CFD simulations for the prediction of roughness effect on ship hydrodynamic characteristics is quite satisfactory and it can be concluded that this method can be used for the evaluation of hull roughness effects on ship hydrodynamic performance.

Table III: The validation study for fouling with barnacles

k, μm	R_T, kN CFD	P_D, MW CFD	η_P CFD	R_T, kN Present method	P_D, MW Present method	η_P Present method
0	1523.2	27.00	0.697	1523.2	27.00	0.697
24	1799.5	31.39	0.708	1802.6 (0.18 %)	31.95 (1.80 %)	0.697 (-1.59 %)
63	1956.5	34.03	0.710	1964.2 (0.39 %)	34.82 (2.31 %)	0.697 (-1.88 %)
84	2011.8	34.97	0.710	2020.6 (0.44 %)	35.82 (2.42 %)	0.697 (-1.94 %)
149	2134.7	37.06	0.711	2145.3 (0.50 %)	38.03 (2.61 %)	0.697 (-2.06 %)
165	2157.9	37.47	0.711	2169.3 (0.53 %)	38.45 (2.62 %)	0.697 (-2.04 %)
174	2170.3	37.70	0.711	2182.1 (0.54 %)	38.68 (2.60 %)	0.697 (-2.00 %)
194	2195.7	38.15	0.711	2208.6 (0.59 %)	39.15 (2.62 %)	0.697 (-1.98 %)
388	2373.9	41.40	0.708	2394.8 (0.88 %)	42.45 (2.54 %)	0.697 (-1.61 %)
460	2423.3	42.31	0.707	2445.3 (0.91 %)	43.35 (2.45 %)	0.697 (-1.50 %)
489	2441.5	42.62	0.707	2462.2 (0.85 %)	43.64 (2.40 %)	0.697 (-1.52 %)

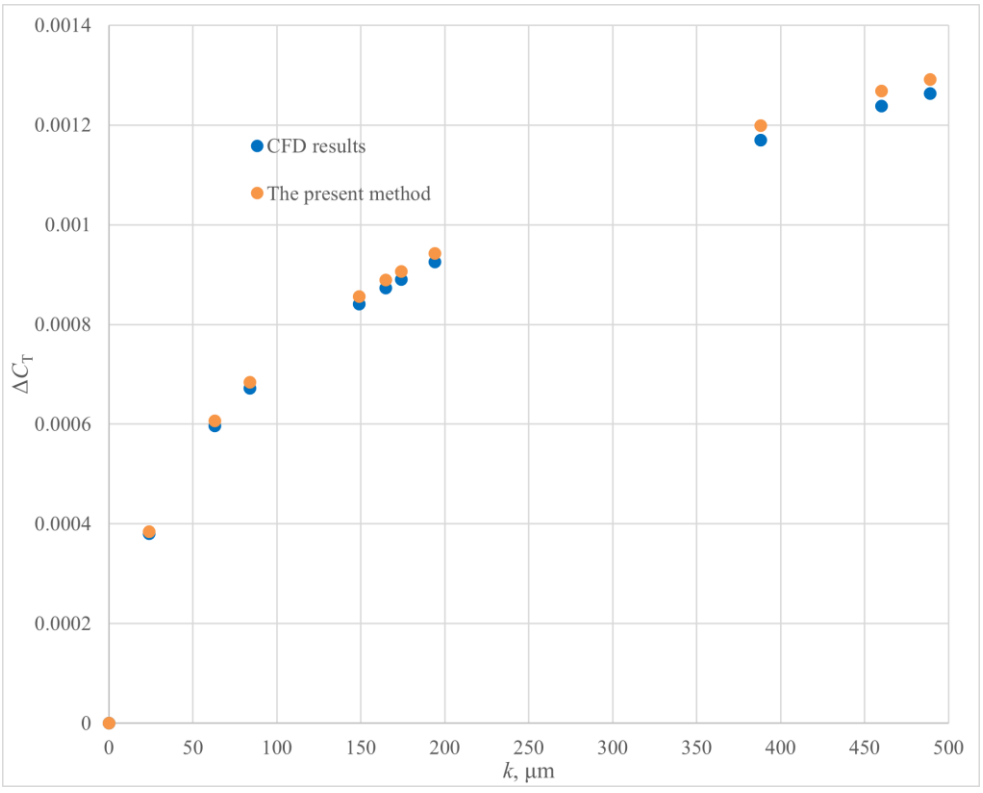

Fig.2: The validation study for fouling with barnacles, KCS

3. Results and discussion

This section is organized in two parts: case study in which the speed and loading condition dependency of the most common performance value: power deviation is demonstrated, and two examples from in-service data in the end of dry-docking (DD) period are analyzed in order to further discuss the challenges associated with the performance values for ship performance monitoring.

3.1. Demonstration of speed and loading conditions dependency of power deviations

To demonstrate speed and loading condition dependency of power deviations, two sets of towing tank test results are utilized: one for post-panamax containership and one for very large LPG carrier. Due to the confidentiality the main particulars of these two vessels could not be presented within this paper. The extrapolated results of towing tank tests for containership are available for design and ballast loading condition and speeds from 22 kn up to 30 kn (depending on loading condition), while for LPG carrier results are available for design, scantling and ballast loading conditions.

As already mentioned, power deviations of effective power will be the same as deviations of delivered power using the method presented in Section 2. In a case where ship propeller is also fouled, propulsive efficiency will decrease, *Farkas et al. (2020d), Song et al. (2020a)*, which will mean that deviations of delivered power are higher for such case than deviations of effective power.

The speed and loading condition dependencies of power deviations are evaluated for fouling with barnacles characterized with surface condition M10%, Table I. The obtained results for containership are presented in Table IV, while the obtained results for LPG carrier are presented in Table V. Longitudinal discretization of equivalent flat plates were made using very fine mesh (points were placed every 1 cm). The obtained power deviations for both cases are presented in Fig.3.

From the obtained results it is clear that power deviations experience quite high loading condition dependency as well as speed-dependency. Speed dependency is more pronounced in for the containership in design loading condition where power deviation deviates from average value by 19.4 % at the lowest speed and by -28.2 % at the highest speed, while for ballast condition power deviation deviates from average value by 7.3 % at the lowest speed and by -9.9 % at the highest speed. Speed dependency for LPG carrier is also present: power deviation for design condition deviates from average value by 5.4 % at 16 kn and by -10.8 % at 19 kn, for scantling condition deviates from average value by 3.2 % at 16 kn and by -4.5 % at 18 kn, while for ballast condition power deviation deviates from average value by 9.3 % at 13 kn and by -7.9 % at 20 kn.

Table IV: Results for containership

Loading condition	Speed, kn	$1000 \times C_{TS}$	$1000 \times \Delta C_T$	Power deviations, %
Design	22	1.830	0.692	37.80
Design	23	1.846	0.694	37.57
Design	24	1.894	0.690	36.41
Design	25	1.983	0.678	34.20
Design	26	2.121	0.658	31.02
Design	27	2.211	0.627	27.05
Design	28	2.317	0.583	22.58
Ballast	24	2.566	0.581	22.64
Ballast	25	2.600	0.578	22.22
Ballast	26	2.633	0.574	21.81
Ballast	27	2.651	0.570	21.33
Ballast	28	2.671	0.563	20.72
Ballast	29	2.718	0.554	19.96
Ballast	30	2.777	0.542	19.00

Table V: Results for LPG carrier

Loading condition	Speed, kn	$1000 \times C_{TS}$	$1000 \times \Delta C_T$	Power deviations, %
Design	13	1.896	0.692	36.48
Design	14	1.864	0.706	37.87
Design	15	1.849	0.717	38.76
Design	16	1.846	0.726	39.29
Design	17	1.864	0.731	39.19
Design	18	1.986	0.718	36.16
Design	19	2.117	0.704	33.24
Scantling	13	1.909	0.702	36.79
Scantling	14	1.888	0.715	37.89
Scantling	15	1.877	0.726	38.67
Scantling	16	1.876	0.734	39.14
Scantling	17	1.900	0.738	38.85
Scantling	18	2.010	0.728	36.24
Ballast	13	2.196	0.731	33.29
Ballast	14	2.278	0.729	31.99
Ballast	15	2.367	0.724	30.60
Ballast	16	2.416	0.725	30.00
Ballast	17	2.435	0.729	29.92
Ballast	18	2.446	0.733	29.98
Ballast	19	2.469	0.736	29.79
Ballast	20	2.578	0.723	28.05

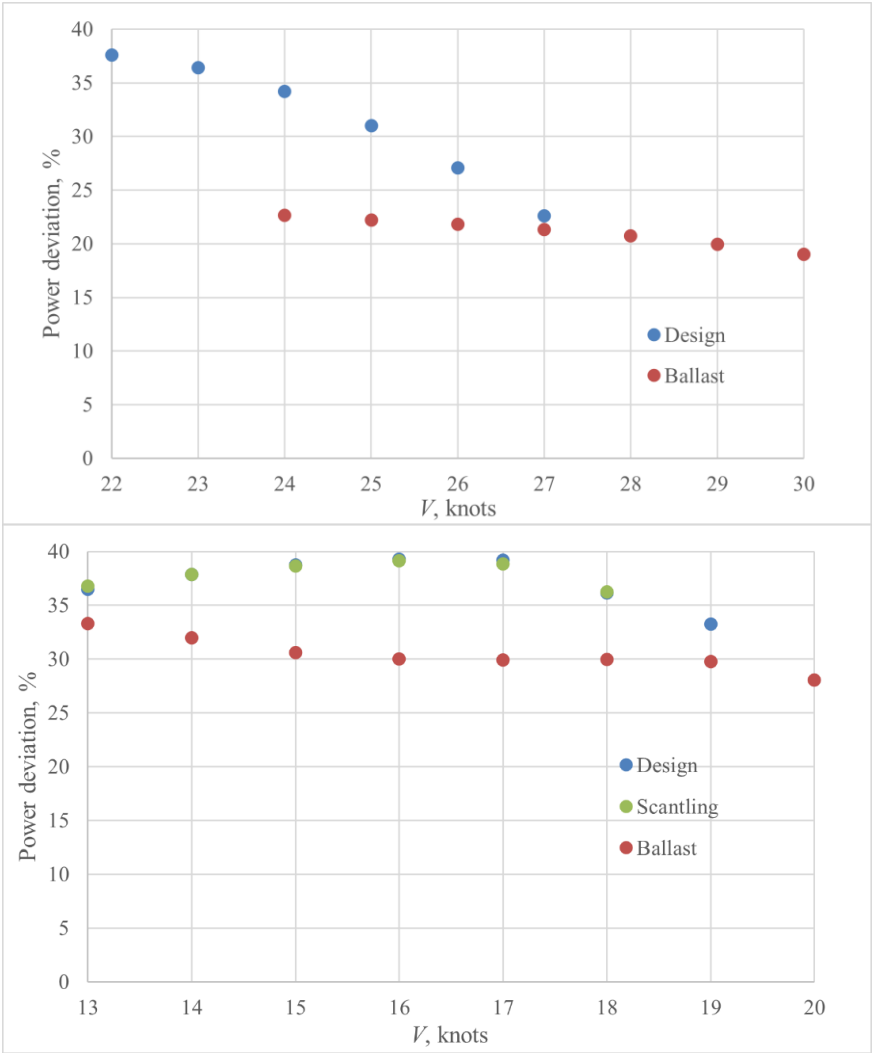

Fig.3: The obtained power deviations for containership (upper) and LPG carrier (lower)

The maximum power deviation is usually obtained for lower speeds where viscous resistance is dominant, while the minimum of power deviations is always obtained at the highest investigated speed. However, there are cases where the maximum power deviation will not always be obtained for the smallest investigated speed, which can be explained by the fact that with the increase in speed ΔC_F increases as well, due to higher roughness Reynolds number, k^+.

From Tables IV and V and Fig.3, it is also evident that power deviations depend on loading condition of a ship. While there is no obvious difference between scantling and design loading conditions for the LPG carrier, power deviations are significantly different for ballast loading condition. Thus at 16 kn for scantling and design loading condition power deviation value is equal to 39.1 % and 39.3 %, while for ballast loading condition power deviation is equal to 30 %.

The same difference between design and ballast condition is noticed for containership, where the power deviation value for design condition at 24 kn is equal to 36.4 %, while for ballast condition is equal to 22.6 %. From the obtained results it can be concluded that power deviations for design and scantling loading condition can be considered as one – laden condition and then there is no big loading condition dependency. However, it is important to distinguish power deviations obtained for ballast and laden conditions, because in ballast condition, significantly lower values of power deviations are obtained for same hull surface condition for the investigated ships. For homogeneous fouling present on the entire wetted surface area, it can be assumed that power increase for same fouling condition and same speed will always be higher in laden condition. This is supported by the fact that form factor value, as well as total resistance coefficient is usually higher in ballast condition in comparison to laden condition, because ship is usually optimized for design loading condition, while ΔC_F will not be significantly affected by loading condition.

Therefore, during averaging power deviations - which is prerequisite for calculating PI, one has to be careful if ship changes its operational profile, because the final value of calculated PI will be significantly affected by speed and loading condition dependency.

3.2. Examples from in-service data

Both speed-dependency and loading conditions dependency of power deviations will cause significant amount of scatter in performance plot if not treated adequately. In order to make additional support for such claim, in-service data in the end of dry-docking (DD) period of two crude oil tankers have been analyzed. Due to the confidentiality of in-service data and coating info, only limited information can be provided. Both vessels were coated with a non-Hempel self-polishing copolymer (SPC) coating and during the DD period several underwater events occurred, including propeller and hull cleanings. Only last two voyages before DD were analyzed: laden and ballast voyages, which occurred without any idle periods nor underwater events between them. It should be noted that for both ships first laden voyage took place (3 weeks for Ship 1 and 2 weeks for Ship 2) and then ballast voyage took place (3 weeks for Ship 1 and 4 weeks for Ship 2). After ballast voyages both ships went immediately to DD.

In-service data was processed and measured shaft power was filtered and environmentally corrected. Consequently, the shaft power under steady-state conditions, corresponding to calm water condition, was obtained. Furthermore, the Hempel's Digital Twin model, which represents ship performance model, is used for building up reference performance level for the clean ship. Hempel's Digital Twin model is capable of making predictions of reference performance level for both ballast and laden conditions, and by scaling the model to data from the first year after DD, a reliable estimate for the clean ship performance is obtained for all loading conditions. Using the environmentally corrected shaft power and reference power level estimated with Hempel's Digital Twin model, power deviation value for every datapoint which survived filtering can be calculated, as well as power increase (difference of average power deviation in analyzed voyage and in reference period), Table VI. What is more, in-docking conditions of the two analyzed ships are presented in Table VII. Note that propellers of both ships were not fouled due to several propeller polishing during the DD period.

As can be seen from Table VI, both ships during the voyages have kept relatively constant speed and for Ship 1 this speed was quite similar in both voyages, around 12.5 kn, while for Ship 2 the speed slightly varied depending on the voyage. Therefore, it can be concluded that the results for Ship 1 indicate solely loading condition dependence, while for Ship 2 both speed and loading condition dependence is present.

Table VI: Results for two analyzed ships

Voyage	Average speed, kn	Standard deviation of speed, kn	Power increase, %
Design, Ship 1	12.3	0.56	26.5
Ballast, Ship 1	12.7	0.72	20.6
Design, Ship 2	12.9	0.64	17.0
Ballast, Ship 2	13.9	0.68	32.2

Table VII: The in-docking condition of analyzed ships

Area	Hard fouling	Weed	Slime	Corrosion	Coating damage
Ship 1 – boottop	/	/	/	10 %	5.5 %
Ship 1 – vertical bottom	2.5 % Moderate	65 % Moderate	10 % Light	6 %	1.5 %
Ship 1 – flat bottom	0.5 % Light	/	/	/	/
Ship 2 – boottop	/	/	/	10 %	6 %
Ship 2 – vertical bottom	1 % Light	30 % Moderate	40 % Light	3 %	20.5 %
Ship 2 – flat bottom	/	/	/	/	/

By checking the in-docking condition, it is clear that Ship 1 was more fouled than Ship 2. However, if the average power increase for these last two voyages combined is calculated, for both ships roughly same value is obtained: 23.3 %. This suggests that it can be quite challenging to estimate hull surface condition using averaging of power deviations without any checks of speed or loading conditions dependency.

There are several reasons which explain the final result. First of all, fouling could grow during the voyages and also in between them, but since there were no idle periods, it can be assumed that this increase over one and a half months would not be significant. Secondly, for Ship 1 where we can monitor loading condition dependence more clearly than for Ship 2, for laden voyage higher power increase is obtained, even though ballast voyage occurred after it. This supports the result presented in the previous section and highlights the difficulties which one could face if a simple averaging of all power deviations is used, regardless of loading condition. The opposite trend was obtained for Ship 2, where higher power increase was obtained for ballast voyage, which also occurred at higher speed and after laden voyage. So even though there is for sure some speed-dependency bias within this result and also some time dependency bias, significantly higher power increase value is obtained in ballast voyage. By checking report of in-docking condition in more detail, interesting pattern was noticed for these two ships. Namely, while fouling was relatively homogenously dispersed along the hull of Ship 1, the highest amount of fouling for Ship 2 was actually present significantly below the laden draught and mostly all fouling was present below the ballast draught. Since percentage of surface coverage were given for laden draught in Table VII, it is obvious that those percentages would be significantly higher for ballast draught for Ship 2 and would directly cause higher power increase value. This demonstrates the importance of heterogeneous fouling patterns which typically occur during DD periods and clearly explains why significantly higher power increase is obtained in ballast voyage for Ship 2 in comparison to laden voyage. To sum up, even if there would not be any physical loading condition dependence (which is not the case), additional problem related to heterogeneous fouling could potentially cause significant challenges during the simple averaging process.

Therefore, during the ship performance analysis, especially when standard performance values are used, it is important to analyze the obtained performance indicators always with speed-dependency and loading conditions dependency on the mind. Additionally, within this study it was considered that propeller is not fouled, which could be the case if propeller polishing is regularly performed. However, in a case of fouled propeller, additional source of uncertainty would be imposed on the obtained results. There are several proposals in the literature regarding the separation of hull and propeller degradation, one of them is presented in *Carchen and Atlar (2020)*, but in order to get accurate result thrust must be measured, which is more difficult in comparison to measurements of shaft torque. Because of this, still there are not that many cases in the shipping industry where thrust measurements are performed. Consequently, in a case where propeller polishing is not regularly performed, the one has to accept additional level of uncertainty in some of the obtained performance indicators.

There are some proposals in the literature and shipping industry for performance values or performance indicators which are less speed dependent or loading condition dependent, however they rely on additional modelling, which will increase the uncertainty of the obtained results in the end from different perspective.

4. Conclusion

Within this study, a relatively simple numerical method is used to predict the effects of idealized homogeneous fouling conditions on the delivered power of a ship. The method is validated by comparisons of the obtained results with results of CFD simulations published in the literature for one containership, bulk carrier and tanker ship and fouling with barnacles. Thereafter, on a case of one containership and one LPG carrier, it was clearly demonstrated that the effect of speed-dependency and loading conditions dependency should not be neglected during the averaging process. To additionally support such claim, two examples from in-service data are further analyzed. Within this analysis, it is clearly demonstrated that aside from physical speed and loading condition dependency, the most common performance value can be also significantly affected by heterogeneity of hull fouling. It can be concluded that both speed-dependency and loading condition dependency of power deviations will cause significant amount of scatter in performance plot if not treated adequately. Therefore, it is always important that the obtained results of performance analysis are interpreted by experts with thorough understanding of underlying methods and models as well as their potential pitfalls or challenges.

References

BERTHELSEN, F.H.; NIELSEN, U.D. (2021), *Prediction of ships' speed-power relationship at speed intervals below the design speed*, Transportation Research Part D: Transport and Environment 99

BERTRAM, V. (2017), *Some Heretic Thoughts on ISO 19030*, 2nd HULLPIC Conf., Ulrichshusen, pp. 4-12, data.hullpic.info/hullpic2017_ulrichshusen.pdf

CARCHEN, A.; ATLAR, M. (2020), *Four KPIs for the assessment of biofouling effect on ship performance*, Ocean Eng. 217

DALHEIM, Ø.Ø.; STEEN, S. (2020), *A computationally efficient method for identification of steady state in time series data from ship monitoring*, J. Ocean Eng. and Science 5(4), pp.333-345

DEMIREL, Y.K.; TURAN, O.; INCECIK, A. (2017a), *Predicting the effect of biofouling on ship resistance using CFD*, Applied Ocean Research, 62, pp.100-118

DEMIREL, Y.K.; UZUN, D.; ZHANG, Y.; FANG, H.C.; DAY, A.H.; TURAN, O. (2017b), *Effect of barnacle fouling on ship resistance and powering*, Biofouling, 33(10), pp.819-834

ESMAILIAN, E.; KIM, Y.R.; STEEN, S.; KOUSHAN, K. (2023), *A new power prediction method using ship in-service data: a case study on a general cargo ship*, Ship Technology Research, pp.1-22

FARKAS, A. (2021), *Numerical modelling of the effects of biofouling on ship resistance and propulsion characteristics*, PhD thesis, University of Zagreb

FARKAS, A.; DEGIULI, N.; MARTIĆ, I. (2020a), *An investigation into the effect of hard fouling on the ship resistance using CFD*, Applied Ocean Research 100

FARKAS, A.; DEGIULI, N.; MARTIĆ, I. (2020b), *Impact of biofilm on the resistance characteristics and nominal wake*, J. Engineering for the Maritime Environment 234(1), pp.59-75

FARKAS, A.; DEGIULI, N.; MARTIĆ, I.; ANČIĆ, I. (2020c), *Performance prediction method for fouled surfaces*, Applied Ocean Research 99

FARKAS, A.; SONG, S.; DEGIULI, N.; MARTIĆ, I.; DEMIREL, Y.K. (2020d), *Impact of biofilm on the ship propulsion characteristics and the speed reduction*, Ocean Engineering 199

FARKAS, A.; DEGIULI, N.; MARTIĆ, I. (2021), *A novel method for the determination of frictional resistance coefficient for a plate with inhomogeneous roughness*, Ocean Eng. 237

GRANVILLE, P.S. (1958), *The frictional resistance and turbulent boundary layer of rough surfaces*, J. Ship Res. 2(4), pp.52-74

GRANVILLE, P.S. (1987), *Three indirect methods for the drag characterization of arbitrarily rough surfaces on flat plates*, J. Ship Res. 31, pp. 70-77

GUNDERMANN, D.; McLAUGHLIN, D., (2019), *When ISO19030 Fails: Utilizing Basic Machine Learning/Data Fitting Methods for Performance Analysis without Reference Data*, 4th HullPIC Conf., Gubbio, pp.220-228, HullPIC2019_gubbio.pdf

GUPTA, P.; RASHEED, A.; STEEN, S. (2024), *Correlation-based outlier detection for ships' in-service datasets*, J. Big Data, 11(1), 85

ISO (2016), *ISO 19030 - Measurement of changes in hull and propeller performance*, Int. Standard Org., Geneva

OLIVEIRA, D.R.; GRANHAG, L.; LARSSON, L. (2018), *Performance Values vs. Speed – A Declaration of Independence?*, 3rd HullPIC Conf., Redworth, pp.80-92, data.hullpic.info/hullpic2018_redworth.pdf

OLIVEIRA, D.R.; GRANHAG, L.; LARSSON, L. (2020), *A novel indicator for ship hull and propeller performance: Examples from two shipping segments*, Ocean Eng. 205

SCHMODE, D.; HYMPENDAHL, O.; GUNDERMANN, D. (2018), *Hull Performance Prediction beyond ISO 19030*, 3rd HullPIC Conf., Redworth, pp.135-140, hullpic2018_redworth.pdf

SFIRIS, P.; DEMIREL, Y.K.; AVLONITIS, V.; PAGONI, S., (2023), *Navigating Energy Efficiency Dilemmas in the CII Era*, 8th HullPIC Conf., Pontignano, pp.171-187, http://data.hullpic.info/HullPIC2023_Pontignano.pdf

SONG, S.; DEMIREL, Y.K.; ATLAR, M. (2020a), *Penalty of hull and propeller fouling on ship self-propulsion performance*, Applied Ocean Research 94

SONG, S.; DEMIREL, Y.K.; ATLAR, M. (2019), *An investigation into the effect of biofouling on the ship hydrodynamic characteristics using CFD*, Ocean Eng. 175, pp.122-137

SONG, S.; DEMIREL, Y.K.; ATLAR, M.; DAI, S.; DAY, S.; TURAN, O. (2020), *Validation of the CFD approach for modelling roughness effect on ship resistance,* Ocean Eng. 200

SVENSEN, T.E. (1983), *A Techno-Economic Model of Ship Operation with Special Reference to Hull and Propeller Maintenance in the Face of Uncertainty,* Vol. 1. University of Newcastle Upon Tyne

TASKAR, B.; ANDERSEN, P. (2021), *Comparison of added resistance methods using digital twin and full-scale data,* Ocean Eng. 229

What? Sea Trials on a Vessel with Jet Engines? Yes!

Dmitry Ponkratov, Siemens Digital Industries Software, London/UK, dmitry.ponkratov@siemens.com
Rui Lopes, Chalmers University of Technology, Gothenburg/Sweden, rui.lopes@chalmers.se
Arash Eslamdoost, Chalmers University of Technology, Gothenburg/Sweden, arash.eslamdoost@chalmers.se
Rickard Bensow, Chalmers University of Technology, Gothenburg/Sweden, rickard.bensow@chalmers.se
Miles Wheeler, Siemens Digital Industries Software, Seattle/USA, miles.wheeler@siemens.com

Abstract

Computational Fluid Dynamics (CFD) calculations at ship scale are very popular nowadays. International Maritime Organisation (IMO) recognised CFD for speed and power prediction in 2021 but suggested an intensive validation process (later enhanced by IJACS in 73 procedures) to ensure numerical simulations provide adequate results. Nevertheless, all existing ship scale validation cases were developed during self-propulsion sea trials (what would be an alternative, right?). However, it would be nice to look at performances and efficiencies, not only the combined system hull+propeller but also separately to have a deeper look at the components. Hence, full-scale resistance trials (bare vessel hull without a propeller) would be desired. But how to perform them? Recent brainstorming concluded that these trials (with tugboats?) are very difficult to execute. Surprisingly, the solution was not found looking ahead, but actually in the past! Brilliant researchers managed to solve this puzzle in an elegant way 75 years ago. They proposed and installed jet engines on a specially prepared vessel to perform resistance trials without propellers (who needs propellers if you have jet engines?). In 2024, this unique test case made a triumphal return to maritime science and gathered the largest community of CFD practitioners to compare and validate their results. This paper outlines the main steps of the unique sea trials and CFD comparison.

1. Introduction

JoRes Joint Research Project (www.jores.net) was launched in 2019 with the aim of performing sea trials on actual vessels and collecting data for CFD validation. The data collection methodology was more stringent than the usual sea trial procedures. In addition to the ISO15016 standard of sea trials conduction, it was essential to pay significant attention to details usually omitted during, for example, vessel delivery sea trials—for example, hull and propeller roughness measurements.

Another wish was noted during the project preparation phase: ship-scale resistance trials (on a vessel without propellers). These trials would significantly enhance the knowledge and understanding of ship performance because they could help to decouple the hull and propeller performance. The question is how to perform these trials. One of the options would be to tow the subject vessel with another vessel. For example, this approach was successfully executed by William Froude, *Froude (1874)*, with the famous towing experiments of HMS Greyhound. Another noticeable experiment of this kind was the towing tests of HMS Penelope in 1974, *Canham (1974)*. Unfortunately, this kind of experiment has a significant disadvantage – the towing vessels ahead of the subject vessel create wake and waves, which makes the measurements of the subject vessel not scientifically accurate. Another option would be to find a place with significant current and moor the subject vessel there. But again, the speed profile of these measurements would not be the same as for the “clean” resistance tests.

So, the JoRes team thought that nowadays, it is practically impossible to perform these kinds of tests and more time would be needed to develop more innovative solutions in the future to solve this puzzle. Surprisingly, the solution was found by chance, and it was in the past rather than the future.

2. Sea trials on Lucy Ashton in 1950-1951

On 8 September 1950, people living on the Gareloch lake in Scotland were puzzled by the weird sound. They thought a jet plane was flying somewhere at a lower altitude, but the sky was clear. They were surprised to see a vessel with four jet engines sailing in the lake…

Lucy Ashton was a paddle steamer in service in Clyde, UK, from 1888. She retired from service in 1949 and was acquired by BSRA (British Ship Research Association) to perform full-scale resistance measurements. For this purpose, the machinery, paddlewheels, and deckhouses were removed, four jet engines were installed on the deck, and a sound-resisting wheelhouse was constructed. Two large steel-hinged flaps were fitted to stop the vessel.

Denny (1951) shows details of jet installation, thrust measurement methods and instrumentation for the trials (ship speed, wind speed and direction, rudder angles, automatic observer (a panel of instruments in the wheelhouse was photographed every 10 s), and two pitot logs). Thrust gauges were calibrated before and after each day's trials. Double runs were made in Gareloch, Scotland. The water temperature and density were measured, the draughts measured before and after trials, and dynamic trim was noted using a trim board.

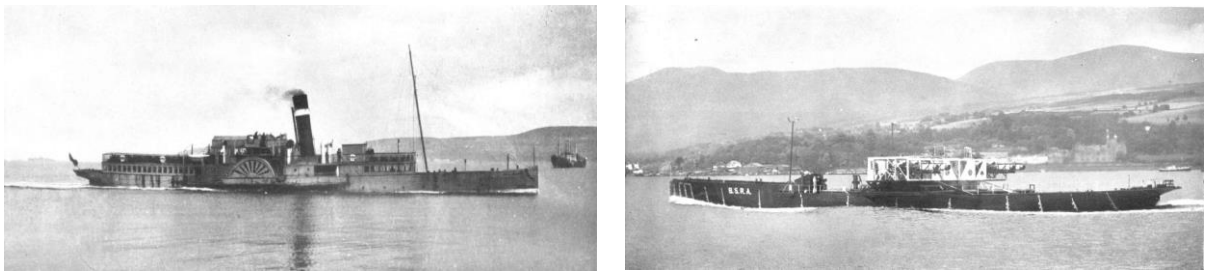

Fig.1: Lucy Ashton as a paddle steamer (left) and transformed into a research vessel (right)

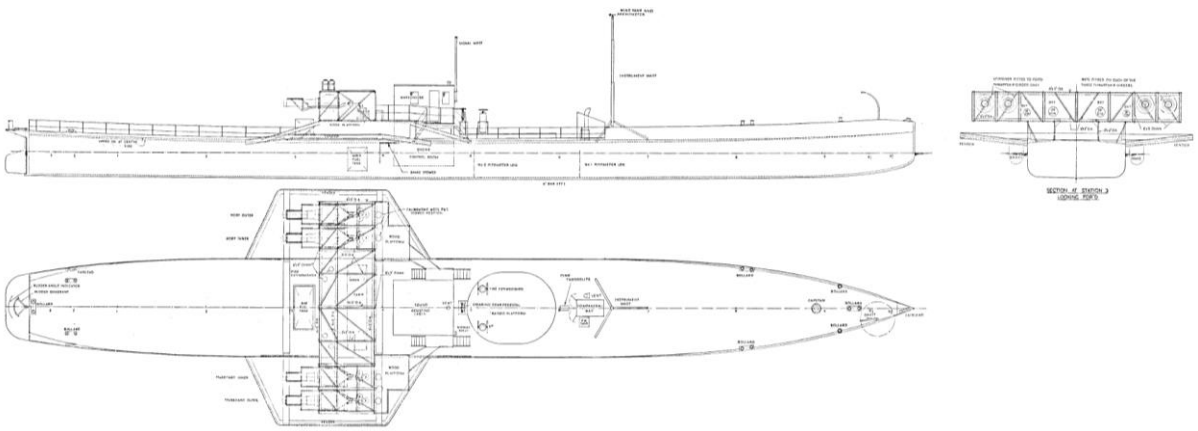

Fig.2: General arrangements of the Lucy Ashton with four jet engines

Fig.3: 3D model of the hull created in 2024 based on the drawings

Full program of the trials included (5-15 kn):

1. Clean naked hull having a red oxide paint surface and sharp seams (the shell plates had flush butts): *Denny (1951)* and *Conn et al. (1953)*.
2. As (1) above but with a bituminous aluminium paint surface: *Denny (1951)* and *Conn et al. (1953)*.
3. Clean hull with red oxide paint surface and dummy twin-screw bossing: *Lackenby (1954)*.

4. Clean hull with red oxide paint surface and dummy twin-screw "A" brackets and shafts: *Lackenby (1954).*
5. Clean naked hull having a red oxide surface and seams faired off with a plastic composition: *Denny (1951)* and *Conn et al. (1953).*
6. As (5) above but with a bituminous aluminium paint surface: *Denny (1951)* and *Conn et al. (1953).*
7. Naked hull with bituminous aluminum paint surface allowed to foul for about one month: *Smith (1955).*
8. Acceleration and retardation tests: *Smith (1955).*

2.1. Hull lines

No original drawings were found in 1950, so the offsets were carefully measured while the vessel was on a slip. The hull was in good condition. The wetted surface area, including the rudder and bar keel, was measured as 4,488 sq ft (416.95 m^2). Hull lines and offsets are shown in *Conn et al.* (1953). In 2024, based on these offsets, Chalmers University built a new 3D geometry for the CFD simulations, Fig.3.

2.2. Hull roughness measurements

Two thin layers of "filler" or rivet cement and two coats of ordinary red oxide paint were applied to make it comparable with freshly painted plates of a new steel vessel. The only excrescences on the hull were the longitudinal overlapped seams of 1/4 in (6.35 mm) thickness.

Two roughness records were taken at the ten stations on both sides when in the dock before and after trials. Three types of instruments were used: a wall gauge, an aerofoil gauge, and a talysurf machine.

The measured equivalent sand grain roughness (Ks) was reported as follows:

1. Sharp seams with red-oxide paint (normal clean service condition) Ks 0.0038 in (97 μm)
2. Faired seams with red-oxide paint: Ks = 0.0029 in (74 μm)
3. Sharp seams with bituminous aluminium paint: Ks = 0.0029 in (74 μm)
4. Faired seams with bituminous aluminium paint (smooth hull surface tested): Ks 0.0023 in (58 μm)

2.3. Uncertainty analysis

At 10 kn, speed measurement accuracy was in the order of one-tenth of one per cent. Thrust accuracy is approximately ±5lb for each engine. At 5 kn (2 engines), the error was 1.5% of resistance, and at top speed, 14.75 kn (4 engines), 0.17%. Rudder angles are negligibly small.

2.4. Model tests

Six models of lengths 9, 12, 16, 20, 24, and 30 ft (2.7 m, 3.6 m, 4.9 m, 6.1 m, 7.3 m, and 9.1 m) corresponding to the scales 1/21.167. 1/15.875. 1/11.906, 1/9.525, 1/7.938, and 1/6.35 were built. The following conditions were considered for a few scale models:

1. Sharp seams with red-oxide paint (normal clean service condition)
2. Faired seams with red-oxide paint
3. Sharp seams with bituminous aluminium paint
4. Faired seams with bituminous aluminium paint (smooth hull surface tested)

The tests were first made without trip wires and then repeated with trip wires of 0.036 in (0.9 mm) diameter fitted at 5% of the length abaft the stem. (the effect of trip-wire was very small, varying from a maximum of 2% on the 9 ft (2.7 m) model to a fraction of 1% on the larger models). The 30 ft (9.1 m) model was tested in deep (18 ft or 5.5 m) and shallow water (11 ft 6 in or 3.5 m) conditions.

2.5. Ship model correlation with bossings and shaft brackets

Additional trials were performed with bossings and shaft brackets, which were simulated with sheet steel weldments. The ship trials were carried out with the hull in normal service conditions (clean hull, sharp seams with red-oxide paint). Model tests with bossings and shaft brackets were performed on six models: 9 ft, 12 ft, 16 ft, 20 ft, 24 ft, and 30 ft (2.7 m, 3.6 m, 4.9 m, 6.1 m, 7.3 m, and 9.1 m).

2.5. Sea trials with fouled hull

In addition to the trials outlined above, additional trials were performed to investigate the effect of fouling on resistance corresponding to various periods of immersion at different times of the year.

Faired seams, the vessel had a bituminous aluminum paint surface and no special anti-fouling properties (equivalent sand grain roughness Ks = 0.0023 in or 58 μm).

Trials on 1 May 1951 – 24 days out of dock (equivalent Ks = 0.0046 in or 117 μm).
Trials on 7 June 1951 – 30 days out of dock (equivalent Ks = 0.007 in or 178 μm).
Trials on 4 June 1951 – 58 days out of dock (equivalent Ks = 0.0135 in or 343 μm).

2.6. Acceleration and retardation trials

Acceleration and retardation trials were performed, from which the virtual mass of the ship was determined.

Two sets of acceleration and retardation trials: the first on 1 May (24 days out of the dock) and the second on 7 May 1951 (30 days out of the dock):

1. 1 May tests: 5 complete tests (two with a speed of 12 kn and three with a speed of 14.5 kn).
2. 7 May tests: one at speed 13.75 kn and the other at 14.5 kn.

2.7. Boundary layer measurements with pitot tubes

Two pitot logs were fitted close to the middle line: N1 72 ft 6 in (22.098 m) and N2 97 ft 4 in (29.67 m) aft of the forward perpendicular.

For these measurements, only the following results are available:

1. N1 Clean hull, sharp seams, and red-oxide paint (5.45, 10.07, and 14.24 kn); Boundary layer thickness at N1 pitot is in the order of 12 in (0.3 m).
2. N2 Clean hull, faired seams and aluminum paint (10.18 kn) and after 58 days out of dock (10.3 kn). Boundary layer thickness at N2 pitot is in the order of 18 in (0.46 m).

2.8. General conclusions made by the authors in 1951

1. Fairing the seams reduced the total resistance by about 3%.
2. Painting the hull with smoother bituminous aluminium paint instead of red oxide reduced the total resistance by a further 3%.
3. A general but light scattering of small barnacles (about 1/8 in high) on the flat bottom in association with a band of fine grasses on the sides gave rise to an increase in the measured resistance of 42%, 29%, and 21% at speeds of 6, 12 and 14 kn, respectively. This corresponds to an increase in the estimated skin-frictional resistance of 50%.
4. The added virtual mass of the ship was on the order of 5%, and there was no significant variation in speed.

3. Lucy Ashton CFD workshop 2024

On 25 September 2024, a group of researchers entered a room at the Chalmers University of Technology in Gothenburg, Sweden, to discuss the CFD results of the first ship-scale resistance workshop…

As discussed in the previous chapter, BSRA collected impressive information about Lucy Ashton in 1950-1951. They initially intended to understand hull performance under various conditions (different paints, bossings, brackets, and fouled conditions) and establish correlations with model test predictions. At that time, they could not foresee the development of numerical methods and the high demand for validation cases. Nevertheless, accurate reporting of all the details in 1950-1951 papers made using these results for CFD validation possible.

3.1. Case description document developments

Based on the careful analysis performed by Chalmers University, the case description documents for CFD calculations were developed. Because the sea trial results represent very comprehensive datasets, it was decided to simplify the simulation case for the first workshop (there is an idea to have a series of workshops to consider all the measured cases). Before announcing the CFD workshop, a preliminary study was made, *Lopes et al. (2025)*, to ensure the test case was suitable for the workshop simulations. So, the requirements for the first workshop include only smooth hull calculations (zero roughness). Aerodynamic resistance was not included.

Three sets of results were expected. The first set was a grid refinement study, using grids prepared by Chalmers University and provided to the participants. The second set consisted of simulations at ship scale for different speeds, and the third set was comprised of simulations at a constant Froude number for varying model sizes.

3.2. Geometry file

Based on the offset table and hull lines published by *Conn et al. (1953)*, a 3D CAD model was generated, Fig.3. This model did not include overlapping steel plates but included the actual sagging of the vessel, as that was reproduced in the measured offsets. The geometry was prepared in various file formats.

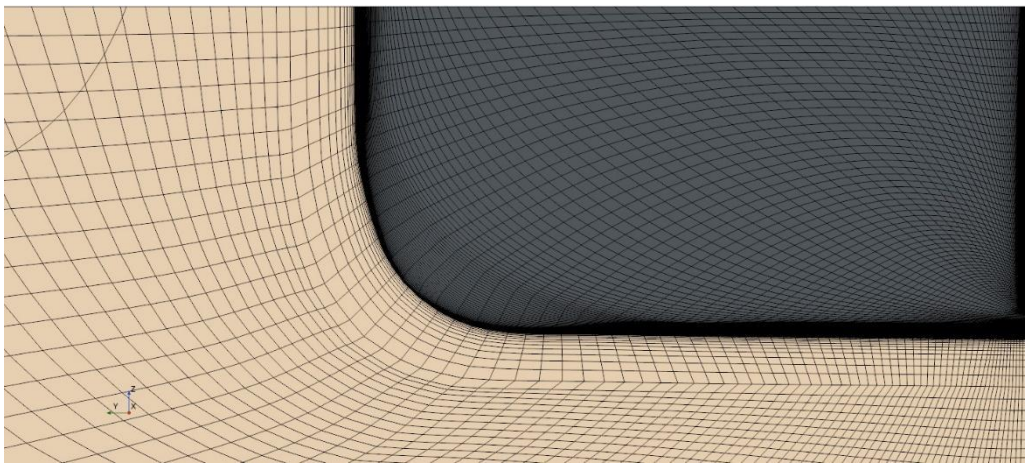

Fig.4: Structured mesh around Lucy Ashton's numerical model

3.3. Workshop announcement and execution

The announcement was made in early 2024 and attracted significant attention from the maritime industry. Many companies showed interest and signed up for the workshop. Even though the original BSRA reports 1950-1951 were in the public domain, the workshop organisers did not specify which

vessel it was and how the trials were performed. This was done deliberately to make the workshop with blind results. Of course, it is impossible to guarantee that no one could find and use the original reports. Still, it is believed the probability is relatively low as this test case is not widely known in the industry (have you heard about it before?). In the end, 47 results were submitted to Chalmers University before the deadline.

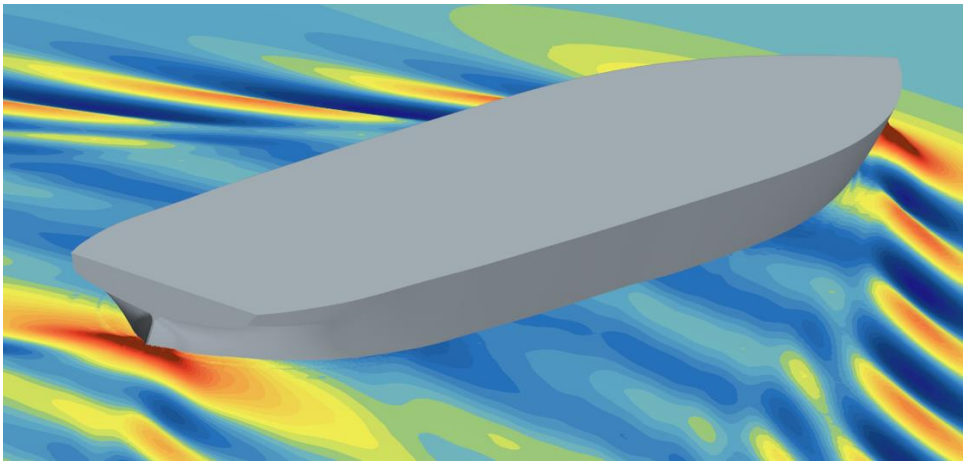

Fig.5: Simulation of Lucy Ashton trials in CFD

3.4. Workshop results

On 25 September 2024, the participants met at the Chalmers University to discuss the results. Some came in person, and some joined online. A comprehensive analysis was performed, and the workshop proceedings will be available shortly. Fig.6 shows the results of the sea trials as reported in the 1950s documents. Additional work is being done to post-process these sea trial results according to the modern ISO15016 procedure, so the curve in Fig.6 may shift a bit.

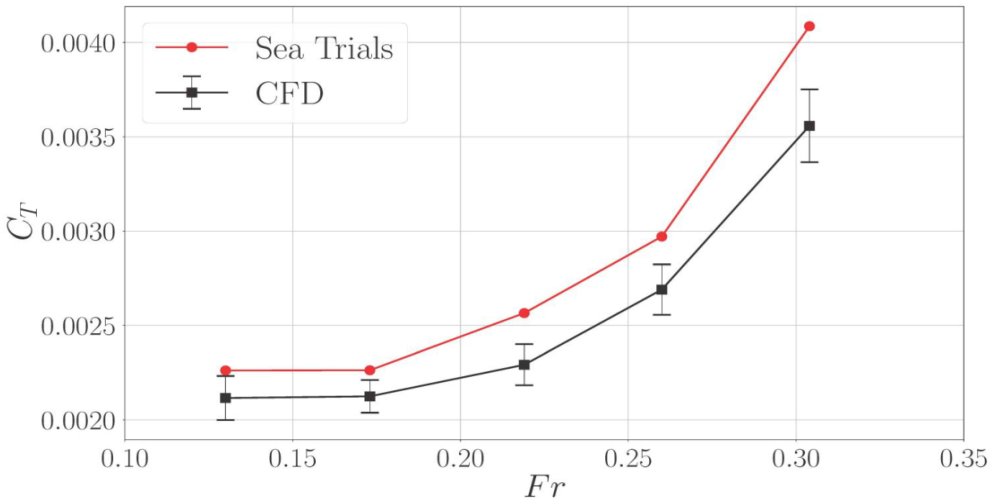

Fig.6: CFD results (smooth hull) vs. 1950 sea trials (post-processed under 1950th methods)

The key results are:

1. The predicted CFD values were below the sea trials curve, which is logical as the CFD runs were performed with the hydrodynamically smooth hull (zero roughness).
2. As seen at the previous self-propulsion workshop, there is a noticeable spread of submitted results. Nevertheless, the standard deviation of all the results (the total ship resistance with the rudder) is on the order of 5% (5.5% at Fr=0.13, 4.09% at Fr=0.173, 4.75% at Fr=0.219, 4.97% at Fr=0.26 and 5.42% at Fr=0.304).

4. Conclusions

Numerical methods open a new and exciting opportunity to help the industry design and build a new generation of ships. The key characteristic of this digital revolution is the ability to simulate and optimise a vessel numerically before the vessel is actually built. The challenge of this approach is the validation of digital tools – how to make sure the predicted performance will be the same as that of the actual as-built vessel. To close this gap, a set of validation cases is needed in the industry to ensure the high performance of digital tools. Even though a few self-propulsion cases were developed within the JoRes project (www.jores.net), the remaining gap was the ship scale resistance measurements, which can help decouple the hull and propeller performance at actual Reynolds numbers. Even though it is nearly impossible for the present and potentially the future, apparently, it was made in the past. The brilliant researchers at BSRA (British Ship Research Association) performed these trials on the vessel Lucy Ashton in 1950-1951 by installing four jet engines on the deck. Detailed reports of these unusual trials made it possible to use this dataset for CFD ship-scale resistance simulations in 2024.

Based on 40 submitted datasets, a reasonable standard deviation of 5% was achieved for the blind simulations (participants did not know the trials' results). This increased confidence in CFD methods, pushing the boundaries of CFD acceptance even further.

Additional workshops are planned to explore the remaining results (various roughnesses, bossing, and brackets) reported in the original reports.

Acknowledgement

We would like to respect and recognise the brilliant researchers of the British Ship Research Association who performed and contributed to the extraordinary Lucy Ashton trials in 1950-1951.

References

CANHAM, H. (1974), *Resistance, Propulsion and Wake tests with HMS 'PENELOPE'*, Trans. RINA, April, pp.61-94

CONN, J.F.C.; LACKENBY, H.; WALKER, W.P. (1953), *B.S.R.A. Resistance experiments on the "Lucy Ashton". Part II - The ship-model correlation for the Naked Hull Conditions*, Proc. Spring Meeting of the Institution of Naval Architects, London

DENNY, M.E. (1951), *B.S.R.A. Resistance experiments on the "Lucy Ashton". Part I - Full-Scale Measurements*, Int. Conf. Naval Architects and Marine Engineers, London

FROUDE, W. (1874), *On experiments with HMS Greyhound*, Trans. Inst. Naval Architects, p. 36

LACKENBY, H. (1954), *B.S.R.A. Resistance experiments on the "Lucy Ashton". Part III - The ship-model correlation for the shaft-appendage conditions,* Proc. Autumn Meeting of the Institution of Naval Architects, Torquay

LOPES, R.; ESLAMDOOST, A.; JOHANSSON, R.; ROYCHOUDHURY, S.; BENSOW, R.; HOG-STROM, P.; PONKRATOV, D. (2025) *Resistance prediction using CFD at model- and full-scale and comparison with measurements*, Ocean Eng. 321

SMITH, S.L. (1955), *B.S.R.A. Resistance experiments on the "Lucy Ashton". Part IV - Miscellaneous Investigations and general Appraisal*, Proc. Spring Meeting of the Institution of Naval Architects, London

Bridging Minds and Machines: Can Neural Networks Harness the Insight of Naval Architecture Models?

Wojciech Górski, Enamor, Gdynia/Poland, wojciech.gorski@enamor.pl
Aleksandra Hein, Enamor, Gdynia/Poland, aleksandra.hein@enamor.pl
Liliana Jarmakowska, Enamor, Gdynia/Poland, liliana.jarmakowska@enamor.pl
Aleksandra Karolik, Enamor, Gdynia/Poland, aleksandra.karolik@enamor.pl
Dominik Leśniak, Enamor, Gdynia/Poland, dominik.lesniak@enamor.pl
Jan Talka, Enamor, Gdynia/Poland, jan.talka@enamor.pl

Abstract

Neural networks have emerged as powerful, state-of-the-art tools for modelling complex system behaviours and dependencies. Predicting the power requirements of sea-going vessels, with all its environmental complexity, seems like an ideal challenge for such an approach. Can we solely relay on the ability of the Machine Learning tools to prepare the models of system that has been a subject of complex simulations, statistics research, towing tank experiments? How can we merge the knowledge of more than 200 years of Naval Architecture discipline and combine it with power of modern Machine Learning algorithms to create a truly robust, hybrid approach? As the resemblance of human's ability to learn new skills, the primal goal of neural network algorithms is to minimize the error rates. Our ability to assess these error rates highly depends on the experiments conducted during our learning process, which are influenced by the operational conditions we're able to record and examine. This can lead to a tendency to optimize accuracy of our predictions specifically for the tested environment, potentially overlooking the global domain. The purely neural network-based approach will be tending to minimize error rates in operating conditions where most data has been recorded. However, if we move beyond these familiar conditions our predictions can become highly error prone. Embedding the information about physics-based models describing vessel's operation characteristics can help us to predict scenarios where very little data has been available for training, enhancing model robustness across a broader range of conditions. Research is focusing on implementation of the capabilities of neural networks to model complex systems basing on recorded data and combining the knowledge of physics-based models developed through hundreds of years of human activity in naval architecture research. By combining data-driven insights with established principles from the Naval Architecture models, this research aims to create hybrid approaches, that enhance predictive accuracy for conditions not covered by training data.

1. Introduction

According to UNCATD Review of maritime transport *United Nations (2024)*, due to political and economic events imposing vessel rerouting the average distances travelled per ton of cargo sustained the increasing trend with a shift from an average of 4675 miles recorded in 2000 to 5186 miles in 2024. Despite the technological advancements in maritime transportation efficiency, the challenges of accurate route planning and technical performance monitoring are becoming more important for remaining competitive on the maritime transport market for charterers, brokers and ship technical managers. In order to support effective route planning and situation awareness for technical performance, the high-quality operational data can be utilized with state-of-the-art machine learning technologies to build vessel-operation model describing technical performance characteristics. The complexity of vessel's operation environment and associated phenomena has been a subject of centuries of the naval architecture research domain. Recent advancements in machine learning technology have led to a growing interest in the field of regression problem-solving techniques. This has resulted in a growing potential for describing multidimensional environments where limited knowledge is available, or where the accurate modelling requires time-consuming and numerically intensive simulations. This has consequently led to the demonstration of regression problem-solving techniques as an accurate means of describing complex systems such as seagoing maritime vessel's propulsion power requirements. However, due to common nature of learning algorithms several challenges have been found resulting in limited confidence

of the model's predictions. These challenges have formed new questions from the users and increasing presence of artificial intelligence in technology domain also imposed limited confidence to the model's predictions. In circumstances where critical decision-making exerts an influence on market competitiveness, reliance on data-driven modelling can be expected to increase if the model prediction confidence rates can be supported. It has been proven by *Parkes et al. (2021)* that regression neural network models for ship's performance solution lose the prediction accuracy for regions of input parameters, where less training data were available and alternative methods has been developed & investigated to overcome this problem. The possibility of combining the semi-empirical knowledge of the ship's propulsion power requirements investigated over centuries of naval engineering with the regression solving neural network approach is also investigated as one of the methods to increase the reliability of model predictions, where limited operational data could have been collected and limited knowledge of the physics laws governing system behaviour in complex environment can be found or is resource demanding to be simulated *Leifsson et al. (2008)*. This approach further referred as grey box modelling is investigated for the accuracy of power prediction in voyages conducted in loading state parameters not covered by the training data. Two approaches for grey box modelling are investigated and compared with power prediction of the high-resolution data recorded by the data collecting system installed onboard merchant vessel. Research aims to explore the potential of accuracy increase for power prediction models that can be used for voyage optimization and performance monitoring tasks with high focus on increasing and assessing the confidence level for the model predictions in the states that were not covered by the training data.

2. Input Data Quality Assessment & Dynamic states identification

Before approaching performance model training task, the input data quality needs to be monitored and investigated for sensor failures or unreliable readings. It is vitally important to identify sensor failures or unreliable reading and exclude them from training datasets in order to avoid false input-output relationships being utilized in training algorithms. Moreover, when utilizing high-resolution data, the training dataset is expected to also cover dynamic transition states recorded by the sensors e.g. changes of the Main Engine RPM setpoints, where vessel's acceleration and whole system reaction needs to be taken into account in order to avoid this training data being used for modeling input-output relationships. This type of data cleaning requires preparation of algorithms allowing RPM setpoint changes detection. This can be found particularly challenging as the variance of recorded high-resolution RPM data also tends to increase in bad-weather conditions or when operating in unsteady conditions, where additional environmental parameters are contributing to added resistance. In order to mitigate those challenges, the two-state RPM setpoint changes filters have been developed allowing to detect RPM setpoint changes in both steady and unsteady operating conditions.

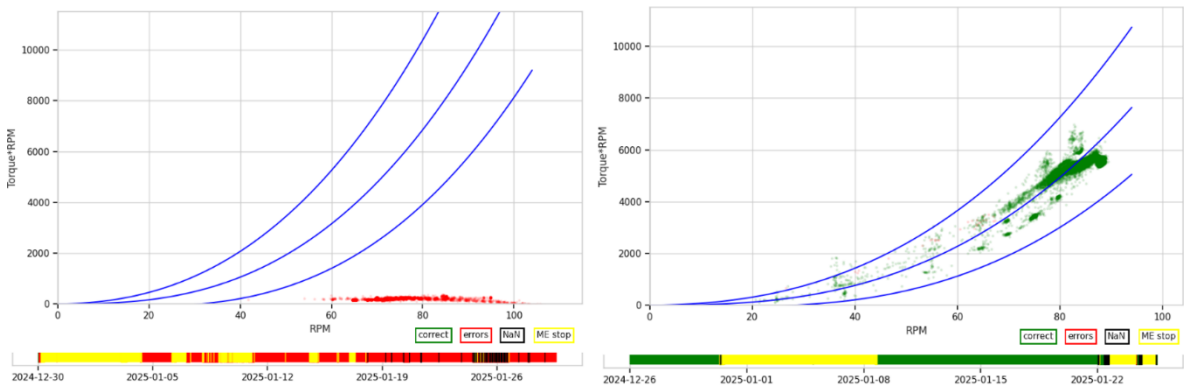

Fig.1: Torque meter sensor diagnostic results, faulty sensor(left), correct sensor reading(right)

2.1. Unsteady operating conditions filter

The threshold determining the unsteady conditions has been evaluated basing on environmental factors partially based on *ITTC (2014)* procedures & recommendations describing environmental conditions

limitations for conducting sea trials. Additional parameter referring to the current speed vector perpendicular to the ship movement direction has been introduced as proposed replacement to the difference between speed through water and speed over ground. Thanks to this parameter more data has been classified as steady conditions, where despite increased difference between speed measured from speed log sensor and GPS receiver, low RPM variances has been observed.

The unsteady operating conditions filter has been based on following parameters :

- $Hw \leq 1.5 \cdot \sqrt{\frac{L_{pp}}{100}}$
- $\begin{cases} V_w < 28\ kts\ for\ L_{pp} > 100m \\ V_w < 22\ kts\ for\ L_{pp} \leq 100m \end{cases}$
- $V_{y,current} \leq 0.5\ kts$
- $h > \left(3 \cdot \sqrt{B \cdot T}\ , 2.75 \cdot \frac{V_{STW}{}^2}{g}\right) max$

Hw – Significant Wave height [m]
L_{pp} – Length between perpendiculars [m]
V_w – Wind speed Relative [kn]
B – Ship's Breadth [m]
T – Draught at midship [m]
$V_{y,current}$ – Current speed vector perpendicular to the ship movement direction [kn]
h – Water Depth [m]
V_{STW} – Speed Through Water [kn]
g - acceleration due to Earth's gravity (9.81 m/s^2)

It is worth noting that the train dataset with identified steady and unsteady conditions is not subjected to rejection of the unsteady conditions data at this phase. The classification results will be utilized further for benefits of the dynamic state filter application. The presence of recorded unsteady conditions is important for further modeling of the adverse weather conditions effect on shaft power requirements.

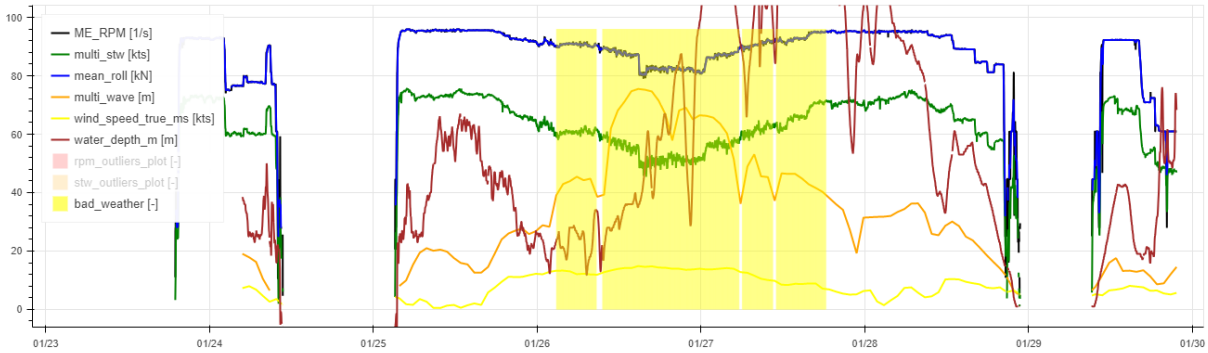

Fig.2: Indication of unsteady conditions (yellow) with visible increase of RPM variance & speed reduction

2.2. Dynamic States filter

The dynamic states filter aims to categorize dataset for speed transition time periods recognition. The change of RPM setpoint is detected basing on speed of RPM change with different threshold depending on previously identified steady or unsteady state. It has been observed that for unsteady states much higher variances of the recorded RPM have been observed and leaded to false detection of the RPM setpoint change. Nevertheless, changes of RPM setpoints in adverse weather conditions are still detected within different levels of threshold for speed of RPM change.

As the Main Engine control system is able to change the operating conditions in relative short time, the overall system reaction for new propeller RPM setpoint takes more time to achieve steady condition.

The additional delay filter for steady condition has been proposed to overcome this phenomena. The reaction time can be assessed by observations of other parameters like STW and shaft torque altering to steady level after the RPM setpoint change. Example of the high-frequency data capturing such effects of RPM setpoint changes can be found in Fig.3.

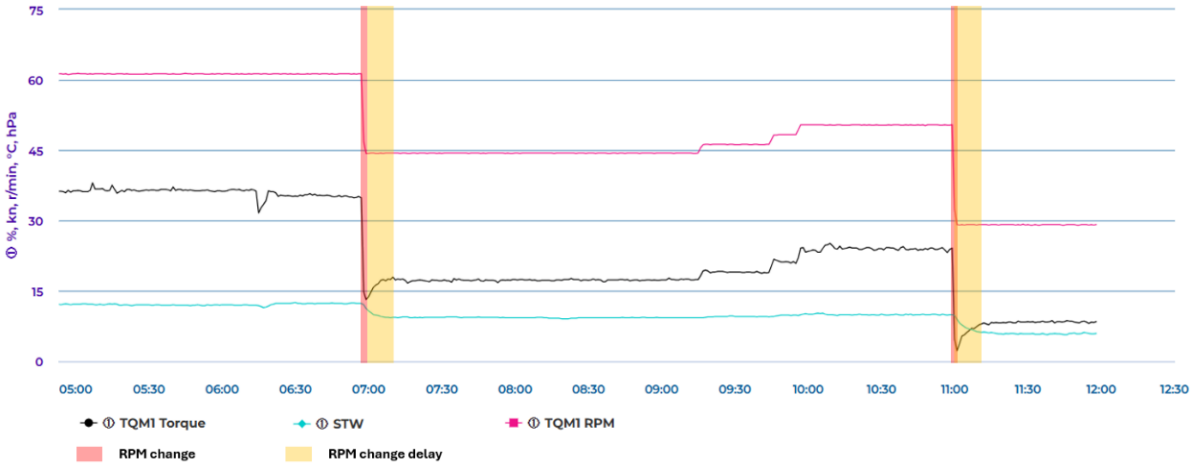

Fig.3: Detected RPM setpoint changes (red), dynamic effect on torque and STW variation (yellow)

In result of dynamics states data filtration & cleaning the transient states can be identified and rejected from training dataset, the effect of reduced scattering can be observed on examples of power/speed plots, Fig.4. It is noticeable that less dense operating points reflecting temporary operating states were identified and rejected from training dataset in order to avoid their contribution in modelling process.

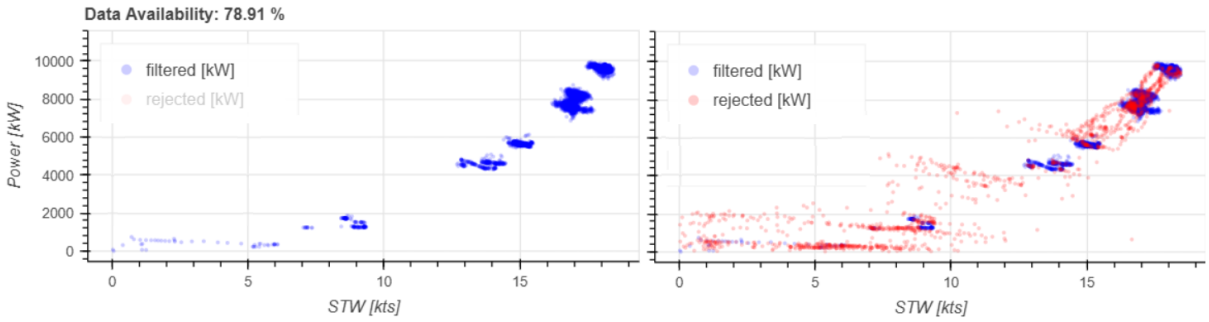

Fig.4: Effect of dynamic state filter. Data after filtering (left), data before filtering (right)

3. Grey Box Modelling Approach

The Regression error metrics utilized during neural network-based models can induce heavy influence of available test data set on accurate representation of the ground truth representing true input-output relationships as presented by *Parkes et al. (2025)*. To overcome this problem, it has been proposed to introduce limited knowledge of the physical models used in naval architecture to predict power requirements and to represent the influence of external environmental conditions on the added resistance. The process of embedding physical laws into the model learning process is realized in two different manners. Their difference lies in the interaction between the part driven by known physical laws, the input features and the target variables of the neural network model.

3.1. White Box Model

The isolated part representing known physical dependencies further referred as white box is subjected to first step of model preparation including adjustment of variables representing following physical parameters during model training process:

- L_{pp} - length between perpendiculars [m]
- B - Beam [m]
- E_1 - Angle of entrance of the waterline [deg]
- E_2 - Angle of run of the waterline [deg]
- C_b - block coefficient [-]
- K_{yy} - non-dimensional radius of gyration of pitch [% LPP]
- H - Ship's Height[m]
- C_d - Wind Resistance Coefficient [-]
- D - Propeller Diameter [m]
- $J(\eta_{max})$ - Advance Ratio for Propeller Max. Efficiency [-]
- η_{max} Propeller Max. Efficiency [%]

Although those physical parameters can be retrieved from ship's particulars data, at this stage the white box model tuning has been proposed. The process allows adjusting the physical parameters during learning stage within scope of certain high and low limiting values derived from typical characteristics of merchant vessels parameters. It's also assumed that part of this initial values is unknown or there's limited knowledge of their current state, such as for maximum propeller efficiency. If some of these parameters are specified by the model user, their limits can be regulated or they can be treated as non-trainable parameters of the white box model. The process of white box model training involves utilization of physics-based models describing vessel's added resistance due to wind, wave and shallow water. The remaining part of hull's resistance is represented by the Frictional Resistance relationships based on estimated hull's wetted surface. Functions representing laws governing added resistance has been based on following references:

- Calm Water resistance: *Papachristou et al. (2024)*

$$R_{friction} = \frac{1}{2} \cdot C_V \cdot \rho_w \cdot S_{wetted} \cdot v_{STW}^2$$

where :
C_v - viscous resistance coefficient, ρ_w - water density (1025.0 kg/m^2), v_{STW}- speed through water, S_{wetted}- wetted hull surface.
Wetted hull surface has been approximated using Denny-Mumford's formula.

$$S_{wetted} = L_{pp} \cdot (1.7 \cdot T + B \cdot C_B)$$

T - ship's draft

- Wind Resistance: *Det Norske Veritas (2014)*

$$R_{wind} = \frac{1}{2} \cdot \rho_a \cdot C_d \cdot S \cdot \sin(\alpha) \cdot V_w^2$$

where :
R_w - added resistance due to wind, ρ_a - air density (1.206 kg/m^2),
S - projected area of the member normal to the direction of the force,
α - angle between the direction of the wind and the axis of the exposed member or surface,
V_w - wind speed relative to the ship
Projected area S has been approximated using formula:

$$S = (H - T) \cdot B$$

- Wave Resistance: *Wang et al. (2021)*

$$R_{wave} = R_{AWM} + R_{AWR}$$

where :
R_{AWM} - motion induced component of resistance, R_{AWR} - wave reflection component of resistance.

$$R_{AWM} = 3859.2 p_w g {\zeta_A}^2 \frac{B^2}{L_{pp}} C_b^{1.34} K_{yy} a_1 a_2 a_3 \omega^{b_1} e^{\frac{b_1}{d_1}(1-\omega^{d_1})}$$

g - acceleration due to Earth's gravity (9.81 m/s^2), ζ_A - wave amplitude a_1,a_2,a_3 b_1,d_1 and ω - parameters dependent on ships length, beam, block coefficient, speed, draft, wave height, wave direction and wave period.

$$R_{AWR} = \sum_{i=1}^{4} R_{AWR\,i}$$

$R_{AWR\,i}$- added wave reflection resistance components dependent on waterline geometry, speed, hull geometry, wave parameters.

- Shallow Water Resistance: *ITTC (2021)*, basing on *Raven's (2019)* method:

$$\frac{C_V}{C_{Vdeep}} = 1 + 0.57 \cdot \left(\frac{T}{h}\right)^{1.79}$$

Added shallow water resistance can be described as:

$$R_{shallow\,water} = \left(\frac{C_V}{C_{Vdeep}} - 1\right) \cdot R_{friction} = 0.57 \cdot \left(\frac{T}{h}\right)^{1.79} \cdot R_{friction}$$

where :

C_V - viscous resistance coefficient, C_{Vdeep} - viscous resistance coefficient in unrestricted waters, h - water depth (m)

Wave making resistance has been excluded from the scope of white box modelling due to its high complexity and lower contribution to hull resistance at Froude numbers, where most operational data can be collected, as mentioned by *Bertram and Marioth (2024)*. The total predicted shaft power within the white box model is given by the formula:

$$P_{shaft\,(white\,box)} = (R_{environment} + R_{friction}) * V_{STW}/\eta_{propulsion}$$
$$R_{environment} = R_{wind} + R_{wave} + R_{shallow\,water}$$

The process of data flow within white box model training can be described by the following algorithm:

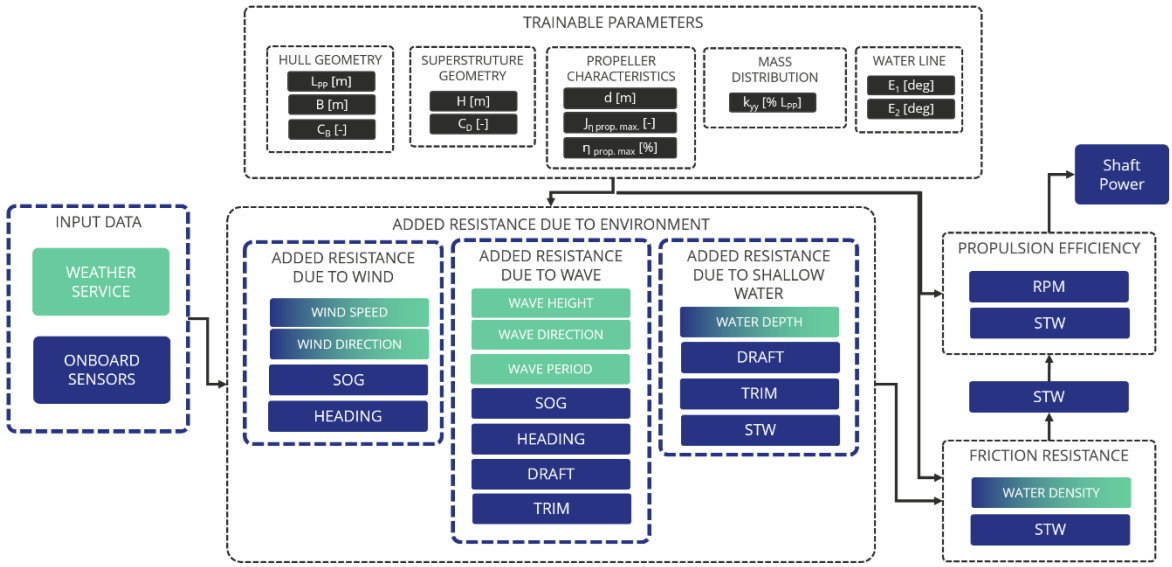

Fig.5: Whitebox model training parameter and data flow diagram

Although the learned white box variables might differentiate from the true vessel's parameters their role allows to tune the relationships within known laws governing power requirements allowing to increase white box model accuracy at the first step.

3.2. Serial Grey Box Model

The physics-based model is coupled with a neural network model in two different scenarios. The serial grey box approach is based on a white box model that provides an initial estimate of the shaft power, which is then used as an additional input feature for the neural network model part, referred to as the black box model.

$$P_{shaft\ (Greybox\ serial)} = P_{(black\ box)}(BB\ features, P_{shaft\ (white\ box)})$$

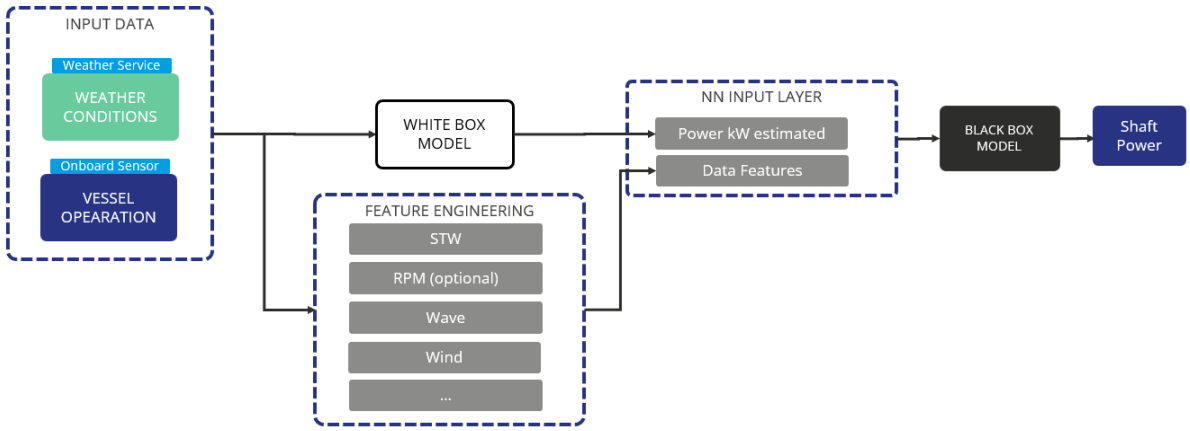

Fig.6: Serial Grey Box Model Diagram

Within scope of this approach the physics-based shaft power estimation provides additional information to the neural network contributing to the more accurate input-output relationships modeling. It is assumed that for regions where very limited amount of training data were available those input-output relationships will provide better estimation accuracy than the pure black box modeling approach.

3.3. Parallel Grey Box Model

The second grey box modelling approach is known as parallel grey box. This approach assumes that the black box part is responsible for modelling the difference between the initial estimated shaft power prediction provided by the white box part and the recorded true shaft power values. With the same level of input features available for the black box it is assumed to provide ability of capturing more precise relationships between input variables representing environmental conditions being able to correct the inability of white box model to precisely represent the input-output relationships.

$$P_{shaft\ (Greybox\ parallel)} = P_{shaft\ (white\ box)} + \Delta P_{(black\ box)}(BB\ features)$$

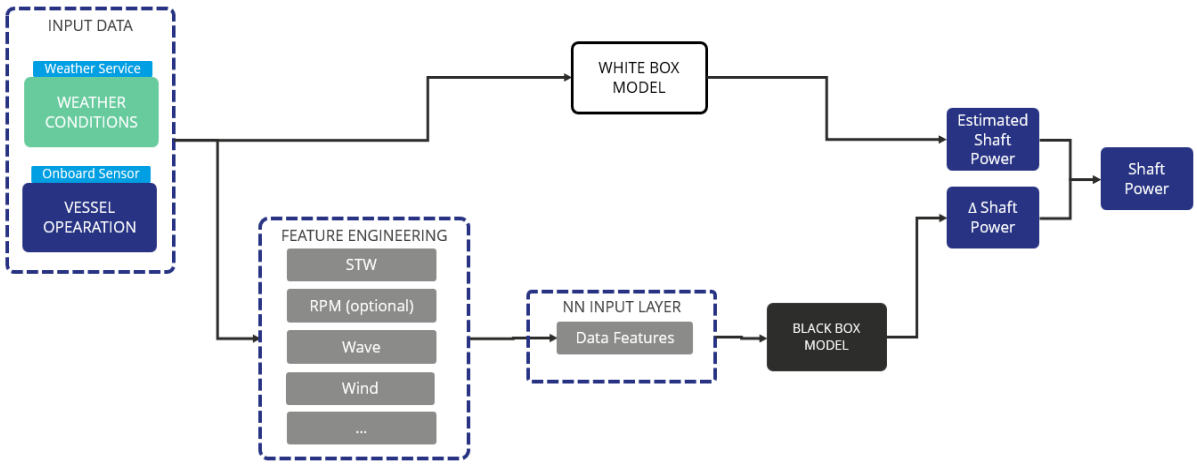

Fig.7: Parallel Grey Box Model Diagram

Similar to the serial grey box, the parallel grey box is assumed to have the ability to increase the prediction accuracy for the regions where little train data was available over pure black box prediction accuracy in that region.

3.4. Grey box method validation with artificial dataset

In order to represent the problem and test the alternative learning algorithm with an indication of the potential advantage of the physics influenced grey box models over pure black box, an artificial dataset has been generated involving white box model-known law given by simple artificial speed and shaft power dependence:

$$P_{Shaft} = STW^2$$

To the one-dimensional dependency, the additional artificial influence of wind speed on added shaft power has been included with following dependency rule:

$$P_{added} = C_D \cdot {V_w}^2 \cdot S$$

where :

C_D – Wind Resistance Coefficient
V_w – Wind Speed
S – Projected area of the member normal to the direction of the force

The artificial training dataset has been generated with two dense regions of data availability in order to resemble the problem of non-uniform distribution of training data. Two datasets were generated with normal distribution patterns for resemblance of the data collected at lower and higher speeds. The amount of data has been distributed by 75 % of the dataset recorded in higher speeds and 25 % of data recorded at lower speeds. The power- speed curves were generated for three models representing power prediction for zero wind speeds with mean absolute percentage errors for each power-speed curve.

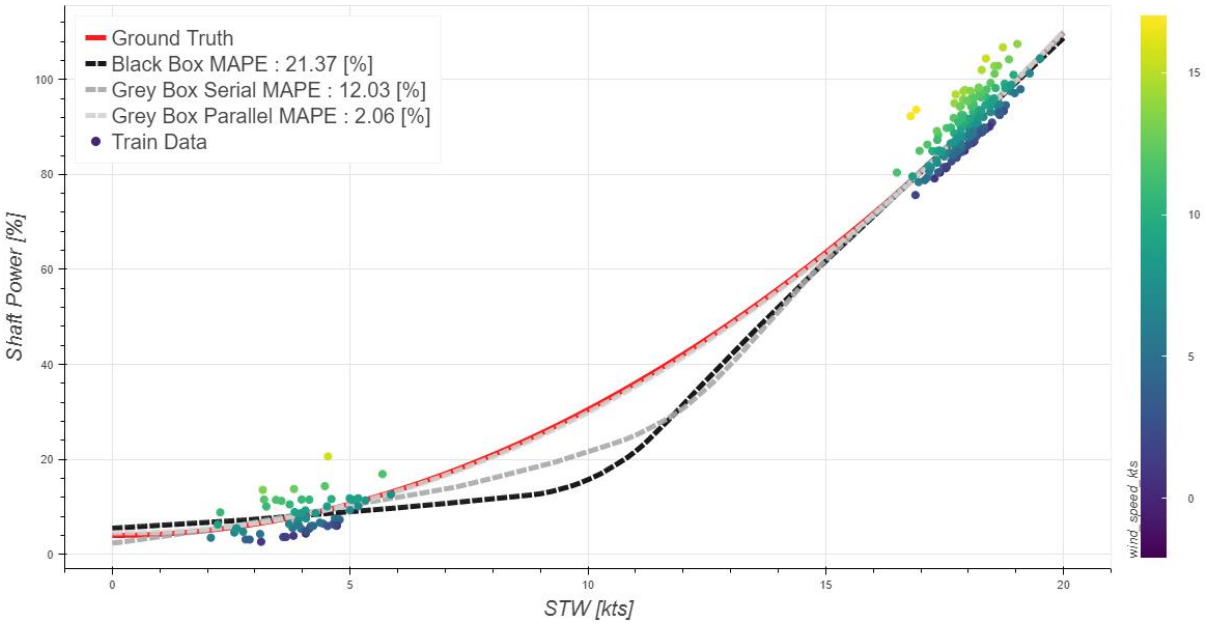

Fig.8: Artificial dataset and power-speed curves from different model predictions

The artificial dataset has presented high advantage of the grey box modelling approaches over the pure black box model. It is noticeable, that the data availability significantly influenced the black box model causing it to strongly deviate from the ground truth relations in the region, where no training data was available. The superiority of parallel grey box over serial grey box can also be observed, but it is not assumed as conclusive at this level due to the simplified method of artificial dataset generation.

4. Confidence Level assessment for Performance Models

The assessment of the reliability of neural network predictions is highly important when predictions will be employed in critical decision-making processes supported by machine learning models. In classification problems the neural network models confidence estimation has been the subject of extensive research, with a range of methods having been proposed. However, research on the application of such measures in regression model applications remains limited as mentioned by *Shin and Koo (2021)*. To address this problem, an alternative way of confidence level assessment in shaft power prediction has been proposed. Basing on knowledge of the basic rules governing environmental conditions and propulsion power requirement gained though industry's research on the aspects of vessel's hydrodynamics and seakeeping, the key parameters allowing to establish the environmental domain limits were selected. It is acknowledged that the resistance of the hull can undergo substantial alteration within the domain of the vessel's draft and trim. These parameters are identified as the parameters of operational optimisation, with the objective of minimising the resistance of the hull. These parameters were selected as the domain definition, in conjunction with STW, which is recognised as the third most significant model feature. Remaining environmental-dependent parameters are assumed to be subjects of further data filtering methods even if their influence on added resistance can be higher than change of draft, trim or STW. The model user shall have the possibility of power requirement estimation regardless of the vessel's loading conditions, with given confidence rates.

The estimation of model's prediction confidence level is based on the availability of the training data within domain of operational parameters of the estimation. The measure describes amount of test data points within training data domain in scope of the selected parameters. In order to pre-define the domains of training data, the clustering methods has been utilized. The methods were previously assessed as useful for vessel's operational datasets classification by *Górski et al. (2021)*. The train datasets are subjected to clustering within the scope of three dimensions of operational parameters. The test datasets are then assessed for their affiliation within the clusters of training data. In instances where test datasets may be allocated to multiple clusters, the affiliation rate is calculated for all potential clusters. Consequently, the highest rate is taken into account. The clustering domains are represented in form of convex hulls. To store the information about classified train datasets, the apexes of convex hulls of identified clusters can be saved for further predictions. To check if new data point is inside the hull, it is check if adding it to the cluster (reduced to apexes of hull) will change a convex hull volume. If the volume of convex hull has been extended, the point was identified as external to the assigned convex hull. Otherwise, the point is inside the convex hull and is regarded as affiliated with the given cluster.

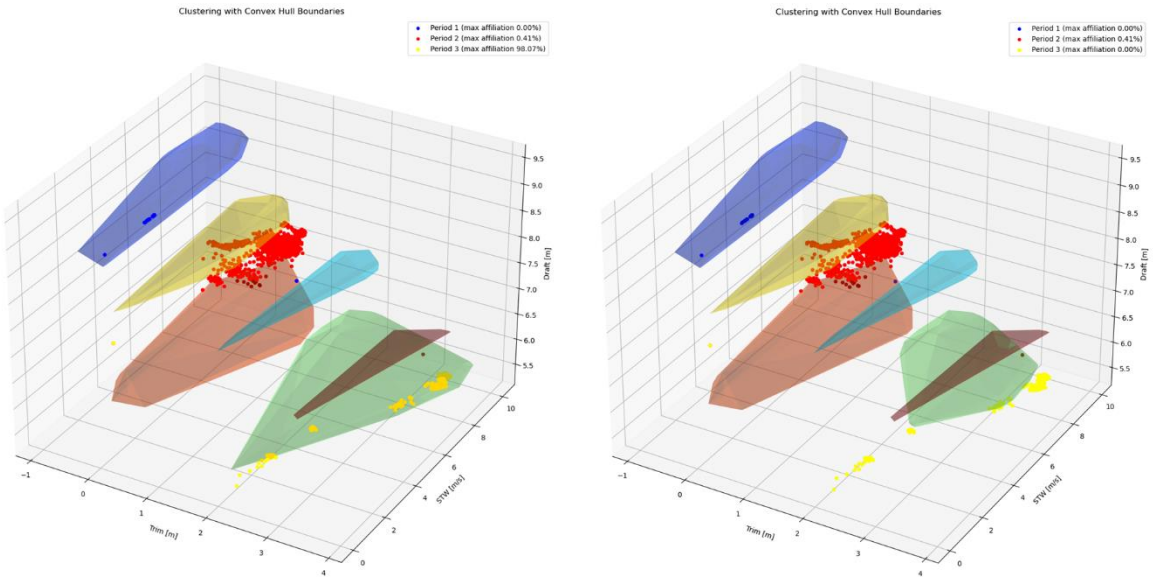

Fig.9: Training dataset Clusters with Test Periods data points max affiliation rates. Cluster with one voyage period artificially excluded from the training dataset resulting in zero affiliation rate for Period no. 3 (right)

5. Comparison of Prediction Accuracy

The model accuracy assessment has been prepared basing on data set collected by SeaPerformer system installed onboard ocean going 1700 TEU container vessel. The selection of container vessel has been dictated by the higher challenge of shaft power prediction posed by significant changes of cargo to wind exposed structure and their influence on added wind resistance, irregular loading conditions causing higher variance of draft & trim in consecutive voyages and more frequent changes of RPM setpoints dictated by the operational characteristics with requirements of reaching precise ETA's at the container terminals. Two train dataset cases were proposed for selected test period in order to validate the change of accuracy basing on training dataset availability. The training dataset has been investigated upon similar operational draft & trim conditions and the close matching voyages has been excluded from the train dataset in order to form second train dataset with no data recorded in close conditions. For the test period next voyage has been selected in order to minimise other time dependent factors like hull fouling on prediction accuracy assessment. The affiliation rates for both train datasets were assessed as 0% and 98.07%. The resulting convex hulls are presented in Fig.9. Selected test period has been represented by yellow points. Despite close presence of the similar draft & trim conditions in voyages conducted in the past, their operating conditions were found to be different and this can be particularly seen on the 3-dimensional graphs. This type of high variance of the loading conditions can be found frequent for container vessels.

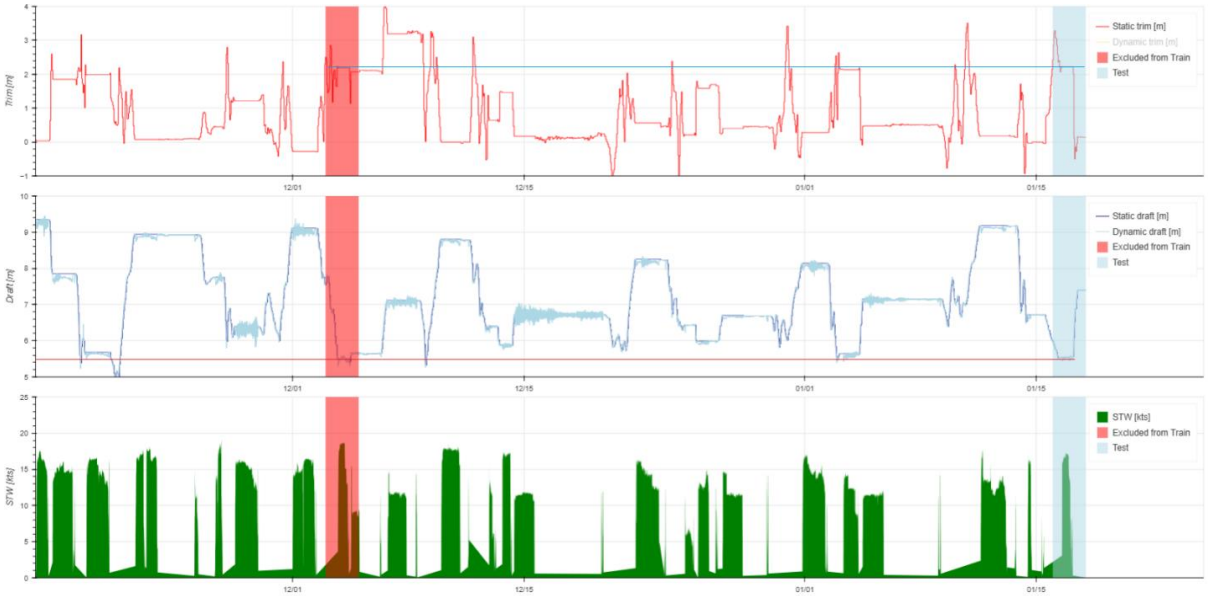

Fig.10: Timeline graph of the train & test (blue) data with excluded similar voyage (red)

Training dataset consists of 1 minute resolution data from 62 days of vessel's operation. Subject to dynamic state filtering, where identified dynamic states were rejected from training, resulting dataset consisted of 93.34% of initial data. Two train datasets with high and zero affiliation were used for model training and validation against test dataset. This approach aimed for representing two scenarios with high and zero test data availability in similar operation conditions. It is noticeable that two grey box models were able to predict shaft power with lower error rates, than black box models for both test cases. It is also seen that there's significant accuracy improvement for the test case where no train data were available when using grey box models over the black box model. There's no big difference between two grey box modeling approaches for zero affiliation test case, however there's a noticeable superiority of serial grey box prediction accuracy over parallel grey box for high affiliation test case.

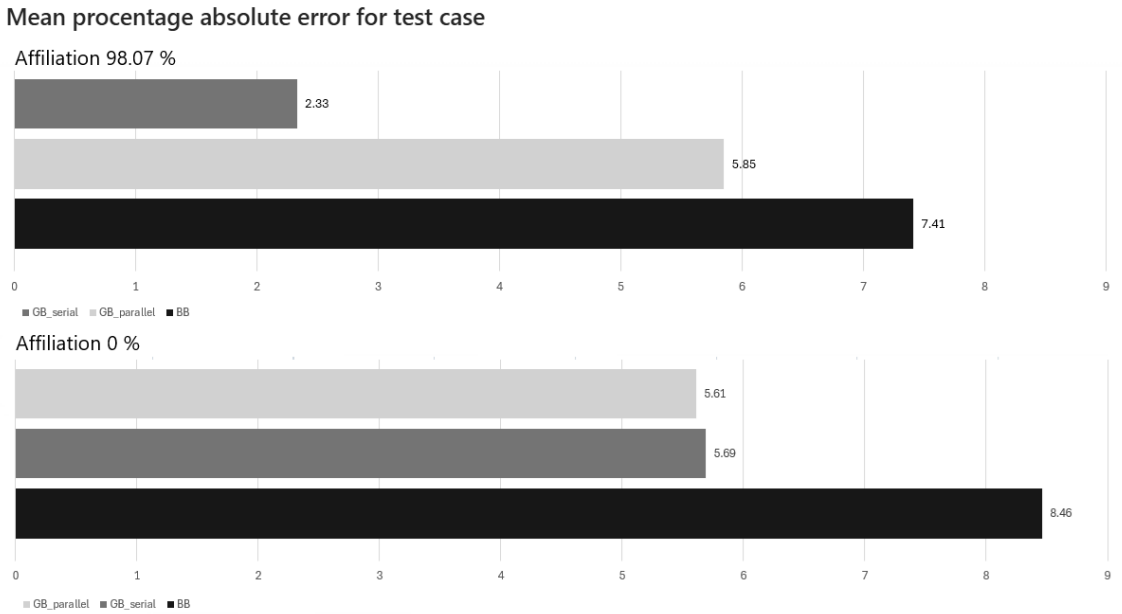

Fig.11: Comparison of model's prediction error rates for two test case datasets

The experiment demonstrates the considerable potential of integrating physics-based knowledge into the machine learning process to enhance the accuracy of power prediction. Results based on real, high-resolution operational data are partially confirming the superiority of grey box modeling achieved on artificial dataset experiment. To validate this finding, further research will be expanded to cover a more extensive range of test cases, involving different vessel types and operational datasets.

Acknowledgement

We would like to express our gratitude for a financial support received within Eurostars-3 project "Integrated Voyage Optimization" (proposal No. 1982), InnovativeSMEs/2/4/2023 (Project No. in Poland).

References

BERTAM, V., MARIOTH, R. (2024), *Third-Power Law – Friend or Foe?*, 9th HullPIC Conf., Tullamore, pp.5-10, http://data.hullpic.info/HullPIC2024_Tullamore.pdf

DET NORSKE VERITAS (2014), *DNV-RP-C205: Environmental conditions and environmental loads*, Det Norske Veritas, pp.70-71

GÓRSKI, W.; MICHNIEWICZ, J.; SZLENDAK, A. (2021), *Using unsupervised machine learning for building ship performance reference model*, 6th HullPIC Conf., Pontignano, pp.132-141, http://data.hullpic.info/HullPIC2021_Pontignano.pdf

ITTC (2014), *Recommended Procedures and Guidelines Preparation and Conduct of Speed/Power Trials*, Revision 4, Int. Towing Tank Conf.

ITTC (2021), *The Specialist Committee on Ships in Operation at Sea (SOS), Final Report and Recommendations to the 29th ITTC*, Int. Towing Tank Conf.

LEIFSSON, L.Þ.; SÆVARSDÓTTIR, H.; SIGURÐSSON, S.Þ.; VÉSTEINSSON, A. (2008), *Grey-Box Modeling of an Ocean Vessel for Operational Optimization*, Simulation Modelling Practice and Theory Volume 16, Issue 8

PAPACHRISTOU, G.; ANTONOPOULOS, G.; DIMITROKALLI, A.; DOULGERIDIS, A.; LOIZOU, E.; MANDITSIOS, G. (2024), *Enhancing Linear Models Vessel Performance Prediction through Domain-Informed Feature Engineering and Data Pre-processing*, 9th HullPIC Conf., Tullamore, pp.94-110, http://data.hullpic.info/HullPIC2024_Tullamore.pdf

PARKES, A.I.; SOBEY, A.J.; HUDSON, D.A. (2021), *Towards Error Measures Which Influence A Learners Inductive Bias To The Ground Truth*, https://arxiv.org/pdf/2105.01567

PARKES, A.I.; SOBEY, A.J.; HUDSON, D.A. (2025), *More Consistent Learnt Relationships In Regression Neural Networks Using Fit To Median Error Measure, Engineering Applications of Artificial Intelligence*, Engineering Applications of Artificial Intelligence 144

RAVEN, H.C., (2019), *Shallow-water effects in ship model testing and at full scale*, Ocean Eng. 189

SHIN, D.W.; KOO, H.I. (2021), *Confidence Estimation Method For Regression Neural Networks*, Ajou University, Suwon

UNITED NATIONS, (2024), *Review Of Maritime Transport*, United Nations Conference On Trade And Development

WANG, J.; BIELICKI, S.; KLUWE, F.; ORIHARA, H.; XIN, G.; KUME, K.; OH, S.; LIU, S.; FENG, P. (2021), *Validation study on a new semi-empirical method for the prediction of added resistance in waves of arbitrary heading in analyzing ship speed trial results*, Ocean Eng. 240

Hydrodynamics of Biofilms and Soft Fouling: Parametrization using High-Fidelity Computations

Elias Balaras, George Washington University, Washington DC/USA, balaras@gwu.edu

Abstract

Today there is an incomplete understanding on how biofilms and soft fouling contribute to the generation of hydrodynamic drag. The main roadblock is the absence of a basic understanding of the impact of such fouling to the turbulent boundary layer, and whether the utilization of the same parametrization strategies used in calcareous fouling would be effective. In this paper we will address this question using topography-resolving direct numerical simulations informed by laboratory experiments. The complex fluid-structure interactions between biofilms and/or streamers and the turbulent boundary layer are directly resolved utilizing our in-house solver and leadership HPC resources. We will discuss the impact of soft fouling on near-wall turbulence, as well as strategies to modify existing correlations related to hydrodynamics drag.

1. Introduction

Biofouling takes place in the parts of a naval vessel submerged in sea water and exposed to marine organisms which colonize these surfaces leading to excess fuel consumption because of the increased hydrodynamic resistance. The corresponding shaft power of a full-scale ship due to various fouling conditions can increase by up to 85%, compared to a hydraulically smooth hull, *Schultz (2007)*. Today, roughness correlations encapsulating numerous datasets obtained over the years are typically utilized to predict the drag penalty over a rough wall. They assume an increased momentum deficit coming from the drag on the roughness elements, which has an impact on the standard law-of-the-wall represented by the roughness function, ΔU^+, see for example *Chung et al. (2021)*. The latter allows for the extrapolation of laboratory data to full-scale Reynolds numbers utilizing scaling laws for smooth-wall boundary layers. The roughness function, however, depends on the details of the topography and the Reynolds number. Over the years multiple experimental and numerical studies for canonical, rough surfaces (i.e. uniform distributions of cylinders, hemispheres, pyramids etc.) provided estimates of the proper hydrodynamic roughness scale that shows the strongest correlation with the roughness function. Direct application of such correlations to biofouling roughness can lead to erroneous predictions, given that biofouling topographies exhibit specific surface properties that are not common in other types of roughness, *Dehn et al. (2017)*.

For calcareous biofouling involving barnacles and/or tubeworms there have been several studies investigating their hydrodynamic impact. *Schultz (2005)* conducted a study to investigate the frictional resistance of different antifouling coatings utilizing actual barnacle-fouled topographies and found that the silicon-based surfaces where the ones to result in the highest skin-friction values. *Monty et al. (2016)* reported experimental measurements in boundary layers over a rough wall populated by tubeworms and estimated the final drag penalty on a ship using scaling analysis. To reconstruct a realistic biofouling surface, they assembled the final roughness by using repeated tiles of scanned fouled coupons. To assess the drag impact of barnacle-type topographies, *Kaminaris et al. (2023)* used direct numerical simulations (DNS) and concluded that the highest contribution to the total drag arose mainly from the pressure force imposed by the organisms (even up to 88%). *Sarakinos and Busse (2019)* performed DNS of turbulent channel flows over barnacle-type topographies with light clustering and observed that the frontal solidity has the highest impact on the roughness function for low planar solidity topographies.

For soft fouling, however, we have an incomplete understanding as to how it contributes to the generation of hydrodynamic drag. In addition, fouling release (FR) and antifouling (AF) hull coatings that help control hard fouling, such as barnacles and tubeworms, are often ineffective at preventing soft fouling, see for example *Molino and Wetherbee (2008)*. As a result, there is a need to develop a better understanding of the impact of such fouling to the turbulent boundary layer and whether the utilization

of the same parametrization strategies used for calcareous fouling would be effective to predict hydrodynamic resistance. Soft fouling, which is also referred to as slime, tends to be one of the first types of fouling to occur. They are typically composed of bacterial cells and diatoms, with the latter being the dominant species. Depending on the geographic location, type of surface and local hydrodynamics the structure of the biofilm varies significantly. Its thickness ranges from micrometers to millimeters, and when it grows under shear it is composed of thin flexible filaments called *streamers*. Today it is generally assumed that soft fouling results in minimal reduction in ship performance and therefore if found during a hull inspection is not considered a reason to clean the hull. Recent work, however, shows biofilms can induce a steep drag penalty. *Murphy et al. (2018)* studied biofilms consisting of very low stiffness streamers grown under shear in a channel flow configuration. They found that the mean velocity profile exhibits a standard log-law region with the expected downward shift found in rough-wall flows. The resulting equivalent sand-grain roughness height, k_s, was of the order of 8.8 mm, and significantly larger than the physical height of the biofilm (1.7 mm). They speculated that this dramatic increase in drag was due to the flapping streamers and possibly the compliance of the biofilm layer.

In this paper we will address these questions using topography-resolving DNS informed by laboratory experiments. The complex fluid-structure interactions between biofilms and/or streamers and the turbulent boundary layer are directly resolved utilizing our in-house solver and leadership HPC resources. We will discuss the impact of soft fouling on the near-wall turbulence, as well as strategies to modify existing correlations related to hydrodynamics drag.

2. Methodologies

We will consider the case of a fully developed turbulent channel flow, where one of the walls is covered by a flexible canopy consisting of an array of filaments randomly distributed to match the desired open area ratio. The coordinates x,y, and z represent the streamwise, wall normal and spanwise directions respectively. The incompressible fluid flow is governed by the Navier-Stokes equations:

$$\frac{\partial \mathbf{u}}{\partial t} + \mathbf{u} \cdot \nabla \mathbf{u} = -\nabla p + \frac{1}{Re} \nabla^{2\mathbf{u}} + \mathbf{f} \qquad (1)$$

where **u** is the velocity vector, p is the pressure, **f** is a force that accounts for the fluid structure interaction, and $Re=U_bH/\nu$ is the Reynolds number based on the kinematic viscosity of the fluid, the bulk velocity U_b and the channel half height H. The dynamic deformations of the filaments are governed by an inextensible Kirchhoff rod model, see for example *Huang et al. (2007)*.

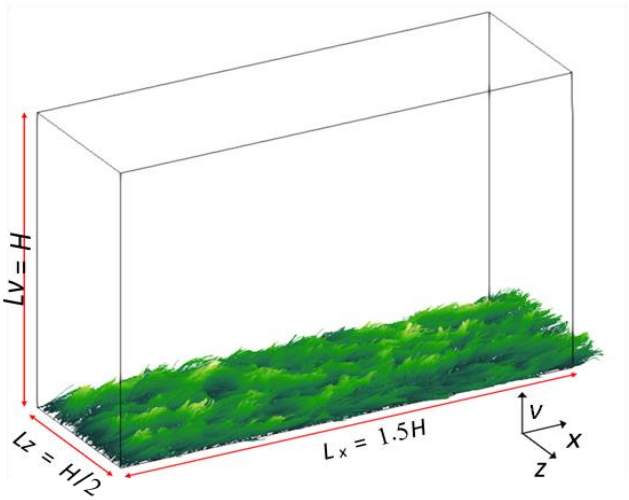

Fig.1: Computational domain of turbulent channel with filaments at the bottom wall. The subset shows a schematic illustration of the Lagrangian markers at the core of the filaments used for the kinematics and the triangular mesh used in the fluid structure interaction.

The Kirchhoff rod model is well suited to model such structures, because it enables control of the undeformed shape and flexibility among other parameters to match the characteristics of the bio-inspired canopies considered in the present study. The governing equation for a flexible inextensible filament is written in Lagrangian non-dimensional form as:

$$\frac{\partial^2 X}{\partial t^2} = \frac{\partial}{\partial s}\left(T\frac{\partial X}{\partial s}\right) - \frac{\partial^2}{\partial s^2}\left(\gamma\frac{\partial^2(X - X_u)}{\partial s^2}\right) + Fr\frac{g}{g} - \alpha \cdot F_l + F_r \qquad (2)$$

where s is the arclength, going from 0 at the bottom of the filament to L_f at the tip, X = ($X(s,t)$,$Y(s,t)$,$Z(s,t)$) the position, T the tension force along the filament axis, F_l the fluid force exerted on the filament, and F_r the repulsive forces between nearby filaments. In Eq.(2), $\alpha = \rho/\rho_s$ denotes the ratio of the density of fluid to that of the filament. The second term on the rhs of Eq. 2 represents the bending force and X_i denotes the undeformed state of the filament. The constant, $\gamma=\Gamma/\rho_s U^2 L^2$ is a dimensionless parameter (Γ and ρ_s are the bending rigidity and density of the filaments respectively) that represents the ratio of the bending to inertial forces.

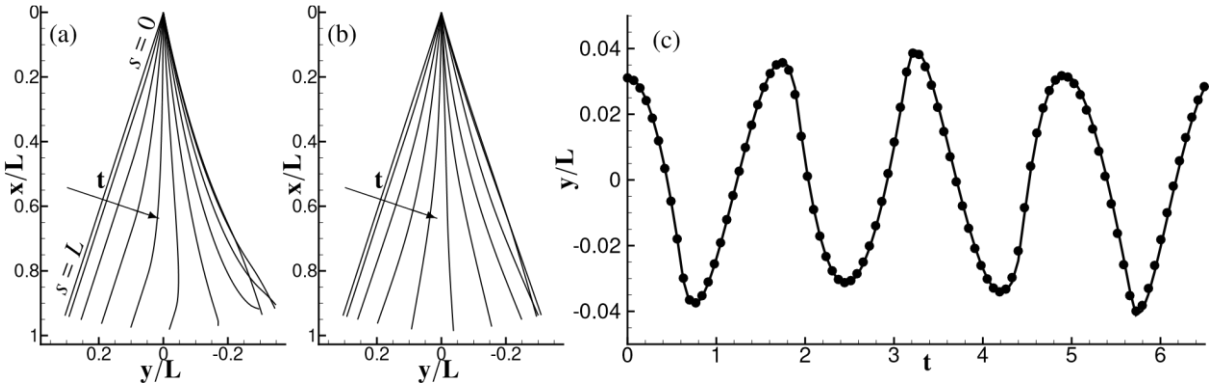

Fig.2: Motion of a hanging filament at various time instants starting at $t = 0$ and separated by $\Delta t = 0.3$. The motion is from left to right. a) $\gamma = 0$ (no bending force) and b) $\gamma = 0.1$. c) Time history of the free end of a hanging filament with $\gamma = 0$ and $\theta_0 = 0.01\pi$. Lines represent: • numerical solution, - analytical solution.

The inextensibility condition is expressed by:

$$\frac{\partial X}{\partial s} \cdot \frac{\partial X}{\partial s} = 0 \qquad (3)$$

The tension force, *T*, in Eq.(2) is determined by the constraint of inextensibility by solving the Poisson equation:

$$\frac{\partial X}{\partial s} \cdot \frac{\partial^2}{\partial s^2}\left(T\frac{X}{\partial s}\right) = \frac{1}{2}\frac{\partial^2}{\partial t^2}\left(\frac{\partial X}{\partial s} \cdot \frac{\partial X}{\partial s}\right) - \frac{\partial^2 X}{\partial t\,\partial s} \cdot \frac{\partial^2 X}{\partial t\,\partial s} - \frac{\partial X}{\partial s} \cdot \frac{\partial}{\partial s}\left(\gamma\frac{\partial^2(X - X_u)}{\partial s^2} - F + F_r\right) \qquad (4)$$

At the free end ($s = L$) the boundary conditions for the filaments are $T = 0$, $\partial^2 X/\partial s^2 = (0,0,0)$ and $\partial^3 X/\partial s^3 = (0,0,0)$. At the bottom wall the filaments are clamped, and the boundary conditions are $\partial T/\partial s = 0$, $X = X_{wall}$ and $\partial X/\partial s = (0,1,0)$. A staggered grid is used in the Lagrangian coordinate system, with the tension defined on the faces and the other variables defined on the nodes. All spatial derivatives are approximated using second order central finite differences. For the time advancement of the kinematics all terms except the bending and repulsive forces are treated implicitly.

To validate the Kirchhoff rod model, we performed simulations of a hanging filament without ambient fluid under a gravitational force. The filament is initially held stationary at an angle θ_0 from the vertical

and released at $t = 0$. The initial position of the filament is given by $X(s,t = 0) = L \cdot cos(\theta_0)$ and $Y(s,t = 0) = L \cdot sin(\theta_0)$, where x is the direction of the gravity. At the hanging end a simply supported boundary condition is used, namely $\partial T/\partial s = 0$, $X = X_{wall}$ and $\partial X^2/\partial s^2 = (0,0,0)$. The motion of the filament with ($\gamma = 0.1$) and without ($\gamma = 0$) bending force at various time steps is shown in Fig.2. The motion is from left to right. In the simulations $L = 1$, $Fr = 10$ and $\theta_0 = 0.1\pi$. In the absence of a bending force the filament is very flexible, and the free end rolls up towards the right at the end of the rightwards motion. When $\gamma = 0.1$ the filament maintains its predeformed shape throughout the motion and the roll-up is inhibited. The motion in this case resembles more that of a pendulum. An analytical solution for the motion of the filament exists when the swing amplitude is small and the bending force is neglected, *Huang et al. (2007)*. Fig.2c compares the analytical solution with the simulation ($\gamma = 0$, $\theta_0 = 0.01\pi$), where the free end position of the filament is plotted. The agreement is excellent.

In the classical immersed boundary technique, the filament would be represented by a triangular surface mesh and there would be at least 10 or more Eulerian grid points across the diameter to resolve the flow. An immersed boundary force is mathematically defined such as to satisfy the correct velocity at the surface of the filament. However, since the filaments are very thin, the computational cost of this approach would be prohibitively expensive. In the present simulations the filaments are represented by a set of markers along the filament core line and the Eulerian grid resolution is approximately equal to the virtual filament diameter. The interaction force between the fluid and the filament is then calculated as:

$$F(X) = c \cdot (U(X) - \mathcal{I}[u(X)]) \cdot dV_{Lag} \tag{5}$$

where $\mathbf{U}(\mathbf{X})$ is the velocity of the filament at the Lagrangian marker location $\mathbf{X}$ and $\mathcal{I}[u(X)]$ is the fluid velocity at the Lagrangian marker location interpolated from the Eulerian grid points surrounding the marker. dV_{Lag} is the volume associated with each Lagrangian marker. The coefficient c was properly adjusted to give the same total drag force as a fully resolved simulation around a filament with a virtual shell of an equivalent diameter. The force is then spread back to the Eulerian grid points surrounding the marker ($\mathbf{f}$ in Eq.(1)) using the same weights as in the interpolator operator.

$$f(x) = \mathcal{S}[F(X)] \tag{6}$$

Note that the linear force in Eq.(2) is simply the force per unit filament length, namely $F_l = F/\Delta s$, where Δs is the Lagrangian grid spacing.

A collision model was used to account for short-range interactions between filaments and between a filament and a wall, *Schmid et al. (2000)*. Due to large number of filaments markers calculating the distance between each filament marker would be prohibitively expensive. We therefore used a different approach. In particular, at each timestep each marker was mapped to the Eulerian grid. Then if a Eulerian grid contained one or more markers and had a neighboring Eulerian cell which also contained one or more markers a repulsive force was applied to all those markers as follows:

$$F_r = c_{r_1} \cdot exp\left[-c_{r_2} \cdot \frac{|\delta X_{l,m}| - 2r}{d_r}\right] \cdot \frac{\delta Xij}{|\delta Xij|}, |\delta X_{l,m}| \leq d_r \tag{7}$$

where $\delta\mathbf{X}_{l,m}$ is the distance vector from marker m to marker l or the wall, and d_r is the threshold separation distance set to 2 Eulerian grid cells. Typically, both coefficients c_{r1} and c_{r2} are sensitive to the flow conditions and are determined empirically, *Schmid et al. (2000)*. For filaments that are very flexible, such as the ones considered in this study, we found that the coefficient c_{r1} can be automatically set to the sum of the magnitude of the fluid forces acting on each marker:

$$\boldsymbol{c_{r_1}} = |\boldsymbol{F_f}|_i + |\boldsymbol{F_f}|_j \tag{8}$$

while $c_2 = 1.0$. This method automatically ensures that the repulsive force is always larger than the local fluid force pushing a filament towards another, but not excessively large to cause instabilities.

The equations governing the fluid flow are advanced in time using a semi-implicit projection method, where all terms treated explicitly are advanced using a 3^{rd} order Runge-Kutta scheme, and all terms treated implicitly are advanced using a 2^{nd} order Crank-Nicholson scheme. All spatial derivatives are discretized using second-order central differences on a staggered grid. A weak coupling schemes was utilized to couple the two sets of equations. The code is parallelized using a domain decomposition approach in the streamwise direction.

3. Problem setup

A turbulent channel flow case is considered where the filaments are located on the bottom wall. Fig.1 shows the setup of the simulation along with the filaments in a deformed state. The computational domain extends $1.5H \times 1H \times 0.5H$ in the streamwise, wall normal and spanwise directions respectively, where H denotes the half-channel height. The pressure gradient was adjusted to maintain a constant bulk velocity U_b. The grid utilizes $400 \times 200 \times 282$ points in x, y and z respectively. No-slip boundary conditions were imposed on the bottom and top walls while periodic boundary conditions were used in the streamwise and spanwise directions. When a portion of a filament crossed over one end of the domain in either x or z direction it was copied in a periodical fashion at the other end.

A total of six simulations were carried out with different canopy coverage ratios and Reynolds numbers. Table 1 lists the cases along with relevant parameters. The Reynolds number based on the half channel height and the bulk velocity varied from $Re_b = 20000 - 80000$. The filaments have a length $l = 0.125H$ and a virtual diameter $d = 0.0015625H$ resulting in a slender ratio $l/d = 80$. The Cauchy number defined as $Ca = \rho d h^2 U^3/2\gamma$ and representing the ratio of fluid forces to bending force is 100000, which means that the filaments are very flexible. The ratio of filament to fluid density $\alpha = \rho_f/\rho = 1.2$ approaching the neutrally buoyant state. The solidity parameter defined as $\lambda = n_f ld/(L_x L_z)$, where n_f is the number of filaments, l and d are the filament length and virtual diameter, and L_x and L_z is the extend of the domain, varied from 1.3 and 2.6, corresponding to 20% and 40% coverage respectively. A total of 5000 and 10000 filaments were used in the $\lambda = 1.3$ and $\lambda = 2.6$ cases respectively with each filament represented by 100 markers.

4. Discussion

First, we analyze the effect of the flexible canopy on the mean velocity profiles. Fig.3 shows the profile of the streamwise velocity averaged over time and homogeneous directions for the different Reynolds numbers and solidity parameters. The ensemble average position of the filaments, calculated by averaging all the filament position relative to their root, is also shown for reference while the inflection points and the canopy tip are indicated by open circles and dashed lines respectively. In general, as the solidity parameter decreases the canopy deflects more and the velocity profiles exhibit a smaller momentum deficit closer to the wall. Also, in agreement to what has been observed in the literature the velocity profiles exhibit two distinct inflection points, one very close to the wall and a second one closer to the canopy tip. The inner inflection point is reminiscent of that attained in an anisotropic porous medium, *Rosti et al. (2018)*, while the outer one is typically associated with the drag discontinuity near the canopy tip and the formation of turbulent mixing layers, *Raupach and Thom (1981)*. The outer inflection point typically matches the location of the canopy tip, *Foggi Rota et al. (2024)*, *He et al. (2022)*, although in several studies the latter is not directly computed form the data. In our simulations we found that the outer inflection point is always below the canopy tip. However, as the solidity parameter increases the inflection points moves closer to the canopy tip. The difference in this behavior is most likely attributed to the different canopy properties, which in our case tends to be considerably more flexible and with larger length to thickness ratio for the individual filaments.

The structure of the mean velocity profiles above points to the presence of two distinct layers inside and outside the canopy, that may or may not follow classical turbulent boundary layer scaling laws. Prior work in this area, *Foggi Rota et al. (2024)*, suggests the use of different velocity scales in each regime.

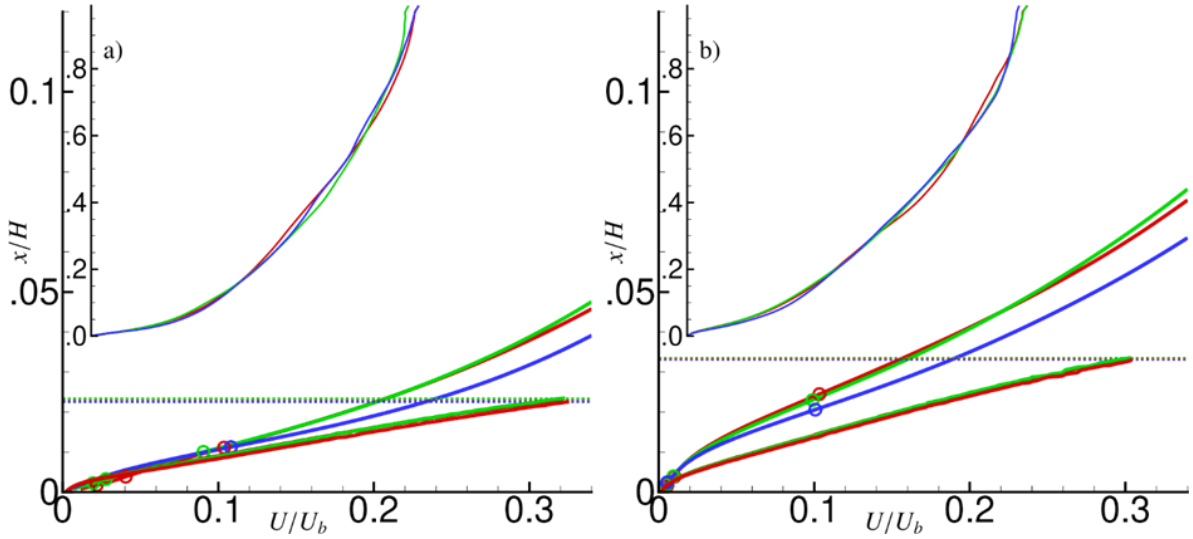

Fig.3: Profiles of the streamwise velocity averaged over time and space shown for solidity parameter of a) λ=1.3 b) λ=2.6. The ensemble average filament position is also shown for reference. The subset shows the velocity profile plotted over the full channel height. The inflection points are shown with open circles and the canopy tip is indicated with dashed lines. Lines represent: — ; Re_b = 80000, —; Re_b = 40000, —; Re_b = 20000.

Table I: Summary of cases

Case	Re	λ	α	*Ca*	k/H	k_+	k_{s+}	k_s/H	ΔU^+	k_s/k
A	20000	1.3	1.2	1e5	0.024	33.3	158.3	0.10	9.1	4.75
B	40000	1.3	1.2	1e5	0.024	68.9	357.0	0.10	11.0	5.18
C	80000	1.3	1.2	1e5	0.024	130.4	566.8	0.10	12.2	4.34
D	20000	2.6	1.2	1e5	0.035	51.7	319.4	0.20	10.8	6.18
E	40000	2.6	1.2	1e5	0.035	99.2	581.0	0.20	12.2	5.85
F	80000	2.6	1.2	1e5	0.035	192.5	1073.0	0.20	13.7	5.58

The friction velocity at the wall, $u_{\tau,in} = (\tau_w/\rho_f)^{1/2}$ is typically used for the, slow, viscous layer inside the canopy boundaries, while for the flow outside the canopy the friction velocity $u_{\tau,yvo}$ at the location of a virtual origin, y_{vo}, is computed. The latter is the distance from the wall that best matches the following logarithmic law:

$$\frac{U}{u_{\tau,y_{vo}}} = \frac{1}{\kappa} log\left(\frac{(y - y_{vo}) \cdot u_{\tau,y_{vo}}}{\nu}\right) + B - \Delta U^+ \qquad (9)$$

where k = 0.41 is the von Karman constant, B = 5.2 and ΔU^+ is the roughness function representing the downward shift in the log-law profile. Eq.(9) is a nonlinear, implicit function that can be used to determine the value of y_{vo}, which is typically assumed to be located between the first and the second inflection points. We found that multiple choices of y_{vo} yielded a log-law fit in some region outside of the canopy. Fig.4 shows contours of the velocity shift, ΔU^+, in Eq. 9 in the y_{vo} vs y coordinate space for the case with λ = 2.6 and Re_b = 80000. The range of the virtual origin extends from the bottom wall all the way up to the canopy tip and the outer flow starts above the canopy tip. The isolines are generally curved but there exist areas where they ΔU^+ remains constant indicating the potential presence of a shifted log-law. While there are horizontal isolines at the low-end of y_{vo}, the range is very short. We therefore determined the choice of the virtual origin by maximizing the range over which the velocity profiles exhibit a log-law fit.

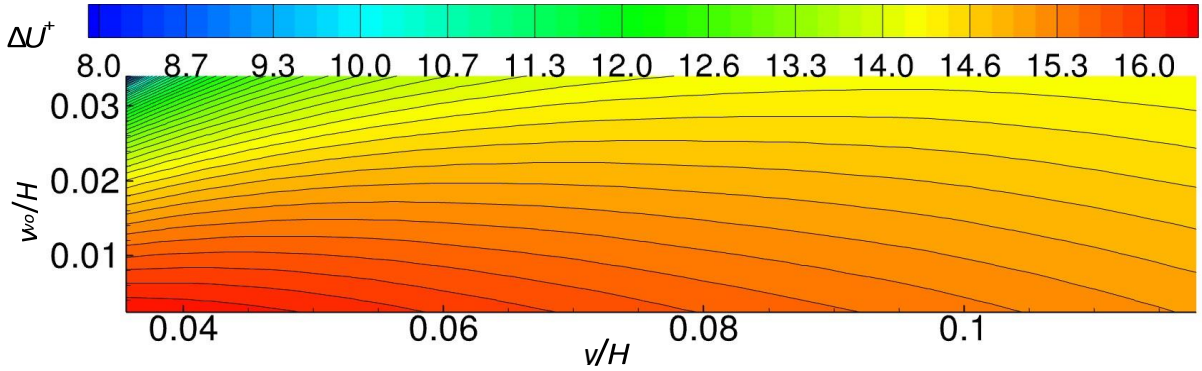

Fig.4: Profiles of the streamwise velocity averaged over time and space shown for solidity parameter of a) λ=1.3 b) λ=2.6. The ensemble average filament position is also shown for reference. The subset shows the velocity profile plotted over the full channel height. The inflection points are shown with open circles and the canopy tip is indicated with dashed lines. Lines represent: —; Re_b = 80000, —; Re_b = 40000, —; Re_b = 20000

Fig.5 shows the velocity profiles scaled by $u^{in}{}_\tau$ on the left and by $u_{\tau,yvo}$ on the right. Only below $y^+ < 1$ do the velocity profiles collapse from all the different simulations collapse and exhibit the typical linear scaling $U/u_{\tau,in} = yu_{\tau,in}/\nu$. This agrees with previous work by *Foggi Rota et al. (2024)* where only the first few very close to the wall observe the same trend. When scaled with $u_{\tau,yvo}$ all velocity profiles have a shifted log law. The starting point and the range of the log law region vary among the simulations, but it appears to be centered around $y^+ \sim 100$. The corresponding ΔU^+ or each case is listed in Table I. Note that the exact value of ΔU^+ depends on the choice of κ, B and the y_{vo} in Eq.(9), but the change in ΔU^+ was less than 5%.

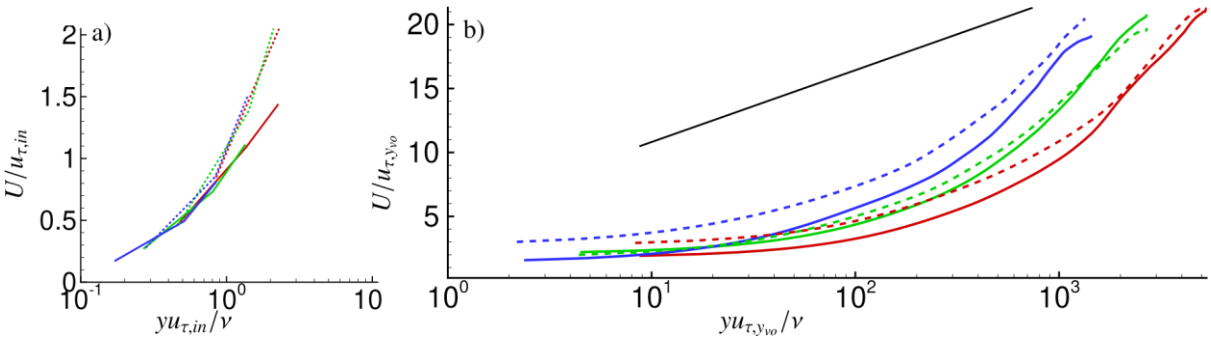

Fig.5: Profiles of the streamwise velocity averaged over time and space and scaled by a) $u\tau_{,in}$ and b) $u\tau_{,yvo}$. Lines represent: — analytical log law for smooth turbulent channel, —; Re_b = 80000 and λ = 2.6, —; Re_b = 40000 and λ = 2.6, —; Re_b = 20000 and λ = 2.6, - -; Re_b = 80000 and λ = 1.3, - -; Re_b = 40000 and λ = 1.3, - -; Re_b = 20000 and λ = 1.3

The roughness function depends on a physical measure of the surface roughness as well as the Reynolds number, see e.g. *Schultz (2007)*. In the case of flexible canopies the average canopy height, k is a reasonable choice. Table I lists the k values for all different cases. In Fig.6a, the roughness function ΔU^+ is plotted as a function of the average canopy height $k^+ = ku_{\tau,yvo}/\nu$ for all cases. For comparison, the uniform sandgrain roughness results by *Nikuradse (1950)* have been added.

The results follow the slop of the sandgrain roughness data in the fully rough regime although the roughness function is significantly larger. A common roughness scale, typically utilized in the literature for fixed roughness topologies, is the equivalent sandgrain roughness height, k_s, which is the height that produces the same roughness function as the uniform sandgrain roughness by *Nikuradse (1950)* in the fully rough regime. The value of $k_s{}^+$ can be determined using the log-law intercept for a uniform sandgrain surface in relative roughness form, *Flack et al. (2007)*:

$$B - \Delta U^+ + \frac{1}{\kappa} ln k_s^+ = 8.5 \qquad (10)$$

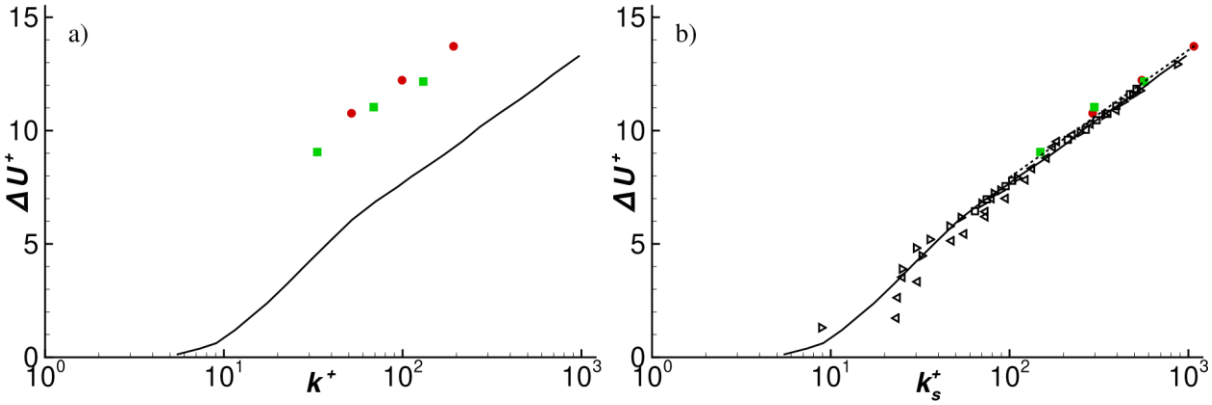

Fig.6: Roughness function results for the flexible canopies simulations. Experiments for a variety of roughness surfaces is also plotted for comparison. a) Dimensionless roughness height k^+ based on average canopy height and b) equivalent sand grain roughness height k^+_s. Lines and symbols represent: ■; flexible filaments λ = 2.6 ■; flexible filaments λ = 1.3, —; uniform sand exp. *Nikuradse (1950)*, ▷ sandpaper roughness exp. *Flack et al. (2007)*.

First, k^+_s is computed using Eq.(10) for each solidity parameter only at the highest Reynolds number to ensure that it's in the fully rough regime. The value of k_s is then obtained from: $k_s = k_s^+ \nu/u_{\tau,yvo}$. For the lower Reynolds numbers k_s^+ was calculated assuming that the equivalent roughness height k_s is universal for a specific coverage. This definition has been shown to collapse the function roughness results in the fully rough regime from different roughness shapes as shown in Fig.6b. The equivalent roughness height for the flexible canopy simulation is shown with red and green symbols. It ranges from 200 to 1000 placing it well within the fully rough regime. Agreement with other types of roughness is good suggesting that the equivalent roughness height can also be applied to flexible canopies. The ratio of the equivalent roughness height to the canopy height, k_s/k, is listed in Table I. The ratio ranges from 4.75 to 6.18 which is large.

The dynamics of the near-wall turbulent flow differ from what is observed over smooth walls. For the case of rigid canopies for example, the formation of coherent spanwise rollers has been reported, *Nepf (2012)*. These structures are the product of a Kelvin–Helmholtz (KH) instability caused by the discontinuity of the drag at the canopy tip. The KH instability triggers the formation of large spanwise-coherent rollers that develop at the canopy tip, and evolve into large, elongated structures in the streamwise direction. Today, in most cases these structures are identified either statistically by analyzing the spatial co-spectra of the velocity fluctuations, or by visualizing the velocity fluctuations, see for example *Monti et al. (2020), Jimenez et al. (2001)*.

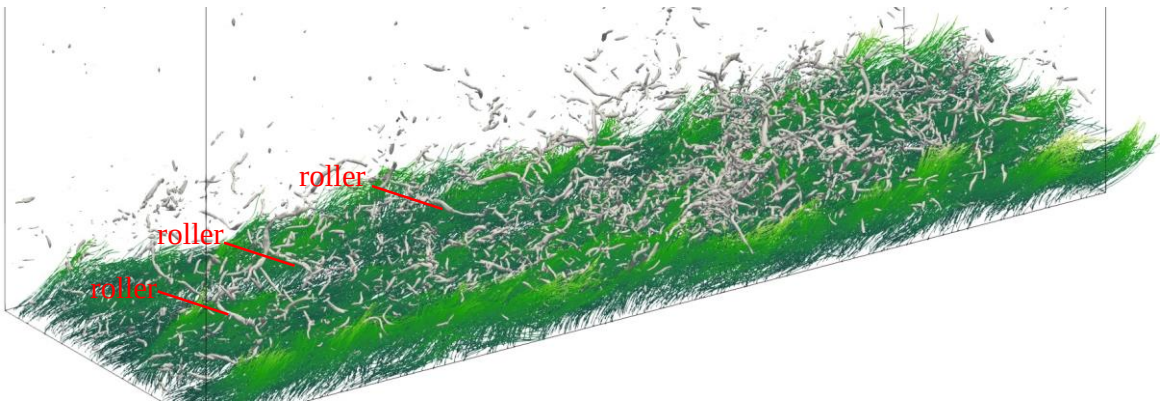

Fig.7: Flow visualization using the Q-criterion of the vortical structures in the flow. The flexible filaments are also shown at the bottom wall and they are colored by their vertical coordinate.

Fig.7 shows an instantaneous snapshot of the flow from the simulation at Re_b = 80,0000 and λ = 2.6. Here, we visualize the turbulent structures by plotting an iso-surface of the second invariant of the

velocity gradient tensor, or Q criterion. The flexible canopy is also shown for reference and colored by the vertical coordinate (darker green at the bottom and lighter green away from the wall). A lot of vortical structures are visible throughout the flow. Three spanwise rollers are clearly indicated by arrows in the figure. These rollers form at the local canopy tip. Their extend in the spanwise direction appears to be comparable to the filament length.

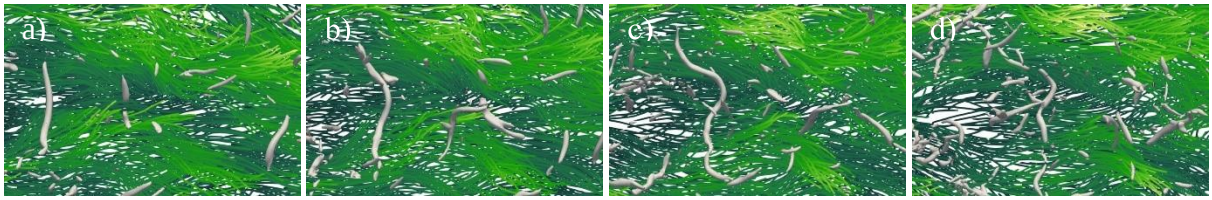

Fig.8: Flow visualization using the Q-criterion showing the evolution in time (at four different instances starting from left to right) of a spanwise roller formed at the canopy tip.

Other spanwise vortices are also visible above the canopy tip as well as a plethora of streamwise oriented vortical structures. An evolution of a spanwise roller is clearly traced in Figure 8. The roller is initially coherent in the spanwise direction. Due to the high shear different parts of the roller are advected at different speeds and the rollers starts to bend along the span until it resembles a horseshoe like vortex. The vortex quickly breaks down into smaller vortices.

References

CHUNG, D.; HUTCHINS, N.; SCHULTZ, M.P.; FLACK, K.A. (2021), *Predicting the drag of rough surfaces*, Annual Review of Fluid Mechanics 53, pp.439-471

DEHN, C., HOLM, E., CHANG, P., VARGAS, A., STORMS, S. (2017), *An approach for the scanning and construction of biofouled surfaces to be used for drag measurements*, 30th American Towing Tank Conf., West Bethesda, MD, pp.1-14

FLACK, K.A.; SCHULTZ, M.P.; CONNELLY, J.S. (2007), *Examination of a critical roughness height for outer layer similarity*, Physics of Fluids 19, pp.95-104

FOGGI ROTA, G.; MONTI, A.; OLIVIERI, S.; ROSTI, M.E. (2024), *Dynamics and fluid–structure interaction in turbulent flows within and above flexible canopies*, J. Fluid Mechanics 989, A11

HE, S.; LIU, H.; SHEN, L. (2022), *Simulation-based study of turbulent aquatic canopy flows with flexible stems*, J. Fluid Mechanics 947, A33

HUANG, W.X.; SHIN, S.J.; SUNG, H.J. (2007), *Simulation of flexible filaments in a uniform flow by the immersed boundary method*, J. Computational Physics 226, pp.2206-2228

JIMENEZ, J.; UHLMANN, M.; PINELLI, A.; KAWAHARA, G. (2001), *Turbulent shear flow over active and passive porous surfaces*, J. Fluid Mechanics 442, pp.89–117

KAMINARIS, I.K.; BALARAS, E.; SCHULTZ, M.P.; VOLINO, R.J. (2023), *Secondary flows in turbulent boundary layers developing over truncated cone surfaces*, J. Fluid Mechanics 961, A23

MOLINO, P.J.; WETHERBEE, R. (2008), *The biology of biofouling diatoms and their role in the development of microbial slimes*, Biofouling 24, pp.365–379

MONTI, A.; OMIDYEGANEH, M.; ECKHARDT, B.; PINELLI, A. (2020), *On the genesis of different regimes in canopy flows: a numerical investigation*, J. Fluid Mechanics 891, A9

MONTY, J.P.; DOGAN, E.; HANSON, R.; SCARDINO, A.J.; GANAPATHISUBRAMANI, B.;

HUTCHINS, N. (2016), *An assessment of the ship drag penalty arising from light calcareous tubeworm fouling*, Biofouling 32

MURPHY, E.A.; BARROS, J.M.; SCHULTZ, M.P.; FLACK, K.A.; STEPPE, C.N.; REIDENBACH, M.A. (2018), *Roughness effects of diatomaceous slime fouling on turbulent boundary layer hydrodynamics*, Biofouling 34, pp.976–988

NEPF, H.M. (2012), *Flow and transport in regions with aquatic vegetation*, Annual Review of Fluid Mechanics 44, pp.123-142

NIKURADSE, J. (1950), *Laws of flow in rough pipes*, NACA-TM-1292

RAUPACH, M.R.; THOM, A.S. (1981), Turbulence in and above plant canopies, Annual Review of Fluid Mechanics 13

ROSTI, M.E.; BRANDT, L.; PINELLI, A. (2018), *Turbulent channel flow over an anisotropic porous wall - drag increase and reduction*, J. Fluid Mech. 842

SARAKINOS, S.; BUSSE, A. (2019), *An algorithm for the generation of biofouled surfaces for applications in marine hydrodynamics*, Recent Advances in CFD for Wind and Tidal Offshore Turbines, pp.61-71

SCHMID, C.F.; SWITZER, L.H.; KLINGENBERG, D.J. (2000), *Simulations of fiber flocculation: Effects of fiber properties and interfiber friction*, J. Rheology 44, pp.781-809

SCHULTZ, M.P. (2005), *Frictional Resistance of Antifouling Coating Systems*, J. Fluids Eng. 126, pp.1039-1047

SCHULTZ, M.P. (2007), *Effects of coating roughness and biofouling on ship resistance and powering*, Biofouling 23, pp.331–341

Lidar Application on board for Improved Wind Measurement

Jan Wienke, DNV, Hamburg/Germany, jan.wienke@dnv.com
Jakob Eisenhart Rothe, DNV, Hamburg/Germany, jakob.von.rothe@dnv.com

Abstract

Wind measurement on board of ships is typically performed by cup anemometers. For higher accuracy, the application of lidar systems is proposed. The first application has already been made for performance measurement on board of ships with wind assisted propulsion systems (WAPS). In the future, there will be an increasing number of WAPS installations and thus a strong demand for performance verification. This verification will be based both on short-term sea trials and on mid-term performance monitoring during in-service operation. The application of lidar systems will be essential for obtaining reliable results from such measuring campaigns. With long-term experience in the application of lidar systems in the offshore wind industry, DNV is ready to assess and verify and to plan and perform such measuring campaigns.

1. Introduction

A new revision of the ISO guideline 15016 on speed/power trials was published at the beginning of February 2025. To improve the reliability of the results, the various corrections due to environmental conditions were reassessed. Wind correction can be improved by imposing stricter limits on the maximum acceptable wind speed or by improved sensors. Ultimately, a combination of these measures was agreed upon: with better sensors, higher wind speeds are acceptable. This means that the fixed installed cup anemometer can still be used for the speed/power trials, but ultrasonic sensors or lidar systems are recommended by the guideline and offer operational advantages.

2. Uncertainty from wind speed measurement

For performance measurements, the measured wind speed is applied for correction of the measured shaft power regarding the additional wind resistance. This is part of the corrections due to environmental conditions which include in addition to the true wind the wind waves, swell, current and water temperature and density. The size of the different corrections depends on the actual environmental and ship conditions. For example, for very large container ships during newbuilding sea trials, the wind resistance is usually the dominant correction due to the high deckhouse.

Currently, wind measurement on-board of ships is performed with cup anemometers. A fixed installed sensor is usually mounted on top of the light mast on the deckhouse. Simply changing the anemometer type will not be sufficient to improve the accuracy. The measuring location is of importance, the applied wind profile over the height and the wind coefficients to calculate the force from the measured wind speed affect the results as well. It should be kept in mind that the force is proportional to the square of the wind speed and therefore sensitive to the measured values.

The application of lidar systems offers several advantages with a remote measurement of undisturbed wind at different levels. Nevertheless, for newbuilding sea trials following the ISO standard, the best accuracy will be achieved for trials in low wind conditions. The same applies to performance monitoring during a ship's operation: the best accuracy can be achieved by filtering the data and removing measured data for higher wind speeds.

Therefore, lidar application will remain an exception for these ISO newbuilding sea trials. In addition to the improved accuracy of the sea trial results themselves, another point should be considered. The application of a lidar during sea trials offers the option to calibrate the fixed installed cup anemometer, thereby improving accuracy during in-service performance monitoring. Eventually, the available data need to be extended by numerical calculations to cover a sufficient range of different

wind speed and direction. This option of anemometer re-calibration during sea trials is only relevant for ships that do not distinctly change their shape depending on the loading condition. For example, container ships experience significantly different disturbances in the airflow at the anemometer position when there are no containers in front of the deckhouse.

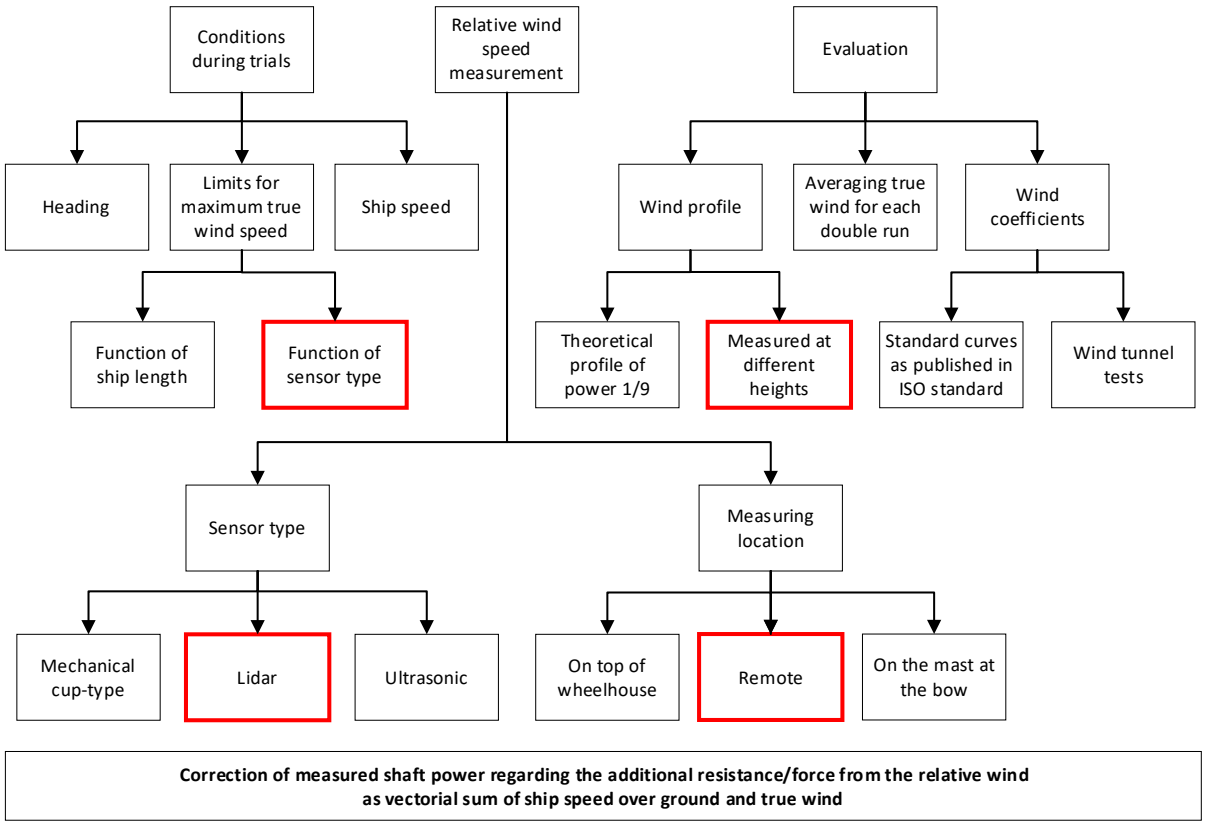

Fig.1: Factors influencing the accuracy of the wind correction for speed trials

Although performing measurements during calm wind conditions is the preferred approach, this is not always possible or even desired. The increasing popularity of WAPS installations raises the demand for performance measurements at true wind speeds of 15 knots and more. And in this case the accuracy is twice as important because the wind force is not only used to correct the measured propulsion power is also the relevant input for the thrust of the WAPS.

The ITTC sea trials procedure for assessing the power savings from wind assisted propulsion highly recommends the application of lidar systems. DNV believes that such short-term verification of WAPS performance requires lidar wind measurement. A short-term measurement provides only limited insight into the actual savings during operation; therefore, a monitoring system should provide further data during operation. If the application of lidar is not possible for monitoring during operation, calibrating the fixed installed wind sensor by the lidar measurements during sea trials, combined with numerical calculations, can potentially improve the accuracy and applicability of the in-service measured data.

3. Lidar systems

Lidar (**Li**ght **d**etection **a**nd **r**anging) is becoming a buzzword, representing very accurate wind speed measurement. However, not every system is suitable for on-board application, and some systems already provide useful features for the installation on board. To allow for comparison of different available lidar systems, the working principle of these measuring devices is explained below in condensed form, along with an overview of their application in the wind energy industry.

Lidar systems for wind speed measurements usually apply infrared lasers, namely in the near infrared spectrum between 780 nm and 3000 nm (corresponds to 3.85 to $1 \cdot 10^{14}$ Hz). The range above 1350 nm is not visible to the human eye, but the near infrared range can be detected by electronic image converters.

The laser beam is emitted into the atmosphere, where it is scattered by particles in the air. A portion of the photons is backscattered and received by the detector, a spectroscope that allows for frequency analysis. The frequency shift between emitted and backscattered signal is due to the Doppler shift, enabling the determination of the speed of the scattering aerosols along the beam direction (often called LOS, the line of sight) from the frequency shift.

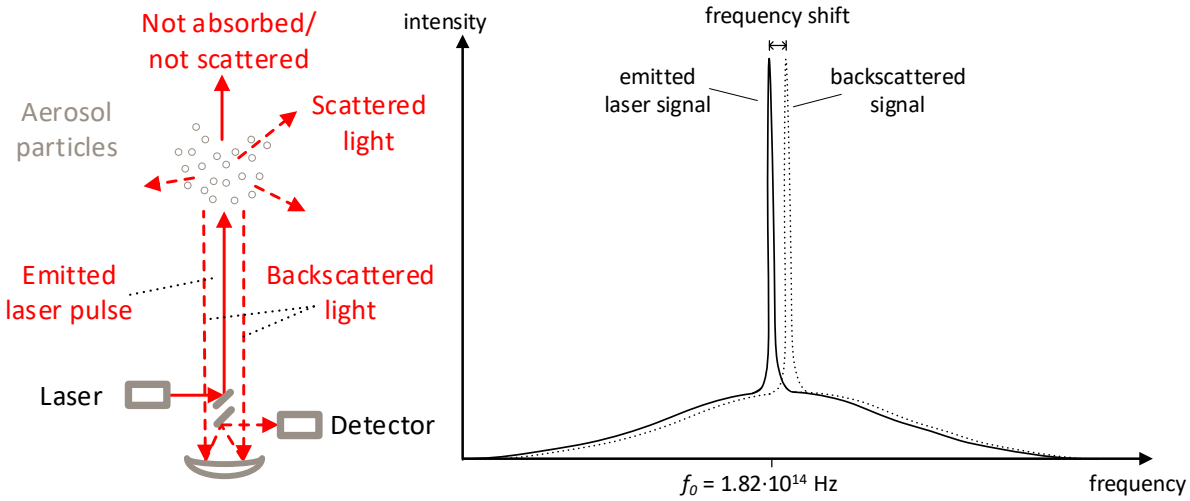

Fig.2: Lidar set-up and detected signal

To identify the velocity of the wind, at least three one-dimensional measurements in different directions are needed. In practice, this can be achieved using a single laser with different inclination angles. Two different methods are usually applied: swinging or rotating the laser.

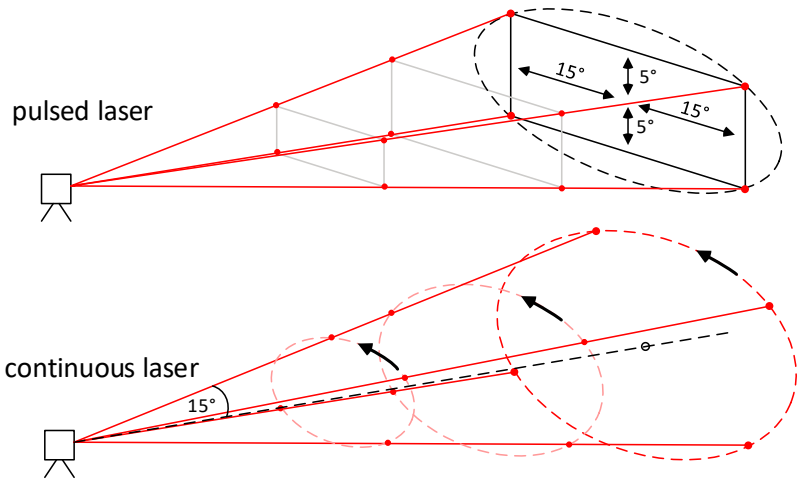

Fig.3: Doppler beam swinging and velocity azimuth display wind field reconstruction

The Doppler beam swinging (DBS) technique uses a pulsed laser. The beam is directed in 4 different directions, typically ±15° in horizontal direction and ±5° vertically relative to the centre. A plane is spanned by the four beams, and assuming that the wind velocity is equal within this area, the three components of the wind velocity can be determined. The distance of the plane from the laser is defined by the runtime of the backscattered signal, allowing for the investigating of different planes with the same beam by distinguishing between different runtimes.

However, a continuous laser is applied for the velocity azimuth display (VAD) method. With an arrangement of prisms and mirrors, the laser beam rotates around the centre line at a constant angle, creating a conical trajectory. Different measurement heights are scanned consecutively by changing the focus of the laser beam.

The orientation of the laser can either be horizontal or vertical. In the wind industry, vertically arranged lidar systems are widely applied. On one hand, these lidar systems are used for wind resource assessment, meaning the pre-construction evaluation of a location's potential. On the other hand, the vertical orientation allows for the identification of wind profiles along the height with measurements at different levels. Lidar systems for the vertical orientation are usually ground based.

Fig.4a: Vaisala WindCube
(ground based 4-beam pulsed DBS lidar)

Fig.4b: ZXTM
(ground based continuous-wave VAD lidar)

An alternative arrangement is nacelle mounted lidar systems. These devices are horizontally aligned and are mounted on the top of the nacelle of a wind turbine. The lidar is oriented ahead to measure the inflow of the turbine at multiple distances. The extremely short-term shadowing of the fast-passing blades can be neglected. These lidar arrangements are used for power performance tests (PPT) during the commissioning and operation of wind turbines. The lidar signal can even be used as input for the wind turbine's control system. Measuring at different distances from the wind turbines allows for the determination of the induction zone, the distance within which the wind field is already affected by the wind turbine. A typical value for the minimum distance for an undisturbed wind field is 2.5 times the diameter of the wind turbine's rotor.

Fig.5a: Vaisala WindCube Nacelle
(4-beam pulsed DBS type nacelle lidar)

Fig.5b: ZXTM
(continuous-wave VAD type nacelle lidar)

4. Measuring campaign preparation

Calibration of the lidar is needed to ensure the lidar unit´s functionality and to quantify the measurement uncertainty. The standard reference instrument for calibrating lidars is the cup anemometer. This type of anemometer provides high accuracy as a calibration reference since the cup

anemometers are calibrated in a wind tunnel under controlled conditions before installation in the field on a test mast. A re-calibration of the cup anemometers in the wind tunnel is carried out every two years.

The calibration process of nacelle lidars follows IEC 61400-50-3. It combines a laboratory and a field test. In the laboratory, the scan geometry of the nacelle lidar is verified. The angle between the original and the actual laser beam orientation is measured with an integrated inclinometer. The accuracy of this measurement is verified by geometric verification of the angle in the laboratory. Several tilt and roll angles are investigated for this verification.

The field test involves comparing the wind speed measured by the lidar with the values from the cup anemometer. The cup anemometers are installed on two test masts and measure in horizontal direction. The lidars are mounted on a lattice mast at a height of 25 or 30 metres and are oriented so that two laser beams are in the horizontal plane, with each beam pointed close to a reference cup anemometer.

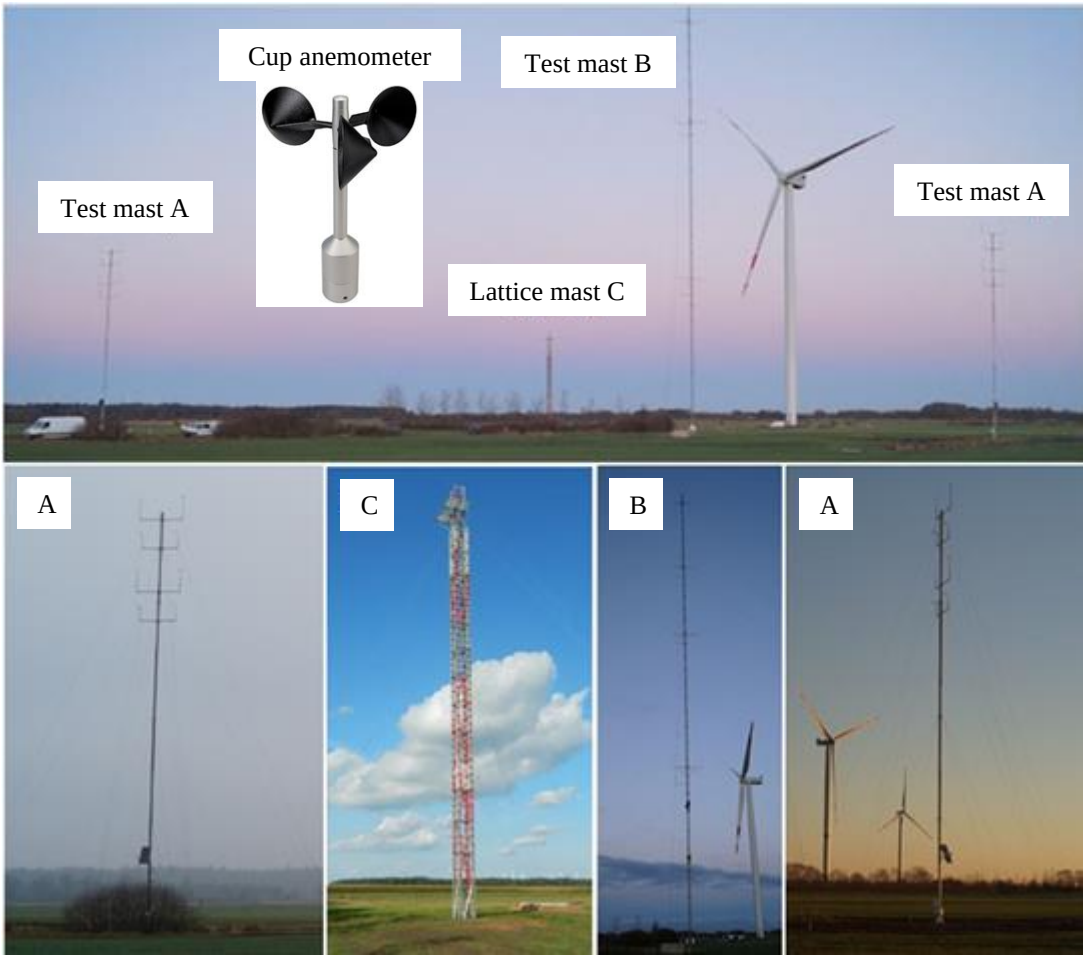

Test mast A: Reference masts with cup anemometers for nacelle lidar calibration with height of 30 m
Test mast B: Reference mast for calibration of ground based lidars with height of 100m
Lattice mast C: Lattice mast for mounting of nacelle lidars with height of 30 m

Fig.6: DNV lidar test site for calibration in Northern Germany

The IEC standard requires a set of data in the range from 4 to 12 m/s with 0.5 m/s intervals. For each interval, a minimum of five valid 10 minutes averages must be sampled to complete the calibration. The duration of a campaign depends on the wind conditions at the test site and usually takes between 6 weeks and 6 months. A new calibration is carried out prior to each measuring campaign or every 2 years. The performance of the lidar calibration is a DAkkS accredited service offered by DNV.

5. Challenges for measuring campaigns on board of ships

The first difference compared to onshore measurements is the restricted space on board. This makes it very difficult to install cup anemometers with sufficient distance from any structure for undisturbed wind flow at the measuring location. Additionally, long pivot arms are subject to engine or propeller induced vibration on board, which restricts the options for a suitable arrangement.

The IEC standard provides detailed mounting guidelines for measurement instruments. For example, a cup anemometer on a lattice mast with a cross section of 0.6 m should be mounted in a distance of 2.55 m. However, even at this distance, there is still a significant range of wind directions that is disturbed by the mast.

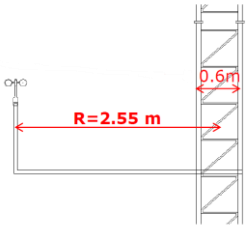

Fig.7: Required lever arm length for a side mounted anemometer according to IEC standard

The consequence from the restricted space is the recommendation for a remote measurement of the undisturbed wind field, meaning the application of lidar for accurate and reliable wind speed measurement.

Another difference compared to onshore measurements is the movement of the ship. The speed along the course can easily be corrected (speed over ground is relevant in this regard and not speed through water) but rolling and pitching of the ship needs additional measurements of the inclination. Data from the inclinometer of the lidar can be applied for this correction.

It is notable that lidar systems are even installed on buoys. In this case vertical arrangement of the laser beam is applied for offshore wind resource assessment. Correction of the buoy movement is essential for this application.

Fig.8: Floating lidar

Another challenge is the data transfer. In case of in-service monitoring application of lidar, it is possible to continuously send the 10 minutes wind speed average values to shore only and to download the detailed high frequency data later in port.

6. Measuring campaign outline

Although for shipping there are no obligatory guidelines in place for power performance tests to assess WAPS, it makes sense to borrow guidance from the on- and offshore wind industry. Lidar is a standard tool in this branch.

Nacelle lidar systems are particularly suitable for on-board application. Planning trials for the verification of WAPS performance, it must be distinguished between short-term sea trials and in-service performance tests. The attended sea trials allow for immediate assessment of relevance and accuracy of the measured values and for first estimation of actual WAPS performance. Unattended in-service tests offer more flexibility regarding the variable wind conditions. A combination of short-term trials and mid-term monitoring promises the most robust results.

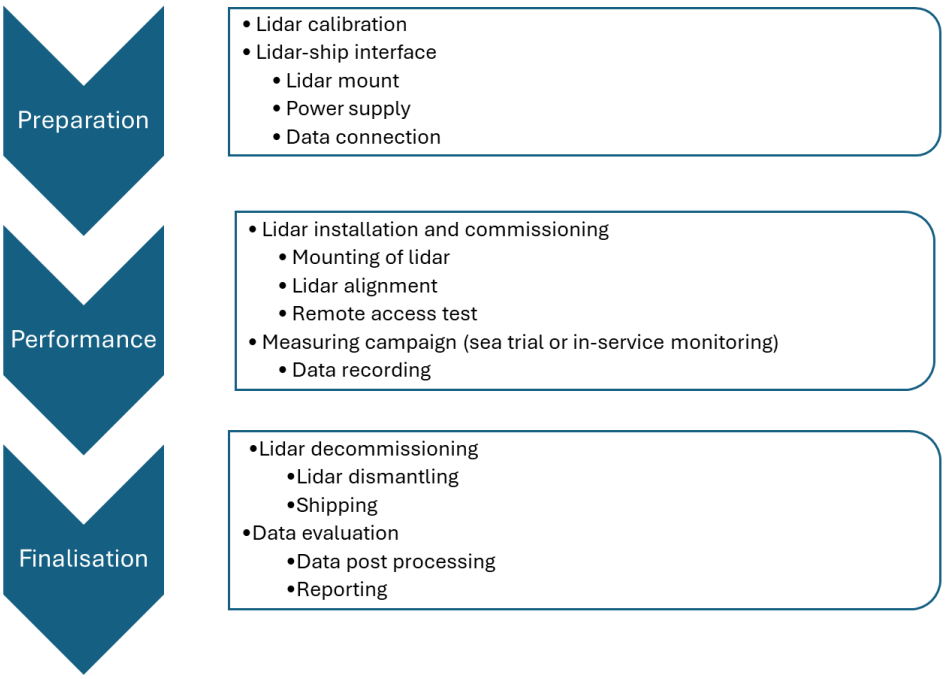

Fig.9: On-board lidar measuring campaign procedure

During performance trials, a detailed recording of the environmental and ship conditions is required. This includes wave and swell height and direction measurements, water temperature and density, air temperature and pressure and drafts, trim and heel of the ship. The new revision of the ISO 15016 proposes the application of a wave buoy when the ship is stopped before and after the test runs.

DNV provides a Vaisala WindCube Nacelle lidar for the wind velocity measurement. This is a four-beam pulsed DBS system. The lower beam pair is aligned in horizontal direction for the even keel condition of the ship. This arrangement allows for the measurement of wind speed and direction at 12 different distances between 40 and 700 m, enabling for all ship sizes wind speed measurement in front of the bow in an undisturbed wind field. In this configuration, the upper beam pair is inclined by 10° and allows for identification of the wind profile.

Regarding the wind speed, the relevant ship speed is the speed over ground as measured by DGPS. For the performance assessment and the power savings by WAPS, the ship speed refers to the speed through water. The difference between both speed values is the current. For sea trial measurements following ISO 15016, the identification of the current can be realized by a series of double runs with reciprocal heading. For sea trials with WAPS, a variation of the heading is required to investigate different relative wind speed and angles. Therefore, a combination of current identification from double runs and comparison with speed log data is proposed for WAPS performance trials.
During in-service operation, performing double runs is not practical, and an assessment of the current must be based on the DGPS speed and the speed measured by the speed log. For WAPS that can be deactivated in short time (rotor sails or suction sails), the WAPS performance can be assessed by comparing subsequent intervals with active and passive sail. If the time between the two measuring intervals is short, the variable current might be negligible.

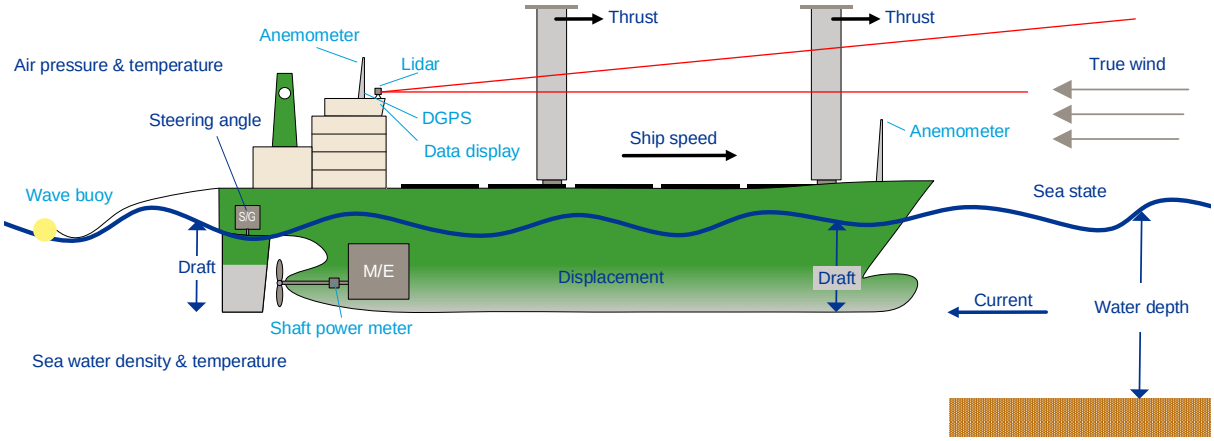

Fig.10: Measuring set-up for WAPS performance verification sea trials

7. Conclusion

The application of lidar on board of ships with wind assisted propulsion is required for best accuracy in WAPS performance verification. DNV has combined experience and capacity from the shipping and wind industry to support our customers in this verification task, starting from calibration of lidars to the performance and evaluation of on-board measurement campaigns.

DNV's common approach is to apply a nacelle lidar for on-board measurements which allows for precise measurement of horizontal wind speed and direction around and ahead of the ship, independent of relative wind direction. Additionally, the wind profile is measured at the same time.

Up to now, there are no binding guidelines in force for the WAPS performance verification. From regulatory perspective, the focus on actual reduced fuel consumption is sufficient. The fuel saving is a direct consequence from the WAPS application but is determined by averaging over some time and different conditions. For a direct assignment of wind conditions to the resulting thrust from the WAPS, a more detailed investigation is required. Procedures for these investigations, such as calibration requirements, can be based on existing guidelines in the wind industry.

References

ISO 15016:2025 (2025), *Ships and marine technology – Specifications for the assessment of speed and power performance by analysis of speed trial data*

ITTC 7.5-04-01-02 (2024), *Sea trials for assessing the power saving from wind assisted propulsion*

IEC 61400-50-3:2022 (2022), *Wind energy generation systems – Use of nacelle-mounted lidars for wind measurements*

IEC 61400-12-1:2017 (2017), *Wind energy generation systems – Power performance measurements of electricity producing wind turbines*

WEITKAMP, C. (2005), *Lidar – Range-resolved optical remote sensing of the atmosphere*, Springer, New York

Ship Sensor vs Weather Provider Environmental Data – A Comparative Study

Margarita Pournaraki, Prisma Electronics, Athens/Greece, m.pournaraki@prismael.com
Athanasios Sampos, Prisma Electronics, Athens/Greece, a.sampos@prismael.com
Stefanos Chartomatzidis, Prisma Electronics, Athens, Greece, schartom@prismael.com
Christos Giordamlis, Prisma Electronics, Athens/Greece, christos@prismael.com

Abstract

A high-frequency data collection system is able to monitor continuously and accurately the performance of the vessel where it is installed. The Weather Station of the vessel is the source of real but relative measurements for weather condition. Weather data may also be acquired from external weather providers using the vessel coordinates to position the vessel on the weather model grid and calculate the corresponding weather forecast parameter values. In this paper a comparative study of vessel's sensor measurements vs data from an external weather provider is presented. Furthermore, the effect of the differences between the different data sources and their impact on performance analysis (ie KPI calculated values) is examined and quantified.

1. Introduction

The performance of a ship underway is significantly influenced by its operating environment, including wind, sea currents, and waves. Accurate and timely environmental data are crucial for calculating and analysing important key performance indicators (KPIs) such as power deviation, engine load margin etc, enabling effective vessel monitoring and performance assessment. Weather data can be collected through crew visual observations , ship sensors (like an anemometer) for measuring wind, or weather providers that extract the parameters from the global weather grid using the ship position coordinates and related time as input. The later, when they correspond to a present time forecasting, are referred as nowcast data. In principle, these methods are not comparable due the following facts:

- Weather is changing per time and location, and the crew observe the weather on a given time and position, which may not be efficient for calculations,
- Sensors are measuring continuously but all measurements are related to their proper positioning and to ship's speed and heading.
- Weather forecasts used may have uncertainty especially when weather is changing.

This study compares wind measurement data obtained from the shipboard sensor with wind nowcast data provided by a weather provider. The research aims to assess the accuracy of wind nowcast data and explore the impact of such data on ship performance KPIs. A real case study will be presented to demonstrate how weather resolution can influence the calculation of a specific KPI.

To facilitate this analysis, the study leverages the LAROS™ High Frequency Data Collection System by Prisma Electronics, which enables high-frequency data acquisition from various systems, instruments and sensors, like the shipboard anemometer. In addition, LAROS advanced APIs allow automated synchronization with weather provider data in parallel with the vessels' anemometer. The powerful analytical and visualization capabilities of LAROS™ Data Analysis Software (DAS) are utilized for in-depth data exploration.

2. Anemometer vs Nowcast Data

Accurate measurement of wind speed and direction on a moving ship presents unique challenges. Shipborne anemometers, while crucial for various applications, are subject to two primary sources of error: The accuracy of the sensor itself and the distortion of the wind flow around the ship body.

Reliable Data from the anemometer itself is a complicated task. Modern sensors typically have accuracy smaller than 2% at wind speeds of approximately 10 m/s. However, this accuracy must be maintained through regular calibration and proper maintenance to ensure reliable measurement when the weather is normal.

Ship's superstructure significantly distorts the airflow around the vessel. This distortion, particularly pronounced around the bridge where anemometers are commonly mounted, leads to inaccurate wind speed readings. Studies like those conducted by *Moat et al. (2005),* utilizing Computational Fluid Dynamics (CFD) simulations and generic ship models (tankers, bulkers), have shown significant discrepancies between free-stream wind speeds and the actual wind speeds experienced by the anemometer due to the ship's structure.

These studies provide valuable insights into the magnitude and nature of this airflow distortion and some of the results are appeared at Fig.1 and Fig.2. As the anemometers measure the wind flow at the point they are positioned above the bridge, their measurements correspond to the modified air stream, which introduces this bias. The distortion of wind speed measurements directly affects the accuracy of true wind calculations.

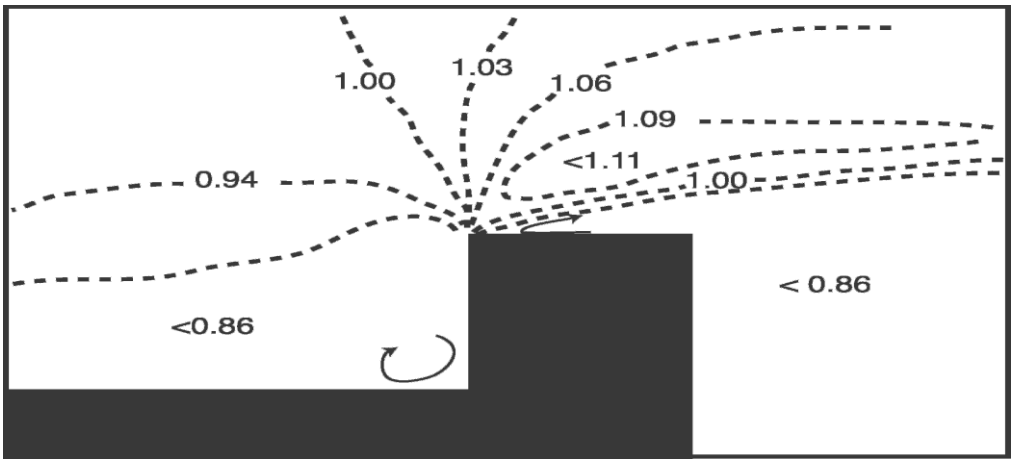

Fig.1: The normalized wind speed along the centerline of the generic ship for a bow-on flow (from left to right). The contours indicate the normalized wind speed (i.e., the measured wind speed as a fraction of the free-stream wind speed). The arrows indicate regions of recirculation *Moat et al. (2005)*

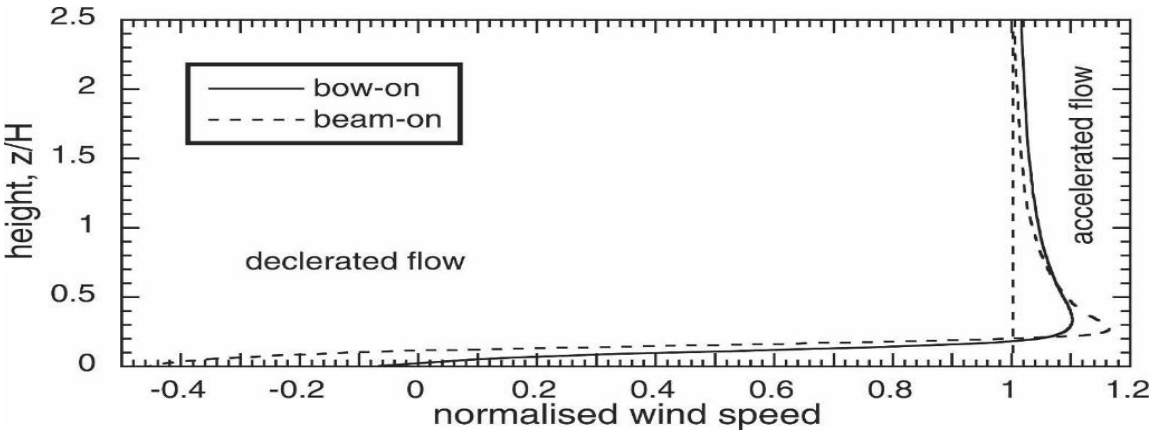

Fig.2: Vertical profiles of normalized wind speed at a distance of x/H 0.3 from the upwind leading edge (located at x 0 z). The heights have been normalized by the step height, H. For beam-on flows, H is the bridge-to-waterline height and for bow-on flows, H is the bridge-to-deck height. A negative normalized wind speed indicates flow reversal. The vertical dashed line indicates the region where the wind speed is equal to the free-stream wind speed *Moat et al. (2005)*.

Weather providers typically deliver nowcast data for marine environments, which encompass a range of environmental parameters beyond just wind speed and direction. These parameters often include:

- Wind: Speed and direction
- Sea Currents: Speed and direction
- Waves: Height, period, and direction
- Swell: Height, period, and direction
- Air Pressure: Atmospheric pressure
- Seawater Depth: Bathymetry information
- Temperature: Air and seawater temperature
- Salinity: Seawater salinity

To provide relevant data for a specific vessel, weather providers utilize the vessel's coordinates (latitude and longitude) at specific timestamp to pinpoint its position within the weather model grid. Weather models generate data on a grid, with each grid point representing a specific location and time. To determine the weather parameters at the vessel's exact location, sophisticated interpolation techniques are applied. These techniques utilize the data from surrounding grid points to estimate the values at the vessel's position. Some indicative factors that affect the accuracy of the data are:

- The accuracy of the data that feed the model (ie effect of the distance of the closest meteorological station or Buoy from the ship's location or the validity of the Voluntary Observing Ship reports).
- The accuracy of the model itself.
- The interpolation or extrapolation techniques for distance and time.

Haranen et al. (2017) demonstrated a strong correlation between wind speed and direction data obtained from nowcast providers and those data measured by onboard ship sensors (anemometers). This correlation seems to provide a valuable tool for data quality assessment but not all the times. Significant deviations from the expected correlation can indicate potential issues with the ship's anemometer, such as calibration errors, sensor malfunctions, or interference from the ship's superstructure or, weather model's inaccuracy at vessel's location. When onboard sensor data is deemed reliable (i.e., exhibiting a strong correlation with crew observations and nowcast data), it should be prioritized for performance analysis due to their higher accuracy and the fact that are real. In cases where onboard sensor data are unreliable or unavailable then, nowcast data can provide a suitable alternative for performance analysis, offering relatively accurate wind information for the vessel's location.

3. Data Selection and Acquisition

3.1. Onboard Data Selection

For this study, the following data were collected from the vessel:

- Speed Over Ground (SOG): The vessel's speed relative to the ground.
- Speed Through Water (STW): The vessel's speed relative to the water.
- Relative Wind Speed and Direction: Measured by the onboard anemometer.
- Heading: The vessel's heading at each data point.
- Static Drafts (Fore & Aft): Used to determine the anemometer height above sea level.
- Propeller Shaft revolutions (RPM).
- Propeller Shaft Power.
- Main Engine Fuel Oil Consumption.

True wind speed and direction were calculated using the formulas outlined in ISO 19030-2 Annex E, which account for the vessel's speed and heading. The recorded drafts were utilized to calculate the

anemometer's height above sea level. This information was then used to apply the velocity profile formula specified in ISO 19030-2 Annex E to adjust the measured wind speed to a standard height of 10 meters above sea level. The analysis encompasses a four-month period, spanning from July 1, 2024, to November 1, 2024.

3.2. Data Acquisition

All data were collected using the LAROS™ system, an advanced Holistic High-Frequency Data Acquisition System developed by Prisma Electronics. LAROS™ provides an independent and transparent approach to signal processing and data gathering, enabling the connection of wireless/wired smart collectors to various sensors, SCADA systems, instruments and equipment across the vessel, in order to have structured, synchronized and on sensor's edge related data. The system collects and processes signals for their quality on the spot (implementing edge computing) from multiple points/sensors; then it creates the related datasets in a synchronized manner. All collected data are finally transmitted to a central server for storage and further processing. Collected data are transmitted to the vessel's headquarters in real-time for further analysis and data driven decision support. Fig.3 shows the LAROS$^{TM©}$ system's architecture.

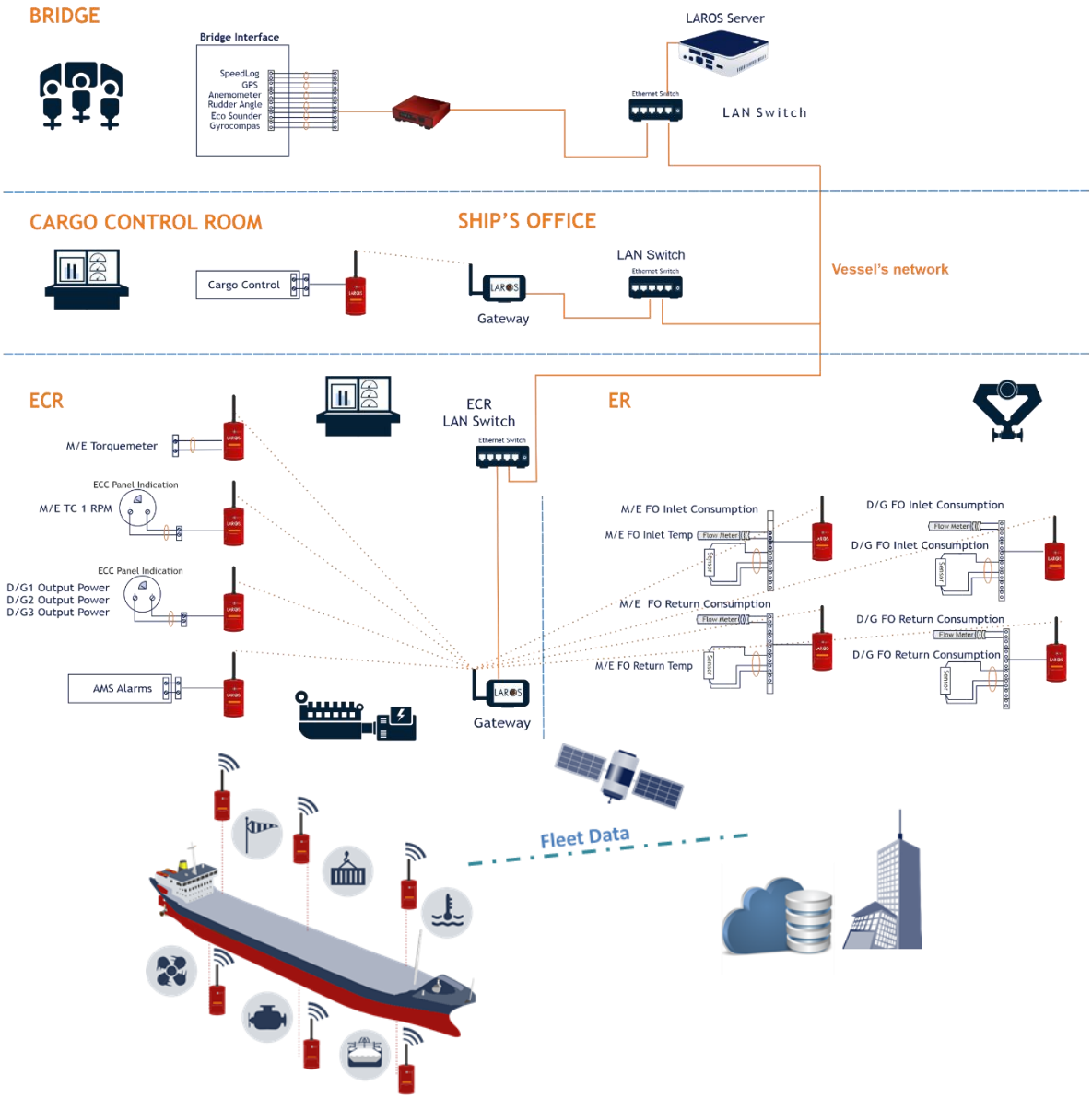

Fig.3: Graphical representation of LAROS$^{TM©}$ system

The system can collect data with a high temporal resolution like per 15 seconds or minute, potentially as frequently as every three seconds or sensors' ability. The accuracy of the collected data is dependent on the accuracy of each individual sensor or equipment that provides the specific measurement but in principal, this is becoming a matter of smaller importance when data from those sensors are used as related time series.

LAROS™ system was integrated with a weather provider to receive nowcast data. The specific provider delivers meteorological and oceanographic data for specific vessel positions, including near-past analysis and forecasts up to 168 hours ahead. For atmospheric parameters, the provider utilizes the NCEP Global Forecast System with a 0.50° resolution. The model is updated every six hours (00:00 UTC, 06:00 UTC, 12:00 UTC, 18:00 UTC). Wind speed at 10 meters (WPWS) and wind direction (WPWD) were retrieved from the nowcast data at an hourly basis using the vessel's coordinates and timestamp as input. The retrieved nowcast data were synchronized with the ship sensor recordings within the LAROS™ system.

3.3. Vessels Selections

Table I summarizes the key characteristics of the twelve bulker vessels included in the analysis. To enhance the reliability of the onboard sensor measurements, the selection process prioritized newer vessels. Furthermore, the analysis focuses on three distinct vessel types, with comparisons drawn among sister vessels within each type. The ratio of the anemometer height above the bridge to the height of the accommodation structure is included. This parameter is used for elaborating further on the potential impact of the airflow distortion on the anemometer readings. Same cell color represents sister vessel.

Table I: Selected vessels summary data

A/A	Type	DWT	Built (year)	z/H
1	Ultramax	63500	2021	0.86
2	Ultramax	63500	2022	0.86
3	Ultramax	61200	2022	0.78
4	Ultramax	61200	2022	0.78
5	Ultramax	61200	2023	0.78
6	Ultramax	61200	2023	0.78
7	Kamsarmax	82000	2023	0.57
8	Kamsarmax	82000	2023	0.57
9	Kamsarmax	82000	2022	0.57
10	Kamsarmax	82000	2023	0.57
11	Kamsarmax	82000	2024	0.57
12	Kamsarmax	82000	2023	0.57

4. Data Analysis

Data analysis and KPI calculations were performed using the LAROS™ Data Analytics (DAS) software, a powerful application developed by Prisma Electronics. DAS offers a user-friendly interface for analyzing and visualizing large volumes of data. Its advanced capabilities extend beyond basic algebraic calculations, enabling the creation and calculation of new data parameters using Boolean conditions and time-based functions. The parameters that were calculated using the received data are:

- **True Wind Speed (TWS) and Direction (TWD**): Calculated using the vessel's speed, heading, and relative wind data.
- **Wind Speed Difference (ΔWS)**: The difference between the true wind speed measured by the ship's anemometer (TWS) and the wind speed provided by the weather provider (WPWS).
- **Wind Speed Ratio (WSR):** The ratio of the true wind speed measured by the ship's anemometer to the wind speed provided by the weather provider (TWS/WPWS).

- **Root Mean Square Error (RMSE) of Wind Speed:** Calculated as the square root of the mean squared difference between TWS and WPWS.
- **Power Deviation:** The deviation between the actual measured shaft power and the theoretical shaft power predicted based on sea trial data for the same vessel speed, expressed as a percentage.
- **Engine Load Margin:** The percentage of available engine load capacity to overcome additional resistance encountered during operation.
- **Fuel Consumption per Nautical Mile:** The amount of fuel consumed by the main engine per nautical mile of advance, expressed in Kilograms per nautical mile (Kg/nm).
- **Propulsion Efficiency:** The nautical miles travelled per kilowatt-hour of energy produced by the main engine (nm/kWh).

4.1 True wind speed vs Wind Speed from Weather Provider

The relationship between TWS derived from the anemometer measurements and WPWS was investigated at two resolutions of 1-minute and 1-hour. The 1 min resolution utilized all recorded and calculated data, capturing the high-frequency variations in anemometer measurements. The 1-hour resolution involved calculating hourly averages of both TWS and WPWS. Due to the hourly update frequency of the weather provider data, WPWS remained constant within each hour, while TWS exhibited continuous fluctuations based on anemometer measurements. This resulted in a less clear correlation between the two datasets at the 1-minute resolution, as depicted in Fig.4. By averaging data over one-hour intervals, the impact of high-frequency fluctuations in TWS was mitigated. This resulted in a more consistent and comparable dataset, leading to a stronger correlation between hourly averaged TWS and WPWS, which, although it is statistically correct, in represents a degradation of the true weather condition information in order to adapt to the low WP data resolution.

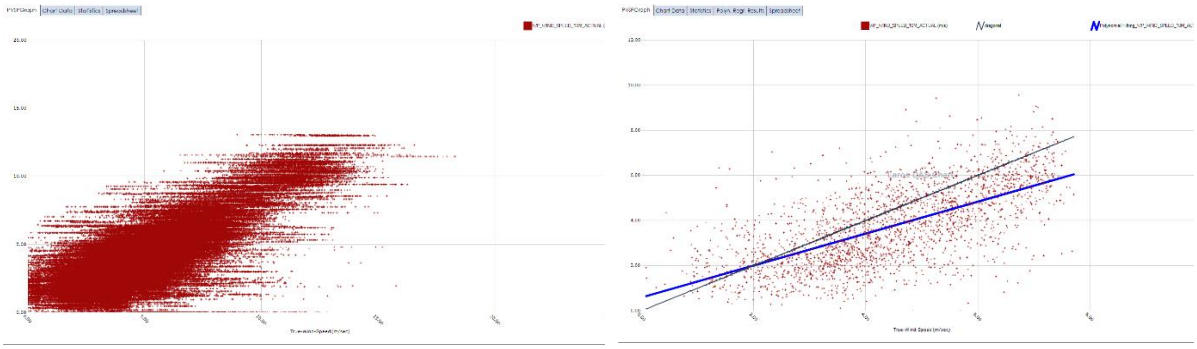

Fig.4: TWS vs WPWS with 1min and 1 hr resolution

Table II: Pearson's correlation coefficient of anemometer true wind speed vs WP wind speed.

A/A	Vessels	Corr. Coef. 1 min resolution	Corr. Coef. 1 hr resolution
1	Vessel 1	-0.41	0.60
2	Vessel 2	0.27	0.82
3	Vessel 3	0.08	0.92
4	Vessel 4	0.23	0.80
5	Vessel 5	0.18	0.91
6	Vessel 6	0.06	0.80
7	Vessel 7	0.20	0.82
8	Vessel 8	0.02	0.85
9	Vessel 9	0.31	0.83
10	Vessel 10	0.03	0.71
11	Vessel 11	0.06	0.78
12	Vessel 12	0.13	0.77

Table II demonstrates this effect, indicating that the Pearson correlation coefficient, a measure of the linear relationship between two variables, was more meaningful when calculated using the hourly averaged data. The high-frequency fluctuations in TWS at the 1-minute resolution obscured the underlying correlation between the two wind speed measurements. On the other hand, the 1 hour resolution cannot represent the vessels true weather condition, as it changes within the 1-hour period, which may degrade the accuracy of the performance evaluation.

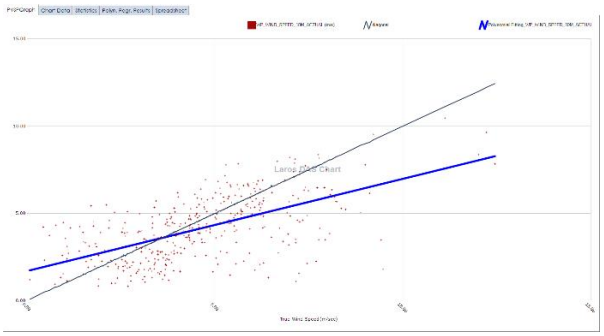

Vessel 1

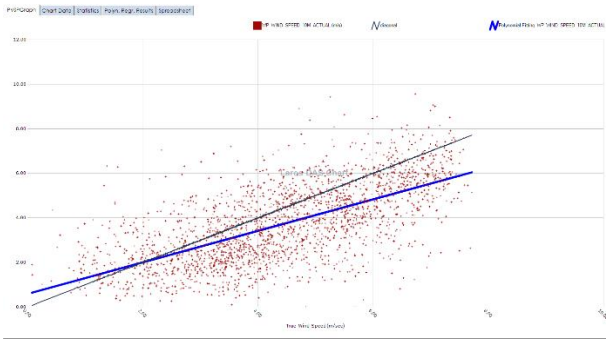

Vessel 2

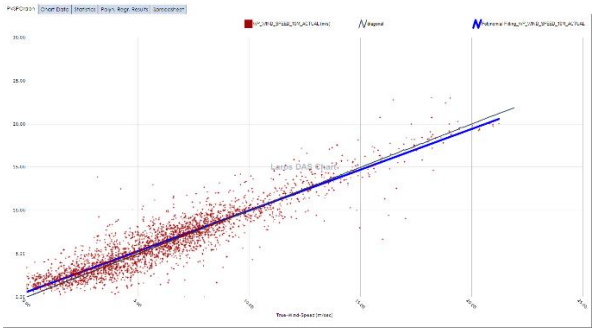

Vessel 3

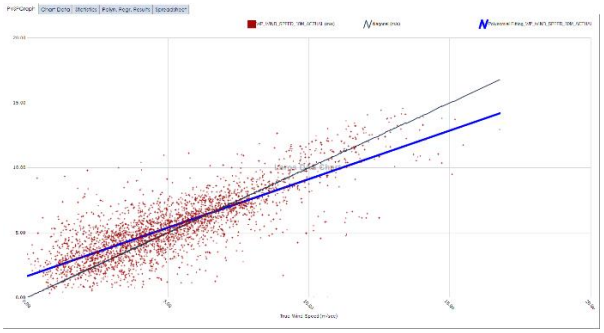

Vessel 4

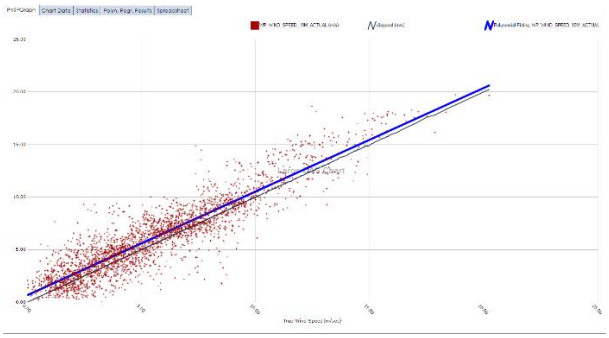

Vessel 5

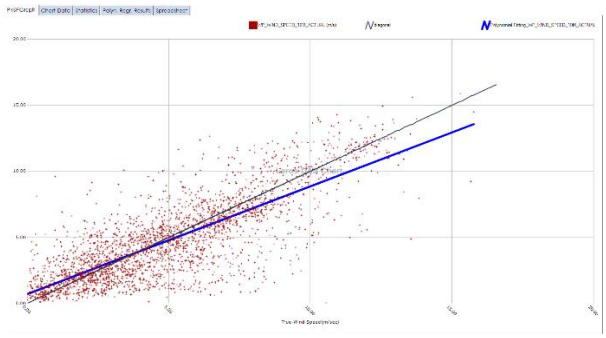

Vessel 6

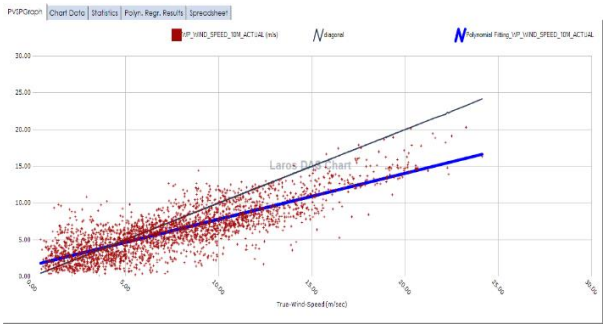

Vessel 7

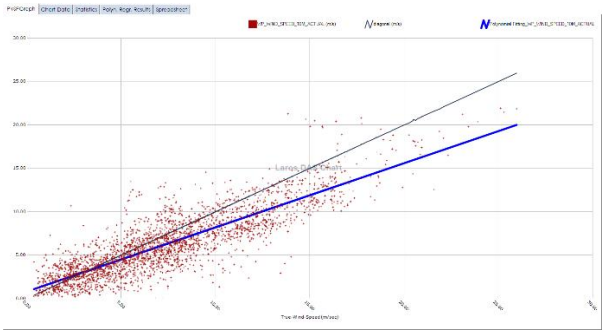

Vessel 8

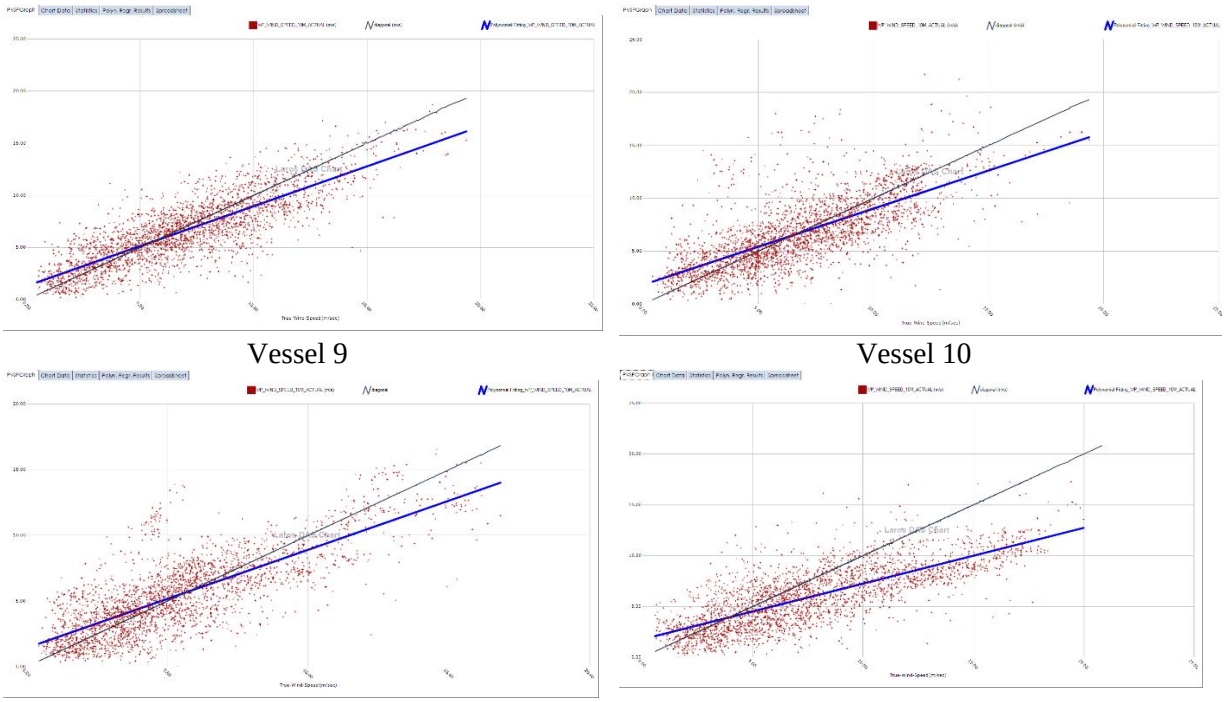

Vessel 9 Vessel 10

Vessel 11 Vessel 12

Fig.5: Weather Provider wind speed vs anemometer wind speed with 1 hr resolution

Scatter plots were generated for each vessel, plotting TWS on the x-axis and WPWS on the y-axis, using 1-hour resolution data. Linear regression curves and a diagonal line (representing perfect agreement between TWS and WPWS) were overlaid on each plot for visual comparison. The plots revealed that at lower wind speeds, WPWS values tended to be larger than TWS values. The opposite is revealed at higher wind speeds. Potential Contributing Factors may be:

- **Anemometer Accuracy:** The accuracy of anemometers can vary depending on the wind speed, potentially leading to different relative errors at different wind speeds.
- **Ship Structure Interference:** The impact of ship structure on airflow can also vary with wind speed, potentially influencing anemometer readings differently at different wind speeds.
- **Influence of Ship Speed:** At lower wind speeds, the vessel's speed contributes more to the relative wind experienced by the anemometer. This can introduce variability in TWS measurements, especially within the anemometer's accuracy range.
- **Errors on Weather Models:** The accuracy of models used for weather forecasting on given locations can vary depending on the microclima there, distance from the weather station that is feeding the model and many other issues, potentially leading to larger relative errors when wind is getting stronger.

The relationship between TWS and WPWS calculated as the ratio (WSR) of the two values (TWS/WPWS) was visualized for all vessels using bar graphs, for further analysis. The WSR values were binned into intervals of 0.1, ranging from 0 to 5. The 1 hour resolution data were used for this analysis. The bar graphs in Fig.6 present the duration of occurrence (i.e., number of observations) of WSR values within the specific intervals. The length of each bar represents the duration. Although most values are close to the average ones, the WSR ratio may spread from 0.1 to 5, indicating cases where true onboard measurements differ significantly from the weather provider wind speed values.

Average WSR values were calculated for each vessel using both 1-minute and 1-hour resolution data. In order to focus on more representative wind conditions, the analysis was further refined by filtering the data to include only wind speeds within the 2-5 Beaufort range. Average WSR values were compared between sister vessels to identify potential variations in wind speed measurements.

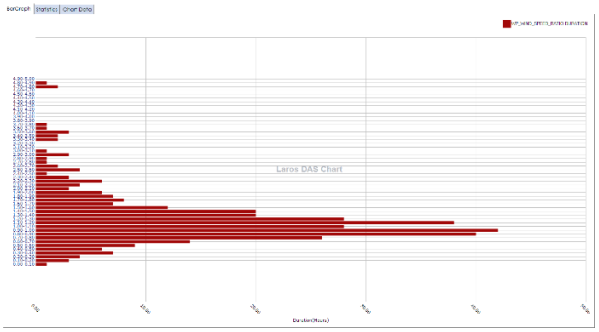

Vessel 1

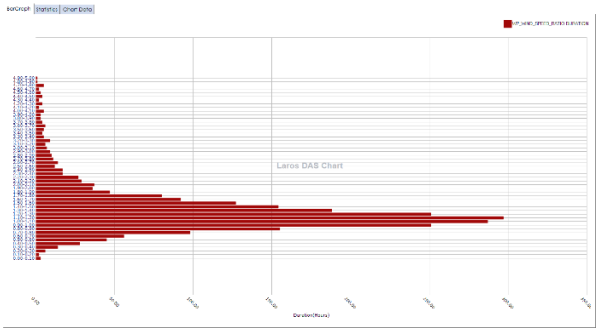

Vessel 2

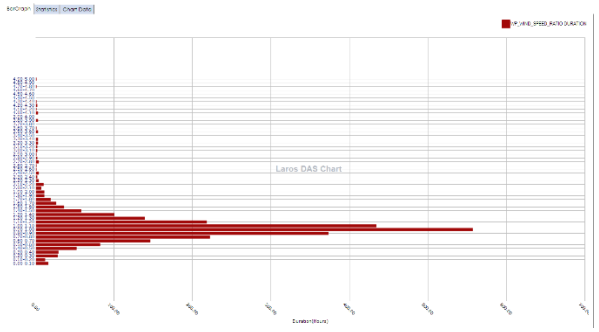

Vessel 3

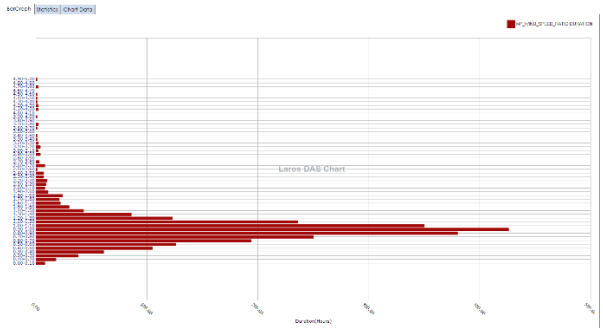

Vessel 4

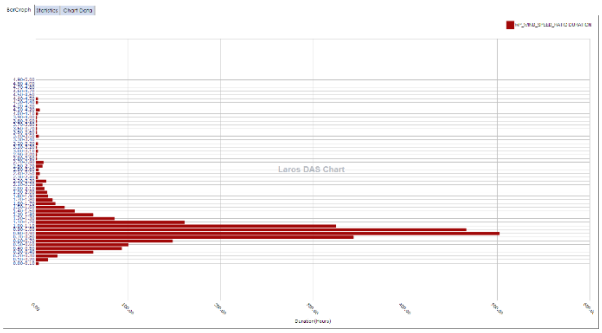

Vessel 5

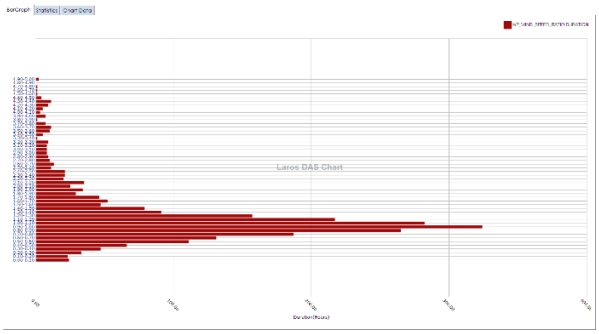

Vessel 6

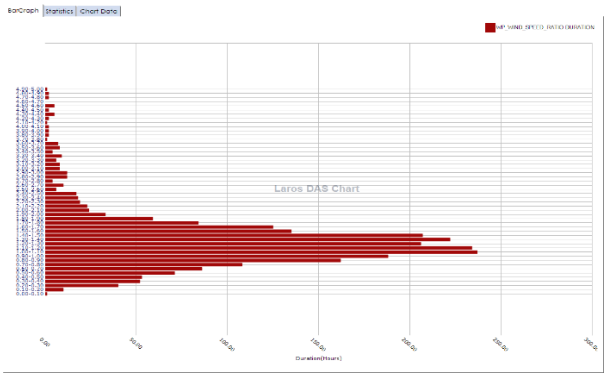

Vessel 7

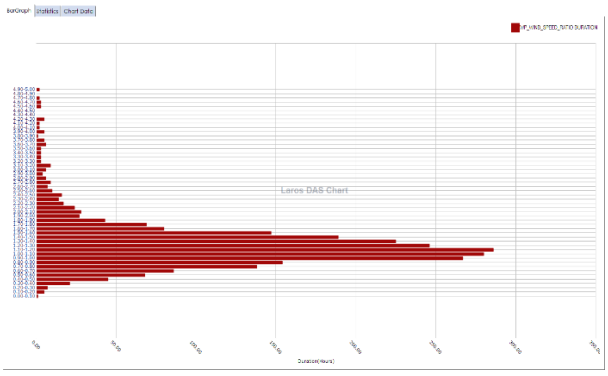

Vessel 8

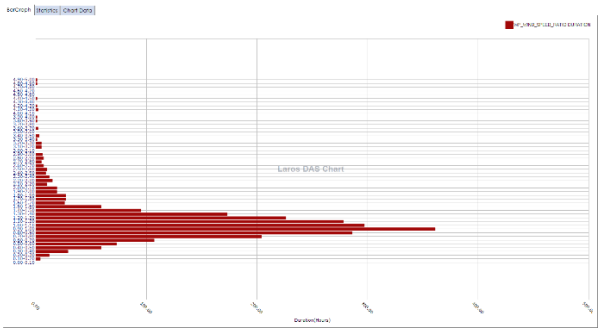

Vessel 9

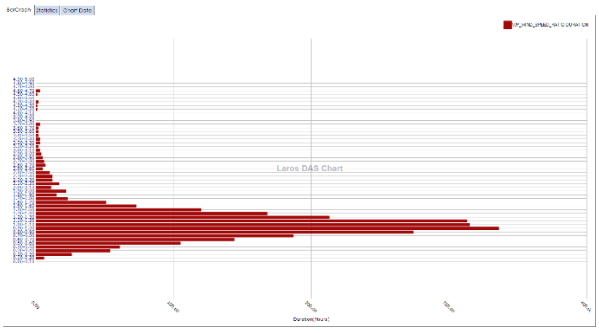

Vessel 10

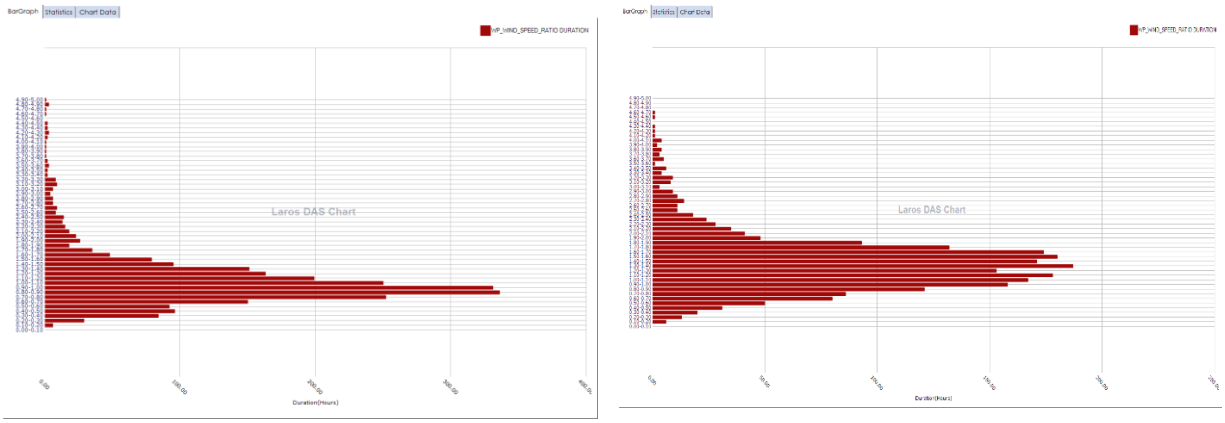

Vessel 11 Vessel 12

Fig.6: WSR duration of appearance

The calculated average WSR values were compared to the values predicted by the simulation model developed by *Moat et al. (2005)*. For vessels 1 to 6, the simulated WSR value from *Moat et al. (2005)* was 1.08. For vessels 7 to 11, the simulated WSR value was 1.11. Table III presents the calculated average WSR values for each vessel, incorporating the different resolutions (1-minute, 1-hour), data filtering (2-5 Bft), and comparisons with sister vessels and the *Moat et al. (2005)* simulation results.

Table III: Wind Speed Ratio deviation from simulation

Vessels	WSR simulation	WSR 1 min resolution	WSR 1 hr resolution	Deviation 1 hr res. (%)	WSR 1 hr res. 2-5 Beaufort	Deviation 1 hr res. 2-5 Beaufort (%)
V 1	1.08	1.34	1.35	19.76	1.40	22.98
V 2	1.08	1.50	1.50	28.18	1.56	30.69
V 3	1.08	1.02	1.01	-6.42	1.07	-1.23
V 4	1.08	1.01	1.01	-7.01	1.05	-2.88
V 5	1.08	1.07	1.07	-0.94	1.13	4.27
V 6	1.08	1.38	1.36	20.76	1.51	28.64
V 7	1.11	1.45	1.45	23.47	1.54	27.79
V 8	1.11	1.35	1.35	17.74	1.40	20.66
V 9	1.11	1.16	1.16	4.30	1.17	5.01
V 10	1.11	1.14	1.14	2.47	1.14	2.79
V 11	1.11	1.14	1.14	2.59	1.19	6.64
V 12	1.11	1.53	1.53	27.40	1.55	28.58

The observation of the values at Table III may lead to the following conclusions:

- The average WSR values (TWS/WPWS) were consistently greater than 1 for all vessels, indicating that, on average, the true wind speed measured by the ship's anemometer was higher than the wind speed estimations provided by the weather provider.
- Despite the inherent limitations of WPWS (not representing true free-stream wind), with a sufficiently large volume of data, the WSR average should primarily depend on vessel-specific characteristics. This assumption allows for meaningful comparisons between the calculated WSR values and the simulation results derived by *Moat et al. (2005)*.
- Deviation of the calculated WSR from the simulation derived WSR is below 10% for half the vessels and this factor must be always in consideration.
- For vessels 3 to 5, the deviation between the calculated WSR values and the simulation values was below 10%, suggesting good agreement between the measured and simulated wind speed relationships. The sister vessel 6 had over 20% deviation. Since a consistency for 3 of 4 sister

vessels was observed, the vessel 6 deviation may be due to a sensor problem or sailing on areas where weather models are not fine-tuned.

- For the vessels 7 to 12, the agreement with the simulation results was less consistent, with half vessels exhibiting deviations below 10% and half showing deviations more than 20%. At this case, it may not be conclusive whether the simulation results work well. On the other hand it may be like a proof that nowcast data accuracy is not consistent, questioning their use for performance or efficiency analysis. In comparison ship sensors, when calibrated and maintained, deliver data with transparency, which explains their behaviour.
- For sister vessels 1 and 2 the deviation from the simulation is 20 to 30%. We observe a consistent deviation, but the reason for it remains unclear. Further investigation is needed to determine the underlying cause.
- Filtering the data to include only wind speeds within the 2-5 Beaufort range had a minor impact on the absolute WSR values but did not significantly alter the overall conclusions of the analysis.

Table IV presents the average difference between TWS and WPWS. Since the differences between TWS and WPWS can be both positive and negative, the simple average difference does not accurately reflect the magnitude of the discrepancies. To provide a more meaningful assessment, the average of the absolute differences and the Root Mean Square Error (RMSE) were also calculated.

The analysis revealed a correlation between the magnitude of the difference ΔWS and the ratio WSR. Smaller differences generally corresponded to WSR values closer to 1. The absolute differences between TWS and WPWS and corresponding RMSE were typically in the range of 2-3 m/s. This magnitude of difference which is of the order of 1 Beaufort suggests that using TWS or WPWS for performance analysis may result in different conclusions, particularly for certain KPIs.

Table IV: Wind Speed Ratio deviation from simulation

Vessels	ΔWS m/s	ΔWS m/s (abs)	RMSE m/s	ΔWS 1 hr resolution m/s	ΔWS (abs) 1 hr resolution m/s	RMSE 1 hr resolution m/s
V 1	0.48	1.46	1.96	0.49	1.37	1.80
V 2	0.87	1.46	1.88	0.87	1.34	1.71
V 3	-0.24	1.44	1.97	-0.24	1.11	1.53
V 4	-0.37	1.48	2.04	-0.37	1.26	1.70
V 5	-0.59	1.48	1.94	-0.59	1.24	1.62
V 6	0.19	1.65	2.28	0.17	1.42	1.96
V 7	1.32	2.47	3.18	1.33	2.29	2.90
V 8	1.10	2.11	2.78	1.08	1.92	2.48
V 9	0.33	1.78	2.37	0.33	1.56	2.02
V 10	0.10	2.00	2.82	0.10	1.79	2.48
V 11	-0.08	1.71	2.32	-0.08	1.54	2.06
V 12	1.71	2.72	3.47	1.72	2.53	3.21

4.2 KPIs calculation and filtering

Four KPIs were evaluated for the analysis period:

- **Power Deviation**: The deviation between the actual measured shaft power and the theoretical shaft power predicted based on sea trial data for the same vessel speed, expressed as a percentage.
- **Engine Load Margin**: The percentage of available engine load capacity to overcome additional resistance encountered during operation.

- **Fuel Consumption per Nautical Mile**: The amount of fuel consumed by the main engine per nautical mile of advance, expressed in Kilograms per nautical mile (Kg/nm).
- **Propulsion Efficiency**: The nautical miles travelled per kilowatt-hour of energy produced by the main engine (nm/kWh).

For each KPI, the average values were calculated using both 1-minute and 1-hour resolution data for all vessels. Further analysis aimed to assess the influence of data filtering (anemometer vs. weather provider wind speed) on the calculated KPI values. Data were filtered for wind speeds within the 0-4 and 4-8 Bft range. The 4-8 Bft filtering was included because it represents a significant amount of the time, during which these wind conditions were encountered by the vessels, as presented at Table V.

Table V: Time period of encountered weather

Vessels	0-4 Bft time (%)	4-6 Bft time (%)	6-8 Bft time (%)	8-12 Bft time (%)	4-8 Bft time (%)
V 1	74.46	24.67	0.87	0.00	**25.54**
V 2	66.03	30.65	3.32	0.01	**33.97**
V 3	54.87	36.14	7.82	1.18	**45.13**
V 4	66.93	29.48	3.55	0.04	**33.07**
V 5	60.76	33.04	5.88	0.32	**39.24**
V 6	65.27	30.67	3.94	0.11	**34.73**
V 7	42.41	38.66	16.20	2.74	**57.59**
V 8	44.82	38.46	14.88	1.83	**55.18**
V 9	46.17	42.63	10.70	0.51	**53.83**
V 10	46.54	43.31	9.76	0.38	**53.46**
V 11	63.65	30.16	6.01	0.18	**36.35**
V 12	42.71	37.61	17.80	1.87	**57.29**

The KPIs were calculated using two wind speed sources for filtering:

- Anemometer wind speed (TWS)
- Weather provider wind speed (WPWS)

The deviations of the KPI values obtained using anemometer wind speed (TWS) filtering, were compared to the corresponding values obtained using weather provider wind speed (WPWS) filtering. These deviations are presented in Tables VI to XII. Note that some vessels lacked certain sensors (e.g., flowmeters, torquemeter), resulting in missing data (void cells) for some KPIs in the tables. For one KPI (Fuel consumption per nautical mile) contour graphs have been created for three sister vessels, presenting this KPI versus TWS and WPWS. To investigate the influence of the wind speed only, the data were filtered for laden condition, head wind direction and 11-12 kn vessel speed.

4.2.1 Power Deviation

Table VI: Power Deviation 4-month average 0-4 Bft filtering

Vessels	1 min res	Anem filtered 1 min res	WP filtered 1 min res	Dev. 1 min res (%)	1 hr res	Anem filtered 1 hr res	WP filtered 1 hr res	Dev. 1 hr res (%)
V 1	50.59	49.71	51.48	**-3.56**	50.93	49.35	52.01	**-5.39**
V 2	17.70	15.14	15.25	**-0.72**	18.48	15.33	15.71	**-2.44**
V 3	58.10	48.57	50.68	**-4.34**	66.63	49.09	54.34	**-10.70**
V 4	21.63	19.03	18.49	**2.83**	22.20	18.21	18.77	**-3.05**
V 5	11.19	8.02	8.65	**-7.82**	11.58	6.41	8.44	**-31.59**
V 6	26.74	20.27	19.83	**2.18**	27.68	19.47	20.60	**-5.77**

V 7	24.47	16.68	20.91	**-25.34**	26.89	15.20	21.59	**-42.03**
V 8	22.20	13.24	16.49	**-24.61**	22.73	12.72	16.69	**-31.18**
V 9								
V 10	17.27	9.70	14.20	**-46.35**	18.22	9.14	14.16	**-54.94**
V 11	50.40	38.61	45.29	**-17.29**	52.13	35.81	44.51	**-24.30**
V 12								

Table VII: Power Deviation 4-month average 4-8B filtering

Vessels	1 min res	Anem filtered 1 min res	WP filtered 1 min res	Dev. 1 min res (%)	1 hr res	Anem filtered 1 hr res	WP filtered 1 hr res	Dev. 1 hr res (%)
V 1	50.59	51.08	48.03	**5.97**	50.93	54.68	47.86	**12.47**
V 2	17.70	21.83	22.45	**-2.82**	18.48	24.14	23.31	**3.45**
V 3	58.10	65.03	60.42	**7.09**	66.63	79.95	71.43	**10.66**
V 4	21.63	26.64	24.94	**6.37**	22.20	31.50	26.27	**16.59**
V 5	11.19	14.72	14.24	**3.26**	11.58	17.22	14.88	**13.60**
V 6	26.74	33.05	37.09	**-12.21**	27.68	38.25	38.06	**0.48**
V 7	24.47	27.57	27.84	**-0.97**	26.89	32.23	31.47	**2.35**
V 8	22.20	26.76	27.89	**-4.22**	22.73	29.61	28.68	**3.16**
V 9								
V 10	17.27	22.26	21.71	**2.48**	18.22	26.49	23.48	**11.36**
V 11	50.40	64.97	54.29	**16.44**	52.13	78.62	60.13	**23.53**
V 12								

Based on Tables VI and VII, we observe the following:

- KPI values are influenced by the choice of wind speed data source (anemometer vs. WP).
- Using WP data generally results in higher KPI values compared to anemometer data when either 0-4 Bft or 4-8 Bft filtering is applied.
- While some deviations are found significant, the actual differences in KPI values are typically below 5%. This may be considered as a deviation factor when WP is used for calculations.
- Even small deviations can be important when KPIs are used for comparison and benchmarking.

4.2.2 Engine Load Margin

Table VII: Engine Load Margin 4-month average 0-4 Bft filtering

Vessels	1 min res	Anem filtered 1 min res	WP filtered 1 min res	Dev. 1 min res (%)	1 hr res	Anem filtered 1 hr res	WP filtered 1 hr res	Dev. 1 hr res (%)
V 1	2.56	1.45	2.61	**-80.19**	1.11	1.72	2.73	**-59.21**
V 2	9.44	9.91	9.91	**0.03**	9.71	10.29	10.18	**1.11**
V 3	6.20	8.50	8.53	**-0.37**	6.34	8.83	8.61	**2.47**
V 4	-15.39	-15.17	-15.18	**-0.10**	-16.24	-15.47	-15.97	**-3.25**
V 5	6.27	6.76	6.75	**0.15**	6.14	6.67	6.59	**1.22**
V 6	10.67	11.60	11.56	**0.42**	10.17	10.74	10.56	**1.70**
V 7	-0.87	1.93	1.72	**10.87**	-0.68	3.31	1.86	**43.72**
V 8	-1.68	0.20	-0.25	**225.36**	-2.16	-0.24	-0.74	**-204.55**
V 9								
V 10	2.36	5.12	4.08	**20.30**	2.32	5.68	4.26	**25.01**
V 11	8.30	10.59	10.37	**2.09**	7.69	9.58	9.35	**2.42**
V 12								

Table VIII: Engine Load Margin 4-month average 4-8 Bft filtering

Vessels	1 min res	Anem filtered 1 min res	WP filtered 1 min res	Dev. 1 min res (%)	1 hr res	Anem filtered 1 hr res	WP filtered 1 hr res	Dev. 1 hr res (%)
V 1	2.56	-0.43	2.48	**118.69**	1.11	-0.96	2.31	**340.79**
V 2	9.44	8.99	8.72	**-15.51**	9.71	8.65	7.79	**10.01**
V 3	6.20	5.07	5.19	**-1.28**	6.34	4.42	5.01	**-13.17**
V 4	-15.39	-16.71	-16.19	**2.71**	-16.24	-18.59	-17.18	**7.61**
V 5	6.27	5.73	5.85	**1.56**	6.14	5.52	5.82	**-5.36**
V 6	10.67	9.49	9.35	**0.20**	10.17	9.05	9.51	**-5.12**
V 7	-0.87	-1.05	-1.83	**49.31**	-0.68	-1.04	-2.06	**-98.42**
V 8	-1.68	-2.34	-2.75	**26.46**	-2.16	-3.24	-3.18	**1.94**
V 9								
V 10	2.36	0.89	0.66	**-89.57**	2.32	0.35	0.47	**-33.91**
V 11	8.30	6.75	7.18	**1.67**	7.69	5.04	6.86	**-36.15**
V 12								

The analysis of the values at Tables VII and VIII shows the following:

- A small impact on KPI values was observed when filtering for good weather conditions. A larger deviation in KPI values was observed at 1-hour resolution and for 4-8 Bft filtering. Therefore, the choice of the wind speed source may affect the vessel performance comparison at higher sea states.
- While some observed deviations in KPI values appear large, a closer examination reveals that these are often influenced by the small absolute values of the KPIs themselves. This can amplify the relative difference, even when the actual absolute differences in engine load margin is small. On the other hand small differences can be important when comparing sister vessels for performance and efficiency.

4.2.3 Fuel Consumption per Nautical Mile

Table IX: Fuel Consumption per Nautical Mile 4-month average 0-4 Bft filtering

Vessels	1 min res	Anem filtered 1 min res	WP filtered 1 min res	Dev. 1 min res (%)	1 hr res	Anem filtered 1 hr res	WP filtered 1 hr res	Dev. 1 hr res (%)
V 1	57.37	57.37	66.43	**12.83**	66.43	64.40	56.47	**12.32**
V 2	59.23	59.23	58.79	**0.64**	58.79	57.07	57.34	**-0.47**
V 3	64.32	64.32	64.85	**1.08**	64.85	59.61	59.58	**0.05**
V 4								
V 5	58.00	58.00	57.73	**-0.15**	57.73	55.79	56.58	**-1.42**
V 6	61.58	61.58	61.09	**-0.01**	61.09	58.23	59.48	**-2.13**
V 7	70.53	70.53	70.59	**-4.29**	70.59	61.01	65.67	**-7.63**
V 8	61.80	61.80	61.72	**-2.18**	61.72	55.99	58.96	**-5.31**
V 9	63.38	63.38	63.50	**-2.97**	63.50	57.17	60.02	**-4.98**
V 10	63.05	63.05	62.81	**-1.35**	62.81	59.59	61.15	**-2.62**
V 11	55.60	55.60	55.28	**-1.02**	55.28	52.71	53.42	**-1.34**
V 12	71.81	71.81	72.13	**-0.74**	72.13	69.09	69.10	**-0.02**

Table X: Fuel Consumption per Nautical Mile 4-month average 4-8 Bft filtering

Vessels	1 min res	Anem filtered 1 min res	WP filtered 1 min res	Dev. 1 min res (%)	1 hr res	Anem filtered 1 hr res	WP filtered 1 hr res	Dev. 1 hr res (%)
V 1	57.37	76.47	58.36	**23.68**	66.43	74.75	58.33	**21.97**
V 2	59.23	61.60	60.28	**2.14**	58.79	62.30	60.49	**2.91**
V 3	64.32	66.44	65.15	**1.93**	64.85	68.36	65.79	**3.76**
V 4								
V 5	58.00	59.32	58.93	**0.65**	57.73	59.77	58.89	**1.47**
V 6	61.58	64.52	64.34	**0.28**	61.09	65.89	63.88	**3.04**
V 7	70.53	72.46	73.47	**-1.39**	70.59	73.44	74.47	**-1.41**
V 8	61.80	64.57	65.40	**-1.29**	61.72	65.66	65.67	**-0.02**
V 9	63.38	65.93	65.40	**0.80**	63.50	67.81	66.09	**2.54**
V 10	63.05	64.65	65.12	**-0.72**	62.81	65.64	65.33	**0.47**
V 11	55.60	57.17	57.03	**0.24**	55.28	58.90	56.92	**3.37**
V 12	71.81	73.37	74.29	**-1.25**	72.13	74.09	74.75	**-0.89**

Based on the observations from Tables IX and X, the following conclusions can be drawn:

- With average values, small deviations are appeared which may suggest that the choice of wind speed data source has a limited impact on the calculated KPI for most vessels. On the other hand, even small differences may affect vessel comparison and benchmarking of sister vessels. There is one vessel exhibiting a deviation over 20%, which triggers further investigation.

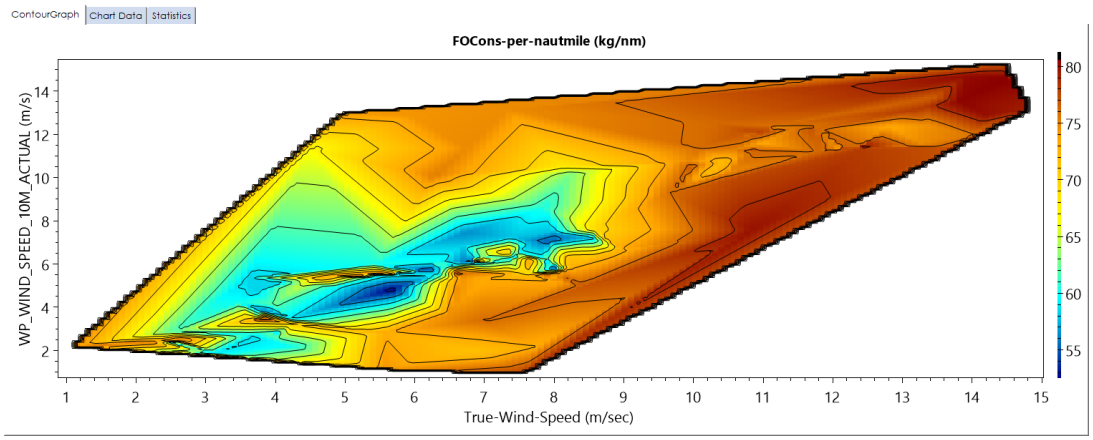

Fig.7: Vessel 3 Fuel Consumption per Nautical Mile-Speed 11-12 kn, Head Winds, Laden

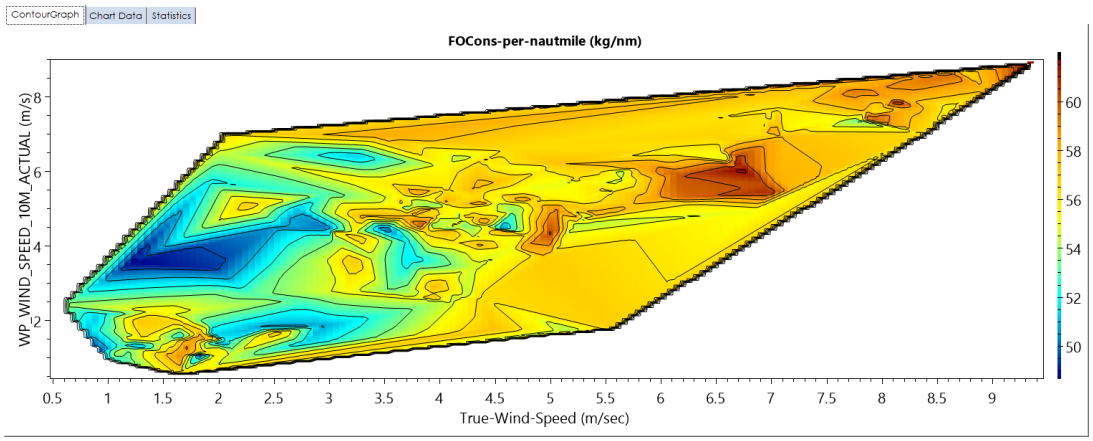

Fig.8: Vessel 5 Fuel Consumption per Nautical Mile-Speed 11-12 kn, Head Winds, Laden

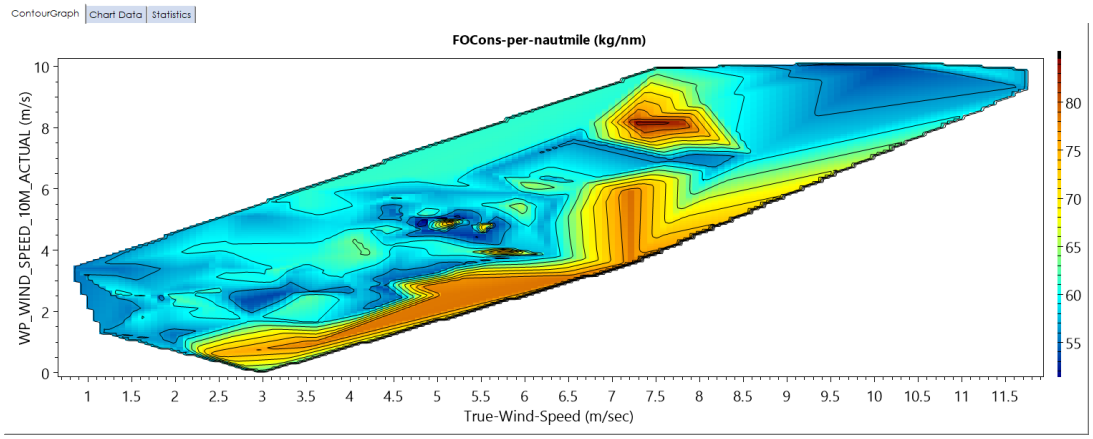

Fig.9: Vessel 6 Fuel Consumption per Nautical Mile-Speed 11-12 knots, Head Winds, Laden

- KPI values need to be reconsidered in order to represent actual sailing condition of the vessel. With this in mind the contours plots of Figs.7 to 9 present more accurately the sensitivity of the KPI to the wind speed source. After vessel speed and wind direction filtering, it is valid to assume that the magnitude of the KPI is mostly affected by the weather conditions. We may observe that the consumption per nautical mile follows more consistently the TWS than the WPWS values. This proves that when reliable data from sensors are available, more advanced calculations may reveal helpful outcomes for decision-making and justify vessel behaviour.

4.2.4 Propulsion Efficiency

Table XI: Propulsion Efficiency 4-month average 0-4 Bft filtering

Vessels	1 min res	Anem filtered 1 min res	WP filtered 1 min res	Dev. 1 min res (%)	1 hr res	Anem filtered 1 hr res	WP filtered 1 hr res	Dev. 1 hr res (%)
V 1	6.37	5.64	6.50	**-15.33**	5.51	5.75	6.73	**-17.00**
V 2	5.92	6.00	6.03	**-0.53**	6.15	6.48	6.39	**1.43**
V 3	6.18	6.65	6.96	**-4.70**	6.25	7.02	7.39	**-5.32**
V 4	6.42	6.50	6.46	**0.59**	6.65	6.80	6.67	**1.86**
V 5	5.96	6.09	6.09	**-0.11**	6.07	6.39	6.28	**1.69**
V 6	5.91	6.02	6.08	**-0.95**	6.19	6.72	6.56	**2.40**
0V 7	4.52	4.87	4.72	**3.15**	4.54	5.06	4.77	**5.81**
V 8	5.11	5.52	5.31	**3.89**	5.16	5.81	5.39	**7.28**
V 9								
V 10	5.49	5.62	5.65	**-0.50**	5.54	5.77	5.78	**-0.26**
V 11	6.22	6.56	6.41	**2.29**	6.37	6.93	6.66	**3.93**
V 12								

Table XII: Propulsion Efficiency 4-month average 4-8 Bft filtering

Vessels	1 min res	Anem filtered 1 min res	WP filtered 1 min res	Dev. 1 min res (%)	1 hr res	Anem filtered 1 hr res	WP filtered 1 hr res	Dev. 1 hr res (%)
V 1	6.37	4.41	6.06	**-37.63**	5.51	4.52	6.08	**-34.50**
V 2	5.92	5.58	5.69	**-1.97**	6.15	5.50	5.72	**-3.93**
V 3	6.18	6.03	6.09	**-1.06**	6.25	5.80	6.12	**-5.47**
V 4	6.42	6.23	6.28	**-0.79**	6.65	6.30	6.40	**-1.59**
V 5	5.96	5.78	5.79	**-0.21**	6.07	5.74	5.79	**-0.83**
V 6	5.91	5.35	5.36	**-0.22**	6.19	5.28	5.52	**-4.72**

V 7	4.52	4.40	4.37	**0.68**	4.54	4.35	4.34	**0.42**
V 8	5.11	4.76	4.73	**0.68**	5.16	4.63	4.70	**-1.52**
V 9								
V 10	5.49	5.31	5.24	**1.35**	5.54	5.33	5.20	**2.44**
V 11	6.22	5.70	5.81	**-1.89**	6.37	5.54	5.96	**-7.59**
V 12								

The observation of the values at Tables 10 to 12 may lead to the following conclusions:

- The KPI values in good sailing conditions generally exhibit small sensitivity to the source of the wind speed data.
- The deviation in KPI values is generally larger when using 1-hour resolution compared to the 1 min resolution.
- When filtering in the range of 4-8 Bft deviation is increased.

4.2.5 Special Case

A special case where the data resolution affected significantly a KPI calculation is presented below. Subject values correspond to vessel V7 and were recorded in November 2023. A screenshot is used from LAROS™ DAS software, Fig.7. Measurements correspond to 1 min resolution. As can be noticed, while applying the 0-4 Bft filter some values of power deviation passed through although it is clear that the general environmental conditions are not changed and the vessel behavior was aligned with those conditions (high power and consumption). These sort lasting, below 4 Beaufort anemometer values, affected the monthly power deviation calculation giving a misleading result. To overcome this the 15 min average wind speed in Beaufort has been used aiming to filter data for good weather conditions.

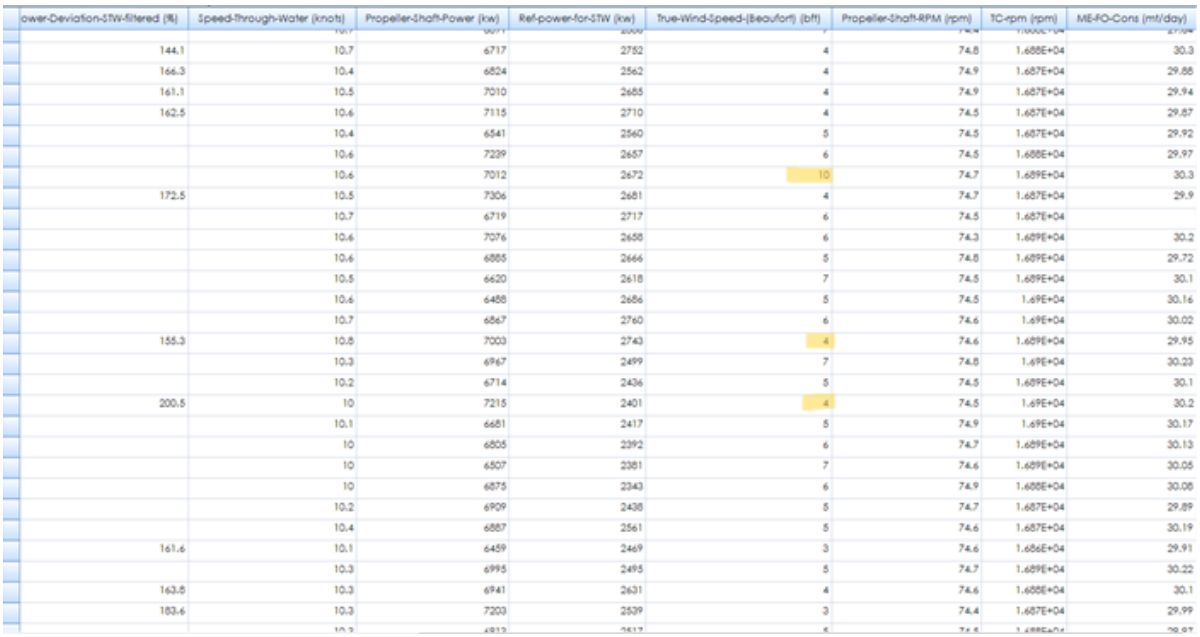

ower-Deviation-STW-filtered (%)	Speed-Through-Water (knots)	Propeller-Shaft-Power (kw)	Ref-power-for-STW (kw)	True-Wind-Speed-(Beaufort) (bft)	Propeller-Shaft-RPM (rpm)	TC-rpm (rpm)	ME-FO-Cons (mt/day)
144.1	10.7	6717	2752	4	74.8	1.68E+04	30.3
166.3	10.4	6824	2562	4	74.9	1.67E+04	29.88
161.1	10.5	7010	2685	4	74.9	1.68E+04	29.94
162.5	10.6	7115	2710	4	74.5	1.68E+04	29.87
	10.4	6541	2560	5	74.5	1.68E+04	29.92
	10.6	7239	2657	6	74.5	1.68E+04	29.97
	10.6	7012	2672	10	74.7	1.69E+04	30.3
172.5	10.5	7306	2681	4	74.7	1.68E+04	29.9
	10.7	6719	2717	6	74.5	1.68E+04	
	10.6	7076	2658	6	74.3	1.69E+04	30.2
	10.6	6865	2666	5	74.8	1.69E+04	29.72
	10.5	6620	2618	7	74.5	1.69E+04	30.1
	10.6	6488	2686	5	74.5	1.69E+04	30.16
	10.7	6867	2760	6	74.6	1.69E+04	30.02
155.3	10.8	7003	2743	4	74.6	1.69E+04	29.95
	10.3	6967	2499	7	74.8	1.69E+04	30.23
	10.2	6714	2436	5	74.5	1.69E+04	30.1
200.5	10	7215	2401	4	74.5	1.69E+04	30.2
	10.1	6681	2417	5	74.9	1.69E+04	30.17
	10	6805	2392	6	74.7	1.69E+04	30.13
	10	6507	2381	7	74.6	1.69E+04	30.05
	10	6875	2343	6	74.9	1.68E+04	30.08
	10.2	6909	2438	5	74.7	1.68E+04	29.89
	10.4	6887	2561	5	74.6	1.68E+04	30.19
161.6	10.1	6459	2469	3	74.6	1.68E+04	29.91
	10.3	6995	2495	5	74.7	1.69E+04	30.22
163.8	10.3	6941	2631	4	74.6	1.68E+04	30.1
183.6	10.3	7203	2539	3	74.4	1.68E+04	29.99

Fig.7: Effect of anemometer wind measurement fluctuation on KPI calculation

5. Conclusions and Future Work

The quality of ship data is important for accurate technical performance evaluation. Sensor accuracy or the vessel superstructure may influence wind data accuracy from ship's anemometer. Nowcast wind data from weather providers may substitute anemometer data for general purpose statistical analysis, although they might not be true. In general, comparing nowcast data with onboard data for a vessel or sister vessels, may give insights on potential sensor issues that need attention. From the current study, where data from 12 vessels for a 4 month period were analyzed, the following were derived:

- Anemometer and weather provider wind speeds exhibit significant correlation at 1-hour resolution.
- Weather provider wind speeds exhibit significant variation from anemometer in changing weather conditions and should be used with caution for performance analysis.
- At some cases the, predicted with CFD simulation, influence of ship superstructure on the anemometer accuracy is confirmed. Consistent behaviour across sister vessels suggests reliable anemometer readings. Significant discrepancies warrant further investigation for potential sensor issues if the weather provider data are accurate.
- Average absolute difference and RMSE between the two data sources are relatively big (around 2-3 m/s or the order of 1 Bft). This suggests that the choice of data source may affect overall true performance analysis.
- Some KPIs are affected more and other less by the wind data source when filtering was applied. These variations generally do not significantly alter overall performance analysis conclusions but may affect comparison and benchmarking among vessels. The choice of the proper KPI might be significant if only WP wind data are available.
- The wind data source affected more the deviation of the KPI averages for winds over 4 Bft. Performance analysis at over 4 Bft weather conditions is important, since these weather conditions represent a significant proportion of the vessels' voyage time.
- In specific cases, using high-frequency anemometer data may introduce noise and compromise filtering, potentially impacting KPI calculation accuracy. Using proper tools, these cases may be identified in order to apply filtering with lower resolution.

For future work, a similar study for sea current calculated as vessel speed over ground minus speed through water vs sea current from the weather provider is recommended. Additionally introducing sensor reliable timeseries and weather provider data into AI models, may exploit further the relationship between true and model weather parameters and enhance performance assessment with tools that today are available only to LAROS$^{TM©}$ users.

Acknowledgement

We express our special gratitude to the shipping company Laskaridis Maritime for the data provision and their insightful contribution.

References

HARANEN, M.; MYOHANEN, S; DRAGOS, S.C. (2017), *The Role of Accurate Now-Cast Data in Ship Efficiency Analysis*, 2nd HullPIC Conf., Ulrichshusen, pp.25-38, http://data.hullpic.info/hullpic2017_ulrichshusen.pdf

ISO (2015a), *Ship and marine technology - Measurements of changes in hull and propeller performance, Part 1: General Principles*, ISO/CD 19030-1, Int. Standard Org., Geneva

ISO (2015b), *Ship and marine technology - Measurements of changes in hull and propeller performance, Part 2: Default method*, ISO/CD 19030-2, Int. Standard Org., Geneva

LAROS$^{TM©}$ by Prisma Electronics

MOAT, B.; YELLAND, M.; MOLLAND, A. (2006), *Quantifying the airflow distortion over merchant ships: part II: application of model results*, J. Atmos. and Ocean. Tech. 23, pp.351-360 https://journals.ametsoc.org/downloadpdf/view/journals/atot/23/3/jtech1859_1.pdf

THEMELIS, N.; SPANDONIDIS, C.; GIORDAMLIS, C. (2019), *Data acquisition and processing techniques for a novel performance monitoring system based on KPIs*, IMAM Conf., Varna

The Use of Ship Navigation Data to Validate and Boost the Accuracy of AI Data-Driven Oceanic Models

Agathe Dupont, Nicolas Le Paih, Evangelos Moschos, Alexandre Stegner,
AMPHITRITE, Palaiseau/France, agathe.dupont@amphitrite.fr
Karine Abel-Michaux, Marianne Avoustin, GENAVIR, Plouzané, France

Abstract

The reliability of ocean currents is not sufficiently taken into accounts in ship route optimization and post-voyage analysis for vessel performance modeling. In order to quantify the accuracy of the various ocean forecasting models, we have collected several hundred thousand of in-situ measurements in order to build up a reference base for validation and training of our AI-data driven models over several navigation zones. These measurements come from drifting buoys, ADCP measurements or are calculated from high-frequency navigation data from several vessels across the globe. Our analyses indicate that the reliability and accuracy of the Operational high-Resolution Currents forecAst (ORCAst) that we have developed exceed those of standard numerical models that are most widely used by the shipping industry. Our work presents case studies quantifying the benefits of high-resolution oceanic current data in different regions for fine scale routing as well as for better estimation of the speed through water for ship performance analysis.

1. Introduction

Surface currents affect all ships across the globe. Adverse currents slow ships down, increasing fuel consumption as vessels compensate to maintain their Estimated Time of Arrival (ETA). Conversely, favorable currents enhance a ship's speed over ground, allowing temporary power reduction while maintaining the ETA. However, it is very difficult for numerical models to correctly localize ocean currents or eddies, which are much smaller than anticyclones or atmospheric storms.

A survey carried out by Amphitrite in 2023, questioning captains of commercial vessels, allowed us to highlight this difference between MetOcean variable predictions, *Moschos et al. (2024).* Almost eighty vessel captains replied - among others - to the question "What is your opinion on the reliability of Weather and Ocean Forecasts? ". Not surprisingly, while wind and wave data were deemed of good reliability by 70% and 66% of respondents correspondingly, only 7% of captains thought the same about ocean currents data at their disposal. On the contrary a 35% believes that the current data available today are of poor reliability.

How then can we assess and improve reliability of ocean current forecasts? Contrary to numerical modelling, satellite observations of the sea surface topography deduce daily information on sea surface currents, *Chelton et al. (2001,2011), Ballarotta et al. (2019)*. Moreover, recent studies using advanced Machine Learning methods have shown that satellite altimetry including the new SWOT mission can be complemented by additional satellite information provided by other sensors such as infrared or visible observations to provide reliable, high-resolution ocean surface data: *Moschos et al. (2023), Martin et al. (2023), Kugusheva et al. (2024), Ciani et al. (2024), Fablet et al. (2024) ; Garcia et al. (2025*). This new generation of AI models, which fuse various satellite observations, is set to revolutionize ocean forecasting. However, the performance of these new forecasting models needs to be precisely validated. Validation metrics need to be adapted to the needs of maritime navigation. The performance of these models needs to be assessed in high-traffic areas, where currents impact on ship speed and hence fuel consumption. The use of navigation data from merchant ships or data from oceanographic campaigns is very useful in this respect. In addition to validation, these data can also be used for the final training and the fine-tuning of AI models.

This new generation of high-precision ocean data enables a new form of short-term optimal routing that fully exploits the potential of surface currents. Traditional weather routing, primarily employed

for trans-oceanic voyages, allows ships to avoid major storms and adverse sea conditions. However, for short-sea shipping, especially in enclosed seas, coastal areas, or channels, more intricate routing is required. Several examples of short-term optimal routing were first presented in the Mediterranean Sea by *Moschos et al. (2024)*. Fine scale routing, using oceanic currents, might also be relevant for trans-oceanic voyages. Even in the middle of the North Atlantic Ocean or at the tip of South Africa veins of currents can be used to speed up a ship's journey.

This paper demonstrates that employing reliable ocean current forecasts at high-resolution can improve the optimal ship routing strategies while also enhancing vessel energy efficiency modelling. By employing surface drifters released all over the globe during oceanographic campaign and vessel data sailing in various area, we can quantify precisely the accuracy of the surface current forecast provided by our ORCAst AI-based model. These novel and reliable ocean current data allow for a short-term optimal routing solution with a low cost, low risk and significant gains in fuel consumption. This can offer a competitive advantage for shipping companies in the general context of the recent introduction of the Carbon Intensity Index (CII) by the IMO, the EU ETS regulations or the use of bio-fuels or e-fuels that will lead to significant additional costs in a green-fuel future.

2. Ocean currents: in-situ measurements

Direct measurement of offshore surface currents has always been a challenge for oceanographers. These currents can vary on spatial scales of a few tens of kilometers and temporal scales of a few days. In-situ measurements can be highly accurate, but they are still very sparse and do not provide an instantaneous map of currents, even over a very small area of a hundred square kilometers. These in-situ measurements are nevertheless necessary to test and validate numerical models, but they can also be used to train a new generation of deep-learning models, as we shall see later. The most commonly used in-situ measurement methods are described below.

2.1. Surface drifters

For many years, meteorological and oceanographic institutes have been deploying drifting buoys to automatically measure the Sea Surface Temperature (SST). These buoys are attached to floating anchors that drift with ocean currents. The SST measurements and the GPS position of these drifting buoys are transmitted by satellite every hour, aloowing to track their trajectory and measure their mean drift speed with an accuracy of a few centimeters per second (i.e. less than a tenth of a knot).

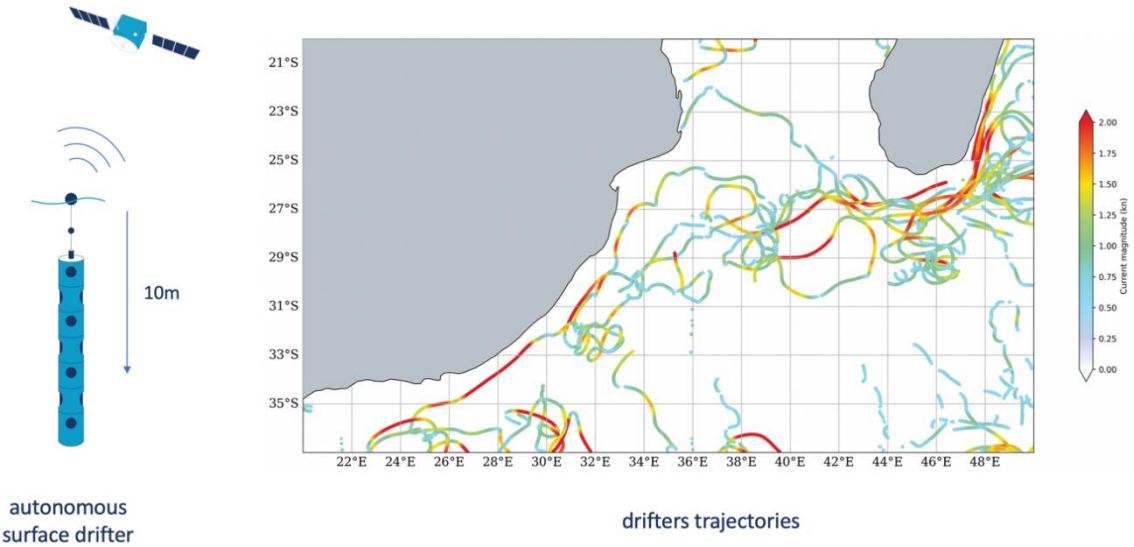

Fig.1: Trajectories and velocities of the surface drifters used for validation between the Cape of Good Hope and Mozambique Channel at the tip of South-Africa. More than 20 170 in-situ measurements of the surface velocity (at 10m) were collected in 2023. The color indicates the magnitude of the current intensity.

Drifting buoys with floating anchors that extend ten meters below the surface allow us to measure the surface currents that impact cargo ships. In order to filter-out fast inertial waves we compute a daily average speed. As the number of buoys is very limited, these daily measurements are few in number, and several months of data must be accumulated to obtain a statistically representative set. The map in Fig.1 shows the measurement points taken over one year (2023) in the Cape of Good Hope region, which is a major shipping route between the Indian Ocean and the South Atlantic. In this area, the current dynamics are complex and very intense, with current speed often exceeding 2 or 3 knots. However, even with more than 20 170 measurements points drifters are sparse and there are many white zones where no measures have been taken.

2.2. Vessel Mounted ADCP

Acoustic Doppler Current Profilers (ADCP) measure water movement by interpreting sound waves ("pings") transmitted by the instrument and subsequently reflected back to the instrument from particles in the water, such as sediment, plankton or other small particles. They rely on the Doppler effect to determine the speed and direction of those passively moving particles, or "scatterers," thereby determining the speed and direction of the currents as well. The Vessel Mounted ADCP measures the speed and direction of currents at multiple depths from the vessel to the seabed. The number of cells (i.e., depth layers) and the instrument's range are determined by the frequency of the ADCP. A 75KHz VM-ACDP can measure currents down to 1000m with a vertical resolution of 10-20m, while a 1000Hz instrument can measure surface currents down to 30m with a vertical resolution of 0.5-1m. In one or two days' sailing, an oceanographic vessel can then cross several times current veins and/or eddy structures. Unlike drifting buoys, we can use VM-ADCP measurements to position these dynamical structures and characterize horizontal velocity gradients with high precision.

2.3. X-Band radar

Recent technology, based on an imaging X-band radar, provides direct measurement of ocean surface current. Digitized radar images are processed with 3D fast Fourier transform (FFTs) to compute a 3D-power spectra of surface gravity waves. The doppler shift induced by the surface currents causes the energy in the 3D spectra frequency planes to be located on ellipses, rather than circles. Based on the power distribution in the wavenumber-frequency spectra, the current vector and the vessel Speed Through Water (STW) can be estimated, *Gangeskar (2018a,b), Bertelsen (2020)*. When the wind induced surface gravity waves generates a minimal level of sea surface roughness, current can be measured in a large area covered by the radar images, in front of the ship and at a reasonable distance from the vessel hull. Today, only a few commercial vessels are equipped with this technology but they already allow us to accurately test the reliability of various ocean forecasts models along several shipping routes. In this study we use the data collected during seven voyages of bulk carriers, crossing the Mediterranean Sea in 2023, equipped with the MIROS WAVEX system.

2.4. Ship navigation data

An increasing number of ships are now equipped with automatic high-frequency navigation data recording systems. This represents a significant advance over the data available with standard noon-reports. It is then possible to use navigation data, recorded and average every 5 or 15 minutes along the ship's route. While GPS data is relatively accurate for speed (SOG) and course (COG) over the bottom, this is not always the case for heading and, above all, the Speed Through Water (STW). *Ikonomakis et al. (2021)* has demonstrated the limitations of vessel speed-log measurements (STW) which are heavily influenced by the hull, fouling, air bubbles turbulences or inaccurate calibration, *Antola et al. (2017), Haranen et al. (2017).*

2.4.1 Speed log recalibration

STW measurement is strongly affected by the displacement of the water around the hull, and therefore by the vessel's draught. Therefore, the standard speed log needs to be re-calibrated for each port-

to-port trip. The first correction consists in correcting a constant offset on speed. Fig.2 shows the STW measurement made by a standard electromagnetic speed-log and the same STW measurement made by a Doppler Velocity Log (DVL) which measures water speed several meters below the hull. This DVL measurement is unaffected by the ship's hull or draught, and is therefore taken as a reference measurement. Precise calibration of this instrument, carried out by the GENAVIR quality team, shows that the margin of error is around 0.5% of the speed range. For a speed of around 15 knots, this corresponds to a precision of less than 0.1 knots. The speed variations measured by the two sensors are almost similar along the entire route, but offset by a constant value. A shift of 0.8knots on the STW measured by the electromagnetic speed-log along the whole voyage is the first correction to be applied to this sensor.

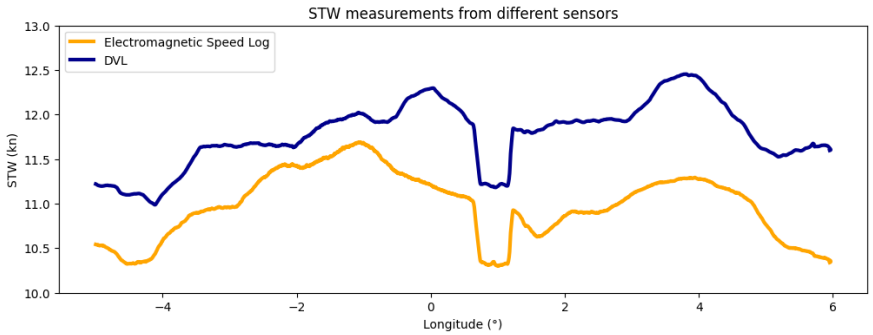

Fig.2: Speed Through Water (STW) measurement with two different sensors on the same vessel for a 5 days transit. The blue line corresponds to the Doppler Velocity Log (DVL), while the yellow line corresponds to the electromagnetic speed log. The mean difference between the two averaged STW, along this transit, is of 0.82 knots.

We introduce a specific method to evaluate the offset error and recalibrate the STW measurement, *Moschos et al. (2024)*. To do so, we use our HIRES-CURRENTS data and select, along the ship track, the points were surface current are weak (i.e. current intensity < 0.1 knots). For such low values of the surface current and when the angle (heading-COG) is less than 6°, we should expect SOG=STW. We then compute, for these selected points, the mean value of the offset <SOG-STW> per voyage and correct the speed through water STWc=STW + <SOG-STW> to get on average <SOG-STWc> = 0.

2.4.2 Current impact along the ship track

We can then compute for each voyage, thanks to these high frequency navigation data, the current impact along the ship track. In other words, how the surface current, acting on the whole hull, will modify the ship's speed (SOG). Fig.3 shows an example of this current impact ΔU=SOG-STWc for a 23000 TEU container ship crossing the Mediterranean Sea from Port-Said to Gibraltar in august 2023 at a mean sailing speed of 18 knots. As expected, the container ship is slowed down by almost 2 knots of facing currents induced by a recurrent anticyclonic gyre in the Alboran sea, just before the Gibraltar strait, *Renault et al. (2012)*. However, all along the route several speed fluctuations from 0.5 to 1 knot, induced by fine scale coastal currents, can be measured. On average the cumulated current impact along this voyage is about -0.5 knots. This will have a non-negligible impact on the mean voyage speed and the ETA at Gibraltar will be delayed by 3 hours in comparison with the ETA computed by the ECDIS that doesn’t account for oceanic currents.

The accurate estimation of the current impact ΔU is crucial for precise ETA prediction and for reliable voyage or speed optimization. But it is also important for post voyage analysis when vessel performance management is concerned or to evaluate hull and propeller designs, the efficiency of hull coating, the hull and propeller cleaning.

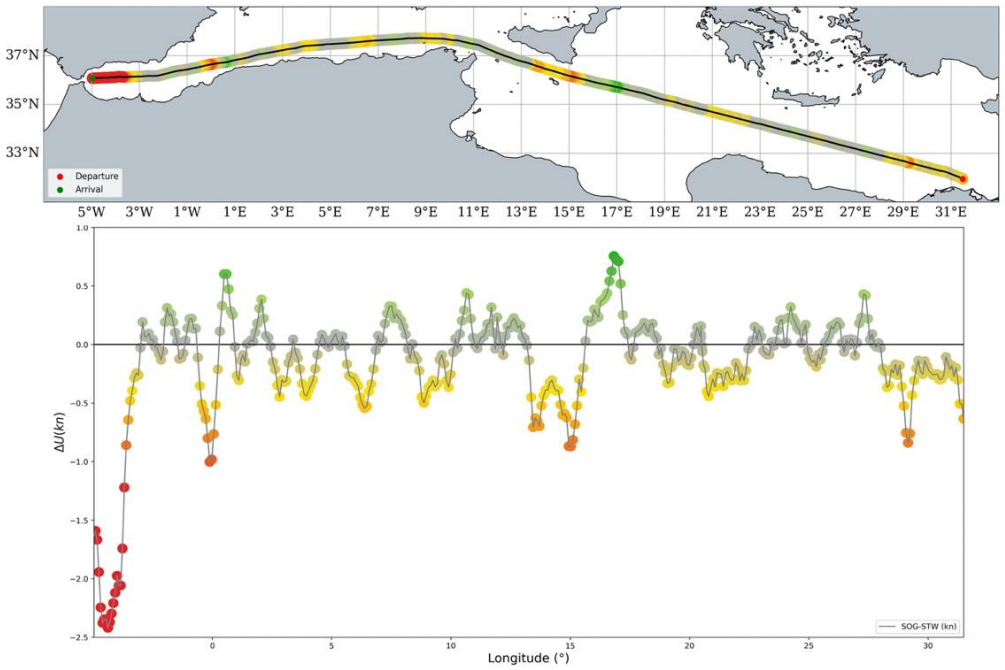

0

Fig.3: The route followed by the container ship from Port-Said to the Gibraltar strait from 21/08/2023 to 26/08/23 (upper panel). The colors indicate the intensity of the current impact ΔU=SOG-STW: green correspond to positive currents while red and yellow ones to adverse current along the ship route.

3. Ocean current forecast: numerical model

Our past survey of ship captains revealed that, according to their experience at sea, ocean current forecasts are perceived as much less reliable than the wind and wave forecasts. For 70% of captains, the reliability of ocean current forecasts is average or poor, *Moschos et al. (2024)*. This is because it is very difficult for ocean numerical models to correctly localize currents veins or eddies, which are much smaller than anticyclones or atmospheric storms. The typical diameter of a storm is around 1000 km, whereas an oceanic eddy is ten times smaller. In addition, there are far fewer measurements in the ocean than in the atmosphere to correctly initialize ocean numerical models.

This leads to an inaccuracy of several tens of nautical miles in the positioning of the main current veins and ocean meanders. This explains the large discrepancies between the predictions of the main operational models and the slowdowns or accelerations induced by real currents on ships. The example below shows localizations of eddies and meanders in the Cape of Good Hope region (same area as Fig.1), predicted by two different ocean general circulation models on the period, Fig.4. The intensities and the localizations of the eddies and meanders looks similar at large scale, when we look in details significant differences appear between the two models. If we plot the current impact for a vessel sailing at 16 knots along the main shipping line in this area (Figure 4 bottom panel) we can quantify the differences between these two currents data. The forecasts for the first half of the route, between 38°E and 50°E of longitude, seems similar (with different current intensities), they differ significantly for the second half along the South African coast where the current impact can be reversed.

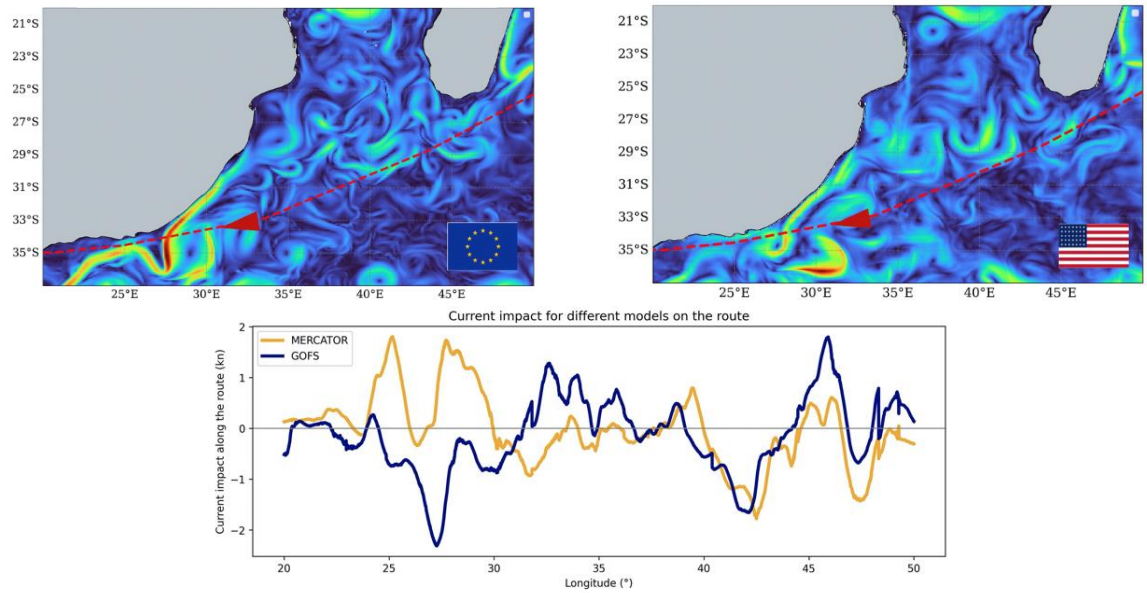

Fig.4: Nowcast of surface current intensity on May, 21, 2023 according to two global operational oceanic models distributed by the EU's (top left) and by the US's (top right) maritime services. The red dashed red line corresponds to the mean ship route from Asia to the UE or the US. Significant differences of the current impact ΔU=SOG-STW can be seen all along this trajectory between these two models (bottom) for a ship sailing at 15 knots.

4. Validation metrics

Various in-situ data can be used to validate surface current data and forecasts. We have chosen to combine current measurements made by drifting buoys, VM-ADCP measurements obtained during oceanographic campaigns and some measurements made by an X-band radar system installed on certain commercial vessels. Only currents of sufficient intensity have been included in this reference base. We have arbitrarily chosen an amplitude greater than half a knot, considering that below this value the precision of the measurement is not sufficient, and that these weak currents will have little impact on the bottom speed of ships which generally sail above 10 knots.

To compare these reference data with the different ocean forecasting models, we need to choose appropriate metrics. We have chosen two specific metrics to quantify both current direction and intensity errors.

We first compute the error angle θ between the measured velocity vector of the reference data and those forecasted by the different models. Small values of θ indicate sea surface currents that remain along a similar direction with the in-situ measurements, while larger values of θ will indicate a strong misalignment or even opposite current direction! The percentage of misalignment angle among all measurements are split in four colors-categories: deep green - excellent (θ <15°), light green - correct (15°< θ <45°), orange - inaccurate (45°< θ <90°) and red-wrong (90°< θ).

A second metric is based on the error vector: the difference between the measured velocity components and the forecast velocity. We compute the amplitude of this error vector and we normalized it by the mean amplitude of all the measured velocities used in the reference data set for the studied area. Therefore, we built a dimensionless error parameter, the Normalized Error Vector Amplitude (NEVA) which take into accounts directional and amplitude errors of the surface currents forecasts.

$$NEVA = \frac{\left\|\vec{V}_{model} - \vec{V}_{measured}\right\|}{avg\left(\left\|\vec{V}_{measured}\right\|\right)}$$

As for the error angle parameter, we split the NEVA parameter in four colors-categories: deep green - excellent (NEVA<30%), light green - correct (30%<NEVA<60%), orange - inaccurate (60%<NEVA<100%) and red-wrong (100%<NEVA).

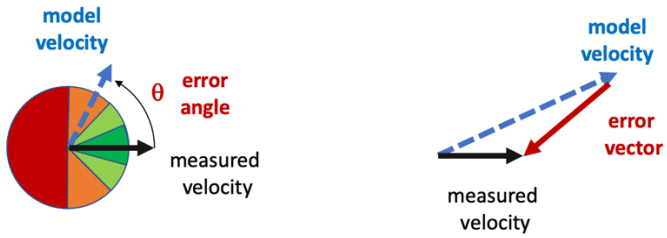

Fig.5: We compare both error angle (left) and Normalized Error Vector Amplitude (NEVA) (right) of measured surface currents (black arrow) with direction of the model forecast (blue arrow).

5. ORCAst: a high-resolution AI data-driven oceanic model

Since the early 2020s, research teams at major technology companies have been revolutionizing weather models by developing deep learning systems for operational atmospheric forecasting such as Google's GraphCast, *Lam et al. (2022)*, Microsoft's Climax, *Nguyen et al. (2023)*, or NVIDIA's FourCastNet, *Pathak et al. (2022)*. The AMPHITRITE R&D team, which comes from France's AI and oceanography research laboratories, develops similar forecasting models for the ocean. However, our deep learning systems are specialized models, trained specifically to predict ocean surface currents rather than a complete 3D model of the ocean. This specialization boosts the reliability of our Operational High-Resolution Current Forecasts (ORCAst) model providing high-resolution ocean data, *Garcia et al. (2025)*. The ORCAst deep learning framework produces 1/30° high-resolution 7-day forecasts of ocean currents in the global ocean.

5.1. Model architecture and training strategies

Our flexible approach allows us to fuse multivariate observations of the ocean such as in-situ measurements of currents (i.e. surface drifters), satellite altimetry, and satellite imaging of sea surface temperature and chlorophyll-a, to improve the spatial resolution and prediction of the temporal evolution surface currents, *Kugusheva et al. (2024), Garcia et al. (2025)*. However, training a model that leverages the diverse range of oceanographic observations—such as sparse in-situ measurements, satellite altimetry, and high-resolution satellite imagery—is challenging due to the differing temporal coverage and resolutions of these data sources. To overcome these difficulties, we train our model using a multiple stage training strategy, to learn a first approximation the geostrophic currents from standard altimetry fields as ground truth, and to progressively refine the learning using scarcer, but more precise or direct observations: SWOT and finally in-situ velocity measurements.

KaRIn altimetry from SWOT provides exciting opportunities for precise reconstruction of the sea surface dynamics. SWOT provides 120 km-wide swaths of high-resolution observations (*NASA/JPL*). This precision allows observation of mesoscale/submesoscale oceanic patterns. We have shown that training our model using the new generation of SWOT data, available since 2023, as targets led to significant improvements. However, only one satellite is presently in orbit, its revisit time period is 21 days, which leaves important areas unobserved. Finally, adding sparse in-situ measurements finetune the intensities of the surface currents forecast.

5.2. Model accuracy in comparison with standard ocean global circulation models

We use the validation metrics, detailed in section 4, to perform a quantitative inter-comparison of the accuracy of the ORCAst model with two operational ocean models widely used by maritime stakeholders. These two numerical models represent the state-of-the-art operational ocean forecasting system provided by the EU (Mercator/Copernicus) or US (GOFS/NOAA) maritime services. We choose

for this validation the specific region between the Cape of Good Hope and the Mozambic channel, Figs.1 and 4. This is an area of strong currents along a major shipping route between Asia and EU or the US. We have collected in this area more than 24 000 in-situ measurements points obtained from autonomous drifters or vessel mounted ADCP between 2022 and 2024. This set of reference data, independent of the data used during the learning phases of ORCAst, enables us to test the accuracy of our 7-days forecasts. Fig.6 shows that, in this area, the accuracy (corresponding to good or excellent label) of several numerical models of the ocean does not exceed 45-60%. This low level of reliability makes it impossible to carry out a fine-scale ship routing to avoid adverse currents and to navigate in more favorable regions. Regardless of the optimization algorithm, if the ocean data is poor, ship routing will be unreliable. However, our AI data-driven ocean forecast provide a much higher accuracy, always higher than 60% and up to 80%. Moreover, the percentage of excellent forecasts is increased by 60% while the percentage of wrong forecasts is divided by two or three. Similar scores were also found in the Mediteranean Sea and the Northern Atlantic regions, *NN (2025)*.

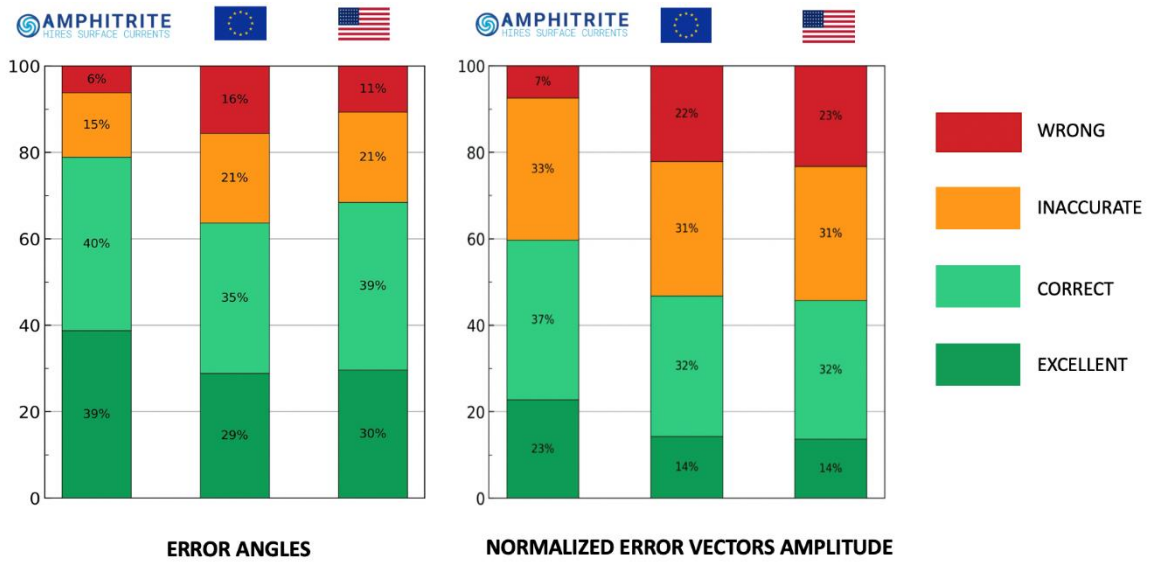

Fig.6: Comparison of the distribution of the error angles (left panel) or the Normalized Error Vector Amplitude (right panel) of surface currents between the 7 days forecast of HIRES-CURRENTS (first column) and those of two standard ocean models of global ocean (second and third columns). The percentage of misalignment angle or NEVA amongst all measurements are split in four colors-categories: deep green = excellent ($\theta<15°$ or NEVA<30%), light green = correct ($15°<\theta<45°$ or 30%<NEVA<60%), orange = inaccurate ($45°<\theta<90°$ or 60%<NEVA<100%) and red = wrong ($90°<\theta$ or NEVA>100%).

6. Accurate SOG forecast along the Suez-Gibraltar route

For a container-ship, compliance with the ETA is a major operational constraint. Apart from any optimization of the ship's route, optimizing speed for a given ETA reduces fuel consumption and CO_2 emissions. In calm sea conditions, as often encountered in the Mediterranean Sea, the current is the main cause of error in the ETA calculation. Therefore, to optimize the speed setting, it is necessary to anticipate, a few days in advance, the changes in the bottom speed (i.e. SOG) caused by currents. The example below, on the Concorde's route in August 2023 (same as Fig.3), shows how the surface current modifies the SOG. Our HIRES-CURRENT forecasts (green line in Fig.7), is very close to the surface current impact measured by the ship.

To quantify the accuracy of the current impact along the ship route we compute the following error index:

$$Error = \frac{RMS(|\Delta U_{model} - (SOG - STW_c)|)}{MEAN(|SOG - STW_c|)}$$

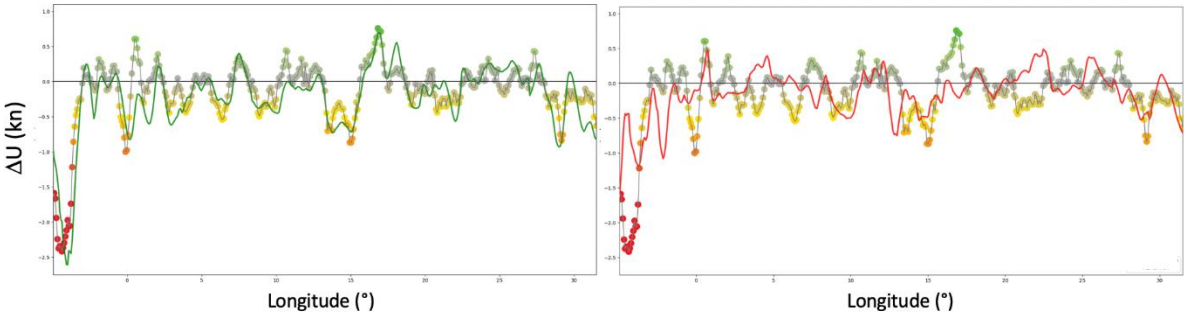

Fig.7: Comparison between the measured current impact ΔU=SOG-STW$_c$ and the forecast of our AI data-driven model HIRES-CURRENTS (green line) or the forecast of two global operational oceanic models distributed by the EU's (red line) or by the US's (pink line) maritime services.

This error index is normalized by the mean amplitude of the measured current for the whole data-set: $\Delta U_{mean} = MEAN(|SOG - STW_c|) = 0.52\ knots$. We filter out from the analysis the low values of surface currents ($|SOG - STW_c| < 0.25kn$) having a small impact on the SOG. We analyzed six voyages of container ships along the main Mediterranean shipping line from Port-Said (i.e. exit of the Suez-Canal) to the Gibraltar strait from August to October 2023. We have completed this first study (Moschos et al. 2024), with the analysis of navigation data from slower ships, two bulk-carriers that crossed the Mediterranean between November 2022 and March 2024. These ships are equipped with the WAVEX system, which provides accurate STW data. To improve the reliability of the dataset, we filtered out inconsistent measurements. Table I provides the error on the current impact according to the surface current forecasts provided by the state-of-the-art of Ocean Global Circulation Models: Mercator (E.U.), GOFS (U.S.) and MFS (Italian regional model).

Table I: Error index of the current impact for various surface current forecasts: the HIRES-CURRENTS provided by ORCAst AI model and the surface currents of three state-of-the-art operational ocean models provided by the marine service of the E.U, U.S. or Italy (IT).

Ship	***Voyage***	***Mean vessel speed (knots)***	***ERROR INDEX***			
			HIRES-CURRENTS	E.U.	U.S.	IT
Container Ships 23 000 TEU						
Container-ship 1	Suez->Gibraltar	17.8	**0.66**	1.12	0.99	1.13
Container-ship 1	Gibraltar->Suez	17	**0.63**	0.95	1.02	1.04
Container-ship 2	Suez->Gibraltar	18.5	**0.66**	1.07	1.06	0.83
Container-ship 3	Gibraltar->Suez	15.8	**0.51**	0.83	0.92	0.75
Container-ship 4	Malta->Suez	14.4	**0.48**	0.6	0.88	0.84
Container-ship 5	Suez->Gibraltar	18.2	0.83	**0.82**	1	0.89
AVERAGE			**0.70**	0.91	0.98	0.91
Bulk-carriers 34 700 GT						
Bulk-carrier 1	Gibraltar->Suez	12.1	**0.45**	0.85	0.79	0.74
Bulk-carrier 1	Suez->Gibraltar	11.6	**0.86**	1.03	0.99	1.07
Bulk-carrier 1	Suez->Gibraltar	10.9	**0.79**	1.01	0.84	-
Bulk-carrier 2	Malta->Gibraltar	10.9	**0.82**	0.89	1.17	0.93
Bulk-carrier 2	Gibraltar->Suez	12.7	**0.71**	0.90	0.83	0.85
Bulk-carrier 2	Suez->Gibraltar	11.7	**0.66**	1.06	0.70	0.87
AVERAGE			**0.71**	0.96	0.89	0.89

For almost all the voyages (92%) the HIRES-CURRENTS forecasts have a higher score than any of the numerical model available for this area, with an error reduced, on average, by 30%. For the few other cases, the accuracy of the HIRES-CURRENTS is roughly the same as the OGCM. It can be seen that these different numerical ocean forecasting models have identical scores, and none is significantly better than the others. This quantitative analysis of the navigation data of various ships using different sensors type to measure the STW confirms that the AI data-driven ocean forecast, based on various satellite observations, provide a much higher accuracy than standard numerical models.

7. Easy fuel savings with short-term optimal routing

Our latest high-precision data enables a new form of short-term optimal routing that fully utilizes the potential of ocean currents. In the example below, we have analyzed a voyage where the gain is mainly due to surface currents. Here, we consider the route of a bulk carrier passing the Cape of Good Hope, with a speed of 13 knots, prescribed by its charter contract, for transport from Asia to Europe.

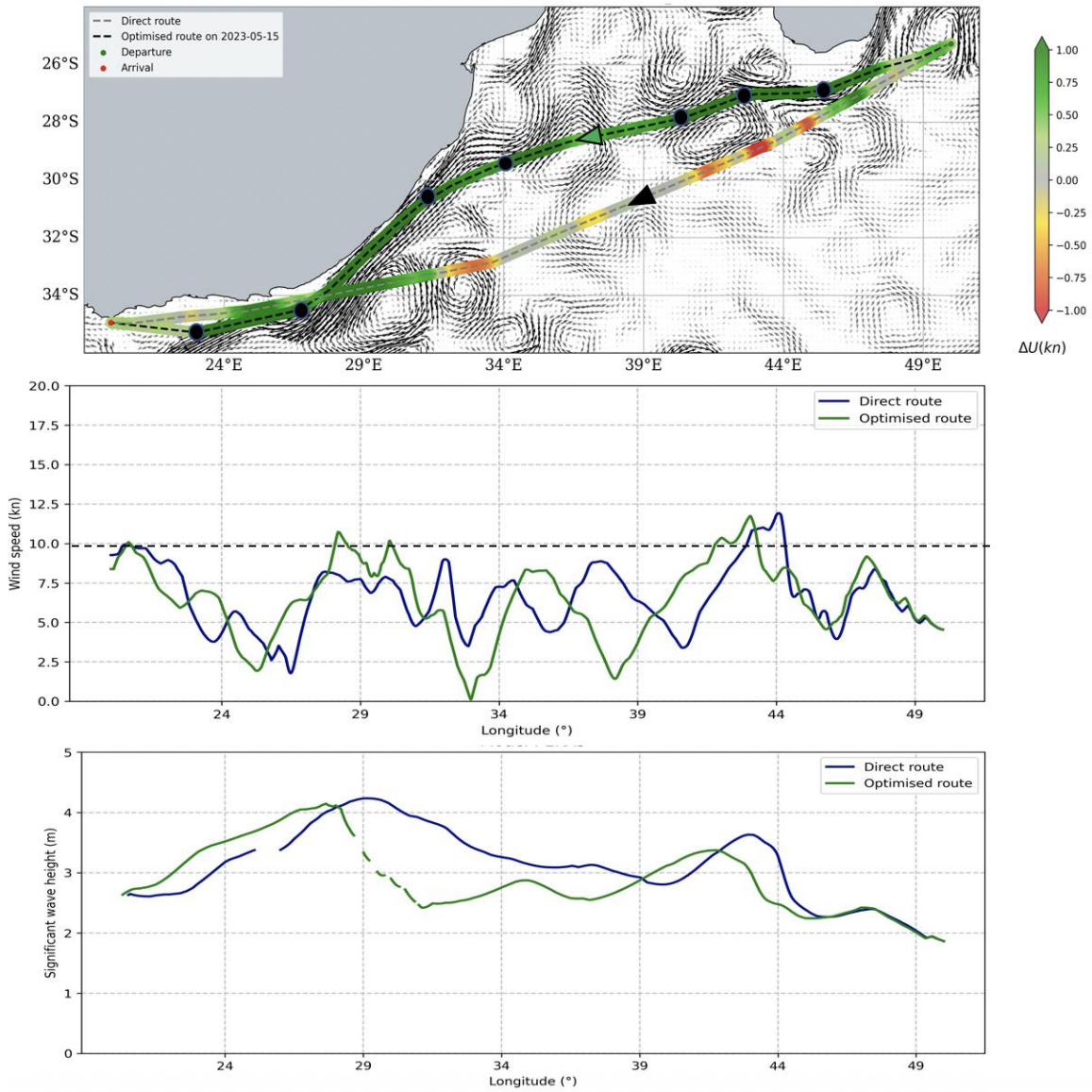

Fig.8: Surface current impact (ΔU=SOG-STW) along direct and optimized route of a bulk carrier with speed STW=13 kn (upper panel). The surface currents (black arrows) are plotted the 15 of May 2023, when the ship is in the middle of the journey. The middle and the lower panels indicate the amplitude of the wind and the wave field simultaneously for the direct (blue line) and the optimized route (green line). The black dotted line corresponds to the standard limit of 10-knots winds for calm seas.

On this stretch of the route, south of the Mozambique Strait, the ship will cross an energetic area with several strong eddies and meanders, which will slow her down upstream of the Agulhas Current. If, on the other hand, it chooses a longer route, passing further north and then following the coast of South Africa, it will benefit from positive currents along this optimized route, which will increase its speed by an average of one knot for 5 days! The extra distance of this optimized route will then be more than offset by this significant speed gain. Analysis of historical weather data in this area shows a easterly wind flow with moderate winds (<10 knots) on both routes, and southwest wave field that will be slightly favorable on the optimized route. As wind and wave conditions are almost identical on both routes, the calculated gain is mainly due to ocean currents. The gain in ETA at the Cape of Good Hope is of the order of 5-6 hours over a 5-day trip, which corresponds to a fuel saving of 4.4%, but if this gain is then used to reduce the ship's speed before arrival at its destination port (i.e. Just In Time arrival) the fuel saving can climb to 8-12%, depending on the ship's consumption curve. For a bulk carrier with a daily consumption of 25T of fuel oil, this can represent a saving of $5500 to $8200 (assuming an IFO price of 550$/ton) with just 5-6 additional waypoints on its route. The reduction in CO_2 emissions can also reach 30 to 46 tons thanks to this short-term optimal routing.

8. Conclusion

Present operational numerical models, frequently used for forecasting oceanic conditions along a ship voyage, present limitations in reproducing oceanic currents with high reliability. On the contrary, the fusion of multiple satellite observations with AI-based models provides oceanic current data that are characterized by statistically smaller errors, especially for regions with strong currents. Precise validation of our high-resolution oceanic current forecasts with a reference data-set of in-situ measurement and navigation data shows that the accuracy of HIRES-CURRENTS, generated by the ORCAst AI model, extends far beyond the state-of-the-art of ocean forecasting system. This new generation of accurate, high-resolution ocean data is now available for all the world's oceans, thanks to recent advances in ocean remote sensing and improved deep learning methodology. HIRES-CURRENTS data can be used to enhance operational routing applications, as well as to monitor ships' consumption curves. It's a low-cost, low-risk solution for the shipping industry.

Acknowledgements

We acknowledge the contributions of the Fleet Center of CMA-CGM in Marseille/France, the decarbonation team of CARGILL international and the contribution of GENAVIR, the operator of the French oceanographic fleet. We thanks all these partners for their active contribution in this work, providing vessel data used for the analysis, discussing the methodology and providing insights on shipping and weather routing practices.

References

ANTOLA, M.; SOLONEN, A.; PYÖRRE, J. (2017), *Notorious speed through water*, 2nd HullPIC Conf., Ulrichshusen, pp.156-165

BERTELSEN, V.; GANGESKAR, R.; PRYTZ, G.; SCHMITD (2020), *Accurate Voyage Sea State and Weather Measurements Improve Performance-Based Vessel Management*, 5th HullPIC Conf., Hamburg, pp.157-171

CIANI, D.; FANELLI, C.; BUONGIORNO-NARDELLI (2024), *Estimating ocean currents from the joint reconstruction of absolute dynamic topography and sea surface temperature through deep learning algorithms*, EGUsphere, pp.1–25

FABLET, R.; CHAPRON, B.; LE SOMMER, J. ; SEVELLEC, F. (2024), *Inversion of Sea Surface Currents From Satellite-Derived SST-SSH Synergies With 4DVarNets*, J. Advances in Modeling Earth Systems, 16(6):e2023MS003609

GANGESKAR, R. (2018a), *Verifying High-Accuracy Ocean Surface Current Measurements by X-Band Radar for Fixed and Moving Installations*, IEEE Trans. Geosci. Remote Sens. 56/8, pp.4845-4855

GANGESKAR, R.; PRYTZ, G.; SVANES BERTELSEN, V. (2018b), *On-Board Real-Time Wave & Current Measurements for Decision Support*, 3rd HullPIC Conf., Redworth, pp.223-233

GARCIA, P.; LARROCHE, I.; PESNEC, A.; BULL, H.; ARCHAMBAULT, T.; CHARANTONIS, A.; BEREZIAT, D.; STEGNER, A. (2025), *ORCAst: Operational High-Resolution Current Forecasts*, Submitted to Artificial Intelligence for the Earth Systems *(*AIES*)*

HARANEN, M.; MYOHANEN, S.; SEBASTIAN-CRITEA, D. (2017), *The Role of Accurate Nowcast Data in Ship Efficiency Analysis*, 2nd HullPIC Conf., Ulrichshusen, pp.25-38

IKONOMAKIS, A.; NIELSEN, U.D.; HOLST, K.K.; DIETZ, J.; GALEAZZI, R. (2021), *How good is the STW sensor? An account from a larger shipping company*, J. Marine Science and Eng. 9(5)

KUGUSHEVA, A.; BULL, H.; MOSCHOS, E.; IOANNOU, A.; LE VU, B.; STEGNER, A. (2024), *Ocean Satellite Data Fusion for High Resolution Surface Current Maps*, Remote Sensing 16/7, p. 1182

LAM, R.; SANCHEZ-GONZALEZ, A.; WILLSON, M.; WIRNSBERGER, P.; FORTUNATO, M.; PRITZEL, A.; RAVURI, S.; EWALDS, T.; ALET, F.; EATON-ROSEN, Z.; HU, W.H.; MEROSE, A.; HOYER, S.; HOLLAND, G.; STOTT, J.; VINYALS, O.; MOHAMED, S.; BATTAGLIA, P. (2023), *GraphCast: Learning skillful medium-range global weather forecasting*, Science 382/6677, pp.1416-1421

MARTIN, S.A.; MANUCHARYAN, G.E.; KLEIN, P. (2023), *Synthesizing Sea Surface Temperature and Satellite Altimetry Observations Using Deep Learning Improves the Accuracy and Resolu tion of Gridded Sea Surface Height* Anomalies, J. Advances in Modeling Earth Systems 15(5): e2022MS003589

MOSCHOS, E.; IOANNOU, A.; DUPONT, A., STEGNER, A. (2024), *Towards Optimal Ocean Routing: Leveraging Vessel Data for Ocean Current Reliability*, 9th HullPIC Conf., Tullamore, pp.213-222

NASA/JPL and CNES (2024), *The SWOT_L3_LR_SSH product, derived from the L2 SWOT KaRIn low rate ocean data products* 666 *[Dataset]*, https://doi.org/10.24400/527896/A01-2023.018

NGUYEN, T.; BRANDSTETTER, J.; KAPOOR, A.; GUPTA, J.K.; GROVER, A. (2023), *ClimaX: A foundation model for weather and climate*, https://doi.org/10.48550/arXiv.2301.10343

PATHAK, J.; SUBRAMANIAN, S.; HARRINGTON, P.; RAJA, S.; CHATTOPADHYAY, A.; MARDANI, M.; ANANDKUMAR, A. (2022), *Fourcastnet: A global data-driven high-resolution weather model using adaptive Fourier neural operators*, arXiv preprint arXiv:2202.11214

RENAULT, L; OGUZ, A.; PASCUAL, G.; VIZOSO, G.; TINTORE, J. (2012), *Surface circulation in the Alborán Sea (western Mediterranean) inferred from remotely sensed data*, J. Geophys. Res. 117

Out of Control – How External Factors Influence the Reliability of Hull Condition Monitoring

Falko Fritz, Albis Marine Performance, Hamburg/Germany, falko.fritz@albis-mp.com

Abstract

This paper discusses the influences of vessel instrumentation, operation schemes and sea areas on the accuracy of hull condition monitoring. Based on experience, the same vessel performance model may show greatly differing ranges of data scatter and reliability depending on external factors beyond the control of the data analyst. Some of the common influences are discussed, before presenting mitigation strategies and approaches to improve the confidence in the results.

1. Introduction

In general, hull condition monitoring works by measuring a ship's speed through water and the corresponding delivered power as primary parameters, and monitoring if that power demand increases over time. This principle is defined in ISO 19030:2016, Part 1, *ISO (2016)*. Since other factors like vessel draft, weather conditions, etc. also influence the vessel's hull resistance, further secondary parameters are recorded in addition. A mathematical vessel model is then used to make the data comparable over time, meaning filtering and normalizing them to a pre-defined set of reference conditions.

The three general steps in the process are shown in Fig.1. The relevant data are recorded on board the vessels, sent to an onshore server where they are processed and evaluated using the vessel model, and then the results are displayed or reported to the ship owner or operator for their considerations and taking action if needed.

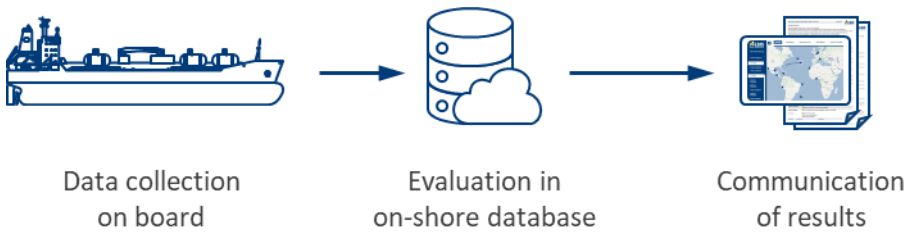

Fig.1: General approach to hull condition monitoring

Out of these three steps, the data processing and vessel modelling are in the hands of data analysts and their expertise. The instrumentation on board the vessel may be recommended by the data specialists, but the decisions are made by the ship owners. The importance of a meaningful integration of the sensors on board was highlighted in *Fritz (2023)*.

The communication of the results and their implementation in decision making is the third vital part of the process. In this paper, however, the focus will be on data acquisition and modelling, and more specifically on the topic which factors can be influenced by the data experts, which are beyond their control and how that influences the quality of the results.

2. Hull Condition Monitoring Results Achieved with Grey Box Modelling

2.1. Measuring the Primary Parameters

Many ships today are equipped with shaft torque meters and/or fuel meters. Sometimes these devices are specifically bought with performance monitoring in mind, or for the purpose of documenting shaft power limitations with regards to the EEXI framework, *IMO (2021)*. According to ISO 19030:2016

Part 3, alternative methods like mass flow meters may be used to measure the energy required to keep the vessel at its intended speed. Why this method may be preferrable is also discussed in *Fritz (2023)*. In many cases, the fuel or shaft power meters are recommended or selected in agreement with the data analysts.

The speed log to measure the ship speed through water on the other hand is typically chosen and installed independently of the goal of vessel performance monitoring. Its quality is often much harder to influence by the team responsible for hull condition monitoring.

2.2. Albis Grey Box Modelling

Albis Marine Performance has been using a grey box model for vessel performance analytics since 2011. It is based on the third-power law also known from the admiralty formula, which states that the required propulsion power of a vessel rises to the cube of its speed through water. The benefits and limitations of this simple approximation were *Bertram and Marioth (2024)*. To achieve realistic results, a grey box model combines the theoretical structure with empirical parameters derived from measurement data. This vessel model has been continuously enhanced and improved since its first application and it's the backbone of Albis' current vessel performance modelling. But despite its tested and proven design, there are cases where its results are less than ideal, as shown in the following chapter.

2.3. Scatter in Exemplary Fuel Consumption Trends

Figs.2 to 4 show exemplary hull condition monitoring graphs of three different vessels. Each data point is the median result of a calendar day and when they exceed a limit that is equivalent to a 5% speed loss, they are highlighted in yellow as a warning.

All three ships are equipped with highly reliable Coriolis mass flow meters, the same Albis V-PER software for data acquisition and processing, and the results were created using the same grey box vessel performance model as explained above. The measured main engine fuel consumption rates were extrapolated to a set of reference conditions that include a pre-defined ship speed, draft and good weather conditions.

It becomes evident that the quality and informative value of the results differs greatly even though they were calculated with the exact same grey box model. The reasons for the vastly differing data scatter are found in influences beyond the control of the data analysts, as described in the following chapter.

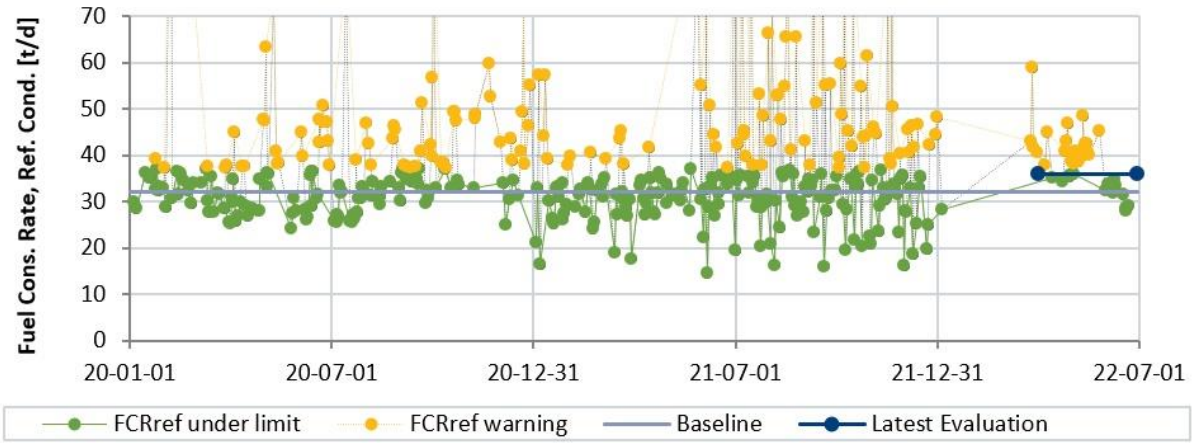

Fig.2: Vessel 1, exemplary normalized fuel consumption graph with significant scatter

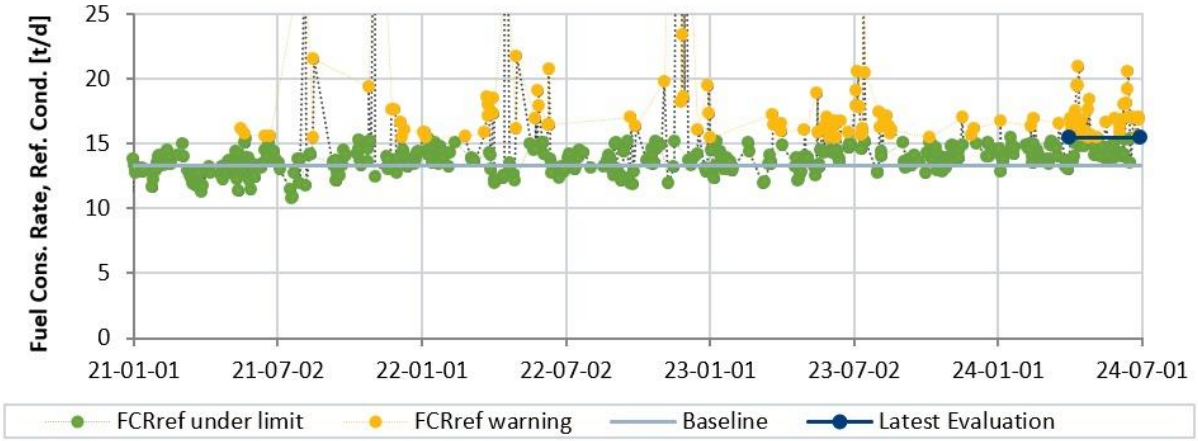

Fig.3: Vessel 2, exemplary normalized fuel consumption graph with typical scatter

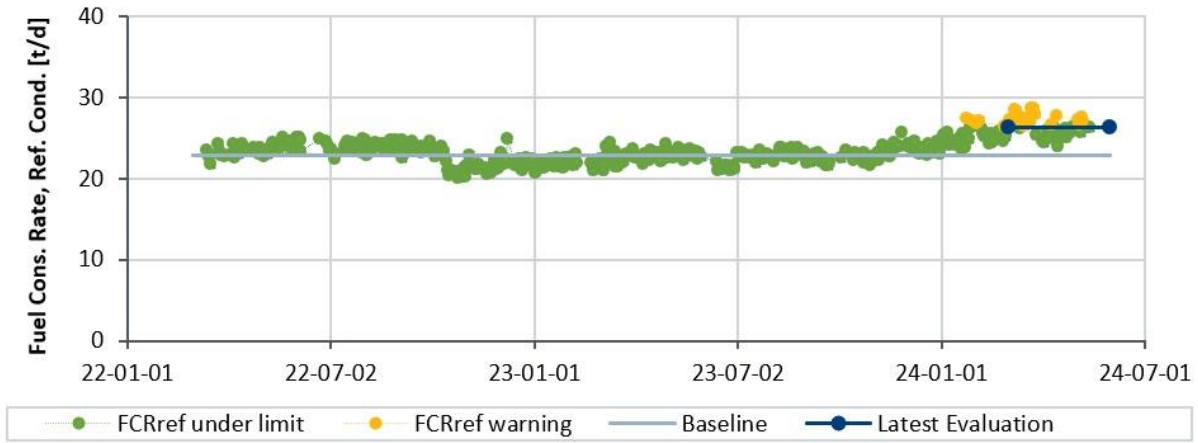

Fig.4: Vessel 3, exemplary normalized fuel consumption graph with very low scatter

2.4. Comparison of Exemplary Vessels

The three exemplary vessels differ by type, but more importantly by their operational schemes and the functioning of their respective speed logs.

- Vessel 1 is a 230 m long bulk carrier that operated mainly in the Gulf of Mexico, where there are strong and shifting surface currents. Many passages are short, there is a significant influence of maneuvering time when approaching or departing from ports and the ship speed varies. Most importantly, though, the speed log was unreliable to a degree that the GPS speed over ground had to be used for the vessel performance evaluations.
- Vessel 2 is a 160 m long tanker that operated globally. Its speed and sea conditions varied. A very accurate speed log allowed the ship speed through water to be recorded with high confidence. Due to longer passages, there was a smaller share of maneuvering compared to the bulk carrier.
- Vessel 3 is a 140 m long RoRo vessel that operated between Spain and Morocco, crossing the Strait of Gibraltar several times each day. There are strong surface currents in this area, but thanks to a reliable ship speed log their influence on the results was minimal. Since the ferry is bound by a strict schedule, many crossings were done at very similar speeds. Traversing the same body of water at the same speed in opposite directions is very comparable to the standardized double-runs used during speed trials according to ISO 15015:2025, *ISO (2025).*

Table I summarizes the influences in direct comparison; Fig.5 shows the operating area of each vessel.

Table I: Main influences on data quality of vessels 1, 2 and 3

	Vessel 1	Vessel 2	Vessel 3
Vessel Type	Bulk carrier (230m)	Tanker (160m)	RoRo vessel (140m)
Main Area	Gulf of Mexico	global	Strait of Gibraltar
Vessel Draft	varying	varying	small variances
Ship Speed	varying	varying	small variances
Sea Currents	strong	varying	strong
Speed Log	unreliable	accurate	accurate
Operation	short passages, no distinct pattern	longer passages, no distinct pattern	very short passages, strict pattern

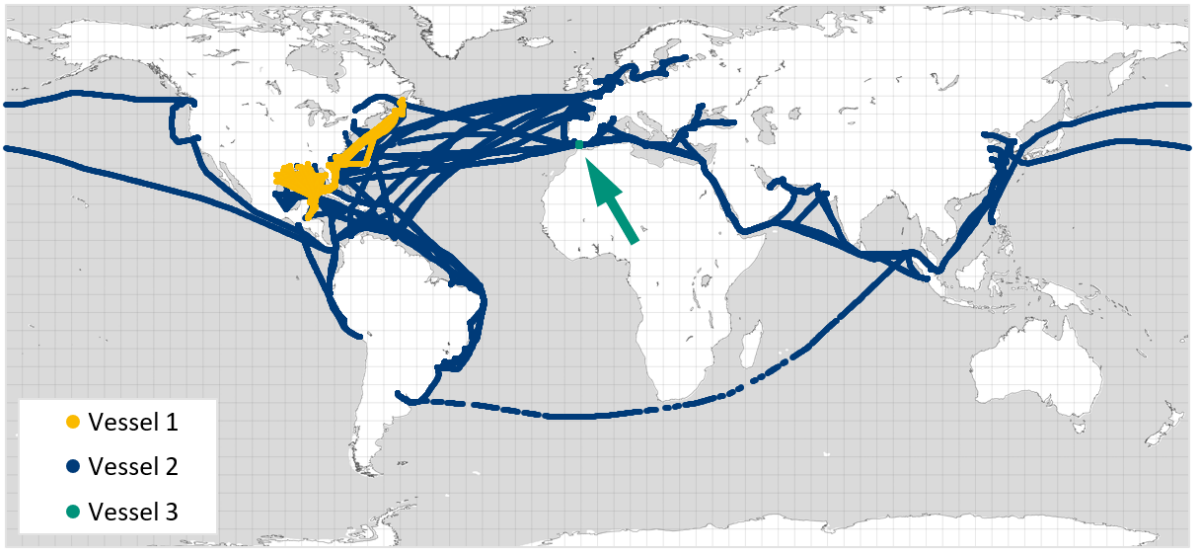

Fig.5: Operating areas of vessels 1, 2 and 3

3. Compensating the Influences Beyond the Control of Data Analysts

3.1 Surface Currents in Weather Data

The main reasons for data scatter in the results are linked to determining the ship speed through water accurately. Due to the cubic dependency of propulsion power and speed, a 1.5% error in the speed recording is about as detrimental as 5% inaccuracy from a shaft power or fuel meter.

Global re-analysis results from weather data providers include the surface currents and can be accessed for each position of the vessel. A vectorial addition of these to the recorded GPS vessel data make it possible to generate a virtual speed through water that's independent of the ship speed log. However, the surface currents in the weather data have a limited resolution both in time and geographical grid. Since the currents break down into smaller eddies and turbulences, the accuracy of this method is also limited. In addition, the weather models based on satellite data can only evaluate the water surface, while the currents that actually affect the vessel's hull remain hidden, *Fritz (2023)*.

The surface currents in weather data should therefore rather be seen as a method to create applicable correction functions for the ship speed log rather than to replace it altogether.

3.2 AI Models

As mentioned in chapter 2.2, the grey box vessel model applies correction functions to fundamental, physical dependencies like the third-power law. Establishing empirical parameters for these corrections becomes increasingly harder when different influences superimpose each other and cannot be evaluated independently. This is typically the case in poorer weather conditions. In the same way as fuel consumption warrants in charter agreements are usually limited to max. 4 Bft wind conditions, fuel consumption predictions become more and more erratic at higher wind speeds and sea states.

In the Albis model, the datasets recorded at 5-12 Bft are therefore filtered out and only 0-4 Bft conditions are used for vessel performance evaluations with the grey box model. This reduction of total data increases the potential scatter. Individual outliers impact the daily medians more if there are fewer valid data points in total.

Finding patterns in data with many variables is a strong point of AI models. Therefore they are well suited to widen the range of valid data and include weather conditions that were inaccessible without AI. Fig.6 shows a greatly simplified, qualitative comparison of grey box vs. AI model accuracy depending on weather and the respective limitations. Including data points between 5-7 Bft wind conditions increases the volume of valid data significantly and thereby helps to reduce data scatter.

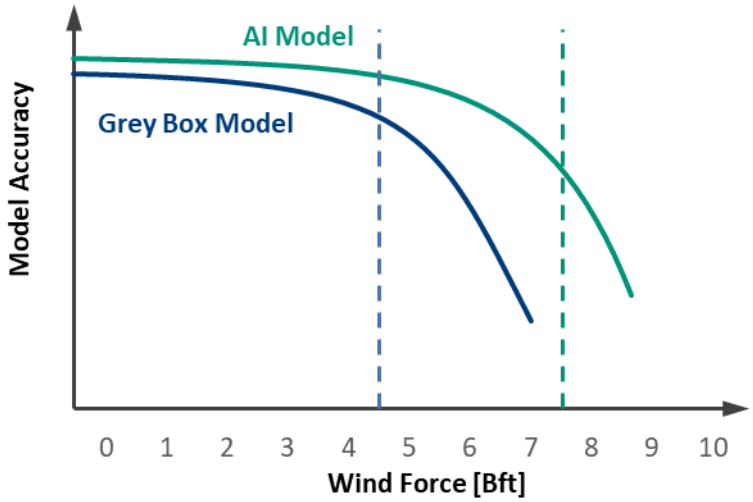

Fig.6: Simplified accuracy of grey box and AI models in different weather conditions

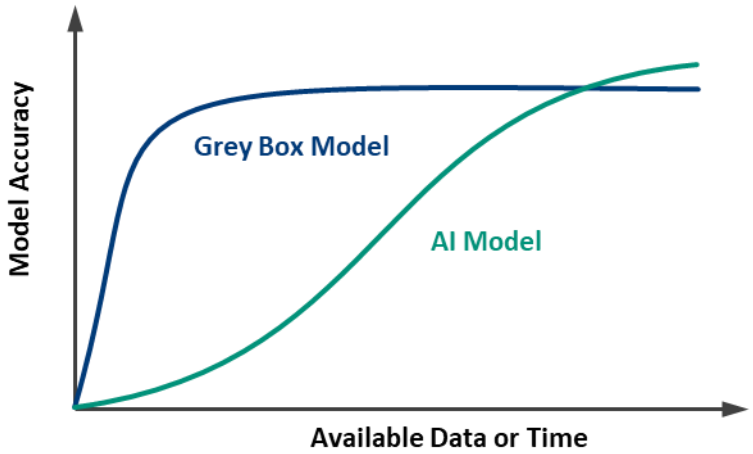

Fig.7: Simplified accuracy of grey box and AI models with increasing data volume over time

The disadvantage of AI models is their dependency on training data, though. While grey box models have a limited set of model parameters that may be estimated at first and then refined when the first

data of a new vessel become available, the complex multi-dimensional problems solved with AI require a much larger volume of training data to begin with. A typical grey box model may be adjusted to a new ship type rather quickly. Though after being fully parametrized, it also reaches its final capacity and does not improve any further. AI models on the other hand continue to improve over time, as more and more training data become available. Fig.7 shows a greatly simplified comparison of grey box and AI models with regards to available data.

However, the lack of training data in AI modelling is not only a concern when a vessel was newly added to the fleet of evaluated vessels. It also becomes relevant when the vessel operates in conditions that were hardly included in the training data, like e.g., certain speed ranges or weather situations that were not encountered before. The drop in the AI modelling accuracy at 8-10 Bft in Fig.6 may be due to the increasingly unpredictable sea states at higher wind speeds, or simply a result of the fact that ship crews generally avoid these conditions and there are hardly any training data available.

In essence, AI models are very well suited to interpolate within a data cloud with many dimensions and a large volume of data, but grey box models may still have the edge on them when it comes to extrapolating to previously uncharted territory. In shipping, this may e.g. be the case with ultra slow steaming that's only used infrequently.

The AI model also benefits greatly from high quality data during the training phase. If there are too many interferences and the random data scatter is too high, the AI results will be rather erratic as well.

3.3 Hybrid Intelligence

Since both the traditional grey box modelling and AI have advantages, it makes sense to use either model at its strongest. The Albis Hybrid Intelligence modelling approach combines the experience of human experts with artificial intelligence. As shown in Fig.8, the vessel data are processed both in the tested and proven grey box model and in a state-of-the-art AI algorithm. A set of boundary conditions is then applied to merge the outcome of both into a result with less data scatter and higher confidence than either model individually.

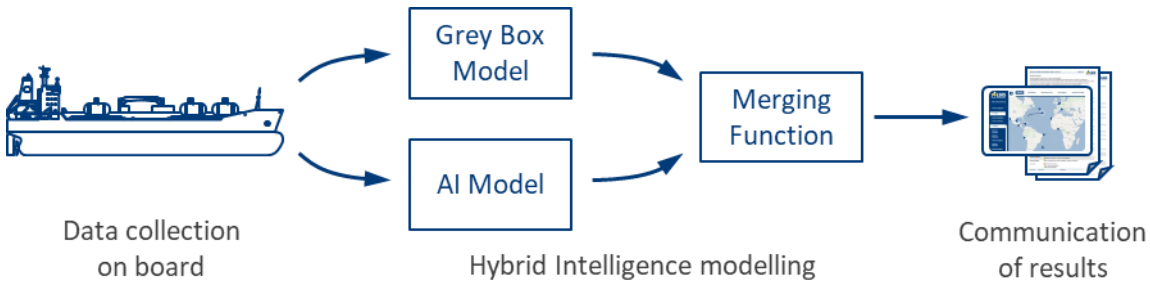

Fig.8: Albis Hybrid Intelligence modelling approach

Even at an early stage of development, results at Albis have already shown that the valid data used for hull condition monitoring can be increased by 70% and the scatter reduced by 40% when an AI algorithm is used in parallel to the grey box model. However, this result was achieved with vessel data that included reliable ship speed through water readings. It is questionable if the same would be possible if that variable was as unreliable as it was on the exemplary vessel 1 in chapter 2.3.

4. Conclusion

The area of vessel operation, trade schemes and typically also the quality of the ship speed through water data are beyond the control of the data analysts that report hull fouling trends or the effectivity of hull cleanings to the ship managers. Yet, these factors have a major influence on the quality of the results. To some extent, they can be compensated by accessing additional data and employing AI models. These come with their own challenges, though. AI algorithms require sufficient training to be

effective. When ships operate in conditions they hardly encountered before or their data were already erratic in the training phase, the AI results may be misleading. Cross-referencing them with a more robust, proven grey box model helps to mitigate these drawbacks and achieve better quality results that can be used with high confidence.

References

BERTRAM, V.; MARIOTH, R. (2024), *Third-Power Law – Friend or Foe?*, 9th HullPIC Conf., Tullamore, pp.5-10, http://data.hullpic.info/HullPIC2024_Tullamore.pdf

FRITZ, F. (2023), *Data Recording on Board – Are We Getting it Wrong from the Start?*, 8th HullPIC Conf., Pontignano, pp.62-69, http://data.hullpic.info/HullPIC2023_Pontignano.pdf

IMO (2021), *2021 Guidelines on the shaft / engine power limitation system to comply with the EEXI requirements and use of a power reserve*, IMO MEPC.335(76) Annex 9

ISO (2016), *Ships and marine technology – Measurement of changes in hull and propeller performance*, ISO 19030-1:2016, Int. Standard Org., Geneva

ISO (2025), *Ships and marine technology – Specifications for the assessment of speed and power performance by analysis of speed trial data*, ISO 15016:2025, Int. Standard Org., Geneva

Comparison between Three Methods of Monitoring Carbon Dioxide and Other Gases from Vessels

Paul O'Brien, Protea, Peterborough/UK, paul.obrien@protea.ltd.uk

Abstract

Comparison between three methods of monitoring Carbon Dioxide (CO_2) and other gases from vessels. These include direct monitoring of the exhaust, calculation from engine load and metered fuel, the data has been collected over several weeks on the five engines on a cruise ship. The direct measurement monitoring system uses in-situ multi component gas analyser (CO_2, CH_4, SO_2, NO_x, H_2O) and an averaging pitot tube flowmeter. The Continuous Emission Monitoring System (CEMS) reports CO_2 in kg/hr enabling a comparison of the CO_2 calculated from the engine fuel flowmeters and engine load in kg/hr.

1. Introduction

In 1997, the International Convention for the Prevention of Pollution from Ships (MARPOL), https://www.imo.org/en/about/Conventions/Pages/International-Convention-for-the-Prevention-of-Pollution-from-Ships-(MARPOL).aspx, was expanded with the addition of Annex VI, titled "Regulations for the Prevention of Air Pollution from Ships." This annex aims to reduce emissions from vessels and lower the carbon intensity of the shipping industry. Its primary goal is to limit air pollutants from ships, thereby mitigating their impact on both local and global environmental issues.

As of recent years, the marine industry is a significant contributor to global emissions, accounting for approximately 2-3% of global CO_2 emissions. The emissions from maritime shipping mainly consist of carbon dioxide (CO_2), nitrogen oxides (NO_x), and sulphur oxides (SO_x), which can have serious health and environmental impacts, including acid rain and global warming.

The European Union (EU) has been proactive in addressing the environmental impact of shipping, establishing frameworks to monitor and reduce marine emissions. In 2015, the EU introduced Regulation (EU) 2015/757, *EU (2015)*, which mandates the monitoring, reporting, and verification (MRV) of CO_2 emissions from vessels. The regulation aims to provide a more transparent and accurate view of emissions from ships and lays the foundation for future reductions. The regulation is designed to promote energy efficiency in shipping by enabling better tracking and management of emissions.

The inclusion of shipping in the EU Emissions Trading System (ETS), https://climate.ec.europa.eu/eu-action/eu-emissions-trading-system-eu-ets_en, under the European Green Deal marks a significant step in extending the EU's climate policies to maritime emissions. From 2024 onwards, ships will be required to purchase emissions allowances for their CO_2 emissions, creating a financial incentive for the industry to adopt cleaner technologies and reduce its carbon footprint. This integration aligns maritime operations with broader decarbonisation efforts, encouraging greater efficiency and investment in sustainable solutions.

A key element of Regulation (EU) 2015/757 is its focus on the direct measurement of emissions, specifically Method D, which requires ships to measure their fuel consumption and CO_2 emissions using onboard monitoring systems. This method ensures a high degree of accuracy and reliability in emissions data, making it essential for compliance with EU regulations.

While Method D offers the advantage of precise, real-time emissions data, it also presents certain challenges. The cost of implementing onboard measurement systems can be a burden for shipping companies, especially smaller operators. Additionally, the complexity of ensuring consistent, high-quality data across the fleet can be a constraint. However, the method's benefits in terms of

transparency and accuracy far outweigh the challenges, as it allows for better-informed policymaking and more effective emissions reductions.

The objective of this study was to demonstrate that the direct measurement of emissions using exhaust gas monitoring systems provides a reliable, accurate, and practical method for quantifying and reporting CO_2 mass emissions. By utilising real-time exhaust gas analysis, this approach offers a viable alternative to traditional estimation methods, ensuring greater transparency and compliance with regulatory requirements.

2. Protea's background

Protea's initial venture into the marine industry began in 2005 with the assessment of exhaust gas cleaning system (EGCS) efficiency on the MS Pride of Kent. This pioneering project laid the foundation for Protea's ongoing commitment to improving emissions monitoring and management in the maritime sector. Since then, Protea has installed hundreds of exhaust gas analysers onboard vessels, primarily for the measurement of SO_2, CO_2, and their ratio, as specified in the IMO Resolution MEPC.340(77) – 2021 Guidelines for Exhaust Gas Cleaning Systems.

As pressure on the maritime industry to monitor and reduce greenhouse gas (GHG) emissions continues to grow, Protea has expanded its focus to support these evolving demands. We are actively engaged in cutting-edge research and development (R&D) projects, including Carbon Capture and Storage (CCS) technologies, to drive innovation in emissions reduction. Additionally, we have partnered with SailPlan, whose Vessel Efficiency Data Platforms incorporate mass emissions measurements, providing valuable insights for optimising vessel performance and compliance.

3. Functional description and methodology of the monitoring system

Measuring mass emissions typically involves using an in-situ analyser, and a flowmeter, Fig.1.

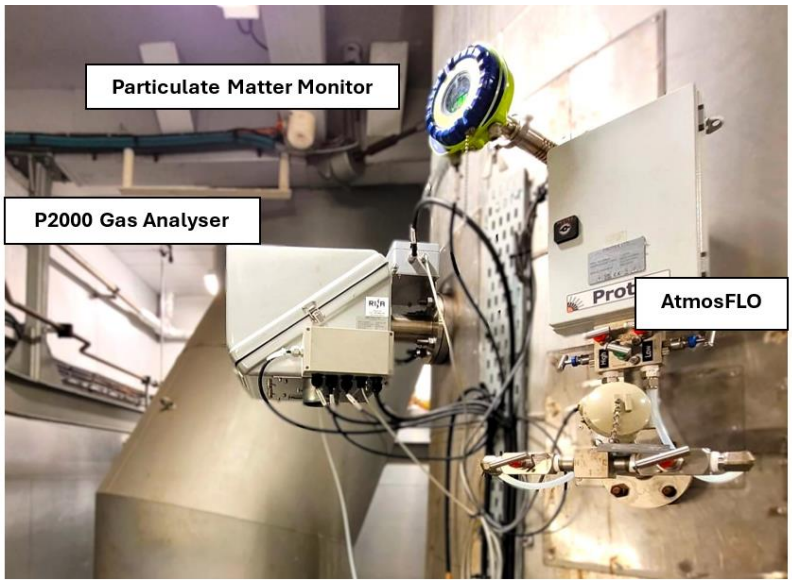

Fig.1: Overview of Direct Emissions Monitoring System

The P2000 in-situ analyser is installed directly within the exhaust or stack, where it continuously measures the concentration of certain pollutants in the gas stream, Fig.2. The in-situ probe of the analyser is placed in the process duct, with a sample cell made of sintered panels that allow the gas to pass through. A beam of filtered infrared (IR) radiation from the Analyser Unit (AU) passes through the cell, reflects off a retro-reflector, and returns to a detector, doubling the path length for absorption. Each gas component absorbs IR radiation at specific wavelengths, and the concentration is determined by the absorption level measured at the IR detector.

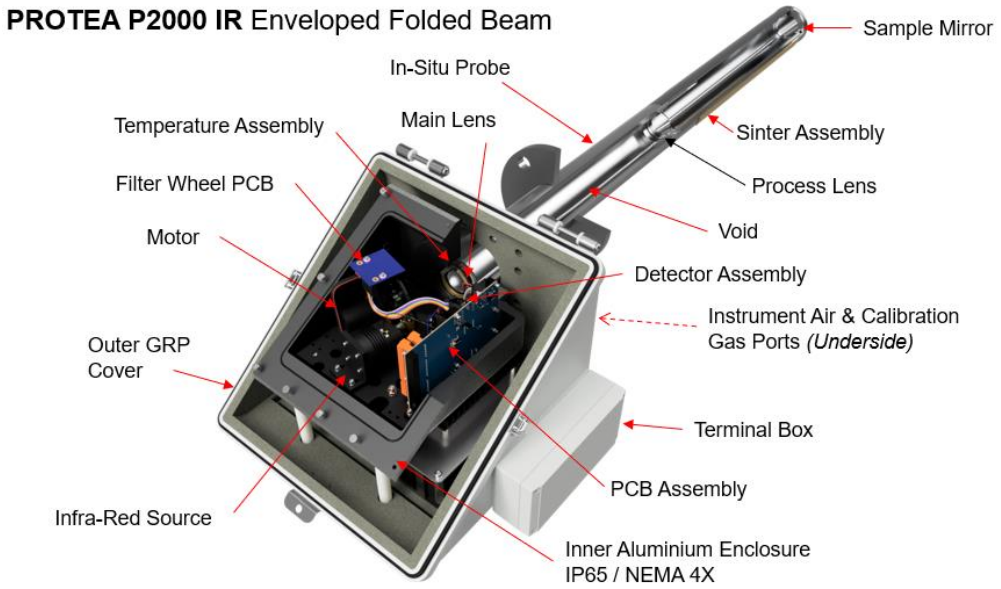

Fig.2: Protea 2000 schematic

The atmosFlo flowmeter measures the volumetric flow rate of the exhaust gas in the stack or duct, Fig.3. The flowmeter is installed at a point where it can accurately capture the flow profile of the gas. It measures the velocity and, combined with the cross-sectional area of the stack, calculates the volumetric flow rate of the gas (often in units like cubic meters per second or cubic feet per minute).

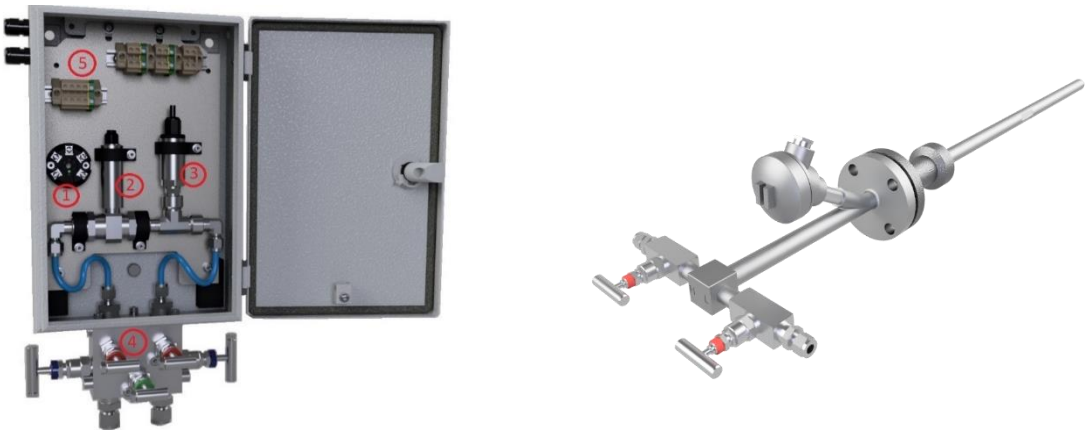

Fig.3: atmosFlo Schematic

4.1. Calculation of mass emission

To determine the mass emissions (for CO_2 for example), the concentration measured by the in-situ analyser and the flow rate measured by the flowmeter are combined. The key steps are:

1. Obtain the volumetric flow rate from the flowmeter (e.g., m^3/hr).
2. Measure the CO_2 concentration (as a percentage) using the in-situ analyser.
3. Convert the CO_2 concentration to mass:, using the molecular weight of CO_2 (44 g/mol) and the ideal gas law to convert the concentration from ppm or percent to mass per unit volume (e.g., kg/m^3).
4. Multiply the flow rate by the CO_2 concentration to get the mass flow rate of CO_2 (e.g., kg/s or tons/hour).

Example formula: CO_2 Mass Emission Rate= Flow Rate (m^3/hr) × CO^2 Concentration (kg/m^3)

This gives the mass of CO_2 emitted per unit time.

4.2. Corrections

The measurements need to be corrected for variations in temperature and pressure to ensure accuracy. This is done automatically in the software, as both the P2000 IR and the atmosFlo are equipped with integrated PT100 temperature sensors and pressure transducers. These sensors allow the measurement data to be corrected to Standard Temperature and Pressure (STP) conditions, ensuring consistency in the mass flow calculations.

Standard Temperature and Pressure (STP) are typically defined as:

- Temperature: 0°C (273.15 K)
- Pressure: 101.325 kPa (1 atm)

The correction factor for gas flow measurements to adjust for non-standard conditions is given by the following formula:

$$Q_{STP} = Q_{measured} \times \left(\frac{P_{measured}}{P_{STP}}\right) \times \left(\frac{T_{STP}}{T_{measured}}\right)$$

where: Q_{STP} = Corrected flow rate at standard conditions
$Q_{measured}$ = Measured flow rate
$P_{measured}$ = Measured pressure (kPa)
P_{STP} =101.325kPa (standard pressure)
$T_{measured}$ = Measured temperature (Kelvin)
T_{STP} =273.15K (standard temperature)

This formula ensures that the measured gas flow is normalized to STP, allowing for consistent and comparable emission data across varying environmental conditions. This method provides real-time, continuous monitoring of mass emissions, ensuring compliance with environmental regulations and facilitating emissions reporting.

4. Comparative Data from Secondary Monitoring Method (Method C)

The first method for comparing CO_2 mass emissions using the direct measurement approach involves assessing emissions against onboard measured fuel flows. Data from all flow meters connected to relevant CO_2 emission sources are aggregated to determine total fuel consumption over a specific period. This method (Method C) is outlined in Regulation (EU) 2015/757, which governs the monitoring of CO_2 emissions from maritime transport.

Method C relies on the measured fuel flows recorded onboard. Data from all Coriolis flowmeters associated with relevant CO_2 emission sources is aggregated to determine the total fuel consumption over a specific period. This aggregated fuel consumption is then used to calculate CO_2 emissions using the formula:

$$Fuel\ Consumption \times Emissions\ Factor$$

This calculation provides a basis for comparison with the direct measurements obtained by Method D.

5.1. Study results

For this study, data was provided by one of our partners, Sailplan, which supplies a marine operations and efficiency data platform for vessel operators. The vessel which was used in the study was equipped with five main engines, each fitted with Protea's emission monitoring system. Additionally, Coriolis flowmeters were installed on each engine, enabling a direct comparison with Method C.

For the vessel, the emissions factor is based on the fuel type (diesel), which corresponds to 3.206 kg CO_2/kg fuel, as specified in the 2018 Guidelines on the Method of Calculation of the Attained Energy Efficiency Design Index (EEDI) for New Ships, Resolution MEPC.308(73).

Fuel oil type	C_F (t-CO_2 / t-Fuel)
Diesel/Gas oil (e.g. ISO 8217 grades DMX through DMB)	3.206
Light fuel oil (LFO) (e.g. ISO 8217 grades RMA through RMD)	3.151
Heavy fuel oil (HFO) (e.g. ISO 8217 grades RME through RMK)	3.114
Liquefied petroleum gas (LPG) (Propane)	3.000
Liquefied petroleum gas (LPG) (Butane)	3.030
Liquefied natural gas (LNG)	2.750
Methanol	1.375
Ethanol	1.913
Other (……)	

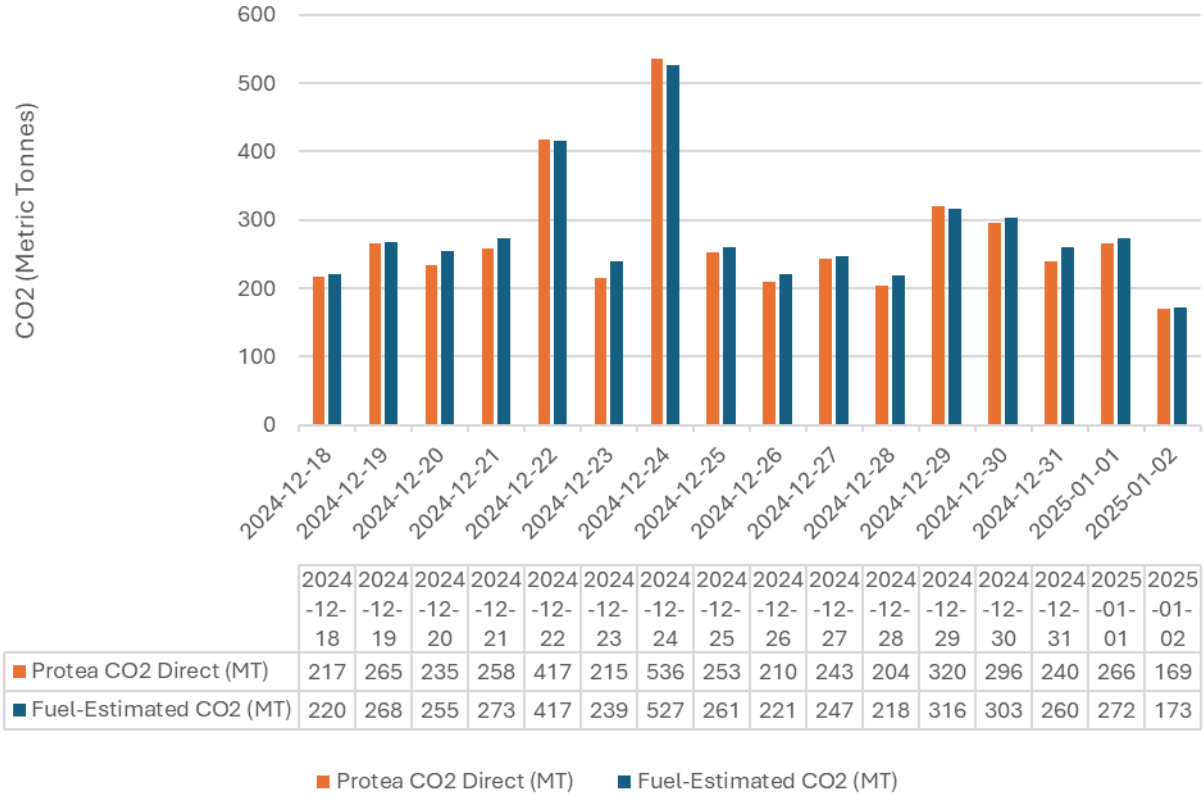

	2024-12-18	2024-12-19	2024-12-20	2024-12-21	2024-12-22	2024-12-23	2024-12-24	2024-12-25	2024-12-26	2024-12-27	2024-12-28	2024-12-29	2024-12-30	2024-12-31	2025-01-01	2025-01-02
Protea CO2 Direct (MT)	217	265	235	258	417	215	536	253	210	243	204	320	296	240	266	169
Fuel-Estimated CO2 (MT)	220	268	255	273	417	239	527	261	221	247	218	316	303	260	272	173

Fig.4: Vessel total mass CO2 emissions per day (MT)

Fig.4 illustrates the daily CO_2 emissions for the vessel, combining the CO_2 emissions from all running engines, presented in metric tons per day, comparing both Direct CO_2 emissions and Fuel-based calculations. This comparison is crucial, as the total daily mass of CO_2 emissions is commonly used for annual reporting, typically expressed as CO_2 emissions per distance or per unit of transport work. To calculate the daily CO_2 emissions in metric tons from the direct CO_2 measurement, the average CO_2 measurement in kg/hr is applied.

$$Tons\ per\ day\ = (\frac{Avg\ kg\ per\ hour}{1000}) \times 24$$

Fig.5 illustrates the trendline for daily CO_2 emissions for the *vessel*, presented in metric tons per day, comparing both Direct CO_2 emissions and Fuel-based calculations. The R^2 value (0.993) shows an excellent correlation between both the direct and fuel-based calculations for daily Mass Emissions of CO_2 for the 16-day period.

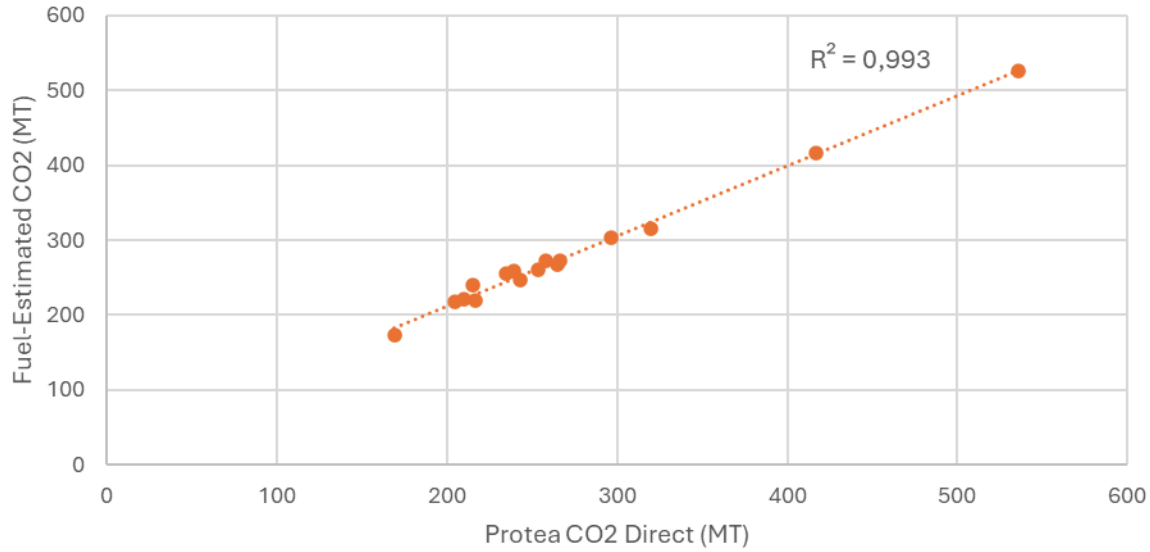

Fig.5: Total mass CO_2 emissions per day (MT)

The R^2 value, or the coefficient of determination, is a statistical measure that indicates how well the variation of one variable explains the variation of another. It is commonly used in regression analysis to assess the goodness of fit of a model.

Fig.6 illustrates the CO_2 mass flow for the vessel, combining the CO_2 emissions from all running engines, presented in kilograms per hour (15 min average), comparing both direct CO_2 emissions and fuel-based calculations.

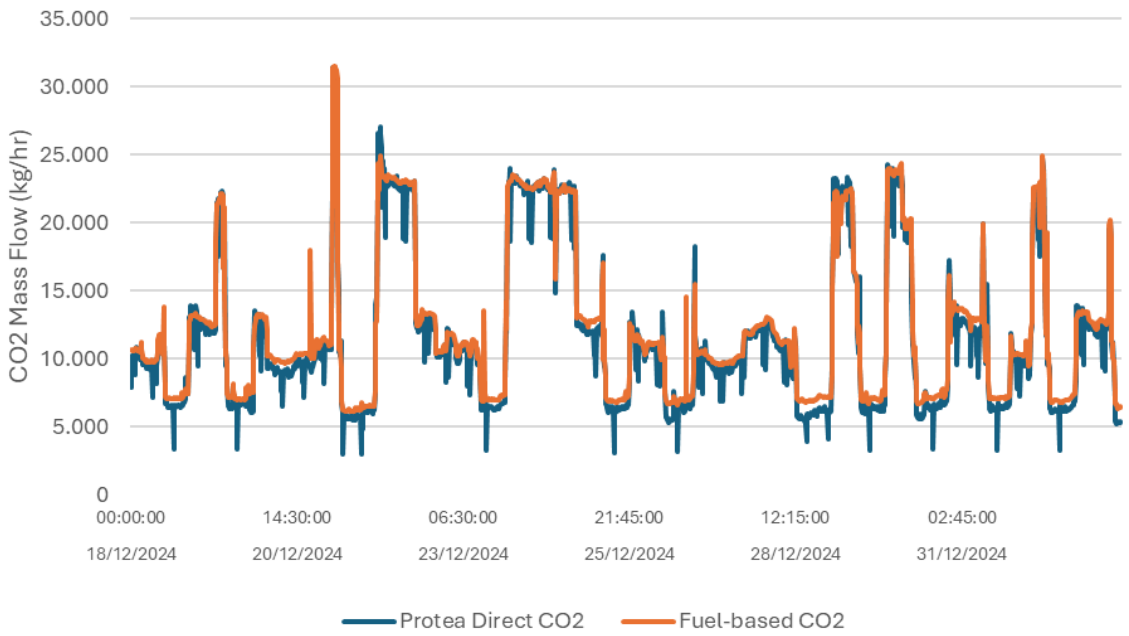

Fig.6: CO_2 Mass flow comparsion (kg/hr)

The scatter plot below illustrates the trendline for CO_2 mass flow for the Vessel, presented in kilograms per hour, comparing both direct CO_2 emissions and fuel-based calculations. The R^2 value (0.9732) shows an excellent correlation between both the direct and fuel-based calculations for mass flow of CO_2 for the 16-day period.

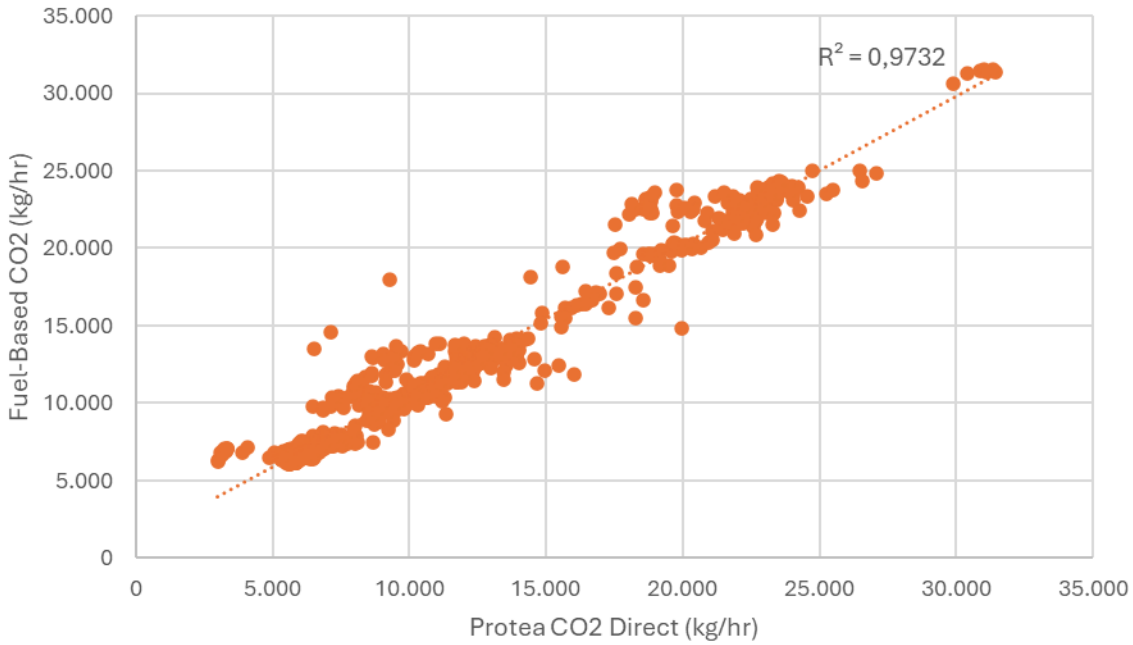

Fig.7: CO_2 mass flow comparison (kg/hr)

5.2. Comparative Data from Third Monitoring Method (load-based calculation)

The third method used for comparison against direct measurement was an engine-load based calculation. This approach estimates CO_2 emissions based on the real-time engine active power (kw) using a line fit equation. The relationship between load and emission rate is derived from the engine bed test report specific to the engine's make and model.

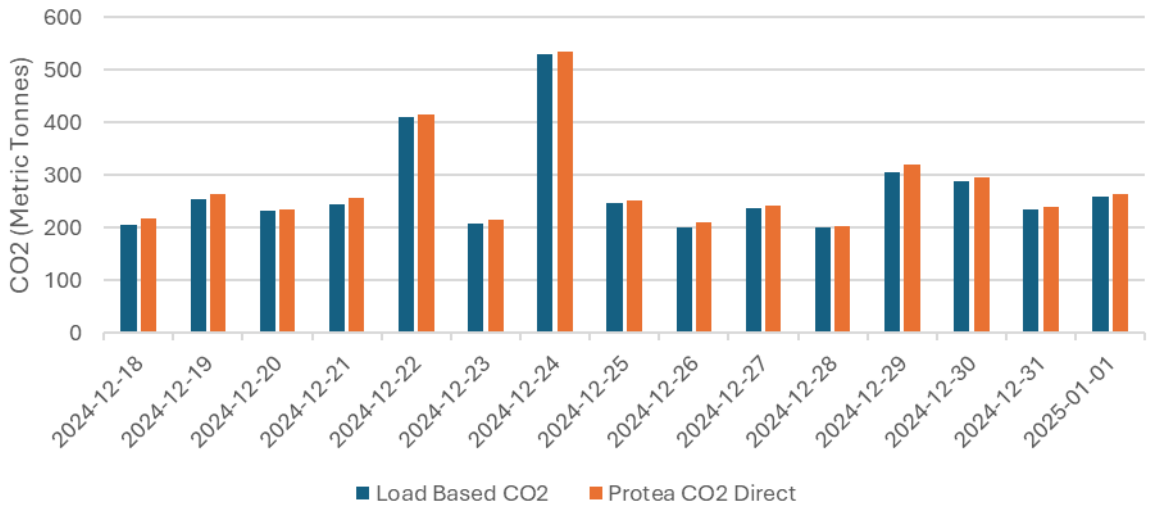

Fig.8: Total mass CO_2 emission per day (MT)

Fig.8 illustrates the daily CO_2 emissions for the vessel, combining the CO_2 emissions from all running engines, presented in metric tons per day, comparing both direct CO_2 emissions and load-based calculations. The scatter plot below illustrates the trendline for daily CO_2 emissions for the vessel, presented in metric tons per day, comparing both direct CO_2 emissions and fuel-based calculations.

The R^2 value (0.9984) shows an excellent correlation between both the direct and Load-based calculations for daily Mass Emissions of CO_2 for the 16-day period.

Fig.9 illustrates the CO_2 mass flow for the vessel, combining the CO_2 emissions from all running engines, presented in kilograms per hour (15 min average), comparing both direct CO_2 emissions and load-based calculations.

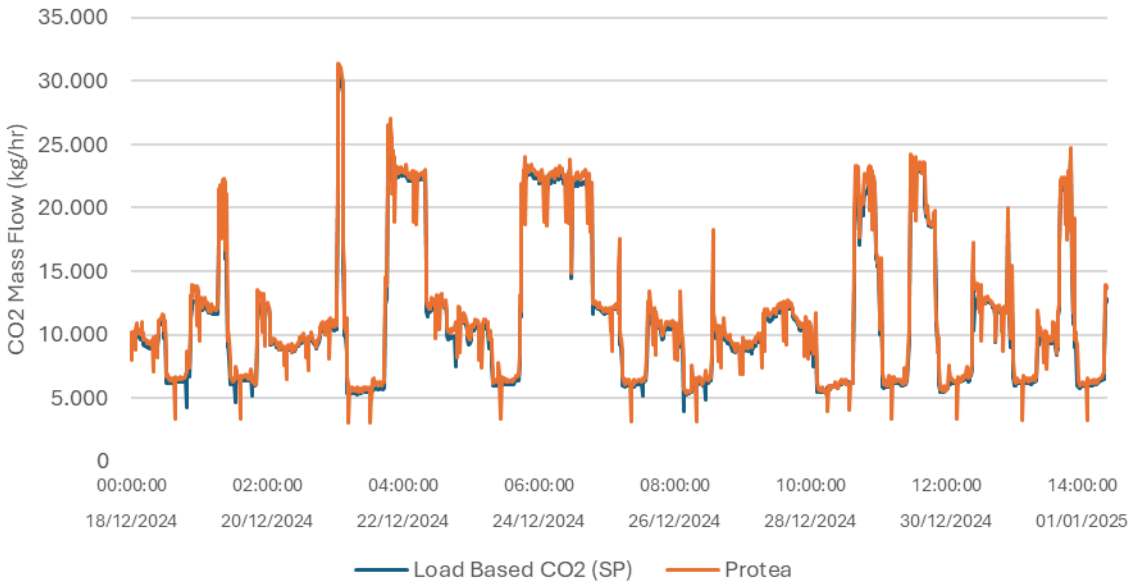

Fig.9: CO_2 mass flow comparison (kg/hr)

Fig.10 illustrates the trendline for CO_2 mass flow for the vessel, presented in kg/hr, comparing both direct CO_2 emissions and load-based calculations. The R^2 value (0.9776) shows an excellent correlation between both the direct and fuel-based calculations for mass flow of CO_2 for the 16-day period.

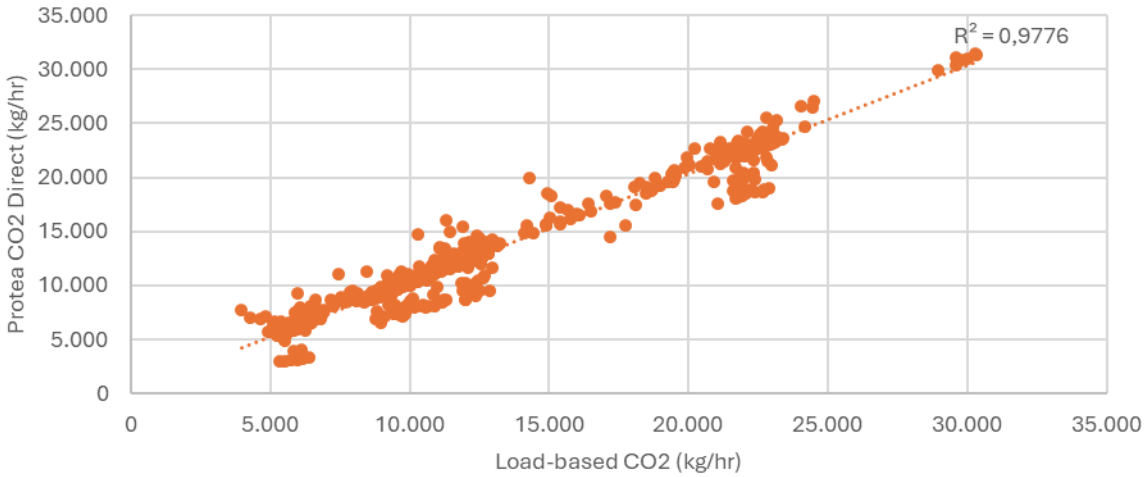

Fig.10: CO_2 mass flow comparison (kg/hr)

5.3. Evaluation and interpretation of results

Over the 16-day period since the visit to the vessel, the CO_2 mass emission data has demonstrated a strong correlation (greater than 95%) between the direct method D, the fuel-based calculated ethod C and the load-based calculated method. This correlation is observed in both the total daily emissions (measured in metric tons per day) and the trended 15-minute averages (measured in kg/hr).

Considering that this data represents the combined emissions from all five main engines (excluding Engine 3, which was inoperative), the results are robust and significant.

Notably, the direct measurement method recorded a daily average 3.5% lower than fuel-based estimates. This suggests that relying on Method C for EU ETS could lead to an overestimation of CO_2 emissions. This may be due to the fact fuel-based estimates assume complete combustion of the available hydrocarbons into CO_2. The combustion efficiency of a marine diesel engine typically ranges from 95% to 98%, *Zhou et al. (2022),* depending on engine design, operating conditions, and fuel quality. While marine diesel engines are highly efficient in converting fuel energy into useful work, not all hydrocarbons are fully oxidised to CO_2. Some incomplete combustion products, such as carbon monoxide (CO), unburned hydrocarbons (HC), and particulate matter (PM), *Lapuerta et al. (2002),* are always present in exhaust emissions.

6. Conclusion

The comparative analysis of CO_2 emissions data for the vessel demonstrates a strong alignment between the direct measurement method (Method D), the fuel-based calculation method (Method C), and the load-based calculation method. Over the 16-day monitoring period, the correlation between direct measurements and the calculated methods exceeded 95%, with R^2 values of 0.993 for the fuel-based method and 0.9984 for the load-based method in daily mass emissions (tons per day). These high correlation values confirm the reliability of direct measurement for quantifying CO_2 emissions.

The results are significant for compliance, performance evaluation, and reporting under frameworks such as the Energy Efficiency Design Index (EEDI).

The primary limitation of this study is the relatively short data collection period of 16 days, which may not fully capture long-term operational variations, or maintenance-related influences on CO_2 emissions. Additionally, the study is limited to five engines from a single vessel, restricting the generalisability of the findings to a broader fleet or different engine configurations. Variability in operational profiles, fuel quality, and external environmental factors such as sea state and weather conditions could introduce uncertainties that may not be fully accounted for within this dataset. Moreover, discrepancies between direct measurements and calculated emissions may arise from assumptions and simplifications inherent in the calculation method, including reliance on engine test bed data that may not fully reflect real-world performance. Instrumentation accuracy, and potential calibration errors in direct measurements also present sources of uncertainty.

The use of direct CO_2 measurement via gas analysers offers several advantages over traditional calculation-based methods. One of the primary benefits is real-time measurement, allowing for immediate data acquisition and analysis without the need for post-processing or estimations based on fuel consumption. This enables faster decision-making in emissions monitoring and compliance reporting. Additionally, direct emissions monitoring provides a more representative measurement when fuel additives or carbon capture abatement equipment are installed, as these technologies can alter the relationship between fuel consumption and actual emissions. In such cases, fuel-based calculations become obsolete, as they do not account for post-combustion CO_2 reductions or changes in emission composition.

Additionally, gas analysers can simultaneously measure multiple gases, including carbon monoxide (CO), nitrogen oxides (NO_x), methane (CH_4), and sulphur dioxide (SO_2). This multi-gas capability provides significant operational and regulatory benefits:

- Methane Slip Monitoring: In dual-fuel and gas engines, unburned methane emissions (methane slip) are a growing concern due to methane's high global warming potential. Real-time CH_4 monitoring allows operators to assess and optimise combustion efficiency to minimise emissions, *ICCT (2020)*.

- Engine Maintenance and Diagnostics: NO_x and CO measurements provide valuable insights into combustion efficiency and engine health. Increased CO emissions may indicate incomplete combustion, while NO_x levels can be used to assess engine tuning and compliance with IMO Tier III or other regional regulations.
- Fuel Quality Assessment: SO_2 emissions are directly linked to the sulphur content of the fuel used. Continuous monitoring of SO_2 can help verify compliance with MARPOL Annex VI sulphur limits and detect fuel quality issues that may affect engine performance or emissions control systems, *LR (2023)*.

By integrating direct measurement technology, vessel operators can enhance emissions reporting accuracy, optimise engine performance, and ensure compliance with evolving environmental regulations.

Acknowledgements

We extend our gratitude to the team at SailPlan for their invaluable assistance and support throughout this study. Their platform and data were essential in making this research possible.

References

EU (2015), *Regulation (EU) 2015/757 on the Monitoring, Reporting, and Verification of CO_2 emissions from ships*, European Commission, eur-lex.europa.eu

ICCT (2020), *Methane Slip from LNG Ships: Issues and Mitigation Strategies*, https://theicct.org

LAPUERTA, M.; ARMAS, O.; BALLESTEROS, R. (2002), *Diesel Particle Size Distribution Estimation from Digital Image Analysis*, Aerosol Science and Technology 36(11), pp.1140-1151

LR (2023), *Understanding Emissions Monitoring and Compliance for the Maritime Industry*, Lloyd's Register, London, https://www.lr.org

ZHOU, S.; ZHOU, Y.; WANG, Y. (2022), *Combustion and Emission Characteristics of Marine Diesel Engines Using Alternative Fuels: A Review*, Applied Energy 310

Real Vessel Data Challenge: A First-of-a-Kind Workshop on Modeling, Insights and Actionable Outcome

Vasileios Tsarsitalidis, ErmaTech, Athens/Greece, V.Tsarsitalidis@ermafirst.com
Dmitry Ponkratov, Siemens, London/UK, Dmitry.Ponkratov@siemens.com
Nikolaos Tsoulakos, Laskaridis Shipping, Athens/Greece, Tsoulakos@Laskaridis.com

Abstract

The "Real Vessel Data Challenge" initiative is an effort to establish a benchmark for evaluating modeling capabilities among vendors of maritime systems. This workshop challenges participants to analyze real-world vessel data, focusing on tasks such as developing baseline models, estimating fouling effects, and assessing data quality. By providing standardized datasets and encouraging collaborative analysis, the challenge aims to foster innovation and knowledge sharing in the maritime industry. The paper outlines the initiative's objectives, structure, expected outcomes, and milestones, emphasizing its potential to enhance decision-making tools for shipowners and improve methodologies for system vendors.

1. Introduction

Long-term monitoring data has become popular since ISO 19030 was introduced, while even the most reluctant shipowners have installed torque meters after ShaPoLi and practically all are collecting data. Although the ISO is a good start, there is no clear and agreed procedure on how to post-process the data to get meaningful, detailed results which could be transformed into a practical decision-making process, especially in realistic conditions when the data do not have ideal quality and/or distribution. A lot of companies offer long-term monitoring analysis, but there is a wide variety of challenges (i.e. data quality, operational profile, weather effects etc.) and a variety of different needs (i.e. on time hull cleaning, predictive maintenance, impact of ESDs, routing, model predictive control etc.), so it is not necessarily clear how it can tangibly and measurably help shipowners. However, the post-processing of this collected data presents a formidable challenge - one that is not just technical but also multifaceted.

Ship performance teams encounter a variety of issues when dealing with long-term monitoring data: inconsistencies in quality, gaps in datasets, and diverse analytical needs ranging from predictive maintenance to routing decisions. These challenges make it difficult for companies to identify the most effective solutions for their specific requirements. Recognizing this gap, the Real Vessel Data Challenge emerges as a response.

This workshop offers a platform where participants can analyze standardized datasets derived from real vessel operations. The dataset provided includes ISO 19030-compatible data along with ship particulars and event labels from a 76000 tdw Bulk Carrier inviting researchers, engineers, and analysts to explore various aspects of maritime performance. Participants will be tasked with generating baseline models for both clean and current conditions, estimating fouling effects, and critically assessing the quality of the collected data.

Beyond its technical objectives, this challenge fosters a collaborative environment that encourages knowledge sharing among maritime professionals. By providing a forum for diverse methodologies and approaches, it promotes innovation and cross-fertilization of ideas within the industry. The event not only addresses current challenges but also paves the way for future advancements in maritime data analysis.

2. Workshop Objectives

The workshop is designed as an inclusive forum for maritime professionals, researchers, and analysts

from diverse backgrounds to collaborate on pressing challenges in marine data analysis. The objectives of this initiative are broad and multifaceted, aiming not only to address specific research questions but also to foster a sustainable community of practice.

1. Promote Cross-Disciplinary Collaboration: Bring together experts from various fields such as data science, engineering, economics, and policy-making to tackle complex maritime issues collectively.
2. Enhance Research Capacity: Provide researchers with access to unique datasets, and a collaborative platform to conduct high-quality studies on maritime sustainability and safety.
3. Support Open Science Practices: Encourage transparency by sharing datasets, methodologies, and results publicly through an online repository, fostering reproducibility and trust among participants.
4. Foster Innovation in Data Analysis: Offer opportunities for participants to explore new methods and tools for analyzing marine data, addressing gaps in current methodologies.
5. Encourage Peer Learning and Networking: Create a space for knowledge exchange where professionals can share their expertise, learn from others' experiences, and build valuable professional networks.
6. Contribute to Policy Development: Use insights gained from the analysis to inform policy decisions related to maritime safety, environmental regulations, and sustainable practices.
7. Recognize Excellence in Research: Highlight outstanding contributions through awards or recognitions, motivating participants to produce high-quality work.
8. Ensure Ethical Data Usage: Establish clear guidelines for data use to protect confidentiality and ensure responsible sharing among participants.
9. Provide Accessible Resources: Compile a repository of datasets, tools, and detailed analysis reports accessible to future projects, serving as an enduring resource for the field.
10. Encourage Continuous Improvement: Gather feedback post-event to refine subsequent iterations, ensuring each challenge builds on previous successes and lessons learned.
11. Align with Global Initiatives: Integrate findings into broader global efforts in marine conservation and sustainability, contributing to a larger movement towards responsible maritime practices.
12. Facilitate Open Dialogue on Challenges: Create a space for open discussions on encountered obstacles, fostering collective problem-solving and identifying areas needing improvement in methodologies.
13. Ensure Long-Term Accessibility: Archive all materials on a dedicated website for ongoing accessibility and utility post-event.
14. Encourage Feedback for Improvement: Continuously seek participant feedback to enhance the challenge's design and outcomes, ensuring each iteration is better than the last.

By encompassing these objectives, the workshop aims not only to address current challenges in marine data analysis but also to build a lasting community committed to advancing maritime research and sustainability.

3. Challenge Details

For the first installment of this challenge, the choice was made to test the modeling capabilities of the participants for one vessel with relatively good quality of data. More challenging data, and/or more diverse sources that would test the generalization capabilities, will be discussed in future workshops, after evaluation of “simple” capabilities is clarified and established.

Real time (per minute) data of approximately one year will be shared in the form of a csv file. These data will include the following metrics: Draft, Trim, Speed (GPS and Log), Power, RPM, Torque, Turbocharger RPM, Fuel Consumption, and weather data. Along with these data, Daily (noon Report) data will be shared, while ship particulars and sea trials and shop test data will also be shared after anonymization. Cleaning events will also be shared. Based on these data the participants will be required to:

1. Generate baseline models for the vessel in clean condition and current condition: Participants will utilize the datasets provided, to create two baseline models: one representing the vessel in its clean condition and another reflecting its current (latest) operational state. The resulting models will be expressed in the form of Speed-Power Curves, for different drafts, in a predefined (template) format, which will be shared for ease of comparison.
2. Estimate fouling effects in terms of added power and/or speed loss: This involves analyzing how fouling accumulates by assessing the increase in resistance or required power to maintain speed, as well as any potential speed loss. These estimates will be delivered as extra columns to the dataset given
3. Simulate current conditions: Provide estimates of Power and/or Consumption, for periods when these data are missing, when possible.
4. Methodology Comparison: The challenge provides a platform for comparing different modeling approaches, allowing participants to showcase their tools and methodologies effectively. Participants will be allowed to make multiple entries, if they desire, to showcase the capabilities and particularities of different methods / algorithms.
5. Optionally attempt to distinguish hull from propeller fouling: Participants may explore differentiating between fouling effects on the hull and those on the propeller. This optional task adds depth by pushing the methodologies to attempt differentiating between contributors using latent effects.
6. Produce data quality/uncertainty reports: This requires evaluating the consistency, cleanliness, and completeness of the provided data. Participants must identify any gaps or anomalies and quantify uncertainties inherent in their models. Clear documentation here ensures transparency and trust in the analysis results.
7. Open Discussion: Where the participants will be able to comment and/or showcase deeper insights they are willing to share.

By addressing these tasks, participants will share insights into how operational conditions evolve over time and the effectiveness of various mitigation strategies for fouling-related performance issues.

4. Evaluation Criteria / Scoring

To ensure fairness and comparability, the following measurable criteria will be used:

1. Accuracy: Measured using Mean Absolute Percentage Error (MAPE) compared against an undisclosed baseline model generated through Computational Fluid Dynamics (CFD), calibrated using towing tank report.
2. Trend Consistency: Assessed by evaluating how well models maintain consistency over time, particularly during periods of operational changes or environmental variability.
3. Robustness: Tested by exposing models to data quality issues such as outliers and missing values, assessing their ability to provide reliable insights.

Participants will also be encouraged to propose alternative metrics for evaluation during the workshop discussions, ensuring that the challenge remains a dynamic platform for continuous improvement.

5. Milestones Description

Release of Data (May 2025):

- The dataset comprising high-frequency measurements from a 76,000 DWT bulk carrier over a year will be made available to participants via a secure online platform or physical media. (TBA)
- Participants are expected to download the dataset and begin preprocessing it for analysis.

Submission Deadline for Analyses and Reports (December 2025):

- Participants will have from May 2025 until December 2025 to analyze the provided data and submit their findings. This period allows ample time for thorough analysis, model development, and reporting.
- Submissions are expected in a standardized format to ensure consistency across participants and easy comparison.

Compiling Workshop Results (February 2026):

- After the submission deadline, all received analyses and reports will be reviewed and compiled into a comprehensive report by an independent panel of experts (TBD).
- This compilation will summarize key findings, evaluate methodologies used, assess data quality and uncertainty metrics, and provide actionable insights for stakeholders in the maritime industry.

Workshop Presentation (March 2026):

- A workshop will be held in the next HullPIC to present the compiled results and discuss with participants and guests.
- This event will foster collaboration and provide a platform for open discussion on challenges faced during data analysis, potential improvements in methodologies, and future directions.

Publication of Final Report (April 2026):

- The final report will be published online, accessible to all registered participants and industry stakeholders. It will serve as a benchmark document highlighting the achievements of the challenge.
- Based on the level of interest, discussion and outcomes of this first challenge, the next challenges will be defined.

4. Considerations

- Feedback Incorporation: Workshops' feedback will be used to enhance the challenge's effectiveness, ensuring continuous improvement in future iterations. At least one meeting will be arranged, to openly discuss issues or concerns before the submission of analyses.
- Participant Diversity: In order to attract a diverse range of participants from various backgrounds and expertise levels, which will enrich discussions and lead to comprehensive insights, participation and access to the datasets and results will be kept free and open.
- Evaluation Criteria: Clear criteria for evaluating models and reports will ensure fair assessment based on consistent standards. An open forum for the discussion and establishment of fair and unbiased criteria will be established and kept open to all.
- Communication Channels: Establishing forums or discussion boards will facilitate collaboration, allowing participants to share ideas and seek clarification throughout the challenge period. The specific platform(s) (i.e. website, discord server etc.) will be announced soon.

Acknowledgements

The Real Vessel Data Challenge owes its gratitude to Laskaridis Shipping for their generous support. Special thanks are extended to Nikos Tsoulakos and Adm. George Christopoulos for their invaluable contribution and their ongoing commitment to advancing maritime technology. Last but not least many thanks are to be extended to Volker Bertram, for his support, patience and flexibility, that allowed the room for this announcement.

Sea Trials Analysis Joint Industry Project: Past, Present & Future

Gijs D. Struijk, MARIN, Wageningen/the Netherlands, g.d.struijk@marin.nl
Rob Grin, MARIN, Wageningen/the Netherlands, r.grin@marin.nl

Abstract

The successful development of speed/power trial methodology in the Sea Trials Analysis Joint Industry Project (STA JIP) in 2004 - 2006 led to adaptation in ITTC, IMO and ISO standards. As such the much-needed harmonisation of the methodology was achieved within the industry. This paper offers the background of the speed/power trial standard, treats the current state of affairs and presents the future work planned in the follow-up project: STA-2 JIP. The aim of this project is to achieve a more accurate and reliable determination of the actual, full-scale speed/power performance of ships, both from speed trials and in-service measurements. Thereto, the project aims to improve the current protocol for speed/power trials and secondly to develop an in-service performance protocol. Within the project, uncertainties associated with in-service performance will be charted, offering a starting point for defining the project's priorities. Improvements and new developments of different correction methods are foreseen, as well as the development of a new in-service test protocol.

1. Introduction

The determination of in-service performance of ships continues to be an important aspect, both in acceptance of newbuilds as well as in evaluating existing operations. Prior to each ship's delivery, speed/power trials are conducted to verify contractual agreements on performance between the owner and the yard, as well as to verify compliance to IMO MEPC EEDI regulations. While the performance is to be evaluated in ideal conditions (no wind, waves or current, etc.), trials are often done in non-ideal conditions due to time constrains. Corrections for the effect of wind, waves, current and other effects are therefore needed to arrive at the performance level in ideal conditions.

Once the vessel enters service, its speed, power, fuel consumption, etc. are nowadays often logged by a performance monitoring system and used for reporting total consumption levels. Also here, it is of interest to evaluate not only total consumption, but to zoom in on the power requirement of the ship in different operational scenarios and compare them to predictions made before. This promises to offer validation of prediction techniques and could lead to improved understanding of phenomena at play in real operational conditions. This comes with its own challenges however. While one can choose to only select voyage segments with very benign weather conditions—getting rid of the associated uncertainties of weather effects on the performance—the main remaining uncertainty is the speed through water.

While during a speed/power trial reciprocal runs are performed to obtain the speed through water to an acceptable accuracy, no owner is willing to spend half a day on a commercial voyage to perform such runs. So, while a lot of challenges are similar in trials and operations, the operational constraints add a specific challenge in obtaining the speed through water during normal commercial operations.

2. Past & present of speed/power trials

In the past, many different speed/power trial protocols were developed. For instance: *Taniguchi-Tamura (1966), BSRA (1964,1978), Jinnaka (1982), SNAME (1989), Schmiechen (1991), Kracht (1999).* In 2002 ISO published the first edition of ISO15016, using analysis method based on the propeller open water diagram and a wide choice of wave added resistance correction methods. The experience with this (and previous) method were adverse, as analysed performance levels were often not confirmed in operation.

Identifying the need for improvement, MARIN, together with industry partners, initiated the Sea Trial Analysis Joint Industry Project (STA-JIP) in 2004 with the objective of developing reliable, practical

and transparent guidelines for analysing speed/power trials. Both the trial procedures and methods for analysis were on the agenda for improvement. Work was done by extensive tank and wind tunnel testing and CFD to improve the corrections for wind, wave and shallow water, as well as the Direct Power Method to translate everything in corrections on power. Further, focus was given on the issue of translating ballast draught results to (contract) design draught performance.

With the STA Recommended Practice for Speed Trials published in 2006 as international industry standard. After thorough review the ITTC adopted the methodology in their 2012 recommended procedures and guidelines. These and the later 2014 version were adopted by MEPC for EEDI.

Meanwhile, the ISO revised their ISO15016 to also follow the same methodology. Both STA-Group and ITTC participated in the ISO Working Group to contribute available methods and validation data. The 'iterative method' was introduced next to the existing 'Mean of Means' method to eliminate the effect of current. In 2015 MEPC adopted the ISO15016:2015 for EEDI. Meanwhile, the STA-Group had developed and released STAIMO software as freeware (https://staimo.com). This software is still maintained and available for use by yards, owners, trial specialists and verifiers worldwide.

Over the last decade since, incremental progress has been made by both the ITTC and ISO working groups. The SNNM method, *Liu and Papanikolaou (2020)*, for correction of waves was validated by the ITTC. The Raven Shallow Water Method, *Raven (2022)*, replaced the Lackenby method, *Lackenby (1963)*. The boundary layer exponent of 1/9 is adopted for height conversions of true wind. The ISO15016 was updated in 2025, after a three-year revision process conducted by TC8/SC6/WG17 comprising more than 40 international experts. The update includes endorsements for modern measurement techniques (wave buoy, wind LiDAR, ultrasonic anemometers) as high-fidelity inputs needed for the updated correction methods.

Although steady progress is shown the last decade, the working groups and committees do not have the possibility to conduct new research, merely review the status quo in literature. Furthermore, it is recognised that there exists room for improvement in bringing today's methods to a higher standard using the present-day knowledge.

3. Proposed project: STA-2

With the above observations, MARIN is taking the initiative to start a new phase of research in the field of full-scale ship performance and proposes the STA-2 JIP. The overall objective of the proposed project is to:

Aim for more accurate and reliable determination of the actual, full-scale speed/power performance of ships, both from speed/power trials and in-service performance measurements.

Thereto, the project will aim at the following objectives:

- Determine uncertainty of the current standard for contract speed/power trials, and if beyond target uncertainty, reduce uncertainty by focusing on the items which contribute most to the uncertainty
- Evaluate state-of-the-art measurement techniques, including drafting guidelines and best-practices for electrical power measurements for cases where mechanical power measurement is not possible
- Develop accurate, reliable and easy to use correction methods for wind, waves and current
- Update and improve the contract speed/power trial protocol
- Develop an in-service performance test protocol
- Validate the above developments in measurement techniques, correction methods and test protocols by conducting dedicated high-fidelity test campaigns

- Deliver free software for the analysis of contract speed/power trials
- Actively promote and support adaptation of new protocols by ISO, IMO and ITTC

The project will work on both improving the method for contract speed/power trials and developing an in-service test protocol for evaluating the performance of ships operating with cargo on a schedule. Both approaches share correction methods that will be updated within the project as well, Fig.1.

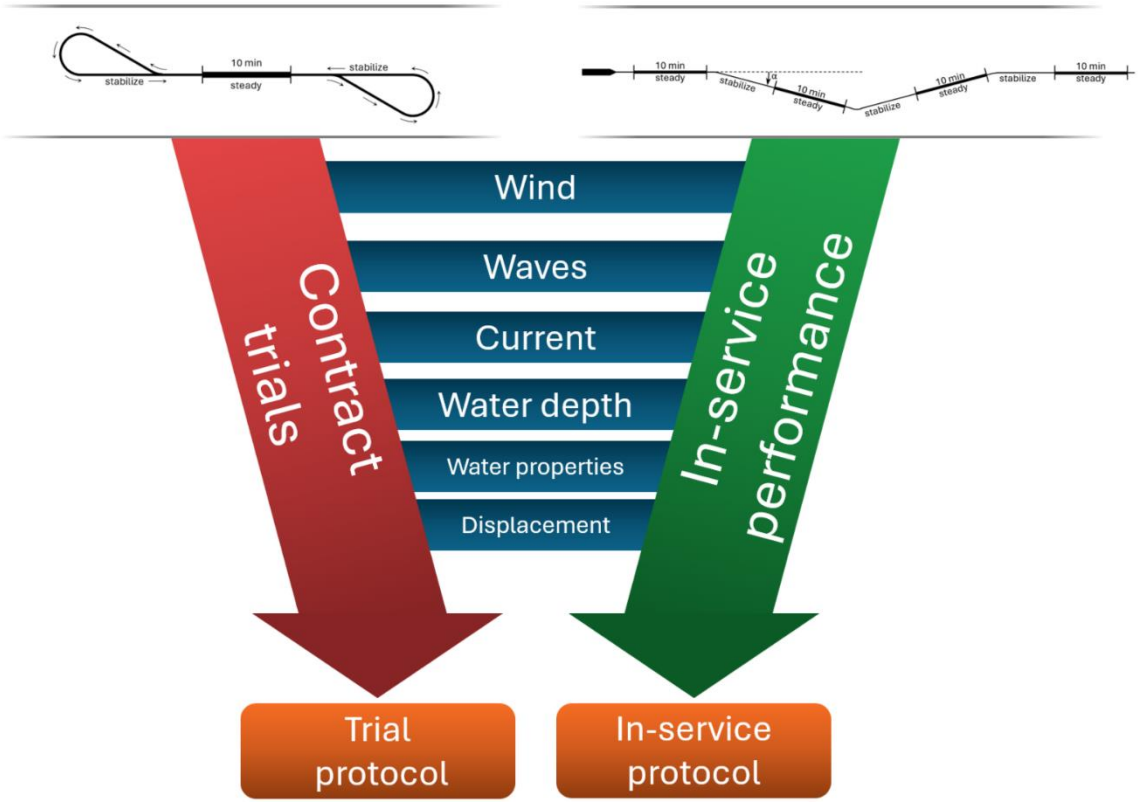

Fig.1: Project scope for both contract and in-service protocol and their shared correction methods, leading to two test protocols

The project will be divided into the following five work packages:

WP1	Aspects of uncertainty
WP2	Measurement techniques and test protocols
WP3	Correction methods
WP4	Validation trial campaigns
WP5	Procedures, implementation & dissemination

The following sections discuss each work package.

3.1. WP1 - Aspects of uncertainty

Within the first work package of the project the components contributing to the uncertainty in speed/power trials and in-service performance test results will be identified. From there, priority can be given to the aspects that contribute most to the uncertainty. Te results of this work will give input and priorities for the other work packages. In addition, a feasibility study will be performed to include (standardised) uncertainty analysis in the contract and in-service protocols.

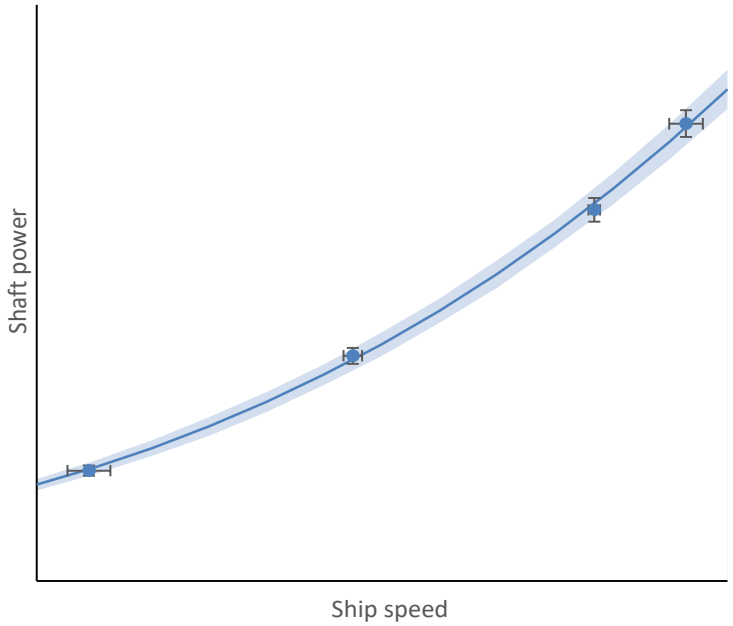

Fig.2: Example of uncertainty in a speed-power trial result

3.2. WP2 - Measurement techniques and test protocols

Besides measuring the correct things at high precision and correcting results to ideal conditions as best we can, the way we conduct any tests contributes greatly to the accuracy and usefulness of the results. Sometimes, trials that were not conducted correctly provided unusable results. For instance, above weather limits, no proper steady-states were achieved before staring a measurement run, high current fluctuations, local effects within the runs, etc.

Contract trials protocol

For contract trials, it is important to have a practical protocol that is both easy to carry out correctly and well-described so as to not contain ambiguities. The protocol will be further developed with clearer descriptions and less ambiguities. Where possible, definitions will be developed on matters such as:

- when the vessel achieves steady state,
- guidance on lengths of approach runs,
- how to measure and calculate the ship's loading condition,
- which heading to choose for the runs (wind, wave).

Furthermore, we expect to investigate the requirement to return to track in a reciprocal run, and if possible, arrive at a set of requirements under which one can sail in opposite heading without returning to track, Fig.3.

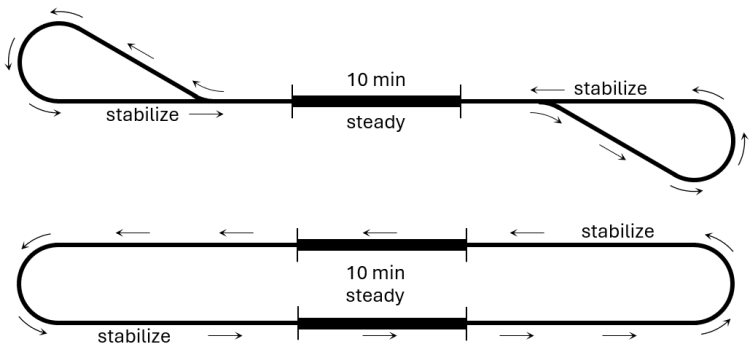

Fig.3: Reciprocal runs: using Williamson turns (upper) or simple 'paperclip' track (lower)

In-service performance protocol

To be able to derive a good baseline performance from an in-service measurement, care needs to be taken to limit uncertainties on the results arising from both weather conditions and measurement accuracy. While taking into account that the ship's schedule is not affected by performing dedicated tests.

Besides influences from weather, we can identify the ship's speed through water (STW) as one of the dominant contributors to the uncertainty. Although Doppler or electromagnetic speed logs are fitted for this purpose, it has been observed they are too unreliable for the purpose of evaluating a vessel's speed/power performance, *Hasselaar (2012).*

To overcome this shortcoming in available measurement techniques, a test protocol will be developed from which the vessel's STW can be derived in a similar fashion as by reciprocal runs, but without the need to hamper the schedule by performing a return run. The proposed protocol uses steady runs at heading deviations much smaller than 180°, resulting in a zig-zag patterned track, Fig.4, from which the current vector, and consequently STW, can be derived by vector calculus. The expectation for this protocol is that it will only yield usable results in very favourable weather conditions, thus needing more restrictive requirements on limiting wind speed and wave height. Within this WP, supported by WP4's validation campaigns, the conditions and limits for application will be developed.

The final deliverable for this task will be a written protocol with which ship operators can instruct their crews to incorporate these tests in their transits to allow regular testing of their ship's in-service performance.

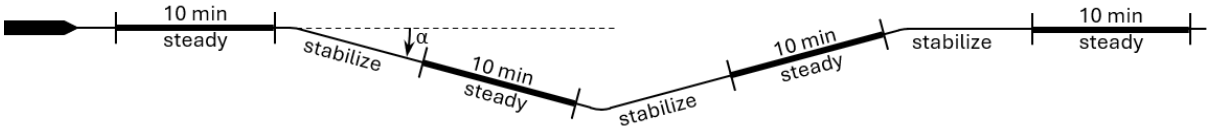

Fig.4: Proposed in-service protocol using a zig-zag pattern

Measurement techniques

Where possible and deemed promising, tasks on evaluating the effectiveness and accuracy of measurement techniques will be carried out. Comparisons of new technology to old, or high-fidelity to low-fidelity approaches can be made by incorporating multiple measurement techniques in the validation campaigns of WP4.

Electrical power measurements

It is expected that future propulsion arrangements will incorporate more 'integrated propulsion systems' such as thrusters and pods where access to a driving shaft for mechanical power measurement by strain gauge system is limited or impossible/impractical. For such cases, one needs to rely on other means of obtaining the propulsion power, such as electrical power measurements. Experience has shown however that this often does not align well with the actual mechanical power output to the propeller. This issue needs addressing to make the protocol future proof.

It is foreseen that this task will deliver guidelines/best-practices on where and how to measure electrical power to a propulsor.

3.3. WP3 - Correction methods

In this work package, the correction methods will be evaluated and improved, depending on the priorities coming from WP1.

Wind

Together with waves, the effect of wind is typically one of the bigger corrections to arrive at ideal

conditions. Given that the relative (apparent) wind speed and direction are properly measured (WP2), the correction for wind consists of:

- Wind averaging
- Correction for the position of the anemometer
- Calculation of wind added resistance using wind coefficients

For each of the three steps, there is potential for improvement. The need for wind averaging can be mitigated once we can arrive at undisturbed measurement location or technique. Regarding the height correction, in the current standard, ISO15016:2025, a 1/9th profile is used. However, recent research from both on board and stationary wind profile measurements over sea suggests much steeper profiles, *Dhomé (2020), Hasager et al. (2013).* This needs to be evaluated for the case of speed/power trial situations.

Waves

As wind, waves is often one of the dominant corrections. Within ISO15016:2025 the following three correction methods are allowed: transfer functions from model tests, SNNM and STAWAVE-1, *Grin (2014)*. From several studies it is shown that all three methods have their own pros and cons. The starting point within this task is to evaluate the presently available approaches for a wide range of ship types and identify shortcomings and areas for improvement.

In trial conditions, the wavelength is typically short when compared to the ship length. It is therefore important to have an accurate prediction in these conditions. It has already been identified that some of the methods do not perform well in the short-wave region. The left plot in Figure 6 shows an example for the KVLCC2, a 320 m tanker. In 2023 MARIN performed model tests for the ITTC benchmark study (results to be published) in which four test setups were evaluated (grey lines in left-hand plot). When compared to three empirical methods it is shown that results vary considerably. The right-hand plot shows the empirical methods in ballast condition (no test results available).

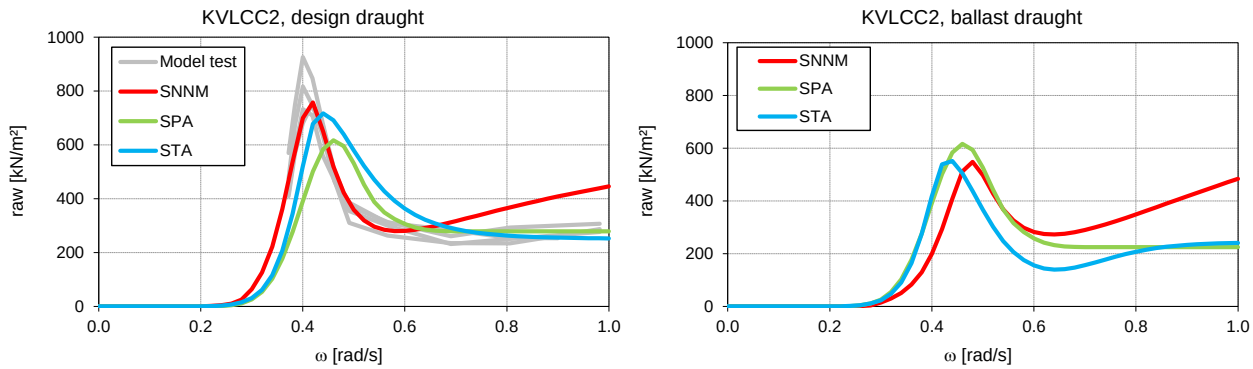

Fig.5: Transfer function of wave added resistance for the KVLCC2 at design draught in head waves (left plot) and KVLCC2 at ballast draft (right plot)

Within this task, a new (semi-)empirical method will be developed that gives a good prediction in both long and short waves, for all wave directions, and for all displacement type hull shapes. The method should be robust, easy to implement and use, and require as few as possible and readily available input parameters. This task can be a joint effort with interested participants.

The method will be validated with available datasets within MARIN and with limited seakeeping model tests, focusing on short waves and for conditions and ship types in which the dataset is not conclusive. Within the basic scope there is probably sufficient budget to perform tests for two ship types. Furthermore, universities and other institutes will be invited to validate the method with their own dataset, in order to avoid bias and ensure industry wide acceptance.

In the current standard (ISO15016:2025) numerical approaches like CFD are not allowed for wave correction in the ISO procedure, contrary to for instance the wind correction. A feasibility study will be performed if it is possible include this option in future protocols. This includes recommendations for verification and validation of these methods and a blind benchmark.

Current
To arrive at the needed STW from the measured speed over ground by GNSS instruments, the speed trial method uses the double run protocol to obtain the current component in the ship's heading direction. To derive the current component in the ship's direction from this, either the mean of means (MoM) method using sets of four runs per propeller setting or the iterative method can be used. The latter was introduced to enable users to use fewer runs while getting an acceptable result.

In the present standard, the method for iterative current correction can be used with fewer datapoints than strictly necessary, resulting in an underdetermined system of equations. This has raised concerns about the soundness of the method, and will be investigated. If needed, an improved method will be developed.

For obtaining the STW for in-service performance evaluation, the zig-zag run protocol will be developed as described in WP2.

3.4. WP4 - Validation trial campaigns

This work package aims to support the above WP2 and WP3 by carrying out dedicated measurement campaigns on a number of vessels in different scenarios. Ship owners and operators within the project are encouraged to facilitate measurement campaigns on their vessels within this work package.

Validation campaigns are aimed to employ high-fidelity approaches: e.g. using state-of-the-art equipment such as wind LiDAR, wave radar and wave buoys (as well as visual wave observations), anemometers, etc. This way, the resulting data will be of high fidelity as well as offer a verification of lower-fidelity approaches and equipment. Specific to STW validation (in-service protocol, revised iterative method), in-situ high-fidelity current measurements by stationary current measurements are foreseen.

The above-described approach deliberately exceeds the practicality constraints of the target protocols, such that the aimed pragmatic approach of the protocols can be tested. Stated differently: "Will the simple zig-zag protocol deliver STW to sufficient accuracy?" can only be answered when a high-fidelity ground-truth is available for STW or current.

3.5. WP5 - Procedures, implementation & dissemination

Procedures
For the contract trials, an updated trial protocol will be written to incorporate all the project's findings. The goal is to arrive at a clearly written, pragmatic procedure.

For the in-service protocol, the new approach will be written to be fit for implementation with on board crew.

Update trial software (STAIMO)
The current STAIMO software for the analysis of speed/power trials will be modernized and brought into line with the updated trial standard.

Dissemination & adaptation (ITTC, IMO, ISO)
Publications of our progress and findings will be made where deemed effective to inform industry and regulators and facilitate the adaptation of the project's recommendations.

Furthermore, liaison with ITTC, IMO and ISO will be pro-actively undertaken to ensure the project's work is known and reviewed within these bodies, and considered within their future updates of recommendations, procedures, and standards.

3.6. JIP participation

The project initiative has received strong interest from many organisations in the maritime industry worldwide, like ship owners, ship operators, shipyards, research institutes and classification societies.

The work is conducted as a Joint Industry Project (JIP), executed by MARIN. Results and costs are shared with participating organisations. Participants gain exclusive access to project results, software, and other resources through a confidential project website. All findings remain confidential for three years after completion, with any publications communicated in advance to all participants.

The advantages for all participants are to participate in large scale R&D with leverage on costs. All participants could be actively involved in the definition of the final scope of work and learn from the experiences of other participants. The project is currently open to interested parties. For more information or to sign up, please contact the authors at STA-2@marin.nl or visit MARIN's JIP page.

4. Conclusions

The evolution of speed/power trial methodologies through the Sea Trials Analysis Joint Industry Project (STA JIP) has led to significant advancements in standardization, shaping international guidelines such as those of ITTC, IMO, and ISO. While considerable progress has been made, challenges remain in further refining the accuracy and reliability of speed/power performance evaluations, both during contract trials and for in-service performance.

The proposed STA-2 JIP aims to address these challenges by improving existing the trial protocol, developing a standardized in-service performance evaluation method, and enhancing correction techniques for environmental influences. By leveraging state-of-the-art measurement technologies and conducting high-fidelity validation campaigns, the project seeks to reduce uncertainties and ensure practical, implementable solutions for ship operators, yards, and regulators.

Collaboration through this Joint Industry Project offers an opportunity for stakeholders to contribute to and benefit from cutting-edge research, leading to more precise and efficient performance assessments. Ultimately, the advancements from STA-2 JIP will strengthen the industry's ability to evaluate ship efficiency under real-world conditions, supporting sustainability goals and regulatory compliance.

References

BSRA (1978), *Standard Method of Speed Trial Analysis*

DHOMÉ, U.; KUTTENKEULER, J.; SEGALINI, A., (2025), *Observation of the atmospheric boundary layer over the Atlantic and its effects for wind propulsion*, J. Wind Engineering & Industrial Aerodynamics 258

GRIN, R. (2014), *On the Prediction of Wave-added Resistance with Empirical Methods*, J. Ship Production and Design 30/4, pp.1–11

HASAGER, C.B.; STEIN, D.; COURTNEY, M.; PEÑA, A.; MIKKELSEN, T.; STICKLAND, M.; OLDROYD, A. (2013), *Hub Height Ocean Winds over the North Sea Observed by the NORSEWInD Lidar Array: Measuring Techniques, Quality Control and Data Management*, Remote Sensing, pp.4280–4303

HASSELAAR, T.W.F. (2012), *Water speed log research - STW measurement validation based on*

performance data MV Belgian Express, SPA-JIP report 23200-12-TM

ISO (2015), *Ships and marine technology - Guidelines for the assessment of speed and power performance by analysis of speed trial data*, ISO15016:2015

ISO (2025), *Ships and marine technology - Specifications for the assessment of speed and power performance by analysis of speed trial data*, ISO15016:2025, third edition

ITTC (2012), *Speed and Power Trials*, ITTC Recommended Procedures and Guidelines 7.5-04-01-01.2

JINNAKA, T. (1982), *On a method of analysis of ship speed trial results of ships*, WSNAJ, N°. 64

KRACHT, A. (1999), *Evaluation of trial tests*, IWSH '99, Wuhan

LACKENBY, H. (1963), *The effect of shallow water on ship speed*, The shipbuilder and marine engine-builder

LIU, S.; PAPANIKOLAOU, A. (2020), *Regression Analysis of Experimental Data for Added Resistance in Waves of Arbitrary Heading and Development of a Semi-Empirical Formula*, Ocean Eng. 206

RAVEN, H.C. (2022), *A correction method for shallow-water effects on ship speed trials*, MARIN, https://www.marin.nl/en/publications/a-correction-method-for-shallow-water-effects-on-ship-speed-trials

SCHMIECHEN, M. (1991), *The Method of Quasisteady Propulsion and its Trial on Board the Meteor*, VWS Bericht Nr.1184/91

SNAME (1989), *Guide for Sea Trials*, SNAME, Chapter 4.0

STA (2006), *Recommended practice for speed trials*, STA-JIP report 18200-2-TM

TANIGUCHI, K.; TAMURA, K. (1966), *On a New Method of Correction for Wind Resistance Relating to the Analysis of Speed Trial Results*, Report of the Performance Committee, Appendix 11, 11th ITTC, Tokyo

A Study on the Prediction of Hull Cleaning Effects using Deep Neural Network

Beom Jin Park, Korea Research Institute of Ships and Ocean Engineering, Daejeon/Republic of Korea, baracude@netopia.re.kr
Joon-Hyong Lee, Korea Research Institute of Ships and Ocean Engineering, Daejeon/Republic of Korea, joonh.lee@kriso.re.kr
Myoung-Soo Kim, Korea Research Institute of Ships and Ocean Engineering, Daejeon/Republic of Korea, mskim@kriso.re.kr
Donghyun Park, Kyung Hee University, Seoul/Republic of Korea, pdh@khu.ac.kr
Jae-Yoon Jung, Kyung Hee University, Seoul/Republic of Korea, jyjung@khu.ac.kr

Abstract

Recent advances in AI and availability of a ship's operational data makes AI based models to be used in ship performance analysis. Continuing from using DNN (Deep Neural Network) model to predict a ship's performance, this paper presents a study on using DNN model to predict the effects of hull cleaning on a ship's performance. Using operational measurement data during an extended period of operation including multiple hull cleaning, a DNN model is developed to predict fuel consumption of a ship from input variables consisting of ship's speed, external weather condition, number of hull cleanings performed since last drydocking and total anchoring period. The model is applied to ship operation data and the results show possibility for using the model for deciding optimal hull cleaning period.

1. Introduction

Ship operators and owners face difficult situations today from regulatory requirements for preventing greenhouse gases and environmental protection. Current regulations such as CII (Carbon Intensity Index) and FuelEU Maritime require ship operators to meet certain criteria for CO_2 emission, which can be met usually by increasing ship operational efficiency and reducing fuel consumption, unless using alternative fuels.

Hull cleaning has been frequently used and well known to increase ship operational efficiency but there has not been enough study to predict quantitative gain from hull cleaning. If decrease in fuel consumption by increased hull efficiency from hull cleaning can be quantitively predicted with a certain accuracy, it will be possible to perform cost benefit analysis on hull cleaning and decide optimal hull cleaning period.

In this study, DNN-based FOC prediction model is applied to predict fuel consumption after hull cleaning. First, DNN-based FOC prediction model is trained using ship operational data. Then performance degradation during operation and fuel consumption after hull cleaning is predicted with the trained model.

2. DNN-based FOC prediction model

A DNN architecture is used to develop an FOC prediction model. DNNs have been actively used in many studies because they can automatically extract representative features without generating complex handcrafted features, which typically require a considerable amount of expert knowledge, *Tarelko and Rudzki (2020)*, *Anh Tran (2021)*, *Zou et al. (2022)*. Consecutive nonlinear calculations of the DNN by stacking several hidden layers allow large and complex problems to be solved, *Uzair and Jamil (2020)*.

The architecture of the FOC prediction model is shown in Fig.1. The DNN architecture comprises of an input layer, three hidden layers, and an output layer. The layers comprise of several nodes connected with weights to be summed in each node using a nonlinear function, ReLU (Rectified Linear Unit),

Agarap (2018). The last hidden layer is connected to the input layer via a shortcut connection, *He et al. (2015)*, where the inputs are summed to the outputs of the last hidden layer during model training. This allows the model to be optimized more easily as only the residual information, excluding the original information added by the connection, is to be learned.

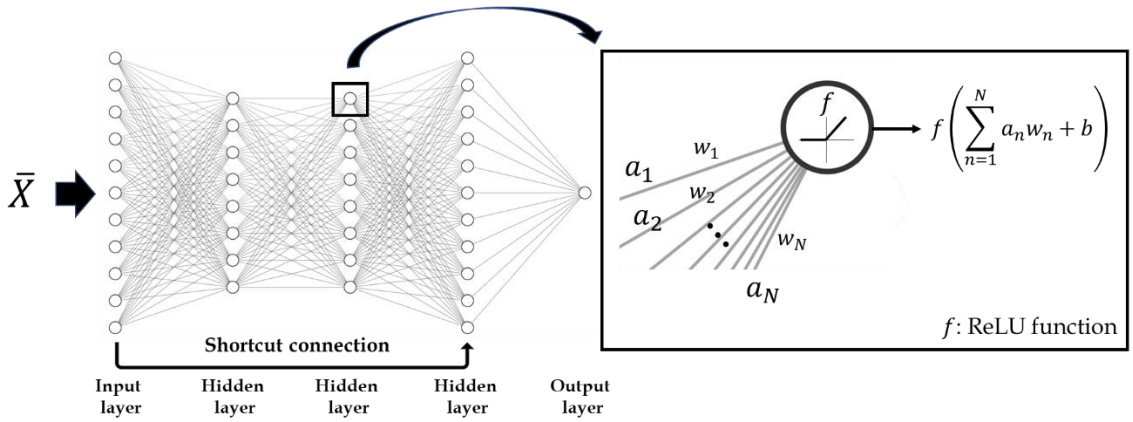

Fig.1: Architecture of DNN-based FOC prediction model

Detailed description of the model and how it was trained ship operation data is already discussed already in *Park et al. (2024)*.

3. Performance degradation prediction

3.1. Prediction model

In order to predict performance degradation, a new feature called CAE (Cumulative Anchoring Effect) is developed, based on the well-known assumption that the degradation of performance due to hull fouling is significantly affected by the length of the anchoring and the water temperature of the anchorage site.

$$CAE_n = (no.of\ anchoring\ days)_n \times (water\ temp.of\ anchoring\ site)_n, \quad (1)$$

where n represent n-th anchoring.

The amount of performance degradation is then estimated as the difference between the predicted FOCs obtained using the input data with the original CAE and initial CAE, as shown in Fig. 2. The FOC prediction model, F, predicts the FOCs in the k-th journey leg, $\hat{y}_k$, using the input features $\bar{X}_k$ including the CAE, which is denoted as A. If the CAE is changed to 0, which implies that the state of the ship returns to the past when no anchoring effects are accumulated, then the prediction model F generates a lower FOC, $\hat{y}'_k$. The percent decrease in the predicted FOCs is quantified as the amount of performance degradation of the k-th journey leg.

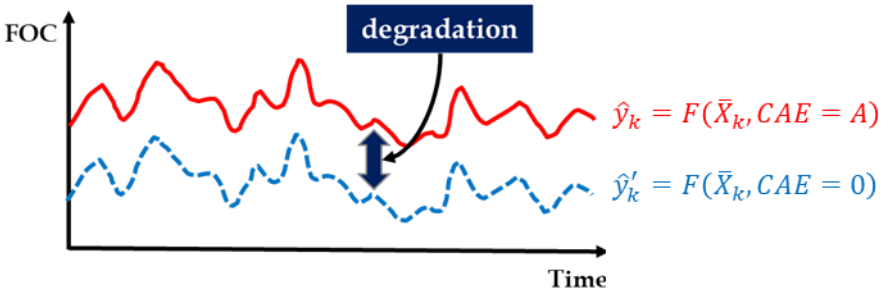

Fig.2: Estimation of ship performance degradation

3.2. Prediction results

Details of prediction results using the prediction model in 3.1 is already discussed in *Park et al. (2024)*. Fig.3 summarizes prediction results. Green trend lines indicate estimated ship operation performance degradation (SOPD), the blue line indicate actual performance degradation. While the trend lines follow general trends, it is not accurate enough to predict performance degradation of each leg of the journey.

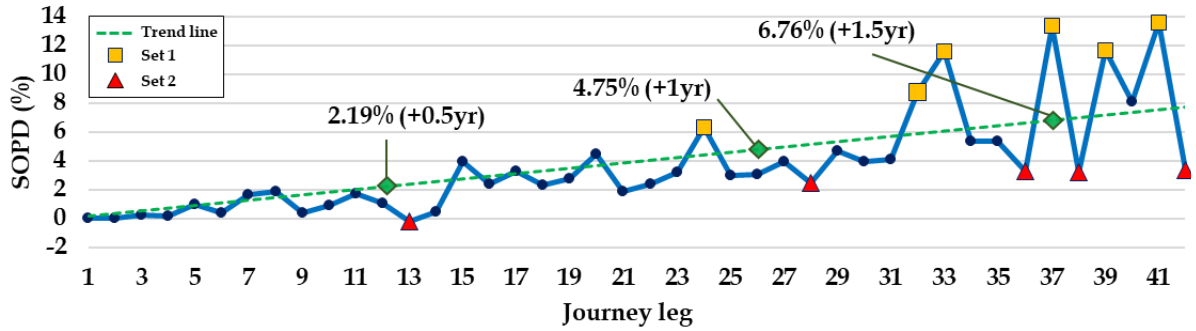

Fig.3: Estimated performance degradations at each journey leg

4. Hull cleaning effects prediction

4.1. Prediction model

For predicting hull cleaning effects, similar concept and performance degradation is applied. Since CAE represents performance degradation from new hull condition, hull cleaning will decrease CAE value. In this study, it is assumed that hull cleaning will have the effect of resetting the value of CAE to 0, meaning that the hull will return to the condition after drydocking.

4.2. Prediction results

The hull cleaning prediction is applied to the operational data of the same ships which is used for performance prediction and degradation as in chapters 2 and 3. Table I summarizes prediction results.

Table I: Hull cleaning prediction results

Vessel	Vessel type	Hull cleaning type	Hull cleaning effects	Average hull cleaning effects
A	Bulk carrier	Propeller polishing	3.84%	3.76%
		Propeller polishing	3.67%	
B	Tanker	Hull cleaning and Propeller polishing	1.35%	1.35%
C	Container	Propeller polishing	10.96%	11.18%
		Propeller polishing	11.39%	

While the prediction results for the same ship are consistent, results between different ships are inconsistent. Therefore, prediction results are only reliable for the same ship, which data is used for the training, and it is difficult to predict general hull cleaning effects. Also, since it is not possible to measure exact performance gain from hull cleaning, validation of the prediction results is difficult.

5. Conclusions

In this study, DNN based performance prediction model is used to predict performance degradation and hull cleaning effects prediction. While the proposed model has potential for the application of

performance prediction, performance degradation prediction and hull cleaning effects prediction, there is not yet enough validation to be used for ship operators.

More study will continue for the validation of prediction results, as well as introducing a factor to the degree of hull cleaning, such that the hull cleaning is not always assumed to return hull condition to after drydocking.

If performance degradation and hull cleaning effects prediction is able to be validated, it will be easily used for cost benefit analysis to decide optimal period for hull cleaning.

Acknowledgement

This research was supported by a grant from Korea Research Institute of Ships and Ocean Engineering Endowment project of "Development of evaluation technology for ship's performance in extreme environment" funded by Ministry of Oceans and Fisheries (1525014865, PES5091).

References

AGARAP, A.F. (2018), *Deep Learning using Rectified Linear Units (ReLU)*, https://arxiv.org/abs/1803.08375v2

ANH TRAN, T. (2021), *Comparative analysis on the fuel consumption prediction model for bulk carriers from ship launching to current states based on sea trial data and machine learning technique*, J. Ocean Eng. and Science 6/4, pp.317-339

HE, K.; ZHANG, X.; S. REN, S.; SUN, J. (2015), *Deep Residual Learning for Image Recognition*, http://image-net.org/challenges/LSVRC/2015/

PARK, P.; LEE, J.; KIM, M.; JUNG, J.; PARK, D. (2024), *DNN based Ship Performance Prediction Model and its Comparisons with Conventional Model*, 9th HullPIC Conf., Tullamore, pp.170-178, http://data.hullpic.info/HullPIC2024_Tullamore.pdf

TARELKO, W.; RUDZKI, K. (2020), *Applying artificial neural networks for modelling ship speed and fuel consumption*, Neural Comput. Appl. 32/23, pp.17379-17395

UZAIR, M.; JAMIL, N. (2020), *Effects of Hidden Layers on the Efficiency of Neural networks*, 23rd IEEE International Multi-Topic Conf., INMIC

ZHOU, T.; HU, Q.; HU, Z.; ZHEN, R. (2022), *An adaptive hyper parameter tuning model for ship fuel consumption prediction under complex maritime environments*, J. Ocean Eng. and Science 7/3, pp.255-263

Wind Assisted Propulsion: Hidden Performance Traps

Inno Gatin, Cloud Towing Tank, Zagreb/Croatia, inno.gatin@cloudtowingtank.com
Robert Keser, Cloud Towing Tank, Zagreb/Croatia, robert.keser@cloudtowingtank.com
Vuko Vukčević, Cloud Towing Tank, Zagreb/Croatia, vuko@cloudtowingtank.com

Abstract

Installing sails onboard of cargo vessels is one of the tools within the decarbonisation toolbox. Whether a classic wing-sail or a Flettner rotor, the installed sail generates thrust by harvesting the energy of the wind. Sounds simple! However, the thrust the sail generates comes at a cost, and not just the cost of installing and operating the device: it also generates a transversal force, which the vessel needs to counteract. She does so by generating an opposite hydrodynamic transversal force, which in turn comes at its own cost: induced resistance of the hull. This paper deals with the details of the induced hull resistance due to sail action, and how it affects the efficiency of wind-assisted propulsion.

1. Introduction

The basic principle of wind-assisted propulsion is simple: the sail converts wind energy into a useful thrust force. The thrust force assists the propeller in maintaining the speed of the vessel, lowering its output and required engine power. This is entirely true only in one special case: when the vessel sails dead downwind (provided that wind speed is higher than ship speed). If there is an angle between heading and wind, it becomes more complicated. Sailing dead upwind is also simple: the sail in that case cannot produce any useful thrust and is giving resistance instead. Since these two special cases are not of particular interest, it might be important to understand the details of a more realistic case.

When the vessel sails at an oblique angle relative to the wind, transversal forces are generated by the sail. These forces need to be opposed, or otherwise the vessel would drift. The counteracting force comes from the hull and appendages, but it comes at a cost. To produce a hydrodynamic side force, the hull induces additional drag. Adding to this, both the sails, and the hull, produce yaw moments acting on the vessel. In general, these moments will not be in equilibrium, which would mean that the vessel is unable to maintain course. That is what the rudder is for! But again, deflecting the rudder to compensate for the yam moment induces additional drag. In short, there is a cascade of effects caused by wind propulsion that induces additional drag which is not trivial to predict. The hydrodynamic transversal forces and moments of the hull are highly dependent on the hull shape.

In this paper we will look at the balance of aerodynamic and hydrodynamic forces at play, acting on a ship that sails in beam wind. The subject is a 230 m bulk carrier with a typical design. More details on this study can be found in *Tomljenović (2023), Tomljenović et al. (2024).*

2. How does sail-assisted propulsion work: simple (incorrect) version

Usually, when thinking about sail-assisted propulsion, we imagine a situation shown in the sketch in Fig.1. The force $F_x Sail$ generated by the sail, helps propel the vessel forward, and together with propeller thrust T compensates for the hydrodynamic resistance of the hull $F_x Hull$. This, however, is an incomplete and misleading representation of wind-assisted propulsion.

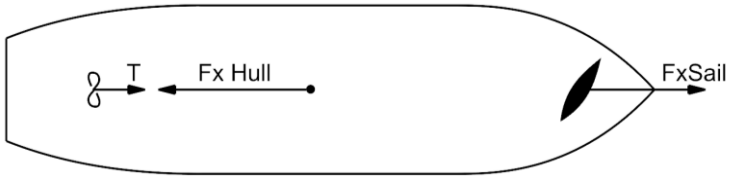

Fig.1: Sail-assisted propulsion: simple version

3. How does it actually work: understanding the forces and moments acting on the hull

In reality, the full story is a bit more complex, and here are important details that need to be considered. Fig.2 shows a sketch of the different moments and forces acting on a hull during wind-assisted sailing in beam winds. The orientation of vectors and the moments in the sketch are realistic. For example, hydrodynamic moment of the hull $Mz\ Hull$, is working in the direction of increasing the drift angle. This is characteristic of full hulls such as bulk carriers. Table I shows the description of all symbols shown in the figure.

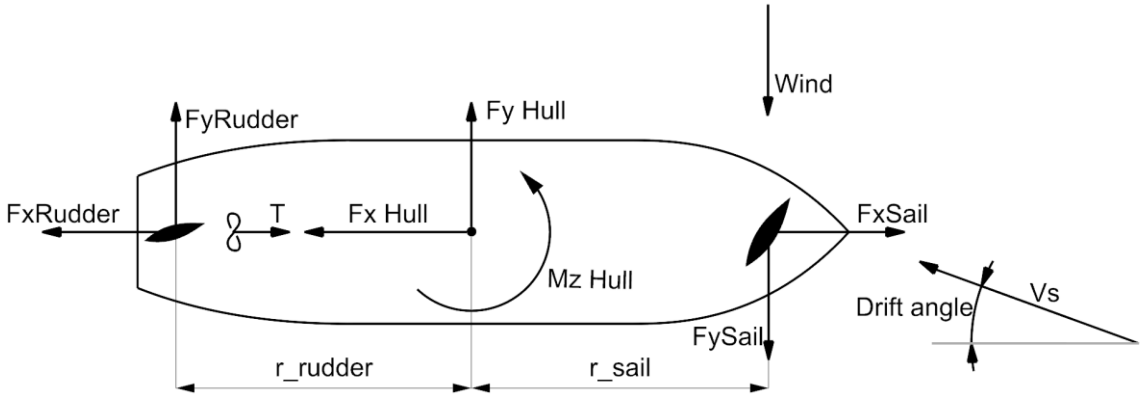

Fig.2: Moments and forces acting on the hull, the rudder and the sail

Table I: Nomenclature

COG	Centre of gravity of the vessel
$F_x\ Hull$	Hydrodynamic resistance force acting on the hull in its longitudinal X direction
$F_y\ Hull$	Hydrodynamic sway force acting on the hull in its transversal Y direction
$F_t Hull$	Total resistance of the hull, calculated as a vector sum of the F_x and F_z components.
$M_z\ Hull$	Hydrodynamic yaw moment acting around the hull's COG around the vertical Z axis
$F_x\ Rudder$	Hydrodynamic resistance force acting on the rudder in longitudinal X direction
$F_y\ Rudder$	Hydrodynamic sway force acting on the rudder in transversal Y direction
r_{rudder}	Arm between the rudder and COG
$F_x\ Sail$	Aerodynamic resistance force acting on the sail in longitudinal X direction
$F_y\ Sail$	Aerodynamic sway force acting on the sail in transversal Y direction
r_{sail}	Arm between the sail and COG
T	Propeller thrust force
V_s	Ship speed

What follows is a brief description of how the different forces interact, necessary to understand this paper. For easier understanding, the equations written below are expressing force components with their scalar values, where the signs follow from the image above. This makes them a bit less general, but easier to follow.

All forces and moments acting on the vessel must be in equilibrium, in order for the vessel to sail at a constant speed and course. Since our goal is to compare the propeller thrust T with and without sail-assisted propulsion, we need to calculate the required thrust in wind-assisted sailing. Obviously, thrust is acting in the longitudinal direction and cannot compensate for any transversal forces. For this reason, the transversal hydrodynamic forces acting on the hull and rudder must compensate the transversal sail force:

$$F_y Hull + F_y Rudder - F_y Sail = 0. \quad (1)$$

Further, the thrust needs to compensate both the hull resistance (usual resistance + induced resistance due to the drift angle) and rudder resistance:

$$T = F_x Hull + F_x Rudder - F_x Sail. \quad (2)$$

The vessel needs to have a constant course and not rotate around its vertical axis; hence the moments need to be in equilibrium as well:

$$M_z Hull - r_{rudder} \cdot F_y Rudder - r_{sail} \cdot F_y Sail = 0. \quad (3)$$

In the sketch, the sail is positioned at the bow. This is no accident: most full-hull form ships will have the sails placed in the fore. The reason behind this is the fact that in this arrangement the sails help compensate the hydrodynamic moment of the hull, which is typically larger than moment generated by the sails. The rudder needs to compensate for the remaining difference.

4. Achieving equilibrium in sail-assisted propulsion

Now that we understand the basic conditions that need to be fulfilled, so let us take a closer look at the details. How does the vessel achieve equilibrium in practice? Here is the order in which different quantities change and adjust themselves:

1. Wind starts blowing from the beam.
2. Sail starts generating aerodynamic forces $F_x Sail$ and $F_y Sail$, which push the vessel sideways, as well as forward.
3. As the vessel starts moving sideways, a hydrodynamic reactive force $F_Y Hull$ starts developing. The vessel moves forward too, so the net effect is that the vessel sails with a deflection angle, called the drift angle, as denoted in Fig.2.
4. Along with $F_y Hull$, hydrodynamic moment acting on the hull, $M_z Hull$, also starts developing. This causes the vessel to turn further towards the wind.
5. The helmsman, or the autopilot, compensates for the change in heading by deflecting the rudder. The rudder deflection is increased until the vessel stops rotating.
6. At this point, the equilibrium is established.

When assessing the effect of wind-assisted propulsion, this equilibrium condition needs to be compared against baseline condition without the sail. Obviously, to do that accurately, we need to assess $F_x Rudder$ and $F_x Hull$ accurately. To estimate these, we first need to know which drift angle the vessel needs to have in order to achieve transversal equilibrium (Eq.$F_y Hull + F_y Rudder - F_y Sail = 0.$ (1), and then the required deflection angle of the rudder to compensate for the yaw moment of the hull to satisfy Eq. $MzHull - r_{rudder} \cdot F_y Rudder - r_{sail} \cdot F_y Sail = 0.$ (3. The drift angle of the vessel is a crucial quantity and influences total resistance of the hull significantly. Vessels that are not equipped with a vertical fin keel (such as the ones used in sailboats), and especially those with a high block coefficient, will need to drift with a significant angle to achieve a meaningful $F_y Hull$. This drift angle will increase the total resistance and reduce the potential gains of sail-assisted propulsion.

5. Example: Wind-assisted propulsion of a 230 m bulk carrier

An example study is conducted using CFD on a bulk carrier. The vessel is 230 m long, 33 m wide, with a design draft of 14.6 m and 93 000 tons of displacement. She has a conventional hull form with a bulbous bow, Fig.3. Ship speed of 12.5 knots is considered.

The CFD study is divided into several phases:

1. Self-propulsion simulations of deflected hull with neutral rudder:
   The purpose of this step is determining hydrodynamic moments and forces on the hull at different drift angles. For this purpose, simulations for at least three different drift angles are conducted to obtain a curve that describes how different forces and moments depend on drift

angle. The simulations include the rudder in neutral position, since the rudder changes the pressure field around the hull and significantly influences its hydrodynamic moments and forces. The outcome of this phase are graphs showing $F_x Hull + FxRudder$, $F_y Hull + F_y Rudder$ and $M_z Hull + M_z Rudder$ versus drift angle, shown in Figd.4 to 6. Note that the longitudinal force Fx reduces with drift angle, but the total resultant resistance force $Ft = \sqrt{F_x^2 + F_y^2}$ increases.

2. Self-propulsion simulations at zero drift angle with deflected rudder:
In this step, rudder forces relative to its deflection angle when working behind the ship are determined. In these simulations, the vessel is sailing at zero drift angle. Along with the rudder force, which then produces the corresponding rudder moment, the deflected rudder induces a hydrodynamic moment acting on the hull (despite its zero drift angle). This induced moment is a consequence of the modified pressure field on the stern of the hull due to the deflected rudder. Fig.6 shows the resulting graph, showing the combined hydrodynamic moment of the rudder and hull.

Fig.3: Profile view of the bulk carrier

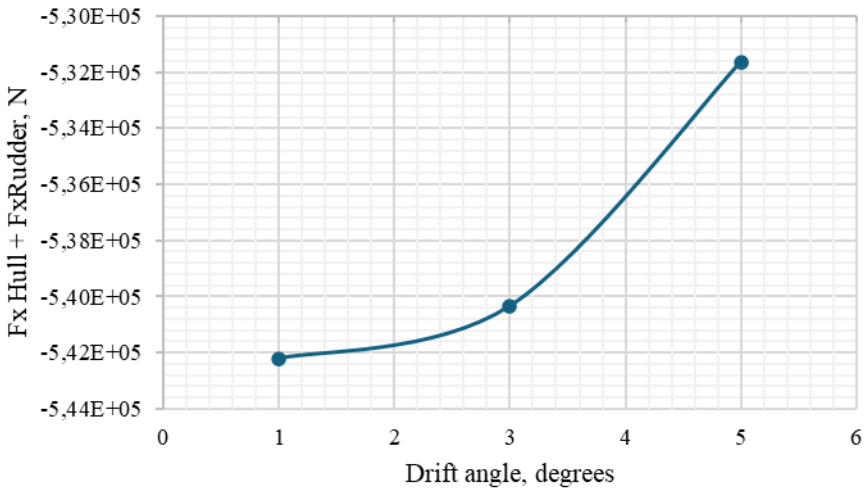

Fig.4: Longitudinal hydrodynamic force acting on hull and rudder at different drift angles of hull

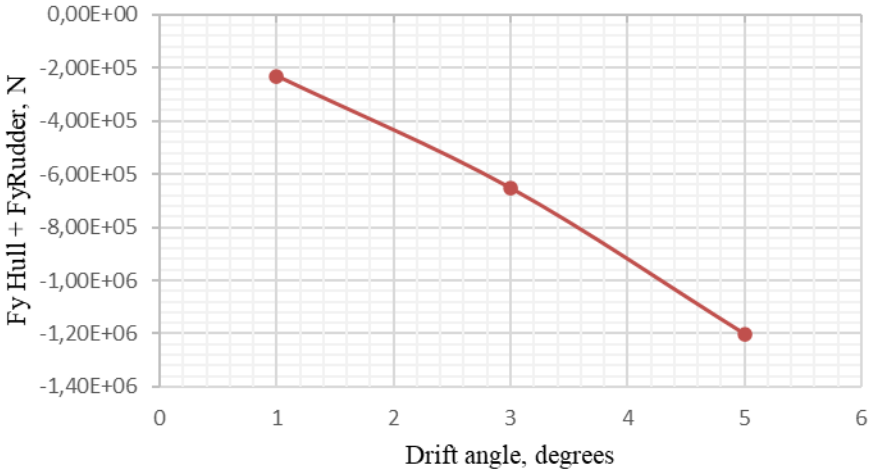

Fig.5: Transverse hydrodynamic force acting on hull and rudder at different drift angles of hull

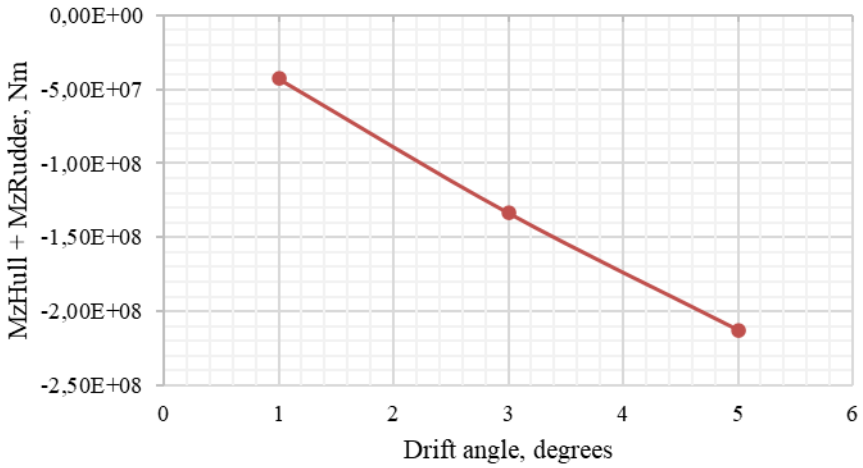

Fig.6: Hydrodynamic yaw moment acting on hull and rudder at different drift angles of hull, with rudder in neutral position

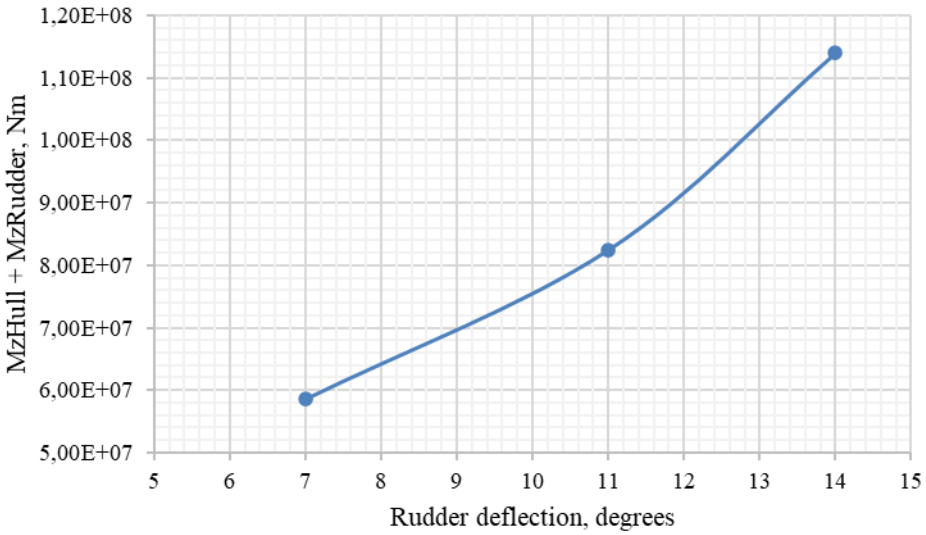

Fig.7: Hydrodynamic yaw moment acting on hull and rudder at zero drift angle of hull, with deflected rudder

Note that the above procedure assumes that the rudder force is not strongly affected by the deflection angle of the hull and that forces and moments obtained from these two sets of analyses can be linearly superimposed. Propeller action is considered in this analysis, since the propeller wash significantly impacts the flow behind the stern and rudder forces.

Once the above tests are completed, all necessary hydrodynamic data is available for planning the number of sails that can be installed, and for predicting the possible benefits of wind-assisted propulsion.

Determining the thrust and side force generated by the sail/s

This information typically comes from the sail vendor. The analysis needs to be limited for a certain assumed wind direction and strength. In case of our example, a strong beam wind is assumed, at which a single sail is estimated to offer 5 tons of thrust (49 kN) and a transversal force of 233.4 kN. The vertical moment of the sails will depend on their placement on the vessel, since this determines the arm relative to centre of gravity.

Determining the number and placement of sails

Using calculated graphs, maximum number and position of sails can be determined. Comparing graphs in Figs.6 and 7, it can be observed that rudder deflection can compensate the hydrodynamic moment of the hull for drift angle of up to about 2.3°: At deflection angle of 14°s, the rudder moment is M_z=1.14e+8 Nm, Fig.7. Reading the hull drift angle that corresponds to this moment from Fig.6 yields the drift angle of around 2.3°. This is the maximum drift angle that the rudder can compensate, without any help from the yaw moment generated by the sails. On the other hand, the $FySails$ needs to be compensated by the hull. For a single sail, the hull needs to be deflected by around 1° (reading from Fig.5 for a force of 233.4 kN). Further, the deflection angle is around 2.1° for two sails, 3.2° for three, and around 4.2° for four sails.

If relying on rudder deflection alone for compensating the moment, it would only be possible to install two sails. Luckily, the sails can be placed in the front part of the hull, and aid in maintaining the course of the vessel. Fig.8 shows the profile view of the vessel. Sails can be retrofitted on top of transversal bulkheads, as denoted with red circles and numbers. The red X denotes the location of the centre of gravity. Sails installed forward of the centre of gravity will aid in maintaining the course of the vessel. Placing one sail at location 2, and two sails at location 1, yields a compensating sail moment of M_zSail =4.06e+7 Nm.

As mentioned, the hull drift angle for three sails is 3.2°. The corresponding moment of the hull and rudder, Fig.6, is around -1.4e+8 Nm. Adding the moment of the sails, the moment that the rudder needs to compensate is 4.06e+7 – 1.4e+8 = 1.04e+8 Nm. The corresponding rudder deflection angle is around 12.8°, Fig.7. This is a high, but manageable rudder angle. Therefore, it can be concluded that this is a feasible but also maximum number of sails that can be installed.

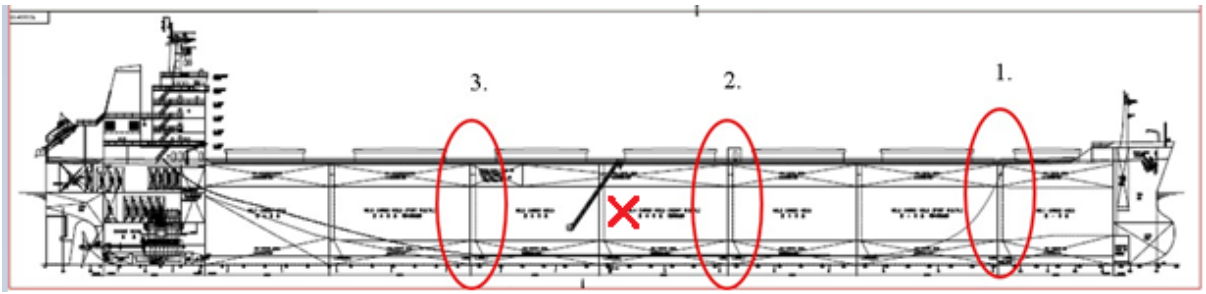

Fig.8: Profile of the ship with marked locations for potential sail installation. The red x marks the centre of gravity. Two sails can be placed at each longitudinal location.

Calculating power gains obtained with wind-assisted propulsion

Finally, we can predict power savings using wind-assisted propulsion. For this purpose, additional CFD simulations are conducted where the vessel is simulated at exactly 3.2° drift angle, and with a deflected rudder, to predict the required thrust and propeller power. Baseline power consumption is also calculated for a vessel sailing at zero drift angle without sails. Table II shows the summary comparison.

From the table, it can be seen that the total hull resistance increased by almost 17% when using sails. This increase is due to the induced resistance of the hull at the non-zero drift angle, and rudder deflection. Indeed, most sail-generated thrust (107 out of 147 kN) is used for compensating the induced resistance. Useful sail thrust is further reduced by induced rudder resistance, where the final impact in terms of thrust reduction is around 17 kN.

This means that in this particular case, only 12% of sail-generated thrust is being utilized. Despite this, the reduction in delivered propeller power is almost 6%.

Table II: Comparison of conventional and wind-assisted propulsion

	Conventional propulsion	Wind-assisted propulsion	Difference, %
Sail thrust, $F_x Sails$ [kN]	0	147.0	
Rudder deflection [deg]	0	12.8	
Drift angle [deg]	0	3.2	
Total resistance F_t [kN]	529.3	636.9	16.9%
Propeller thrust, T [kN]	650.2	633.0	-2.7%
Delivered propeller power, [kW]	5227.1	4944.9	-5.7%

4. Conclusion

A detailed analysis of wind-assisted propulsion is given in this paper, with the focus on induced hydrodynamic drag. Analysis is performed on an example bulk carrier, representative of a full-form vessel that could be a candidate for a wind-assisted propulsion retrofit. In this case, no underwater retrofit is planned, in form of hydrodynamic lifting surfaces such as vertical fin keels or similar.

The following observations are made from this analysis:

1. The sail area that can be installed is limited by the high hydrodynamic moment induced on the hull when sailing with a drift angle. Sails need to be installed in the forward part to aid in reducing this moment.

2. Due to a high drift angle and poor lift-to-drag ratio of the hull, total hull resistance increases significantly. This reduces the useful portion of the sail-generated thrust.

3. For the present example in ideal beam wind conditions, only **12%** of sail-generated thrust is being utilized to reduce the propulsion power, while the remaining 88% is used to compensate for induced drag of the hull and rudder.

4. The resulting power savings is **5.7%**.

In conclusion, the following is suggested:

1. Retrofitting the underwater hull together with the sails, in form of vertical keels or similar, to improve the lift-to-drag ratio of the hull.

2. Taking careful consideration of induced hydrodynamic drag within wind-assisted propulsion feasibility studies.

References

TOMLJENOVIĆ, I. (2023), *Numerical Analysis of Self-Propulsion of a Bulk Carrier with Wind Assisted Propulsion*, University of Zagreb. https://urn.nsk.hr/urn:nbn:hr:235:439004

TOMLJENOVIĆ, I.; GATIN, I.; VLADIMIR, N. (2024), *CFD Simulations of Self-Propulsion of a Bulk Carrier with Wind-Assisted Propulsion by OpenFOAM*, Global Conf. on Naval Architecture and Ocean Engineering, pp.734–48

Continuous Performance Measurement of Wind Propulsion

Juhan Voutilainen, Norsepower, Helsinki/Finland, juhan.voutilainen@norsepower.com
Ville Paakkari, Norsepower, Helsinki/Finland, ville.paakkari@norsepower.com

Abstract

Wind propulsion is gaining momentum as a means of producing low-carbon propulsion energy for ships, helping to reduce shipping emissions. However, one challenge remains: how to measure the performance of sails on a continuous basis. This issue has both commercial and regulatory implications. In this paper, a novel methodology for measuring sail performance is introduced, along with full-scale results demonstrating the methodology's applicability.

1. Introduction

In recent years, wind propulsion has emerged as a promising solution for low-carbon propulsion in the maritime sector. As international shipping faces increasing pressure to decarbonize and meet upcoming environmental regulations, alternative propulsion technologies are gaining attention. Among these technologies, rotor sails are leading the way. The integration of modern rotor sails into ship designs has the potential to significantly reduce fuel consumption and emissions by harnessing the renewable energy of the wind.

Despite the growing interest and advances in wind-assisted propulsion systems, one key challenge remains unresolved: the continuous and reliable measurement of sail performance in real-world operations. This challenge is critical not only from a technical standpoint but also for its commercial and regulatory implications. Ship operators and stakeholders require accurate performance metrics to evaluate the economic viability of wind propulsion technologies to optimize their usage. Similarly, regulatory bodies must have accurate real-time sail performance data to correctly credit ships for the installed low-carbon propulsion.

To address this gap, this paper introduces a novel methodology for measuring the performance of sails under full-scale operational conditions. The proposed approach is designed to overcome limitations of performance predictions of analytic formulas and other modelling-based methods.

2. Why is continuous performance measurement needed?

Continuous measurement can be seen as logical development step for the rather novel technology of modern sails. Without continuously measuring the performance of the sails, assessing the real benefit, reliability, and compliance with regulations is difficult and inaccurate. The continuous performance measurements are necessary to:

1) Validate performance claims made by vendors
2) Monitor optimal performance of the system over time
3) Sustain continuous development of both wind propulsion systems and the overall ship designs
4) Enable overcoming the “owner-charterer” dilemma
5) Enable considering wind as an energy source in a regulatory context

Validating the performance promises from the sail vendors is challenging without access to continuous real-time performance data. Options without the continuous performance data are limited to full-scale point testing of computational models or purely computational tools, both of which are prone to significant errors.

It has been shown in *Paakkari (2025)* that small bias in sail control can lead to significant drop of sail performance, which can be unnoticed in full-scale spot testing, and obviously in computational tools.

In the study, anemometer bias was selected as an example to show how just 30° error in orientation of the sensor can lead to performance loss of over 50%. This loss would yield only 6% mean difference between the ideal performance and the results from five control points at sea trials.

Time spares no one and leaves its mark on us all. Without continuous monitoring, it is impossible to detect performance drift over time. Monitoring the performance data enables corrective actions and maintenance immediately after any decrease in performance is noticed. The same data can be used for studying and improving the sails, and the whole sail-ship system, in real life conditions.

All the benefits of the continuous performance measurements are not purely technical. The maritime industry is striving towards lowering carbon emissions of shipping. A crucial aspect of this are the efforts done in lowering the carbon intensity of the energy mix used onboard. Continuous measurement of the produced sail benefit enables the real-time information about the contribution of the wind propulsion to the total produced energy of the ship. The information simplifies the work of regulators, owners and charterers by making the process of accounting for wind energy in different contexts straightforward and transparent.

3. Method

The presented method requires inputs from sails and ship to function. Certain measuring equipment needs to be available, both on sails and ship, to provide necessary data. Required inputs for the system are sail thrust force $F_{x,sail}$, sail lateral force $F_{y,sail}$, ship's shaft thrust force $F_{x,prop}$, and ship's shaft power P_{prop}. Fig.1 illustrates the required signals from sails and ship. Sail thrust and lateral force measurement require thrust measurement system. Shaft power and thrust meters are required for providing ship data. Measurement arrangement for the sail forces, and the principles of the method are further explained. Shaft power and thrust measurements are well established and instrumentation is widely available.

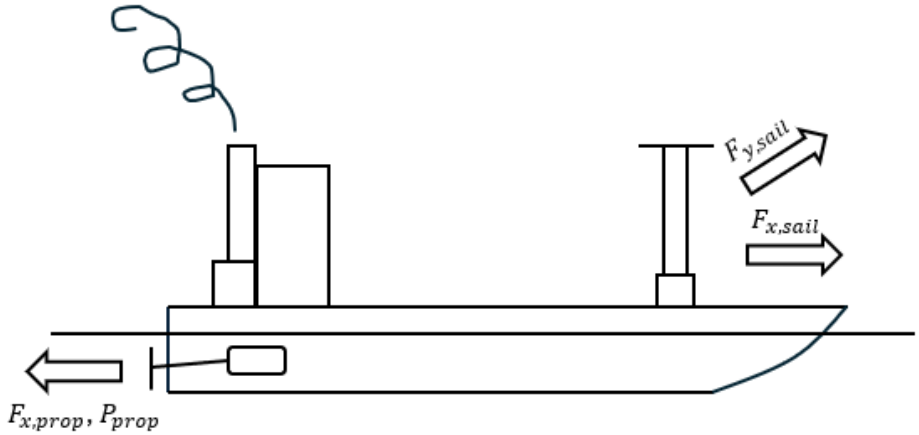

Fig.1: Required signal inputs for the continuous measurements

3.1. Measuring sail forces

Accurately measuring the sail performance requires continuous measurement feedback of the forces produced by the sails. The thrust measurement system deployed on NPRS is based on measuring the surface pressure on the sail with pressure transducers. This measured surface pressure field is then used to calculate the force magnitude and direction applied by the sails.

The pressure-based measurement system can be considered the most direct measurement of the magnus effect. The measurement principle has been earlier used in academia in wind tunnel tests, *Bordogna (2020)*. The surface pressure measurement can be expressed as p(θ), which is the function a pressure measurement obtained from angle θ. The force per meter acting on a sail is obtained by integrating the

pressure p(θ) over the circumference.

$$\frac{\boldsymbol{F_{RS}}}{h} = \int_0^{2\pi} p_k(\theta)\boldsymbol{n}\, r\, d\theta \tag{1}$$

The total force is obtained by integrating over the sail height

$$\boldsymbol{F_{RS}} = \int_0^{H}\int_0^{2\pi} p_k(\theta)\boldsymbol{n}\, r\, d\theta\, dh \tag{2}$$

The total force can be divided into thrust and lateral force. Thrust force and lateral force are used in the formulation of continuous measurement and are referred as $F_{x,sail}$ and $F_{y,sail}$ respectively.

3.2. Net main engine power demand reduction

The main engine equivalent power produced by the sails is defined as a contribution of the sails to the total propulsive force of the ship at any given moment:

$$P_{prop,sail} = \frac{F_{x,sail} \times V}{\eta} \tag{3}$$

Where V is the ship speed and η is the total propulsive efficiency of the ship. To overcome the issue of defining the total propulsive efficiency, a new parameter called Power ratio, PR_{Sail}, is defined. This power ratio describes the share of sail propulsion in the overall ship propulsion:

$$PR_{Sail} = \frac{P_{prop,sail}}{P_{prop}} \tag{4}$$

With the assumption of constant total efficiency in both the relationship further develops:

$$PR_{Sail} = \frac{P_{prop,Sail}}{P_{prop}} = \frac{\frac{F_{x,Sail} * V}{\eta}}{\frac{F_{x,prop} * V}{\eta}} = \frac{F_{x,sail}}{F_{x,prop}} \tag{5}$$

And further:

$$P_{prop,sail} = \frac{F_{x,sail}}{F_{x,prop}} * P_{prop} \tag{6}$$

From the relation above, we note that all the variables are such, that it is possible to directly measure them. $F_{x,sail}$ is measured from the sail pressures, and P_{prop} and $F_{x,prop}$ are measured from ship's shaft line. Hence the measurement principle used to measure the $P_{prop,sail}$ is very straightforward. This is a significant advantage, as it allows using a limited number of sensors and enables a transparent measurement setup with minimal amount of complicated post-processing.

However, forces produced by rotor sails affect the dynamics of the ship. Well known phenomena are lateral force induced drift, heel, and yaw moment, which may increase the total resistance of a ship. Simultaneously, sail induced thrust affects the efficiency of the propeller.

Lateral forces and the resulting yaw moment must be balanced by opposite hydrodynamical forces. Resulting yaw moment is strongly affected by location of the sails on the ship. Yaw moment is being balanced by increasing rudder angle. Lateral force pushing the ship sideways balances out when resulting drift induces enough opposing side force. Due to tall structure of the sails the lateral force acts

well above the deck, creating considerable heeling moment, which is balanced by rotation of the hull. All these balancing forces may increase the total resistance of a ship. On other hand, forward thrust reduces propeller loading affecting ships open water efficiency and can cause positive influence.

Whenever comparing the case of the ship with sails to (real or imaginary) case without the sails, the rotor sail impact on ship dynamics should be considered. When deriving Eq.(6), total efficiency was, for convenience, assumed to be same for sail and propeller propulsion. The total efficiency η consists of hull, open water propeller, relative rotative, shaft, and engine efficiencies. In terms of force balance between sail and propeller propulsion, the hull and open water efficiencies are being affected when comparing the two propulsion sources. Thrust produced by the propeller is always subject to added resistance due to its influence on the flow around ship's aft body. The effect is taken into consideration by applying thrust deduction coefficient. In terms of sail forces, two main sources of impact on ship dynamics can be defined as lateral force and change of open water propeller efficiency. With the proposed effects in consideration Eq.(6) becomes as follows:

$$\Delta \mathrm{P}_{\mathrm{sail,ind}} = \frac{F_{x,sail} - \Delta S}{F_{x,prop} * (1-t)} * P_{prop} \tag{7}$$

Where ΔS denotes the rotor sail impact on ship dynamics including the lateral force and efficiency change. t denotes thrust deduction factor. The thrust deduction factor is derived either from the model tests of the ship or using semi-empirical relations such as Holtropp-Mennen. The rotor sail impact on ship dynamics ΔS can be derived either by full-scale, model-scale or numerical experiments and is unique for each ship.

3.4. Wind propulsion net benefit

Rotor sails consume power in order to generate thrust. Wind propulsion net benefit simply deducts sail used power from the net main engine power demand reduction.

$$\Delta \mathrm{P}_{\mathrm{sail,ind,net}} = \frac{F_{x,sail} - \Delta S}{F_{x,prop} * (1-t)} * P_{prop} - P_{sail,cons} \tag{8}$$

Where $\Delta \mathrm{P}_{\mathrm{sail,ind,net}}$ is wind propulsion net benefit, and $P_{sail,cons}$ is the power consumed by sail system. As a result, indicator for the net benefit of the sail system is achieved and can be used for operational optimization.

4. Results

Before testing the methodology on a real ship, purely computational desktop feasibility study of the method was performed. Desktop evaluation has no contact with any real ship and is done to just study the theoretical accuracy of the methodology. Desktop evaluation and the real ship analysis are both done to net main engine power demand reduction i.e., the sail force effects on the achieved power are taken into consideration through ΔS, but sail consumed power $P_{sail,cons}$ is neglected. During the full-scale campaign, the sail was run using auxiliary power source, thus neglecting the $P_{sail,cons}$ is justified for getting exact comparison of shaft power with and without the sail. Results of both, desktop study and the study on a real ship, are presented next.

4.1. Desktop evaluation

The study was done by using 3 DOF model to represent a ship. The model is a low-fidelity program based on force equilibrium in longitudinal and lateral directions, and moment balance around centre axis. The rotor sail thrust is used to decrease the load required from the ship's propeller. In addition to thrust force, rotor sails produce also lateral force and yawing moment. The additional lateral force will cause the ship to drift and the yawing moment will be cancelled with rudder action. The drift and rudder

angle will increase the ship's resistance, and the additional impact should be considered when evaluating the required main engine power. These effects can be considered by solving the force and moment equilibrium equations in surge, sway and yaw directions. The model was validated against results in *Kramer and Steen (2022)* with corresponding hydrodynamical derivates and lateral forces.

The same ship model as for the validation of 3 DOF model was used to perform the numerical feasibility study. It is important to note that the used ship model has nothing to do with SC Connector and was selected purely for desktop evaluation of accuracy of the continuous measurement methodology. Determination of the correction ΔS was carried out using numerical approach. Required propulsion powers, for various wind conditions, with and without rotor sails were calculated with 3 DOF method, achieving directly the power saved by rotor sails. These calculations can be referred to numerical ON/OFF tests as the principle is same as in full-scale. Results were compared to results calculated by net main engine power demand reduction $\Delta P_{sail,ind}$. By comparison, good understanding about precision of the presented method is obtained.

Fig.2 presents the percentual error between directly calculated power savings ΔP_{direct} from numerical ON/OFF tests of the 3 DOF model, and net main engine power demand reduction $\Delta P_{sail,ind}$. Same sail locations as in work of Kramer & Steen, i.e., $X/L = 0, 0.25, 0.4$ were used, where L is length of a ship and X is the location of the sail, measured as distance from midships to bow. Each data point represents different wind condition, providing wide variety of sail thrust and lateral forces. The ratio between thrust produced by sails and ship propulsion is expressed with $T_{ratio,sail}$. The value highlights the great variety of different operating conditions.

Majority of the data points are within ±5% of difference. Highest deviating single points for $X/L = 0, 0.25, 0.4$ indicate respectively -40.49%, -26.23%, and -26.85% difference between $\Delta P_{sail,ind}$ and the directly derived savings from 3 DOF. The mostly deviating data points are from wind conditions, where the sails produce almost only lateral force. In such cases the power produced by sails is low and the error percentage gets overly amplified. Root mean square error (RMSE) value for the cases with sail located at $X/L = 0, 0.25, 0.4$ are 4.61kW, 3.81kW, and 3.65kW respectively, which is low in context of ship propulsion.

Due to low RMSE values, and its sensitivity to higher deviations, it can be reasoned that the deviating data points from the borderline wind conditions are not significantly affecting the precision of the method. All the most deviating data points are underpredicting the sail generated power, making the method slightly conservative. Influence of the signal errors on the precision of the methodology was analysed and no degradative influence on robustness was found.

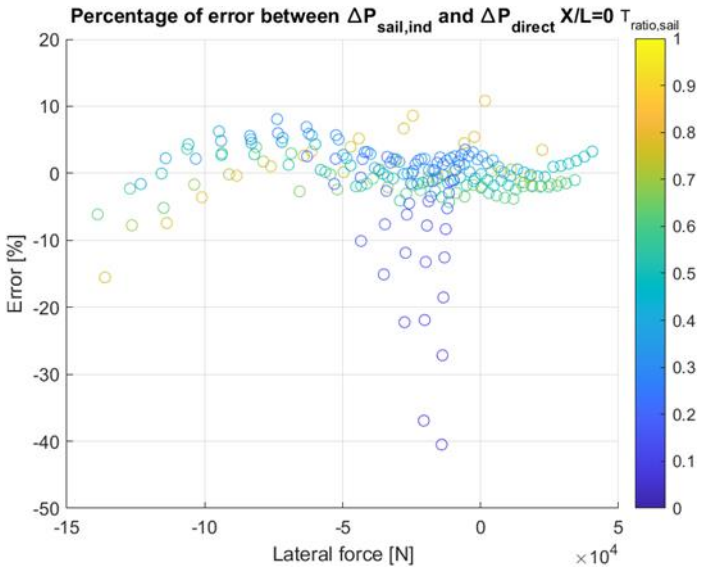

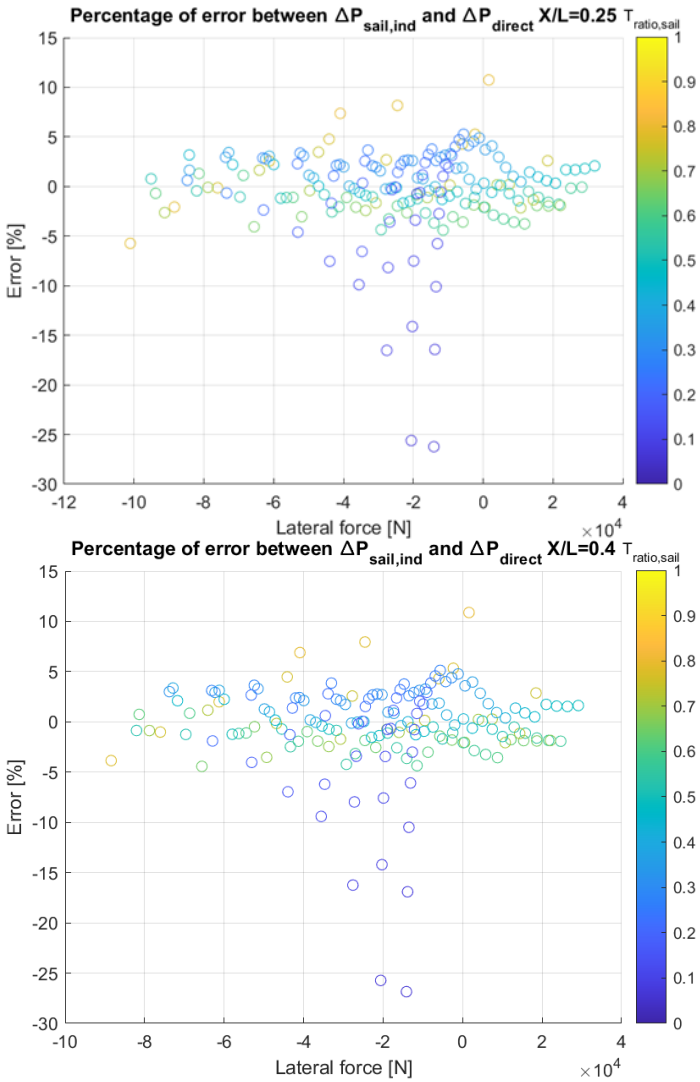

Fig.2: Error between $\Delta \mathbf{P_{sail,ind}}$ and $\Delta \mathbf{P_{direct}}$3 DOF

4.2. Full-scale tests

Experimental test campaign was conducted onboard of Ro-Ro vessel SC Connector at the North Sea. The vessel has overall length of 154.50 m, and gross tonnage of 12803. Vessel is equipped with two 35x5 m rotor sails. The test campaign was conducted using only the fore sail. During the campaign ΔS was derived with the full scale experimental approach. ON/OFF measurements were used to compare results of ΔS corrected net main engine power demand reduction $\Delta P_{sail,ind}$, and ΔP_{direct} i.e., the power reduction defined by ON/OFF tests. Procedure of ON/OFF testing was similar to the one described in ITTC 7.5-04-01-02 “Sea trials for assessing the power saving from wind assisted propulsion - guidelines”, *ITTC (2024)*. The vessel’s speeds during the tests varied between 9-15 knots, providing a good range describing different operational conditions. The ship is equipped with control-lable pitch propeller. For the purpose of the trials, the propeller rpm was kept constant, and the adjustment to speed was carried out by changing the propeller pitch.

Tests were performed in varying wind conditions, with the aim to gather diverse data points representing different combinations of sail thrust and lateral forces. The amount of data is rather small but gives an understanding of the capabilities of the discussed method. Experienced wind conditions varied from apparent wind speeds between 7 to 16 m/s, and apparent wind angles from very headwinds to complete tailwind. Encountered wind conditions give rather a good sweep over different sail forces. Reduction in required shaft power varied from 260 kW to over 900 kW, and percentage of wind propulsion from total varied between 7 and 38%. The achieved power reductions during the campaign should not be

seen as average savings potential for the rotor sail technology onboard. Each test points represent only the very moment when the measurement was conducted.

Accuracy of the net main engine power demand reduction $\Delta P_{sail,ind}$ was assessed by comparing the results with ON/OFF tests at the same time instance. To achieve normalized results vessel's speed was kept constant during ON and OFF phases of the test cycle. If same speed could not be achieved, speed correction to the ON/OFF results was applied by using speed-power curve. On average velocities within 0.2 knots were achieved during ON and OFF cycles. The largest deviation was 0.93 knots. It was observed that used speed-power curve was not predicting well the influence of such big difference, and the results for this point were inaccurate. Thus, the point was removed from the data set, and the velocity difference guideline was tightened to avoid collecting more points with such difference.

The result of comparison is presented in Fig.3. X-axis represents the power saving results achieved by ON/OFF tests, and Y-axis the power savings achieved by the $\Delta P_{sail,ind}$ methodology at the same instance. Tests points in the figure demonstrate correlation between the two results. Part of the test runs were used for defining ΔS correction. These points are excluded from power predictions and expressed as dependent measurements. The perfect match between the results would mean that the trendline drawn through the independent predicted points would have a slope of one. The results have good correlation, even some scatter can be observed.

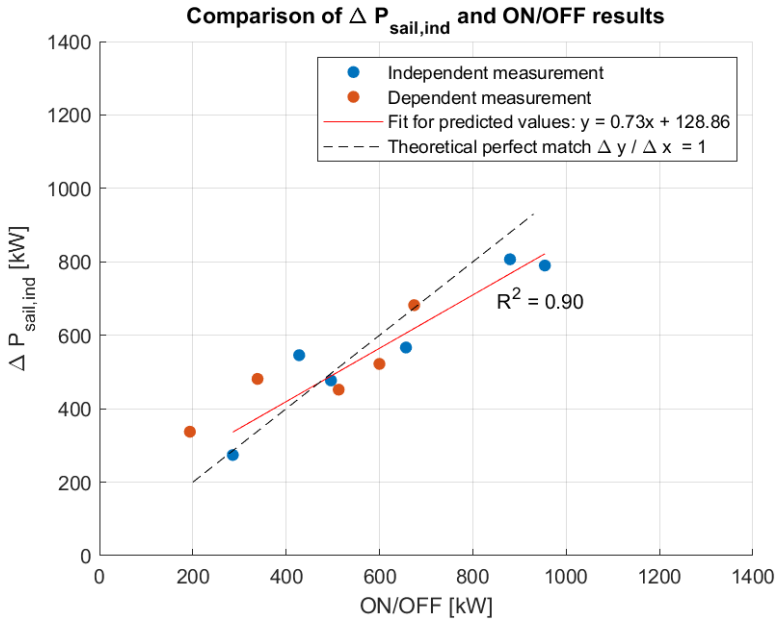

Fig.3: Comparison between $\Delta P_{sail,ind}$ and ON/OFF test results

Table I: Errors of independent measurement points

ON/OFF [kW]	ΔP sail,ind [kW]	Error [%]
427.9	545.8	-21.6
954.3	790.0	20.8
879.6	806.9	9.0
495.9	477.0	4.0
656.7	566.8	15.9
285.7	274.0	4.3
Ave: 616	**576.7**	**6.9**

Measurements are done in real life sea conditions during normal operation of the vessel, thus certain level of scatter is unavoidable. Coefficient of determination R^2 shows that the variation of data is well

explained by the trendline. Error of independent predicted points, presented in Table I, vary from 4% to -21.6%. Positive values represent underpredicted $\Delta P_{sail,ind}$ values and negative overpredicted. Values from the $\Delta P_{sail,ind}$ are mostly underestimating the generated power. Root mean square error of the whole data is 74 kW, which can be seen as low in the context of full-scale ship power measurements.

5. Discussion

Development and implementation of new continuous measuring technology in wind propulsion industry plays a crucial role in increasing the understanding and attractiveness of the sail technologies. Promising results in real life sea conditions have been achieved with the methodology presented in this work. The chaotic operational environment of ships should be considered when interpreting the results and the differences. It is fair to say that perfect match will never be achieved.

Current data shows slight conservativity in obtained measurement points. Mostly power is slightly underpredicted compared to the ON/OFF results. Underprediction can be seen in Fig.3 from the slope for independent values being below one. Currently, the slope has clear deviation from the perfect match of one, but with the size of the dataset, and the distribution of the current points, the slope is very prone to changes. Single points have deviation up to -21.6%, but greater focus should be placed on the average of the predicted power, which is 6.9%, as single points are prone to errors.

Clearly, the experimental dataset used for validation of the method is still small. The reached accuracy with such short campaign can be seen as a success. The accuracy is expected to grow with increasing amount of data. Work to collect more data is ongoing at the very instance of writing this document. Simultaneously third-party validation process is ongoing.

The theoretical challenge of the presented methodology is in accounting for the impact of sail forces on the ship behaviour and efficiency, and in correctly accounting for speed difference in ON/OFF testing. Deploying the continuous measurement system requires understanding the behaviour of the ship under influence of the sail forces. Defining the influence directly from the vessel through sea trials data is proving to be functional approach. Another approach is defining the sail impact by modelling the ship behaviour with computational tools. Validation of the computational approach is under work and will be topic of separate publication.

Important practical aspects are strongly related to calibration of measurement equipment. Accurate readings are necessary to achieve accurate results, thus calibrating all the required measurement equipment before deploying the continuous measurement system is a matter of priority.

6. Conclusion

Results seen until now provide very promising insight about the presented continuous measurement system. Average power reductions between the results from full-scale ON/OFF tests and the continuous predictions differed by 6.9%. Wind conditions, vessel speed, and the proportion of wind propulsion varied greatly during the campaign, highlighting the capability of the continuous methodology across various operational ranges and conditions

The dataset is still small, but results are showing good correlation with the full-scale ON/OFF results. Ongoing full-scale campaigns and third-party validations will add reliability to the method. It can be expected that the continuous measurement will be new standard for assessing the performance of the wind propulsion systems in shipping industry in the near future.

Acknowledgement

Data for this study was achieved by full-scale experiments onboard Ro-Ro vessel of Sea Cargo AS. Their efforts and interest in developing wind propulsion technology is highly appreciated.

References

BORDOGNA, G. (2020), *Aerodynamics of wind-assisted ships - Interaction effects on the aerodynamic performance of multiple wind-propulsion systems*, PhD thesis, TU Delft

ITTC (2024), *Recommended Procedures and Guidelines. Sea Trials for assessing the power saving from wind assisted propulsion*, https://www.ittc.info/media/11974/75-04-01-02.pdf

KRAMER, J.V.; STEEN, S. (2022), *Simplified test program for hydrodynamic CFD simulations of wind-powered cargo ships*, Ocean Engineering, Trondheim

PAAKKARI, V. (2025), *White paper: How simple errors can destroy the sail performance*, Norsepower, https://www.norsepower.com/app/uploads/2025/02/How-simple-errors-can-destroy-the-sail-performance.pdf

Assessing and Rating the Performance when Chartering Unknown Bulk Carrier Vessels

Richard Marioth, Idealship, Itzehoe/Germany, rm@idealship.de

Abstract

When a vessel charter is considered, ship operators need to estimate the fuel performance of unknown vessels. Although limited data is publicly available to assist in this assessment, it can be leveraged with specific calculation models. This paper explains first how Fuel Consumption clauses of Charter Party agreements work. Then the publicly accessible data sources and different methodologies for estimating the vessel fuel performance prior fixture are reviewed. Finally, the paper presents the results of a case study involving ten bulk carrier vessels, demonstrating the effectiveness of the various estimation methods in real-world applications.

1. Introduction

1.1. Importance of the question

In the past decade, rising fuel costs and increasingly stringent regulatory frameworks, such as Fuel EU EU Emissions Trading System (EU ETS) and Carbon Intensity Indicator (CII), have heightened the need for ship operators to accurately assess the vessel's performance before making decisions. Understanding a vessel's fuel efficiency and compliance capabilities has become essential for managing operational costs and adhering to environmental regulations. Furthermore, some commercial charterers prioritize vessels that can transport cargo with minimal carbon dioxide emissions, reflecting the growing demand for sustainable shipping practices.

Whether negotiating new charter contracts, assessing transport costs, joining a pool, or considering the purchase of a second-hand vessel, a solid understanding of a vessel's performance can strengthen the negotiation position, significantly influence financial outcomes, and ensure compliance with evolving industry standards.

1.2. Impacts on vessel performance and how it changes over time

Many stakeholders and environmental factors impact the current vessel's performance. To estimate the consumption of an unknown vessel, these factors need to be considered somehow. The main factors are:

- The Design of the vessel: Hull and Propeller Designs and dimensions will have different hydrodynamic properties and thus propulsion fuel consumption values.
- Paint performance: The antifouling and roughness degradation over time can have a high impact on the frictional resistance of the vessel. Also, Hull Cleaning actions will have an impact on this, as frequent reactive cleanings can reduce the effectiveness of the antifouling and increase the vessel's roughness.
- Biofouling pressure: The fouling pressure of the global area where the vessel was operated in the past. It can be quite different as Marine species grow more in warm regions and the likelihood of getting a fouled hull increases significantly with the duration of an idle stay in such waters.
- Machinery maintenance: The maintenance condition of the ship machinery can have a particular impact on its fuel efficiency. This has an effect but can hardly be measured without detailed vessel operational data.
- Wear & tear and mechanical damages to the ship hull and propeller over time are other effects that can scarcely be measured.

Different disciplines are involved in keeping vessel performance at its optimum. Hence, it is challenging to correctly account for all these aspects when predicting the performance of an unknown vessel.

2. The CP Description

2.1. About a Charter Party

A Charter Party contract is a written charter agreement between the disponent owner and merchant or cargo owner. That contract places the owner's vessels at the charterer's disposal and regulates mutual terms and obligations. The Charter Party is a legally binding and internationally recognised document. The owners are being paid in the form of freight for voyage charters, and in our case, for the specific period charters, the owners remunerations are being known as hire, *Plomaritou (2014).*

There are many types of Charter Parties, but this chapter will concentrate on Time Charters and Trip Time Charters for the specific vessel's performance descriptions. The Charter Party is a legally tricky agreement with many particular variations, which this study cannot fathom in this document in detail. Thus, the study concentrates on standard forms (like BIMCO), clauses, specific wording and attributes that one finds in such forms, *Wilson (2010).*

2.2. Vessel Performance clauses within charter parties

The so-called "vessel performance" is part of the Charter Party "Vessel Description" clause, usually part of the Charter Party Rider and Annex. This clause describes the vessel's particulars and how to read or interpret them. Often, in the period charter, such a description may be a separate Annex with the Ship's Particulars, General Arrangement plan, and many other documents that the charterer may request during the negotiation phase. An example of a typical description is shown in Fig.1.

SPEED / CONS (INCLUDING A/E)

BALLAST : ABT 14.00 KNOTS ON ABT 25.00 MTS VSLFO + ABT 0,1 MTS LSGO

LADEN : ABT 13.00 KNOTS ON ABT 25.00 MTS VSLFO + ABT 0,1 MTS LSGO

ECO SPEED / CONS (INCLUDING A/E)

BALLAST : ABT 12.00 KNOTS ON ABT 17.00 MTS VSLFO + ABT 0,1 MTS LSGO

LADEN : ABT 11.00 KNOTS ON ABT 17.00 MTS VSLFO + ABT 0,1 MTS LSGO

PORT/ANCHORAGE CONSUMPTION:

IDLE: ABT 3.00 MT VSLFO

WORKING: ABT 6.50 MT VSLFO

FINAL DESCRIPTION TO BE ADJUSTED BY OWNERS WITHIN 90 DAYS AFTER DELIVERY BUT TO BE MAXIMUM +/- 5% FROM THE PROVIDED DESCRIPTION. IN CASE OF LARGER DISCREPANCIES CHARTERERS AND OWNERS TO DISCUSS IN GOOD FAITH.

SPEED AND CONSUMPTION IS BASIS ACTUAL "GOOD WEATHER" PERIODS DEFINED AS: MAX WIND FORCE BEAUFORT SCALE 4 AND/OR MAX DOUGLAS SEA STATE 3 (TOTAL COMBINED (SEA AND SWELL) CORRESPONDING TO 1.25 METERS SIGNIFICANT WAVE HEIGHT) WITH NO ADVERSE CURRENTS AND/OR SWELL WITH VESSEL AT DESIGN DRAFT. FAVORABLE CURRENTS NOT TO BE FACTORED IN WHEN ASSESSING VESSEL'S PERFORMANCE. ONLY VOYAGES EXCEEDING 48 HOURS TRANSIT TIME FROM SEA PILOT TO SEA PILOT - EXCLUDING A PERIOD OF 12HRS AFTER COSP/PRIOR EOSP - ARE TO BE TAKEN INTO ACCOUNT WHEN ASSESSING VESSEL'S PERFORMANCE. PASSAGES WITH RESTRICTED VISIBILITY AND/OR WHEN NAVIGATING IN CONGESTED WATERS, STRAITS, NARROW WATERS, AND/OR MANOEUVERING, ENTERING OR LEAVING PORTS ARE TO BE EXCLUDED. FOR A STEAMING PERIOD TO BE CONSIDERED A GOOD WEATHER ONE, ALL TIME FROM NOON TO NOON HAS TO BE IN GOOD WEATHER AS DEFINED ABOVE. EXTRAPOLATION OF "GOOD WEATHER" PERFORMANCE FOR "BAD WEATHER" PERIODS IS NOT ALLOWED. 5 PCT ALLOWANCE FOR ABT IN BOTH CASES IN OWNERS FAVOR

THE VESSEL SHALL HAVE THE LIBERTY TO USE MDO/MGO FOR MANEUVERING IN/OUT OF PORTS, STARTING OF A/E, NAVIGATING IN SHALLOW/RESTRICTED/BUSY WATERS, CANAL AND RIVERS. GENERATOR ENGINES TO CONSUME DIESEL OIL IN CASE OF PART LOAD. WHEN VESSEL IS PERFORMING BALLAST WATER TREATMENT, MANEUVERING ON DEPARTURE/ARRIVAL, BALLASTING/DE-BALLASTING EXCHANGE AND HOLDS CLEANING WHILE AT SEA OR PORT THE TOTAL CONSUMPTION OF THE VESSEL WILL BE INCREASED BY ABT 4 MT. CHARTERERS ARE NOT ENTITLED TO RETAIN ANY AMOUNTS FROM HIRE PAYMENTS IN CONNECTION WITH ALLEGED PERFORMANCE CLAIMS.

BUNKERS SPECIFICATIONS: RMG 380 AND DMA OR DMB ISO 8217:2017 AS PER ISO/PAS 23263:2019 MIN. VISCOSITY 2 CST AND ALWAYS IN COMPLIANCE WITH ANY APPLICABLE SULPHUR CONTENT REQUIREMENTS, (NET CALORIFIC VALUES ALWAYS 10200 KCAL/KG). CHARTERERS MAY PROVIDE THE VESSEL WITH BUNKERS OF ISO 8217:2012 SPECIFICATION AS PER ISO/PAS 23263:2019 ALWAYS IN COMPLIANCE WITH ANY APPLICABLE SULPHUR CONTENT REQUIREMENTS, WHEN/WHERE BUNKERS OF ISO 8217:2017 SPECIFICATION IS NOT AVAILABLE.

BUNKERS SPECIFICATIONS: RMG 380 AND DMA OR DMB ISO 8217:2017 AS PER ISO/PAS 23263:2019 MIN. VISCOSITY 2 CST AND ALWAYS IN COMPLIANCE WITH ANY APPLICABLE SULPHUR CONTENT REQUIREMENTS. CHARTERERS MAY PROVIDE THE VESSEL WITH BUNKERS OF ISO 8217:2012 AS PER ISO/PAS 23263:2019 ALWAYS IN COMPLIANCE WITH ANY APPLICABLE SULPHUR CONTENT REQUIREMENTS, WHEN/WHERE BUNKERS OF ISO 8217:2017 SPECIFICATION IS NOT AVAILABLE. IF ISO 8217:2012 IS NOT AVAILABLE, CHARTERERS MAY PROVIDE THE VESSEL WITH BUNKERS OF ISO 8217:2010. IF ISO 8217:2010 IS NOT AVAILABLE, CHARTERERS MAY PROVIDE THE VESSEL WITH BUNKERS OF ISO 8217:2005.

ALL DETAILS ABOUT

Fig.1: Example of the CP Description attributes

Most period Charter Parties have the following descriptions regarding the vessel's speed and consumption relation - serving as strict reports filtration parameters, *Plomaritou (2014)*:

I. Main descriptors:
   - Bunker Grade: description of the allowed bunker grades in ISO (8217/2010) format,
   - "About" statement to indicate not precise descriptions, usually in wording like "About" shall mean an allowance of plus/minus 0.5 knots for speed and/minus 5 per cent for fuel oil/diesel oil / low sulphur gas oil consumption.
   - Weather range, so-called "Good Weather Conditions" for the description. In most contracts, it is up to a wind 4 Beaufort force and Douglas Sea state 3. Often, the significant wave height is additionally restricted to 1.25m.
   - The central description part is the speed vs. consumption pair. In most cases, total consumption is the sum of the Main Engine, Auxiliary Engines, and Boiler. Some cases have, however, ME-only descriptions. The speed-consumption pair may be divided into Maximum / ECO / Super ECO and Super Slow Steaming parts. Some Charter Party agreements have only a "single speed" description.
   - The central part may be divided into "warranted" and "without guarantee" speeds and consumption pairs.
   - In the case of the ME-only speed-consumption description, the Auxiliary Engine consumption should be defined when at sea.
   - Description of Auxiliary Engines consumption in port divided into "Idle" and "Working" phases.

II. Additional CP description attributes. The additional array of filtration wordings may include phrases like:
   - "with no adverse currents and no current factor": excluding the periods with adverse currents. Sometimes, with additional "as recorded in ship log books," which would exclude the hindcast as a weather source.
   - "favourable currents not to be taken into account"
   - "not exceeding summer draft and even keel" without an exact description of what laden and ballast may indicate.
   - "excluding any voyage under 36 hours duration."
   - "subject to good weather days of 24 consecutive hours."
   - excluding "periods during reductions of speed for safety, sailing in piracy areas, in congestion, in reduced visibility, manoeuvring or sailing in shallow/restricted waters, when loaded with deck cargo and when approaching/entering/leaving ports, rivers, canals, etc."
   - “any gain over and above the minimum warranted performance to be set off against loss on time and/or consumption.”
   - “no excessive hull fouling due to anchoring" or similar wording to exclude long idle times without cleaning.
   - "No extrapolation allowed" - a significant and harsh statement disallowing the extrapolation of "good weather" calculations into "bad weather" periods.
   - "vessel entitles to use more diesel oil in narrow/shallow/busy waters and engine starting/stopping" without giving specific values or ranges.

Calculation methodologies or mathematical formulas are usually not part of the Charter Party. Instead, it is formulated using the long and unclear methodology used during arbitration and legal disputes. As the main "about" description and various matrix of used attributes vary significantly, the interpretation and these quasi-performance calculations are unclear and open the doors for different interpretations between the owner and charterer. Apart from that, as given in the media, the weather worldwide has worsened during the last few years, finding the "good weather" days is becoming more and more difficult during the voyages. Additional attributes practically filtrate out most of the good weather days, rendering that pseudo-methodology statistically impotent to establishing the vessel's performance.

2.3 Consequences of used consumption methodologies

The CP description is a legal promise from owners to charterers, used in voyage calculations and impacting the Profit & Loss tools, including planned bunker price calculations vs. actual fuel consumption. Note that the CP descriptions are usually set when the contracts between owners and charterers are signed and not adjusted within the contract timeframe until there are specific provisions regarding post-drydocking performance. Furthermore, owners often do not sufficiently consider the impacts on vessel performance described in this study under 1.2. This also has to do with how charter contractors operate, *Nugroho (2005)*. One can determine the difference between the measured fuel performance based on noon reports and the Charter Party consumption figures as a CP overconsumption percentage:

$$Average\ CP\ Overconsumption = \frac{FC_{NoonReports}(Draught, Speed, Weather)}{CP_{Consumption}(Draught, Speed, Weather)}$$

Fig.2 shows the average CP Overconsumption estimation for a fleet of 55 bulk carriers over a 5-year Dry Docking period of the bulk carrier chartering company partnered for this study.

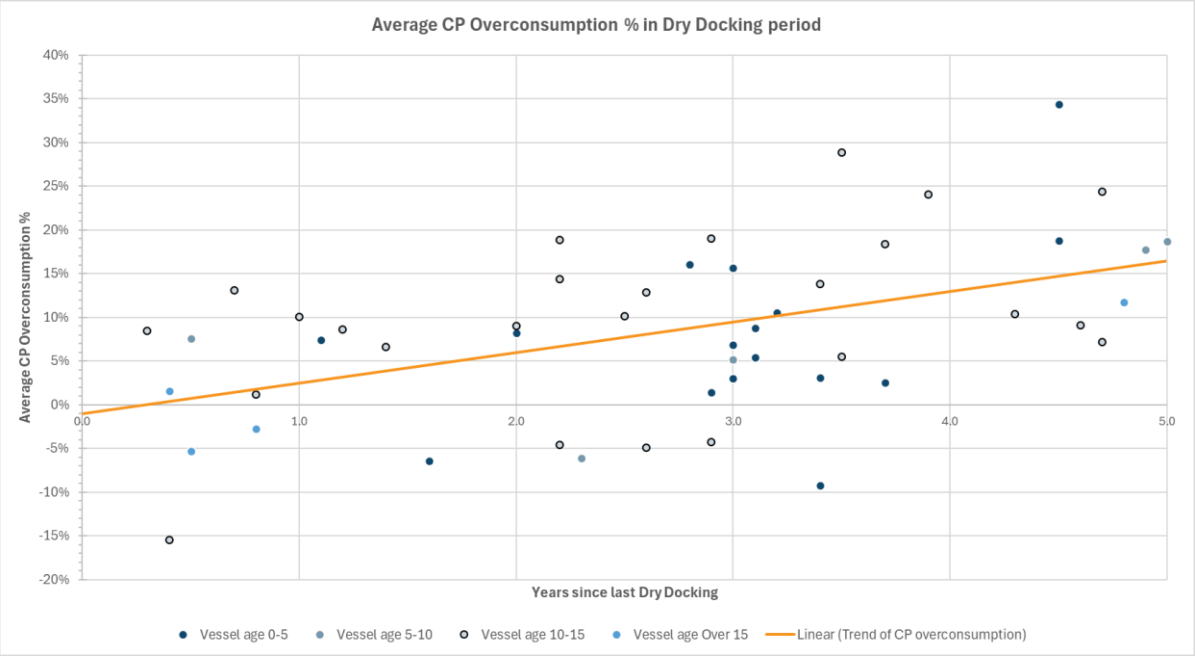

Fig.2: Charter Party overconsumption within a Dry Docking period (each point shows one vessel)

One can observe that the overconsumption compared to the Charter Party agreement gets higher as time passes since the last Dry Docking. The linear trendline of the graph shows an average overconsumption percentage rising to about 3.5% yearly since Dry Docking. It has to be said that the presented graph includes owners doing due diligence in recalibrating descriptions before starting a new charter and owners not calibrating descriptions at all.

The current practice of relying on Charter Party consumptions for vessel operations is impractical. Some improvement could be made by accounting for performance degradation over time. Owners and charterers should incorporate an assumed degradation slope into the "vessel performance" clauses, ensuring a more accurate reflection of fuel efficiency within the Dry-Docking period.

The reluctance to take steps towards improving chartering processes is based mainly on the lack of proper scientific and legal sound approaches to the calculation process. Without such a robust scientific assessment and an effective incentive structure, the potential for performance improvements and CO_2 reduction will largely remain untapped. This needs to change. Addressing these issues with a more

scientific and structured approach can help improve accuracy, efficiency, and sustainability in vessel operations, *Bonello and Smith (2019).*

Due to the limited quality and reliability of the Charter Party fuel tables, charters shall pre-evaluate a vessel based on available data before the fixture. Available methodologies for this are analyzed in the following chapters.

3. Available data and performance prediction methods

3.1. Publicly available data

Estimating fuel performance for unknown vessels relies on the availability and accuracy of public data sources. One can get base information about vessel designs from general web portals like the one from IHS Markit. Such databases provide general vessel information like the dimensions, engine types, build year, and some retrofit history. One needs to keep in mind that certain information might not be up to date. It is also important to note that these sites do not directly offer fuel performance data; however, vessel characteristics are needed for performance prediction calculations.

Furthermore, there is a variety of providers that offer AIS Position Data. Automatic Identification System (AIS) data is critical for tracking vessel movements and operational patterns. One can identify the speed profile, operational area, and distance travelled by analysing AIS data. One should keep in mind that AIS was developed for vessel identification and practically as a helpful tool to improve collision avoidance; thus, the input needs to be understood in this context. For instance, draught information will more likely be the maximum draught than the mean draught of the vessel. Also, Officer On Watch manually updates such information, and there can be many instances where AIS manual inputs are wrong or never adequately updated.

In addition to general information about the vessel and its current operational patterns, one can obtain some Emission data for it in case the vessel travelled to Europe. EU Monitoring, Reporting, and Verification (MRV) data is publicly available and discussed further in chapter 3.6.

These sources collectively provide a framework for assessing vessel fuel performance. However, the effectiveness of the estimations hinges on the integration of data from the varied sources into coherent models that reflect the complexities of vessel operations. Each source has its strengths and limitations, understanding these is key to making an optimum forecast of fuel performance analysis.

3.2. Predictions using the EEDI and EEXI

The EEDI was adopted by the International Maritime Organization (IMO) in 2011 as part of the MARPOL Annex VI regulations and entered into force on 1 January 2013, *IMO (2011)*. It was developed to promote energy-efficient ship design by setting minimum efficiency requirements for new ships. In essence, it serves as a theoretical CO_2 emission score.

The IMO introduced the EEXI as part of the same regulatory framework to extend efficiency principles similar to those of existing vessels. Unlike the EEDI, which applies to new ships, the EEXI establishes a standardized approach for assessing the energy efficiency of vessels already in operation. This is achieved by setting technical efficiency baselines that existing vessels must meet to comply with emission reduction targets, *IMO (2021)*.

EEDI and EEXI values are not publicly available but can be requested within a chartering process. Apart from that, an equivalent efficiency measure can be calculated according to the regulations set by IMO. In principle, this is done in the Existing Vessel Design Index (EVDI), a proprietary metric developed and used by RightShip. EVDI is fundamentally based on the EEDI concept but adapted for existing vessels where complete design data might not be available. RightShip uses EVDI to rate vessels on a carbon efficiency scale (A–E), where A represents the most efficient ships and E the least.

For the purposes of this study, the EEDI values used are derived based on available data, utilizing EEXI as a reference where necessary to maintain consistency in assessing vessel efficiency. This approach is conceptually similar but may not be identical to the EVDI methodology.

3.3 Predictions using the Carbon Intensity Indicator (CII)

Similarly to EEXI, the International Maritime Organization (IMO) adopted the Carbon Intensity Indicator (CII) regulations in 2021 as part of amendments to MARPOL Annex VI. Accordingly, these regulations entered into force on November 1, 2022, and became mandatory for all ships starting January 1, 2023, *IMO (2022).* The CII Index is calculated from a simple formula:

$$CII_{Attained} = \frac{Annual\ Fuel\ Consumption \times CO_2\ Emission\ Factor}{Annual\ Dist.\ Sailed \times Design\ Tonnage\ of\ the\ Vessel}$$

The calculation data are reported under the IMO Data Collection System (DCS). Based on the reference CII value estimated for 2019 and reduction factors, the attained CII within a year is further divided into 5 ratings from A to E based on calculated limits. Failure to meet a D or E rating imposes additional corrective plans for the owner in the Ship Energy Efficiency Management Plan (SEEMP).

Unfortunately, IMO-DCS data are not publicly available, and owners are not sharing the attained CII values with charterers. When asked, owners refuse to share "entry" CII values pre-charter as the Charter Party CII clauses generally calculate the AER value only within the chartered period, and based on that, the clause is evaluated. So, no pre-entry CII value sharing is necessary in such a scenario. As the CII is still an operational parameter, the paper will briefly examine the benefit of including it in the pre-charter assessment.

3.4. Empirical model using Linear Regression of Microsoft Excel

Within this study, an Excel-based linear regression model to predict vessel fuel performance, measured as the total fuel consumption per 24 h at a speed of 11.5 kn, scantling draft, and a weather condition of BF4 all Dir, was developed. Linear regression is a statistical method that models the relationship between a dependent variable and one or more independent variables. The model assumes a linear relationship between fuel performance and selected vessel attributes. So:

$$Fuel\ Performance = \beta_0 + \beta_1 \cdot X_1 + \beta_2 \cdot X_2 + .. + \beta_n \cdot X_n$$

- β_0: $Regression\ intercept$
- $\beta_{1\ldots}\beta_n$: $Regression\ coefficients$
- $X_{1\ldots}X_n$: $Selected\ vessel\ caracteristics$

The reference dataset for the linear model had 92 bulk carrier vessels, excluding the 10 test case vessels of Chapter 5. The following parameters were used as vessel characteristics:

- Has Bulbous Bow (Binary: 1 = Yes, 0 = No)
- Displacement (tonnage)
- LOA (Length Overall) (m)
- LBP (Length Between Perpendiculars) (m)
- Beam (m)
- Scantling Draft (m)
- Ballast Draft (Light) (m)
- Deadweight Tonnage (DWT) (tonnes)
- Vessel's Age (@Last Report) (years)
- Main Engine Maximum Continuous Rating (ME MCR) (kW)
- Main Engine RPM at MCR (ME RPM@MCR) (rpm)

These variables were chosen due to their theoretical and empirical significance in fuel consumption estimation.

3.5. Empirical models by vessel performance service providers

In recent years, companies specializing in data technology and vessel performance analytics have developed advanced fuel consumption forecasting algorithms. These models use extensive datasets, including vessel noon reports, high-frequency sensor data, weather conditions, AIS signals, port activities, maintenance records, and vessel specifications. Such algorithms can predict a vessel's fuel consumption across various operational scenarios, even when specific vessel data is absent. As these models process vast amounts of data, they continuously learn and adapt, enhancing their predictive accuracy over time. Continuous refinement through machine learning techniques enables these models to improve accuracy over time, offering a more dynamic alternative to traditional static models. The model of one of these providers is available to the bulk carrier chartering company partnered at this study and is analyzed along with the other methodologies.

3.6. Another potential option: EU MRV

Another methodology for predicting fuel performance is based on EU MRV data as mentioned above. The EU Monitoring, Reporting, and Verification (MRV) system collects fuel consumption and emissions data from vessels above 5,000 gross tonnages operating within the European Economic Area. The database has public access through https://mrv.emsa.europa.eu/#public/emission-report . It allows the analysis of fuel efficiency across different vessel types. A sample of the data which can be extracted from the web portal is shown in Fig.3.

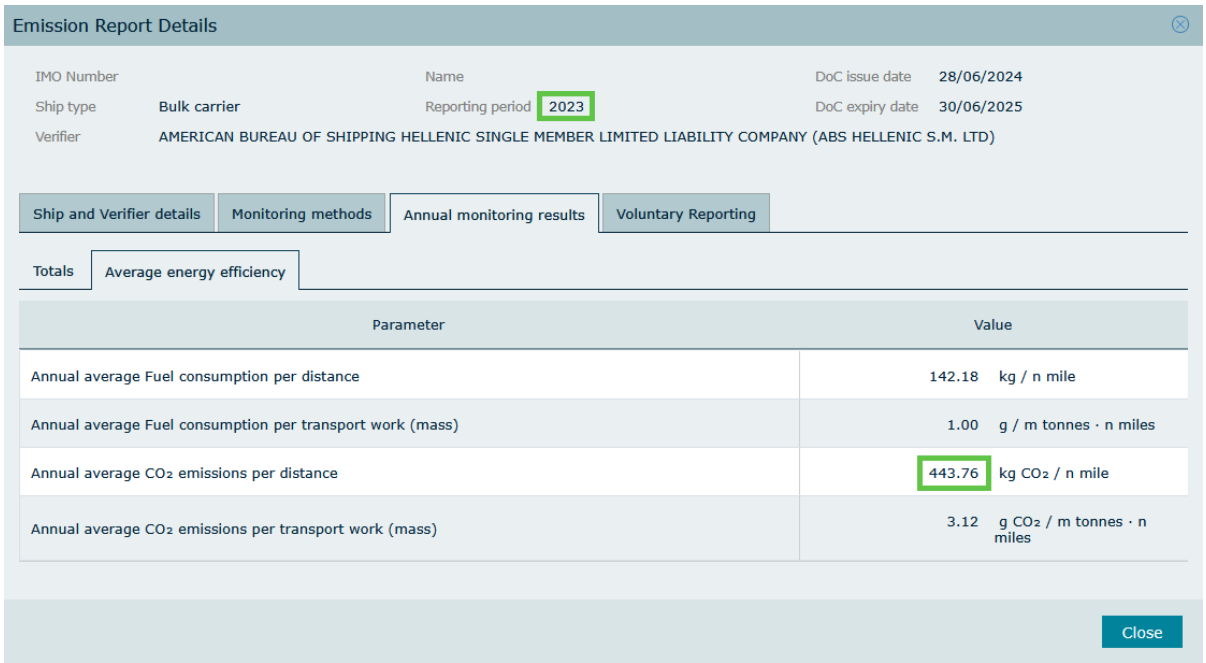

Fig.3: EU MRV data for one of the assessed Bulk carriers

Unfortunately, EU MRV data has limitations, including availability gaps and regional restrictions. Since it only covers vessels operating within the EU framework, its applicability to global fleet performance prediction is constrained. For the bulk carrier vessels analyzed in Chapter 5 of this study, EU MRV data was only available for a few cases. Due to these limitations, methodologies relying on EU MRV data could not further be considered.

4. Results of case study

4.1. Vessels of case study and their Charter Party

A case study was conducted on three sister-class groups of bulk carriers to assess the quality of different approaches for estimating fuel performance. Each sister class was built within a similar timeframe. The objective was to compare the accuracy of these estimation methods. Table I provides an overview of the vessels included in the case study.

Table I: Overview of vessels which are part of the case study

Vessel Tag	LPP [m]	B [m]	$T_{Scant.}$ [m]	DWT [kt]	Vessel's Age [years]	ME MCR [MW]	ME RPM [1/min]	Reference Speed [kn]	Fuel Performance [t/24h] @Ref Speed, Tsummer, BF4 all Dir.
Pan A	222.0	32.3	14.5	81	13.4	11.0	96.0	11.5	29.4
Pan B	222.0	32.3	14.6	81	13.2	11.0	96.0	11.5	30.8
Pan C	222.0	32.3	14.5	81	12.9	11.0	96.0	11.5	27.1
Cape Old A	283.0	45.0	18.2	180	14.7	18.7	91.0	11.5	43.1
Cape Old B	283.0	45.1	18.2	180	15.8	18.7	91.0	11.5	42.2
Cape Old C	283.0	45.1	18.2	180	15.1	18.7	91.0	11.5	50.1
Cape New A	295.2	50.0	18.5	211	3.2	15.7	68.0	11.5	38.7
Cape New B	295.2	50.0	18.5	211	3.1	15.7	68.0	11.5	37.5
Cape New C	295.0	50.0	18.5	211	3.2	15.7	68.0	11.5	36.4
Cape New D	295.2	50.0	18.5	211	3.3	15.7	68.0	11.5	38.9

Fuel Performance is expressed as the total fuel consumption determined at a speed of 11.5 kn under weather conditions equivalent to Beaufort 4, with wind and sea considered from all directions. The fuel consumption figures are then compared to the performance prediction methodologies.

In Fig.4, the total consumption values of the Charter Party agreement are compared to the current Fuel Performance. One can derive a similar conclusion as in Chapter 2.3: The total fuel consumption values of the Charter Party can rarely be met, and the actual fuel consumption is mostly higher.

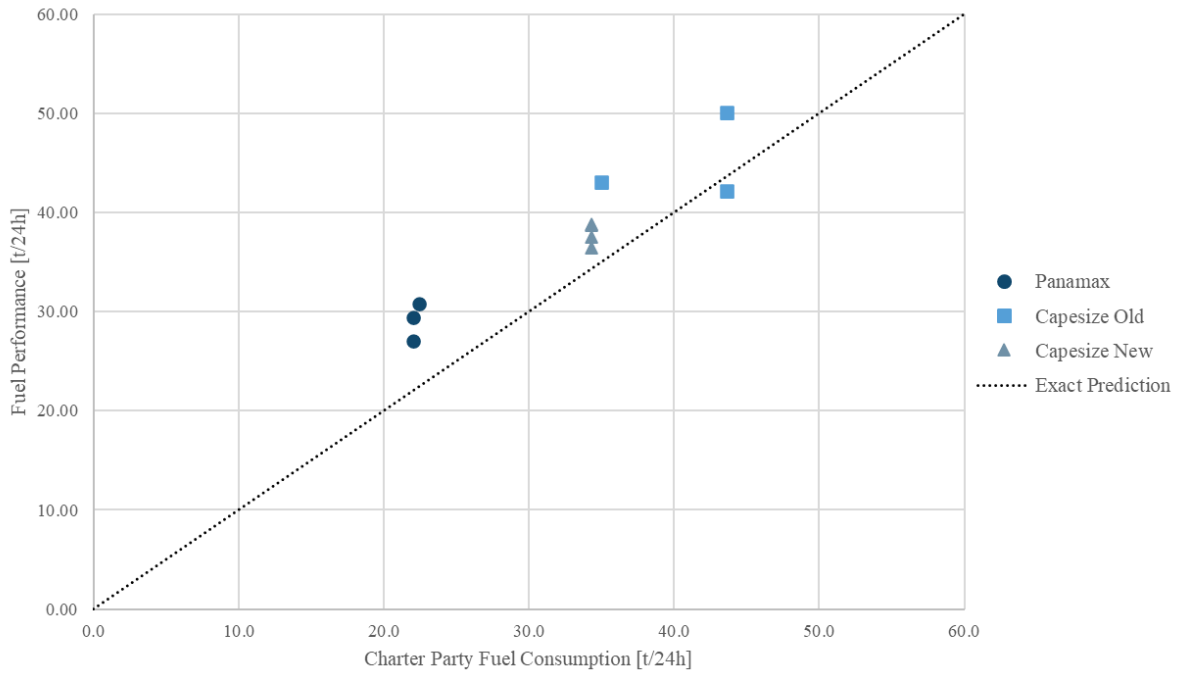

Fig.4: Comparison of the Charter Party figures and the current Fuel Performance

4.2. Calculated EEDI vs. Fuel Performance

Since several vessels in the case study are over 11 years old, not all have an EEDI figure. For those where the figure was absent, an EEDI was calculated using the vessels' EEXI files. The results of the calculated EEDI are compared to the current Fuel Performance values in Fig.5.

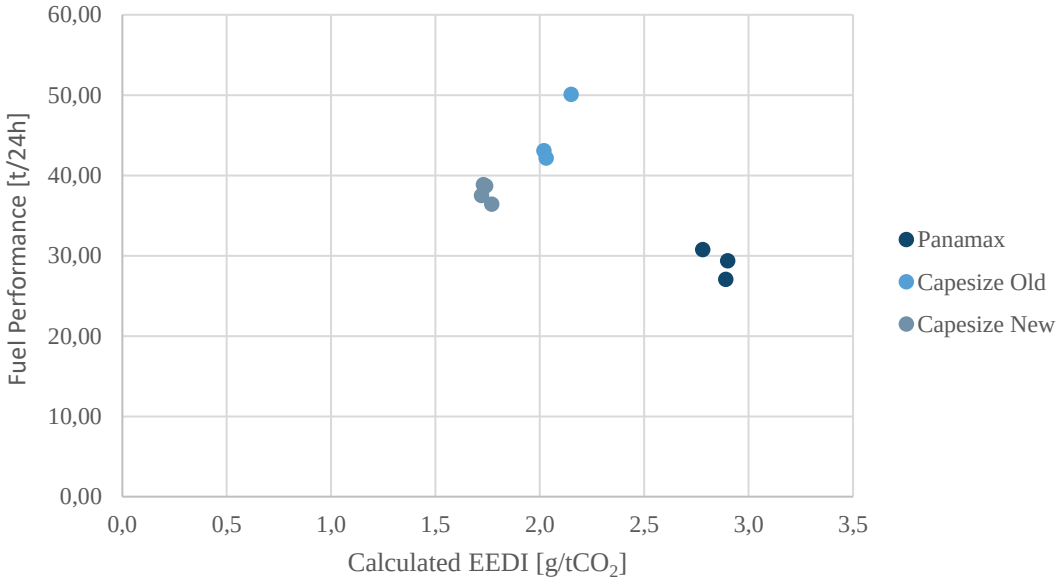

Fig.5: Comparison of calculated EEDI and the current Fuel Performance

As capacity is part of the equation, the EEDI values are comparable only to those of similar vessels. At the Panamax vessel group, an interesting observation can be made: The vessel with the lowest EEDI has a worse fuel performance than her sisters. This discrepancy is likely due to a poorer hull fouling condition of that vessel as compared to her sister vessels. Such operational effects are not part of the EEDI equation. This means that performance prediction methodologies solely based on concepts similar to the EEDI calculation cannot accurately predict operational performance figures for vessels highly impacted by a shipping company's biofouling management skills.

4.3. CII vs. Fuel Performance

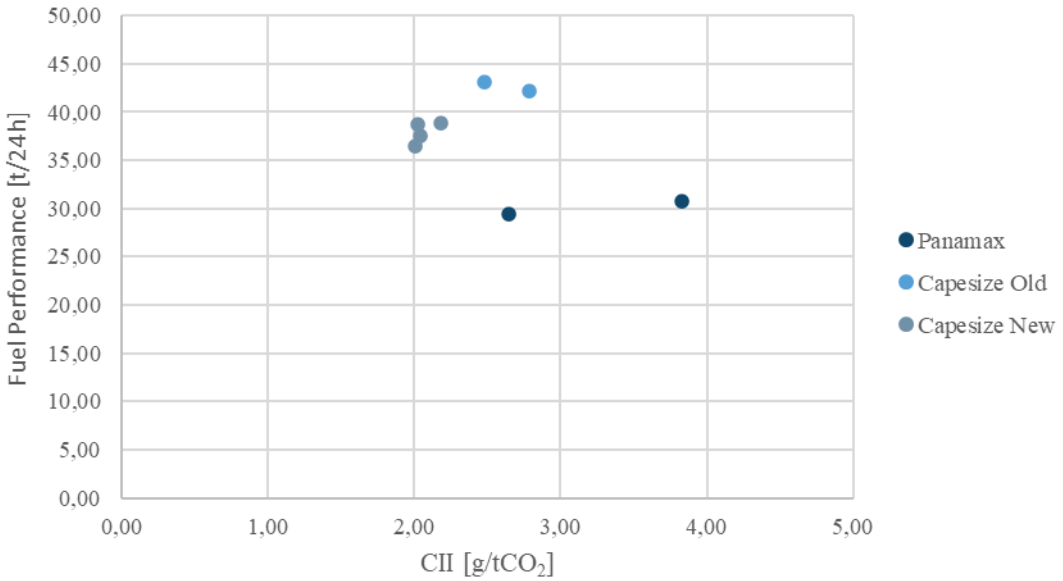

Fig.6: Comparison of CII from 2013 and the current Fuel Performance

The CII values available, when this paper was written, are based on operational data for the year 2023. Some of the figures were not available to the authors. No CII value was available for the vessels “Pan C” and “Cape Old C”. In Fig.6, the fuel Performance for the remaining 8 vessels is shown vs. the CII. Overall, there is no strong correlation between the CII and the current fuel performance. One can observe that the two remaining Panamax vessels have quite different CII values but somewhat similar fuel performance figures. The same goes for older Capsize vessels. Most likely the root cause of the high discrepancy is that the vessels had quite different operational profiles in 2023. The CII rating cannot fully describe the Fuel Performance of a single vessel, compare, *Marioth (2022)*..

4.4. Predictions by Linear Regression Model vs. Fuel Performance

In Fig.7 the linear regression model results are compared with the observed Fuel Performance values of the 10 case study vessels. The model’s prediction accuracy varies across the cases, with deviations ranging from -9.70% to +8.67%.

The linear regression model developed for this paper demonstrates a strong correlation with actual fuel performance, as indicated by the Multiple R-value of 0.926, showing a high degree of association between the predicted and observed values. Additionally, the R^2 value of 0.857 suggests that the model can explain approximately 85.7% of the variance in fuel performance, reinforcing its reliability in capturing key influencing factors.

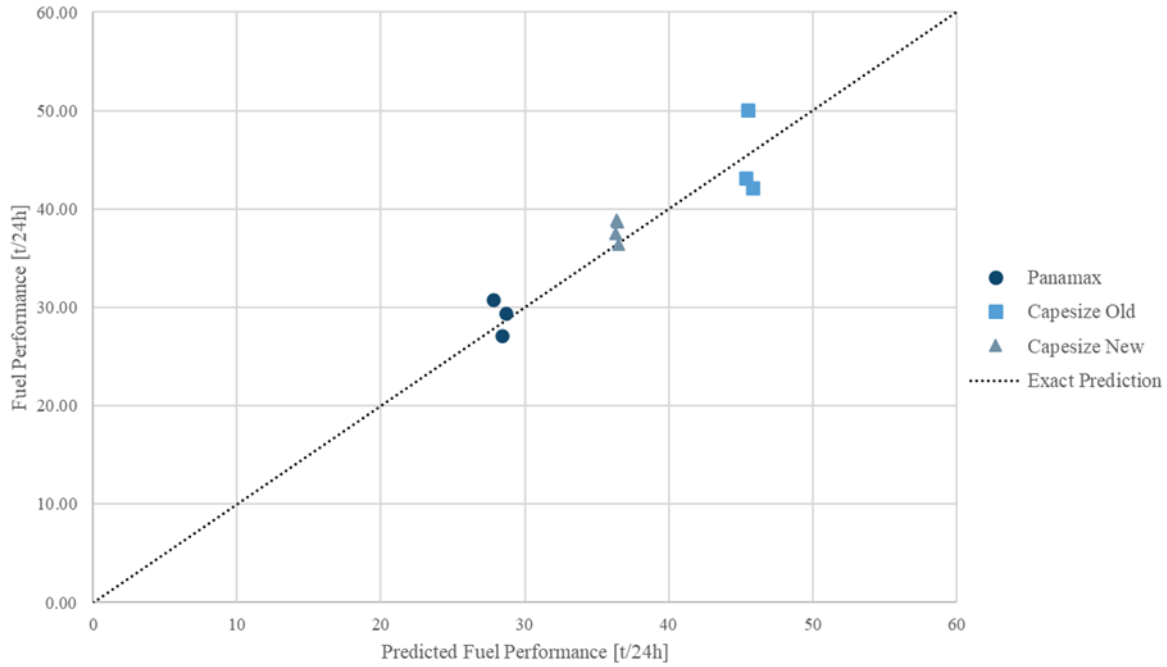

Fig.7: Predicted Fuel Performance through Linear Regression vs. the current Fuel Performance

Despite the strong overall performance, the prediction accuracy varies between vessels, as seen in the prediction error values. While some vessels show minimal deviation (e.g., 0.14%), others exhibit more significant discrepancies, particularly indicating potential influences beyond those captured by the model. Factors like hull fouling pressure and paint conditions may contribute to these variations. Overall, one can already come quite far with such simple models to make better decisions at the pre-charter assessments.

4.5. Predictions of Performance Provider vs. Fuel Performance

In Fig.8, the vessel performance predictions provided by the external service provider, considering unknown vessel conditions, are compared with the observed Fuel Performance values. The results show

a high level of accuracy, with deviations ranging from -7.64% to +7.86% and an average prediction error of only -0.15%.

The standard deviation (4.14%) indicates that while there is some variance in the predictions, the provider's methodology offers a reasonable estimate of vessel performance. The relatively balanced distribution of positive and negative deviations suggests that the model does not exhibit a strong bias toward over- or underestimation.

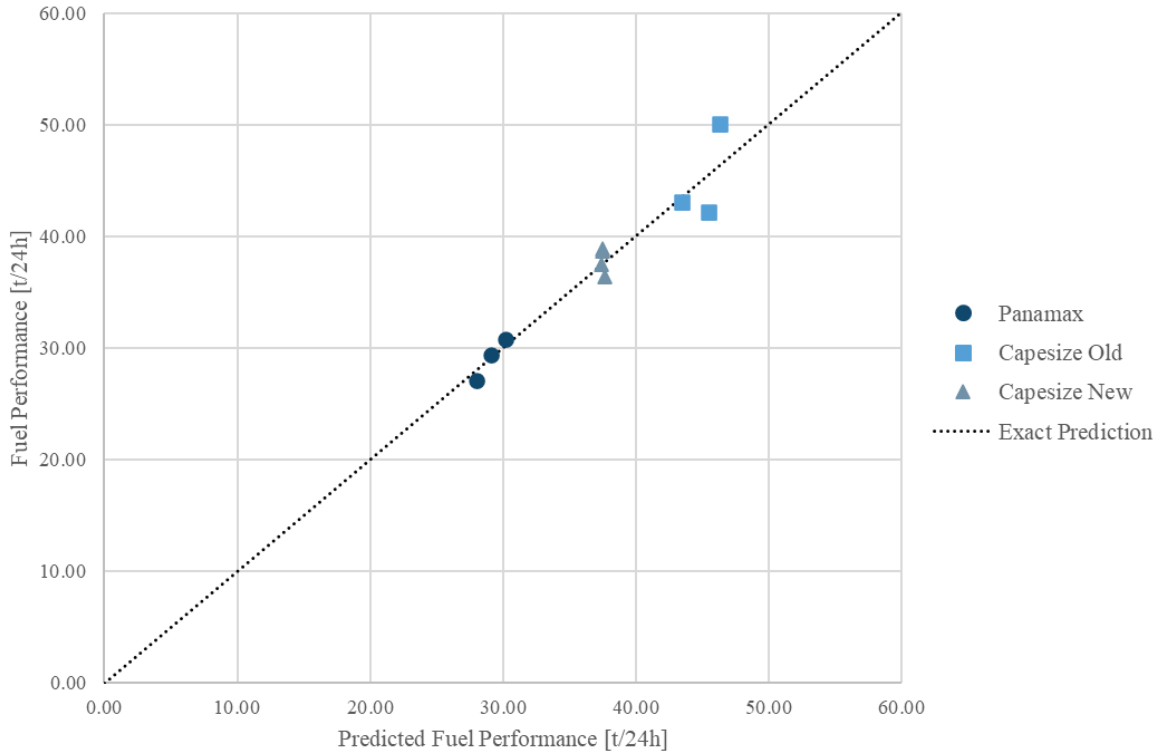

Fig.8: Comparison of the predicted Fuel Performance and the current Fuel Performance

Overall, these results demonstrate that the external performance provider delivers robust predictions. While minor variations remain inevitable due to operational and environmental influences, the provider's methodology is a practical and data-driven resource for performance evaluation.

4.6. Comparison of results

The case study in this paper demonstrates that operational fuel performance of vessels cannot be reliably predicted using the CII or EEDI defined by IMO. The primary reasons for this are the variability in operational profiles and the decline in vessel performance over time, largely caused by hull fouling.

As calculated EEDI and CII can only be compared in a limited way with the used measurement metrics of the study, they are not reviewed further. Instead, Table II shows a comparison of the other approaches of the study. The comparison of different fuel performance prediction methods highlights significant differences in accuracy and reliability. Charter Party (CP) fuel performance values tend to substantially underestimate actual fuel consumption, with an average deviation of -13.7% and a high standard deviation of 8.6%, indicating considerable variability. This makes CP values unreliable for precise operational forecasting.

Empirical models, such as the Excel-based Linear Regression (LR) model created for the study, provide a more structured and data-driven approach, improving prediction accuracy. With an average deviation of -1.8% and a reduced standard deviation of 6.0%, the model offers a reasonable estimate, though there is still some scatter.

Table II: Overview of prediction results

Vessel Tag	Current Fuel Performance t/24h]	Fuel Performance as per Charter Party [t/24h]	Diff. [%]	Fuel Performance as per Excel LR Model [t/24h]	Diff. [%]	Fuel Performance as per External Provider [t/24h]	Diff. [%]
Pan A	29.4	22.0	-25.0%	28.7	-2.5%	29.1	-0.9%
Pan B	30.8	22.4	-27.0%	27.8	-9.7%	30.2	-1.9%
Pan C	27.1	22.0	-18.6%	28.4	4.9%	28.1	3.6%
Cape Old A	43.1	35.0	-18.8%	45.3	5.2%	43.5	0.9%
Cape Old B	42.2	43.6	3.4%	45.8	8.7%	45.5	7.9%
Cape Old C	50.1	43.6	-13.0%	45.5	-9.2%	46.3	-7.6%
Cape New A	38.7	34.3	-11.4%	36.4	-5.9%	37.5	-3.1%
Cape New B	37.5	34.3	-8.6%	36.3	-3.2%	37.4	-0.3%
Cape New C	36.4	34.3	-5.9%	36.5	0.1%	37.7	3.5%
Cape New D	38.9	34.3	-11.8%	36.4	-6.3%	37.5	-3.5%
Average:	-	-	**-13.7%**	-	**-1.8%**	-	**-0.1%**
Standard deviation:	-	-	**8.6%**	-	**6.0%**	-	**4.1%**

The external performance provider's model, currently used for vessel performance monitoring, demonstrates the highest accuracy and consistency. With an average deviation of just -0.1% and the lowest standard deviation of 4.1%, it delivers the most reliable fuel performance estimates, minimizing both bias and variability.

These results demonstrate the need for structured, data-driven methodologies. While empirical models provide a solid alternative, the external provider's approach proves to be the most precise. A continued focus on refining prediction models with real-world operational data will be essential for improving vessel performance assessment and decision-making in the shipping industry.

5. Conclusion

The bulk carriers' Charter Party and embedded legacy pseudo-methodology are potentially the main roadblocks to performance improvement and CO_2 reduction processes. Charter Party contracts should include foreseen Hull & Propeller degradations over time as an immediate improvement. A very important process is simply missing: A high quality and scientific assessment and incentive structure within the Charter Party framework. Legally sound methodologies are needed in the long term to bridge the gap between the owner's and charterers' incentives, *Bonello and Smith (2019).*

The situation requires charterers to carefully pre-assess vessels before the fixture and signature of the Charter Party contract. Providers who only assess the current performance based on technical parameters when the vessel was built, EEDI methodology or similar, have strong limitations as they do not include the impact vessel operation and hull fouling. Without professional performance monitoring pre-assessment, even Excel-based linear regression models to predict fuel performance yield in more viable estimation of fuel performance.

Professional vessel performance software providers using systems based on operational data can provide high quality estimations of the current fuel consumption. Furthermore, the significant changes of hull and propeller performance over time, highlight the importance of continuous vessel performance monitoring for every shipping company.

References

BONELLO, J.M.; SMITH, T. (2019), *Exploring the Effect of Vessel Performance Information Barriers on Decision-Making Practice: A Time Charter Application*, HullPIC Conf., Gubbio, pp.128-142

IMO (2011), Resolution MEPC 203(62), Int. Mar. Org., London

IMO (2021), Resolution MEPC 328(76), Int. Mar. Org., London

IMO (2022), Resolution MEPC.352-354. CII Guidelines, Int. Mar. Org., London

MARIOTH, R. (2022), *How CII ratings (A to E) are linked to energy efficiency*, HullPIC Conf., Tullamore, pp.111-123

NUGROHO, S. (2005), *Concept of Compatibility in Shipping - Fuzzy Set Theory and Case-Based Reasoning Approaches*. TU Berlin

PLOMARITOU, E. (2014), *A Review of Shipowner's & Charterer's Obligations in Various Types of Charter*, J. Shipping and Ocean Eng., pp.307-321

WILSON, J.F. (2010), *Carriage of Goods By Sea*, Pearson Education

Assessment of a Gate Rudder Performance through Full-Scale Monitoring

Paolo Becchi, CETENA, Genova/Italy, paolo.becchi@cetena.it

Abstract

The three-year-long research EU project GATERS has been focused on the assessment of the performance of a new technology aimed to improve the ship efficiency, in terms of speed, fuel consumption, maneuverability and noise emissions. Within this project, a long monitoring campaign has been done to collect data concerning the ship's performance before and after the retrofit. This paper summarizes the results of the full-scale trials and the voyage monitoring up to the assessment of the effective improvement due to the Gate Rudder adoption, passing through the description of the equipment and the analysis procedure used.

1. Introduction

An innovative new energy saving device has been studied and developed in the three years research project GATERS, sponsored by the EC H2020 Programme (ID:860337). The scope of this research was the design, the construction and the full-scale assessment of a gate rudder device on a retrofitted 5500 DWT general cargo. The project has an official sub-license agreement with Wartsila Netherlands BV to utilise the Gate Rudder Patent (EP 3103715) at specific retrofit projects of vessel sizes below 15000 DWT.

In the GATERS project, CETENA leaded the team aimed to design, conduct and analyse the full-scale tests on the target vessel, including sea trials across the retrofit and the whole monitoring campaign. In detail, among the partners involved in the work package group, the on-board sea trials were under the responsibility of Hidroteknik (Hidroteknik yat gemi deniz yapilaritasarim teknolojileri sanayi ve ticaret limited), the off-board sea trials (under water radiated noise tests) were overviewed by Bureau Veritas (Paris) and the monitoring campaign was leaded by CETENA, that uses its own ship performance monitoring system for both the data collection and the results analysis, as published in the related project deliverable.

The assessment covered the most part of the project, the testcase vessel has been equipped with a customized monitoring system before and after the retrofit, to collect performance data of both conventional rudder system (CRS) and the gate rudder (GRS). It made it possible to describe the ship performance about one year before and one year after the adoption of this new technology. During the usual ship operation, the monitoring system automatically collected data from both ship navigation system and specific custom sensors arranged on board by some partners of the project. For the scope of the monitoring campaign, sensors have been arranged on the propeller shaft, the rudder and the fuel pipeline through a new flow meter. All these instruments were coupled with a collection unit located close to the shaft and then up to the wheelhouse acquisition unit through serial connection. Furthermore, the crew has been trained to input the load conditions to monitor also the trim and the ship displacement. Finally, although the wind state has been acquired through ship anemometer, the sea state has been collected separately through a hindcast provider. The data has been saved through daily log files that have been checked and analysed one by one periodically.

Furthermore, custom sea trials have also been conducted across the dry-dock to measure the ship performance in well-known conditions and in accordance with the recommended international procedure ISO15016, as described by *Aktas et al. (2021,2023).* Although the sea trials have been done in full ballast conditions being not possible to reach the laden condition across the drydock, the correlation between the monitoring collected data, the results obtained through the sea trials and finally the numerical predictions performed in the first phase of the project made it possible to assess the performance of the Gate Rudder technology with a reliable estimation of power saving.

1.1. The innovative technology

A gate rudder is an innovative energy saving device ideated in Japan around 2010, it consists of a couple of twin rudders with asymmetric cross-section that are located aside the propeller, the closeness and the interaction between rudders and propeller generates a partial accelerating flow in between like a duct effect with the propeller. This phenomenon induces an additional thrust through the rudders, *Sasaki et al. (2015).* The rudders can also be controlled independently via rudder stock at the top of each, *Sasaki et al. (2015)*, it provides improved manoeuvrability, and seakeeping ability, *Turkmen et al. (2015)*. The system must then be considered as an equivalent propeller for which part of the thrust is generated by the rudders blade without any torque required at the shaft, for this reason it leads to an overall higher efficiency of the system respect to a traditional propeller.

1.2. Feasibility studies

In the last ten years, feasibility studies of this technology have been done through numerical simulations, model scale tests and in some case full-scale sea trials. The following table summarizes a brief and probably not complete description of the vessels used for the investigations done by now. Among all these cases, one of the more relevant applications concerns the twin container vessels Sakura and Shigenobu that have been respectively equipped with a conventional rudder system and a gate rudder system just at the ship delivery, *Sasaki et al. (2019,2020)*. Furthermore, the bulk carrier case provides good indication for low-speed vessel: although the analysis is confined to feasibility studies, the deep numerical investigation and the model test campaigns carried out in SRC (Ship research Center of Japan) show good results in terms of efficiency improvement.

Table I: Feasibility studies of the gate rudder applications

Ship type	name	L_{BP} [m]	V_S [kt]	F_N [-]	Note
Bulk carrier		225.0	14.5	0.158	Feasibility study
Container carrier	SAKURA	101.9	15.5	0.252	CRS at ship delivery 2016
	SHIGENOBU	101.9	15.5	0.252	GRS at ship delivery 2017
General cargo	KOHSIN MARU	68.6	12.8	0.253	Feasibility study
			from	*Turkmen et al. (2016)*	
General cargo	ERGE		12.0	0.214	CRS at ship delivery 2010 GRS retrofitted 2023
			from	*Koksal et al. (2024)*	

The propulsive performance of the gate rudder technology applied on the previously mentioned ships are summarised in the following Table II. The author apologies for the probably not complete and exact data shown that has been collected from the literature available, but it is just important to show the state of art of the order of magnitude of the performance predicted over different kinds of ships.

Table II: Propulsive performance of gate rudders

Bulk carrier			
7-8%		from model tests	*Sasaki et al. (2015)*
Container carrier			
14%	of fuel consumption saving	from sea trials	*Fukazawa et al. (2018)*
14%	of power saving PD in calm water	from sea trials	*Mizzi et al. (2022)*
30%	of power saving PD in rough sea	from monitoring	*Gurkan et al. (2022)*
33%	liter/miles consumption reduction	from monitoring	*Sasaki et al. (2020)*
PREDICTIONS			
8-10%		from study on model test and CFD	*Sasaki et al. (2018)*
Comparison with ITU measurements (model scale)			

1.8%	PE prediction	*Gurkan et al. (2022)*
0.6%	PD prediction	
Comparison with HSVA measurements (model scale)		
11%	PE prediction	
14%	PD prediction	
2%	PD prediction in ballast condition	*Celik et al. (2022)*
6.5%	PD prediction in full load condition	

1.3. The project's testcase vessel

In the GATERS project the assessment of the gate rudder technology has been done through the retrofit of a commercial coastal vessel. M/V ERGE (Ex-JOERG N) is one of eight multi-purpose dry-cargo sister ships, initially commissioned and owned by a German Consortium. It was designed by a German design firm, ABH (ABH Ingenieur Technik GMBH) and was built by the Chinese shipyard Weihai Donghai in 2010-2011. All the eight sister ships have been equipped with conventional rudder systems (CRS) with flaps (Becker type) and 5-bladed, left-handed FPP propellers, *Koksal et al. (2024).* In 2015, one of the GATERS project partners, CAPA, purchased two of these vessels named M/V ERGE, which was selected as the "Target Ship" for the GATERS project and her sister, M/V ERLE. After the purchase, M/V ERGE's capacity increased from 4500DWT to 5500 DWT by increasing her draft by approximately 0.65 m without any engineering modifications to the main hull or propeller or the engine. Bureau Veritas (BV) approved the capacity increase calculations. The ship M/V ERGE underwent a series of full-scale sea trials in 2010 before it was delivered. Following her build, the initial sea trials were conducted in the Yellow Sea of China on February 5th and 6th, 2010, the latter two trials were conducted in 2023 during the GATERS project and before and after the GRS was retrofitted in January 2023 and May 2023, respectively, *Koksal et al. (2024)*. The main dimensions of the target vessel are shown in Table III.

2. Monitoring System

For the assessment of the gate rudder system, a monitoring system was arranged on the target vessel. The monitoring campaign collected the data that could lead to an accurate analysis of the ship performance before and after the retrofit. CETENA provided and arranged its system PM&OTE, developed and maintained since 90's, *Della Loggia et al. (1993), Galli et al. (2014), Becchi (2019).*

The monitoring system was customized and configured for the target vessel. It consisted of one rugged PC with a dedicated software recording the available data on board, proper hardware to acquire in-field signals from torquemeter, shaft RPM, rudder angle, rudder torque and through one serial server. Although the monitoring system was provided by CETENA, the custom sensors were supplied by other partners such BV (shaft and rudder) and University of Strathclyde (flow meter). The arrangement of these instruments was done through collaboration of all the partners involved and the kind support of the crew.

The PC is equipped with a user interface making it possible for the crew to add additional data like payload, draft readings, and the weather condition observed. The PC has been arranged in the wheelhouse to be connected with the signals coming from the integrated navigation system and to be also available for the crew during the navigation. The signals monitored are:

- from GPS: date, time, latitude, longitude, speed over ground, course over ground
- from gyrocompass: true heading
- from anemometer: relative wind speed and direction
- from echo sounder: water depth under keel
- from speed log: speed through water

Table III: Main dimensions of target vessel M/V ERGE

MAIN DIMENSIONS				
			laden	ballast
Length overall	L_{OA}	[m]	89.95	
Length betw. perp.	L_{BP}	[m]	84.95	
Breadth	B	[m]	15.40	
Draught	T_F	[m]	6.46	2.80
	T_A	[m]	6.46	3.80
Displacement	Δ	[t]	7280	3585
Service speed	V_S	[kt]	12.0	
Rudder type			CR	

MAIN ENGINE			PROPELLER		
Type		8L38/32A	Type		FPP
Rated power	[kW]	1960	Speed	[RPM]	147.25
Rated speed	[RPM]	775	direction		left
Gear box ratio		5.263:1	Diameter	[m]	3.42
			Blade number		5
			P/D		0.83
			BAR		0.61

The collection of the signals from all the other sensors arranged in both steering and main engine rooms has been done through a custom cabinet located close to the shaft, portside. The layout of the monitoring system used for the project is shown in Fig.1.

Acquisition unit

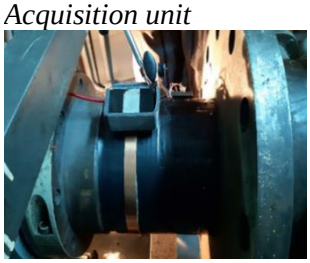

Torquemeter

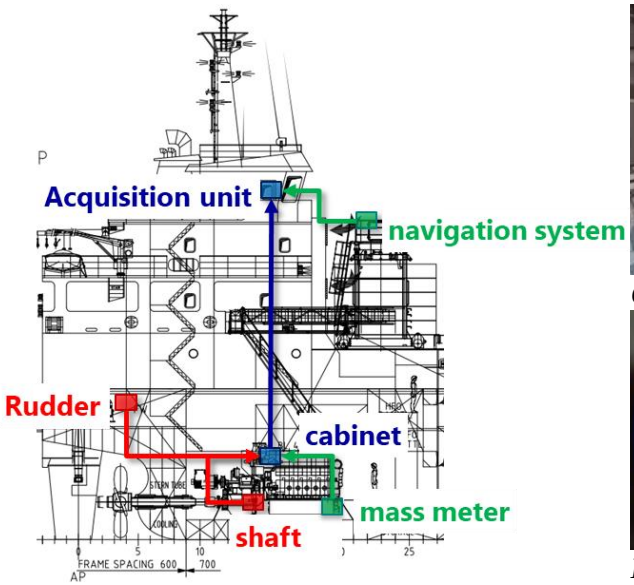

Cabinet

Mass meter

Fig.1: Monitoring system layout

CETENA Performance Monitoring software can acquire signals with a sampling frequency of at least 1 Hz; the effective sampling frequency of parameters from ship systems depends of course on throughput sentences from them. The software can average and store the acquired values with a flexible time interval defined by user (usually every 60 s for this kind of applications) and to save them in proper files. For this reason, the system has been used also for the sea trials done across the retrofit, collecting data every second. Fig.2 shows the user interface that can be used by the crew to take under control the current sailing conditions and the values acquired through specific custom sensors, like the rudders' angle and the fuel consumption. Furthermore, it is also possible to record manual inputs like payload, fuel and estimated weather conditions that represent data that the crew was asked to input at the beginning of any trip.

The monitoring system has been arranged and cabled onboard at the beginning of the project, and it has been made working up to the end of the project, it has been removed some months after the project closure and the data file stored.

3. Methodology

The assessment of the gate rudder has been done through the analysis of data collected in two configurations, that are:

- CRS, the original Conventional Rudder System for which the monitoring campaign started in fall 2021 after complete hull cleaning
- GRS, the new Gate Rudder System that has been retrofitted during dry-dock from January to May 2023. In that occasion a complete hull cleaning has been done as well.

Furthermore, it is important to highlight that retrofit did not affect only the rudder system, but the whole vessel stern, including new propeller, new shaft, two rudders and custom modification of the hull surface at the shaft exit.

Fig.2: Long term monitoring system cockpit

The assessment of the ship's performance in its effective operability has been done through short term monitoring campaigns covering approximately one year for each configuration. Nevertheless, the collected data is affected by uncertainties being the sailing conditions not under control, so particular attention has been paid during the data analysis. Data were continuously recorded and averaged day by day. It means that a single record represents the average of the values collected during a specific time window in which the sailing conditions could be steady or unsteady. Furthermore, even if both the environmental (wind, depth, waves) and the load (displacement, trim) conditions have been measured/input, the effect of their related correction on the results accuracy depends on the analysis method. Although the assessment of the ship performance has been done through a detailed analysis of the data including all the reasonable corrections to improve accuracy, the obtained results can be characterized by approximations due to both the assumptions made and the amount and type of the data recorded. Furthermore, being not possible to carry out custom sea trials in laden conditions, the adopted procedure represents the better way to assess the propulsive performance in usual ship operating conditions.

The adopted methodology is consistent with what is prescribed by ISO19030. Nevertheless, because the ISO procedure published in 2016 considers only the effects of wind and displacement, additional corrections have been developed consistently with ISO 15016 and ITTC 2017. Although a longer monitoring campaign would lead to more consolidated results, the application of the previously

described corrections on the data sets characterized by steady condition makes it possible to define the speed and power through a reduced number of records.

The evaluation of the power curves has been done through the application of some filters making it possible to select only the recorded values consistent with specific constraints, that are: constant sailing conditions, weather conditions not exceeding Bft 3, displacement within 5% the reference value. The resulting data was then fitted through cubic polynomial curve to define the speed-power curve, as usually done for the power assessment, *Fukazawa et al. (2018), Molland et al. (2011), Carlton (2007), SNAME (1988), Saunders (1956).* More details about the procedure used are described in the following.

Once the power curve has been computed, the assessment has been done through the performance comparison in the reference conditions:

- computing the shaft power required by the two configurations (CRS and GRS) to sail the vessel at the reference speed, and then evaluating the power (and FOC) saving
- computing the vessel speed keeping the same shaft power in the two configurations (CRS and GRS) and hence evaluating efficiency in terms of sailing time and fuel saving

An analysis of the performance in terms of fuel oil consumption has been done starting from the evaluation of effective shaft power and a FOC curve that has been defined as the linear curve fitting a specific collected data set (4).

3.1. Constant measured runs

The analysis carried out on the data collected before and after the retrofit was aimed at defining the performance of the vessel in steady sailing conditions, excluding the effect of the weather on the propulsive performance as recommended by the international procedures for the ship in service, *ISO (2016)*. The normative is aimed at the definition of a default method for measuring changes in hull and/or propeller performance of the same ship to itself over a maintenance event, that in this case is the rudder system retrofit.

The method is based on the analysis of data collected onboard, among all the parameters monitored the two primary ones are the ship speed through water V_S and delivered power P_D that must be varied to cover the whole range of the ship speed and must be also constant during each data set considered.

So, the first step of the analysis concerned the definition of 10 minutes long time slots characterized by constant sailing conditions, that are: speed, shaft rate of revolution, rudder angle and heading. The collected data files have been checked one by one using CETENA data analysis software, Fig.3, looking for reliable time slots in which the sailing conditions were constant.

These time slots represent the ‘measured runs’ used for the subsequent performance analysis, and they are characterized by:

- minimum duration equals to 10 minutes
- constant speed over ground
- constant rate of revolution
- constant course over ground
- sea state not exceeding level 3

For each extracted measured run the average values of the sailing conditions have been automatically computed. So, each record used for the power curve computation represents the average value of constant sailing conditions at least 10 minutes long, so no less than 10 raw measured points.

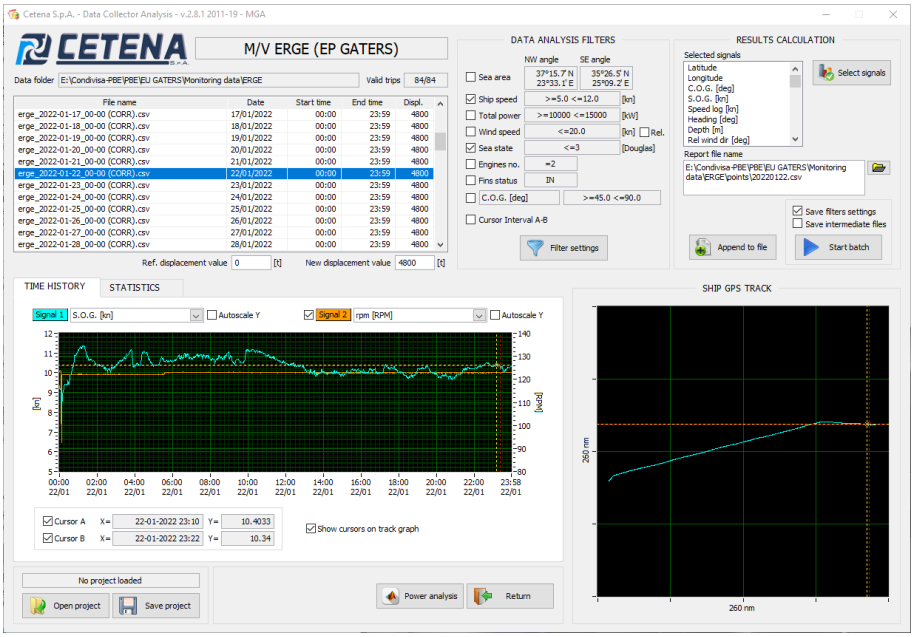

Fig.3: CETENA software for monitored data analysis

3.2. Environmental conditions

The evaluation of the ship performance could not be carried out without some restrictions on the weather conditions encountered during the monitoring campaign. This constraint is due to the need to keep the environmental effects under control, at least as much as possible. The added resistance due to weather conditions far from the ideal ones can lead to an additional power needed that is not easy to be computed in post-processing, and it can lead to misleading results in terms of a reliable power curve. As prescribed by international rules, all the parameters describing the real conditions must be recorded, but only the data set within prescribed limits must be considered.

So, the parameters describing the weather effect acting on the ship performance represent part of the secondary parameters recorded, that are: wind state (direction and magnitude), wave height, period and direction, current components and water depth. Although the wind state and the water depth could be easily measured through the ship's usual instrumentations, for the wave and current data a practical solution has been agreed and adopted. At the beginning of the project the environmental conditions were intended to be measured through specific sensors that would be arranged on the vessel for the whole monitoring campaign periods, but the technical solutions originally considered looked to not fit the expectation required for the data analysis. For this reason, a collaboration with a specific hindcast data provider has been established. Experience with this kind of data and in the same kind of activity has been done in the past ten years by CETENA in CRS, www.crships.org, activities with reliable results confirmed by the community partners.

LaMMA, Environmental Monitoring and Modelling Laboratory for the Sustainable Development, is a public consortium between the Tuscany Region and the Italian National Research Council and it has a specific department for Oceanography. This sector includes activities related to observation systems and modelling of the state of the sea and coastal dynamics, both physical and biogeochemical, to support activities for the protection of the environment and marine ecosystems, safety at sea and in particular navigation, monitoring, management and protection of the coastal strip.

The collaboration between CETENA and LaMMA Consortium included an agreed procedure for the data transferring leading to a quite easy and quick procedure to equip the monitored collected data with the weather conditions. So, stating the weather conditions encountered during the monitoring campaign, it was possible to:

- filter the collected data to consider and analyze only that fulfilling the environmental conditions prescribed by international rule
- correct the ship performance as measured to consider the effect of the weather conditions on the propulsive performance itself.

Nevertheless, being the recommended procedure, *ISO (2016)*, just limited to the wind correction at the moment of the project, some further corrections have been made consistently with *ISO (2015)* to make the evaluation as accurate as possible.

4. Evaluation of FOC curve

To evaluate the relationship between shaft power and the main engine consumption, the data collected during the monitoring campaign has been used to define the fitting curves between the FOC and the power measured at the shaft.

The data used cover the 6 months from the hull cleaning at the beginning of the project for the CRS configuration and the first 3 months after the dry-dock for the GRS.

Fig.4 shows the fitting curves obtained for the two conditions: CRS (red) and GRS (blue). There is a gap between the two conditions across the dry-dock, that can be estimated approximately in 3-4% probably due to maintenance activities on the main engine during the dry-dock, the shaft and propeller retrofit and/or to the differences in hull and propeller cleaning: only underwater cleaning has been done at the beginning of the project while during the retrofitting dry-dock hull cleaning and coating has been carried out. The FOC-Ps curve is just needed to evaluate the FOC value starting from the final speed-power curves in the two conditions, providing the order of magnitude of the fuel consumption can be expected.

4.1. Sea trial across the retrofit

In the two configurations, custom sea trials have been conducted consistently with recommended international procedure for the speed & power assessment of a vessel, *ISO (2015)*. Nevertheless, for a cargo vessel like the project one, the load condition that can be reached at the dry-dock is usually very far from the reference one, that is the full load. Only a full ballast load condition could be used, although inappropriate to represent the usual sailing condition because of the trim and the absence of load. So, the results obtained have been compared with those obtained from numerical simulations carried out in the sea trial condition, just to assess the accuracy of the numerical approach.

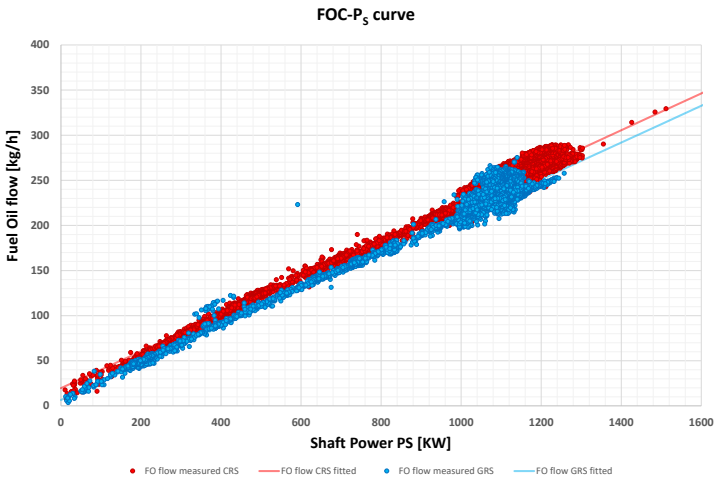

Fig.4: Evaluation of the power vs FOC curve

Although the original plan for the sea trial with CRS concerned the hull cleaning before the tests, the drydock schedule was not available stating the overbooking due to the backlog of COVID-19-related ship maintenance activities. Then the sea trials were done with the hull affected by the medium to heavy slime conditions seen through underwater inspection and a survey during the retrofitting dry-dock. During the retrofit, the hull was cleaned and coated. High value of roughness (300 μm) has been measured, it is considered to be due to the fact that the hull was not shot-blasted during the three coating campaigns over the previous 13 years. It is the reason for the low performance measured in comparison with the sea trial at the ship delivery, *Koksal et al. (2024)*.

4.2. Fuel consumption

The assessment of ship performance could not be done simply through the usage of consumption data because the measured values must be accurately checked and filtered to not include values concerning unsuitable sailing conditions, and then to avoid misleading conclusions. Although fuel consumption is related to the power delivered by the engine and then to the propeller, the performance of the ship through the water must be not confused with the engine performance. The data collected during a monitoring campaign covers all the possible situations in which the vessel is asked to sail, good and weather and depth conditions, maneuvering, anchoring, berthing and cruise conditions. In all these situations, fuel consumption can present different values at the same power at the shaft. Furthermore, the mechanical efficiency in the engine room as well as physical characteristics of the fuel can modify the recorded consumption.

The reason of the possible low accuracy obtained using only the FOC values can be explained through a specific example, using the data collected in June 2023 and after the retrofit, in particular paying attention to what happened on June 9th when the vessel was sailing from Italy to Greece in reduced load condition (5100 t) because in this case the ship had to operate in particular prescribed conditions. In fact, on that day the vessel was moving from Tyrrhenian Sea to Ionian Sea passing through the strait of Messina. Fig.5 shows the track covered by the vessel in that day overlapped with the bathymetric curves.

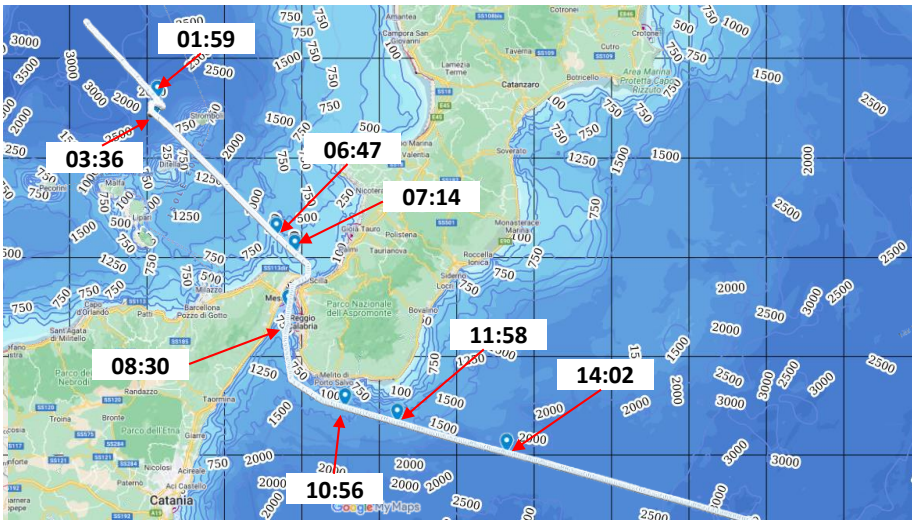

Fig.5: Ship track on 2023 June 9th (GRS)

Fig.6 shows the whole amount of data collected in June 2023 (gray points) in terms of FOC vs shaft power, the black points represent the data recorded on the day considered. It can be noted that there are some points located far from the line fitting the most part of the data, especially those highlighted by the two arrows. The behavior of these values is not due to neither a malfunction of the collection system nor the sensors, but it's just due to the sailing conditions that was not constant.

Fig.7 shows the data collected on the considered day is shown; the diagram represents:

- Shaft power (averaged over 1 minute)
- 3FOC (averaged over 1 minute)
- Rudder angles (maximum and minimum values)
- Speed over ground (averaged over 1 minute)
- Torque (maximum and minimum values)
- Rate of revolutions (maximum and minimum values)

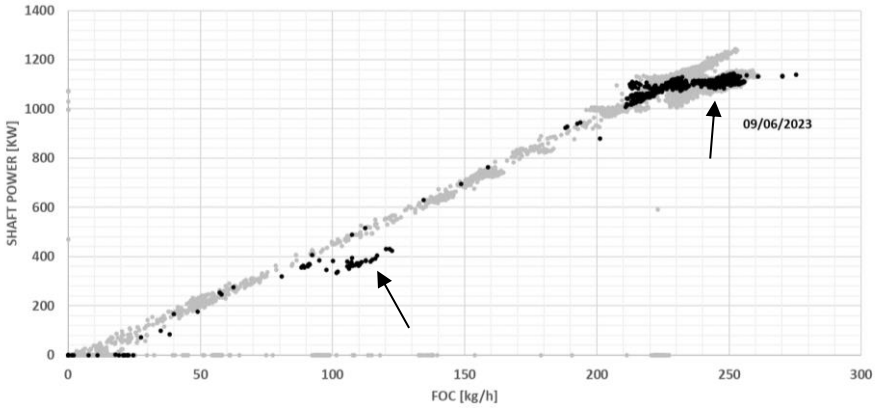

Fig.6: Shaft power vs FOC measured in June 2023

As highlighted by the colored boxes across 14:02, the FOC has an increase of ~5% while the shaft power and the vessel speed are constant. Furthermore, moving up to the end of the day, after 14:02 the spread of the FOC values increases while the power curve looks still constant.

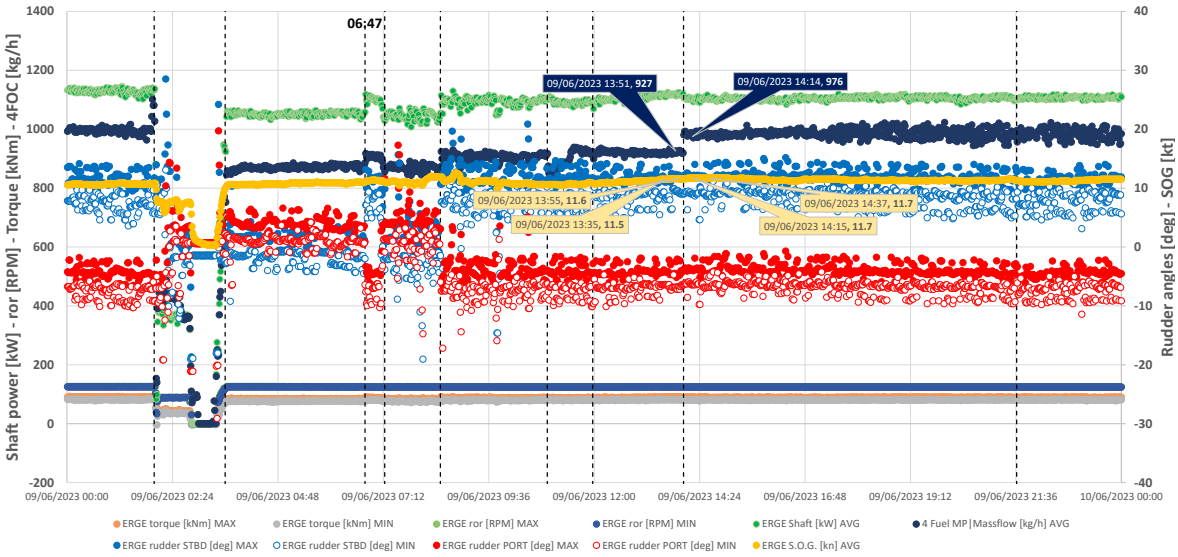

Fig.7: Data collected on 2023 June 9th

Other considerations can be made considering the highlighted time stamps defining specific conditions under which the ship sailed to pass the strait. The conclusion raised from this analysis is that fuel consumption does not represent properly the performance of the vessel, especially if no filter is used to group data related to well defined conditions.

The relationship between fuel consumption and shaft power is linear when the ship is in unsteady conditions, that means maneuver, speed increase or decrease, navigation in constrained area. Otherwise, when the ship is sailing in constant conditions, that means at fixed heading with constant speed, the relationship between FOC and power looks to be not linear: for the same power, different values of FOC have been noticed. This is due to the need to keep the power constant being the ship already sailing

at the desired speed: the consumption needed to reach a vessel speed is higher than that required to keep that speed constant, once it has been reached.

Nevertheless, a rough indication of the order of magnitude of the performance increase obtained through the measured FOC values was done as well.

5. Performance assessment

The evaluation of the speed and power curves have been computed as previously described, considering the data sets extracted through the analysis of the whole amount of collected data.

In all cases, the measured runs considered have been corrected to consider the effect of load and environmental conditions on the speed-power relationship. Then the related curves have been obtained fitting the resulting values with a cubic curve. In the following, the obtained results are shown; furthermore, in the next section the agreement of the adopted methodology with the data collected during the sea trial after the retrofit is shown.

The results presented are related to the expected ship performance in ideal conditions (or as close as possible), in terms of speed and power as recommended by *ISO (2015) and ISO (2016).*

5.1. Ballast condition

The methodology used for the analysis of the monitored data has been applied also in ballast conditions, just for the GRS for which data was available. The scope of this check was just the assessment of the methodology through the comparison with the sea trials results. Fig.8 shows the comparison between the model scale prediction (black line), the sea trials curve (red line) and the power curve obtained through the monitoring campaign. The curves look to be in good agreement, especially considering the usual cruise speed of the vessel not exceeding 10.5 kt. Fig.9 shows the comparison between full ballast curves for CRS and GRS, defined through the sea trial results.

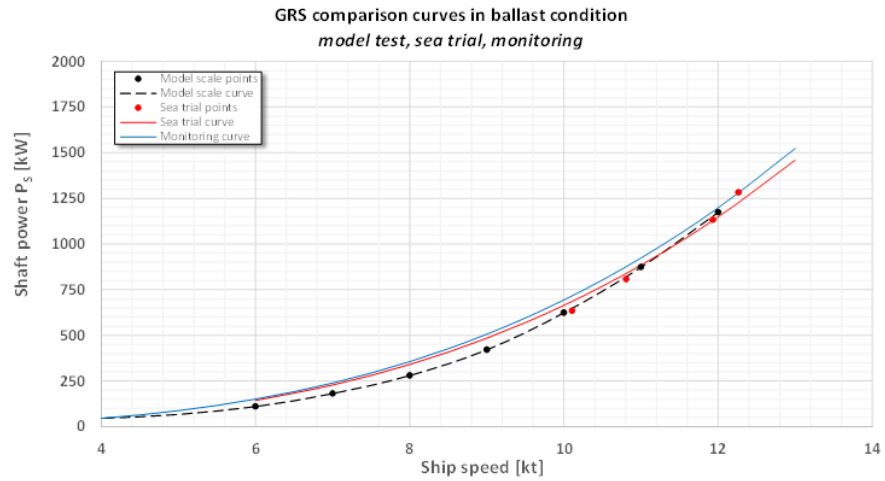

Fig.8: GRS in ballast condition: comparison between sea trials results, model test data and monitoring curve

In the following, the performance measured during the sea trials across the retrofit is analyzed through comparison of the CRS and the GRS for two conditions: at the same speed and with the same shaft power. Although consistently with what prescribed in *ISO (2015)*, the sea trials with CRS have been carried out in not ideal conditions and for this reason the results have been corrected to exclude the environmental effects on the performance. It must be considered that during the sea trial the load (and trim condition) was quite far from that characterizing the full (design) one, in particular:

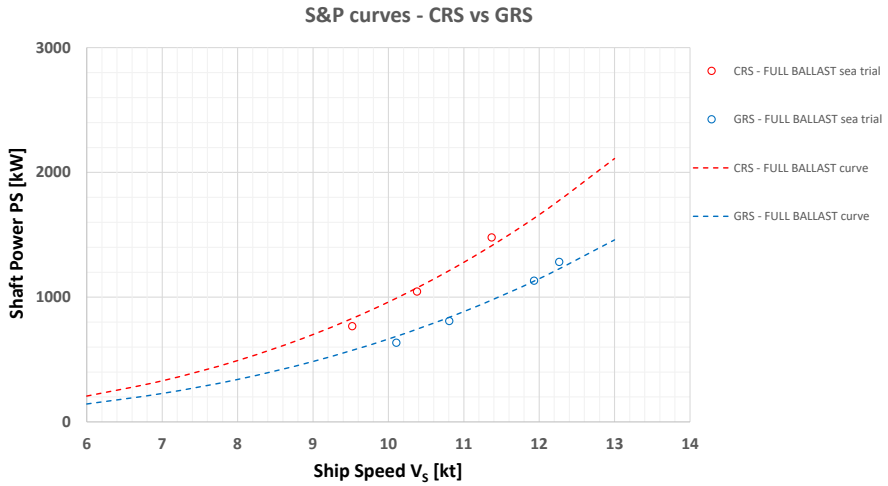

Fig.9: Performance assessment and comparison between CRS and GRS in sea trial condition

Table IV: Full ballast condition (sea trial)

L_{OA}	89.95 m	T	3.300 m
L_{BP}	84.95 m	T_F	3.800 m
B	15.40 m	T_A	2.800 m
		τ	-1.000 m
		Δ	3 585 t

5.2. Full load condition

The full load condition (7500 t) has been analyzed only through the data collected during the monitoring campaign because it was not possible to proceed with S&P sea trial at full load. Nevertheless, the curve obtained has been compared to the predicted one obtained through the model scale test carried out for the GRS condition. Good agreement was found between the curves computed (red: raw data, blue: corrected data) and the model scale results, Fig.10 (right).

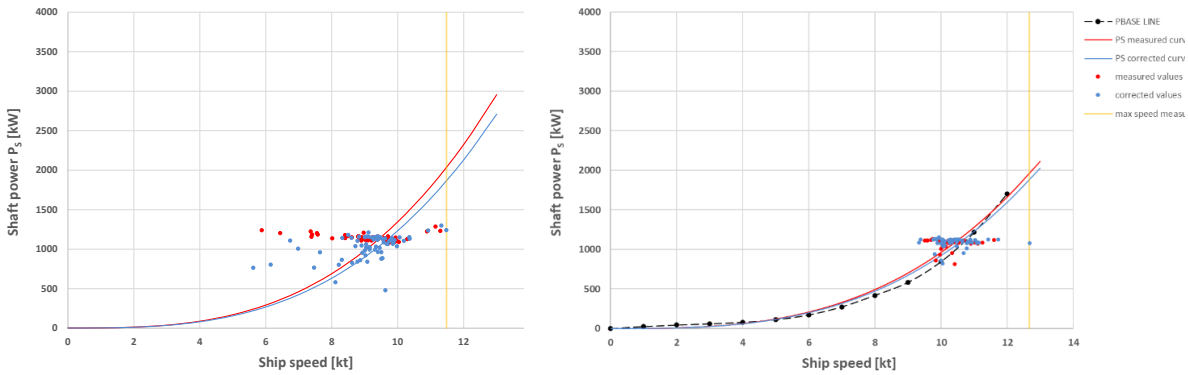

CRS **GRS**

Fig.10: Full load condition – fitting curves for CRS and GRS

The analysis adopted for the evaluation of the S&P curves is based on the use of specific data sets, extracted from the amount of the collected data and referred to constant sailing conditions. The approach is like that used for the official sea trial in which the ship performance is measured over 10 minutes long runs at constant speed, route, shaft speed. These data sets have also been corrected to remove the effect of the weather conditions on the propulsive performance. The evaluation of the S&P is based on the usage of a reduced amount of data (abt 70 for CRS and abt 50 for GRS), representing well established and constant sailing conditions as close as possible to the ideal ones. So, the amount of data

used is considered enough to provide reliable results, taking also into account that each single record used represents the average value of abt. 10 value collected by the monitoring system. Nevertheless, the most part of the data computed is mainly related to the usual cruise conditions adopted by the ship, and hence close to the reference speed that is around 10 kt. Furthermore, the correction methodology has been developed in the more accurate way possible stating the available data, and the points computed are mainly located around specific points even if others look to be far, especially for the CRS.

Fig.10 represents the results obtained through the analysis previously described, where:

- the red points represent the measured run results extracted from the whole monitoring data set
- the blue points represent the measured run results in ideal conditions, and hence the corrected ones
- the solid curves represent the cubic fitting curve representing the raw value (red) and the corrected one (blue)

It can be noted that:

- the cloud of the points computed is focused on the usual sailing conditions, especially for the GRS
- some points are far from the final curves, it can be due to the uncertainty of the collected data (mainly trim and displacement) and to the correction formulation used, although as accurate as possible
- the curves obtained for the GRS are close to the base line (black one), that represents the results obtained from the model scale

Furthermore, the following aspects must be considered:

1. the evaluation of the full load condition curves is based on all the available data for which the displacement is within ±5% of the reference value, as required in *ISO (2016)*, that is in the range: 7125-7875 t (reference value = 7500 t).
2. the analysis adopted does not include any correction for the trim, that depends on what has been input by the crew and it is not the same for the data used for CRS and GRS. It is expected the trim effect can affect the points cloud spread. For the load condition, the trim values are given in Table V.

Fig.11 shows the resulting curves obtained for both CRS and GRS in full load and ballast (trial) conditions, excluding the environmental effect.

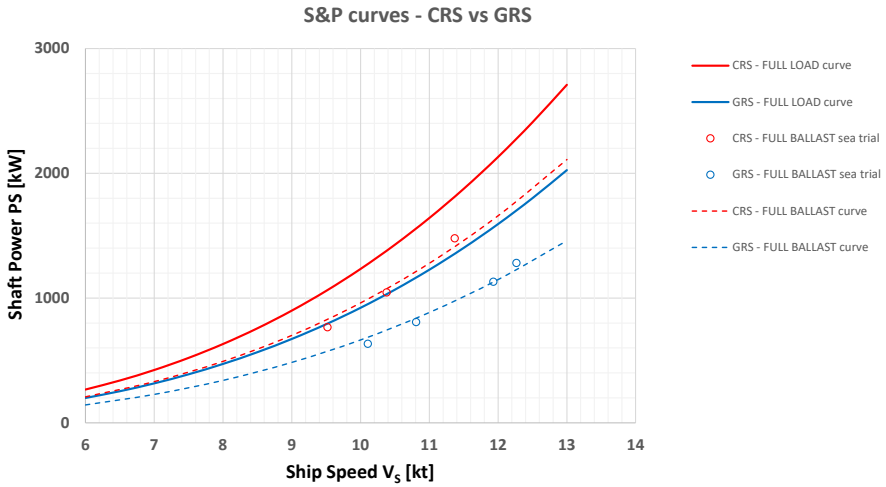

Fig.11: S&P performance in full and ballast condition, CRS vs GRS

Table V: Trim in full load condition

	TRIM (T_F-T_A)	
	min	*max*
CRS	-0.800 m	-0.500 m
GRS	-0.500 m	-0.150 m

5.3. Comparison at the same speed

Once the power curves have been computed for the two rudder systems, the first investigation of the power saving improvement has been done considering the CRS and the GRS at the same speed, to assess the performance of the GRS in terms of power saving. The ship speed considered is that performed by the vessel with CRS in usual operating conditions because it represents the matching point between propeller and engine at maximum continuous rating, covering the most part of the sailing time monitored. The results obtained are shown in Fig.12. Starting from the usual full load sailing condition for the CRS, it can be noted that the adoption of GRS technology can lead to a huge shaft power reduction abt. -25%. Nevertheless, it must be reminded that this comparison is overestimated because of the initial CRS conditions. As introduced, the original configuration was affected by some modifications that obviously lead to a reduced propeller efficiency: in 2015 the ship capacity was increased from 4500 DWT to 5500 DWT through the increase of the draft (0.65 m) without any modification to hull, propeller or engine, *Koksal et al. (2024)*. Furthermore, the original propeller was cropped during the initial trials to reduce the torque, so that it would match the power rating of the main engine, although no clear evidence existed, *Atlar et al. (2024)*. So, stating that in terms of efficiency the design of the propulsion system of the M/V ERGE at the beginning of the project can be considered lower than the original, with the propeller not modified and designed for a reduced full load condition. This is the reason the power reduction computed through monitoring campaigns is considered overestimated; consequently, the comparison with the result obtained through the twin container vessels, *Sasaki et al. (2019)*, that equals to 14% power reduction, looks more consistent.

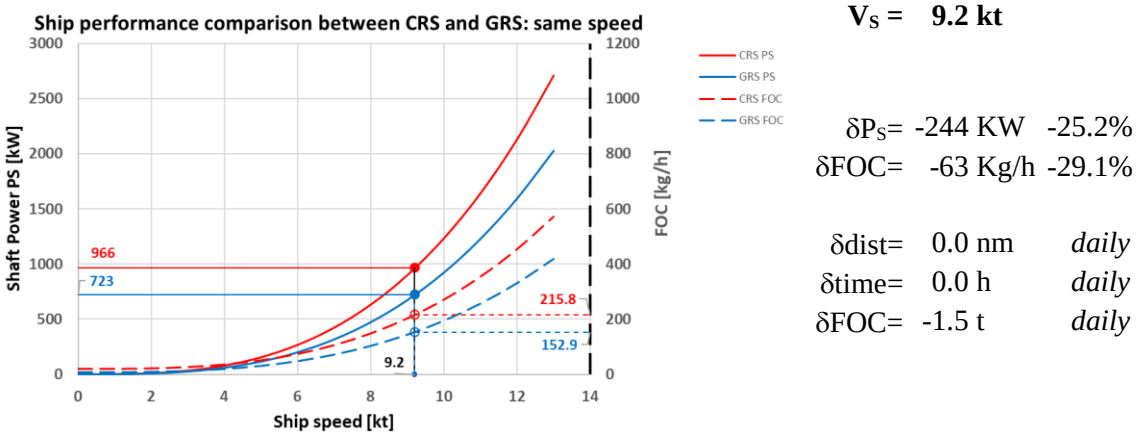

Fig.12: performance comparison at same speed in full load condition

The analysis was extended to the evaluation of FOC predictions, that shows -29% in Fig.12, but the same considerations can be extended to the fuel consumption reduction, including the gap observed between the two FOC curves, that is 3-4%. Nevertheless, it must be considered that this efficiency improvement could be only a virtual one and not feasible, because the reduction of power requirement at the shaft could not be suitable for the engine, that is usually designed to work at the NCR (nominally 85% MCR). A wide modification of the propulsive point of the engine can affect both the efficiency and the mechanics of the engine, with increased maintenance costs. So, this result leads to assessing that a retrofit aimed at the gate rudder adoption makes it possible to derate the engine and then design the propulsion system at a lower power point keeping the usual cruise speed.

5.4. Comparison at the same shaft power

The second phase of the assessment consists of the evaluation of the GRS performance keeping constant the same shaft power that was set during the usual CRS operations. The decision to use this specific propulsive point is related to the engine's continuous rating of the vessel as it was during the project. As described before, because of modifications done on the vessel load and on the original propeller geometry and considering that the hull was not shot-blasted in the three coating campaigns over the previous 13 years, the propulsive points used in CRS operations are surely the more relevant for the engine behavior. So, the prediction has been made fixing the reference shaft power and looking at the GRS improvement in terms of ship speed. At the same delivered shaft power (961 kW, that is the required power to sail at 9.2 kt in CRS condition), the gate rudder can provide a speed increase abt. 0.9 kt, Fig.13. Furthermore, the advantage of using the GRS (on M/V ERGE at NCR) can lead to save 2 hours per day, and then to a couple of advantages: the former is the fuel saved because of both the reduced sailing time and the propulsive efficiency of the GRS itself respect to the CRS, the latter is represented by the sailing time saved in terms of ship operability. From this point of view, it is not possible to estimate a general indication of the increased performance, because it depends on the type of vessel and its operability, but the possibility of reducing the trip duration at the same shaft power implies advantages in terms of ship management. Obviously, the consideration done for the constant speed assessment about the CRS propulsion system efficiency decrease is valid as well.

These results match with the feedback received from the captain in Livorno (ITA) on 2023 September 2nd, that is: "the speed increased from 9.2 kt to 10.0 kt, every day we put two hours saved in the pocket".

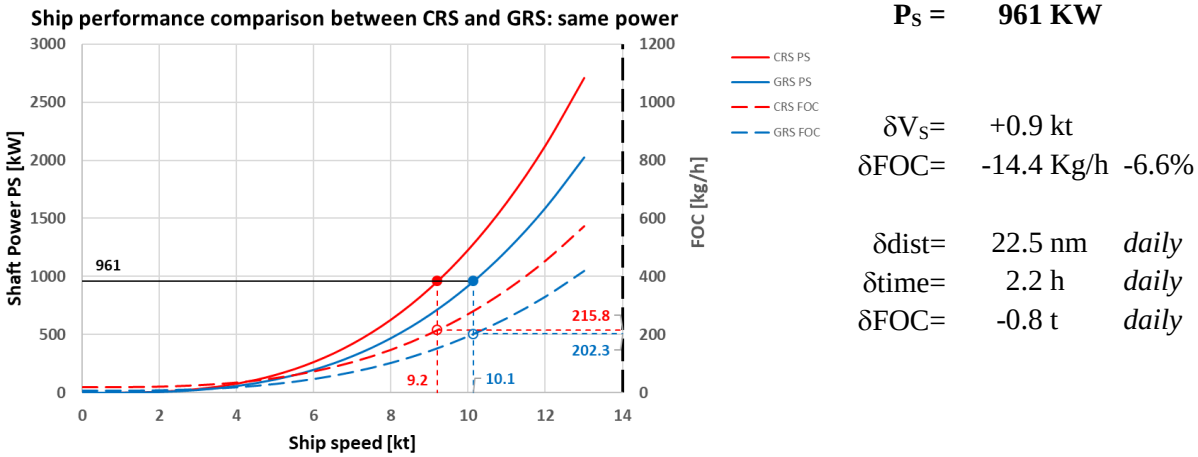

Fig.13: performance comparison at same shaft power in full load condition

6. Assessment through FOC

As previously described in (3), because of the uncertainty of the relationship between the fuel consumption and the ship speed/power the collected data could be used only for a rough estimation of the performance assessment, that is described in this section.

The deep investigation done on the monitored data showed that the assessment of the retrofit cannot be done accurately using the measured values of fuel consumption. The correlation between ship position, maneuvering, speed and fuel consumption showed one more time that the performance of the ship from the hydrodynamic point of view (and then speed and power) are not strictly related to the machinery performance (fuel consumption). At the power level on the shaft, different fuel consumptions were measured because of local and not predictable sailing conditions, it is highlighted especially when the ship is arriving or departing: the consumption measured to reach the same speed looked different. Stating that, although for a rough estimation, it is important to use the fuel consumption values in the better way, without any scaling procedure up to reference conditions (speed and/or displacement) being the scaling law not consistent with the performance of the engine. In the case of the target vessel, for

example, the fuel measured at the same power represents the continuous rating of the engine during usual operation, so the evaluation of a predicted consumption with the CRS at the same speed of the GRS leads to a not reliable and then misleading conclusion, being the engine not able to operate in that conditions.

Usually, the Admiralty coefficient is adopted for power correction and/or prediction, considering different speed and displacement, but although a useful criterion, is a somewhat 'blunt instrument' when used as a performance criterion since it fails to effectively distinguish between the engine and hull-related parameters. The same is also true for the alternative version of this equation, termed the fuel coefficient, in which the shaft horsepower (P_S) is replaced with fuel consumption, *Carlton (2007), Molland (2008), Whipps (1985).* for example, attempted to split the overall performance of the vessel into two components – the responsibility of the engine room and the responsibility of the bridge watch-keepers:

K1 – nautical miles/tonne of fuel (overall performance)
K2 – metres travelled/shp/h (navigational performance)
K3 – grams of fuel/shp/h (engine performance).

In order to reduce the effect of the data spread as observed in (3), the data collection has been analyzed using a specific custom parameter derived from the carbon intensity indicator (CII index) prescribed by *IMO (2021)*, being related to the K3 previously described. As is known, the CII coefficient is computed as the ratio of the total mass of CO_2 emitted to the total transport work, that is the product of the ship's capacity and the distance travelled in a given calendar year:

$$CII_{ship} = \frac{M_{CO_2}}{C \cdot d} \qquad (1)$$

- M_{CO_2} is the total mass of CO_2 emitted and can be computed through the total mass of fuel consumed and the CO_2 mass conversion factor for fuel oil type: $M_{CO_2} = FC \cdot c_F$
- C is the ship's capacity, for general cargo ships it represents the deadweight tonnage (DWT = Δ - LWT)
- d is the total distance travelled in nautical miles

In order to simplify as much as possible the analysis of the data collected, a further parameter has been defined to provide an indication of the fuel consumed during the navigation for each data recorded, excluding any kind of scaling or further computation that, stating the uncertainty shown in 4.2, could lead to misleading results.

So, starting from Eq.(1), and considering that

$M^1_{CO_2}$ mass of CO_2 emitted during a trip long a specific time interval dt
$M^1_{CO_2} = \left[FCO\ \left[\frac{kg}{h}\right] \cdot c_f\ [-] \cdot dt\right]$ being FCO the average fuel oil consumption measured in the time interval dt

d^1 distance covered during the time interval dt in constant sailing condition
$d^1 = V_S \left[\frac{nm}{h}\right] \cdot dt$

Δ ship displacement
$\Delta = LWT + DWT$

dt time step

the CII coefficient can be reformulated for a specific sailing time step as follows

$$CII^1_{ship} = \frac{M^1_{CO_2}}{C \cdot d^1} = \frac{\left[FCO\ \left[\frac{kg}{h}\right] \cdot c_f\ [-] \cdot dt\right]}{(\Delta - LWT) \cdot V_S \left[\frac{nm}{h}\right] \cdot dt} = \frac{FCO\ \left[\frac{kg}{h}\right] \cdot c_f\ [-]}{(\Delta - LWT) \cdot V_S \left[\frac{nm}{h}\right]}$$

$$CII^1_{ship} = \frac{FCO \cdot c_f}{(\Delta - LWT) \cdot V_S} \left[\frac{kg}{t \cdot nm}\right] \quad (2)$$

As previously described, this real-time specific carbon intensity indicator makes it possible to put in relationship the fuel consumption with the performance (speed) and the load conditions (displacement), avoiding any manipulation of the consumption values to referred it at a different and referred power point/ship speed. Nevertheless, although the formulation is quite simple, it must be considered that the knowledge of the right value of both conversion factor and LWT is not relevant for the scope of this work, and they could be ignored leading to a simpler formulation, that is:

$$t_{ml} = 1000 \cdot \frac{FOC}{\Delta \cdot V_S} \qquad (3)$$

with

- FOC is the fuel flow that is the fuel consumption over one hour sailing at the same condition [kg/h]
- V_S is the ship speed and represents the distance covered in one hour sailing at the same condition [kt]
- Δ is the total displacement of the vessel, as declared at departure [t]

The *tml* coefficient represents the amount of fuel needed to move 1 ton over 1 nautical mile, and hence it is related to the speed usually used for the two configurations. It represents a fuel indicator describing the ship as used by the crew, in more efficient ways with both CRS and GRS and consistently with the operating needs.

Fig.14 shows the distribution of the *tml* (fuel tons per mile-load) for the two configurations (CRS and GRS), considering the data collected in the following periods:

- CRS: from 05/12/2021 to 25/09/202
- GRS: from 06/06/2023 to 19/11/2023

Data has been filtered to consider only the propulsive conditions related to the usual continuous rating of the engine. So, consistently with the results obtained in the performance results (see ch.5.4), the assessment through the fuel consumption has been done considering all the measured records close to the nominal continuous rating of the two configurations previously obtained, that are: 9.2 kt for CRS and 10.1 for GRS at full load. The filters applied are related to displacement (±5%), ship speed (±0.5 kt). The threshold applied on the ship speed (1 kt across the reference value) is due to the need to exclude not relevant values for CRS, being its reference speed (9.2 kt) close to slow steaming condition. The comparison has then been done using abt. 6 thousand values for CRS and 9 thousand for GRS.

In the diagram, the *tml* coefficient is plotted referred to the true wind magnitude, as computed through the apparent one measured onboard. Furthermore, the wave height and sea state curves are plotted to describe the weather conditions as they can be expected to be stating the Beaufort scale definition and the over mentioned true wind magnitude as computed. The charts could not be deeply accurate but provide an important indication that is: the performance increase due to the adoption of the GRS technology looks to be constant over the true wind, and hence the weather conditions encountered. In quite condition (true wind close to zero) the values converge on the average values, while increasing the weather condition the spread of the point plotted changes because of the sea state and wind encountered, even if the GRS values vary more than the CRS ones.

Although the reduced spread of the measured values, the consumption of the two configurations is quite

clear and gathered around the average values, represented by the dotted red and blue lines. Nevertheless, apart from the average values it can be noted that the two configurations show another leaning, that in this case are shown by yellow and light blue dotted lines, closer than the average values.

In conclusion, the diagram shows the assessment computed through the measured fuel oil consumption, considering the NCR condition usually adopted by the owner before and after the retrofit in full load, as described in ch.5.4. The measurements have been averaged providing a gap equal to abt. 17%, but different leanings that can be noticed in the points distribution showing a difference abt. 12%. So, as anticipated and previously described in ch.4, the assessment carried out through fuel consumption cannot be accurate enough to provide a reliable indication, contrary to what done through the power analysis done. Nevertheless, a fuel consumption reduction due to the GRS retrofit cannot be neglected and looks really promising.

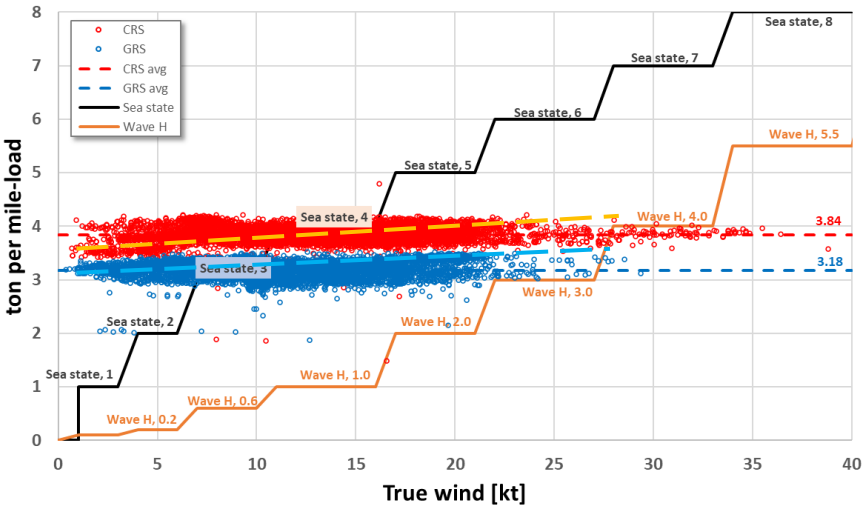

Fig.14: tml vs espected sea state condition

7. Conclusions

The EU project GATERS had the scope of assessing the performance of a new technology aimed at improving ship efficiency, in terms of speed, fuel consumption, maneuverability and noise emission. The project was centered on the design, construction and retrofit of a test case vessel, the general dry cargo M/V ERGE.

One of the key activities done was the monitoring campaign that covered the most part of the project, before and after the retrofit, and that was aimed at collecting the navigation data to be used for the assessment of the GRS performance.

This paper describes the results obtained through the monitoring campaign, in accordance with what is prescribed by the international procedures, that are ISO and ITTC publications. The methodology proposed has been improved with some specific formulations that are not included in the release of these procedures. The analysis led to identify the vessel performance in conditions as close as possible to the ideal ones as recommended by the standard methodologies.

The following main conclusions can be summarized:

- the principle on which the gate rudder is based on generates additional thrust on the rudder blades, without any extra torque at the propeller shaft. For this reason, at the same delivered thrust of a CRS the gate rudder has a higher propulsion efficiency
- the results obtained from the M\V ERGE are really promising, although the CRS condition was affected by previous modifications at the original hull and propeller. This leads to considering

the results being overestimated, even if still good and promising.

- the GRS retrofit can be used for a shaft power reduction or a vessel speed increase, in former case the engine must be derated to optimize its efficiency, in the latter the sailing time is hugely reduced.
- The assessment through fuel consumption cannot be done accurately and without special care in filtering the data and avoiding any scaling law. The proposed fuel parameter (*tml*) is consistent with what suggested in literature, and it shows a not neglectable fuel saving independently from the sea state encountered, over the whole monitored period and for the usual continuous rating conditions adopted by the crew before and after the retrofit. A detailed FOC reduction cannot be determined being the fuel consumption related to the performance of the engine and then not directly to the ship efficiency. Nevertheless, the results obtained just for the target vessel (M/V ERGE) show that it is possible to predict fuel saving in the range 12-17% at the NCR, full load.
- the more relevant improvement due to GRS application is represented by the speed increase, considering the same shaft power of the CRS cruise conditions. In this scenario the vessel can save significant sailing time, that if compared with the CRS implies economic advantages like the reduction of fuel consumption and the improvement of the whole ship's operability.

Acknowledgement

The author would like to thank ing. Carlo Pestelli, from Wartsila Italia S.p.A., Marine Solutions, Engines, Technology-Analysis, for the kind support and experienced discussion concerning the collected data reading, the analysis results and the conclusions.

This paper is based on the Innovation Action Project GATERS, funded by the EC H2020 Program (ID:860337) with independent aims and objectives. The project has an official sub-license agreement with Wartsila Netherlands BV to utilize the Gate Rudder Patent (EP 3103715) at specific retrofit projects of vessel sizes below 15000 DWT.

References

AKTAS, B.; INSEL, M.; SAYDAM, Z.; BRULIARD, F.A.; BECCHI, P., YALCIN, I.; SASAKI, N.; ATLAR, M. (2023), *Dedicated on-board sea trials of the target ship before and after the GRS retrofit*, Deliverable 2.2, GATERS project

AKTAS, B.; GURKAN, A.; ATLAR, M. (2021), *Report of the selected vessels and operational data*, Deliverable D1.1, GATERS project

ATLAR, M.; SASAKI, N.; INSEL, M. ; SAYDAM, Z.; KOKSAL, C.S.; GURKAN, A.; AKTAS, B. (2024), *On the powering performance trials of the GATERS project target ship M/V ERGE*, JSNAOE Autumn Conf.

BECCHI, P. (2019), *ISO 19030: Onboard Monitoring System for Real-time Performance*, HullPIC Conf., Gubbio

CARLTON, J.S. (2007), Marine propellers and propulsion, Butterworth-Heinemann

CELIK, C.; ÖZSAYAN, S.; KOKSAL, C.S.; DANIŞMAN, D.B. (2022), *On the full-scale powering extrapolation of ships with Gate Rudder system (GRS)*, A. Yücel ODABAŞI Coll. Series, Istanbul

DELLA LOGGIA, B.; CAPRINA, G.; TAMURA, K.; VAN DEN BERG, W. (1993), *The on-board monitoring session*, ITTC, San Francisco

FUKAZAWA, M.; TURKMEN, S.; MARINO, A. (2018), *Full-scale gate rudder performance obtained from voyage data*, Istanbul Technical University

GALLI, A.M.; GUALENI, P. ; STRANIERI, G. ; QUALICH, S. (2014), *Monitoring and analysis of the performance data of a RO-PAX ship in the perspective of energy efficiency*, Polish Maritime Research, 21(4), pp.18-26

GURKAN, A.; AKTAS, B.; UNAL, U.O.; ATLAR, M. (2022), *Investigation of Gate Rudder blade design for ship powering using the design of experiment (DoE) method*, Istanbul Technical University

IMO (2021), *Guidelines on operational carbon intensity indicators and the calculation methods (CII guidelines, G1)*, MEPC.336, Int. Mar. Org., London

ISO (2015), *ISO 15016: Ships and marine technology - guidelines for the assessment of speed and power performance by analysis of speed trial data*, Int. Standard Org., Geneva

ISO (2016), *ISO 19030: Ships and marine technology - Measurement of changes in hull and propeller performance*, Int. Standard Org., Geneva

ITTC (2017), *Preparation, conduction and analysis of speed/power sea trials*, Int. Towing Tank Conf.

KOKSAL, C.S.; CELIK, C.; ÖZSAYAN, S.; KORKUT, E.; ATLAR, M. (2024), *Evaluation of the powering extrapolation of a ship with a gate rudder system, including ageing and fouling effects*, Ocean Eng. 313

MIZZI, K.; MUNRO, M.Z.; GURKAN, A.; AKTAS, B.; ATLAR, M.; SASAKI, N. (2022), *The performance prediction and energy saving evaluation for the retrofit of a Gate Rudder system on a general cargo vessel using CFD procedures*, 4th Int. Meeting - Ship Design & Optimization and Energy Efficient Devices for Fuel Economy, Istanbul

MOLLAND, A.F. (2008), *The maritime engineering reference book*, Butterworth-Heinemann

MOLLAND, A.F.; TURNOCK, S.R.; HUDSON, D.A. (2011), *Ship resistance and propulsion*, Cambridge University Press

SASAKI, N.; ATLAR, M.; KURIBAYASHI, S. (2015), *Advantages of twin rudder system with asymmetric wing section aside a propeller*, J. Marine Science and Technology 21, pp.297-308

SASAKI, N.; KURIBAYASHI, S.; ATLAR, M. (2018), *Gate Rudder*, Istanbul Technical University

SASAKI, N.; KURIBAYASHI, S.; FUKAZAWA, M.; ATLAR, M. (2020), *Towards a realistic estimation of the powering performance of a ship with a Gate Rudder system*, J. Marine Science and Engineering 08(043)

SASAKI, N.; KURIBAYASHI, S.; MILES, A. (2019), *Full scale performance of gate rudder*, The Royal Institution of Naval Architects

SNAME (1988), *Principles of naval architecture*, SNAME

SAUNDERS, H.E. (1956), *Hydrodynamics in ship design*, SNAME

TURKMEN, S.; CARCHEN, A.; SASAKI, N.; ATLAR, M. (2015), *A new energy saving twin rudder system - gate rudder*, University of Strathclyde

TURKMEN, S.; SASAKI, N.; ATLAR, M. (2016), *The Gate Rudder application to improve poor course keeping ability of ships*, A. Yücel Odabaşı Colloquium Series, Istanbul

WHIPPS, S.L. (1985), *On-line ship performance monitoring system: operational experience and design requirements*, p.14

Proactive Cleaning: Leveraging Data for a Successful Beginning

Manolis Levantis, Jotun Hellas, Athens/Greece, manolis.levantis@jotun.com
Morten Sten Johansen, Jotun, Sandefjord/Norway, morten.sten.johansen@jotun.com

Abstract

Marine biofouling, the accumulation of microorganisms and organisms on vessels' hulls, significantly impacts vessel performance. According to IMO, proactive cleaning is the periodic removal of microfouling on ships' hulls to prevent and minimize attachment of macrofouling. Jotun, a leader in hull performance, has been one of the first movers in this area with Hull Skating Solutions, offering an always clean hull combining robotics, antifouling and active hull condition monitoring. This paper will delve into key components of the solution, discuss how data are used in order to monitor and optimize proactive cleaning operations and through real-world case studies and in-service performance data demonstrate the significant impact on proactive cleaning on fuel efficiency, environmental sustainability and overall vessel performance.

1. Introduction

Over time, the buildup of biofouling significantly impacts vessel performance, leading to increased fuel consumption and a larger environmental impact Fig.1, *GIA (2021)*. To address this, ship operators apply hull coatings with anti-fouling properties. However, these coatings may not always provide optimal protection due to varying operational conditions or extreme fouling pressure that exceeds the coating's tolerance.

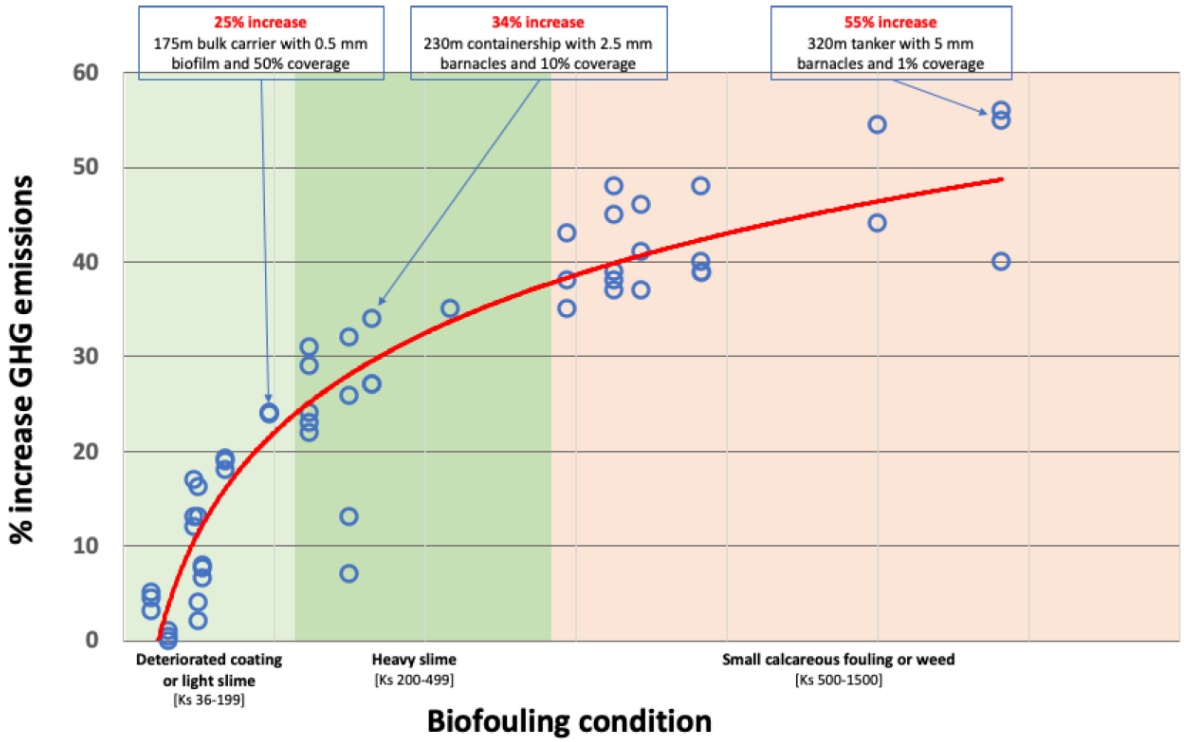

Fig.1: Impact of biofouling on Greenhouse Gas (GHG) emissions, *GIA (2021)*

Several factors can negatively affect hull performance, especially when speed, inactivity periods, and water temperature fall outside the parameters used to specify the coating. For example, bulk carriers, tankers, and

general cargo ships often remain in ports for extended periods. Additionally, some vessels may face delays in berthing due to neap tides. In such cases, shallow waters and temperate environments can accelerate growth of biofouling, posing regular challenges for many shipowners.

According to the IMO's 4th GHG emissions study, *IMO (2020)*, international shipping emitted approximately 919 million tons of CO2 and 21 million tons of other GHGs (including methane, Nox, and SOx) in 2018. The study indicates that 9% of these emissions were due to biofouling, suggesting a potential annual reduction of 83 million tons of CO2 and around 2 million tons of other GHGs. These findings align with other studies, such as the Clean Shipping Coalition's submission to the 63rd IMO Marine Environment Protection Committee meeting, *CSC (2015)*.

For ships experiencing higher biofouling pressure, the additional fuel consumption due to biofouling likely exceeds the 9% average for all ships, indicating significant improvement potential.

Besides applying a fresh coating during dry-dockings, hulls and propellers may occasionally be cleaned in water while in service. This reactive cleaning approach typically occurs when heavy biofouling causes a measurable performance loss. Modern performance monitoring software can measure efficiency loss due to degrading hull performance, prompting for cleaning. However, by this stage, fouling is already a significant issue.

Traditional cleaning, performed manually by divers, remains common but faces increasing scrutiny. While effective at removing biofouling, this labor-intensive and costly process can be challenging to schedule and may lead to off-hire time due to unavailability of divers and necessary logistics. Moreover, manual cleaning often damages the coating (Fig.2, right), leading to accelerated growth of biofouling shortly after. Environmental concerns also arise, as cleaning can release aquatic invasive species and eroded coating materials into the water column (Fig.2, left), harming local ecosystems. Consequently, port authorities have become more restrictive on in-water cleaning, complicating adherence to IMO’s biofouling guidelines. Additionally, manual cleaning poses significant safety risks to divers, with injuries and fatalities reported annually.

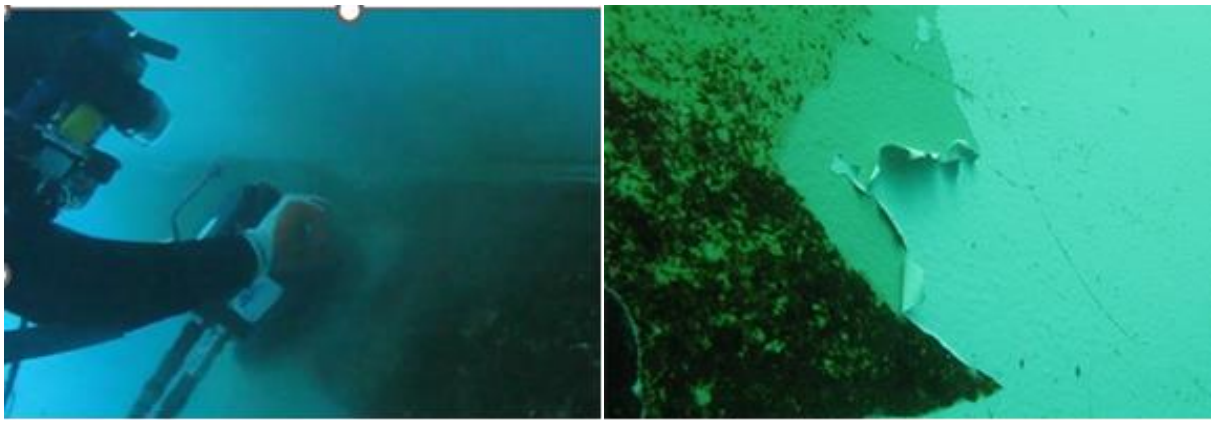

Fig.2: Traditional cleaning releasing fouling and paint particles (left); resultant paint damage (right)

Robotic cleaning, using autonomous or remotely controlled robots, offers an alternative for hull cleaning, with various emerging solutions of differing maturity *Bertram, (2021)*. Many newer robots can capture removed coating and biofouling for proper disposal in port. However, most current cleaning technologies are reactive, designed for use once biofouling has already become a significant problem.

2. Proactive cleaning and the Jotun Hull Skating Solution

To combat biofouling and address the concerns of port authorities regarding the release of invasive species, Jotun has adopted proactive cleaning through its innovative Hull Skating Solutions (HSS). Proactive cleaning, sometimes also referred to as grooming, has been increasingly advocated, e.g. *Hunsucker et al. (2018)*, *Swain et al. (2020)*. Jotun has been active in promoting a corresponding standard for in-water cleaning, *Oftedahl and Skarbø (2021)*, *Oftedahl et al. (2022)*, *Skarbø (2022)*.

Table I: Fouling rating as per IMOs Biofouling Management Guidelines

PPR 10/WP.5
Annex 1, page 16

Table 1: Rating scale to assess the extent of fouling on inspection area

Rating	Description	Macrofouling cover of area inspected (visual estimate)	Recommended cleaning
0	**No fouling.** Surface entirely clean. No visible biofouling on surfaces.	-	-
1	**Microfouling.** Submerged areas partially or entirely covered in microfouling. Metal and painted surface may be visible beneath the fouling.	-	Proactive cleaning may be recommended as further specified in paragraph 9.4
2	**Light macrofouling.** Presence of microfouling and multiple macrofouling patches. Fouling species cannot be easily wiped off by hand.	1-15% of surface	Cleaning with capture is recommended as further specified in paragraph 9.9. It is recommended to shorten the interval until next inspection. If the AFS is significantly deteriorated, drydocking with maintenance and re-application of AFS is recommended.
3	**Medium macrofouling.** Presence of microfouling and multiple macrofouling patches.	16-40% of surface	
4	**Heavy macrofouling.** Large patches or submerged areas entirely covered in macrofouling.	41-100% of surface	

Proactive cleaning involves the removal of biofouling at its early stages, specifically before it progresses to the macro-fouling stage. According to the fouling rating system outlined in Table I of the IMO's biofouling management guidelines *IMO, (2023)* this corresponds to a fouling rating of 1. This proactive approach entails regular hull cleaning while the biofouling is still in the microfouling stage. By removing biofouling at this early stage, significant performance impacts can be mitigated, and the capture and collection of biofouling waste may be not necessary. Importantly, early-stage biofouling can be effectively removed with small shear forces, thereby preventing damage or erosion of the hull coating, preserving its integrity, extending its lifespan, and reducing the need for frequent re-applications.

2.1. Solution elements

Jotun's Hull Skating Solutions (HSS) combine five elements, Fig.3, addressing technical, operational and commercial issues:

Fig.3: The five elements in the Hull Skating Solutions

- **High performance coating** – Jotun's SeaQuantum Skate coating was specifically developed to optimize performance in conjunction with the robotic cleaning technology of the HullSkater robot. The silyl-acrylate based coating is designed to withstand repeated mechanical contact with the specially designed proactive cleaning brushes without experiencing erosion.

- **Proactive condition monitoring** – This is an essential component of predictive hull maintenance, enabling the HullSkater to operate when it is most needed. Jotun's in-house data scientists and marine biologists have developed an algorithm predicting when fouling start to occur on the vessel's hull. This enables the Skate Operator to appropriately time the deployment of the system. As part of the monitoring, vessel performance is analyzed and document using the ISO 19030 standard for hull and propeller performance, *ISO (2016).*

- **Inspection and proactive cleaning** – The HullSkater is the first robotic device specifically designed for proactive cleaning, Fig.4. It has high inspection and cleaning capabilities while effectively removing biofouling without damaging the anti-fouling coating. The HullSkater is always kept onboard in a specially designed in-rail station, Fig.5, with launch and recovery ramp. This ensures constant availability for use whenever the ship is in port or at anchorage. The ship's crew can easily launch and retrieve the device, Fig.6.

- **High-end technical service –** HSS includes highly skilled coating advisors who ensure proper coating application of the high-performance coating, including a comprehensive regime for measuring and documenting the quality of the application process. Every HSS delivery is overseen by a certified project manager, who monitors the application process, and ensures smooth installation and setup of the robotics. Once launched, the HullSkater is remotely operated by dedicated Skate Operators from Jotun, Fig.7.

- **Performance and service level guarantees** – The confidence in Jotun's Hull Skating Solutions allows us to offer performance and service level guarantees fitting the needs of the most challenging operations.

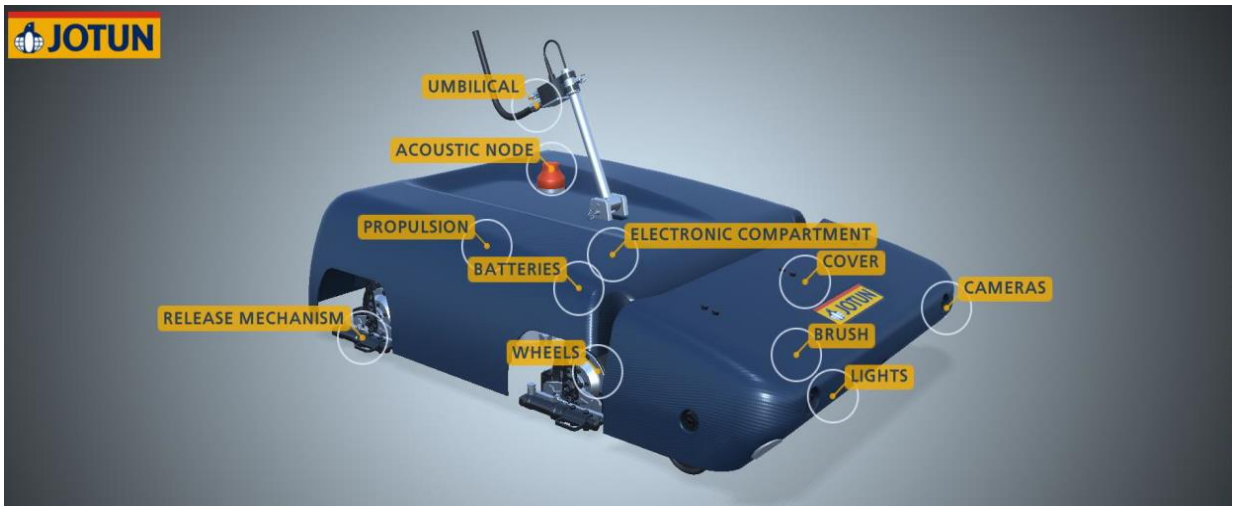

Fig.4: HullSkater robot

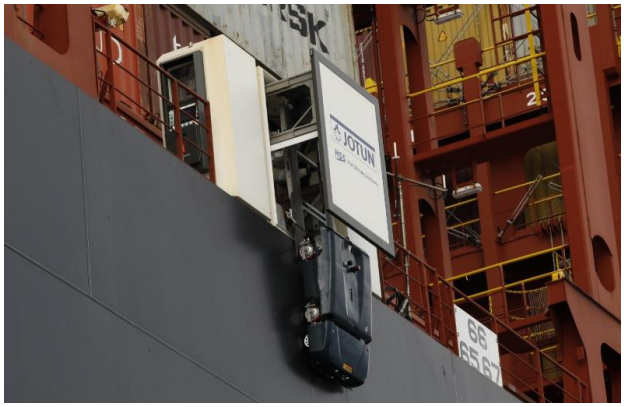

Fig.5: HullSkater in-rail station

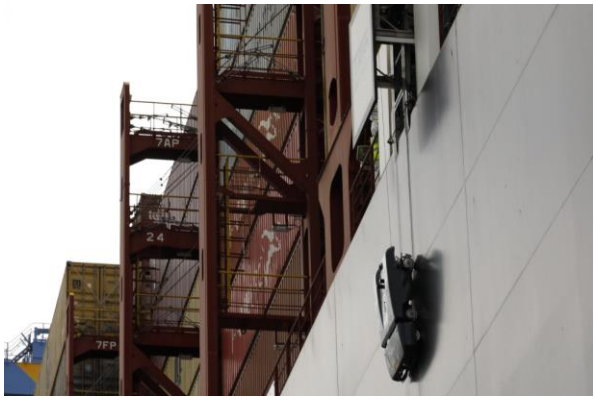

Fig.6: HullSkater being launched

Fig.7: Remote control of HullSkater

2.2. How it works

Jotun Hull Skating Solutions is installed on the vessel at the new build or dry dock yard and remains on board and in operation all through the drydocking cycle, Fig.8.

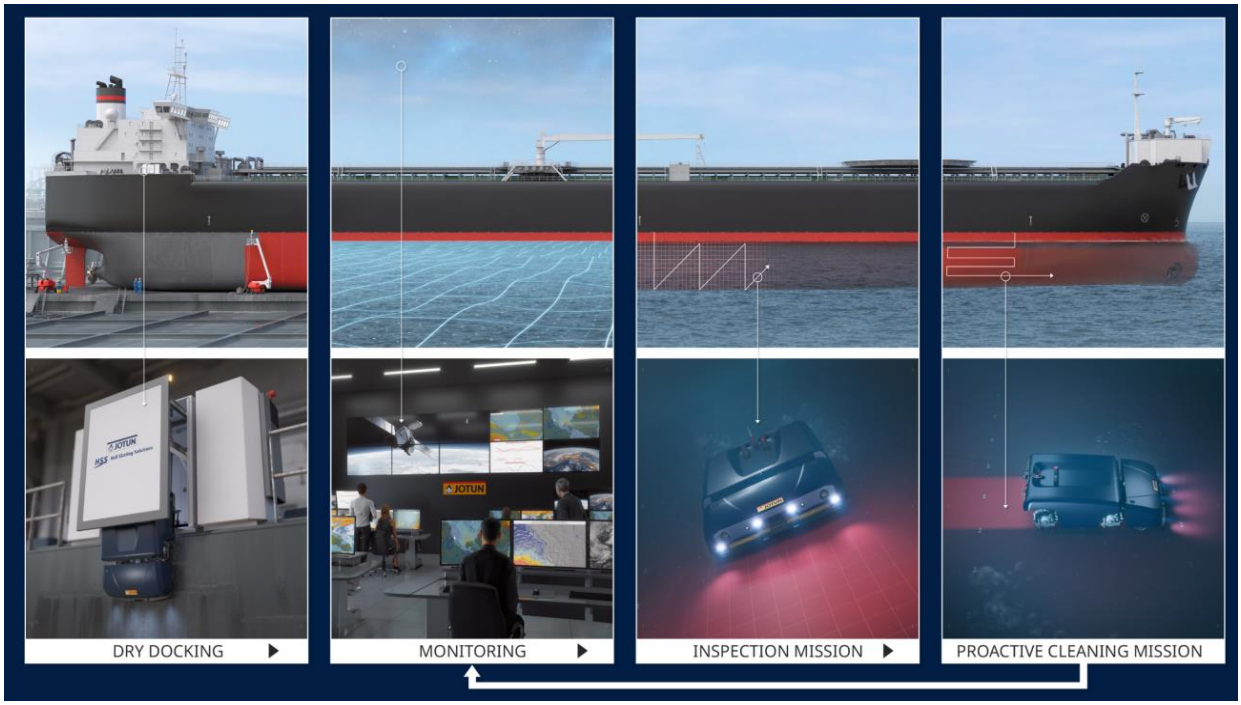

Fig.8: How it works

- **Drydocking:** During drydocking, a certified Jotun Project Manager oversees the painting process and is responsible for installing the HullSkater and the Skate Station.
- **Monitoring:** In addition to performance monitoring adhering to ISO 19030 standard, a fouling prediction algorithm is deployed to predict the probability of fouling based on operational areas and ship operational parameters. The algorithm also identifys when the Skater requires deployment for inspection and potential proactive cleaning missions**.**
- **Inspection Mission:** When the fouling prediction algorithm triggers an alert, the Jotun Skate Operator contacts the ship to schedule an inspection mission. The Jotun HullSkater can be operated in port or at anchor, provided there is sufficient 4G coverage for communication.
- **Proactive Cleaning Mission:** If light slime is detected during the inspection mission, the Skate Operator initiates proactive cleaning. If time constraints preclude a proactive cleaning mission, the Jotun Skate Operator coordinates with the ship to determine the next available opportunity.

3. Leveraging data

In such solutions, correct usage of relevant data is critical for success. Operating the Jotun HullSkater incurs costs. In addition to that, the more inspections and the more pro-active cleaning missions conducted, the more robot maintenance is needed. It is obvious that an optimization process should be applied to keep the number of missions at an optimum level. The ideal scenario is to have a prediction algorithm that would be able to predict accurately the level of biofouling on a vessel's hull and by this trigger a mission only when it is necessary. As previously discussed, this is when biofouling is approaching a fouling rating of 1 as per IMO's biofouling management guidelines. *Levantis et al. (2023)* discussed the challenges faced, when

trying to model antifouling protection – the underlying physics of antifouling coating - and the pressure from the external marine environment.

In that paper, a holistic approach was discussed for developing an accurate fouling prediction algorithm. A better version of this approach is now implemented in Jotun's HullKeeper solution, a platform that enables timely decisions regarding hull maintenance, achieving accuracy levels of up to 80% in predicting biofouling settlement on a vessel's hull. A similar fouling risk algorithm is used in Hull Skating Solution. The key difference in the Hull Skating Solution lies in the fact that coating protection does not need to be modeled, as the coating is always the same, SeaQuantum Skate. Given this, only the marine environment significantly influences the outcome, as the effect of the coating can safely assumed to be the same.

Although this approach may seem simpler, the fouling risk algorithm requires careful tuning to be highly sensitive in the early stages of biofouling. To achieve this, two methods were introduced and will be presented in this study. The first, serving as a baseline, is a basic approach that ignores the influence of the external environment and identifies the optimal number of days after a mission. The second approach incorporates the influence of the external environment.

To determine the optimal number of missions, data from actual vessels already utilizing Hull Skating Solutions were collected. The most crucial information required is the condition of the hull immediately before each proactive cleaning mission. To collect this data, the vessel hull is divided into sections. Each section is then rated based on the IMOs fouling rating scale by the Skate Operator after the completion of each mission, Fig.9. The data used for this study were obtained from 29 vessels (including bulkers, containers, and ROROs) to which, 493 inspection and proactive cleaning missions have been conducted.

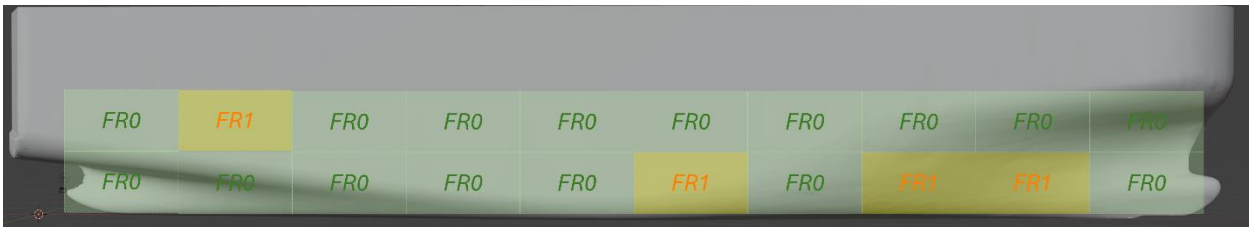

Fig.9: Vessel divided into sections and rated based on USN FR scale

After preparing the data the basic approach is relatively easy. Let x represent the number of days after previous event. A possible mission is considered "justified" if, within 30 days after the theoretical mission, the hull condition is found to be equal to or greater than a fouling rating of 1. On the contrary, a mission is considered as "not justified" if the condition of the hull is found to be in a good state (fouling rating of 0). Based on this, it is possible to calculate the number of "justified" and "not justified" inspections for each value of x. After simulating all possible scenarios with x ranging from 30 to 90 days, the optimal x was determined to be 55 days, with only 38% of missions classified as "justified". This indicates a highly ineffective proactive cleaning strategy, as expected. This outcome can be attributed to the exceptional performance of the ultra-premium coating. The data reveals that the ultra-premium coating consistently maintains the hull below a fouling rating of 1 for extended periods, resulting in a significant number of simulated missions being deemed "not justified."

It is clear from the above that a more effective pro-active cleaning strategy is needed. To address this, an attempt was made to model the biofouling pressure from the environment. The underlying principle is that an inspection mission is conducted only when the risk from the environment exceeds a certain threshold. This can increase accuracy a lot as it accounts for vessels that have not been exposed to significant environmental pressure for extended periods. If so, there is limited or no need to conduct an inspection mission on these vessels.

Levantis et al. (2023) highlighted the complexities when trying to model external risk from the environment. Since this is a highly complicated problem a more simplified approach was selected as a starting point. It is well-established that parameters such as sea water temperature, salinity, chlorophyl, sea water depth, UV light and nutrients have a strong correlation with the presence of biofouling, *Yebra et al. (2004), Arai et al. (2009)*.

Let daily fouling risk Rf be a function (f) of these parameters. The specific form of the function (f) was determined through empirical analysis and involved linear combinations of the environmental parameters. Vessels positions were obtained from AIS data, and corresponding parameter values for any given point in time were retrieved from https://marine.copernicus.eu/. To make sure that the risk is always a value between zero to one for each function (f) the value was divided by the number of parameters used in that function. This normalization step reflects the assumption that the maximum potential risk a vessel can be exposed to within a day is one, while zero represents no risk within that timeframe.

$$Rf(t)=f(T,S,C,D,U,N) / n$$

where: T: Seawater temperature
S: Salinity
C: Chlorophyll concentration
D: Seawater depth
U: UV light intensity
N: Nutrient concentration
n: number of parameters used

Let RT(t1,t2) represent the total risk accumulated between times t1 and t2:

$$RT(t1,t2) = \sum_{t1}^{t2} Rf(t)$$

As in previous approach a potential inspection mission would be classified as “justifiable” if, within 30 days the hull is found to be equal or greater than fouling rating of 1. Given this, the optimum value of RT (risk threshold) must be determined to maximize the number of “justifiable” missions. Fig.10 illustrates the optimization process within a time series. The y-axis represents a possible values of RT function. The three vertical red lines indicate instances of proactive cleaning missions. Since these are actual proactive cleaning missions, they signify that there were parts of the hull that were rated with a fouling rating of 1, classifying them as “justifiable”. The optimization process aims to identify the optimum threshold that would trigger the most “justified” proactive cleaning missions. In this illustrated scenario, the optimum threshold would be located around RT=135, resulting in two “justifiable” and one “not-justifiable” proactive cleaning mission.

After checking all possible combinations of Rf(t) and identifying the optimum RT for each, the best performing model was selected. This accuracy level might be slightly lower than expected for such a sophisticated solution, but it's crucial to acknowledge the inherent complexity of the problem. There are numerous instances where an optimal value may not exist. For example, if only the first two missions are considered in the above example, it becomes evident that an optimal threshold cannot be definitively determined. If the threshold is increased, the result will be one "justifiable" proactive cleaning mission (the first instance) and one "non-justifiable" mission (the second instance). Conversely, if the threshold is decreased, the outcomes will be reversed.

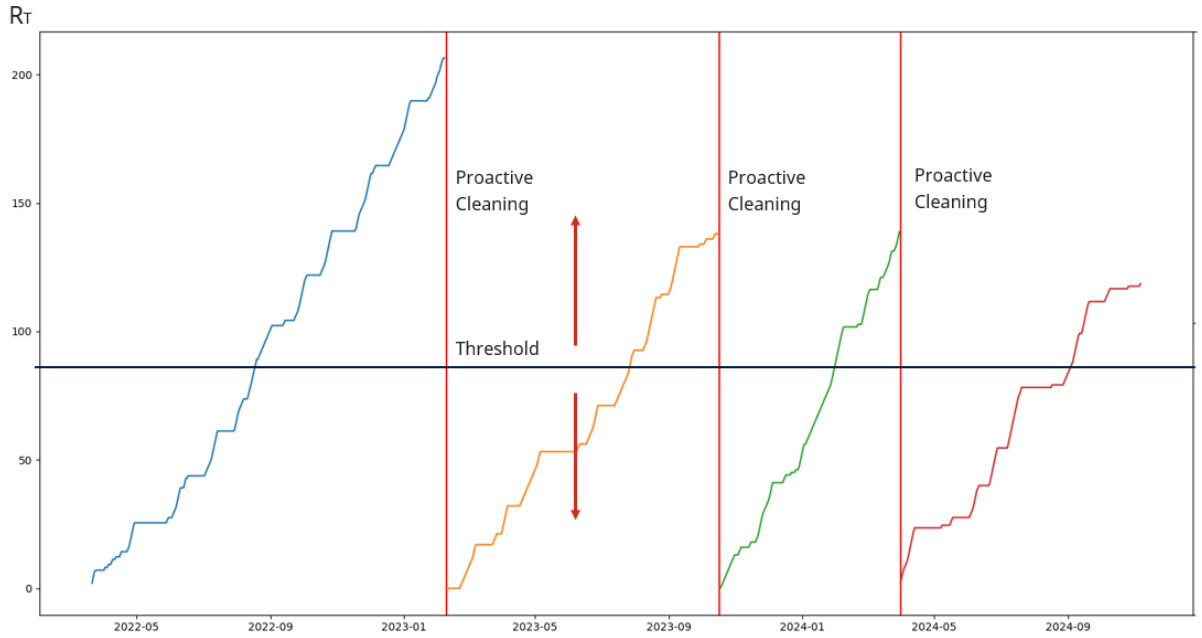

Fig.10: Illustration of the optimization process

4. Delivering on expectations - visual assessment and ISO 19030 analysis

In order to test if the solution is actually delivering an always clean hull, hull performance was evaluated using both visual inspections and sensor data. To measure hull performance from sensor data the ISO 19030 analysis methodology was used. Data from 5 vessels were retrieved. Unfortunately, these vessels didn't have high frequency data, necessitating the use of validated noon data. The sailing periods for vessels A, B, C, D and E are 25, 25, 26, 35 and 29 months, respectively, since they applied Hull Skating Solutions. Vessels A, B and C are large car carriers, vessel D is a container of 13.000 TEU and vessel E is a 60.000 deadweight tonnage bulk carrier.

To validate the noon data, additional sources were utilized. Speed over ground and draft were validated by using AIS data. To exclude the influence of adverse weather conditions, wind speed and sea state was compared against wind and waves data retrieved from https://marine.copernicus.eu/. To validate steady state of speed over a day (as mandated by the ISO 19030 methodology) AIS data were used in order to calculate the standard deviation of speed over ground within a day. Anything above standard deviation of 2 knots was filtered out. Additionally, all possible correlation (speed–power, speed-rpm, speed-fuel oil consumption, rpm-power, rpm-fuel oil consumption, power-fuel oil consumption) were plotted and visually assessed. Clearly erroneous values were filtered out.

As illustrated in Fig.11, all vessels are performing very well, meeting expectations. Hull Skating Solutions in-service performance as per ISO 19030 is expected to be 0.5% over a 60 month period. Vessels A, B, C, D and E in-service performance is 0.15%, 0.32%, 0.02%, 0.25% and 0.22% respectively. It is important to highlight that no downward trend is seen in 4 out of 5 vessels. Vessel B, however, may exhibit a potential downward trend after July 2024. This could be attributed to biofouling accumulation or changes in the operational profile. Upon thoroughly examining the operational profile of vessel B during this latter period, it was found to be operating at a draft two meters lower and one knot slower compared to previous voyages. This discrepancy explains the observed downward trend in performance during this specific period.

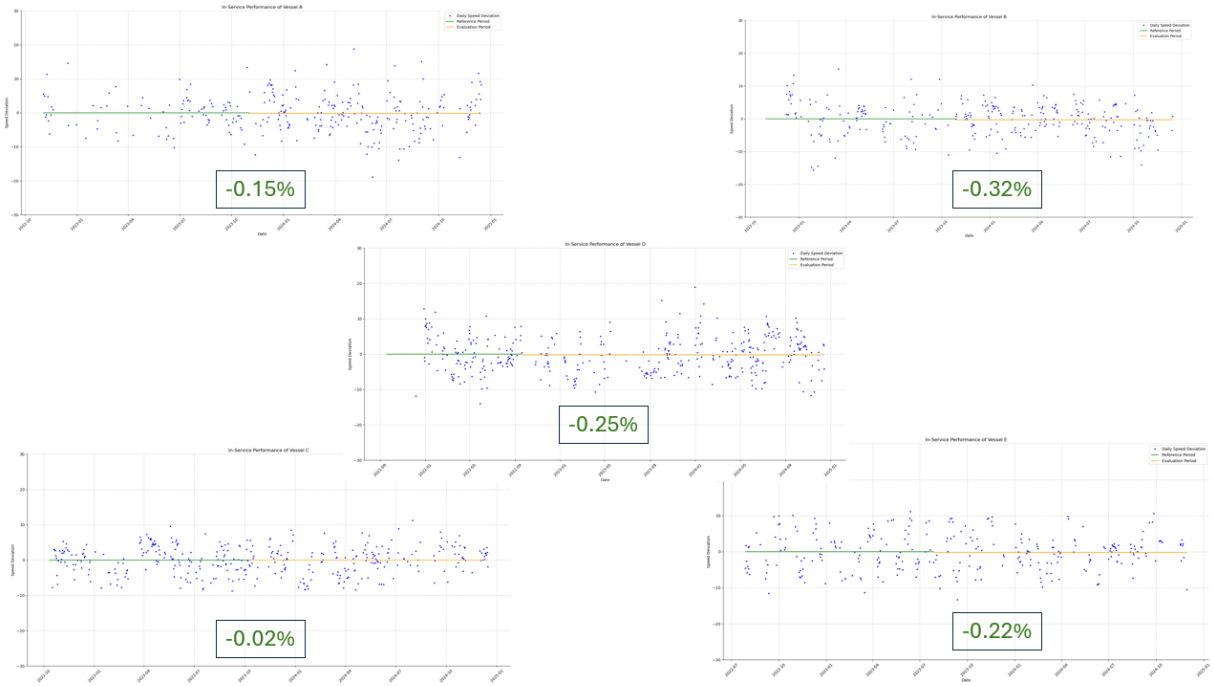

Fig.11: In service performance of Vessels A, B, C, D and E

To strengthen more what was obvious from the data, access to the video footage of the latest inspection from the HullSkater was given. By thoroughly examining the videos and as seen in Fig.12 (representative pictures) all vessels hulls appear to be clean. As expected, sometimes there were some small areas with light slime (FR 1 as per IMO Biofouling Guidelines) where they had to be proactively cleaned.

Fig.12: Representative condition of the hull from Vessels A, B, C, D and E

Acknowledgements

Developing the Hull Skating Solutions would not have been possible without world-class partners, which we gratefully acknowledge. Thanks go to the many colleagues at Kongsberg, Semcon, DNV, Telenor, DNB / EksFin, Wallenius Wilhemsen and our other customer partners joining the exiting journey of this ground-breaking innovation.

References

ARAI, T.; HARINO, H.; OHJI, M.; LANGSTON, W.J. (Eds.) (2009), *Ecotoxicology of antifouling biocides*, Springer, p.315

BERTRAM, V. (2021), *Robotic Hull Cleaning – State of the Art and Roadmap*, 13th HIPER Symp., Tullamore, pp.37-44

CSC (2015), *A transparent and reliable hull and propeller performance standard*, Clean Shipping Coalition submission to MEPC 63, IMO, London, https://bellona.no/assets/sites/3/2015/06/fil_MEPC_63-4-8_-_A_transparent_and_reliable_hull_and_propeller_performance_standard_CSC1.pdf

GIA (2021), *Impact of Ships' Biofouling on Greenhouse Gas Emissions*, Global Industry Alliance for Marine Biosafety, IMO, London, https://wwwcdn.imo.org/localresources/en/MediaCentre/Documents/Biofouling%20report.pdf

HUNSUCKER, K.; BRAGA, C.; ERGODAN, C.; GARDNER, H.; HEARIN, J.; RALSTON, E.; GEOFFREY SWAIN, G.; TRIBOU, M.; WASSICK, A. (2018), *The Advantages of Proactive In-Water Hull Grooming from a Biologist's Perspective*, 3rd HullPIC Conf., Redworth, pp.210-222, http://data.hullpic.info/hullpic2018_redworth.pdf

IMO (2023), *Biofouling Management Guidelines*, Annex 17, page 16, https://wwwcdn.imo.org/localresources/en/KnowledgeCentre/IndexofIMOResolutions/MEPCDocuments/MEPC.378(80).pdf

IMO (2020), *4th IMO GHG Study – Final Report*, IMO, London, https://wwwcdn.imo.org/localresources/en/OurWork/Environment/Documents/Fourth%20IMO%20GHG%20Study%202020%20-%20Full%20report%20and%20annexes.pdf

LEVANTIS, M.; JOHANSEN, M.S.; LEE, R.; CHALAMCHARLA, H. (2023), *Fouling Prediction for Improving Hull Performance-Is it possible?*, 7th HullPic Conf., Tullamore, http://data.hullpic.info/HullPIC2023_Pontignano.pdf

OFTEDAHL, G.A.; SKARBØ, R.C. (2021), *A Way Forward for In-water Proactive Cleaning*, 3rd PortPIC Conf., Hamburg, pp.67-75, http://data.hullpic.info/PortPIC2021_Pontignano.pdf

OFTEDAHL, G.A.; SKARBØ, R.; JOHANSEN, M.S.; ERTSÅS, H.V.; OEPSTAD, C. (2022), *A Way Forward for In-water Proactive Cleaning*, 3rd PortPIC Conf., Hamburg, pp.67-75, http://data.hullpic.info/PortPIC2022_Hamburg.pdf

SKARBØ, R. (2022), *The Clean Hull Initiative One Year Later: Towards an ISO Standard on Proactive Hull Cleaning*, 3rd PortPIC Conf., Hamburg, pp.150-154, http://data.hullpic.info/PortPIC2022_Hamburg.pdf

SWAIN, G.; TRIBOU, M.; GARDNER, H.; HUNSUCKER, K. (2020), *In-Water Grooming of Fouling Control Coatings: From Research to Reality*, 1st PortPIC Conf., Hamburg, pp.29-37, http://data.hullpic.info/PortPIC2020_Hamburg.pdf

YEBRA, D.M.; KIIL, S.; DAM-JOHANSEN, K. (2004), *Antifouling technology—past, present and future steps towards efficient and environmentally friendly antifouling coatings*, Progress in Organic Coatings 50/2, pp.75-104

A Maritime Officers Approach to Vessel Performance

Anders H. Møller, MOL Chemical Tankers, Copenhagen/Denmark,
anders.moller@molchemtankers.com

Abstract

This paper addresses vessel performance in scenarios where there is only manually logged data available from a fleet of vessels with the absolute economy package of measuring devices and no access to third party analysis, naval architect expertise, trim tables or anything like that.

1. Background

Despite the advances in the last couple of decades in the understanding of vessel sensor data quality, increased availability and reliability of weather, current and bathymetry data, development of fouling exposure models, digital twins, trim tables, etc. and the availability of high frequency data from AIS, there are still those in the industry that refuses to join the 21st century.

So, what can one do when faced with these limitations?

That will of course depend on the qualifications that one has, and the answer given in this example is therefore coloured through the lens of a Dual Marime Officers that spent 10 years in Maersk Line before going ashore to pursue a career in vessel performance.

2. Master Data

This is an exercise in what is possible with very limited resources and availability of data for a given vessel. All vessels have the minimum of documentation required to use this approach and there will usually not be any issues getting access to this documentation, even if one is purely a vessel Operator.

2.1. Sea Trial

The sea trial deck/engine contains a lot of data that is important to most vessel model building, but it is not necessary to this approach.

2.2. Main Engine Testbed

The main engine testbed/shop trial forms the foundation for the basic vessel model as this is the richest source of reference data for which there also exists a robust set of measurements that the crew can submit via almost any manual reporting tool.

3. Collecting Data

Your average manual reporting platform will not have fields for reporting the data that is required to use this approach, but is should be relatively simple to add these fields to most reports as they will not have to be mapped to other systems or integrated with anything else as all, except of course that you will have to be able to access the database/repository where the manually reported data ends up.

3.1. Data Gatekeepers

Usually, it will be the vessel operator that receives the manually reported data for review and approval. Their focus will of course be on distance/speed and consumption in relation to any Charter Party Speed & Consumption clauses, other speed and consumption instructions or speed and consumption tables within their voyage management system.

Other data in the report is unlikely to be begiven much attention and is therefore more likely to be approved despite typing errors, deliberate manipulation by crew, misunderstandings by crew on what is supposed to be reported and so on.

3.2. Data Quality Checks

Most systems for manual reporting that are not integral to a vessel performance system have inadequate or no data validation at the point of entry, usually limited to type of data e.g. text or number fields or if we are lucky, order of magnitude checks e.g. between 0.0 and 99.9.

4. Building a Basic Vessel Model

Strictly speaking it is not a vessel/hull model but more of an engine model used to approximate hull and propeller performance.

4.1. Nominal Propeller Curve

The nominal propeller curve describes the relation between the revolutions of the propeller shaft and the load on the propeller shaft as recorded in the main engine documentation. This curve forms the foundation of the basic model and the performance analysis.

4.2. Power Estimation

In the absence of a shaft load measurement, some vessels with newer engines are equipped with Online Performance Measurement Indicator, that optimizes combustion pressure in service, but also gives an engine load measurement. This could be used as a proxy for shaft load, but the following assumes that this measurement is not available either.

4.2.1 Shaft Speed vs Nominal Shaft Load

The relationship between shaft speed and nominal shaft load is a cubic and can be describe as ax3 = b, where a is a constant, x is the shaft speed and b is the shaft load. The constant a can be derived by inserting the main engine Maximum Continuous Rating for shaft speed and shaft load e.g. 6150 kW @ 121 RPM.

$$a = \frac{6150}{121^3} = 0.0034715 \ldots$$

Fig.1 was made in Excel and the blue line represents the 3rd order polynomial regression function build into the graph. The Green line represents the pure cubic relationship described above and as we see there is no significant difference between the two within the range for which data is available in the main engine testbed/shop trial, represented by the orange square, and below that range the pure cubic relationship gives better estimates as it does not go below 0 kW.

4.2.2 Fuel Pump Index vs Shaft Load

The fuel pump index is a measure of the volume of fuel that is injected into the engine and this measurement is of course dependent on the wear and tear on the fuel injection pumps as well as the lower calorific value of the fuel. Normalization for fuel pump wear is not possible with the data available, and for the purpose of this basic model, normalization for the lower calorific value will not be included.

The relationship between fuel pump index and shaft load is relatively close to linear, but not quite since leakage in the pumps increase slightly with increased shaft load and the regression therefore uses a 2nd order polynomial.

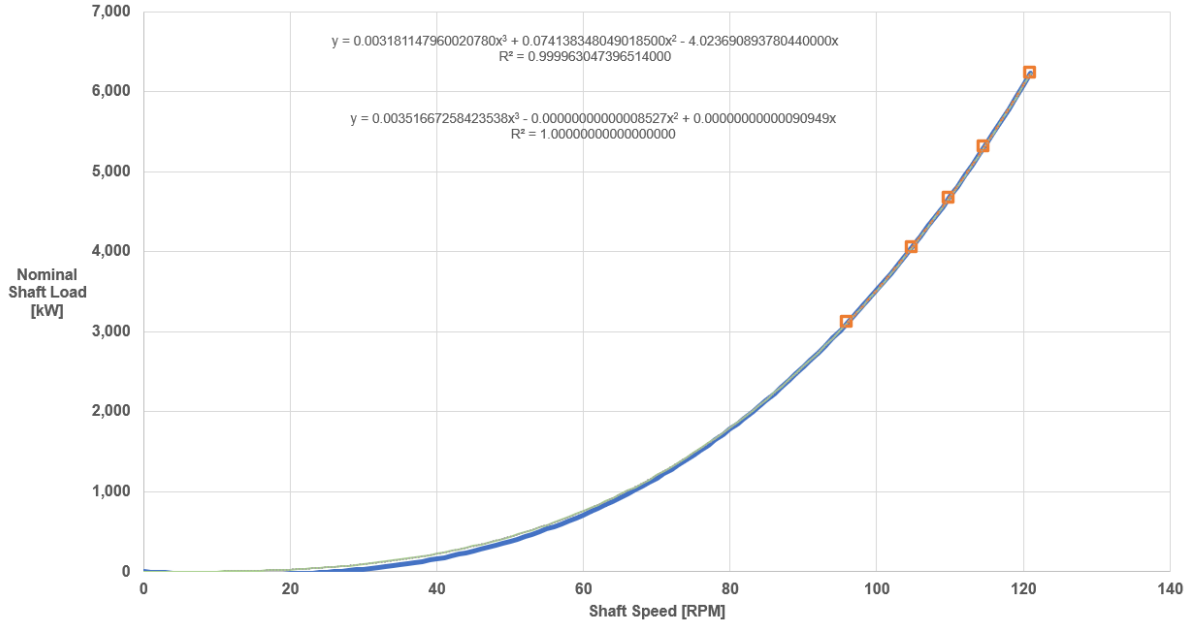

Fig.1: Excel graph showing the relationship between shaft speed and nominal shaft load

Interpolation at lower loads than the data sample present in the main engine testbed/shop trial is reasonably accurate since there are no other external factors influencing it and we can safely assume that a fuel pump index of 0 is equal to a shaft load of 0 kW.

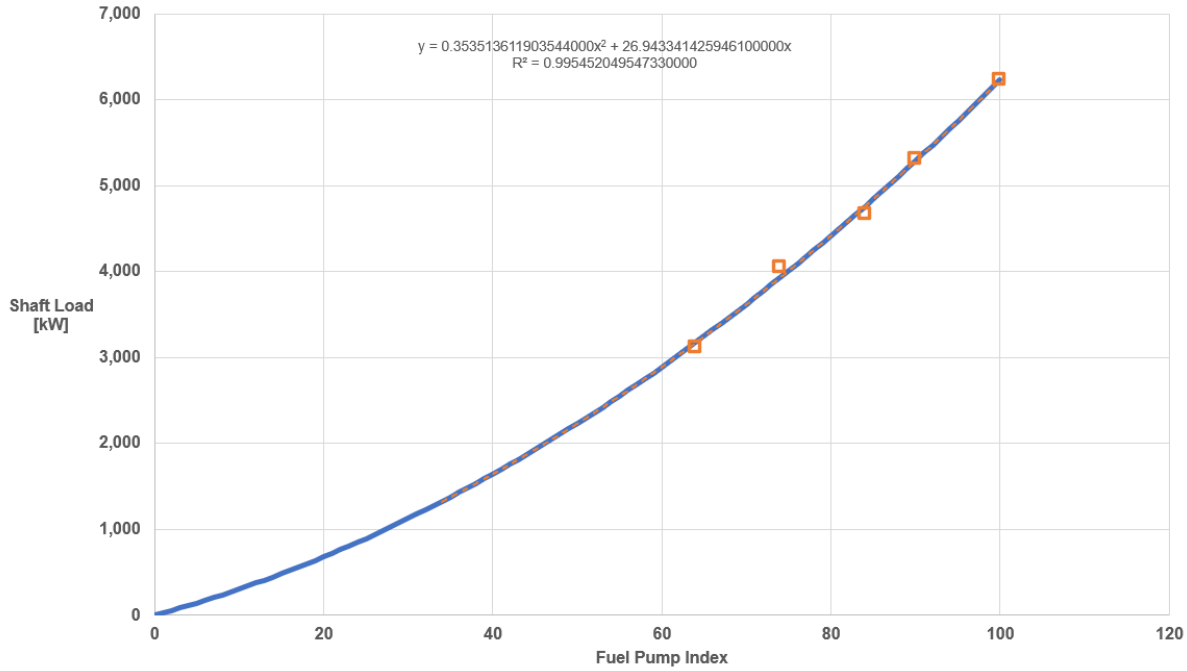

Fig.2: Excel graph showing the relationship between fuel pump index and shaft load

4.2.3 Turbo Charger Speed vs Shaft Load

The turbo charger speed is a measure of the amount of exhaust gas that the engine is producing, and this measurement is of course dependent on the wear and tear on the turbo charger turbine and compressor sides, which will result in lower and higher speeds measured respectively. Normalization for these factors is not possible with the available data.

The relationship between turbo charger speed and shaft load is relatively close to linear, but interpolation at lower loads than the data sample present in the main engine testbed/shop trial should be avoided at least at loads where the auxiliary blower is running.

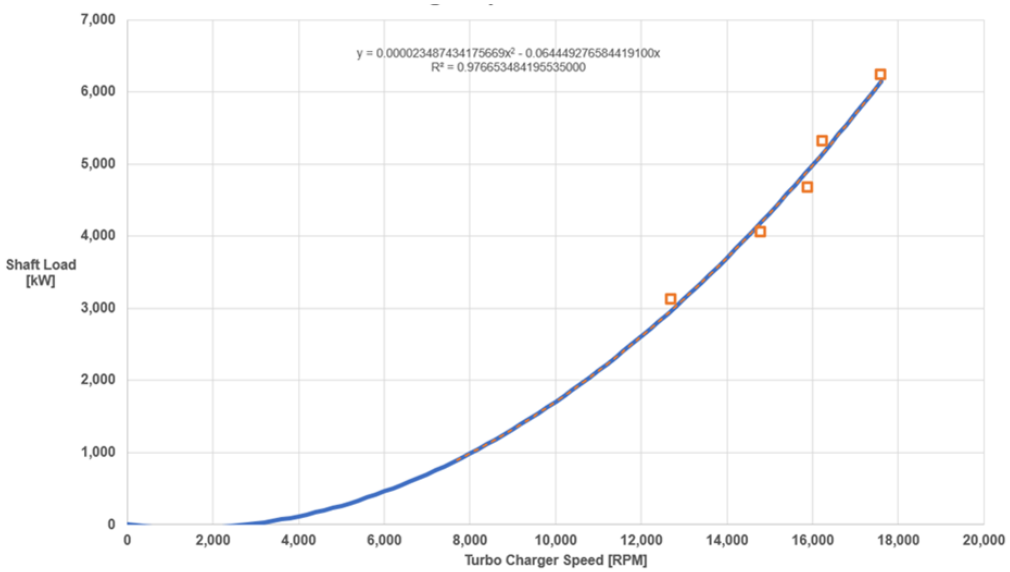

Fig.3: Excel graph showing the relationship between turbo charger speed and shaft load

4.2.4 Scavenge Air Pressure Speed vs Shaft Load

The scavenge air pressure, like the turbo charger speed, is a measure of the amount of exhaust gas that the engine is producing, and is dependent on the same factors, but also on the airflow and filter condition on the compressor side as well as the scavenge air cooler performance. Normalization for these factors are not possible with the available data.

The relationship between scavenge air pressure and shaft load is represented by below 2nd order polynomial and interpolation at lower loads than the data sample present in the main engine testbed/shop trial should be avoided at least at loads where the auxiliary blower is running.

While the fuel pump index and turbo charger speed measurements are both accurate and precise, the scavenge air pressure may be precise but will usually not be very precise as the gauge from which the reading is taken has low granularity.

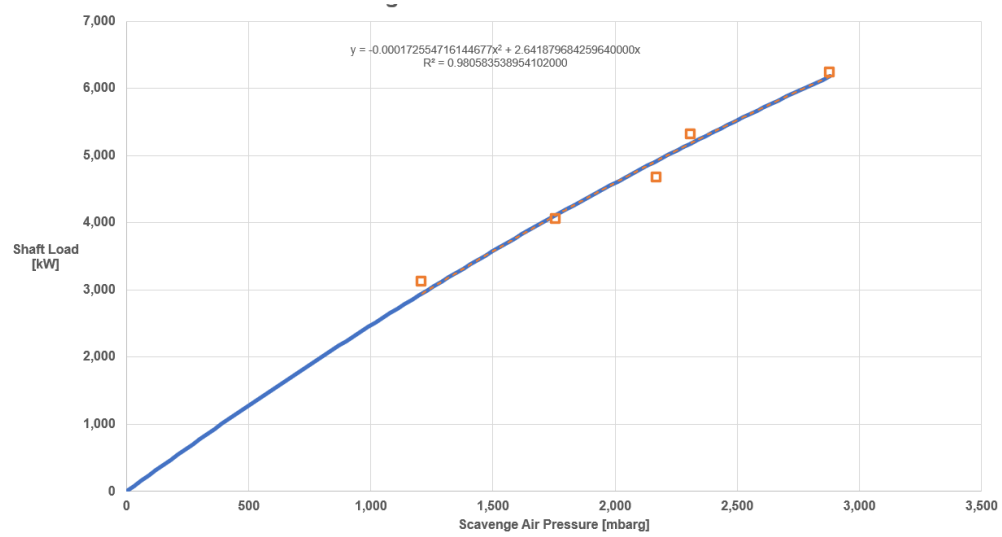

Fig.4: Excel graph showing the relationship between scavenge air pressure and shaft load

4.2.5 Shaft Load vs Specific Fuel Oil Consumption

During the main engine testbed/shop trial, shaft output and consumption is measured along with the environmental conditions relating to its normalization and we can therefore create another 2nd order polynomial describing the shaft load to ISO normalized specific fuel oil consumption.

With the estimated load, as described above, we can translate that to an estimated consumption that may then be compared to the reported consumption.

In below example we see a dataset that was obviously manipulated to show a contract compliant SFOC at the contract point, while being unusually high at loads immediately above or below the contract point.

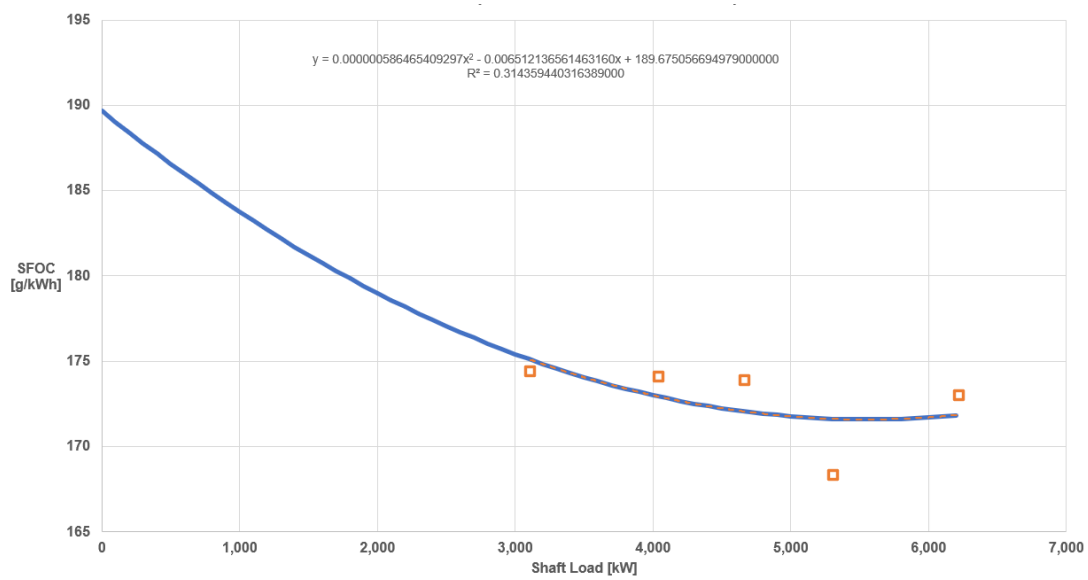

Fig.5: Excel graph showing the relationship between shaft load and specific fuel oil consumption.

4.2.6 Application of Basic Vessel Model in Data Collection Platform

In this example it was possible to implement the calculations described above in the manual data collection tool on board, but just the fields required to collect the data, giving the crew an opportunity to notice data entry errors resulting in unrealistic calculated results.

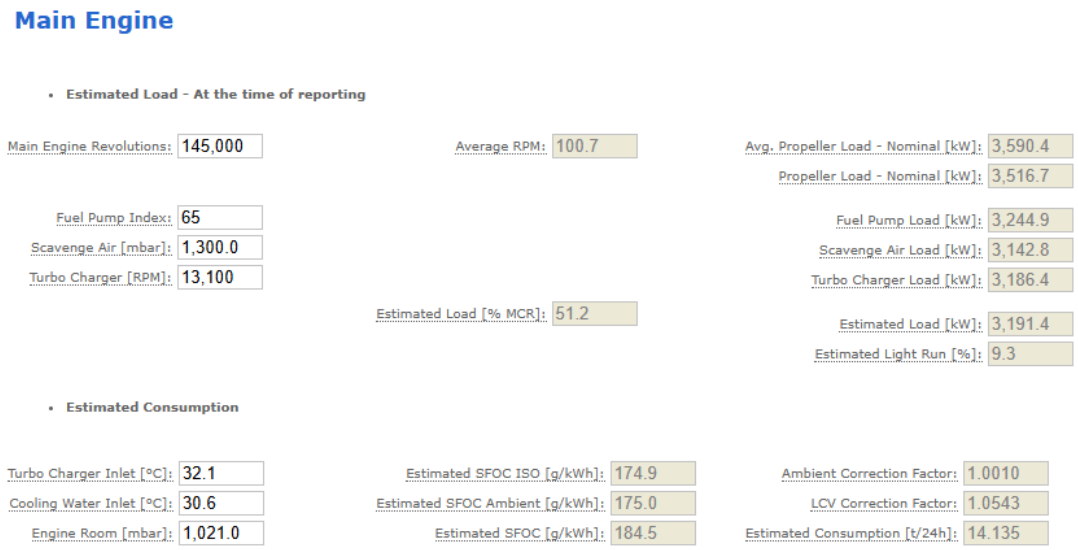

Fig.6: Example of on-board shaft load estimation based on available measurements

In the real world of course, if it can go wrong, it will and despite our best efforts, instructions, guidance and tool tips, crews have other things to do at do not pay attention to those things.

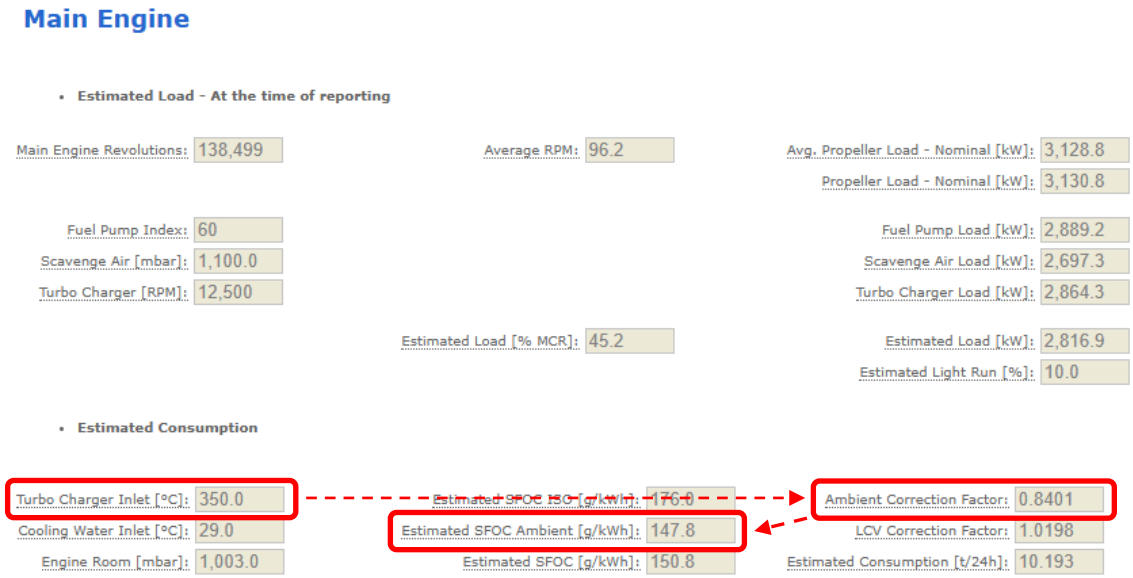

Fig.7: Example of on-board data collection with reporting errors

5. Vessel Performance Analysis

Plotting the development of the light running factor over time, where 10% light running will be plotted as 100 - 10% = 90 in below graph, we can see a development over time as hull and propeller performance deteriorates.
Note that there is of course no normalization for draft, trim, water depth, weather or anything like that.

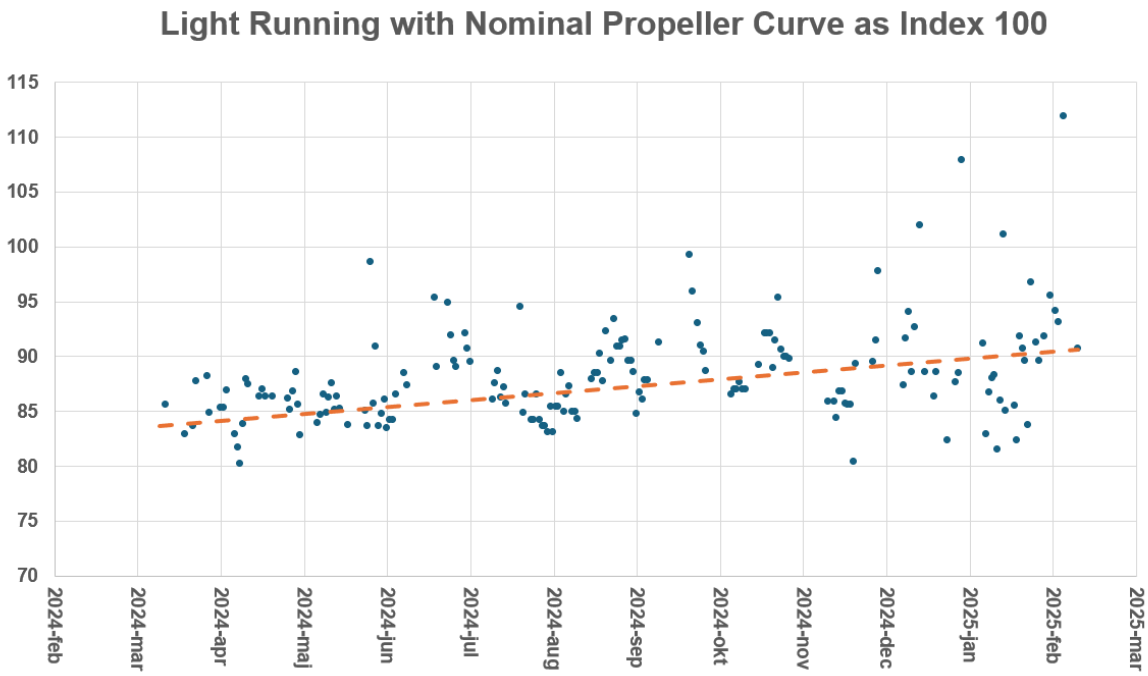

Fig.8: Example of the development of the light running index over time

Looking at the development we see that it is about 84 1st of April and about 90 1st of February giving us a delta of 6/84 ≈ 7% increase in propulsion resistance (assuming 100-16 = 84 or 16% light running as the out of dock performance).

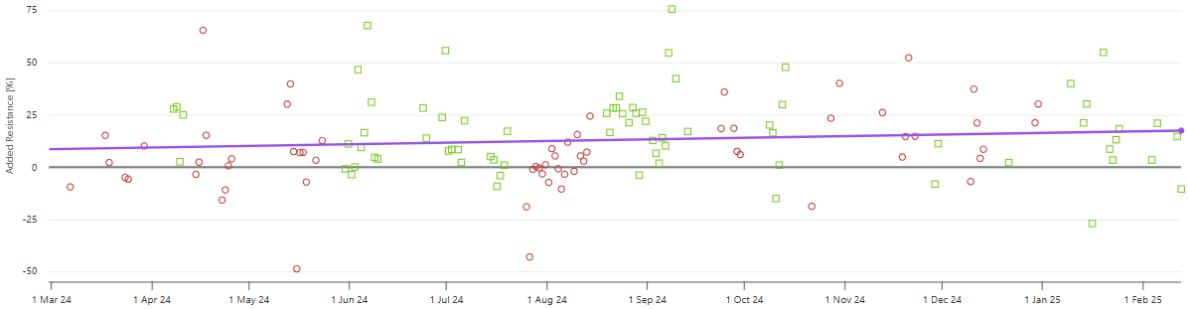

Fig.9: Actual performance system evaluating added resistance development over time

Looking at the same data from an actual performance system we see a development of added resistance from about 10% to about 18% or index 1.10 to 1.18 ≈ 7% increase in added resistance over the period (assuming the 10% added resistance or index 1.1 as the out of dock performance).

Does this mean that we can dispense with all our naval architects, hind cast weather, auto-log data and so on? No of course not, only that it is possible in the absence of an actual performance system to do something rather than nothing. Given the opportunity an actual performance system should always be chosen.

Acknowledgement

Thanks to Richard Marioth for suggesting that I make this presentation, after having heard snippets of it over the past 7 years.

Just How Big Is the Barnacle Fouling Problem for the Global Fleet? Using Hull Inspection Data to Find the Answer

Markus Jönsson, I-Tech, Mölndal/Sweden, markus.jonsson@i-tech.se
Catherine Austin, I-Tech, Mölndal/Sweden catherine.austin@i-tech.se

Abstract

This paper describes the findings of a research study commissioned by I-Tech, based on data provided by Safinah Group, which attempts to further quantify the true scale of barnacle fouling across the global shipping fleet. Data is presented from the assessment of animal fouling prevalence on 685 vessels during hull condition inspections in dry dock between 2015-2024. The results of this study proceed an earlier study presented by I-Tech at HullPic in 2020, wherein the analysis of hull condition data was undertaken, as an indicator for the scale of barnacle fouling on the global shipping fleet, albeit for a smaller sample size of 249 vessels. The impact of the biocide, Selektope on barnacle fouling across a selection of ships inspected during dry docking is also described in this paper.

1. Introduction

Ships spend their working lives sailing through, or sitting in, a watery soup of aquatic micro and macro-organisms. The composition of the watery soup, and its strength varies from area to area on a global scale, determined by several varying factors including light levels, water temperature and pH.

Soon after a vessel enters the water, a natural process occurs whereby microorganisms in the water form a biofilm. After around one week, spores and protozoa, and larvae of macrofouling species attach to the hull. Over the course of a few weeks, larger macrofouling species anchor to the surface and grow.

This process is called biofouling. In the 2023 Guidelines for the control and management of ships' biofouling to minimize the transfer of invasive aquatic species (Biofouling Guidelines), *IMO (2023)*, the International Maritime Organization (IMO) defines biofouling as “the accumulation of aquatic organisms such as microorganisms, plants and animals on surfaces and structures immersed in or exposed to the aquatic environment.” They also state that “biofouling can include pathogens.”

There are approximately 5,000 different fouling species that are found in the world’s oceans. These can be classified into micro fouling which comprise slime fouling and macro fouling which comprises weed fouling and animal fouling (hard, with a shell and soft, without a shell).

In the 2023 Biofouling Guidelines, the IMO defines microfouling as “biofouling caused by bacteria, fungi, microalgae, protozoans and other microscopic organisms that creates a biofilm also called a slime layer”, and macrofouling as “biofouling caused by the attachment and subsequent growth of visible plants and animals on structures and ships exposed to water. Macrofouling is large, distinct multicellular individual or colonial organisms visible to the human eye such as barnacles, tubeworms, mussels, fronds/filaments of algae, bryozoans, sea squirts and other large attached, encrusting or mobile organisms.”

Any organisms anchored on a ship’s hull create increased hydrodynamic drag (added frictional resistance) which significantly decreases vessel performance. Hard (with a shell) animal fouling (noted as calcareous fouling in Fig.2) which includes molluscs, bryozoans, tubeworms and barnacles cause the greatest added resistance penalty in terms of hydrodynamic drag when attached to a vessel’s hull.

This is not good news for ship owners and/or operators attempting to meet global rules around GHG emission reduction in the IMO’s 2023 GHG Strategy, namely a CO_2-per transport work reduction target of 40% by 2030, and a 2050 net zero GHG target. Also, tighter restrictions coming into force on a regional scale around biosafety.

In *GIA (2022)*, a statement in the opening introduction to the report reads: "One of the most significant factors impacting the efficiency of all ships in service is associated with the resistance generated by the friction of water on the ship's hull. Resistance increases when the hull is fouled. Therefore, maintaining a smooth and clean hull free from biofouling is of paramount importance to optimise the energy efficiency of ships."

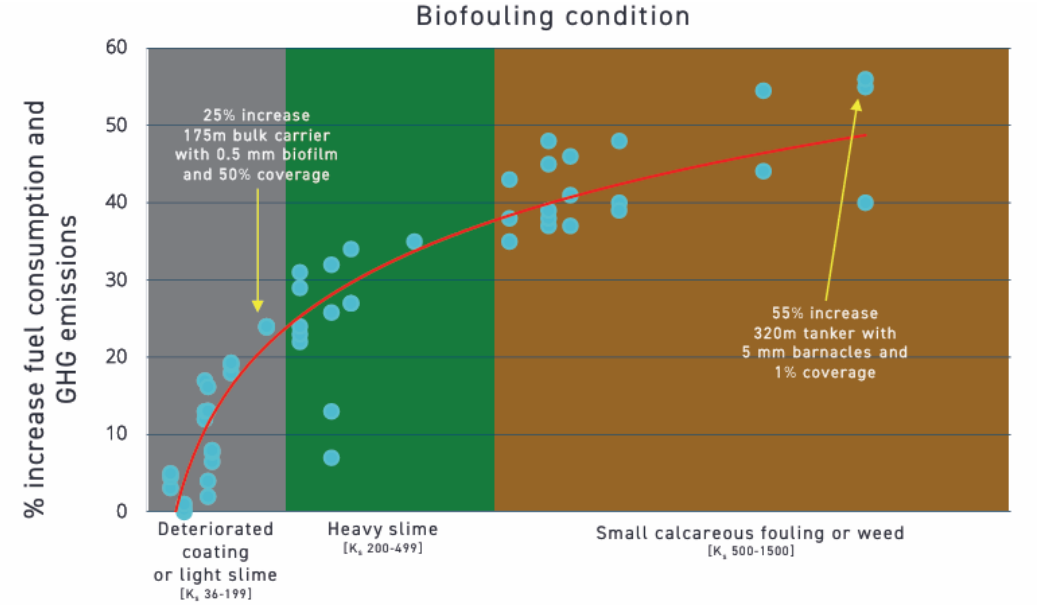

Fig.1: Impact of ship hull fouling on GHG emissions, *GIA (2022)*

Hull condition	**Additional shaft power to sustain speed (%)**
Freshly applied coating	0
Deteriorated coating or thin slime	9
Heavy slime	19
Small calcareous fouling or macroalgae	33
Medium calcareous fouling	52
Heavy calcareous fouling	84

Fig.2: Roughness and fouling penalties for a navy vessel - adapted from *Schultz (2007)*

Fig.3: Barnacles (medium calcareous fouling) on the flat bottom area of a chemical tanker hull

A 2020 study, commissioned by I-Tech based on data provided by Safinah Group, *Hoffmann and Austin (2020)*, found that 40% of ships surveyed for hull condition in a sample size of 249 had more than 20% of their underwater hull flat bottom area covered with hard animal fouling. Approximately 10% of ships inspected in the sample had more than 40% of their underwater areas covered by hard animal fouling.

Swain et al. (2022) calculated that if the underwater portion of all the world shipping fleet could be maintained in a smooth and fouling free condition, then the reduction in CO_2 and other exhaust gasses would be significant. In this study, the estimated hull condition from *Munk et al. (2009)* was used to quantify the reduction in CO_2 emissions if all vessels were maintained in a smooth and fouling free condition:

"1,056 million tons/year (an International Maritime Organization estimate for CO_2e emissions from ships from the 4th Greenhouse Gas study) × 0.7 friction resistance (assuming the average contribution of power from frictional resistance to move a ship is 70%) × [(33% ships with a 10% penalty) + (50% ships with 30% penalty) + (17% ships with 50% penalty)]
= 198 million tons of CO_{2e} or 19% per year reduction of ship emissions."

A hull suffering from heavy biofouling is also extremely impactful on maintenance costs. Costs associated with hull cleaning services must be factored into a ship operator's operating expenditure (OPEX). Repeated cleaning of the hull can also remove layers of the antifouling coating thickness, reducing its service life.

In addition, growing regulatory focus on the transportation of invasive aquatic species by the international shipping fleet can also impact a ship commercially. Some regional regulations are already in force that allow ports to refuse entry of heavily bio-fouled ships, resulting in greater financial costs for the operator.

2. The important role of antifouling coatings

Antifouling coatings act as the first line of defence against micro and macro biofouling organisms. They prolong the life of marine vessels and reduce GHG emissions by keeping the hull surface smooth and with minimal frictional resistance. Careful selection of an antifouling coating product for a ship is essential to ensure it meets the requirements of the ship in terms of its trade routes, activity levels and potential biofouling risk encountered during the coating's service lifetime, which could be up to 60 months.

There are essentially two main types of fouling control technology for commercial vessels, foul release coatings (with or without biocides) and biocidal antifouling coatings.

A biocidal antifouling coating comprises a soluble, or partially soluble, resin system that contains a mixture of biocide(s) effective against a broad range of fouling organisms. They are the most widely used technology for fouling control and account for approximately 90% of the fouling control technology market. These types of antifouling coatings primarily differ by the resin system used, also referred to as 'delivery mechanism', and the level and type of biocides used. The two main types of biocidal antifouling resins are: Controlled Depletion Polymers (CDPs) and Self-Polishing Copolymers (SPCs).

Foul release coatings typically comprise low surface energy silicone polymers. The speed of the vessel produces the hydrodynamic shear needed for the loosely attached fouling to fall off. Some foul release antifouling coating products are biocide-free and some contain biocides.

There are also 'hard coatings' that are based on epoxy technology and are biocide free. These coatings are mainly used for ice-going vessels. They accumulate biofouling quickly but are designed to withstand regular in-water cleaning without damaging the integrity of the coating.

3. The need for antifouling biocides

For centuries, materials or compounds that have an antifouling effect have been used for biofouling prevention on surfaces submerged in water.

Throughout this vast experience in using biocidal compounds, no other solutions have been proven as viable alternatives to meet increasingly tough requirements from the industry on i) application procedures, ii) long-term in-service life (up to 60 months) and iii) coating renewal processes, for the entirety of the global shipping fleet.

Biocidal products have been proven to be the one of the best solutions to meet the environmental and performance requirements for marine vessels operating in a highly competitive commercial environment where vessels sail in waters with varying biofouling risk.

To be effective across the entire range of biofouling micro- and microorganisms, a combination of biocides are generally used within an antifouling coating, referred to as co-biocides.

Today, there are a limited number of biocides that have passed evaluation and are approved for global use in marine coatings. Biocides are approved by the most stringent regulatory schemes in many global regions such as EU, UK, Turkey, Malaysia, South Korea, Japan, China, Australia, New Zealand, Canada, and the USA. The regulatory landscape for new biocidal substances is complex and this is certainly the case for biocidal substances intended for use in marine antifouling coatings. Biocides in use today have been tested, evaluated, and used for more than twenty years.

However, the biological complexity and the high industrial requirements for hull coatings present an increasingly complex challenge for this small, but highly impactful collection of certified biocides. According to data presented by Alistair Finnie at the 2023 International Antifouling Conference, in the listed antifouling coating products in the Lloyd's Register Antifouling Coating Type Approvals database as of August 2023, 10 biocides were used but with 45 different listed combinations, https://www.lr.org/en/services/classification-certification/lr-approvals/.

4. The nature of barnacle fouling

Hard macro-organisms create the greatest added frictional resistance. This type of biofouling also introduces complexities for hull grooming practices. For example, even when cleaning methods that can remove hard fouling are used, the base plates of barnacles and their colonies can remain on the hull. The biofouling success of barnacles is attributable to their adhesion to the hull surface. Barnacle larvae release an oily droplet to clear water from surfaces before sticking down using a phosphoprotein adhesive. This two-component system ensures that the glue can adhere even in the challenging conditions of the ocean, where dissolved ions, varying pH levels, and constant wetness would typically hinder adhesion.

The strength of this glue-like substance is such that mechanical forces are required to dislodge attached barnacles. In the first week after settling, the surface between the barnacle and the hull is very small, and the barnacles constantly release "barnacle" glue to bond to the surface. At this stage, the barnacles can be removed by a hull cleaning without damaging the coating. However, the older and larger a barnacle becomes, the more difficult it will be to remove from the hull without damaging the coating.

Once one barnacle larva attaches to the hull and progresses from cyprid larvae, to juvenile and into its adult life stage, it does not take long for a whole colony of barnacles to follow.

However, avoiding barnacles isn't an easy task. As a rule of thumb, barnacle larvae attach to a ship hull when it is stationary. Since most barnacle species prefer shallow or tidal zones, with 75% of them residing at depths of less than 100 metres, ships sailing in the open ocean or seas are at a lower risk. This means that barnacle fouling risk increases significantly within coastal areas, and if a ship is spending time at anchor, or at very low speeds, typically below 6 knots.

Hoffmann and Austin (2022) presented the results from an examination of idling and barnacle biofouling using in-depth analysis of the global fleet patterns from AIS data for all IMO-registered vessels in the global fleet. This research revealed that the total number of vessels idling has roughly doubled over the

decade 2010-2020 and that depending on season, between 50% - 85% of idling is occurring in water temperatures of above 15ºC).

I-Tech found that 'Fouling Idling', as defined in the study as 'any vessel that is idling for 14 days or more in waters of 15ºC or more', had increased constantly since 2009, with a starting point of 25.4% to a peak of 35.0% in May 2020 in the global fleet.

The study also found that vessels are increasingly idling in so-called biofouling ´hotspots´, where water temperatures above 25°C. Vessels spending most of their time sailing in these regions are at acute risk of excessive hard fouling accumulation.

The conclusion of the study was that antifouling coating products that can offer extended static protection from both soft (slimes) and hard (barnacles) fouling are essential for the adequate protection of the global shipping fleet from biofouling.

5. Selektope® as a barnacle-repelling biocide and its future applications

Improving static performance against barnacle fouling has been a focus for the sector given the severe impact that barnacle fouling has on increasing added resistance and GHG emissions.

The introduction of the biocide Selektope® to the market in 2015 has offered antifouling coatings manufacturers the ability to increase static performance guarantees for coating products.

As an organic, non-metal active agent, Selektope is relatively unique compared to traditional marine biocides. When exposed to Selektope, the swimming behaviour of a barnacle cyprid larva is activated through receptor stimulation, this disables their ability to settle on a surface. The effect of Selektope is temporary and has reversible effects. Any larvae that came into contact with Selektope could still metamorphose into juvenile barnacles with no apparent ill effect. When used in antifouling paints, Selektope can protect all ship types when they are idle or operating at low speeds for extended periods of time, even in extreme barnacle fouling risk areas.

Today, approximately 3,000 ships are sailing with coatings that contain Selektope. SPC antifouling coatings products that contain Selektope are sold by multiple coatings manufacturers.

In SPC biocidal coatings, Selektope binds to pigment and other particles and is continuously released in the same way as other biocides present. The compatibility between Selektope and the paint matrix in the marine coatings industry ensures as slow and steady release secures the antifouling effect for the entire coating service life.

Selektope is a biocide that has highly favourable antifouling properties at low concentrations (nano Molar). To obtain full protection against barnacle fouling, 0.1 - 0.3% w/w of Selektope should be used in a wet paint formulation. That equates around 2 grams of Selektope per litre of paint when 0.1% w/w is used, comparable to 500-700 grams of cuprous oxide used per litre of paint.

Extensive R&D efforts are being undertaken by scientists at I-Tech to incorporate Selektope into foul release coatings (e.g. via attaching Selektope to a polymer chain) with successes achieve to-date.

6. Novel research: determining the true scale of barnacle fouling on the global shipping fleet

In November 2024, I-Tech contracted Safinah Group (Safinah) to independently analyse a dataset comprising hull condition data from 685 vessel inspections. This study updates *I-Tech (2020)* wherein data from 249 vessel inspections were independently analysed by Safinah to quantify the scale of barnacle fouling on the global shipping fleet. There are certain limitations related to the analysis that should be taken into account when interpreting the results and conclusions of this study:

- Certain ship types are better represented in the data, such as tankers.
- The coating technology comparisons in terms of animal fouling do not include any operational history or environmental data,
- In-water cleaning frequency is not taken into account in this study,
- The age of the ships comprising the sample is relatively low so that may have an impact on the choices regarding surface preparation and coating selection.
- Commercial product names or any identifiers linked to the inspected ships have not been disclosed.

Furthermore, the dry dock reports received for data analysis do not provide details as to a vessel's activity and/or static periods. Extended static periods are known to be particularly challenging to both biocidal and foul release coating types.

The data used in the research is based on historical drydock attendance reports / inspections conducted by Safinah during the period 2015 – 2024. This dataset comprised data from 685 individual vessel inspections undertaken from 836 hull-related drydock projects managed and conducted by Safinah in that time period.

The 685 vessels inspected are presented, by type, in Fig.4.

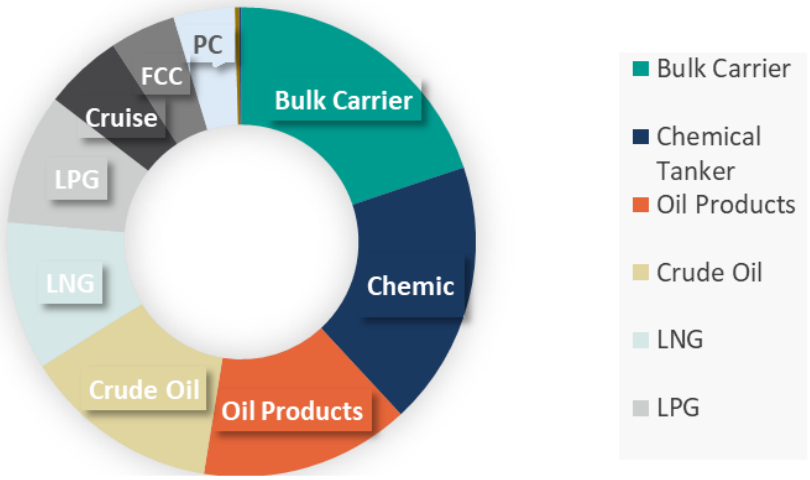

Fig.4: Vessel type distribution

The majority of vessels inspected by Safinah were younger than 10 years. Fig.5 show the vessel age distribution for the total number of dry dock projects undertaken by Safinah. 260 drydock projects were conducted for 0–5-years-old vessels, and 250 drydock projects for 5–10-years-old vessels, respectively.

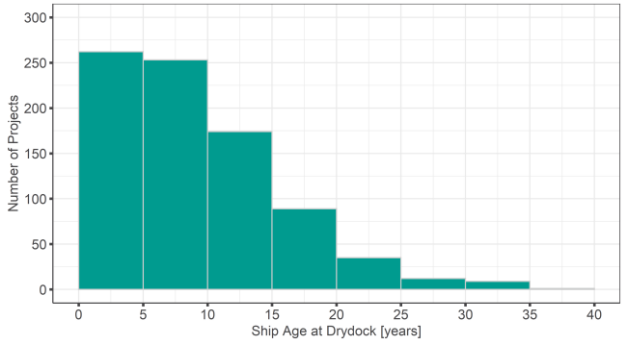

Fig.5: Vessel age distribution

Less than 100 drydock projects were conducted for vessels over 15 years in age and under 50 drydock projects were conducted for vessels aged 20 years and over.

In this study, observations of animal fouling are used as a method to quantify barnacle fouling coverage. Safinah confirms that while the term 'animal fouling' is used for the purposes of this study, animal fouling presence on vessel hulls is pre-dominantly barnacle related.

Fig.6 shows the overall animal fouling coverage by proportion of the total underwater hull area for all vessels inspected during 761 hull-related drydock projects undertaken by Safinah.

- Most dry dock projects found vessels with animal fouling on the underwater hull. Only 140 drydock projects found vessels with <0.1%/<0.1sqm animal fouling coverage on the hull.
- The majority of drydock projects found vessels with 0.1 - 5% animal fouling coverage on the underwater hull.
- More than a third of drydock projects found vessels with >10% animal fouling coverage on the underwater hull.
- 18% of drydock projects undertaken found vessels with >20% animal fouling coverage on the underwater hull.

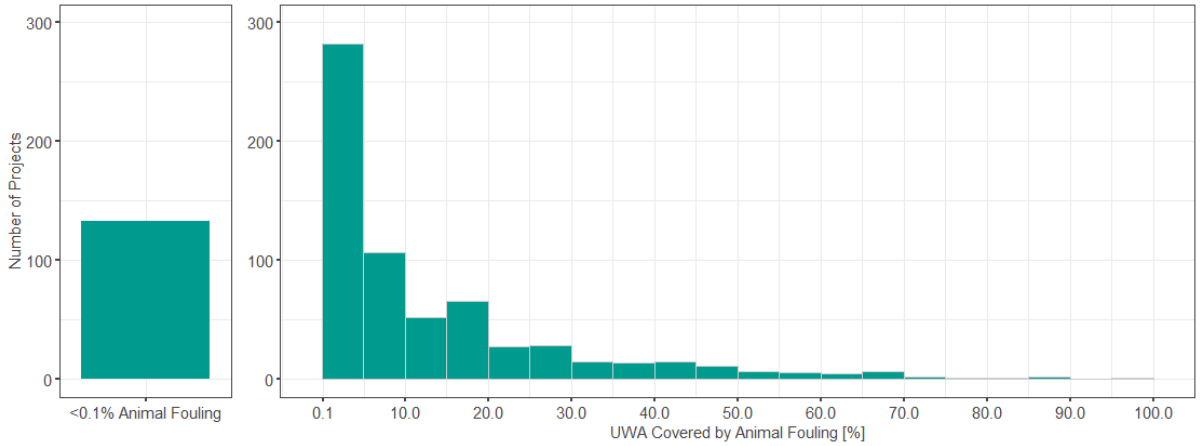

Fig.6: Animal fouling coverage on the underwater for vessels inspected in 761 drydock projects

In Fig.7, the total surface area covered by animal fouling on the hull, plotted as m^2 coverage, is presented. The average underwater hull area in this data sample is 11,600m^2. In terms of animal fouling coverage by m^2 area of hull surface, the highest percentage of drydock projects found vessels with 0.1%-1000m^2 of animal fouling coverage. Fig.7 also shows that for 400 of the 761 drydock projects undertaken; vessels had 0.1-1000 m^2 of animal fouling coverage. Whereas 110 drydock projects found vessels with 1000-2000m^2 of animal fouling coverage. The number of drydock projects where larger surface areas were covered by animal fouling decreases significantly after 4,000m^2.

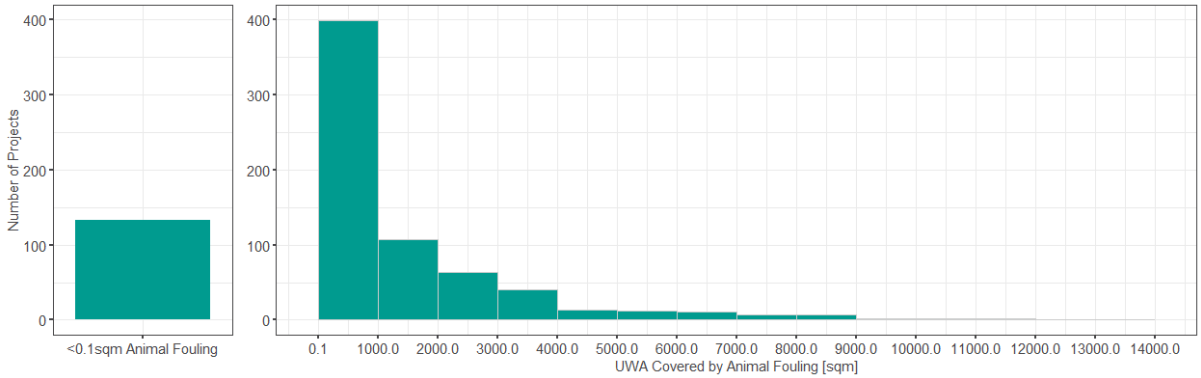

Fig.7: Animal fouling coverage on the underwater hull as m^2

Fig.8 presents a deeper analysis of the level of animal fouling found on vessels inspected by hull area.

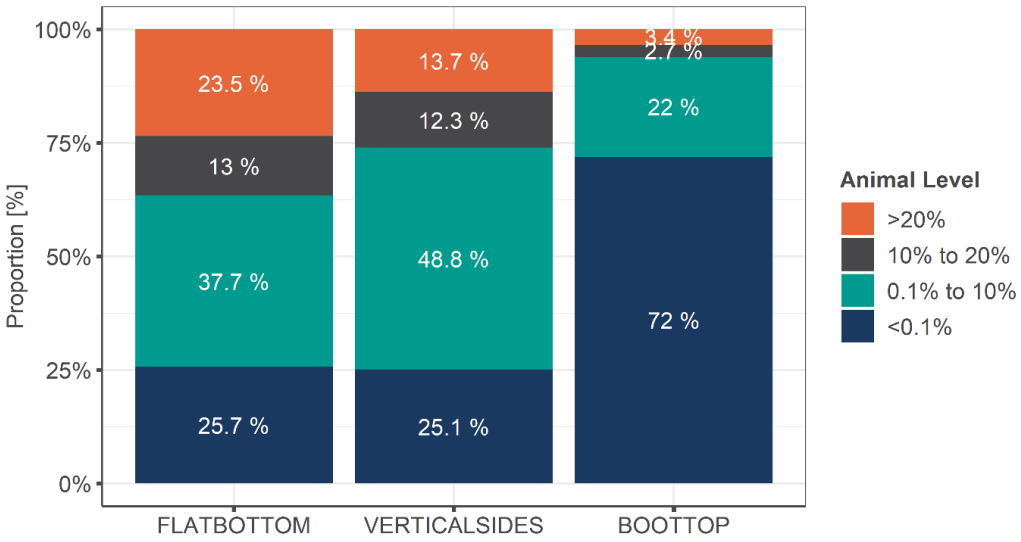

Fig.8: Animal fouling levels by main hull area

The combinations of animal fouling types by hull area are quantified in Fig.9. Fig.9 shows that animal/weed and slime were the most encountered fouling condition on the flat bottom and vertical sides logged for the 685 vessels inspected. Whilst animal fouling, with or without other fouling types, is present on the majority of vessels inspected for vertical sides and flat bottom, animal fouling is more prevalent on the flat bottom hull area.

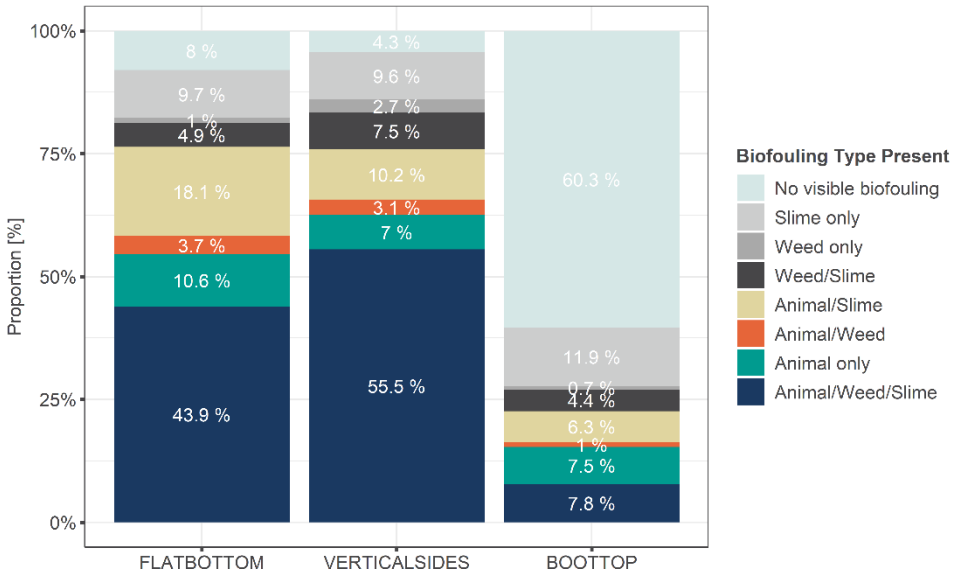

Fig.9: Biofouling type combinations by main hull area

The presence of animal fouling by ship type on arrival in drydock is presented in Fig.10. Fig.10 shows that all vessel types had some level of animal fouling presence on the hull when inspected.

Also, Fig.10 confirms that animal fouling is more prevalent on tankers (product, chemical, crude, LNG, and LPG). The vessel type with the lowest proportion of animal fouling in the data set was containerships, closely followed by Pure Car Carriers (PCC).

Large variations in animal fouling between vessel types can be attributable to a certain degree to different root causes, different paint systems, speed, activity and where the vessels sail (geographically).

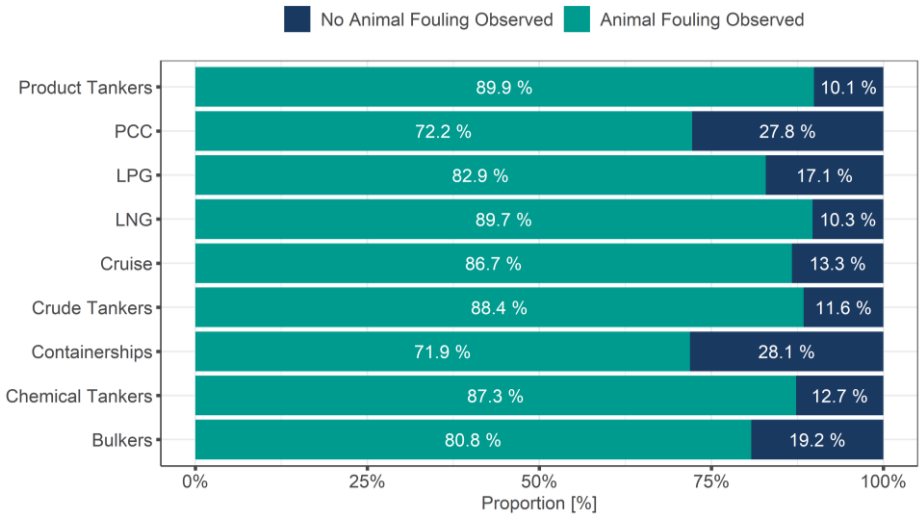

Fig.10: Animal fouling presence by ship type

A further split of the data was made to assess barnacle fouling by relative activity of the vessel types. The split of vessel types by higher activity level and low activity lower is shown in Fig.. While the actual activities of the vessel in the dataset were unknown, the vessels were grouped by relative vessel activity based on typical industry assumptions.

Relatively lower activity	Relatively higher activity
Chemical / Product Tanker	Car Carrier
Crude Oil Tanker (up to 80k DWT)	Crude Oil Tanker (up to >80k DWT)
LPG	Container
Oil Products Tanker	Cruise Ship
	Ferry
	LNG

Fig.11: Vessel types by relative vessel activity

The fouling condition for lower and higher activity vessels in the dataset are presented in Fig.12.

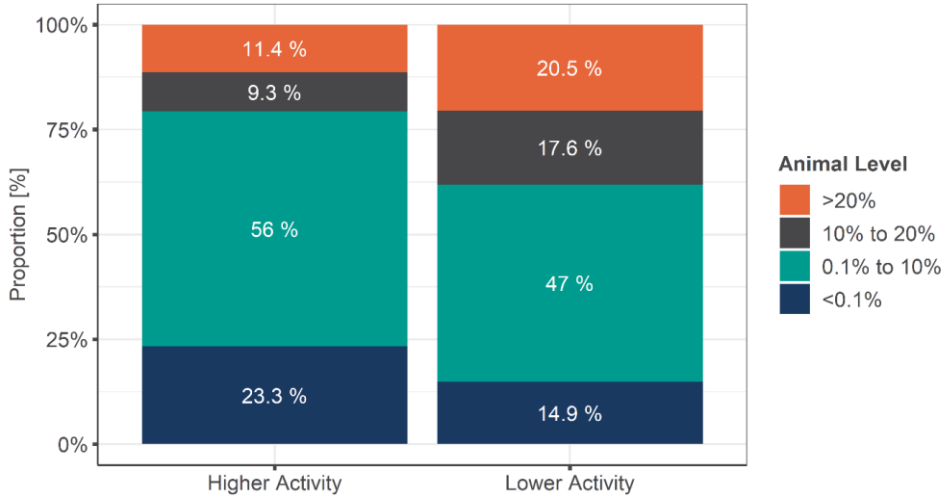

Fig.12: Animal fouling proportion (%) – higher activity vessels versus lower activity vessels

This data shows us that higher levels of animal fouling are more prevalent on lower activity vessels (20.5% on lower activity vessels versus 11.4% on higher activity vessels). Also, we can conclude from the data that larger proportions of the relatively lower activity vessels arrive in drydock with more than 10% of the hull area covered in animal fouling.

In Fig.13, animal fouling presence by hull area for higher activity vessels versus lower activity vessels is presented. These statistics are area-specific rather than ship-specific. Fig.13 shows that animal fouling coverage is significantly greater across the flat bottom of both higher and lower activity vessels compared to the boottop. In lower activity vessels, animal fouling is more prevalent on the flat bottom than on higher activity vessels. However, animal fouling on the vertical sides of both lower activity and higher activity vessels is relatively similar.

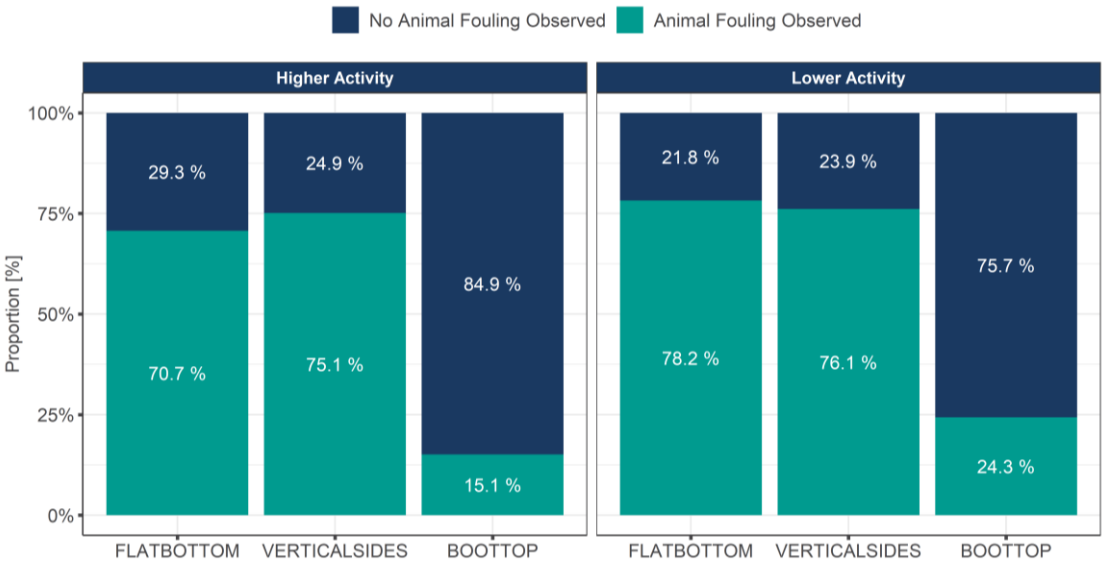

Fig.13: Animal fouling presence by UWA type, higher activity vessels versus lower activity vessels

Polish through can be an issue with biocidal antifouling coating systems. The analysis presented below examines the level of polish through versus animal fouling coverage was conducted to distinguish if one of the potential causes of animal fouling lies in polished through areas of coatings. Fig.14 isolates the levels of polish through and animal fouling. Fig.14 shows that ships with larger areas of polish through tend to arrive in drydock with more animal fouling on the underwater hull. The data also tells us that polish through occurrence is not uniform across vessel areas – the number of observations per each main hull area and polish through level varies. The data presented in Fig.14 also confirms that >20% polish through has a more significant effect on animal fouling on the flat bottom and vertical sides than <20% polish through. Note that even with no polish through, animal fouling is still present on the flat bottom and vertical sides. This confirms that not all animal fouling presence can be reasoned by polished through areas of a coating.

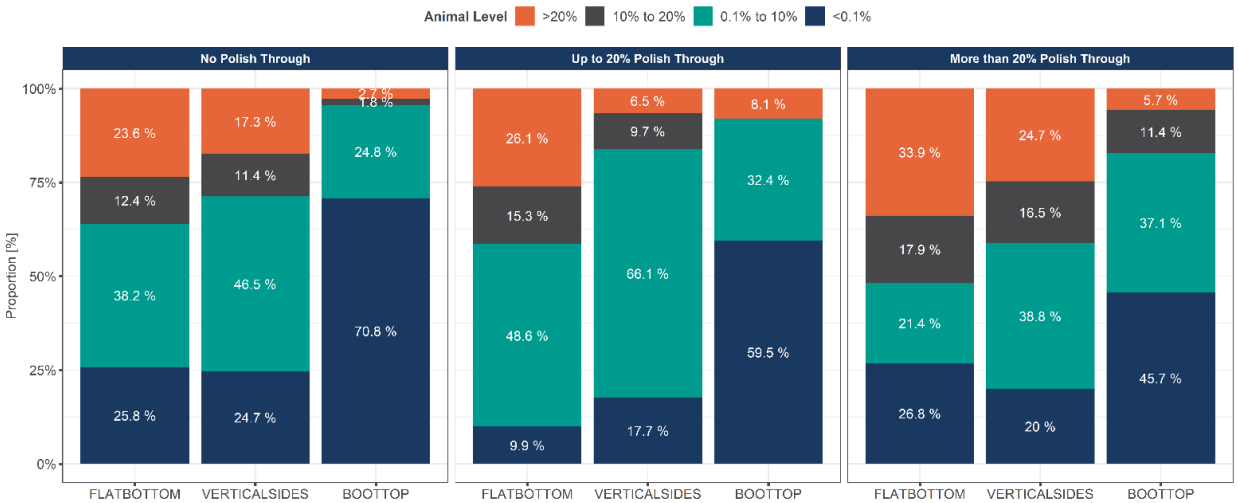

Fig.14: Animal level by main hull area and level of polish through

An analysis of animal fouling presence on conventional biocidal coatings versus foul release coatings was undertaken as part of this study. Also, animal fouling coverage on different grades of antifouling coatings were assessed. Conventional biocidal products were split into 'Perceived Low Technology Level', "Perceived Medium Technology Level' and 'Perceived High Technology Level". Fouling release products (biocidal / biocide-free) are grouped under the 'FRC' technology. The results in Fig.15 indicate that no perceivable difference between technology types can be observed in terms of level of animal fouling, for the ships inspected in this sample, without factoring in ship operating history and environmental conditions.

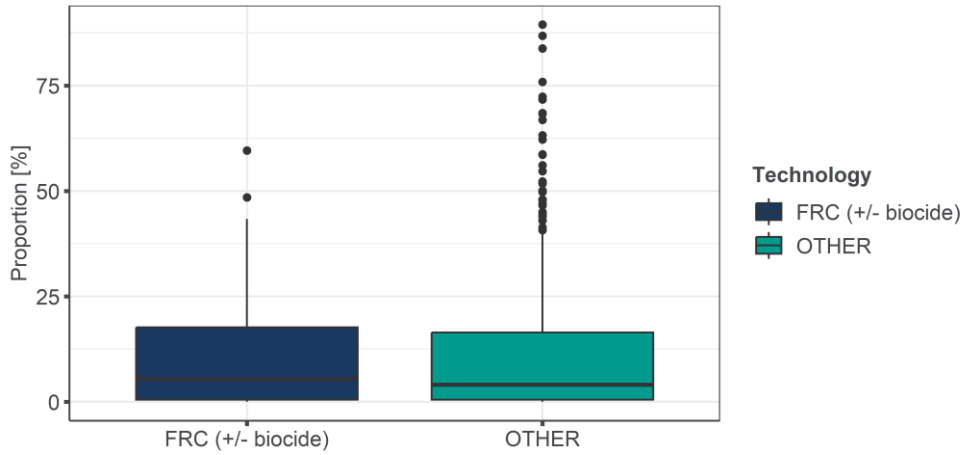

Fig.15: Animal fouling by technology. Foul Release Coating (FRC) (including products with and without biocides) versus conventional biocidal coating products (other).

Fig.16 shows animal fouling prevalence on different coating technology grades.

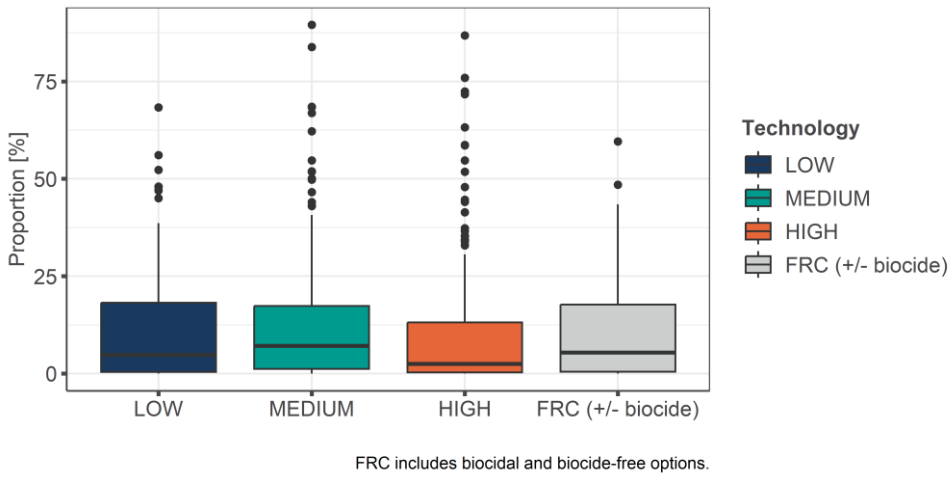

Fig.16: Animal fouling by technology grade (data from 547 dry dock projects)

The data in Fig.17 tells us that high grade coatings are working better in terms of animal fouling prevention than medium or low-grade technologies. Please note, the analysis conducted in this study does not take into account in-docking times, docking cycles and any in-water cleaning events in between dry dockings.

Most foul release coatings can also be regarded as high performing systems. However, the following conclusions can be made based on this data analysis. High performing systems show better performance on average (depicted by the line).

Low and medium systems show similar results however, the lower grade systems are more often used for 2-to-3-year schemes while the medium systems can be used for up to 5 years docking cycles.

As part of the study, Safinah conducted independent analysis of inspections carried out on a small sample of vessels with Selektope-containing antifouling coating products on the underwater hull. A total of 12 ships were inspected. 11 ships had their full underwater hull coated with Selektope-containing antifouling coating products, whereas 1 ship had only the vertical sides of their hull coated with a Selektope-containing antifouling coating product. It should be noted that this is a small sample size and data on in water cleaning events were not available. Therefore, the impact of in water cleaning events is not factored into the analysis. This data analysis confirmed that ships with products containing Selektope arrived in drydock with <10% animal fouling coverage in most cases (10 out of 12 ships inspected).

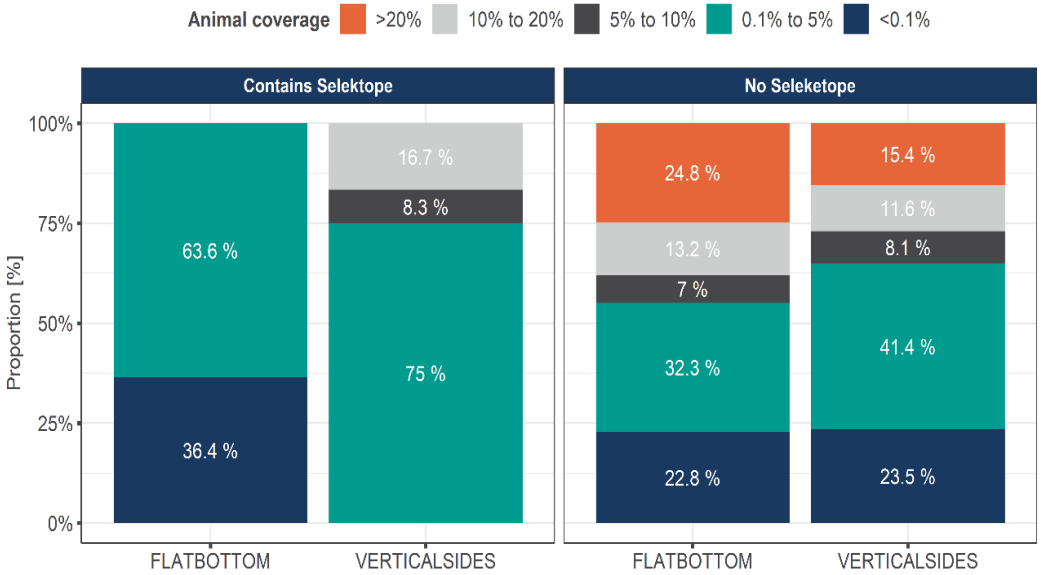

Fig.17: Animal level of ships on arrival with and without Selektope

Two of the vessels inspected had over 10% animal fouling coverage on the vertical sides – one with a little over 10% coverage and the other with 19.6% coverage respectively. The vessel with over 10% animal coverage was a container ship. (60-month scheme with Selektope antifouling coating on the vertical sides and flat bottom). The vessel with over 19% animal coverage was a Suezmax crude oil tanker. Historical AIS data was obtained for the container ship. There were 3 stationary periods over 13 days for the 60 months docking interval, all of which occurred nearly 3 years prior to dry-docking the ship. This suggests that the animal fouling observed is not a direct result of a significant stationary period prior to dry-docking. Analysis of the speed and activity profile of the vessel, over the whole period and year on year, did not reveal any operational anomalies that could be linked to the arrival condition. An overview of the operational history of the vessel is presented below.

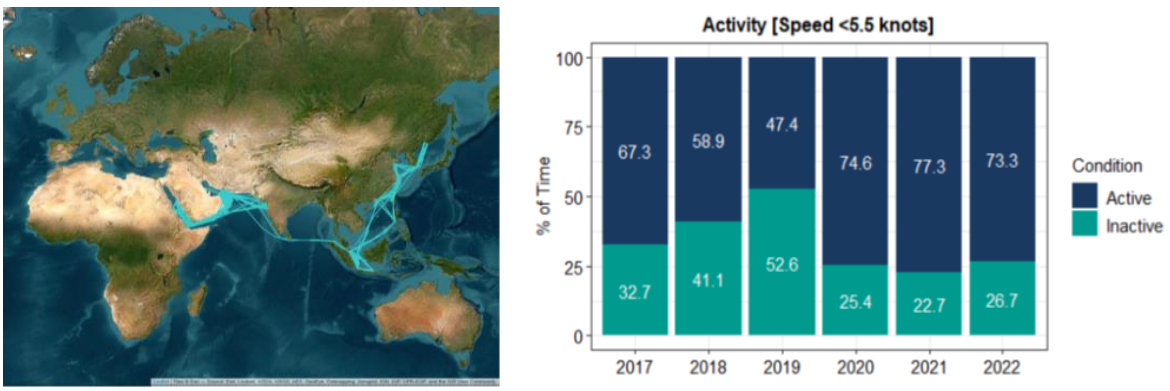

Fig.18: Overview of the operational profile of a containership with ~10% animal fouling coverage (Selektope-containing coating on flat bottom and vertical sides)

Fig.19: Photographs of the arrival condition of a container ship with ~10% animal fouling (Selektope-containing coating on flat bottom and vertical sides)

7. Conclusion

Based on a dataset of 836 dry docking projects wherein the hull inspection data for 685 vessels was analysed, the authors conclude that barnacle fouling is a big problem for the global shipping fleet. The majority of vessels inspected had animal fouling coverage levels of 0.1-5% on their underwater hull and more than a third of vessels inspected had >10% animal fouling coverage. Animal fouling conditions on the flat bottom of vessels inspected was more intense than the authors expected. Although this was not investigated as part of this study, it is possible that the phenomenon is partly due to the practice of using more economic coating systems on the flat bottoms of vessels.

Ships with larger areas of polish through tend to arrive in drydock with more animal fouling however, the data shows that animal fouling was also prevalent on vessel hulls without polish through. This confirms that not all animal fouling can be reasoned by polished through areas of a coating.

The data analysis in this study confirms that high grade coatings are working better in terms of animal fouling prevention than medium or low-grade technologies.

Data analysed for foul release (with and without biocide) versus conventional biocidal coatings showed that no perceivable difference between technology types can be observed in terms of level of animal fouling for the ships inspected in this sample, without factoring in ship operating history and environmental conditions.

Independent data analysis on the vessels using coatings with Selektope showed, in the majority, no barnacle fouling. Although this was not investigated as part of this study, Selektope has been shown to deliver animal fouling settlement protection during long idle periods. The authors conclude that coatings inclusive of the barnacle-repelling technology, Selektope should be used to afford protection against barnacle fouling for vessels at any risk of idling for more than a few days or weeks on both flat bottom and vertical sides.

The evidence from the data set clearly points to a need for further improvement in the current fouling control range in resisting animal fouling to achieve global decarbonization targets.

As the maritime industry moves towards using cleaner, greener, less carbon intensive fuel options, the cost of fuel per metric ton will only increase. Therefore, increased fuel consumption resulting from biofouling accumulation will incur a more expensive cost penalty than today in a not-so-distant future.

Acknowledgements

We thank the University of Gothenburg and the Safinah Group.

References

GIA (2022), *Analysing the Impact of Marine Biofouling on the Energy Efficiency of Ships and the GHG Abatement Potential of Biofouling Management Measures*, GEF-UNDP-IMO Glofouling Partnerships Project and GIA For Marine Biosafety, Int. Mar. Org., London

HOFFMANN, M.; AUSTIN, C. (2020), *Quantifying the Barnacle Fouling Problem on the Global Shipping Fleet*, original research with Safinah Group

HOFFMANN, M.; AUSTIN, C. (2022), *Managing biofouling in shipping - The Idling Challenge*, original research with Marine Benchmark

IMO (2020), *The Control of Harmful Anti-Fouling Systems on Ships (AFS Convention), to Include Controls on the Biocide Cybutryne*, MEPC Vol. 75, Int. Mar. Org., London

IMO (2023), *2023 Guidelines for the control and management of ships' biofouling to minimize the transfer of invasive aquatic species*, Int. Mar. Org., London

I-TECH (2020), *Quantifying the scale of the barnacle fouling problem on the global shipping fleet*, I-Tech, https://selektope.com/wp-content/uploads/2020/12/ITECH-WHITE-PAPER_June-2020-1.pdf

MUNK, T.; KANE, D.; YEBRA, D.M. (2009), *The effects of corrosion and fouling on the performance of ocean-going vessels*, Advances in Marine Antifouling Coatings and Technologies

SCHULTZ, M.P. (2007), *Effects of coating roughness and biofouling on ship resistance and powering*, Biofouling 23, pp.331-341

SWAIN, G.; ERDOGAN, C.; FOY, L.; GARDNER, H.; HARPER, M.; HEARIN, J.; HUNSUCKER, K.Z.; HUNSUCKER, J.T.; LIEBERMAN, K.; NANNEY, M.; RALSTON, E.; STEPHENS, A.; TRIBOU, M.; WALKER, B.; WASSICK, A. (2022), *Proactive In-Water Ship Hull Grooming as a Method to Reduce the Environmental Footprint of Ships*, Front. Mar. Sci.

A Feasible Approach for Cost-Saving Splitting of Wind Propulsion Technology Installations

Sofia Werner, RISE SSPA Maritime Centre, Gothenburg/Sweden, sofia.werner@ri.se
Frederik Gerhardt, RISE SSPA Maritime Centre, Gothenburg/Sweden

Abstract

Wind propulsion offers a promising solution for reducing fuel consumption and minimizing environmental impact. The high initial costs of these installations pose significant barriers, but sharing the investment costs and fuel savings among stakeholders can ease the burden. To achieve an efficient cost-saving split, it is essential to accurately assess the actual fuel savings provided by wind propulsion during operation, a task that is technically not trivial. A few solutions with differing levels of complexity and transparency are offered by OEMs and others. This paper presents an alternative approach designed to be economically feasible, independent, robust, and transparent. Other possible methodologies are described briefly.

1. Introduction

In recent years, wind propulsion technology has gained significant popularity in the shipping industry. Currently, over 50 cargo vessels are equipped with wind propulsion solutions. However, for this number to increase and reach a larger portion of the global fleet, several major barriers must be overcome. One of the primary challenges is the investment cost of wind propulsion installations. To mitigate this, cost-sharing arrangements between owners and charterers, as well as various pay-as-you-save solutions, have been proposed. While these financial models have been utilized in shipping for a long time, assessing the actual savings from wind propulsion once a ship is in operation remains challenging. The savings depend heavily on the wind conditions encountered, which vary based on the geographical area of operation. Additionally, factors such as the frequency of technology usage, idling periods, and ship speed also impact the savings.

To make saving split arrangements or pay-as-you-save models viable, reliable methods for assessing actual savings during operation are essential. This paper discusses various methods for assessing power savings from wind propulsion during service. These methods can be used for splitting savings between stakeholders and for ship owners to monitor the returns on their investments.

Some of the methods discussed are currently in use by the author's organization, while others are still under development. The wind propulsion industry is rapidly evolving, and it is likely that advancements in equipment will soon provide new opportunities for logging and assessing savings. The aim of this paper is to present the current state of available methods and to inspire future developments in this field.

2. Method

2.1. Overview

The conventional method for assessing the effectiveness of energy-saving measures on a ship typically involves logging fuel consumption or performance monitoring. However, this approach presents several challenges for wind propulsion installations. The savings from wind propulsion are highly dependent on wind conditions, making it difficult for most vessels to identify reference periods for comparison. Additionally, retro-fit installations are often carried out alongside other maintenance activities, meaning there is no true reference period with all other variables unchanged. For new builds, there is, of course, no reference period at all. Therefore, traditional performance logging will not be discussed further here. Instead, this paper proposes alternative methods that are better suited to isolating the contribution of wind propulsion technology.

Fig.1 lists the major physical effects that influence the assessment of power savings from wind propulsion. The process begins with the wind, which enables the wind propulsion technology to generate a force. However, this force does not directly translate to fuel savings. To convert the thrust force into fuel savings, we need to understand the ship's propulsive efficiency (η_D) and the engine's specific fuel oil consumption. When wind propulsion technology provides thrust, the propeller gets off-loaded, altering the propulsive efficiency.

The wind propulsion device generates not only thrust force but also side forces. These side forces result in a drift angle and increased rudder angles, leading to additional resistance and changes in propeller inflow.

Various options for continuously deriving power savings in service are suggested in Fig.1, either by measuring or modelling the mentioned effects. Option 1 is the simplest approach, in which nothing is measured in service. The power savings are based on predictions using a generic wind profile or wind statistics for a given route. The inclusion of wind propulsion in EEDI *IMO (2021)*, and the Fuel EU Maritime are examples of this approach. Options 2 and 3 will be discussed in the following sections. Options 4 and 5 require measurement equipment that is not commonly used onboard today. These options will not be discussed further in this work, but they may become relevant in the near future.

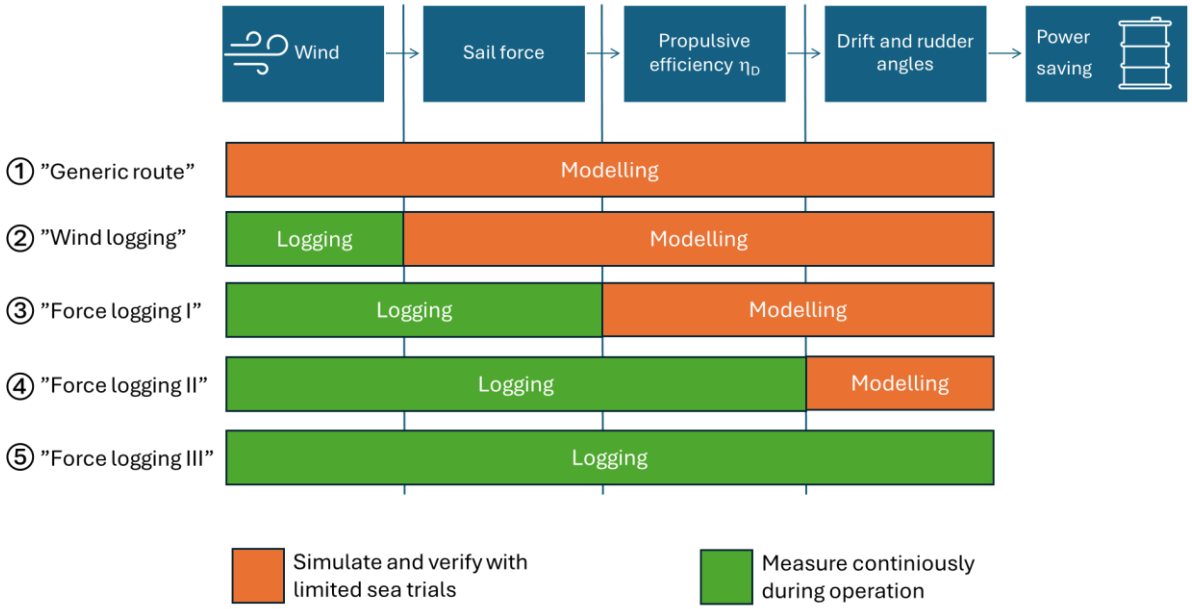

Fig.1: Alternative approaches for in-service monitoring power saving from wind propulsion

2.2. Assessment method based on Wind logging

2.2.1 Process

This method was developed at RISE to address the industry's demand for a cost-effective and robust solution. The procedure involves the following four steps, Fig.2:

1. Prediction of power saving
2. Verification of power saving
3. Agreement
4. Operation, data logging and saving estimation

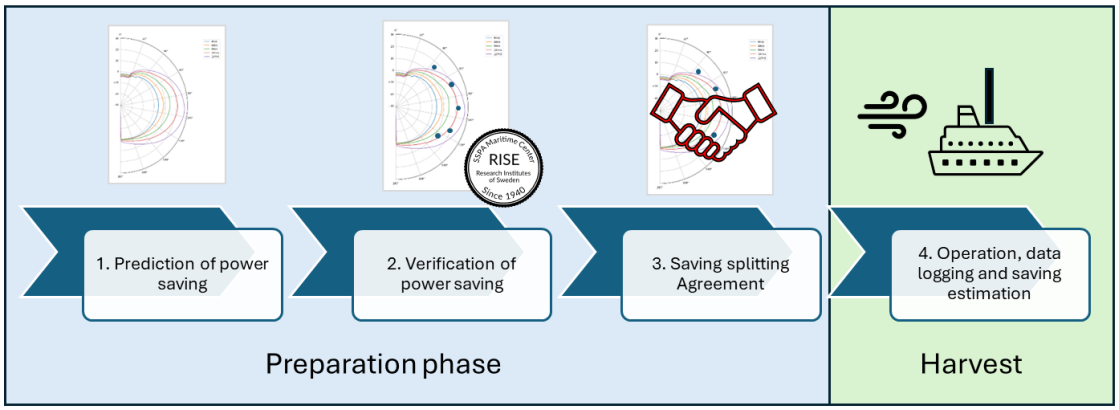

Fig.2: The four steps in the basic method for estimating fuel saving from wind propulsion in service

Step 1. Prediction of power saving

The first step is to predict the power savings of the wind propulsion system under various wind conditions, ship speeds, and draughts. The procedure for such predictions is outlined in ITTC 7.5-02-03-01.9. At RISE, simulations are conducted using the in-house software SEAMAN Winds, which can be performed at different confidence levels, Table I.

Table I: Performance assessment levels of confidence vs complexity

	Typical use	Included physics	Typical tools
Level 0	Technology selection	Stand-alone unit only, no ship	
Level I	Early idea of saving potential	• Generic ship data • Simplified physics	• Database • 1DOF PPP • Voyage simulation
Level II	Business case, Performance expectation, Comparing solutions	• Side force and yaw balance (leeway, rudder angles, heel) • propeller unloading • aerodynamics and hydrodynamic forces from empirical/database • Fixed route	• Database • 4DOF PPP • Voyage simulation
Level III	Business case, Performance expectation for contracts	• Full CFD for aerodynamics and hydrodynamics forces • Fixed route	• CFD and/or wind tunnel • CFD and/or towing tank • 4DOF PPP • Voyage simulation
Level IV	Advanced Performance expectation, complex cases	• Weather Routing • Dynamic effects • Etc	• CFD and/or wind tunnel • CFD and/or towing tank • 4DOF PPP • Voyage simulation

Level I involves only empirical models. Level II mostly mid-fidelity tools and Level III requires substantial CFD work. Level IV adds complexity of route optimisation. For the purposes discussed

here, we recommended between Level II to IV. For the purposes discussed here, we recommend using levels II to IV. The choice of level depends on the ambition of the involved parties and the scale of wind propulsion. For modest power contributions, lower levels may be acceptable.

The simulations produce a Power Saving Matrix, which can be represented as a polar diagram. This diagram illustrates the potential of the wind propulsion system to save propulsion power at various wind directions and speeds. "Saving" here refers to the comparison with the same ship operating without a wind propulsion system, maintaining the same ship speed.

Step 2. Verification of Power Saving Matrix

The next step is to verify the calculated power savings. This is done using the sea trial methodology initially developed by RISE (Werner, 2022) and recently refined into ITTC Recommended Procedures 7.5-04-01-02. Similar to a conventional sea trial, the sea trial for ships with wind propulsion consists of a series of short runs. The main difference is that the outcome is not the absolute value of the speed-power curve, but the power reduction due to the wind propulsion system. The effect of the wind propulsion system is determined by comparing the speed and power of individual runs with and without wind propulsion under the same wind conditions (known as on-off tests). The measured speed difference is then converted to a power difference using the shape of the speed-power curve, with some corrections for speed variations.

The signals to be measured are the same as for a normal speed-power sea trial: ship's speed, power, wind speed, and direction. Unlike normal procedures, the correction for current, usually based on double runs, cannot be applied when wind propulsion is active. To address this, speed trough water is measured using the ship's log if the trial is conducted in an area known to be affected by tidal currents. Since the goal is to derive a speed difference, the relatively poor accuracy of speed logs is acceptable.

The minimum test program includes five wind angles and can be completed within one day. However, the scope can be extended to include a larger number of conditions and can be conducted over a longer period during operation. Typically, the crew can conduct the trial in service based on instructions from RISE, after an initial trial with RISE personnel onboard.

For ships with significant differences in freeboard height between loading conditions, the power-saving matrix and its verification should be conducted under more than one loading condition. Trials should also preferably be conducted at a range of ship speeds.

The purpose of the sea trial is to verify the calculated Power Saving Matrix. If the sea trial results do not match the predicted Power Saving Matrix, the simulation model needs to be updated. However, this is not trivial, as deviations can result from various modelling errors. There are no specific guidelines for this, and it largely depends on the experience and knowledge of the prediction provider.

3. Agreement

All stakeholders are now invited to review the 3rd party verification of the predictions. When all parties agree, the confirmed Power Saving Matrix is from now on locked. This means that the parties do not need to spend further time on arguing or disputing performance claims.

4. Operation, data logging and saving estimation

It is now time to harvest the savings from wind propulsion. During the operation, the following signals are logged onboard:

- Positions and time
- Loading condition or draft
- Wind propulsion state (on or off)

At regular intervals, for example every 6 month, an independent organisation such as a performance monitoring provider or similar, conduct the estimation of energy or fuel saved. This is done in the following way:

i. from the logged positions and time, the hind-cast weather is retrieved from an agreed weather source (such as ECMWF reanalysis data), for the time events that the wind propulsion system was *on*
ii. the estimated fuel saving during the period is derived by combining the agreed Power Saving Matrix with the hind-cast wind.

A Saving Report as the example in Fig.3 is issued to all partis.

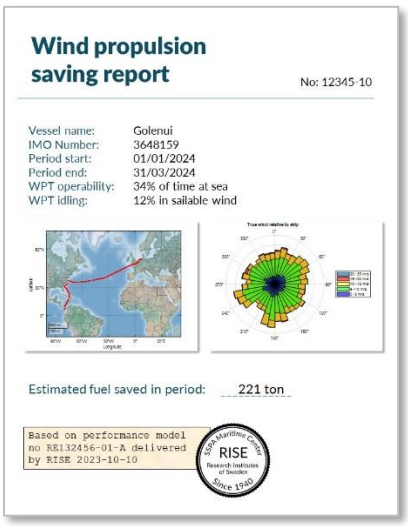

Fig.3: Example of Wind Propulsion Saving Report, derived by a 3rd party using a verified performance model

2.2.2 Pro and cons of the method

The main merit of this method is that all potentially time-consuming discussions and disputes between stakeholders are resolved once and for all in Step 3. After that, the process is very simple and transparent. Furthermore, the process does not require any additional instrumentation, making it both cost-efficient and robust. Relying on a failing or inaccurate sensor for calculating the savings split is not an ideal scenario.

The disadvantage lies in the simplifications of the process. If the sea trial is conducted with a limited scope, poor performance in untested conditions may go unnoticed. Additionally, deterioration of performance over time due to wear, malfunctioning control systems, etc., will not be detected since the verification is conducted only in the initial phase. Moreover, if extensive weather routing is used, it is not entirely accurate to derive power savings based on logged weather, as the vessel without wind propulsion might sail a different route.

Despite these risks, this method can be a attractive solution, especially for moderate wind propulsion systems (wind assistance), offering an attractive balance between cost and accuracy.

2.2.3. Case study

To illustrate the process, we examine a medium range cargo vessel equipped with rotor sails. The vessel operates mainly in Europe, with trading pattern as shown in Fig.4. The estimated average power saving, based on the process described in Section 3, is shown in Fig.4 (right). Note that the saving varies significantly from month to month, depending on the wind that the vessel has met.

Fig.5 shows another example case with a similar wind propulsion system installed on a vessel with world-wide trade. In some periods, the vessel operates in areas with very low wind speeds, which results in low saving or even negative saving, i.e. increased resistance. The latter is due to the rotor which on this vessel cannot be tilted. The resulting power saving is significantly different from the one estimated with the Global Weather Matrix, a generic wind distribution use for EEDI calculation. (In this example, using the Global Weather Matrix gives a higher calculated saving, but it can just as well give a lower.)

These examples illustrate that fuel savings from wind propulsion depend heavily on the actual wind conditions along the route. For ships not on fixed routes, predicting fuel savings beforehand is challenging and relies more on logistical decisions than technical ones. This highlights the importance of estimating actual savings based on experienced weather rather than predictions.

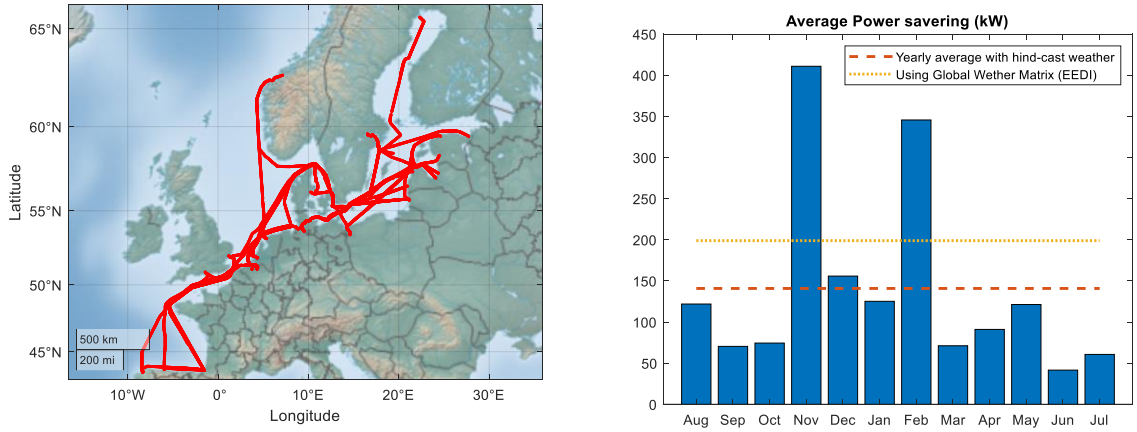

Fig.4: Estimated power saving from wind propulsion based on hind-cast weather (Operation Case 1)

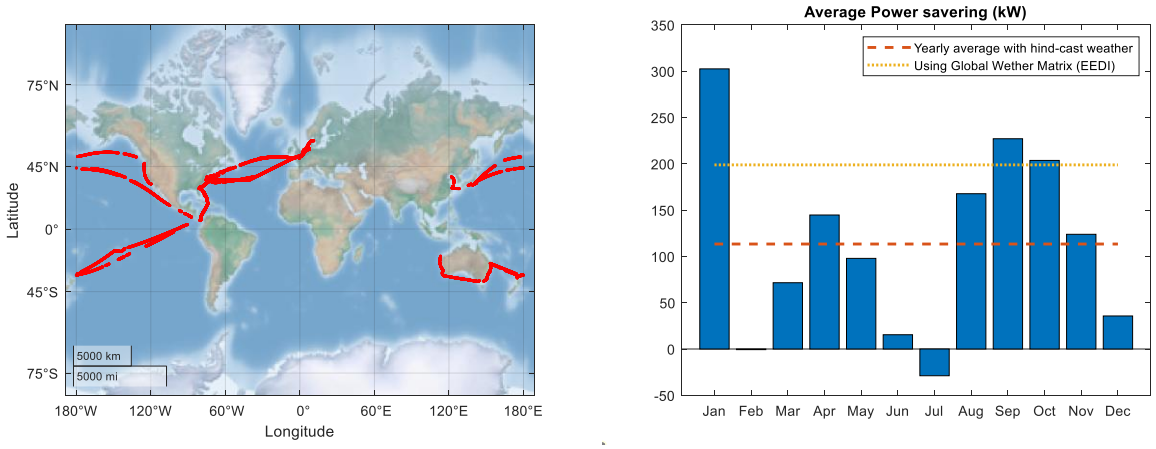

Fig.5: Estimated power saving from wind propulsion based on hind-cast weather (Operation Case 2)

2.2.4. Uncertainties

An uncertainty assessment should be carried out case-by-case. The largest uncertainty sources are the following:

Wind speed. Wind speed is not measured locally on the ship but is obtained from metocean data. Comparing hind-cast wind data with anemometer data from various ships shows that local wind may deviate from hind-cast data, but these differences average out over time. However, in the context of wind propulsion, it is important to remember that the thrust from the sails is proportional to the square of the wind speed. While the average wind speed may be accurate, the squared value may not be. For example, if the wind speed encountered on route in reality deviates by ±10% from the metocean data but the mean is correct, the bias error on the squared wind speed is +1%. This means the thrust force

from the wind propulsion device will be overestimated by 1%, if it is computed using the wind in each time step. This known effect can be compensated for.

Wind direction. Similar to wind speed, the wind direction from metocean has been found to match the local wind measured onboard ships *on average*. Within a ±10° range, the wind propulsion thrust is nearly linear with respect to the wind direction. Therefore, if the average wind direction is accurate, any errors caused by local deviations are likely to cancel out over time.

Performance model incorrect. If the Power Saving Matrix is inaccurate, the estimated fuel savings will also be inaccurate. The Power Saving Matrix is verified through on-off tests conducted during a limited sea trial period. The uncertainty of the sea trial campaign must be assessed on a case-by-case basis. This uncertainty depends on various factors, including the measurement equipment, the presence of currents in the sea trial area, and, most importantly, the range of tested wind speeds and directions, ship speeds and drafts.

Wind propulsion system degradation. Since the Power Saving Matrix is only verified once, the method will not capture degradations of the wind propulsion system or malfunctioning sensors. The uncertainty of this effect is difficult to estimate. Parties concerned about this issue can request additional sea trial verifications at regular intervals.

Drift of total propulsive efficiency η_D. The power saving is approximately proportional to the wind propulsive thrust times ship speed divided by η_D. If η_D changes with time due to fouling, this will affect the amount of power saving that the wind propulsion system generates for the same thrust. Again, the uncertainty of this effect is difficult to estimate. Parties concerned about this issue can request additional sea trial verifications at regular intervals.

2.3. Assessment method based on force logging (level I)

2.3.1. Process

Several providers of wind propulsion solutions now include equipment for measuring the forces generated by their devices. This is a relatively new development area, and there is still limited published information on the accuracy and reliability of these measurements. Nevertheless, this is a clear trend, and we can expect to see more of this in the coming years.

A challenge in using force measurements is that the wind propulsion thrust must be converted to propulsion power savings. The main factors affecting this conversion are the ship's propulsive efficiency (η_D) and the wind propulsion side force, which generates added resistance due to drift and increased rudder angles. Additionally, the wind propulsion device may alter the vessel's aerodynamic drag, resulting in increased or decreased windage. This effect is not well studied yet, but the authors' experience so far suggests that it is secondary. However, more research is needed.

As of now, there are no published guidelines on how this conversion should be done. Below is a suggested approach, though it should be noted that it has not yet been validated in real-life trials.

The proposed procedure involves the following four steps:

1. Predict the power saving using a Power Prediction Program simulation (Level III) as described in Section 2.2 above. From the result, derive a Force-to-power-saving conversion table by listing the result in table containing [Ship speed; Sail-Thrust-force; Sail-Side-force; Ship power-saving]
2. Verify the Force-to-power-saving conversion table in real life using a number of on-off tests (using ITTC 7.5-04-01-02) and comparing with the device’s force measurement. Adjust the conversion table if the result does not match.

3. During service, log continuously the following quantities: [Ship speed; Sail-Thrust-force; Sail-Side-force;]. After filtering and averaging over a suitable time step, use the conversion table to convert the measured force to power-saving in kW.
4. Accumulate the derived power-savings over time to give the energy saving.

2.3.2. Case study

The two ships shown in Fig.6 are used to demonstrate the method. Case A has a moderate installation of rotors sails that gives on average around 7% saving. Case B has a relatively powerful installation of wing sails, giving around 40% savings on average. Fig.7 shows the surface representation of the conversion table for one ship speed. This illustrates that the surface is regular and suitable for interpolation.

Fig.6: Test case A and B

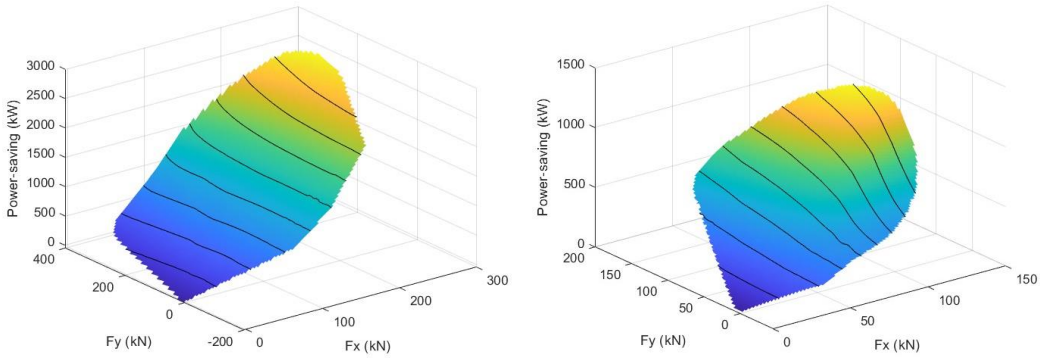

Fig.7: Visualisation of conversion tables for translating wind propulsion thrust force (Fx) and side force (Fy) to power saving. Left for Case A with moderate power saving and right for Case B with substantial power saving from wind propulsion compared to its ship size.

2.3.3. Pro and cons of the method

The primary benefit of continuously logging the wind propulsion device force is that the actual contribution is monitored. This method will detect performance decreases due to malfunctioning sensors, control systems, or other unforeseen degradations over time. However, the disadvantage is the need to install and rely on advanced measurement equipment.

2.3.4. Uncertainties

Just as with the previous method, an uncertainty assessment should be carried case-by-case. The largest uncertainty sources are the following:

Wind propulsion thrust force. The primary source of uncertainty in this method is the thrust force measurement. Currently, there are no publications specifically addressing the accuracy of thrust force measurements. As this is a new technical area, more knowledge is expected to emerge soon.

Wind propulsion side force. The measured side force is used to correct power savings due to added resistance from drift and rudder angles. These are secondary effects, so the accuracy of the side force measurement is not as critical as that of the thrust force. The side force has a minor effect on power savings for ships with small wind propulsion contribution, such as Case A. However, it can have a significant impact on ships with powerful installations or poor yaw balance, like Case B. Whether side force measurements are critical or not can easily be check by comparing results from a PPP in 1DOF and 3DOF.

Ship speed. If the speed log of the actual ship is unreliable, the Speed Over Ground (SOG) can be used. Errors due to currents are likely to even out over time. For small or moderate wind propulsion installations, the relationship between power saving and speed is smooth and well suited for interpolation. Scatter in speed is likely to even out if the average speed is correct over time. However, for ships affected by side force at low speeds, such as in Case B, accurate ship speed measurements are more important.

Conversion table inaccuracy. The conversion table is verified through on-off tests conducted during a limited sea trial period. The uncertainty of the sea trial campaign must be assessed on a case-by-case basis. This uncertainty depends on various factors, including the measurement equipment, the presence of currents in the sea trial area, and, most importantly, the range of tested wind conditions, drafts, and speeds.

Drift of total propulsive efficiency η_D. The η_D is assumed to be constant and assessed through on-off tests during the limited sea trial period when the conversion table is verified. As was discussed earlier in section 2.2.4, the change of η_D over time is not known in general. This could be arranged by using a propeller thrust sensor (leading to method Force logging II mentioned in Fig.1)

4. Conclusions

This paper discusses the continuous assessment of power savings from wind propulsion technologies, which is essential for ship owners to monitor the returns on their investments and for cost-sharing arrangements between owners and charterers.

Two methods for assessing power savings from wind propulsion during service are examined. The first method utilizes hind-cast wind data combined with a performance model. By confirming the performance model through a limited sea trial period conducted by a third party, the risk of contractual disputes between stakeholders during service is minimized. This method is robust and cost-effective but involves some approximations.

The second method involves force measurements on the wind propulsion devices, requiring the conversion of force to power saving or fuel savings. This method captures performance changes over time but also relies on some modelling, which needs to be confirmed through on-off tests during a limited sea trial period.

Delivering these solutions to the shipping companies requires collaboration between several actors: wind propulsion makers to deliver the equipment, performance monitoring and hind-cast weather providers to acquires and post-process logs and wind data, and 3rd party institutes to calculate and verify the performance models.

The development of wind propulsion technologies is new and rapidly evolving. More research is needed on the uncertainties of sea trial methods and the accuracy of force measurements.

Acknowledgement

This work received funds from the European Union's Horizon Europe Research and Innovation programme under grant no. 101096673, ORCELLE.

References

IMO (2021), *MEPC.1-Circ.896, Guidance on treatment of innovative energy efficiency technologies for calculation and verification of the attained EEDI and EEXI,* Int. Mar. Org., London

WERNER, S.; NISBET, J.; OLSSON, F. (2022), *Sea Trial Methodology for Wind Assisted Ships, 7th* HullPIC Conf., Tullamore, pp. 17, http://data.hullpic.info/HullPIC2022_Tullamore.pdf

A Family of Performance-oriented Digital Twins for Maritime Efficiency

Christos Gkerekos, Tom Melamed, Konstantinos Anastasiou, Giovanni Bignardi, Max Cole, Nicola Dotti, Anton Hawthorne, Volodymyr Rospotniuk, Ninety Percent of Everything (90POE), London/UK, christos.gkerekos@90poe.io

Abstract

Within 90POE's OpenOcean STUDIO maritime platform, we use three core models for performance monitoring and optimisation: digital twins for vessel propulsion, performance degradation modelling, and speed-fuel consumption curves under good weather conditions. In this paper, we discuss each model and the advantages of employing multiple distinct models to address our clients' needs. The challenges inherent in validating such models are explored, along with the novel quantitative and qualitative methods developed to ensure their reliability. Case studies are presented to illustrate the practical benefits of these approaches, followed by an examination of challenges encountered during their implementation and a discussion of future directions for research and development in vessel performance monitoring.

1. Introduction

In today's maritime industry, optimising vessel performance is critical for both efficiency and sustainability. This is driven by fluctuating oil prices, stringent emissions regulations, and the introduction of emission trading schemes. By leveraging the increasing availability of large datasets, advancements in cutting-edge machine learning techniques, and greater computing power, the industry can better understand, predict, and optimise vessel performance to reduce operating costs and emissions. This includes predicting vessel degradation, scheduling maintenance, and improving carbon trading positions, ultimately leading to a more efficient and sustainable maritime sector.

Optimising vessel performance offers numerous benefits, including lower operational expenditures (OPEX) and higher profitability. Additionally, it reduces the environmental impact of sailing and mitigates the societal impact of maritime cargo operations.

At 90POE, we have developed OpenOcean STUDIO, a next-generation maritime software platform designed to accelerate the industry's journey toward a more efficient, competitive, and sustainable future. Central to this mission is the deployment of accurate and trustworthy data-driven models that underpin vessel performance optimisation services. Through extensive research and development, we have created advanced digital models that include digital twins for vessel propulsion systems, performance degradation modelling to account for factors like hull fouling and engine wear, and speed-fuel consumption curves calibrated for good weather conditions.

These models allow for the precise analysis and optimisation of propulsive efficiency, enabling proactive maintenance strategies and performance management, as well as crucial insights for voyage planning and fuel optimisation. Seamlessly integrated within OpenOcean STUDIO, the digital models provide the foundation for a suite of tools within the platform that enable customers to make data-driven decisions to improve operational efficiency, enhance competitiveness in the market, and contribute to a more sustainable maritime ecosystem.

In this paper, we will provide an overview of these data-driven models and expand on the working principles of each. We will then elaborate on typical use cases, discussing the strengths and shortcomings of each model. Furthermore, we will present case studies where different models are utilised to predict and/or evaluate using the same underlying historical ship data, highlighting the differences in results and discussing their practical implications in terms of reducing emissions, improving chartering, and optimising maintenance activities.

2. Background

This section provides an overview of the scientific literature pertinent to this paper. First, methodologies relevant to digital twins for predicting power and fuel consumption will be reviewed. Following that, the topic of hull and propeller fouling will be examined, along with the various performance degradation digital twin approaches currently implemented in different settings. Finally, the above findings will be summarised to identify the current trends and gaps, and explain the motivation for the family of digital twins we have developed.

Coraddu et al. (2017) conducted a study comparing white, grey, and black box models to estimate the fuel oil consumption of a Handymax chemical/product tanker. White box models rely on physical process knowledge, while black box models use statistical methods and historical data. They found that grey box models, which combine both approaches, are particularly effective at forecasting fuel oil consumption, even with limited historical data. *Cai et al. (2024)* support this statement, noting that grey box models can achieve higher accuracy using less data than black box approaches. Similarly, *Ma et al. (2023)* performed a similar comparison to conclude that combining grey-box modelling with the SHAP (SHapley Additive exPlanations) framework allows the identification of the most influencing inputs to the model.

Additionally, *Gkerekos et al. (2019), Chen et al. (2024)* investigated black box models and concluded that, given enough data, they can be effective predictors of a vessel's fuel consumption. Similarly, *Jiang et al. (2025)* and *Salazar et al. (2024)* present cutting-edge black box approaches that improve model accuracy in vessel performance modelling applications.

In terms of vessel degradation, *Themelis et al. (2024)* trained tree-based models to predict fuel consumption, including a days-since-drydocking feature allowing them to capture the effect of biofouling on vessel performance. In an earlier approach, *Coraddu et al. (2019)* used unsupervised machine learning models based on Support Vector Machines and k-nearest neighbour algorithms to diagnose hull and propeller fouling conditions, noting that this approach does not require labelled training data. *Huang et al. (2024)* combined a Genetic Algorithm (GA) with Long Short-Term Memory (LSTM) networks to combine the temporal benefits of LSTM networks with physics-informed feature engineering based on the GA.

From the above, it is evident that there is significant research interest in the field of digital twins for predicting power and fuel consumption. The variety of approaches, ranging from white, grey, and black box models to cutting-edge machine learning techniques, underscores the complexity and importance of this research area. This diversity not only makes it a compelling research question but also highlights its critical relevance to consumers and industry stakeholders. Accurate predictions of fuel consumption and vessel performance can lead to substantial cost savings, improved operational efficiency, and reduced environmental impact, making this an essential focus area for the future of maritime operations. These motivations have driven 90POE to develop a family of performance-oriented digital twins that can accurately influence performance-related decision-making at all levels.

3. Methodology

This section outlines the suite of performance-oriented digital twins developed and utilised at 90POE. We will detail their distinct inputs and outputs, highlighting their unique advantages and limitations. This approach will demonstrate the necessity of maintaining a diverse set of digital twins rather than relying on a single, generalised model. At 90POE, we have created specialised digital twins for three key purposes: quasi-physical digital twins for vessel propulsion modelling, models for accurately tracking performance degradation (including hull and propeller fouling) over time, and speed-fuel curves under good weather conditions. Each of these models will be examined in the following sections, illustrating their individual contributions and the overall benefit of employing a comprehensive array of digital twins to enhance maritime efficiency, competitiveness, and sustainability.

3.1. Vessel Propulsion Digital Twins

The aim of the Vessel Propulsion Digital Twins (VPDTs) is to predict power, fuel consumption and engine RPM given a vessel's speed, draft and the ambient sailing conditions. This is achieved by combining a physical propulsion model with knowledge mined from historical sailing data of that vessel.

Combining a physics-first model with historical observations reduces the requisite data points and the corresponding collection window, allowing for better and more localised propulsion models. Moreover, unlike a black-box model, being bounded by a physical model ensures the model remains physically reasonable outside of the areas covered by training data while also increasing model explainability. At the same time, the use of historical observations allows us to build models tailored to specific vessels with accuracy beyond what would be achievable by a traditional first-principles model and without having to resort to full hydrodynamic modelling.

The VPDT model has distinct, physics-first components that capture a vessel's calm water, wind, and wave resistance. These components have weights that depend on a vessel's principal particulars. Furthermore, they also have weights that are learnt or fine-tuned through machine learning, based on the vessel's historical data points.

3.2. Performance Degradation Digital Twins

The aim of the Performance Degradation Digital Twins (PDDTs) is to assess the day-to-day performance and performance degradation of vessels, leveraging the quasi-physical modelling of the VPDT. Using the well-tested, well-explainable VPDT as the backbone of PDDT allows us to retain more data and increase responsivity and historic coverage compared to developing a new, greenfield offering.

As the direct output of the PDDT and its residuals have some inherent noise due to noise in its inputs (e.g. weather hindcast errors, GPS noise, temporary measurement issues) it is too noisy to provide actionable information. For this reason, a Kalman filter layer has been implemented to smooth the noise and provide more trustworthy results.

At a high level, PDDT translates VPDT residuals into a vessel performance indicator. This, of course, means that residuals become a measure of the impact of unknown factors, that cannot be decoupled. A variation in model residuals could be ascribed to several reasons, inter alia: long-term hull/propeller degradation, short-term hull/propeller degradation (e.g. due to prolonged port stays in warm water), temporary vessel issues (e.g. propeller catching fishnets), or unflagged and unfiltered sensor issues.

3.3. Speed-Fuel Curves

The purpose of the Speed Fuel Curves (SFCs) is to address a question similar to that of the combined Vessel Propulsion Digital Twin (VPDT) and Performance Degradation Digital Twin (PDDT) models: determining the amount of fuel a vessel would consume at a given draft and speed. However, unlike the VPDT and PDDT models, which require precise output values, the SFCs aim to provide a reliable "ballpark" estimate under the assumption of good (Beaufort Scale less or equal to 4, Douglas Sea State less or equal to 3) weather conditions. This approach can be based on noon report data corresponding to short data collection windows, allowing for easier adoption. If high-frequency data are available, input data can be cross-checked for accuracy. The data are used to shape a 3D physics-informed surface that links draft, speed, and power/fuel/RPM. Meanwhile, the model's straight-forward nature ensures extensive explainability.

The motivation for this model is to increase the accuracy of charter pricing, enabling ship managers to make data-informed decisions regarding the optimal vessel selection for specific tasks, and to evaluate vessel performance through time snapshots.

3.4. Maritime Efficiency - The Sum is Greater than the Parts

Starting from the same dataset, the information can be presented in three distinct ways to tell different stories. First, it can illustrate the average vessel performance, ignoring the effects of fouling, based on a comprehensive list of inputs. This provides a baseline understanding of how the vessel operates under ideal conditions. Second, the data can highlight the percentage increase in power required from the baseline due to fouling, offering insights into the impact of hull and propeller degradation over time. These two can be combined to create a highly accurate vessel performance digital twin with a strong temporal element. Third, it can show the vessel's current performance over a 6-12 month window in good weather conditions, giving a snapshot of its operational efficiency in recent times.

When combined, these perspectives offer a holistic view of the vessel's power and fuel consumption, the effects of hull and propeller degradation, and fouling impacts. This comprehensive analysis not only aids in understanding the vessel's current state but also provides valuable chartering estimates for the short-term future. By integrating these different aspects, ship managers can make more informed decisions regarding maintenance, operations, and chartering, ultimately enhancing the vessel's performance and profitability.

3.5. Validation

Even for physics-informed models, there is a risk of overfitting to the training data or becoming inaccurate or biased due to sensor issues. To mitigate these risks, we utilise virtual sensors based on different data sources to correct, if possible, or discard readings flagged as unreliable. Additionally, we have built a suite of physicality validation tools designed to stress-test our models and ensure that the results adhere to physical first principles across a wide range of scenarios.

We also perform cross-testing across different voyages to avoid training and testing on the same voyage, ensuring robust model validation. In cases of performance degradation, we use noon report fuel consumption data to validate the overall performance history. Furthermore, extreme cases are flagged for further investigation, suspecting sensor issues.

For speed-fuel curves, we have developed a bespoke validation system that considers both high- and low-frequency observations to ensure our predictions remain accurate. This system helps us maintain the reliability of our models by serving only high-confidence areas within the 3D draft, speed and power/fuel/RPM space.

4. Application Description

In this case study, we select a Cape size vessel and apply our three distinct digital twin models using the same pool of input data points. By leveraging the Vessel Propulsion Digital Twins (VPDTs), Performance Degradation Digital Twins (PDDTs), and Speed-Fuel Curves (SFCs), we aim to demonstrate how different perspectives can tell unique stories about vessel performance.

We begin by providing a general description of the vessel and an overview of the input dataset. Following this, we delve deeper into the methodology discussed earlier, elaborating on how each of these models was specifically applied in this case study. This approach will highlight the practical application of our models and underscore the importance of using a diverse set of digital twins to capture the multifaceted nature of vessel performance.

4.1. Vessel Description & Dataset EDA

A Cape size vessel has been selected for this case study; however, due to confidentiality constraints, its exact details and principal particulars cannot be shared. Instead, typical principal particular ranges for Cape size bulk carriers are provided: length between perpendiculars of about 290 m, design speed of 13 to 15 knots, breadth of around 45 m, draft of around 18 m, and a depth of around 24 m.

The data sources used include noon reports, Automatic Identification System (AIS) data, weather hindcasts, and high-frequency (HF) data collected at minute intervals and averaged into 10-minute windows before analysis. To ensure the accuracy of our analysis, we filter out data during periods of manoeuvring and slow steaming. Additionally, we validate and cross-check data from multiple sources to correct any discrepancies when possible and exclude any unreliable readings.

In total, this case study utilises approximately 6.5 years of data, spanning from about 2 years prior to the vessel's last dry docking to roughly 4.5 years afterward.

4.2 Model Training

In this case study, the VPDTs were trained using one year of data, specifically the most recent 12 months of the available dataset. Speed-fuel curves are trained in rolling 6- and 12-month windows to balance the trade-off between accuracy and responsiveness to changes. For clarity, only the curves based on 12-month windows are displayed to reduce graph clutter. Finally, the PDDTs use the same underlying model as the VPDT, meaning the most recent 12 months of data serve as the performance baseline, aligning with VPDT predictions.

4.3 Model evaluation

For model evaluation, we adopted the symmetric mean absolute percentage error (SMAPE) due to its balanced treatment of forecast errors and robustness to edge cases. Unlike traditional MAPE, which becomes unstable with near-zero actual values, SMAPE normalises absolute errors by the average of actual and forecasted values. This ensures symmetry between over- and under-predictions and bounds errors within a 0–200% range, preventing skewed results from small denominators. SMAPE is defined as:

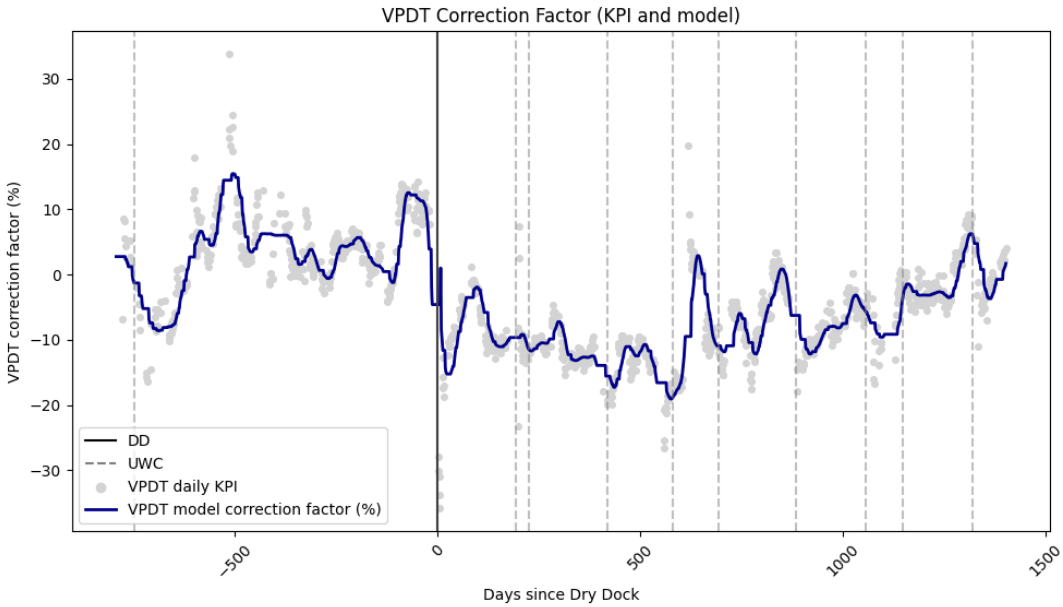

Fig.1: Vessel performance degradation as captured by our Performance Degradation Digital Twin (PDDT). Dry-Dockings (DDs) are marked with solid black vertical lines, and Under-Water Cleaning (UWC) events with dashed grey vertical lines.

$$\text{SMAPE} = \frac{100}{n}\sum_{t=1}^{n}\frac{|F_t - A_t|}{(|F_t| + |A_t|)/2}$$

where n is the number of points available, A_t is the actual value observed and F_t is the value predicted by the model.

SMAPE's key advantage lies in its equitable assessment of prediction deviations: errors of equal magnitude receive identical penalties regardless of direction. This symmetry avoids biases inherent in MAPE, which disproportionately penalises under-predictions when actual values are small. Additionally, the bounded error scale enables consistent cross-model and cross-dataset comparisons, even with volatile baselines, while maintaining sensitivity to meaningful deviations.

5. Application Results & Discussion

Having trained the models as described in Section 4.2 above, the results obtained can be evaluated, both independently and in relation to one another.

Starting with the PDDT, Fig.1 displays the estimated percent power increase due to vessel performance degradation through time, with cleaning events superimposed on the graph. The daily KPI (grey dots) can still be noisy, as described in 3.2. However, the final power increase curve tracks degradation events well, with a minimal amount of noise present, mostly due to weather hindcast and sensor inaccuracies as well as ambient conditions and fuel variations. In the plot, the curve is shown with a 7-day delay: this is the typical delay we use to back test the corrected model performance in hindsight without introducing look-ahead bias in the metrics.

Fig.2 and Fig.3 both focus on the performance of the VPDT, with and without the PDDT contributing performance degradation multipliers. More specifically, Fig.2 shows a SMAPE time series achieved first by the VPDT and then by the combination of VPDT and PDDT. As with the PDDT graph above, a 7-day lag has been applied to the PDDT forecasts. As expected, the SMAPE of the pure VPDT, which was trained on the last year of sailing data, fluctuates significantly over the 5.5 years of the timeline shown, with lower SMAPEs observed towards the end of the time series as that was the training window. Similarly, the two years before the DD exhibit relatively low errors, indicating vessel performance similar to the training window. Unsurprisingly, a high SMAPE is observed during the first two years post-DD as the vessel performance changes significantly during that period. Over the entire period presented, the VPDT model achieved a mean SMAPE of 7.07% and a median SMAPE of 6.50%.

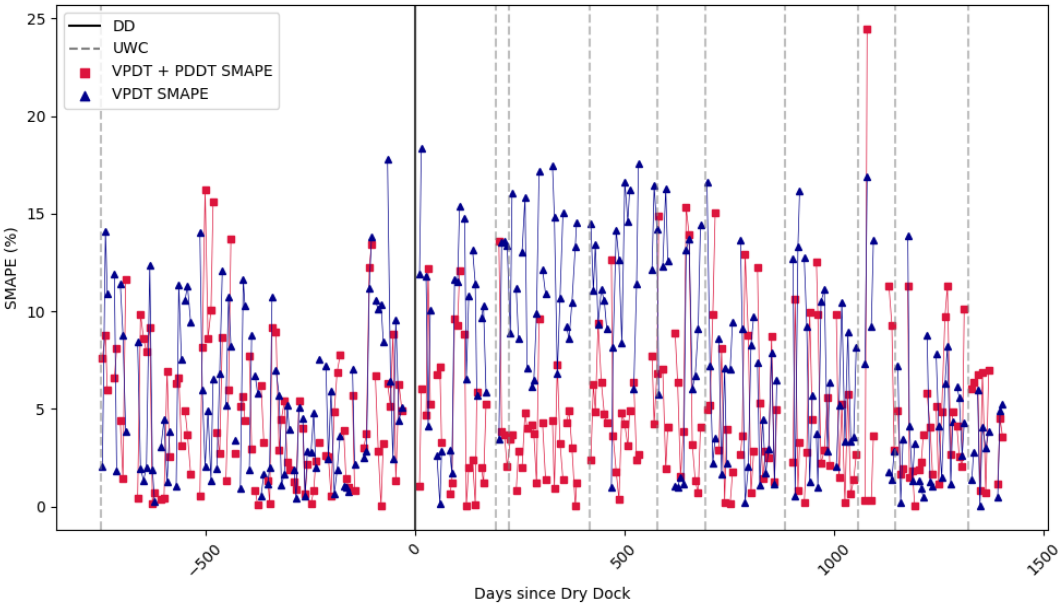

Fig.2: Symmetric Mean Absolute Percentage Errors (SMAPEs) achieved by our Vessel Performance Digital Twin (VPDT) with and without the inclusion of the Performance Degradation Digital Twin (PDDT). Dry-Dockings (DDs) are marked with solid black vertical lines, and Under-Water Cleaning (UWC) events with dashed grey vertical lines.

In the case of the combined VPDT and PDDT, the SMAPEs observed are both lower and evenly distributed, as there is no significant time-dependent variation in the errors. In this case, the combined models achieved a mean SMAPE of 4.77% and a median SMAPE of 3.92%.

A handful of higher-than-usual errors can be observed in both the VPDT and the combined VPDT and PDDT models. These can be attributed to weather hindcast anomalies and other localised sensor issues.

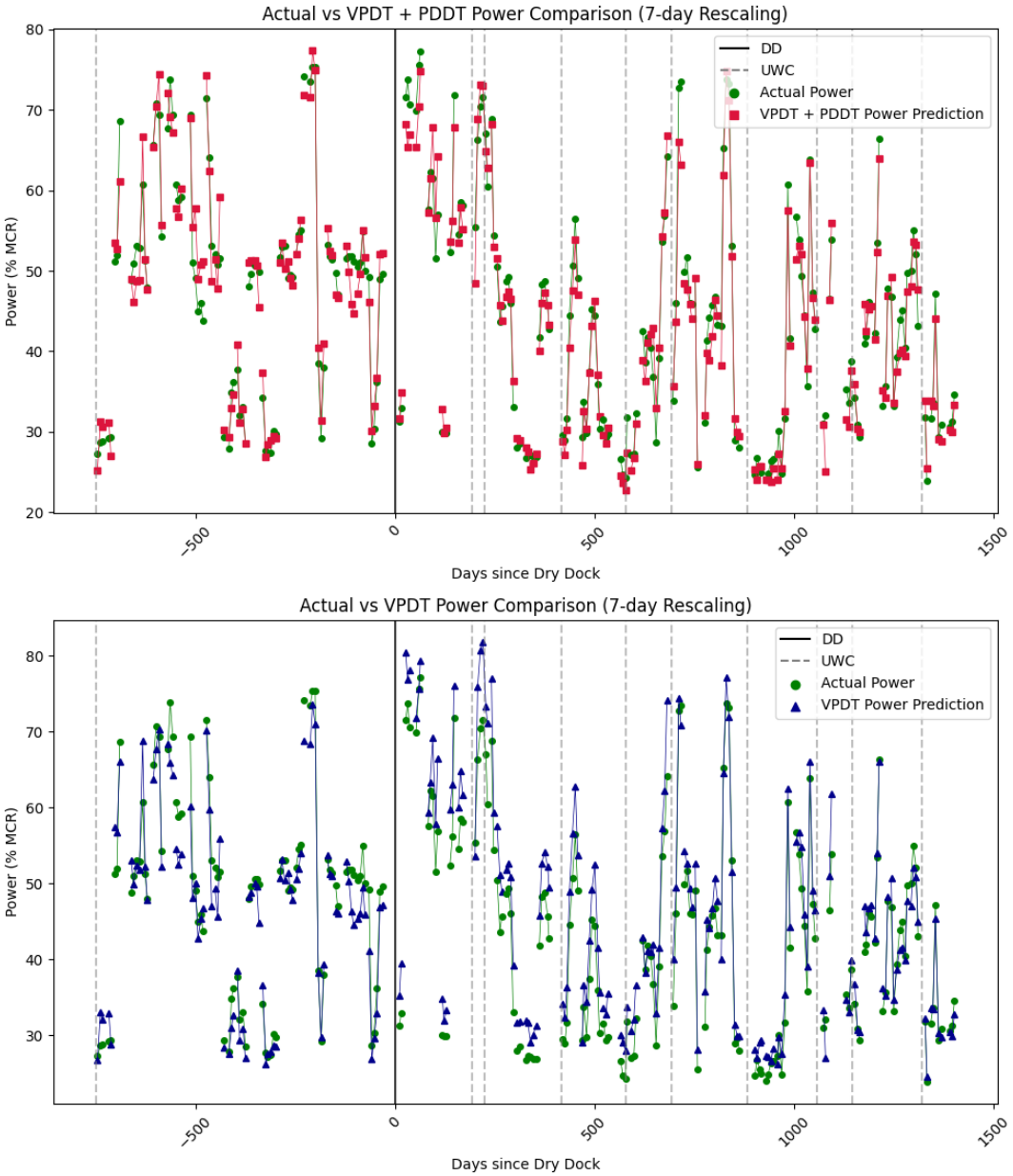

Fig.3: Comparison between Actual and Vessel Performance Digital Twin (VPDT)-predicted powers through time with (top) and without (bottom) the inclusion of Performance Degradation Digital Twin (PDDT). Dry-Dockings (DDs) are marked with solid black vertical lines, and Under-Water Cleaning (UWC) events with dashed grey vertical lines.

The results above are corroborated by those presented in the graph of Fig.3. This graph presents the same time series as above, but instead of comparing the SMAPEs, it compares the actual powers to the power predictions, first of the combined VPDT and PDDT model and then for the VPDT model on its own. To maintain vessel anonymity and facilitate results comparison, the y-axis is expressed in terms of % MCR instead of traditional power units. In the case of the pure VPDT model, as expected,

a power overestimation can be observed in the time window that follows the DD. This is, again, justifiable by the model being trained on the last year of data, i.e., a heavily degraded vessel condition. In the case of the combined VPDT and PDDT, the errors are significantly smaller and without any noticeable bias.

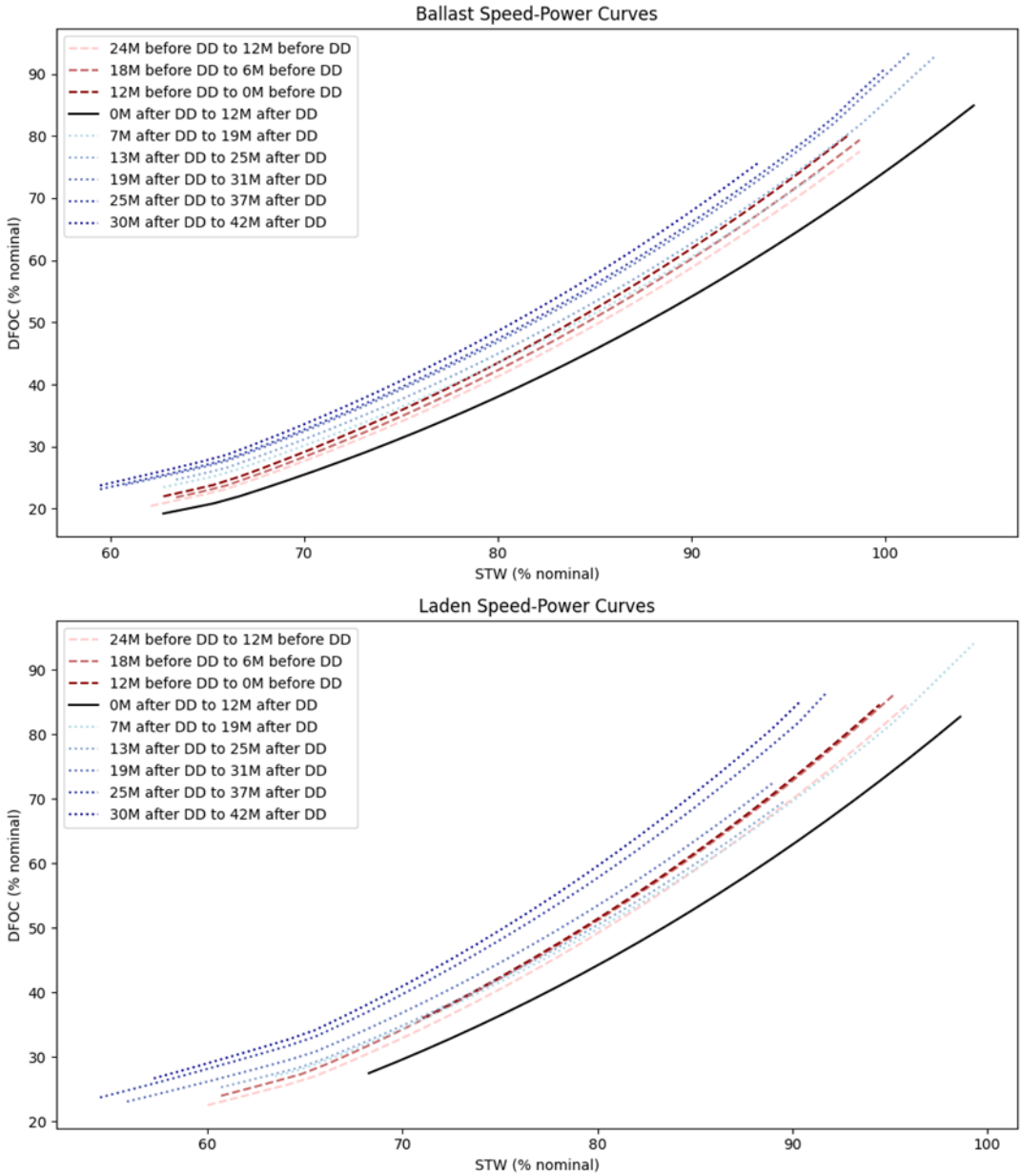

Fig.4: Comparison between speed-fuel curves corresponding to different time windows pre- and post-DD. The solid black lines represent data from a 12-month window immediately following the dry docking (DD), while the dotted blue lines show later curves, and the red hues indicate curves from periods before the DD. Lighter hues denote earlier time windows.

Finally, Fig.4 illustrates the speed-fuel curves' progression over time, with the vessel's two principal load conditions shown separately in the sub-plots. The solid black lines represent data from a 12-month window immediately following the dry docking (DD), while the dotted blue lines show later curves, and the red hues indicate curves from periods before the DD. Lighter hues denote earlier time windows. To maintain vessel anonymity and facilitate comparisons between the two conditions, both

the x and y axes have been normalised against a nominal sea-trial data point. Additionally, the x-axis span of different curves varies depending on the operational profile followed by the vessel during the given time window.

As expected, the speed-fuel curve for the period immediately after the DD shows the lowest Daily Fuel Oil Consumption (DFOC) in both load conditions. A gradual increase in DFOC can be observed in the windows before and after the DD for both load conditions. The current vessel DFOC is higher compared to the last windows before the previous DD, indicating that another DD would be highly beneficial at this point. Furthermore, the fact that the post-DD speed-fuel curves quickly reached and then exceeded the pre-DD DFOC could provide actionable feedback to ship managers regarding the quality of paint chosen, assuming other factors (e.g., long port stays) can be ruled out.

Comparing the vessel performance in Fig.4 to that in Fig.1, we observe similar trendlines with one notable exception. In Fig.1, the vessel maintains comparable performance conditions at both the beginning and end of the timeline. However, for the SFCs produced, the vessel shows more significant degradation towards the end of the timeline. This difference arises because PDDT operates in power-space, while SFCs function in fuel service. Once measurement issues are excluded, this observation can help identify potential engine degradation.

6. Conclusions

This study has demonstrated the effectiveness of using a suite of performance-oriented digital twins to optimise vessel performance. By leveraging the Vessel Propulsion Digital Twins (VPDTs), Performance Degradation Digital Twins (PDDTs), and Speed-Fuel Curves (SFCs), we have shown that different models can provide unique insights into vessel performance, each contributing to a comprehensive understanding of the vessel's operational efficiency.

The results highlight the importance of explainability in Machine Learning models, which we achieve through rigorous validation and sensitivity analysis. This ensures that our models remain trustworthy and reliable, even when applied to complex real-world scenarios. The use of multiple specialised models, rather than a single generalised model, allows us to maintain high accuracy and reliability, addressing specific aspects of vessel performance without compromising the integrity of the overall analysis.

These models are crucial for making informed decisions about vessel maintenance, such as determining the optimal timing for hull and propeller cleaning to maintain efficiency. Additionally, they can be used for route optimisation, ensuring that vessels operate under the most favourable conditions to save fuel and reduce emissions. The Speed-Fuel Curves (SFCs) also play a vital role in charter party agreements by providing accurate estimates of fuel consumption under various conditions, aiding in better contract negotiations and operational planning.

Looking ahead, there are several exciting areas for future research. One key area is improving sensor reliability and developing methods to trust and validate sensor data. Additionally, leveraging our extensive dataset to create typical models for vessels based on their principal particulars could further enhance the accuracy and applicability of our digital twins. These advancements will continue to drive the maritime industry towards a more efficient, competitive, and sustainable future.

In conclusion, the integration of advanced Machine Learning models in maritime operations is not just a glimpse into the future but a necessary step towards achieving significant operational improvements. By continuously refining our models and exploring new research avenues, we can ensure that the maritime industry remains at the forefront of technological innovation.

Acknowledgements

The authors would like to thank the client/shipping company, which shall remain unnamed for confidentiality reasons, for providing the data used in this paper. We also extend our gratitude to our colleagues at 90POE for their support and collaboration. Special thanks go to the members of the data science team for their dedication and hard work in making this research possible.

References

CAI, Z.; LI, L.; YU, L.; LI, C.; SUN, M. (2024), *Diversity, quality, and quantity of real ship data on the black-box and gray-box prediction models of ship fuel consumption*, Ocean Eng. 291

CORADDU, A.; ONETO, L.; BALDI, F.; ANGUITA, D. (2017), *Vessels fuel consumption forecast and trim optimisation: A data analytics perspective*, Ocean Eng. 130, pp.351-370

CORADDU, A.; LIM, S.; ONETO, L.; PAZOUKI, K.; NORMAN, R.; MURPHY, A.J. (2019), *A novelty detection approach to diagnosing hull and propeller fouling*, Ocean Eng. 176, pp.65-73

CHEN, Y.; HUANG, Z.; FENG, L. (2024), *Research on Ship Main Engine Fuel Consumption Model with Data Integration and Noise Cleaning*, IEEE Access 12, pp 154546-154569

GKEREKOS, C.; LAZAKIS, I.; THEOTOKATOS, G. (2019), *Machine learning models for predicting ship main engine Fuel Oil Consumption: A comparative study*, Ocean Eng. 188

HUANG, G.; LIU, Y.; XIN, J.; BAO, T. (2024), *Assessment of Hull and Propeller Performance Degradation Based on TSO-GA-LSTM*, J. Marine Science and Eng. 12(8)

JIANG, X., DAI, Y.; LI, S.; MA, R.; DU, T.; ZOU, Y.; ZHANG, P.; ZHANG, Y.; SUN, P. (2025), *Research on ship speed prediction based on time series imaging and deep convolutional network fusion method*, Applied Ocean Research 154

MA, Y.; ZHAO, Y.; YU, J.; ZHOU, J.; KUANG, H. (2023) *An Interpretable Gray Box Model for Ship Fuel Consumption Prediction Based on the SHAP Framework*, J. Marine Science and Eng. 11(5)

SALAZAR, A.A.; SALAMEH, G.; CHESSE, P.; BULOT, N.; THEVENOUX, Y. (2024), *Improving Fuel Consumption Prediction for Marine Diesel Engines Using Hierarchical Neural Networks and Pulsating Exhaust Models*, Energies 18

THEMELIS, N.; NIKOLAIDIS, G.; ZAGKAS, V. (2024), *Assessment of Hull and Propeller Degradation Due to Biofouling Using Tree-Based Models*, Applied Sciences 14(20)

Accurate Analysis of the Effect of Propeller Cleaning using the Newly Established Vessel Technical Index

Gunnar Prytz, Miros, Asker/Norway, gp@miros-group.com
Alfredo Carella, Miros, Asker/Norway, ac@miros-group.com
Vemund Svanes Bertelsen, Miros, Asker/Norway, vsb@miros-group.com
Michael Schmidt, Copenhagen Commercial Platform, Copenhagen/Denmark, mhs@ccp-platform.com

Abstract

Ship owners, operators, charterers, suppliers and regulators share a profound interest in reducing fossil fuel consumption and associated emissions. The fuel consumption of a vessel is closely linked to numerous technical, operational and weather-related factors. The actual performance of a vessel in a given situation is highly dependent on the technical state of the vessel and the effect of the weather. Traditionally, vessel performance analyses have been tainted with large uncertainties. However, today it is possible to get high-frequency, high-quality weather data and this enables new levels of insight into how vessels perform in real-time. Additionally, the recently published Vessel Technical Index (VTI) recommended practice offers an accurate and transparent method for measuring, evaluating, and verifying the technical performance of ships in service. This paper investigates the effect of propeller cleaning events by utilizing accurate speed through water and sea state data as input into a VTI analysis. With this solution, performance improvements down to a few percent could be accurately identified within just a day of sailing after the cleaning. Furthermore, the implications of this approach in analyzing the effectiveness of energy saving devices are also discussed.

1. Introduction

Vessel performance is a critical aspect of maritime operations, directly influencing resource usage, operational efficiency, environmental impact and overall operational costs. With increasing pressure on the maritime industry to optimize fuel consumption, reduce emissions, and improve profitability, understanding and managing vessel performance has become more important than ever. Accurate data is at the heart of these efforts, enabling operators to make informed decisions that enhance vessel operations and ensure compliance with environmental regulations.

Reliable data on parameters such as speed, fuel consumption and sea state is essential for accurate performance assessment and optimization. However, the challenge lies not only in the collection of such data but also in its interpretation and application. Inaccurate or incomplete data can lead to misguided decisions, resulting in inefficiencies, higher costs, and potential regulatory non-compliance. Therefore, maintaining the integrity and precision of performance data is a fundamental requirement for improving the sustainability and competitiveness of the maritime industry.

IMO has introduced a vessel design efficiency index (EEDI/EEXI) and an operational index (CII). The EEDI/EEXI addresses the vessel efficiency when the vessel was delivered from yard, but the EEDI/EEXI only vaguely indicate the efficiency of a vessel in operation, which can be influenced by hull and propeller deterioration, fouling and retrofit of energy saving devices. The CII is an operational index, which is mainly determined by vessel loading, operational speed, duration of port stays, weather etc. The CII is influenced by the technical efficiency of the vessel, but operational decisions are overshadowing the technical efficiency of the vessel.

DNV (2023) published a Recommended Practice (RP) proposing a Vessel Technical Index (VTI) as a complementary measure. The VTI is pinpointing the technical performance of a ship relative to a reference baseline, e.g. the newbuilt state, thereby eliminating the influence of external operational factors such as the weather and the loading condition. In addition, the VTI RP includes a novel approach for assessing the relevant sources of uncertainty, enabling the users to take informed decisions based on the VTI calculations.

The VTI approach is centered around investigating how the propulsion power of the vessel is transferred to a set of consumers. While the propulsion power is moving the vessel, a significant amount of shaft power may also be lost in countering the effects of the waves in situations with bad weather. The amount of power lost to waves depends on wave height, direction and period. In situations with several wave systems present, each wave component will result in a certain amount of power lost to waves. In some situations, there can even be a positive effect from the waves, e.g. the waves contribute positively to the forward motion of the vessel.

The situation is similar for wind, which can have a considerable impact on the forward motion of a vessel. The effect varies with the wind magnitude and direction. The wind power can be both negative and positive, as is obvious for sailing vessels. For vessels with wind assisted propulsion (WASP) the effects of the wind can be very significant. For such vessels, a VTI analysis can reveal crucial information about the efficiency of the WASP technology in various operational scenarios. Such work is currently ongoing but is beyond the scope of this paper.

The depth of the water also influences the amount of power required to move a vessel forward. In areas with low depth (up to 5-10 times the mean draft of the vessel), more power is required to move the vessel forward than in deep water areas. Furthermore, the ocean water temperature and salinity influence how much power is needed to maintain a certain speed through the water.

In addition to the above, power can be lost by vessel navigation, i.e. when the vessel changes speed or course. Changing the trim state (i.e. the difference between forward and aft draft) may also influence the vessel and the amount of power required to propel the vessel forward.

There is a need to subtract the influences of the environment and vessel navigation in order to arrive at the actual, technical vessel performance. The removal of weather effects is normally referred to as weather normalization, and a specific approach is defined in the DNV RP. Similarly, the normalization procedure for the effects of water temperature and water salinity is also described in this document.

Similarly, navigational effects can be removed by removing time periods where the vessel is changing speed or course. Due to the inherent time lag in such a system, there might be a need to also remove a certain time period (e.g. 30 minutes) after the change in order to allow the vessel speed to settle.

A VTI analysis should be accompanied by high-frequency, high-accuracy data to gain the full benefit from the methodology. The following data is required to calculate the VTI:

- Directional wave spectrum (alternatively wave height, period and direction)
- Speed Through Water (STW)
- Speed Over Ground (SOG)
- Vessel heading
- Wind magnitude and direction (corrected to 10 m height above the sea level)
- Water temperature and (if available) salinity
- Water depth
- Shaft power
- Shaft revolutions
- Vessel draft

The VTI analysis can be performed in real-time if a sufficiently advanced vessel performance system is installed, like the Miros VTI service based on real-time, high frequency, accurate data combined with a full implementation of the DNV RP. Alternatively, the VTI can be performed in retrospect.

Some results from using the VTI approach have already been published *Bertelsen (2021), Guo (2021), Bertelsen (2022). Gupta (2023a)* found that the uncertainty in a VTI analysis could be significantly reduced by using accurately measured sea state data as compared to using less accurate data combined

with hindcast data. Similarly, *Bertelsen (2022)* showed a large difference in accuracy between using accurately measured data and relying on hindcast data. *Gupta (2023b)* further analyzed the uncertainty in VTI using Principal Component Analysis (PCA).

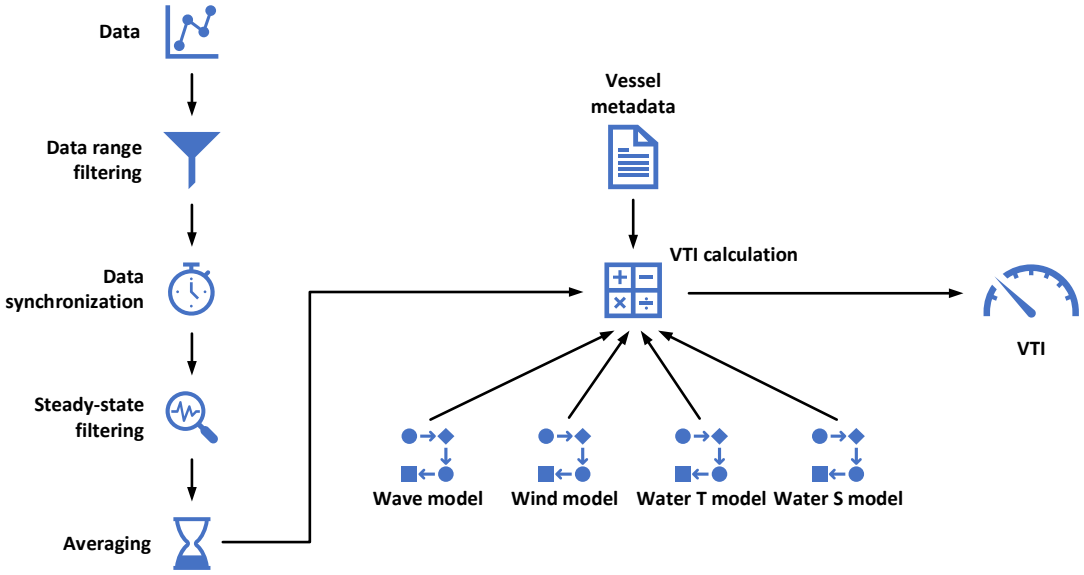

Fig.1: The VTI calculation process

This paper investigates the effect of two propeller cleanings by performing a VTI analysis. The approach combines accurate, high-frequency data on wave, STW and wind with the latest advances in weather normalization methods as described by the DNV RP. In this way, the effect of the propeller cleaning can be isolated from the influence of the weather and other disturbances. In essence, this in practice corresponds to performing a continuous sea trial so that the before and after situations can be quickly compared.

2. Measuring waves, currents and STW based on imaging X-band radar

Radar-based sea state measurements have made significant improvements during the last decade *Gangeskar (2017,2018a,b,c,2019,2021)*. The latest solutions in radar-based sea state measurements can measure both ocean waves, ocean currents and STW accurately under widely varying conditions and with high availability and reliability.

The Miros Wavex solution bases its measurements on radar images covering local areas of interest, in a distance of a couple of hundred meters in front of the vessel. The images are processed using dedicated algorithms to obtain real-time wave spectra, integrated wave parameters, surface current vectors and STW data, *Prytz (2019), Svanes Bertelsen (2020)*.

Specialized DNV type-approved hardware is connected to the analog video signal output from a marine navigation X-band radar to obtain digitized images. Digitized images can also be acquired directly from radars with digital data output (Internet Protocol radars). In addition, Wavex utilizes certain radar image metadata from a GPS and a gyro compass. For further details on the basic components of a Wavex system on a moving vessel, refer to *Prytz (2019)* and *Svanes Bertelsen (2020)*.

3. Analyzing the effect of propeller cleanings

The VTI analysis was performed for two cargo vessels using the following equipment and services:

- Miros Wavex for measurement of directional wave spectra and speed through water
- Miros Edge platform for collection of propulsion data
- Miros VTI service for automatic calculation of the VTI

The Miros onboard system also collected wind data, vessel position and heading. The Miros VTI service collected hindcast water temperature data from the EU Copernicus database. Water salinity was not used in the analysis. Finally, water depth data was also collected from the EU Copernicus service to filter out shallow water situations.

3.1. Propeller cleaning 1

In the first scenario, an LNG carrier (length 295 m and width 46 m) was on a voyage from Tianjin, China to Qalhat, Oman as shown in Fig.2. A hull inspection and propeller cleaning were performed during a one-day stopover in Singapore. Some photos taken during the inspection together with a specification of the fouling identified are shown in Fig.3 and Fig.4.

Fig.2: Vessel route from Tianjin, China to Qalhat, Oman with a one-day stopover in Singapore. The blue part of the voyage is before the cleaning and the red part is after the cleaning.

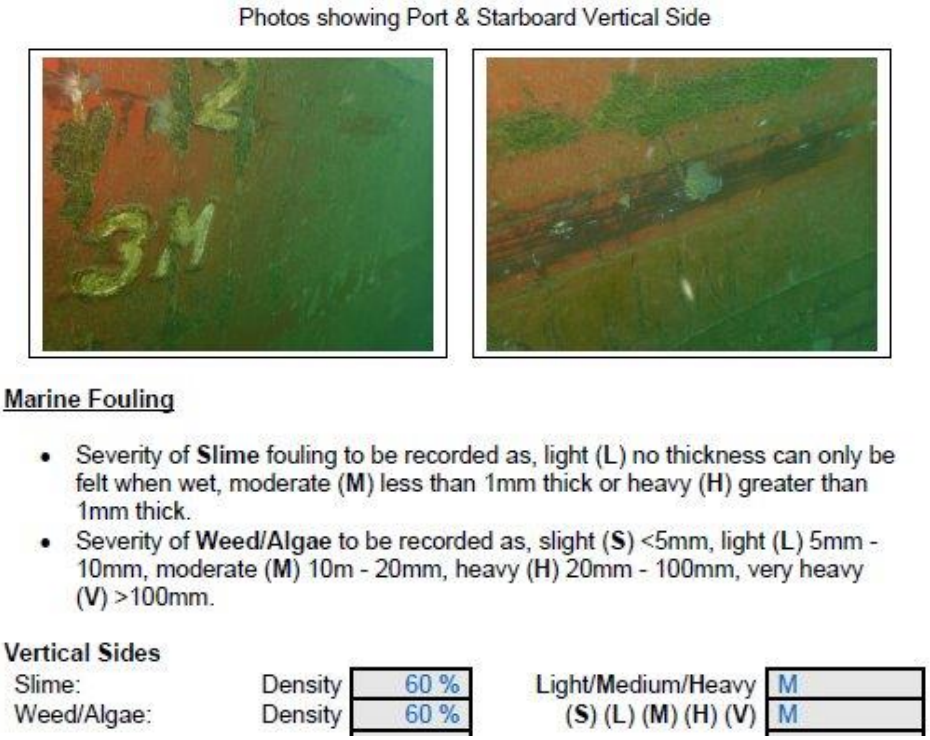

Fig.3: Pictures and specification of the fouling for the port and starboard vertical sides.

The VTI was calculated for the entire voyage as shown in Fig.5. From this depiction of the VTI time series it is difficult to conclude on the changes in VTI due to the propeller cleaning. The distribution of

VTI values was therefore compared together with a statistical analysis of the result. This is shown in Fig.6. As can be seen from the analysis, the VTI was reduced from 1.28 to 1.22 after the propeller cleaning.

3.2. Propeller cleaning 2

In the second scenario, an ultramax bulk carrier (length 200 m and width 32 m) was on a voyage from San Vincente, Chile to Buenaventura, Colombia as shown in Fig.7. A hull inspection and propeller cleaning were performed during a two-day stopover in Callao, Peru. Fig.8 shows pictures of the fouling on the vertical port side of the vessel. As in scenario 1, light hull fouling (slime) was observed. Fig.9 shows pictures of the propeller before and after the polishing. The propeller was found to be moderately fouled (slime, barnacles, sea grass) before the polishing.Fig.3

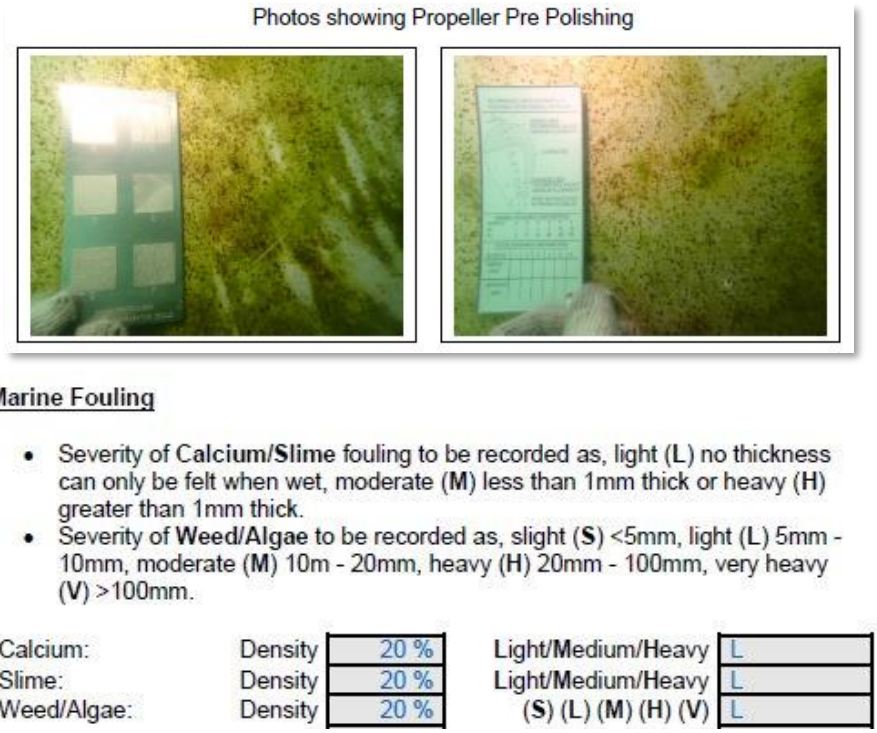

Fig.4: Pictures and specification of the fouling of the propeller before the polishing.

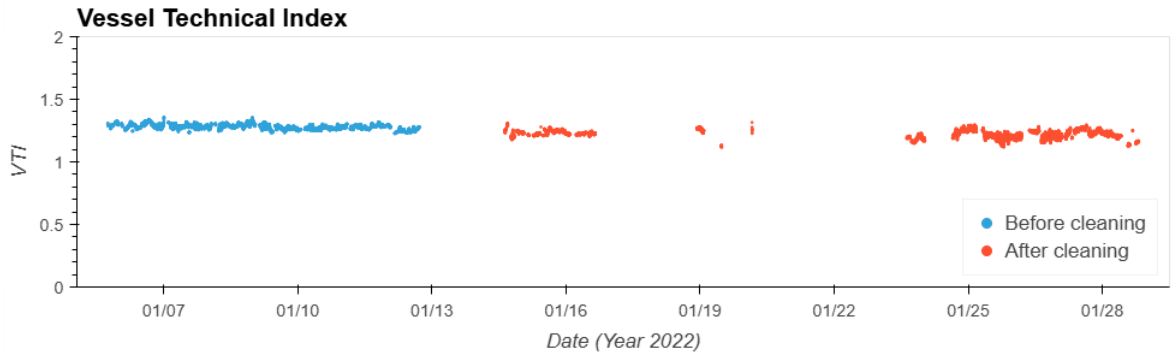

Fig.5: The VTI calculated for the voyage from Tianjin, China to Qalhat, Oman. The missing values are normally due to weather conditions exceeding the allowed limits for the VTI analysis or because of relatively rapid changes in vessel operation or weather conditions.

The VTI was calculated for the entire voyage as shown in Fig.11. As in scenario 1, the distribution of VTI values was compared together with a statistical analysis of the result. This is shown in Fig.12. The VTI was reduced from 1.20 to 1.08 after the propeller cleaning.

4. Discussion

This paper investigated the technical performance of two large cargo vessels before and after propeller cleaning events by applying a VTI analysis methodology. Two hull cleaning events were analyzed. In both cases, the inspection revealed that the vessel only had light fouling on the hull. The propeller was also found to have light fouling in the first case whereas moderate fouling was identified in the second case.

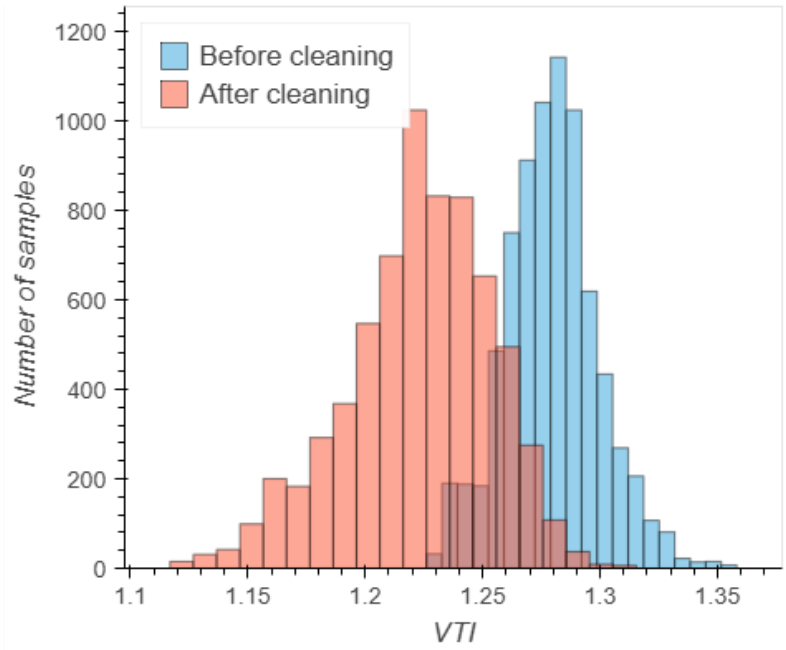

Propeller cleaning 1

Change in VTI statistics

	VTI	
	mean	std
Before	1.28	± 0.02
After	1.22	± 0.03

Fig.6: The VTI distribution before and after the propeller cleaning with the associated statistics shown on the right. The vertical axis shows the number of samples, i.e. the number of minutes with valid VTI calculations.

Fig.7: Vessel route from Vincente, Chile to Buenaventura, Colombia with a two-day stopover in Callao, Peru. The blue part of the voyage is before the cleaning and the red part is after the cleaning.

In the first scenario, the vessel VTI was reduced by 0.06 from a moderately high level of 1.28 prior to the cleaning procedure. In the second scenario, the VTI was reduced by 0.12 from 1.20 to 1.08. The

identified changes were relatively small but statistically significant even with the short time frames of data used in the analysis. The accuracy of the VTI analysis was approximately 0.03 in all scenarios. This shows that it is possible to accurately identify the effect of such cleaning procedures within a short time period of a few days. The analysis was performed using high-frequency, accurate data, and without accurate data, it is unlikely that such small changes in vessel performance could have been identified with sufficient accuracy without looking at much larger time frames.

Fig.8: Pictures of the fouling on the port vertical side

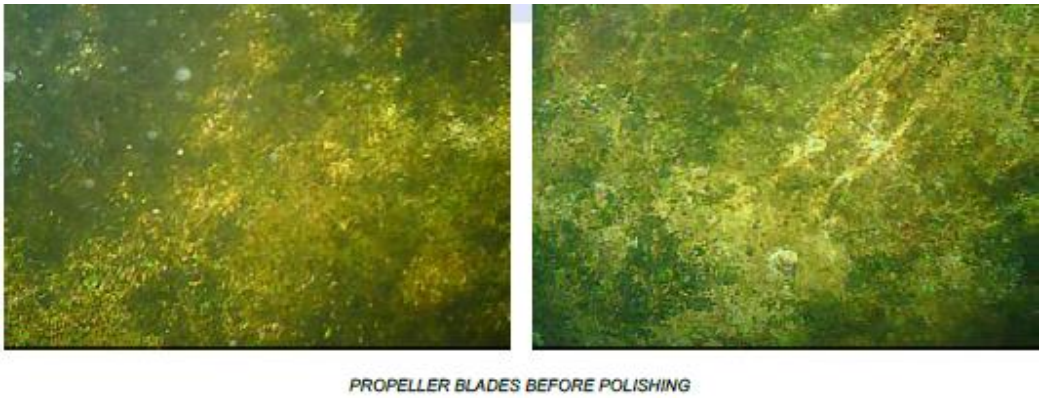

Fig.9: Pictures of the propeller before the propeller polishing

Fig.10: Pictures of the propeller after the propeller polishing

5. Conclusion

The results presented in this paper show that the VTI concept can be used to quickly and accurately analyze the effect of propeller cleanings when used together with accurate data on STW, waves and wind. The VTI methodology can accurately normalize for the impact of weather, vessel operational

changes and navigation effects. It has been shown that a VTI analysis can identify relatively small performance gains by cleaning a lightly fouled propeller. In this case, the cleaning of a lightly fouled propeller led to a reduction in VTI of 0.06. This was accurately identified by analyzing just a very few days of data. The effect of cleaning a moderately fouled propeller was found to be significantly higher with a reduction in VTI of 0.12. The accuracy of the results were 0.02-0.03 VTI points, or 2-3%.

The VTI is therefore a valuable tool for accurate vessel performance analysis that can provide a new level of accuracy in determining the effect of hull cleaning procedures, identifying the effect of energy saving devices and by identifying the actual performance level of a vessel at any time.

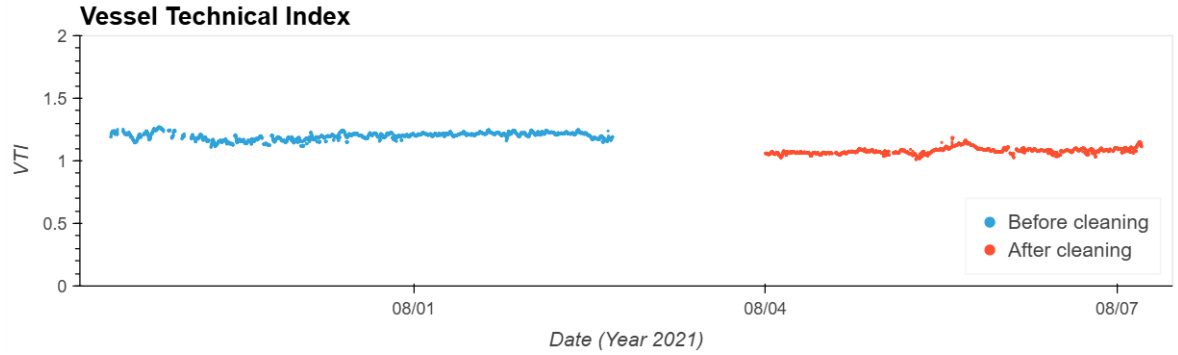

Fig.11: The VTI calculated for the voyage from Vincente, Chile to Buenaventura, Colombia. The missing values are normally due to weather conditions exceeding the allowed limits for the VTI analysis or because of relatively rapid changes in vessel operation or weather conditions.

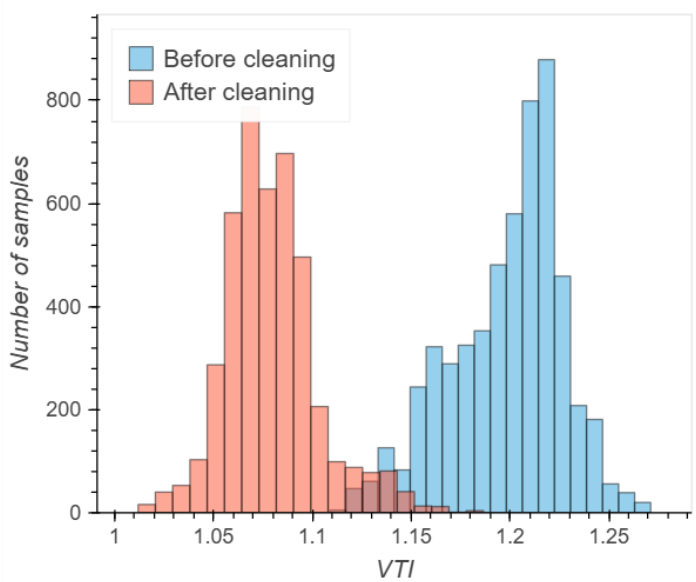

Propeller cleaning 2

Change in VTI statistics

	VTI	
	mean	std
Before	1.20	± 0.03
After	1.08	± 0.02

Fig.12: The VTI distribution before and after the propeller cleaning with the associated statistics shown on the right. The vertical axis shows the number of samples, i.e. the number of minutes with valid VTI calculations.

References

DNV (2023), *Technical ship performance*, DNV-RP-0675, DNV, Hovik

GANGESKAR, R. (2017), *Automatically calibrated wave spectra by the Miros Wavex system – Accuracy verified*, Miros AS, Asker

GANGESKAR, R.; PRYTZ, G.; SVANES BERTELSEN, V. (2018a), *On-Board Real-Time Wave & Current Measurements for Decision Support*, 3rd HullPIC Conf., Redworth, pp.223-233

GANGESKAR, R. (2018b), *Verifying High-Accuracy Ocean Surface Current Measurements by X-Band Radar for Fixed and Moving Installations*, IEEE Trans. Geosci. Remote Sens. 56/8, pp.4845-4855

GANGESKAR, R. (2018c), *Surface Current Measurements from Moving Vessels by Wavex*, Miros AS, Asker

GANGESKAR, R. (2019), *Measuring the speed through water by Wavex*, Miros AS, Asker

GANGESKAR, R. (2021), *Automatic Radar Data Quality Control – Applying Deep Learning, AI to Ocean Wave, Current Measurements*, Sea Technology 62/2, pp. 23-27

GUO, B.; ROGNEBAKKE, O.; TVETE, H.A.; ADAL, C.; STORHAUG, G.; SCHMIDT, M.; BRUSET, T.; PRYTZ, G. (2021), *Setting the standard for evaluation of in-service technical ship performance*, 6th HullPIC Conf., pp.88-105

GUPTA, P.; GUO, B.; STEEN, S.; TVETE, H.A. (2023a), *Reliable Hull Performance Analysis using Vessel Technical Index*, 15th Symp. High-Performance Marine Vehicles (HIPER), Bernried

GUPTA, P.; STEEN, S.; GUO, B.; TVETE, H.A. (2023b), *Evaluating vessel technical performance index using physics-based and data-driven approach*, Ocean Eng.

PRYTZ, G.; GANGESKAR, R.; SVANES BERTELSEN, V. (2019), *Distributing Real-Time Measurements of Speed Through Water from Ship to Shore*, 4th HullPIC Conf., Gubbio, pp.114-127

SVANES BERTELSEN, V.; GANGESKAR, R.; PRYTZ, G.; SCHMIDT, M. (2020), *Accurate Voyage Sea State and Weather Measurements Improve Performance-Based Vessel Management*, 5th HullPIC Conf., Hamburg, pp.157-171

SVANES BERTELSEN, V.; BRUSET, T.; GANGESKAR, R.; PRYTZ, G.; SCHMIDT, M. (2021), *Accurate Speed Through Water Measurements Enable Accurate Vessel Performance Management*, 6th HullPIC Conf., Pontignano, pp.112-123

SVANES BERTELSEN, V.; CARELLA, A.; GANGESKAR, R.; PRYTZ, G.; SCHMIDT, M. (2022), *Vessel Technical Performance Analysis using Accurate Weather and Speed Through Water Data*, 7th HullPIC Conf., Tullamore, pp.260-274

Separating Propeller and Hull Performance with Thrust Measurements

Rasmus Ruff, Vessel Performance Solutions, Lyngby/Denmark, rru@vpsolutions.dk
Kristian Bendix Nielsen, Vessel Performance Solutions, Lyngby/Denmark, kbn@vpsolutions.dk

Abstract

This paper presents the results of utilizing advanced propulsion models to isolate and evaluate the performance of a vessel's hull and propeller individually. This is achieved by leveraging auto-log data, including thrust, torque and fuel measurements, alongside other real-life sensor data. Penalties caused by fouling and wear can thereby be attributed to either the hull or the propeller, supporting more informed operational decisions. To achieve this, a method proposed by Ballegoojen (2019) is used. This requires baselines for the thrust and torque of the vessel. This paper is investigating two different methods to create those baselines: the first is utilizing Vessel Performance Solutions' in-house ship performance Speed-Power models and the second is relying on propeller Open-Water curves and Model test data. The methods were tested on bulk carriers using real-life operational data. The models show that a separation can be achieved, further investigation is needed to improve the understanding of the correlation between the KPI's.

1. Introduction

Today, vessel performance is an advanced technology essential to vessel operations. Operators are interested in reducing their operational costs and greenhouse gas emissions (GHE). In general, vessel performance can be understood as covering many different operation areas. This paper will focus on hull and propeller performance. Over time, the vessel develops fouling and corrosion. On top of this, cavitation can damage the propeller over time. This impacts the vessel's resistance and the efficiency of the propulsion system. Cleaning the hull, using antifouling paints, or polishing the propeller can counteract this impact. These measures can be expensive, so knowing the benefits and comparing them can help to make an informed decision.

The need to investigate the increased resistance due to degradation and fouling can be seen in an example case from *Schultz (2007)* based on an Oliver Hazard Perry-class frigate. The frigate had an increase in shaft power for a heavy calcareous fouled condition of 84% compared to the clean hull condition. Resulting in overconsumption and higher operational cost.

New regulations from the International Maritime Organization (IMO) and local governments increase the pressure on companies to reduce their GHE. In 2023, IMO completed the first revision of its GHE strategy and increased its goal to reduce shipping GHE by 20% compared to 2008 in 2030 and finally to net zero in 2050. They estimate that 5%-15% can be saved by considering vessels hydrodynamic characteristics, which requires regular and timely cleanings of hull and propeller e.g. *DNV (2023)*.

Today, one way to measure the performance of your vessel is to compare the vessel's consumption to a baseline and, by this, monitor the vessel's performance. This approach gives valuable information about the vessel's combined hull and propeller condition, but it does not provide any explicit information about the separate performance of the hull and propeller. Distinguishing between the increased resistance caused by hull and propeller gives the operators a better decision base. This helps to schedule respective hull cleanings and propeller polishes more efficiently. By this the overall consumption of a vessel can be optimized and operational cost and GHE can be reduced.

When talking about hull and propeller resistance, we can gain a misunderstanding of the physical terms behind the words. Hull resistance is the resistance of a ship or floating body needed to be pulled through water. It follows the well-known formula:

$$R_T = \frac{1}{2}\rho C_T S\, V^2$$

Where R_T is the total resistance of the hull, C_T is the total resistance coefficient, S is the wetted surface area and V is the velocity. C_T in this case depends on the hull shape, speed, draft and surface condition of the hull.

When talking about the propeller the focus is not that much on the resistance but the change of efficiency of the propeller. In terms of performance, the efficiency change can be presented as a resistance, as it is increasing the total fuel consumption of the vessel.

2. Ballegooijen approach to separate Hull and Propeller Performance

Ballegooijen (2019) suggests a method to separate hull and propeller performance using the thrust and torque sensors of a vessel and comparing them with a baseline for each sensor. The concept is based on the idea that fouling and surface degradation have different impacts on the thrust and torque of the propeller.

Hull fouling increases the total resistance of the hull. Thereby both the thrust measured and the torque measured should increase similarly when the hull becomes fouled. On the other side, propeller fouling only impacts the efficiency of the propeller. The same thrust is needed to propel the ship, but more torque is needed to convert the engine power to the equivalent thrust. Thereby the changes in torque represents both the propeller and hull condition. The changes of the thrust represent the changes in the hull resistance. To split those from each other, 3 key performance indicators (KPI) are proposed. The first uses torque measurements to give a view over the combined condition of hull and propeller. The second uses the thrust to show the condition of the hull. The third is the difference of both to indicate the propeller condition.

The following changes can be detected disregarding the weather impact.

Thrust sensor:

- Thrust deduction
- Hull resistance

Torque sensor:

- Thrust deduction
- Hull resistance
- Wake fraction
- Propeller efficiency

To be able to compare the torque with the thrust it is needed to convert them into power.

The torque can be converted by applying the power equation for a shaft:

$$P_D = 2\pi n M$$

P_D is the delivered power, n is the number of rotations per second and M is the torque.

The thrust would be normally converted using the following formula:

$$P_T = T \cdot V_A$$

Here P_T is the thrust power and V_A is the wake speed around the propeller. The disadvantage of this formula is that it is difficult to determine the wake speed in an operating vessel, therefore *Ballegooijen* (2019) suggest to use either the speed through water instead, as this is measurable using

a log sensor, or correcting the speed overground for currents. This gives a new parameter, hull power, here V is for the speed in m/s:

$$P_H = TV.$$

Thereby KPIs for the thrust and for the torque can be defined as follows:

$$\text{KPI}_{\text{Total}} = \text{KPI}_T = \left(\frac{P_{\_D}}{\text{Baseline Delivered Power}} - 1\right) \cdot 100\%\Big)$$

$$\text{KPI}_{\text{Hull}} = \text{KPI}_T = \left(\frac{P_H}{\text{Baseline Hull Power}} - 1\right) \cdot 100\%\Big)$$

Assuming KPI_{Total} measures the total change in the propulsion efficiency and KPI_{Hull} measures the change of hull resistance and thrust deduction, the difference of both KPI's shows the changes in the wake fraction and the propeller efficiency. This gives the last KPI for the propeller performance:

$$KPI_{Prop.} = KPI_{Total} - KPI_{Hull}$$

3. Verify KPI's with simulation results

To validate the proposed concept, the KPI will be calculated for results of a computational fluid dynamics (CFD) simulation of a container vessel. Those simulations were conducted by *Song et al. (2020)*. Full-scale simulations of a KRISO reference container vessel with different "hull", "propeller" and "hull and propeller combined" surface roughness was conducted. The CFD results contain the propeller thrust and torque coefficient and wake and thrust deduction for the different roughness. This enables using those results to calculate the KPIs and see the impact of the different roughness on them. As baselines for the hull power P_H and delivered power P_D, the clean hull condition is used. Fig.1a shows the KPIs calculated for hull with different surface roughness applied and Fig.1b shows the KPIs for the propeller with different surface roughness.

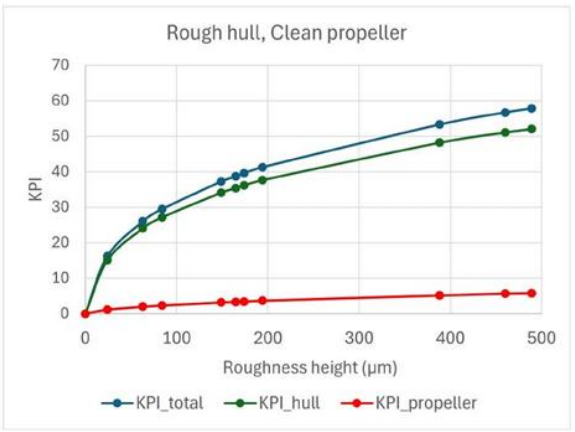

(a) KPI's for different hull roughnesses with a clean propeller.

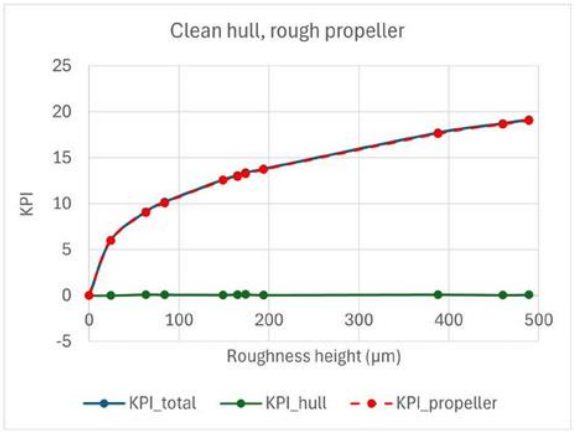

(b) KPI's for different propeller roughnesses with a clean hull.

Fig.1: CFD results for different hull and propeller roughnesses, converted to KPI

The results show that when only the propeller surface is changed, the KPI of the hull is not impacted, only the propeller and total KPIs are increasing. When the hull roughness is increasing, it is impacting both the total KPI, hull KPI and in a smaller degree the propeller KPI.

Fig.2a shows the KPIs when both hull and propeller surface roughness increase. All three KPIs are increasing as expected. Fig.2b shows a comparison of the KPIs for summed separated, meaning

$KPI_{i,Rough\ hull} + KPI_{i,Rough\ propeller}$ and for the combined $KPI_{i,Rough\ hull\ and\ rough\ propeller}$. The combined simulation has higher propeller and total KPIs compared to the sum of the separated simulated roughnesses. This shows that there is an interaction between the hull KPI and propeller KPI.

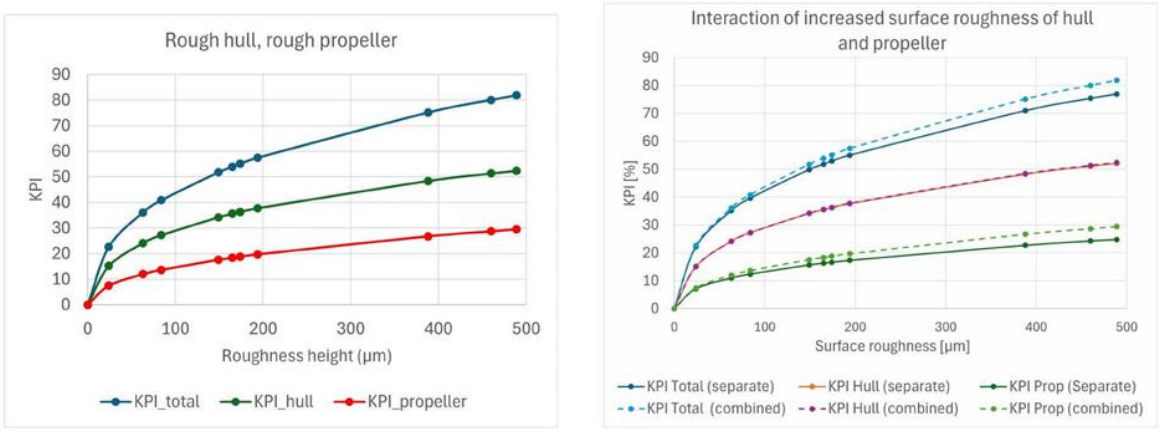

(a) CFD results for different hull and propeller roughnesses.

(b) Interaction of combined change in hull and propeller surface roughness.

Fig.2: Simulated KPIs for hull and propeller for different surface roughnesses. In b) separate is: $KPI_{i,Rough\ hull} + KPI_{i,Rough\ propeller}$ and combined is: $KPI_{i,Rough\ hull\ and\ rough\ propeller}$

The reason for effects on the propeller KPI, when only the hull roughness is changed, comes from the impact the surface roughness has on the wake. Increased surface roughness decreases the wake speed and impacts the propulsive efficiency η_D negatively. The latter consists of the hull efficiency et $a_H = (1-t)/(1-w)$, open water efficiency η_O, and rotative efficiency, all of which depend on the wake fraction. The propeller KPI does not directly measure the propeller's increased resistance. Instead, it measures the change in propulsive efficiency.

4. Baselines

The last section shows that those KPIs can be used to separate the hull and propeller impact and that both are linked with each other through the wake fraction. Even though valuable knowledge of the performance can be gained from those KPIs, to improve decision making of operators.

Total and hull KPI are all based on a baseline. *Ballegooijen (2019)* employs the operational data right after a propeller and hull cleaning event to construct the required baselines. This is obtained by a simple curve fitting over the measured data as follows:

$$P = aV^b$$

Here P is the power, V is the vessel's speed, and a and b are the fitting coefficients. Two baselines for the delivered power and thrust can be created accordingly.

The issue with the baselines using this method is that they are obtained by adjusting and fitting the data to get the expected outcome. However, we believe that the baselines should be built in accordance with the underlying physical models. Therefore, in this project, we use different methods to construct the baselines. In the following sections, these methods are explained.

4.1. Vesper Baseline

The first baseline will be created from a Vesper model. The Vesper software was developed by VPS for vessel performance. Each vessel class gets a model, which includes a digital twin with a speed-draft-power model. This model is calibrated to the ship's sea trial and thereby to its newbuild

condition. A speed-power model can be seen in Fig.3. The model predicts the delivered power for the vessel's full range of operational speeds and drafts. As the Vesper model covers the delivered power, it can directly be used as the delivered power P_D baseline. To adjust it for the hull power, the relation between hull power and delivered power needs to be known. To achieve this, their relation to the effective power P_E is found.

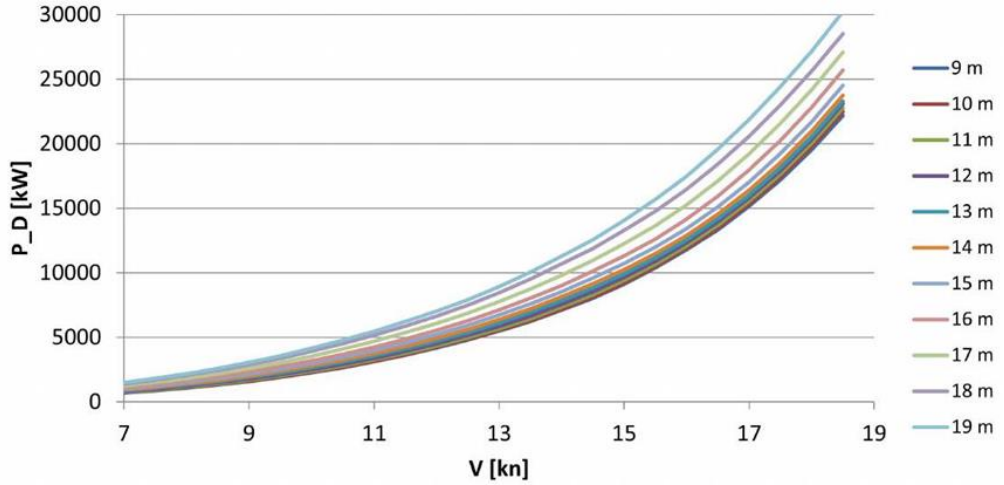

Fig.3: A Vesper speed-power model for different drafts

For the hull power we get:

$$P_E = P_H(1-t)$$
$$P_E = TV(1-t)$$

t is the thrust deduction, presenting the thrust lost coursed by the shape of the hull. To go from delivered power to effective power we get:

$$P_E = P_D\eta_D$$

Combine this to get the relation between delivered power and Hull Power:

$$P_H(1-t) = P_D\eta_D$$
$$P_H = \frac{P_D\eta_D}{(1-t)}$$

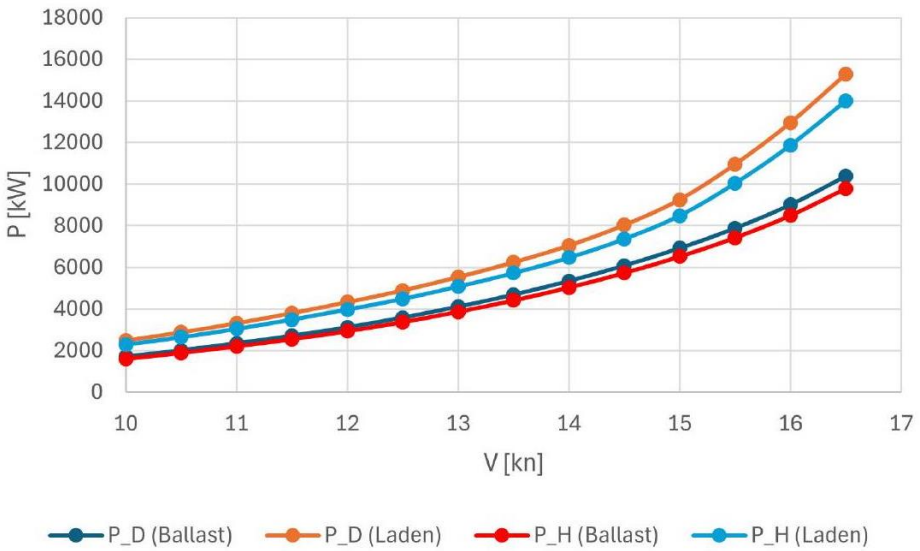

Fig.4: Vesper Baselines for one vessel in ballast and laden condition

A normal range for η_D is from 55% to 75%, *USNA (2020)*. Based on the existing model test it was decided to set the η_D to 0.7. It is important to mention that the η_D depends on the draft and speed, but it is assumed to be constant to simplify the model. The thrust deduction coefficients are taken from model test. For vessels without a model test, the thrust deduction is calculated using the BSRA method e.g. *Pattulo et al. (1971)*, see appendix. The baselines for one of the vessels for laden and ballast can be seen in Fig.4. The hull power is slightly below the delivered power. Fig.5 shows a flowchart describing the process.

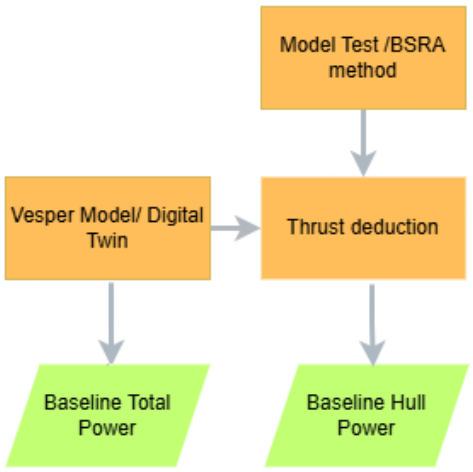

Fig.5: Flowchart showing the creation of the Vesper baseline

5. Open water baseline

The second baseline is obtained based on the propeller characteristics. Those are achieved from open-water tests and model tests. Here, the thrust and torque coefficients of the vessel with the corresponding rotative efficiency are used to calculate the expected delivered power and hull power. As the thrust identity is used for the model test, the torque coefficient is adjusted with the rotative efficiency η_R.

$$P_H = \mathrm{K}_T(J)\rho n_L^2 D^4 V$$

$$P_D = \frac{\mathrm{K}_Q(J)\rho n_L^2 D^5}{\eta_R(V)} 2\pi n_L$$

$K_T = \frac{T}{\rho n^2 D^4}$ and $K_Q = \frac{Q}{\rho n^2 D^5}$ are the propellers Thrust and Torque coefficients, $J = \frac{V_A}{nD}$ is the advancements ratio, ρ is the water density, n_L is the light running rotational speed of the engine. D is the propeller diameter and η_R is the rotative efficiency.

Here K_T and K_Q are functions of J. η_R is a function of the velocity. n_L represents the light running rotations per second, it is calculated based on Vesper Speed Power model, as no relation is given in the available Sea Trials. It can be calculated by using the following formula:

$$n_L = \frac{\mathrm{RPM}_{\mathrm{heavy}}\,(\mathrm{ME}_{\mathrm{load}}) \cdot \mathrm{LRM}}{60} \tag{32}$$

Here, $\mathrm{RPM}_{\mathrm{heavy}}\,(\mathrm{ME}_{\mathrm{load}})$ is the rotational speed of the engine at the current engine power. The heavy RPM curve can be calculated by:

$$\mathrm{RPM}_{\mathrm{heavy}}\,(P) = \left[\frac{P}{\frac{\mathrm{MCR}}{\mathrm{RPM}_{\mathrm{heavy}}\,(\mathrm{MCR})^3}}\right]^{\frac{1}{3}}$$

The MCR is the maximum continuous rating of the vessel engine and RPM_{heavy} (MCR) is the corresponding RPM. Both can be found in the vessel's engine data.

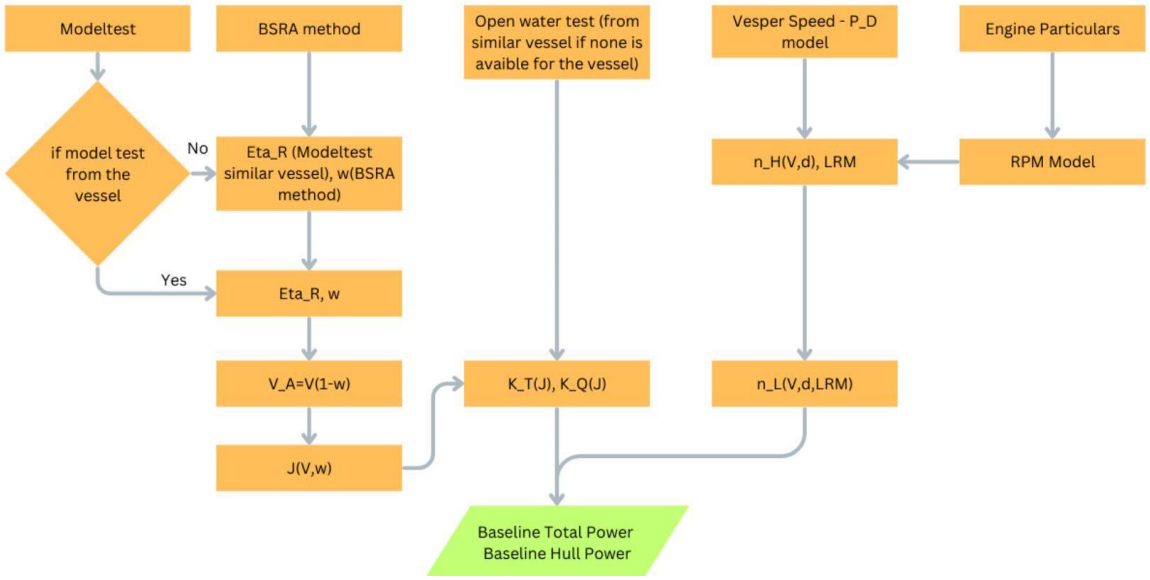

Fig.6: Flowchart of the open water baseline

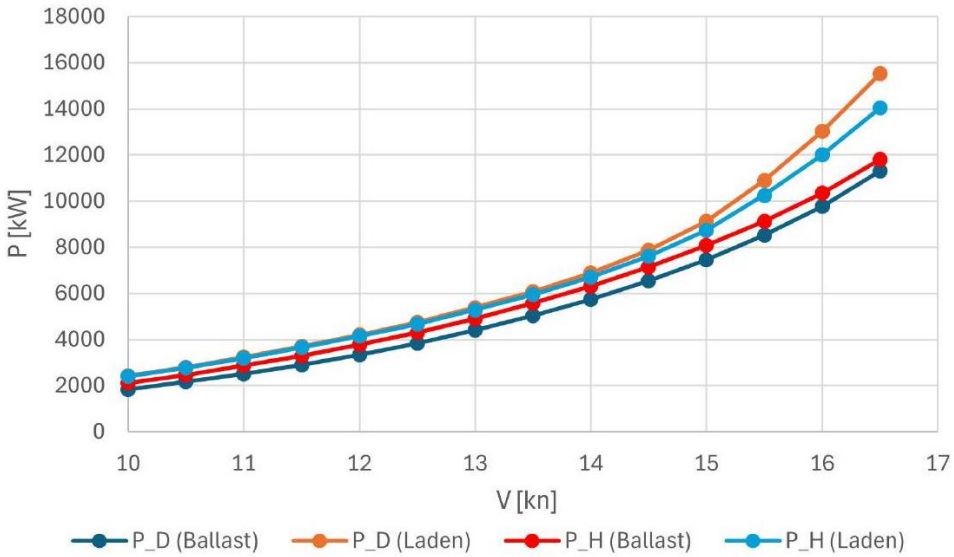

Fig.7: Baselines created by the propeller characteristics for vessel 3

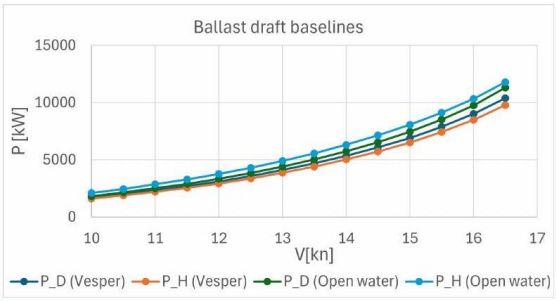

(a) Baselines in ballast condition.

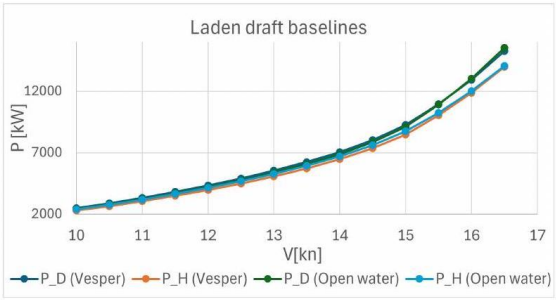

(b) Baselines in laden condition.

Fig.8: Open water and Vesper baselines for one of the investigated vessels. This results in the two baselines. An example for Vessel 3 can be seen in Fig.7. The flow chart for the open water baseline is shown in Fig.6.

The $K_T(J)$ and $K_Q(J)$ are interpolated from the model test for the corresponding advance number J. J is calculated using the propeller dimensions the wake speed and the light running RPM. The wake speed V_a is dependent on the wake fraction. The wake fraction can be interpolated from the model tests or empirically estimated using the BSRA method (see appendix) equation. For the models with model test, the model test data is used. For the vessels without the BSRA method is used.

6. Calculating KPI from operational data

In section 3 the KPIs are calculated based on the CFD results. CFD calculations have the advantage that we know the best condition of the hull and that the forces from weather, currents and other external forces can be controlled. During the operation those external forces need to be determined and the measurements need to be corrected for this. For this study this is done by Vesper. During this study High frequency auto log data is used. To simplify the calculations, the stable periods of the main sensors are detected and the average for those are calculated. Then those values are taken to calculated the measured delivered power P_D and hull power P_H. Both are corrected for the weather and compared to the baseline to calculate their KPI.

Fig.9 shows the flow diagram of this process until the calculation of the KPI.

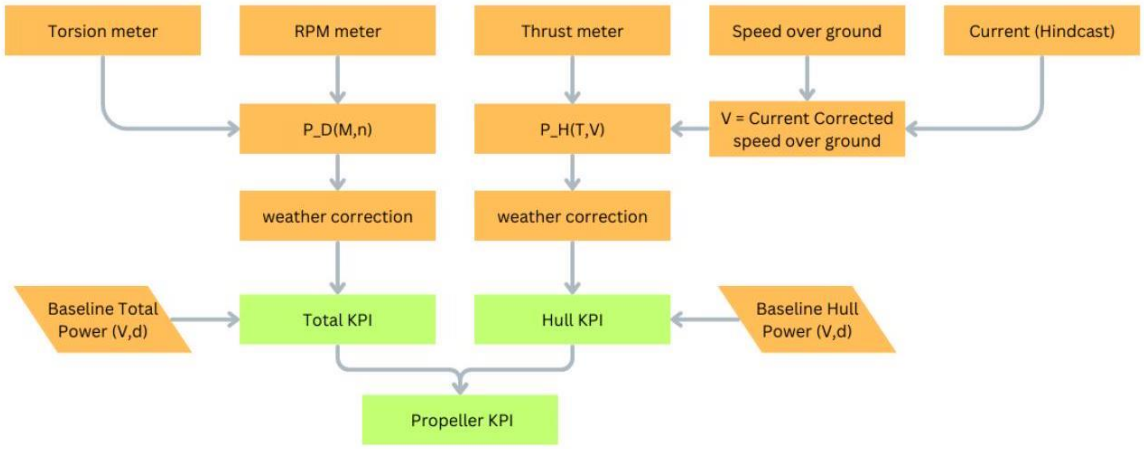

Fig.9: KPI procedure

7. Applying both baselines on operational data

The two baselines were built for 9 bulk carriers and were applied for their auto-log data. Afterwards the KPI average before and after a propeller polish was investigated. It was chosen to focus on propeller polishes. This is done because those events have the main impact on the propeller KPI and total KPI. The hull KPI should stay stable before and after the events.

During the investigation period 11 propeller polishes happened. The results of those events can be seen in Figure 10. The average was taken of the KPI for a period of 30 days before and 30 days after the propeller polish. The results were collected for both baselines. To ensure the quality of the torsion meter the shaft power is also calculated based on the fuel consumption.

Fig.10 shows that the shaft power shows similar results, whether it is calculated from torsion meter or fuel meter. Looking at the open water baseline, the impact on the hull KPI is larger than the impact on the propeller KPI. This shows that the baseline is not able to show the difference between propeller and hull fouling. On the other side looking at the baseline created with the Vesper baselines, the impact from the propeller polish is bigger on the propeller KPI compared to the impact on hull KPI. The average and the median of the hull KPI are close to 0. This can be expected looking at the CFD example shown in Part 3.

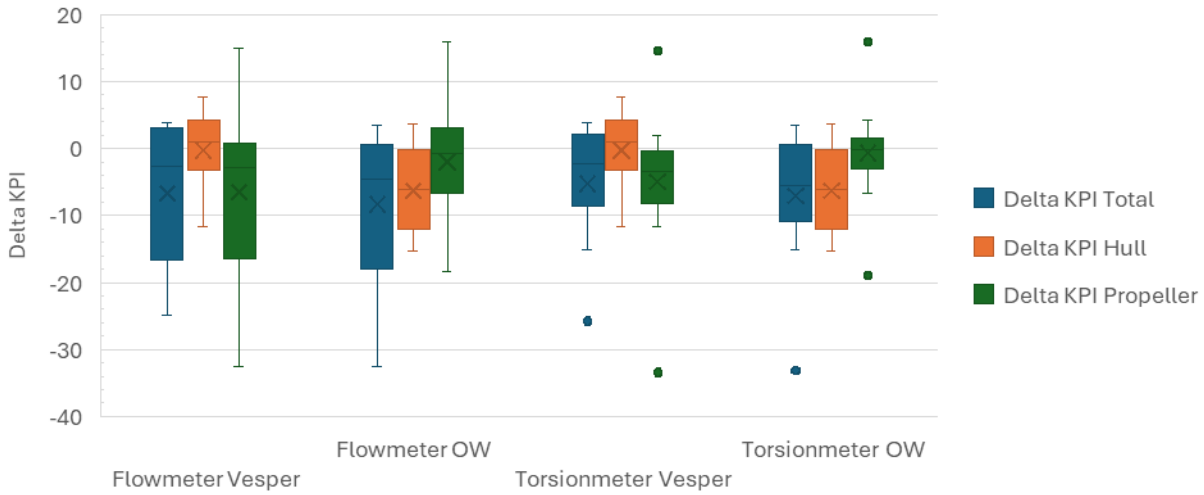

Fig.10: Change of KPIs before and after propeller polish. KPI is based on either the Vesper baseline or the open water baseline. The shaft power is either calculated with fuel consumption or the torsion meter. "OW" refers to the open water baseline. "Vesper" refers to the Vesper Baseline.

The open water baseline is showing unexpected changes of the KPIs over a propeller polish. It is showing a higher decrease of the hull KPI compared to the propeller KPI. This is against expectations. It is also surprising as we would expect model test and open water test to create a precise model. One of the reasons for this could be that the model tests do not always cover the full operational range of drafts and speeds. This can lead to errors in the interpolation of thrust and torque coefficients. Also, it is known that due to different Reynolds numbers and frictional forces the scaling of the wake fraction from model to real live scale can be challenging. Thereby a different wake can impact the baselines.

8. Conclusion and next steps

The KPIs proposed by *Ballegooijen (2019)* can separate the propeller and hull performance. However, an advanced baseline for the hull and total KPI is crucial to gain useful information. To improve the method, the correlation between the hull power and shaft power needs to be better understood, so that a new factor can describe the impact of the hull to the propeller. This can be done by developing a relation between the hull KPI and wake fraction, thereby gaining a better understanding on how the hull condition impacts the flow towards the propeller and its efficiency. Two baselines were proposed. The open water baseline seems to have scaling errors which are not considered, impacting the baselines. Better results are seen when taking the Vesper baseline and applying the thrust deduction to create the hull baseline. This method seems to have the advantage that the thrust deduction is more stable when scaling and is less impacted by the condition of the hull.

To verify those results a bigger study with more events is needed. On top of this, the relation between the hull KPI and the change of wake fraction would be needed to gain a better understanding of how the condition of the hull impacts the propeller efficiency.

Acknowledgement

I would like to thank everyone who helped with this paper. Firstly, the client who allowed using their data anonymously to investigate the KPIs. As this paper is based on my master thesis at DTU, I would also like to thank my supervisors Mostafa Amini-Afshar and Harry Bingham and Dimitris Georgousis for their help and contribution to the project. Lastly, I would like to thank all my colleagues at Vessel Performance Solutions, who helped when help was needed.

References

BALLEGOOIJEN, E.v.; HELSLOOT, T. (2019), *An Approach to Monitor the Propeller Separately from the Hull*, 4th HullPIC Conf., Gubbio, pp.50-55, http://data.hullpic.info/HullPIC2019_gubbio.pdf

DNV (2023), *Maritime Forecast to 2050: Energy Transition Outlook 2023*, DNV, Høvik

HARVARD, S.A. (1983), *Resistance and Propulsion of Ships*, Dept. Ocean Engineering, DTU

MOLLAND, A.; TURNOCK, S.; HUDSON D. (2017), *Ship Resistance and Propulsion*, Cambridge University Press, pp.12-16

PATTULLO, R.N.M.; WRIGHT, B.D.W. (1971), *Methodical series experiments on single-screw ocean-going merchant ship forms. Extended and revised overall analysis*, BSRA Report NS333

SCHULTZ, M.P. (2007), *Effects of coating roughness and biofouling on ship resistance and Powering*, Biofouling 23/5, pp.331-341

SONG, S.S.; DEMIREL, Y.K.; ATLAR, M. (2020), *Penalty of hull and propeller fouling on ship self-propulsion performance*, Applied Ocean Research

USNA (2020), *Course Notes: EN400: Principles of Ship Performance*, https://www.usna.edu/NAOE/_files/documents/Courses/EN400/02.07_Chapter_7-May20.pdf

Appendix

A.1 Wake fraction and thrust deduction

The British Ship Research Association (BSRA) has adapted some empirical formulas found by *Pattullo et al. (1971)* to predict the wake fraction and thrust deduction. Because model tests are not always conducted for vessels or the data is not yet available, it is important to be able to predict the wake fraction or thrust deduction on an empirical basis. The empirical formula for the wake fraction of a single screw vessels, is defined as:

$$w_T = -0.0458 + 0.3745C_B^2 + 0.1590D_W - 0.8635F_R + 1.4773F_R^2$$

Where in D_w is a wake fraction parameter:

$$D_W = \frac{B}{\nabla^{1/3}}\sqrt{\frac{\nabla^{1/3}}{d}}$$

The limit for this method is $C_B = [0.55,0.85], \mathrm{Fr} = [0.12 - 0.36]$: C_B is the block coefficient, F_R is the Froude number, B the vessels beam, ∇ is the displacement volume and d is the draft.

As for the wake fraction, thrust deduction can be determined by self-propulsion test, CFD and empirical estimations. The empirical formula from the BSRA is shown below. BSRA has developed two models, the first one if the pitch and diameter of the propeller are known and the second if they are not known.

$$t = -0.2064 + 0.3246C_B^2 - 2.1504C_B(\mathrm{LCB}/L_{BP}) + 0.1705\left(B/\nabla^{1/3}\right) + 0.1504(\mathrm{P/D})$$
$$t = 0.5352 - 1.6837C_B + 1.4935C_B^2 - 1.6625(\mathrm{LCB}/L_{BP}) + 0.6688D_t$$

where LCB is the longitudinal center of buoyancy forward of 0.5 L as a percentage of L, P/D is the pitch ratio of the propeller and L_{BP} is the length between perpendiculars.

The LCB can be estimated by using the *Harvald (1983)* method:

$$\mathrm{LCB} = -44.17Fn + 9.37$$

Uncertainty Analysis for the New Self-Propulsion Unit at Newcastle University

Gabriela Grasu, Newcastle University, Newcastle upon Tyne/UK, g.grasu2@newcastle.ac.uk
Samir Belhenniche, Newcastle University, Newcastle upon Tyne/UK, samir.belhenniche@newcastle.ac.uk
Rose Norman, Newcastle University, Newcastle upon Tyne/UK, rose.norman@newcastle.ac.uk
Serkan Turkmen, Newcastle University, Newcastle upon Tyne/UK, serkan.turkmen@newcastle.ac.uk

Abstract

In this study, Newcastle University's recently commissioned self-propulsion equipment is used to conduct experiments in the towing tank to test measurement methods and data analysis techniques. The cost and time-effective test campaign acts as a learning tool to benchmark test sensors and analysis methods. Uncertainty levels will be determined by using ITTC's guidelines for self-propulsion test uncertainty analysis. The results provide insight into the prediction accuracy achieved by Newcastle University's new facility, for calm water conditions.

1. Introduction

The International Maritime Organization (IMO) updated its strategy for reducing ship-induced greenhouse gas (GHG) emissions on 7th July 2023. The new strategy aims to reach net-zero GHG emissions from international shipping by, or around, 2050, *IMO (2023)*. To respond to IMO's strategy sustainable propulsion systems (SPSs), energy-saving devices (ESD) and performance monitoring systems need to be implemented for both new and existing ships. A cost-effective approach for assessing the proposed solutions should start with testing scaled-down models, identifying the error sources and understanding the accuracy of the test results as this represents the initial estimate of ship performance and the associated GHG emissions.

An uncertainty sources classification is provided by ISO 19030:2016 Part 1 where the general principles for the measurement of changes in hull and propeller performance are set out, *BSI (2016)*. Investigated uncertainty sources for both full-scale ships and experimental tests are the sensors installed for measuring the variables of interest such as the Doppler speed log, *Dalheim and Steen (2021)* of which the manufacturer's accuracy could become the baseline for the uncertainty analysis and the deployed data acquisition systems (DAQ), *Sogihara et al. (2020)*.

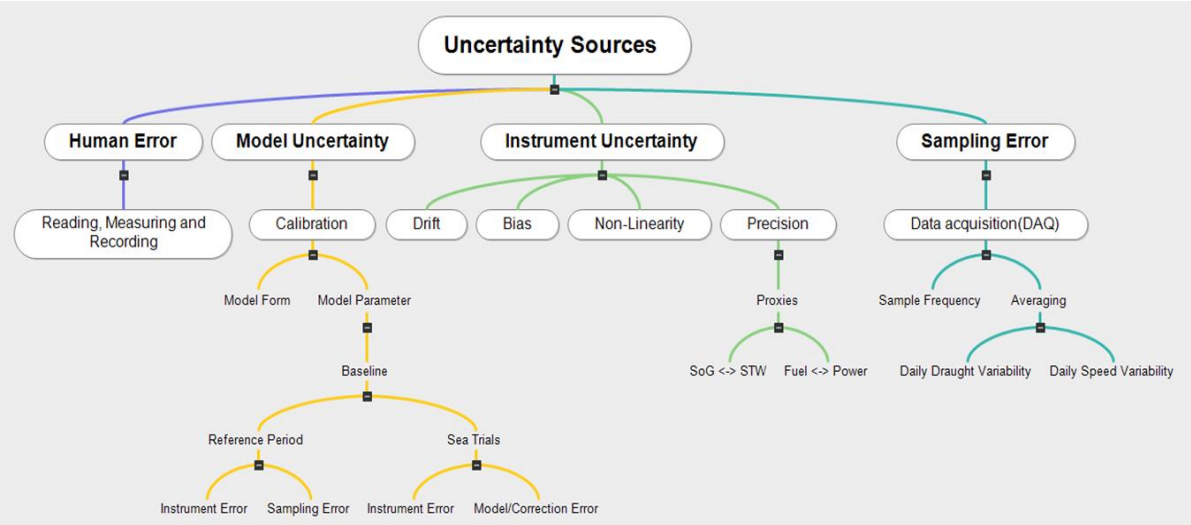

Fig.1: The Uncertainty Sources – An Overall View, *BSI (2016)*

Any full-scale example of power-speed performance shows uncertainty. Firstly, we need to identify the uncertainty sources for obtaining reliable calm water conditions power-speed performance. To assess the efficiency of ESD or any improvements in ship design to reduce GHG emissions, we need to normalise (bring the calm water conditions) the operational power-speed performance measurement. The uncertainty of the full-scale performance estimation or calculation depends on the procedures selected for normalizing the recorded data, *BSI (2016).*

Based on the existing guidelines developed by various institutes and organisations including the American Institute of Aeronautics and Astronautics, American Society of Mechanical Engineers (AIAA/ASME) and Bureau International des Poids Mesures (BIPM), the International Towing Tank Conference (ITTC) developed several specific procedures and guidelines for the uncertainty analysis of model test data providing a robust baseline for uncertainty analysis of ship's self-propulsion tests, *ITTC (2017).*

Through the quantification of the sensitivity coefficients of the individual measured variables, the uncertainty analysis represents a valuable tool for the identification of the dominant sources of error and their influence on the overall prediction accuracy, *Wu et al. (2015).*

The required certainty level of the baseline calm seas conditions, before the evolution to the real seas state of a ship, enables an informed decision to be made regarding the results obtained from the real seas model tests. This study aims to ascertain the accuracy of Newcastle University's new self-propulsion unit and its facility.

2. Uncertainty Analysis

Experiments are typically designed to ascertain the value of a quantity of interest that cannot be directly measured, namely the measurand. Its value is computed based on a measurement equation, namely a data reduction equation, containing the values of elemental variables obtained directly from measurements, *ITTC (2016b).*

$$Y = f(X_1, X_2, \dots, X_N) \tag{1}$$

where Y represents the measurand, $X_1, X_2, \dots, X_N$ represent the N directly measured variables and the function f is the physical law for determining the measurand value but also incorporates all quantities that contribute to the measurand's uncertainty such as the correction factors for $X_1, X_2, \dots, X_N$ and relevant sources of variability.

Measurements will always contain errors. How far a measurement could be from the true value of the measured variable will depend on the type of error accompanying the measurements. Hence, the estimation of the measurand depends on the estimation of the directly measured variables.

$$y = f(x_1, x_2, \dots, x_N) \tag{2}$$

where y represents the estimate of the measurand and $x_1, x_2, \dots, x_N$ represent the estimates associated with the N directly measured variables $X_1, X_2, \dots, X_N$.

The estimates of the directly measured variables will be derived from the systematic errors arising from different sources such as the instrument's precision and calibration and the data acquisition system, and the random errors that are triggered by the uncontrolled elements such as the unsteadiness of the phenomenon being observed, slight fluctuations in the measuring instruments and environment or the operator precision. In the case of systematic errors, namely bias limits, the results could be consistent in a particular direction, low or high. Random errors are described as precision limits, and according to the ITTC guidelines for propulsion tests, *ITTC (2017).* they will be completely aleatory, not exhibiting any obvious trend and as the number of samples increases, they will have a normal Gaussian distribution. The true value of the directly measured variable will remain unknown; however,

uncertainty analysis aims to provide a reasonable estimate of their bias, *B*, and precision limits, *P*, for constructing an uncertainty interval where the true value of the measured variable could be expected to lie with a certain level of confidence. For experimental hydrodynamics, the ITTC guidelines recommend a 95% level of confidence, *ITTC (2016a)*.

Finally, the total uncertainty of the measurand is computed based on the analysis and quantification of the measured variables' total uncertainty interval.

$$u(y) = g(u(x_1), u(x_2), \dots, u(x_i), \dots, u(x_N)) \tag{3}$$

where g represents the generalised form of the law of propagation of uncertainty, $u(y)$ is the uncertainty of the measurand and $u(x_1), u(x_2), \dots, u(x_N)$ are the uncertainties associated with the N directly measured variables $X_1, X_2, \dots, X_N$.

2.1. Standard Uncertainty

There are two methods for obtaining the standard uncertainty of a measurement: Type A and Type B, *ITTC (2016b)*. Both are based on a probability distribution, with the uncertainty quantified by the standard deviation. The Type A method uses the statistical analysis of a series of observations to obtain the components of uncertainty, while the Type B method uses the instrument manufacturer's information, prior experience, or professional judgments.

2.2. Combined Standard Uncertainty

The combined standard uncertainty is determined by implementing the law of propagation of uncertainty with its general equation accounting for both correlated and uncorrelated input quantities. For this study, the input quantities are assumed to be fully uncorrelated, therefore the root sum square of the elementary bias limits will be used to ascertain the combined bias limit of the measured variables. The bias error sources recommended by the ITTC guideline for the self-propulsion test, *ITTC (2017)*, are classified into three categories: calibration, data acquisition, and data reduction, where the latter is applicable only for the corrected values of input quantities and the measurand (the derived value from the measured quantities). Normally, the data acquisition category encompasses the biases associated with the curve fitting and signal conversion from analogue to digital. ITTC recommends a simplified calibration by performing it as an end-to-end process, meaning the wiring, connectors, routing and the data acquisition system are all part of the calibration process. As a result, the bias limit associated with the signal conversion from analogue to digital is accounted for within the bias limit associated with the curve fitting.

The total bias of a directly measured variable, for independent bias error sources, is obtained using the root of the sum of the squares (RSS) arising from each individual source:

$$B(x_i) = \sqrt{B_{std}^2(x_i) + B_{cf}^2(x_i) + B_{ADC}^2(x_i)} \tag{4}$$

where B_{std} represents the bias error introduced by the weights used for the calibration, B_{cf} is the bias error introduced by the curve fit and B_{ADC} is the bias error associated with the analogue-to-digital conversion.

Each directly measured input variable will have a different impact on the variable of interest, the measurand. Their different impacts on the measurand uncertainty are quantified as sensitivity coefficients calculated from the partial derivative of the measurand with respect to the relevant input variable, as seen in Eq.(5).

$$c_i = \frac{\partial y}{\partial x_i} \tag{5}$$

where *y* is the estimate of the measurand and c_i represents the sensitivity coefficient of the input variable x_i.

The combined bias limit of the measurand, for fully uncorrelated input variables is calculated as:

$$B(y) = \sqrt{\sum_{i=1}^{N} c_i^2 \, B^2(x_i)} \tag{6}$$

where *B(y)* is the measurand combined bias limit, c_i is the sensitivity coefficient of the estimated input variable x_i and $B(x_i)$ represents the combined bias of the estimated input variable x_i.

In the case of precision limits, which are calculated using repeat tests, the estimate of a measured variable is obtained by calculating the average, μ, of '*n*' measurements under the same conditions of repeatability:

$$\mu = \frac{1}{n} \sum_{k=1}^{n} x_k \tag{7}$$

where x_k is the k value of the measured variable x.

The standard deviation, σ, characterise the dispersion of the measured variables around the mean and is calculated based on Eq.(8).

$$\sigma = \sqrt{\frac{1}{n-1} \sum_{k=1}^{n} (x_k - \mu)^2} \tag{8}$$

When the curve fitting bias limit is required to be determined with a 95% confidence level, the standard error of estimate (*SEE*) is calculated:

$$SEE = \sqrt{\frac{1}{n-2} \sum_{k=1}^{n} (Y_k - (aX_k + b))^2} \tag{9}$$

where Y_k represents the measured values and $(aX_k + b)$ are the obtained values from the regression equation.

A ±2(*SEE*) interval about the regression curve will contain approximately 95% of the data points and represent the confidence interval on the curve fit.

For a single test, the precision limit of a measured variable can be estimated as the product between the standard deviation σ, derived from multiple tests, and the coverage factor, *k*, corresponding to a 95% confidence level. ITTC recommends 15 measurements for the repeat tests to achieve a coverage factor of two, *ITTC (2017)*.

$$P(S) = k\sigma \tag{10}$$

where $P(S)$ is the single-test precision limit of a measured variable and the coverage factor, *k* represents the inverse student t-test for a degree of freedom equal to $n - 1$.

For a measured variable, the precision limit for multiple tests, *P(M)*, is obtained according to:

$$P(M) = \frac{k\sigma}{\sqrt{M}} \tag{11}$$

where *M* represents the number of tests for which the precision limit is to be established.

The estimation of the measurand's precision limit, for single or multiple tests and fully uncorrelated input variables, is calculated based on *Forgach's (2002)* recommendation:

$$P(y) = \sqrt{\sum_{i=1}^{N} c_i^2 \, P^2(x_i)} \tag{12}$$

The total uncertainty associated with the measurand, is given by the root sum square of the uncertainties in the total bias and precision limits:

$$U(y) = \sqrt{B(y)^2 + P(y)^2} \tag{13}$$

2.3. Data Reduction Equation

A self-propulsion test is primarily conducted to determine the powering requirements of a ship in the presence of a propeller with the thrust deduction factor, t, the wake fraction, w, and relative rotative efficiency, η_R as important propulsion parameters that help designers and researchers to assess in more detail the performance of a ship, *Bertram (2004).*

The analysis conducted within this paper aims to estimate the uncertainty associated with the calculation of the thrust deduction factor, t, as its values are independent of the Froude number, and it will not be changed by the extrapolation process to the full-scale, therefore its accuracy estimation at the model scale provides a good insight for estimating the hull efficiency in the presence of a propeller.

$$\eta_H = \frac{1-t}{1-w} \tag{14}$$

where η_H represents the hull efficiency and w is the wake factor. A smaller thrust deduction factor than the wake factor will yield a hull efficiency greater than unity which will require less power from the propeller resulting in fewer emissions if the prime mover is an internal combustion engine using fossil fuel. Hence, the accurate quantification of the thrust deduction factor is an important stage in the process of emission reduction estimation resulting from the ship design optimisation or implementation of sustainable technologies.

The recommendations of the *ITTC (2017)* guideline for the self-propulsion test were followed to quantify the total uncertainty related to the thrust deduction factor.

The self-propulsion unit was purchased to support Newcastle University's teaching activities. This will ensure that future generations of naval architects and marine engineers have the necessary skills and understanding of a ship performance assessment and the importance of integrating uncertainty analysis into the analysis of experimental tests and full-scale ship operations. The thrust deduction factor data reduction equation was selected for this analysis as it aligns with the existing resources and will ensure a robust baseline in developing an in-house procedure. The thrust deduction factor, t, is expressed as follows:

$$t = 1 - (R_C - F_D)/T \tag{15}$$

where t, namely the measurand, is not measured directly but is determined from T, the measured thrust in the propulsion test, F_D is the calculated external tow force and R_C the resistance corrected for the

difference in temperature between the resistance and propulsion tests. Due to the towing tank location, the water temperature did not differ substantially between the resistance and propulsion tests, hence the difference in total resistance was considered negligible.

The total uncertainty of the thrust deduction factor will arise from the bias and precision limits of the T, F_D and R_C estimations. It is assumed that T, F_D and R_C are fully uncorrelated.

The bias limit of the thrust deduction factor is obtained by applying the law of propagation for uncertainty:

$$B(t) = \sqrt{(\frac{\partial t}{\partial R_C} B(R_C))^2 + (\frac{\partial t}{\partial F_D} B(F_D))^2 + (\frac{\partial t}{\partial T} B(T))^2} \tag{16}$$

where the sensitivity coefficients for the resistance, the external towing force and thrust are calculated as:

$$\frac{\partial t}{\partial R_C} = -1/T \tag{17}$$

$$\frac{\partial t}{\partial F_D} = 1/T \tag{18}$$

$$\frac{\partial t}{\partial T} = (F_D - R_C)(-1/T^2) \tag{19}$$

Similarly, the precision limit of the thrust deduction factor is calculated using the sensitivity coefficients and the precision limits of the T, F_D and R_C estimations:

$$P(t) = \sqrt{(\frac{\partial t}{\partial R_C} P(R_C))^2 + (\frac{\partial t}{\partial F_D} P(F_D))^2 + (\frac{\partial t}{\partial T} P(T))^2} \tag{20}$$

This leads to the total uncertainty of the thrust deduction factor, being:

$$U(t) = \sqrt{B^2(t) + P^2(t)} \tag{21}$$

3. Case Study

This uncertainty analysis aims to estimate the total uncertainty associated with the measurements of the model speed and the input variables required to calculate the thrust deduction factor. The results will be compared with the speed benchmark provided by the standard BS ISO 15016, *BSI (2015)*, and ITTC guidelines for assessing the speed and power performance during sea trials, *ITTC (2024)*.

The self-propulsion test was performed at the Newcastle University Hydrolab and followed the so-called "British Method" which consists of applying an external force to the model, F_D, to compensate for the difference in skin friction coefficients between the model and the full-scale ship. At the same time, it will ensure that the correct propeller loads are achieved during the self-propulsion test, *Bertram (2004)*. However, in our study, the estimated skin friction correction force was used only as a numerical aid for the graphical estimation of the ship's self-propulsion point not for achieving the model's self-propelled equilibrium.

3.1. The Newcastle University Towing Tank

The self-propulsion test was conducted in Newcastle University's towing tank, shown in Fig.2, a teaching facility primarily designed for conducting resistance tests. The towing tank capabilities together with the conditions of the repeated tests for the self-propulsion experiment in calm water conditions are presented in Table I.

Table I: Specification of Newcastle University Towing Tank and Conditions of the Repeat Test

Descriptions	**Units**	**Values**
Length x Width	(m)	37 x 3.7
Water Depth	(m)	1.25
Maximum Carriage Velocity	(m/s)	3.0
Capacity of Load Cell	(N)	50
Gifford Load Cell Precision	(N)	±2.5
R31 Dynamometer Rated Thrust	(N)	±100
R31 Dynamometer Thrust Non-linearity	(%F.S.)	0.15
R31 Dynamometer Rated Torque	(Nm)	±4
R31 Dynamometer Torque Non-linearity	(%F.S.)	0.15
Water Temperature	(deg. C)	14.5
Thermometer resolution	(deg. C)	0.4
Number of Repeat Tests	(-)	15
Samples Interval for Each Test	(s)	0.00062
Total Number of Samples for Each Test	(-)	28655

Fig.2: The Newcastle University's Towing Tank

During the tests, the measurement instruments are powered by a set of Y24-12 YUASA valve-regulated lead acid batteries installed on the carriage unit.

A bare hull resistance test was conducted to obtain the model form factor and the total resistance curve corresponding to the model speeds.

3.2. The Self-Propulsion Unit

The self-propulsion unit, consisting of an electrical motor, flexible shaft and dynamometer, was commissioned from HR Wallingford together with a standard 1.5 m long glass-reinforced plastic (GRP) educational model, which is a generic representation of an offshore support/trawler ship with an approximate overall length of 30 m. This ensures the availability of a wide range of engine types for the full-scale ship. The ship's main particulars are indicated in Table II.

Table II: Ship Main Particulars

Main Particulars	**Unit**	**Full Scale**	**Model Scale**
Scale Factor	(-)	20	
Length Overall	(m)	30.00	1.500
Breadth Moulded	(m)	6.80	0.340
Depth Moulded	(m)	6.92	0.346
Draft	(m)	3.20	0.160
Length Waterline	(m)	28.74	1.437
Volume of Displacement	(m^3)	392.00	0.049
Wetted Surface Area	(m^2)	304.80	0.762
Estimated Design Speed	(knots)/(m/s)	7.00	0.800

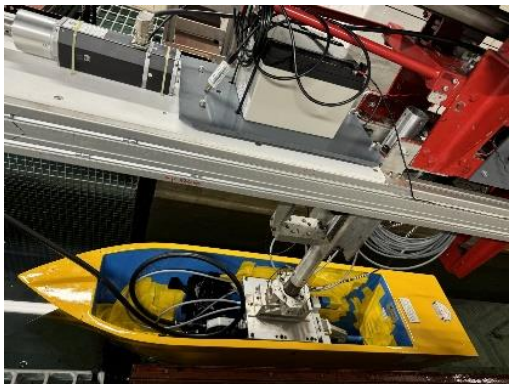

Fig.3: Model and Self-Propulsion Unit Portside View

Fig.4: Model and Self-Propulsion Unit Aft View

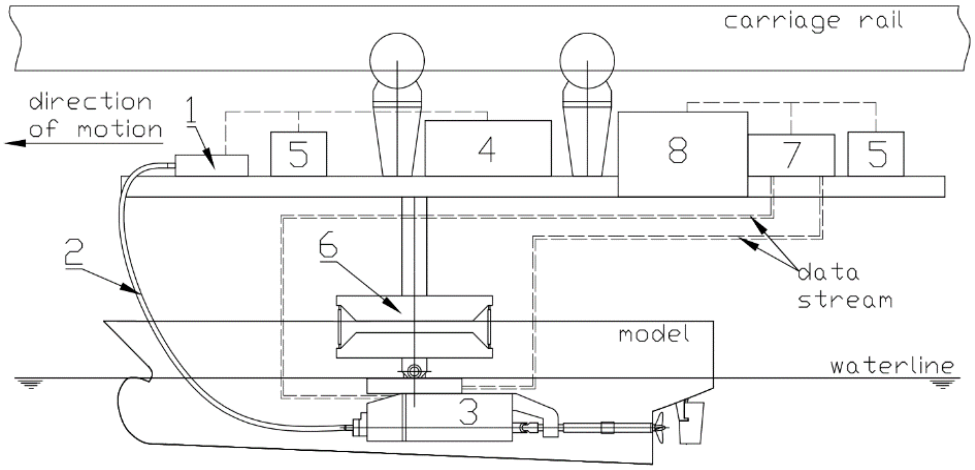

Fig.5: Experimental Set-Up for the Self-Propulsion Test

As a testing apparatus, this self-propulsion model ship will be used for teaching and research at Newcastle University.

For the self-propulsion test, the model was fitted with a stern tube, propeller shaft, mounting brackets for the R31-01 type self-propulsion dynamometer, and a towing point for its connection to the towing platform. The model was set up for the resistance test with the motor installed on the carriage and the dynamometer installed on the model. The propeller rotational speed is transmitted from the motor to the dynamometer through a flexible shaft as illustrated in Figs.3 and 4. The tests were conducted using a three-blade brass model propeller of 75 mm diameter. It was estimated, from the propeller model expanded area ratio, the pitch ratio and measuring its rake angle, as being a Wageningen B series, B3.50. The propeller and dynamometer were not fitted on the ship model for the resistance tests. An equipment list is given in Table III and the diagrammatic representation is in Fig.5.

Table III: The Equipment List Used for the Self-Propulsion Test

ID	Equipment Description
1	Electrical Motor
2	Flexible Shaft
3	R31-01 Dynamometer
4	Electrical Motor Switch
5	Y24-12 YUASA Battery
6	Gifford Load Cell
7	Data Acquisition Unit
8	Laptop with LabVIEW software

4. Preliminary Results and Discussions

4.1. The Model Speed Total Uncertainty

The total uncertainty associated with the measurements of the model speed was calculated through the law of propagation of uncertainty using the bias of the model speed linear regression of the carriage motor rotational speed and the precision limit calculated based on the multiple test runs conducted during the propulsion test. This is presented in Table IV.

The relationship between the mean model speeds achieved during two complete resistance tests and carriage motor rotational speed is shown in Fig.6. The value of the bias limit associated with the linear regression, with a 95% confidence level, is represented by a band about the curve fit with a range of ±2*SEE*. The relationship between the desired model speeds and carriage motor rotational speed, based on the existing table, is illustrated in Fig.7.

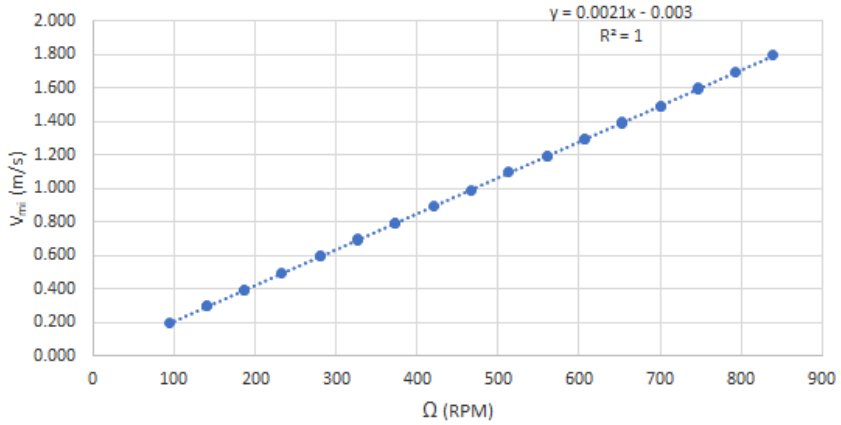

Fig.6: Model Speed - Experimental Linear Regression

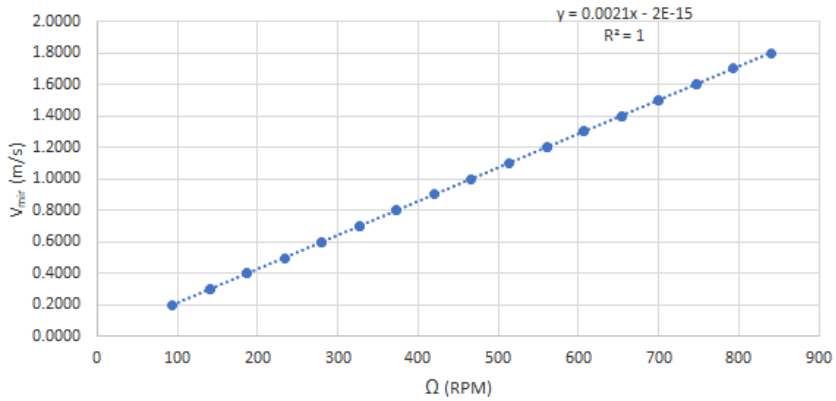

Fig.7: Model Speed – Facility's Linear Regression

The bias and precision limit values obtained were used for the estimation of the model speed total uncertainty and their percentage contributions are illustrated in Table IV.

Table IV: The Model Speed Uncertainty Analysis Outcomes

V_s (m/s)	3.57
V_m (m/s)	0.798
B_V (m/s)	0.012
B_V (%) of U_V(S)	95.96%
B_V (%) of U_V(M)	99.72%
P_V (S)(m/s)	0.0025
P_V (S) (%) of U_V(S)	4.04%
P_V (M) (m/s)	0.0006
P_V (M) (%) of U_V(M)	0.28%
U_V (S)(m/s)	0.012
U_V (S) (%) of V_m (m/s)	1.55%
U_V (M) (m/s)	0.012
U_V (M) (%) of V_m (m/s)	1.52%
U_V (S)(kts)	0.107

The results show that the total uncertainty is marginally greater than 1.5% when expressed relative to the mean model speed of 0.798 m/s. The bias limit from the curve fitting significantly contributes toward the total uncertainty for single and multiple runs. For the extrapolation to the full-scale ship, applying the Froude similarity and returning to absolute numbers, the obtained total uncertainty value is 0.107 knots which satisfies ISO's requirements for ship speed predictions, *BSI (2015)*. Automated means of selecting the carriage motor rotational speed and increasing the accuracy of the analogue to digital conversion may improve the accuracy of the ship speed predictions.

4.2. The Thrust Deduction Factor Total Uncertainty

For obtaining the total uncertainty associated with the thrust deduction factor we first estimate the bias and precision limits for the input variables: thrust T, applied towing force F_D and the corrected resistance R_C. The identification of the significant sources of uncertainties was conducted following the *ITTC (2017)* example for the propulsion test and the guide for experimental hydrodynamics, *ITTC (2016b)*. As we conducted an end-to-end calibration for the Gifford load cell and the propulsion dynamometer, the bias limit due to the data acquisition is accounted for by the bias of the curve fit, hence only two sources of uncertainty were investigated: the bias arising from the tolerance of the calibration weights and the bias of the curve fit.

Table V contains the baseline values of the accuracy for the input variables. They were calculated for Newcastle University's instruments used in the self-propulsion test by following the *ITTC (2021)* recommendation for the instrument's accuracy relative to their maximum capacity and the Newcastle University Hydrolab technician's expertise in obtaining a confidence interval for the measured values utilizing 10% of the instruments' maximum capacity.

Table V: The Baseline Values of the Accuracy for the Input Variables

Source	**Resistance [N]**	**Thrust [N]**	**Torque [Nm]**	**Model Speed [m/s]**
ITTC - 7.5-02-03-02.1 (ITTC, 2021)	0.1	0.2	0.008	-
Newcastle University Hydrolab_min. values	5	5	0.4	0.02
Newcastle University Hydrolab_max. values	45	45	3.6	3

4.3. The Input Variables Bias Limit

Following the in-house procedure, the propulsion dynamometer and Gifford load cell were calibrated in the Newcastle University Hydrolab. The calibration intervals were selected based on the estimated values for the input variables during the resistance and the self-propulsion tests. Therefore, for the positive thrust, the available weights allowed a 3.51 N to 18.51 N calibration range in increments of 5 N. In the case of positive torque calibration, we covered a range between 0 Nm and 1 Nm in increments of 0.5 Nm and for the resistance calibration, the full range of the Gifford load cell was investigated based on the existing curve fit in the data acquisition system. Figs.8 to 11 illustrate the standard uncertainty components for the positive thrust/torque calibration bias limits; the calibration weights accuracy, B_{std} and the curve fitting, B_{cf}.

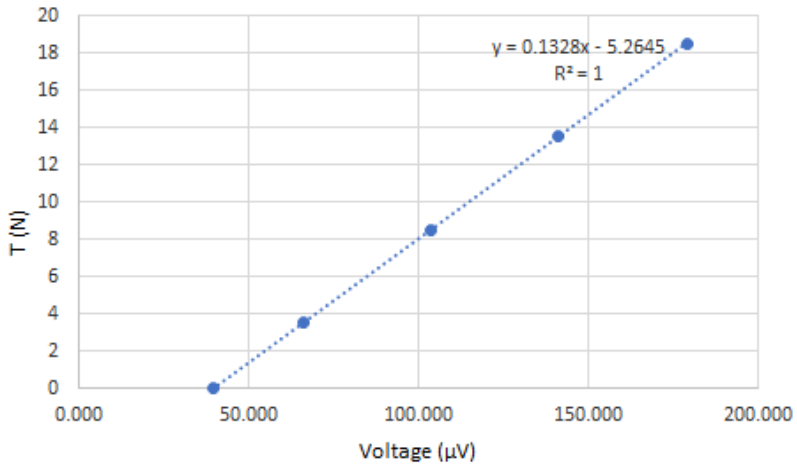

Fig.8: Positive Thrust - Bias Limit from Curve Fitting, B_{cfT}

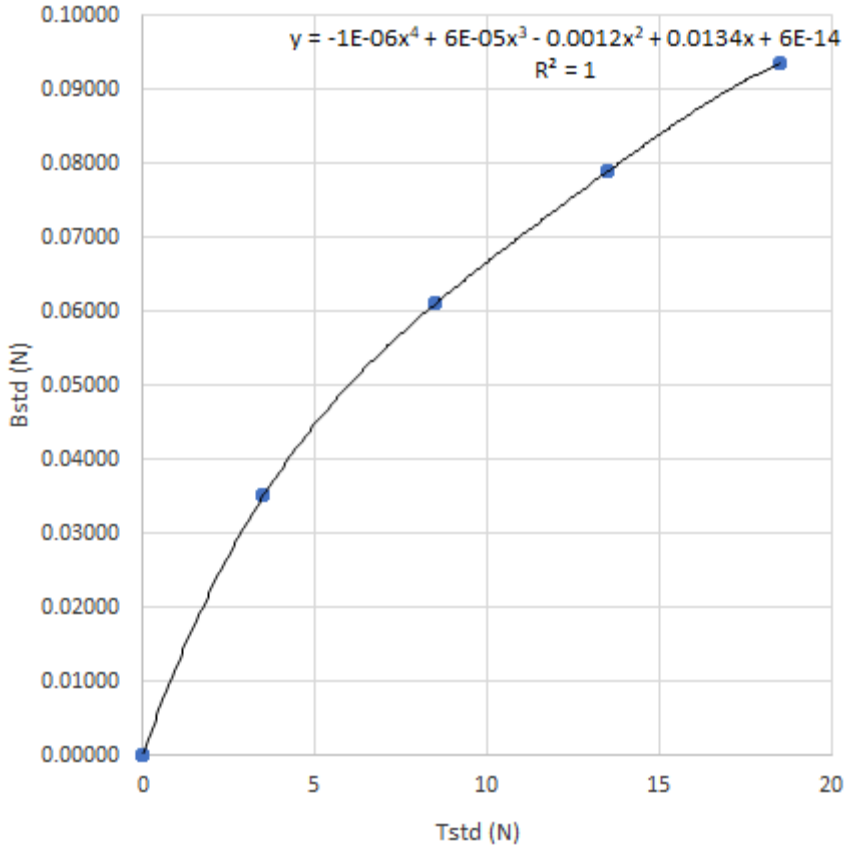

Fig.9: Positive Thrust - Bias Limit from Weights, B_{stdT}

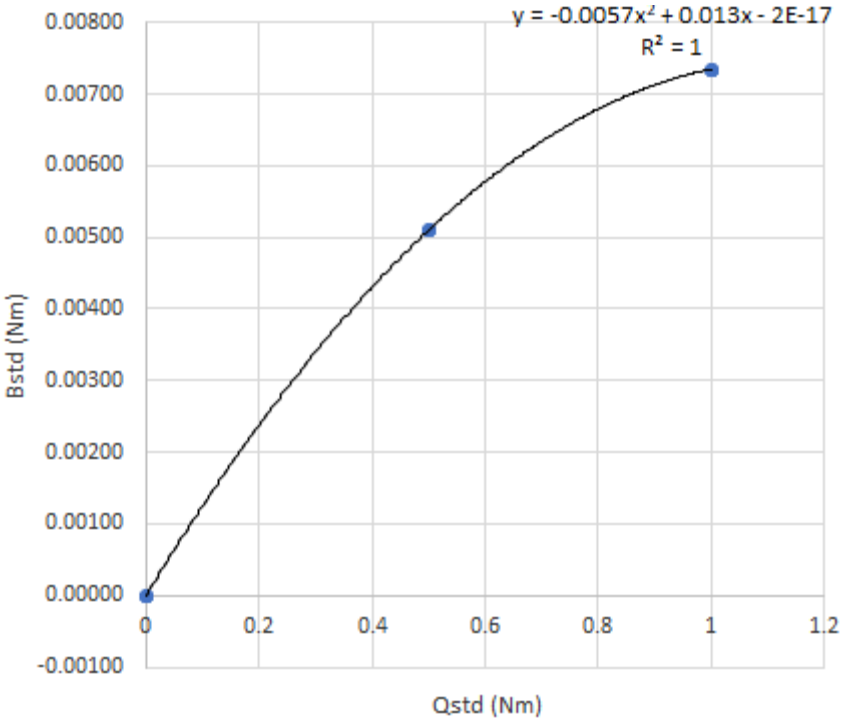

Fig.10: Positive Torque (clockwise rotation) - Bias Limit from Weights, B_{stdQ}

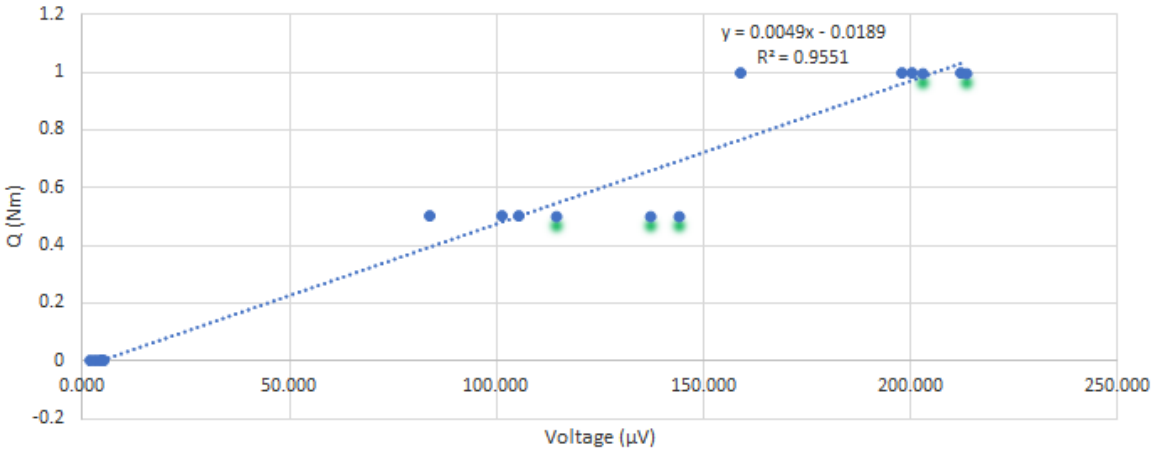

Fig.11: Positive Torque (clockwise rotation) - Bias Limit from Curve Fitting, B_{cfQ}

These bias limits are classified as Type A uncertainties as they were obtained based on the statistical analysis of at least three repeated sets for the dynamometer and Gifford load cell calibration, *ITTC (2016b)*. For thrust calibration, a sample population of 81 data points was obtained and for torque calibration, the sample population was 18 data points.

The total bias limits associated with resistance, thrust and torque calibration were calculated using the RSS of the bias limit from the weights and the curve fitting based on the law of propagation of uncertainty, see Eq.(4).

From Table VI, we observe that the accuracy of the regression curve primarily influences the total thrust and torque bias limit. However, satisfactory results were obtained for the accuracy of the resistance and thrust bias limits corresponding to 0.798 m/s model speed. Improvements in the accuracy of the positive torque bias limit will be achieved if larger torque values are measured.

Table VI: The Results for the Resistance, Thrust and Torque Calibration Bias Limits

V_s (m/s)		3.57
V_m (m/s)		0.798
Corrected Resistance, R_C (N)		1.63
Measured Thrust, T (N)		1.257
Measured Torque, Q (Nm)		0.009
Corrected Resistance, R_C	B_{stdRC} (N)	0.0163
	B_{cfRC} (N)	0.0079
	B_{RC} (N)	0.0181
	% of the Measured Resistance	0.49%
Thrust, T (positive)	B_{stdT} (N)	0.0126
	B_{cfT} (N)	0.0078
	B_T (N)	0.0148
	% of the Measured Thrust	1.18%
Torque, Q (positive)	B_{stdQ} (Nm)	0.0001
	B_{cfQ} (Nm)	0.1836
	B_Q (Nm)	0.1836
	% of the Measured Torque	5%

For the model's mean speed of 0.798 m/s and based on the initial calibration outcomes, the lowest combined bias limit is estimated for the resistance as 0.018 N, with the largest being obtained for the torque as 0.18 Nm.

These obtained bias limits, which are defined as Type A uncertainties, are greater than the *ITTC (2021)* recommendations and the dynamometer thrust full-scale non-linearity of 0.15% which can be associated with a Type B uncertainty, *ITTC (2016b)*. ITTC states that "for high-quality instrumentation and in a well-controlled environment, the Type A uncertainties are usually smaller in comparison to the Type B uncertainties", *ITTC (2016b)* which does not appear to be the case for the measured parameters corresponding to the model speed of approximately 0.8 m/s. Therefore, further analysis is required for higher model speeds.

4.4. The Input Variables Precision Limit

For the determination of the input variables' precision limits, the *ITTC (2017)* recommendations were followed, and five sets of testing (A-E), each containing three consecutive runs were conducted, with the model removed and reinstalled between each set of measurements. The standard deviation obtained from the mean of 15 runs, each representing 28655 data points of the measured parameters, represented the basis for estimating their precision limit. During each run, the model speed and shaft revolutions were constant and representative of the balance point of nominal loading for the specified model speed. The Gifford load cell measured an augmented resistance representing the difference between the model's total resistance corresponding to the selected model speed and the thrust generated by the propeller. For the selected condition, the propeller-delivered thrust and torque were measured by the R31 dynamometer and the results were recorded using LabVIEW software. A summary of the processed data is presented in Table VII.

Table VII: The Summary of the Input Variables Precision Limit

Propeller Speed 14.11 [rps]	**R_C [N]**	**Thrust [N]**	**Torque [Nm]**	**Model Speed [m/s]**
Mean	0.3774	1.2566	0.0091	0.7980
Standard Deviation, σ	0.0362	0.0107	0.0004	0.0012
P(S)	0.0724	0.0215	0.0007	0.0025
P(S) (%) of Mean	19.17%	1.71%	8.16%	0.31%
P(M)	0.0187	0.0055	0.0002	0.0006
P(M) (%) of Mean	4.95%	0.44%	2.11%	0.08%

The calculated precision limit for a single run, P(S), and for multiple runs, P(M), are classified as Type A as they were also obtained based on the statistical analysis of multiple tests, *ITTC (2016b)*. From Table VII we observe that the lower precision limit is achieved for the model speed and the higher precision limit is achieved for the augmented resistance which means that the Gifford load cell provides the lower measurement accuracy. The same precision limit is associated with the corrected resistance and towing force for determining the thrust coefficient factor. Hence, their accuracy could greatly influence the accuracy of the computed thrust coefficient factor. However, their impact on the total uncertainty of the thrust coefficient factor is also dependent on the percentage contribution of the thrust coefficient factor precision limit.

The thrust precision limit is smaller than the torque precision limits indicating that the thrust measurements are more accurate and, comparing with the results obtained for the bias limits, one can affirm that thrust measurements are reliable while the torque measurements lie within the uncertainty band and the propeller needs to deliver a greater torque in order to obtain valid measurements.

The law of propagation of uncertainty is applied for the estimation of the input parameters' total uncertainty by computing the RSS of the bias and precision limits, as shown in Table VIII.

Table VIII: The Summary of the Input Variables Total Uncertainties

Propeller Speed **14.11 [rps]**	**R_C** **[N]**	**Thrust, T** **[N]**	**F_D** **[N]**	**Torque, Q** **[Nm]**	**Model Speed** **[m/s]**
Values	1.63	1.2566	0.575	0.0091	0.7980
Bias Limit, B	0.0181	0.0294	0.0028	0.1836	0.0012
B % of U(S)	5.91%	65.21%	0.15%	99.9984%	95.96%
B % of U(M)	48.5%	96.56%	2.20%	99.9999%	99.72%
P(S)	0.0724	0.0215	0.0724	0.0007	0.0025
P(S) % of U(S)	94.09%	34.79%	99.85%	0.0016%	0.31%
P(M)	0.0187	0.0055	0.0187	0.0002	0.0006
P(M) % of U(M)	51.5%	3.44%	97.80	0.0001%	0.08%
U(S)	0.0746	0.0364	0.0724	0.1836	0.0123
U(M)	0.0260	0.0299	0.0189	0.1836	0.0121
U(S) % of parameter's value	4.58%	2.89%	12.59%	2014.71%	1.55%
U(M) % of parameter's value	1.60%	2.38%	3.29%	2014.70%	1.52%

We can observe that for the model speed of 0.798 m/s, greater measurement accuracies were obtained for model speed, thrust and resistance. When multiple runs are conducted, significant improvements are observed in resistance and the towing force which in turn will improve the accuracy in the determination of the hull efficiency from the computation of the thrust deduction factor.

However, as the obtained value for torque, during this self-propulsion run, is significantly smaller than the absolute value of its total uncertainty, these run measurements should be disregarded. An investigation was conducted to identify the possible sources of error such as the calibration settings and procedure, the regression equation, the equipment installation, the friction in bearings, the geometry/ size of the propeller and the accuracy of the open-water diagram. We selected a new propeller from the Wageningen series, B4.60, to conduct new tests as it was estimated to produce a torque value greater than 0.2 Nm for an average model speed of 0.798 m/s.

Eq.(15) represents the basis for calculating the thrust deduction factor bias and precision limits. The contribution of the input parameters to the total uncertainty is quantified through their sensitivity coefficients obtained from Eqs.(17)-(19) with the total uncertainty of the thrust deduction factor estimation obtained by applying the law of propagation for uncertainty to the data reduction, see Eqs.(16), (20) and (21). The calculations were performed in Excel using *Liu (2023)* matrix example for

the open-water test uncertainty analysis. A summary of the outcomes, for the speeds of interest, is presented in Table IX.

Table IX: Total Uncertainty for the Thrust Deduction Factor

V_s (m/s)	3.57
V_m (m/s)	0.798
Thrust Deduction Factor, t	0.1604
B(t)	0.0245
B(t) (% of U(t)(S))	8%
B(t) (% of U(t)(M))	57%
P(t)(S)	0.0827
P(t)(S) (% of U(t)(S))	92%
P(t)(M)	0.0213
P(t)(M) (% of U(t)(M))	43%
U(t)(S)	0.0862
U(t)(M)	0.0325
U(t)(S) (% of t)	54%
U(t)(M) (% of t)	20%

For single runs, the total uncertainty represents 54% of the computed thrust deduction factor with the precision limit being the most significant source of uncertainty. Significant improvements in accuracy were achieved for multiple runs which represents a good strategy to be implemented as *Forgach (2002)* adopted for their self-propulsion experiments and uncertainty analysis.

In the case of multiple runs, the total uncertainty level is reduced considerably but with the bias limit representing the most significant source of uncertainty with almost 60% contribution towards the total uncertainty. This bias limit is the combined result of the curve fitting from the instruments' calibration. With the dynamometer's manufacturer data indicating it as an accurate instrument, improvements in this direction should aim to balance the trade-offs between the in-house calibration rig and optimisation of procedures and the more expensive calibration fees required by a specialised laboratory.

5. Conclusion

This study presents the uncertainty analysis methodology associated with the self-propulsion tests conducted at the Newcastle University Hydrolab. It provided valuable insights into the importance of integrating uncertainty analysis at the experiment design stage and highlighted the influence of the calibration equipment and procedures on the test outcomes. In addition, it indicated that performing multiple runs could improve the overall accuracy of the results.

The higher accuracy was obtained for the measurement of the model speed with its extrapolation to the full-scale ship satisfying the ISO requirements for ship speed predictions.

The bias and precision limits analysis results were satisfactory for the resistance force and thrust parameters which are essential in the thrust deduction factor calculation. The outcomes indicated that accuracy will significantly improve when multiple runs are conducted and consequently, an accurate estimation of the hull efficiency and emission reductions could be obtained from the ship design optimisation.

The uncertainty levels obtained for the input variables and the thrust deduction factor, based on ITTC's guidelines for self-propulsion test uncertainty analysis, are specific to the Newcastle University facility, at the time of this paper's publication and further work is planned for increasing the accuracy of the results. Using the same propulsion unit configuration, the work will continue to determine the total uncertainty associated with the wake fraction and the relative rotative efficiency to ensure a comprehensive insight into the accuracy of the propulsion parameters required for the ship design

optimisation and its impact on greenhouse gas emission reduction. This will add transparency to the effectiveness of the proposed optimisation.

Acknowledgments

We thank the Engineering and Physical Science Research Council of the United Kingdom for funding this study as part of the main author's PhD (Grant no. EP/W524700/1). The authors thank Newcastle University for its support and the Willis Fund for the monetary contribution in purchasing the self-propulsion unit. This study was also supported by the UK National Clean Maritime Research Hub, funded by the UK Department for Transport (DfT) and Engineering and Physical Sciences Research Council (EPSRC) (Grant no. EP/Y024605/1). The authors gratefully acknowledge advice and support from all members of the Marine Hydrodynamic Team of Newcastle University, in particular, Ian Howard-Row for his professionalism and patience.

References

BERTRAM, V. (2004), Practical ship hydrodynamics, Butterworth-Heinemann

DALHEIM, Ø.Ø.; STEEN, S. (2021), *Uncertainty in the real-time estimation of ship speed through water*, Ocean Eng. 235

FORGACH, K.M. (2002), *Measurement Uncertainty Analysis of Ship Model Resistance and Self Propulsion Tests*, NSWC-CD, https://apps.dtic.mil/sti/tr/pdf/ADA409338.pdf

IMO (2023), *Revised GHG reduction strategy for global shipping adopted*, Int. Mar. Org., London, https://www.imo.org/en/MediaCentre/PressBriefings/pages/Revised-GHG-reduction-strategy-for-global-shipping-adopted-.aspx

ITTC (2016a), *7.5-02-01-01 ITTC - Recommended Procedures and Guidelines, Guide to the Expression of Uncertainty in Experimental Hydrodynamics*, Int. Towing Tank Conf.

ITTC (2016b), *7.5-02-01-01 ITTC-Recommended Procedures and Guidelines, Guide to the Expression of Uncertainty in Experimental Hydrodynamics*, Int. Towing Tank Conf.

ITTC (2017), *7.5-02-03-01.2 ITTC - Recommended Procedures and Guidelines, Uncertainty Analysis, Example for Propulsion Test*, Int. Towing Tank Conf.

ITTC (2021), *7.5-02-03-02.1 ITTC-Recommended Procedures and Guidelines, Open Water Test*, Int. Towing Tank Conf.

ITTC (2024), *7.5-04-01-01.1 ITTC - Recommended Procedures and Guidelines, Preparation, Conduct and Analysis of Speed/Power Trials, Process Control*, Int. Towing Tank Conf.

LIU, P. (2023), *MAR8069 Advanced Naval Architecture - Part 1*, Marine Engineering Course, Newcastle University

SOGIHARA, N.; TSUJIMOTO, M.; FUKASAWA, R.; HAMADA, T. (2020), *Uncertainty analysis for measurement of added resistance in short regular waves: Its application and evaluation*, Ocean Eng. 216

BSI (2015), *BS ISO 15016:2015 Ships and marine technology-Guidelines for the assessment of speed and power performance by analysis of speed trial data*, The British Standards Institution

BSI (2016), *ISO 19030-1:2016 Ships and marine technology. Measurement of changes in hull and propeller performance. General principles*, The British Standards Institution

WU, B.; JI, S.; WANG, W. (2015), *Uncertainty Analysis for Ship Powering Performance Prediction Based on Model Tests*, SNAME Maritime Conv., Providence, http://onepetro.org/snamewmtc/proceedings-pdf/WMTC15/1-WMTC15/D011S003R012/2509920/sname-wmtc-2015-122.pdf/1

Big Data, Little Effort Analysis of Paint and Fouling at Sea

Rune Freyer, Shipshave, Stavanger/Norway, rune.freyer@shipshave.no
Masaki Katafuchi, Shipshave, Stavanger/Norway

Abstract

Hull performance is analyzed with corrected fuel consumption. Or it is estimated by subjective picture analysis from ROVs. A new sensor and software directly measure the hydraulic properties of paint and fouling during transit. By using big data and computer analysis it can answer questions like: Is premium paint worth the added cost in the real world? How do I optimize the cleaning operation? How frequent shall I groom? Shall we spot blast the hull in DD?

1. Introduction

Hull grooming is employed frequently as a proactive maintenance strategy to reduce hull resistance and maintain vessel efficiency. One promising approach is in-transit grooming, where the hull is cleaned while the vessel is underway. The primary motivations for this method include continuous cleaning without disrupting transport schedules, eliminating reliance on third-party suppliers and port authorities, and ensuring gentle interaction with the paint.

Traditionally, hull efficiency has been estimated using indirect methods such as fuel efficiency analysis, video documentation of cleaning operations or inspections with remotely operated vehicles. However, these approaches often suffer from limitations, including low measurement accuracy, inconsistent data collection, insufficient sample sizes for robust statistical analysis, and high operational costs. In contrast, modern industrial processes routinely utilize high-precision measurements and large datasets to optimize performance. Given its significant impact on fuel consumption and environmental performance, hull roughness deserves similarly advanced measurement methodologies.

Recent advancements in inspection and grooming technologies have introduced new possibilities to record high-resolution videos during grooming operations. A new system that measures hull roughness while simultaneously recording videos and performing grooming is now in its semi-commercial stage.

2. The use and analysis of In Transit hull cleaning

In transit hull cleaning was introduced in 2020 for cleaning a hull while operating at ship speeds between 10 and 14knots. The aim is to always keep a clean hull rather than to wait for degrading hull performance. The tools are carried by the ship and operated by the crews. As it is operated offshore, it does not require port permits. A cleaning operation can be performed within hours but depending on ship size and fouling level. The system was first intended for slime, but further R&D has allowed removal of heavy fouling as well, including barnacles. This was exemplified in a study by DNV on two large container vessels that showed fuel savings of 5 and 16%, *Hollenbach (2024)*. The system today is used on container, bulk and tank vessels from 128m to 400m length and with fouling release and self-polishing paints.

A survey conducted at HullPIC 2019, *Schmode et al. (2019),* established that inadequate measurement and analysis was the biggest challenge in hull performance. The ITCH system has been independently proven with indirect analysis methods (traditional fuel efficiency derived analysis), but such analysis can be expensive. Gaining confidence in quality analysis can take years from the first cleaning till the analysis is ready. With FuelEU efficiency penalties being introduced, *EU (2023),* and others in the pipeline, the industry hardly have the time to wait.

Qualitative evaluation is done by watching fouling removal videos that is captured during cleaning operations. At daytime offshore, the water is clear and video quality good. The fouling plumes are immediately carried away and never obstruct the view. The video can be combined with areal coverage plots to get a good impression. The method is however not quantitative, and for hours of watching, some may find an old “Die hard” movie more entertaining.

2.1. Why is roughness measurement important?

Loss of fuel efficiency is a symptom of increasing hull roughness and is the current state of the art in hull efficiency monitoring. However, by measuring the roughness you get hard data, and you can action it by cleaning the hull. Surface roughness is a part of fluid viscous flow equations. If you can’t determine the roughness, you cannot calculate the losses. In shipping we try to derive the roughness from fuel consumption. But weather, waves, current, wind, engine condition, air temperature, water temperature, propeller, trim and loading also play in. Most calculations assume that fouling and paint wear is equally distributed between boot top and bilge, but we know that is not true. The division into paint roughness and hydraulic roughness is also important because it separates effects that can be affected by hull cleaning and effects needing sand blasting of the hull.

2.2. Why measure roughness in the water?

Fouling has organic matter, but mainly consists of water and is “fluffy”. Once fouling gets in dry dock, most of the volume is lost and therefore the hull performance information of a roughness measurement is lost.

2.3. Why measure fouling roughness In-Transit?

Fouling, in particular fibrous fouling has very different volume when the ship is still vs in speed. In speed, it will flow along the hull side and that is what determines resistance in the water. If green grass fouling extends 50 mm from the hull when still, it may not extend more than 3 mm in transit or 0.2 mm in dock.

Biofouling documentation will be increasingly stringent with demands on frequent monitoring for port access. To maintain revenue generation, inspection during transit generates more profits than during standstill.

2.4. Why do we need “big data”?

Traditional roughness measurements are made on hulls with handheld sensors in dry dock. These measurements may be taken with 10s of max hundreds of measurements. Locations will be in accessible locations on the hull. Reliable roughness estimates require thousands or tens of thousands of measurements. The methodology involves measuring the surface before and after cleaning. Immediately repeating such a survey means that the “after” cleaning roughness measure an identical hull condition on the next survey.

2.5. Why does it matter where the fouling is on a hull?

Selection of paint is inaccurate science with cost impact for dock works and fuel consumption. Different hulls in the same trade may be painted with the same paints but experience different results. But this may be because of biological reasons, not the paint. One ship painted with different paints will undergo nearly the same biological conditions. Painting a ship with 4 different paints and locating and measuring the resulting roughness in different depths in a 1-month cycle is possible. One may also analyze where the roughness is. How far up on the bottom do you see fouling? This can even determine if different paints can be used in different parts of the hull. Hull roughness maps can be used as a part of the biofouling management documentation towards port authorities. This can automate the documentation for the crew.

2.6. Why can paint roughness be of value be for planning paint work?

Some paint suppliers for fouling release coatings (FRC) claim fuel efficiency benefits with less paint roughness degradation than others. Others argue that these FRC paints are more fragile. Having roughness measurement on the hull can develop hard numbers on how this acts on my trade pattern. Can big data back it up? And can you quantify the benefits of a premium paint beyond a premium cost? By knowing the condition of the paint on before a dry dock, you get better basis for decision on whether blasting the hull or just a spot blasting the boot top.

2.7 How is roughness measured?

The ITCH-Performance robot measures hull roughness using optical methods. By applying image processing techniques, the ITCH-P robot can measure both hydrodynamic surface roughness and hard-surface roughness. This method provides high-resolution, non-contact measurements that are effective even in underwater environments. While the hard-surface roughness measurements have been tested and validated, the hydrodynamic surface roughness measurements require further verification and validation to ensure their accuracy and reliability.

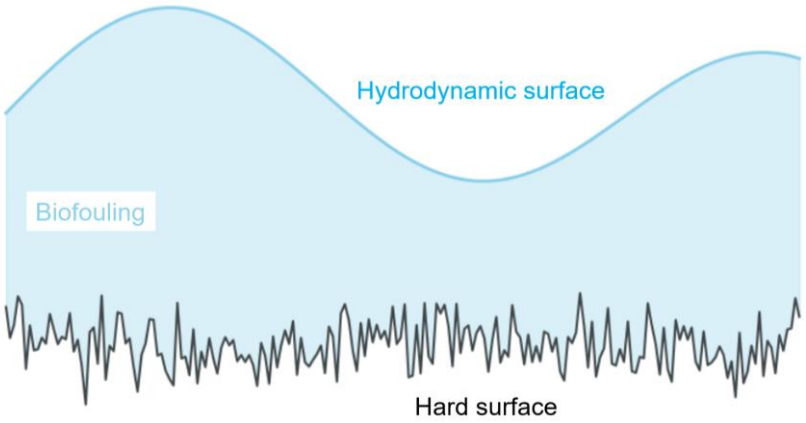

Fig.1: Schematic representation of hydrodynamic and hard-surface roughness. The hydrodynamic surface is influenced by biofouling such as slime, which alters the fluid flow profile, while the hard surface represents the inherent texture of the hull material. The ITCH-Performance robot measures both layers to provide comprehensive roughness data.

3. Case studies

3.1. Single Deployment Analysis

In this section, we focus on a single deployment of the ITCH-Performance (ITCH-P) robot to evaluate the changes in hull roughness before and after a cleaning operation. On the starboard side of a Chemical Tanker with a length of 145 m, cleaning was conducted several times using another ITCH system prior to the deployment of ITCH-P. The ITCH-P robot was deployed after these cleaning operations to assess residual roughness. During this deployment, the ITCH-P recorded 78,739 data points.

ITCH-P does not perform data processing while underwater. Instead, video files captured during deployments are processed post-operation using a designated application once ITCH-P is connected to a laptop. This post-processing enables users to obtain detailed roughness measurements.

To evaluate the changes in hull roughness resulting from the cleaning operation, measurements from the ITCH-P deployment were analyzed. Each ITCH-P deployment included a bow-to-aft movement followed by an aft-to-bow movement. Roughness values recorded during the bow-to-aft movement represented the hull condition before cleaning, while values from the aft-to-bow movement reflected

the post-cleaning condition. Depth sensor readings and the frequencies of the winch spooling the rope connected to ITCH-P were employed to estimate the robot's position throughout both movements. However, the estimation of the horizontal position is yet insufficiently accurate to allocate repeatedly to the resolution of the graphics. Specifically, data such as the spooled rope length, rope tension, and their timestamps were lacking, which constrained the accuracy of the positional estimates. The estimated path of the ITCH-P robot is presented in Fig.2.

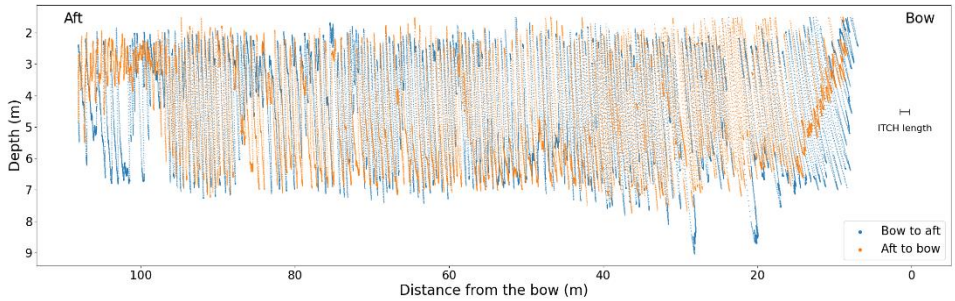

Fig.2: Paths of the ITCH-Performance robot during the cleaning operations on the starboard side. The blue path represents the bow-to-aft movement, while the orange path indicates the aft-to-bow movement during the deployment. Depth readings and winch speed were used to track the robot's position.

The processed roughness data were synchronized with depth sensor readings using timestamps. Figs.3 and 4 illustrate the differences in hull roughness, before and after the cleaning operation, represented by Rt_{25}, mapped to corresponding sections of the hull, each measuring 10 m in length and 1 m in depth.

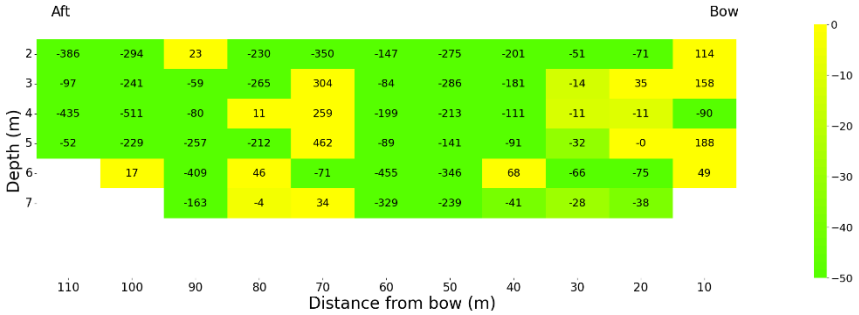

Fig.3: Difference in hydrodynamic roughness (Rt_{25}) mapped to hull sections after the cleaning operation. The color gradient represents the reduction in roughness, indicating effective removal of transparent biofouling.

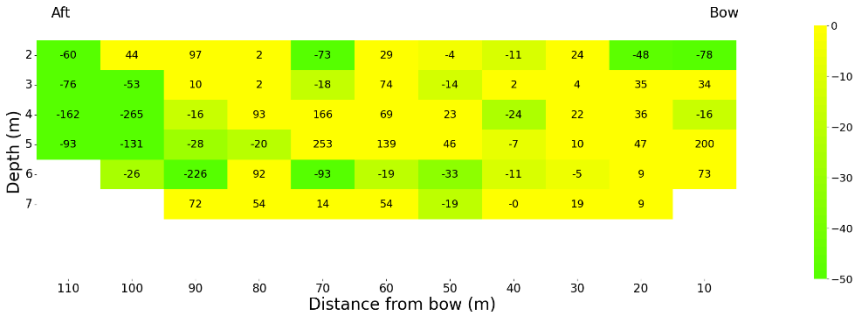

Fig.4: Difference in hard-surface roughness (Rt_{25}) mapped to hull sections after the cleaning operation. The random variations suggest minimal impact on hard-surface materials such as paint and metal.

Fig.3 demonstrates improvements in hydrodynamic roughness, while Fig.4 highlights the variations in hard-surface roughness. These results suggest that the ITCH system effectively reduces hydrodynamic

roughness by removing transparent biofouling, such as slime, without significantly affecting hard-surface materials, including paint, metal surfaces, and barnacles. Note that these figures may also bear inaccuracies due to limitations in estimating the horizontal position of the ITCH-P robot, as mentioned in the previous paragraph.

Fig.5 provides a comparative analysis of average hydrodynamic and hard-surface roughness before and after the cleaning operation, illustrating the substantial reduction in hydrodynamic roughness achieved, while hard-surface roughness remains largely unchanged.

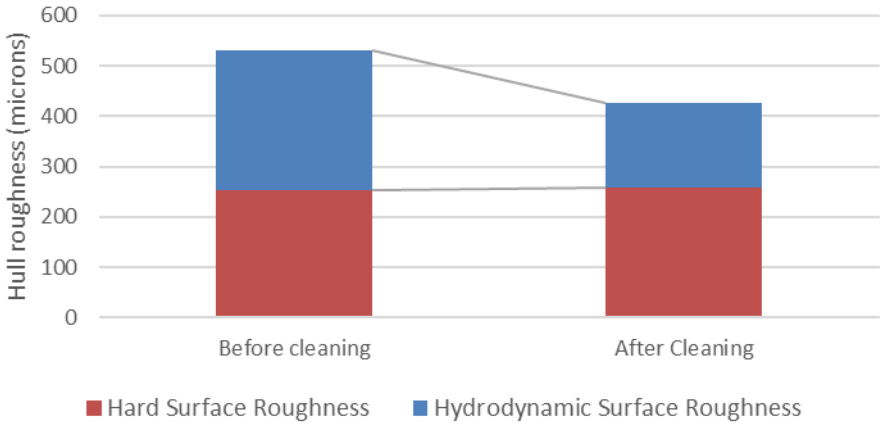

Fig.5: Comparison of average hydrodynamic and hard-surface roughness before and after the cleaning operation. The stacked bar chart shows reduction in hydrodynamic roughness, while hard-surface roughness remains largely unchanged. The 0-point estimation for hydraulic roughness lacks accuracy.

3.2. Transition of Hull Roughness Over Multiple Deployments

This section examines the transition of hull roughness over multiple deployments of the ITCH-Performance (ITCH-P) robot as a part of a test operation. Cleaning tests were conducted five times on the starboard side of a Capesize bulk carrier, with ITCH-P utilized in the first and fourth operations. During these deployments, ITCH-P made roughness measurements, with 130,600 and 113,552 data points processed for the first and fourth operations, respectively.

ITCH-P does not perform data processing while underwater and files captured during deployments were processed post-operation using a designated application once ITCH-P was connected to a laptop. This post-processing enabled users to obtain detailed roughness measurements.

To evaluate the changes in hull roughness resulting from the cleaning operations, measurements from the first and fourth deployments were compared. Specifically, data from the first half of the first operation (bow-to-aft direction) and the second half of the fourth operation (aft-to-bow direction) were analyzed. Depth sensor readings were employed to estimate ITCH-P's position throughout the cleaning process. Fig.6 shows the estimated paths of the ITCH-P robot during the of the above-mentioned operations.

The processed roughness data were synchronized with depth sensor readings using timestamps. Figs.7 and 8 illustrate the mean hull roughness, represented by Rt_{25}, at each depth section before and after the cleaning operations, along with the differences between them. While Fig.7 demonstrates improvements in hydrodynamic roughness at each depth, Fig.8 reveals random variations in hard-surface roughness. These results suggest that the ITCH system effectively reduces hydrodynamic roughness by removing transparent biofouling, such as slime, from the hull without significantly affecting hard-surface materials, including paint, metal surfaces, and barnacles.

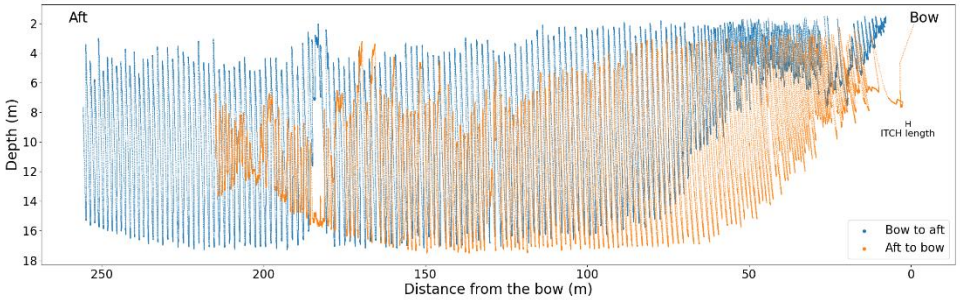

Fig.6: Paths of the ITCH-Performance robot during the first and fourth cleaning operations on the starboard side. The blue path represents the bow-to-aft movement during the first deployment, while the orange path indicates the aft-to-bow movement during the fourth deployment. Depth readings were used to track the robot's position.

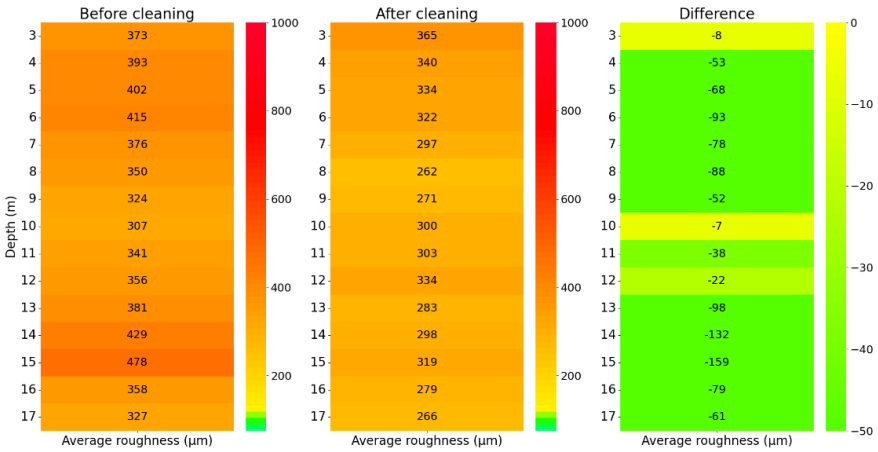

Fig.7: Mean hydrodynamic roughness (Rt_{25}) at varying depths before and after cleaning operations. The left and middle panels show roughness values before and after cleaning, respectively, while the right panel illustrates the reduction in roughness. Decreases in roughness indicate removal of slime and other transparent biofouling.

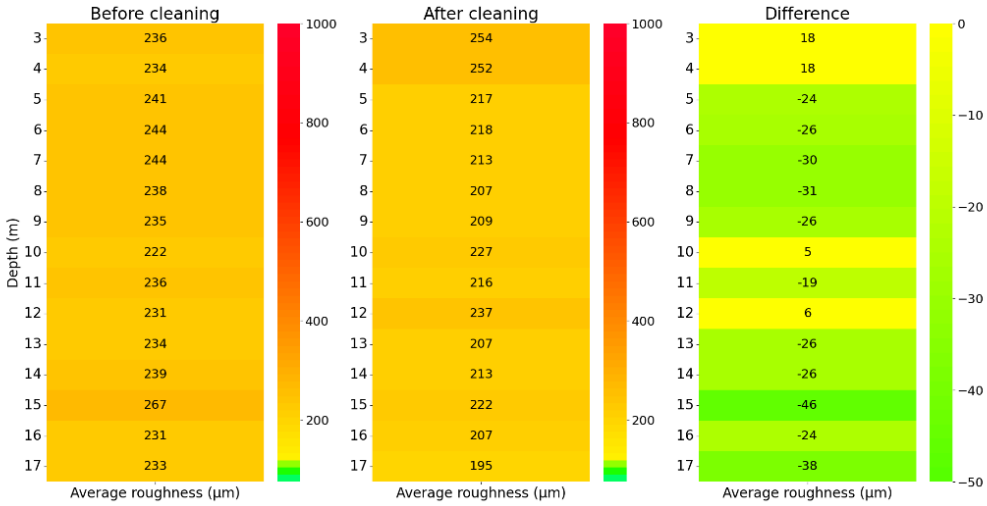

Fig.8: Average hard-surface roughness (Rt_{25}) at varying depths before and after cleaning operations. The left and middle panels show roughness values before and after cleaning, respectively, while the right panel illustrates the differences. The random variations suggest minimal impact on hard-surface materials such as paint and metal. The graphics are more consistent when averaged over vertical distribution.

By using the paths of the ITCH-P robot shown in Fig.6, the roughness values were mapped to the corresponding sections of the hull, each measuring 10 m in length and 1 m in depth. The mean roughness values were averaged within each section, and the overall average hull roughness was calculated using sections covered by both the bow-to-aft and aft-to-bow movements. The transition of roughness values is summarized in Fig.9. The figure demonstrates the successful removal of transparent fouling during the first deployment and suggests further reductions achieved through subsequent cleanings.

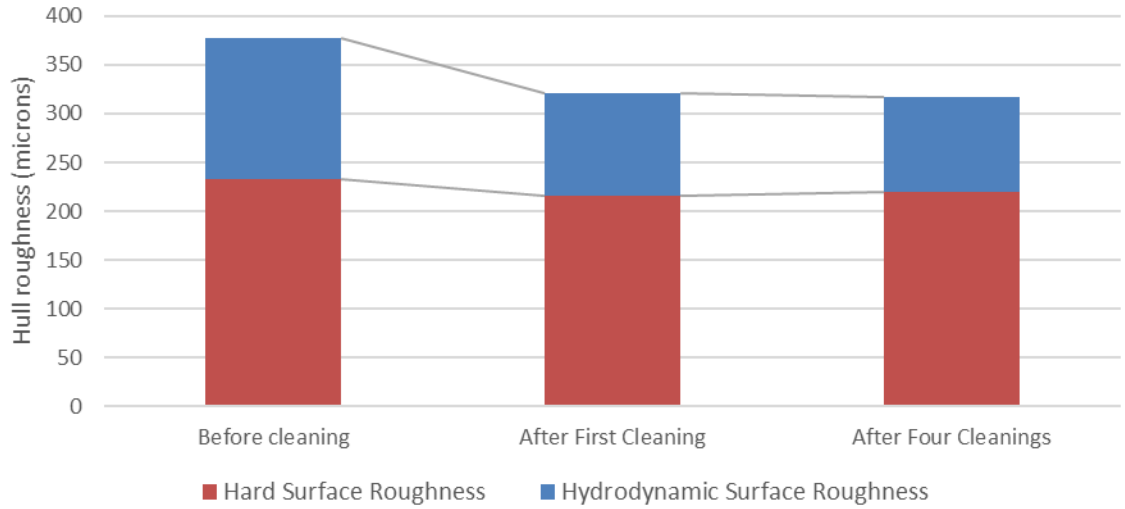

Fig.9: Average hydrodynamic and hard-surface roughness before cleaning, after the first cleaning, and after four cleaning operations. The stacked bar chart shows a significant reduction in hydrodynamic roughness following initial cleaning, while hard-surface roughness remains largely unchanged, indicating selective biofouling removal by the ITCH system. However, it also indicates an irreducible hydraulic roughness measurement bias being a focus of further studies.

4. Conclusions

This paper has presented the deployment and performance of the ITCH-Performance robot in measuring hull roughness through case studies. The analysis demonstrated the system's capability to deliver reliable roughness measurements across different hull surfaces, contributing valuable insights for hull maintenance and performance optimization.

The paper proposes paint evaluation as important. Paints are investments 2-3 orders of magnitude larger than cleanings and lasts for 5 years. Paint selection will benefit of increased quantification to enter in an AI assisted evaluation scenario

The case studies highlighted the effectiveness of the ITCH-Performance system in processing the collected data and extracting key surface parameters such as Rt and Ra for the paint. Additionally, the ITCH-Performance robot can measure significantly more points than traditional hull roughness measurement methods, providing more comprehensive surface characterization. The hydrodynamic roughness measurement (fouling roughness) will never be as accurate as the hard surface, but there is still significant potential improved accuracy.

Future work will focus on refining the measurement algorithms, particularly for hydrodynamic roughness. It will also focus on improving the position estimation of the robot during cleaning operations to make roughness comparisons more accurate and consistent. Increased use and gradual improvement of the technology will enable a technology that is reliable and accurate, not only for paint, but also fouling.

References

EU (2023), *FuelEU Maritime Regulation*, European Commission, https://transport.ec.europa.eu/transport-modes/maritime/decarbonising-maritime-transport-fueleu-maritime/questions-and-answers-regulation-eu-20231805-use-renewable-and-low-carbon-fuels-maritime-transport_en

HOLLENBACH, U. (2024), *Performance Assessment: Assessing the performance of Shipshave ITCH system at Hapag Lloyd container vessels BARZAN and CHICAGO EXPRESS*, DNV

SCHMODE, D.; HYMPENDAHL, O.; BELLUSCI, F. (2019), *Influence of Data Sources on Hull Performance Prediction*, 4th HullPIC Conf., Gubbio, pp.162-171

Operational Data-Driven Nonlinear Regression for Ship Resistance Analysis

Daehyuk Kim, Seoul National University, Seoul/Republic of Korea, daehyuk.kim@snu.ac.kr
Shin Hyung Rhee, Seoul National University, Seoul/Republic of Korea, shr@snu.ac.kr

Abstract

This study employs nonlinear regression analysis on operational data to model ship resistance under real maritime conditions. The methodology categorizes resistance into calm water, wind, wave, and current components, using theoretical models integrated with ship onboard data and weather data. Z-score filtering ensures data reliability by removing outliers. The Trust Region Reflective (TRR) algorithm minimizes the residuals between observed and predicted values. Results indicate significant impacts of wind and wave resistance on ship performance, with added resistance components validated against real-world data, providing insights for improved ship design and operational efficiency. Comprehensive data segmentation enhances model accuracy and prediction reliability.

1. Introduction

Ship resistance studies conducted in controlled environments, like towing tanks and numerical simulations, often fail to account for the complexities of real-world maritime conditions, leading to a discrepancy known as the "sea margin." This margin, accounting for 15% to 20% additional resistance, is a buffer in power calculations but does not explicitly consider diverse environmental factors such as wind, waves, and currents. Early studies have explored added resistance due to these factors. Still, they primarily rely on model test data rather than operational data, highlighting a gap in applying real-world data for accurate resistance modelling, *ITTC (2021)*.

ISO standards like ISO 15016 and ISO 19030 guide ship speed, power measurement, and hull performance maintenance but have limitations in capturing comprehensive operational data, *ISO (2002,2015,2016)*. Recent AI techniques offer potential solutions but face challenges in interpretability and validation. Integrating theoretical models with operational data, including GPS tracking and weather conditions, can bridge these gaps, providing transparent, practical, and reliable full-scale models. These models enhance research, development, and the practical operation of ships, ensuring that theoretical, experimental, and numerical techniques are effectively utilized and compared.

2. Methodology

The mathematical modeling begins with the relationship between a ship's power and resistance. EHP P_E is the power required to overcome the total resistance of the ship R_T as it moves through the water at a given speed V. It does not account for losses in the propulsion system and purely presents the power needed to propel the ship in Eq.(1).

$$P_E = R_T \times V \tag{1}$$

$$P_D = \frac{P_E}{\eta_D} \tag{2}$$

$$P_S \approx P_D \tag{3}$$

$$R_T = \frac{P_S \times \eta_D}{V} \tag{4}$$

This study categorizes the resistance into four components, as shown in Eq.(5): the calm water resistance, the added resistance due to wind, waves, and current.

$$R_T = R_{calm} + R_{wind} + R_{wave} + R_{current} \tag{5}$$

First, the calm water resistance is expressed as the product of water density ρ_w, ship speed V_G, wetted surface area S, and calm water resistance coefficient C_{calm}, as shown in Equation (6). The increase in added resistance due to hull fouling, resulting from increased frictional resistance, can be included in this component. So, the effect of hull fouling would appear as an increase in the calm water resistance coefficient. It is important to note that ship's speed V_G should be considered as SOG rather than STW.

$$R_{calm} = \frac{1}{2}\rho_w V_G^2 S C_{calm} \tag{6}$$

The added resistance due to wind is considered, which is well-defined in ISO 15016, as shown in Eq.(7). ρ_a is the air density, C_{wind} is the coefficient of added resistance due to wind, A_{XV} is the transverse projected area above the waterline including superstructures, and V_{wind} is the relative wind speed. The second term in Eq.(7) is the added resistance due to wind that occurs even when the relative wind speed is zero, caused by the headwind effect as the ship advances at speed V_G. Generally, this component is included in the total resistance of the full-scale ship during power prediction based on model tests *ITTC (2017)*. In this study, we also consider the second term as part of the calm water resistance and exclude it from the added resistance due to wind. To simplify the equation, we transformed the coefficient of added resistance due to wind at zero relative wind direction using a cosine function of the relative wind direction. Thus, the final equation for the added resistance due to wind is shown in Eq.(8).

$$R_{wind} = \frac{1}{2}\rho_a C_{wind}\left(\psi_{wind}\right) A_{XV} V_{wind}^2 - \frac{1}{2}\rho_a C_{wind}\left(0\right) A_{XV} V_G^2 \tag{7}$$

$$R_{wind} = \frac{1}{2}\rho_a A_{XV} V_{wind}^2 C_{wind}\left(0\right)\cos\left(\psi_{wind}\right) \tag{8}$$

$$A_{XV} = A_{ref} + \Delta T \times B \tag{9}$$

$$\Delta T = T_{ref} - T \tag{10}$$

$$V_{wind} = V_{wind,anemometer}\left(\frac{z_{ref}}{z_a}\right)^{1/7} \tag{11}$$

The modeling of added resistance due to waves also follows a non-dimensional approach. In the semi-empirical SNNM method, the non-dimensional transfer function for added resistance from regular waves K_{AW} can be expressed using water density, gravitational acceleration g, ship breadth B, length L, and wave height ζ_A, as shown in Eq.(12), *Wang et al. (2021).* The SNNM method defines the added resistance due to waves as the mean added resistance in regular waves and as the sum of the motion-induced component and the wave reflection-induced component. The non-dimensional transfer function defined in this study is considered to include both components. The empirical formula typically involves complex equations that consider the ship's shape parameter, draft, speed, and wave direction based on a series of data sets, *Liu and Papanikolaou (2016,2019,2020).* In this study, it is defined the transfer function as a function of only non-dimensionalized mean wave length λ / L and the mean relative wave direction ψ_{wave}. To facilitate regression using operational data and simplify the interpretation of results, it is simplified it to a 2nd order polynomial function of two variables, as shown in Eq.(13). The terms $c_{wave,00}$, $c_{wave,10}$, etc.; are the polynomial coefficients.

$$R_{wave} = 4\rho_w g \frac{B^2}{L}\zeta_A^2 K_{AW} \tag{12}$$

$$K_{AW}\left(\frac{\lambda}{L},\psi_{wave}\right)=c_{wave,00}+c_{wave,10}\left(\frac{\lambda}{L}\right)+c_{wave,01}\left(\psi_{wave}\right)+c_{wave,11}\left(\frac{\lambda}{L}\right)\left(\psi_{wave}\right)+c_{wave,20}\left(\frac{\lambda}{L}\right)^2+c_{wave,02}\left(\psi_{wave}\right)^2 \tag{13}$$

$$\lambda=\frac{gT_{wave}^2}{2\pi} \tag{14}$$

ISO 19030 applies the concept of relative water speed concerning the hull by using STW as the reference speed, *ISO (2016).* Conversely, as mentioned in the modeling of the calm water resistance, SOG is used for the reference speed of a ship in the study. Consequently, the reference speed for the added resistance due to current will be defined as the difference between the STW V_W and SOG V_G. By defining the current resistance coefficient $C_{current}$ as shown in Eq.(15) and considering the sign of the difference between STW and SOG, it can be determined the directional influence of the current. If $C_{current}^{+}$ is applied, it indicates the current is assisting by pushing the ship from behind, thereby decreasing the total resistance. Conversely, $C_{current}^{-}$ applies when the current opposes the motion by pushing against the ship from the front, thus increasing the total resistance.

$$R_{current}=\frac{1}{2}\rho_w\left(\frac{C_{current}^{+}+C_{current}^{-}}{2}+\frac{C_{current}^{+}-C_{current}^{-}}{2}sign\left(V_G-V_W\right)\right)\left(V_G-V_W\right)\left|V_G-V_W\right|S \tag{15}$$

Additionally, the sea water density can be determined using sea temperature data from onboard measurements or weather information. It can be accurately calculated the water density by referring to the ITTC sea water density table, *ITTC (2011).* The water density can be incorporated as a function, as shown in Eq.(16). Operational data typically includes the mean draft measured by draft gauges, which can be used to determine the wetted surface area and the transverse projected area. If the design values for the wetted surface area and transverse projected area are known, linear regression can create functions, as shown in Eqs.(17) and (18).

$$\rho_w=f_{\rho_w}\left(sea\ temperature\right) \tag{16}$$

$$S=f_S\left(T\right) \tag{17}$$

$$A_{XV}=f_{A_{XV}}\left(T\right) \tag{18}$$

The non-linear mathematical model for the resistance components is developed in the previous chapter. TRR algorithm is designed to handle non-linear optimization problems, making it the most appropriate and effective method for our needs, *Coleman and Li (1994).* The primary objective of TRR algorithm is to minimize the sum of the squares of the residuals, which are the differences between the observed and model-predicted values. The objective function $f\left(\mathrm{p}\right)$ is mathematically presented in Eq.(19).

$$f\left(\mathrm{p}\right)=\min_{\mathrm{p}}\sum_{i=1}^{n}r_i^2 \tag{19}$$

where r_i is the residual for the the i-th observation, and p is the coefficient vector of dimension m, which is the number of coefficients to be estimated. The residual vector r has dimension n, which is the number of observations.

One of the key features of TRR algorithm is its ability to handle bound constraints on coefficient s. In practical scenarios, certain coefficients must remain within specific limits to reflect realistic physical conditions. The bounds can be defined in Eq.(20).

$$\mathrm{p}_{\mathrm{lower}}\le\mathrm{p}\le\mathrm{p}_{\mathrm{upper}} \tag{20}$$

where p_{lower} and p_{lower} are the lower and upper bounds of the coefficient vector p.

The trust region subproblem is then solved within these bounds, ensuring that the coefficient updates do not violate the specified constraints. The trust region subproblem with bound constraints can be formulated in Eq.(21).

$$\min_{d} \|Jd + r\|^2 + \lambda d^T d \quad \text{subject to} \quad \|d\| \le \Delta \quad \text{and} \quad p_{lower} \le p + d \le p_{upper} \tag{21}$$

where λ is the Lagrange multiplier.

Operational data comes from various sources with measurement accuracies that are often difficult to verify due to the inherent uncertainty in measurement and weather data, *Aldous (2016), Alous et al. (2015)*. Even highly accurate sensors at the time of installation may not maintain that level of precision throughout their operational life. This variability makes it crucial to thoroughly review data for outliers. Outliers can significantly distort outcomes, potentially leading to a substantial decrease in model reliability. Therefore, this study employs a z-score filtering method to systematically identify and iteratively remove outliers that negatively impact our regression analysis, ensuring robust and reliable results, *Rousseeuw and Hubert (2011).*

The z-score method identifies observations that deviate significantly from the mean of the dataset. The z-score for each data point is calculated using Eq.(22).

$$Z_i = \frac{x_i - \bar{x}}{s} \tag{22}$$

where Z_i is the z-score value, x_i is the individual observation, $\bar{x}$ is the mean of the observations, and s is the standard deviation of the observations.

The threshold for determining whether an observation is an outlier based on the z-score is typically set at 1.96, corresponding to a 95% confidence interval.

- If $|Z_i| > 1.96$: The i-th observation is considered an outlier. This means that the observation deviates significantly from the mean and may have a disproportionately large effect on the estimated regression coefficients.
- If: $|Z_i| \le 1.96$: The i-th observation is not considered an outlier. These observations are deemed to have an acceptable level of deviation and are retained in the dataset.

p-value, also known as the significance probability, is used to assess the significance of estimated coefficients and determine which coefficients are statistically meaningful and should be retained in the model. The p-value in statistical hypothesis testing measures the strength of evidence against a null hypothesis. For regression analysis, the null hypothesis typically states that a particular coefficient does not affect the dependent variable, *Kennedy-Shaffer (2019), Maneejuk and Yamaka (2021), Moiseev (2017).*

- Null hypothesis (H0): The coefficient does not significantly contribute to the model.
- Alternative hypothesis (H1): The coefficient significantly contributes to the model.

A small p-value (typically ≤ 0.05) indicates strong evidence against the null hypothesis, suggesting that the coefficient is statistically significant and should be considered reliable. Conversely, a large p-value suggests weak evidence against the null hypothesis, indicating that the coefficient may not be necessary.

For regression coefficient θ_i, p-value is derived from the s-statistic, calculated in Eqs.(23) and (24).

$$t_i = \frac{\theta_i}{SE\left(\theta_i\right)} \tag{23}$$

$$p_i = 2\left(1 - F_t\left|t_i\right|\right) \tag{24}$$

where θ_i is the estimated value of the coefficient and $SE\left(\theta_i\right)$ is the standard error of the estimate. The p-value p_i is obtained from CDF of the t-distribution F_i. The factor of 2 accounts for the two-tailed nature of the test, as it is interested in deviations in both directions from the null hypothesis. Significant coefficients (p-value ≤ 0.05) will likely have a meaningful impact on the dependent variable. They are considered reliable, while insignificant coefficients (p-value > 0.05) do not significantly affect the dependent variable and may be excluded to simplify the model.

3. Subject Ships

Operational data from three ships, identically designed and constructed at the same shipyard, designated as Ships G, I, and K, are used to explore ship resistance characteristics under various service conditions.

Table I: Comprehensive specifications of the subject ships

No.	Symbol	Variable Name	Unit	Value		
				Scantling	Normal ballast	Heavy ballast
1	L_{BP}	Length Between Perpendiculars	[m]	334.00		
2	B	Breadth	[m]	62.00		
3	D	Depth	[m]	29.80		
4	L_{WL}	Length of Waterline (LWL)	[m]	339.90	323.01	327.07
5	T_F	Draft at Forward Perpendicular (FP)	[m]	21.40	10.80	14.03
6	T_A	Draft at After Perpendicular (AP)	[m]	21.40	11.30	14.03
7	T_M	Draft at midship	[m]	21.40	11.05	14.03
8	∇	Displacement	[m^3]	360,537	173,644	225,686
9	S	Wetted surface area	[m^2]	297,75	22,021	24,303
10	S_{BK}	Bilge keel area	[m^2]	127.00		
11	A_T	Transverse area above Waterline	[m^2]	1,223	1,865	1,680
12		LCB from midship, f+	[m]	8.56	13.20	12.97
13		KB	[m]	11.207	5.734	7.302
14	C_b	Block coefficient	-	0.8136	0.7589	0.7768
15	C_p	Prismatic coefficient	-	0.8151	0.7616	0.7790
16	C_m	Midship section coefficient	-	0.9980	0.9960	0.9970
17	C_w	Waterplane coefficient		0.9020	0.8260	0.8547
18		L_{BP} / B	-	5.39		
19		B / T_M	-	2.90	5.61	4.42
20		$L_{BP} / \nabla^{1/3}$	-	4.69	5.99	5.49
21		$S / \nabla^{2/3}$		2.78	2.31	2.41
22		Propeller diameter	[m]	10.70		
23		Number of blades	-	4		
24		Service speed with sea margin 15%	[knots]	14.62	15.75	15.55
25		Main engine MCR	-	21,000 kW x 58.9 RPM		
26		Main engine NCR	-	17,850 kW x 55.8 RPM		

Table I is comprehensive specifications of subject ships. It includes details on how these design

parameters vary under different loading states, such as scantling, normal Ballast, and heavy ballast conditions.

Fig.1 shows the geoplots of the routes for Ships G, I, and K. These ships primarily load cargo on the eastern coast of South America, sail around the Cape of Good Hope at the southern tip of Africa, and mainly unload their cargo on the eastern coasts of South Korea and China, occasionally stopping in the Middle East as well. All three ships operate on the same service route, traveling between the eastern coast of South America and East Asia.

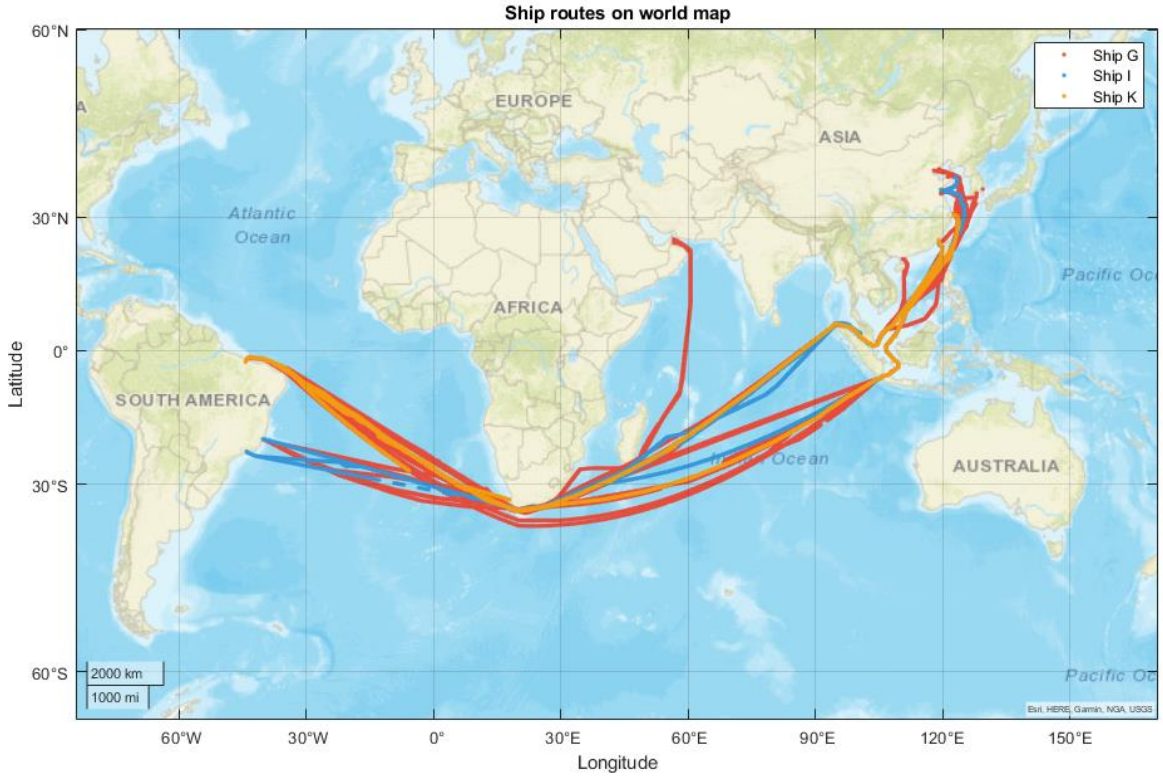

Fig.1: Ship route on world map of Ship G, I and K

4. Results and Discussion

4.1. Normality assessment of residuals for regression analysis

Normality assessment ensures that the assumptions underlying the regression analysis are met, thereby validating the statistical inferences drawn from the model. Non-normal residuals can indicate model misspecification, heteroscedasticity, or the presence of outliers, which can undermine the reliability of the regression results. Therefore, by confirming that the residuals follow a normal distribution, it is enhanced the robustness and credibility of our regression models.

Regression analysis is conducted on the entire datasets for three subject ships over all collection period. Fig.2 shows histograms of the z-score residuals for each ship. To evaluate the adequacy of the regression analysis, KS statistic, skewness, and kurtosis are used as metrics to assess the normality of the residuals. The KS test is a nonparametric test that measures the maximum distance between the sample's ECDF and the ECDF of a reference distribution, typically the normal distribution for regression analysis, *Fasano and Franceschini (1987).* Skewness quantifies the asymmetry of a distribution around its mean. Positive skew indicates a tail extending towards higher values, and negative skew indicates a tail extending towards lower values, *Bai and Ng (2005).* Kurtosis measures the "tailedness" of the distribution or the concentration of values around the mean. Excess kurtosis compares the distribution's kurtosis with a normal distribution with a kurtosis of 3. The statistical calculations for these measures

are in Eqs.(25)-(27).

$$\text{KS Statistic} = \max\left|F_n(x) - F(x)\right| \tag{25}$$

$$\text{Skewness} = \frac{1}{n}\sum_{i=1}^{n}\left(\frac{X_i - \overline{X}}{s}\right)^3 \tag{26}$$

$$\text{Kurtosis} = \frac{1}{n}\sum_{i=1}^{n}\left(\frac{X_i - \overline{X}}{s}\right)^4 - 3 \tag{27}$$

where $F_n(x)$ is ECDF of the residuals and $F(x)$ is ECDF of a normal distribution. X_i is the individual residual values, $\overline{X}$ is the mean of the residuals, and s is standard deviation.

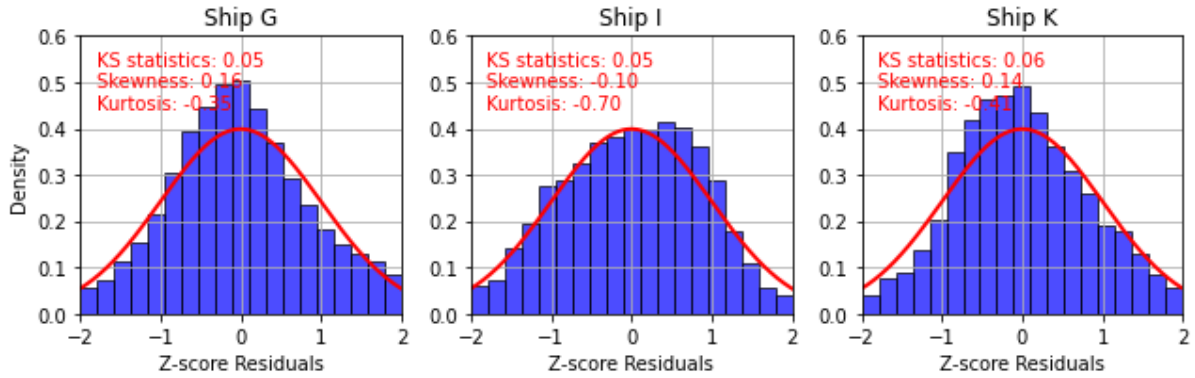

Fig.2: Standardized residual histograms with KS statistic, skewness and kurtosis using entire dataset

4.2. Regression analysis results using entire dataset

Fig.3 shows the scatter plots of the true and predicted total resistance values for Ships G, I, and K using the entire dataset. The percentage RMSE values are calculated to be 12.44% for Ship G, 8.83% for Ship I, and 8.28% for Ship K. These %RMSE values provide a quantitative measure of the regression models' prediction accuracy. Ships I and K exhibit slightly lower %RMSE values than Ship G, indicating that the models for these ships are marginally more accurate in their predictions.

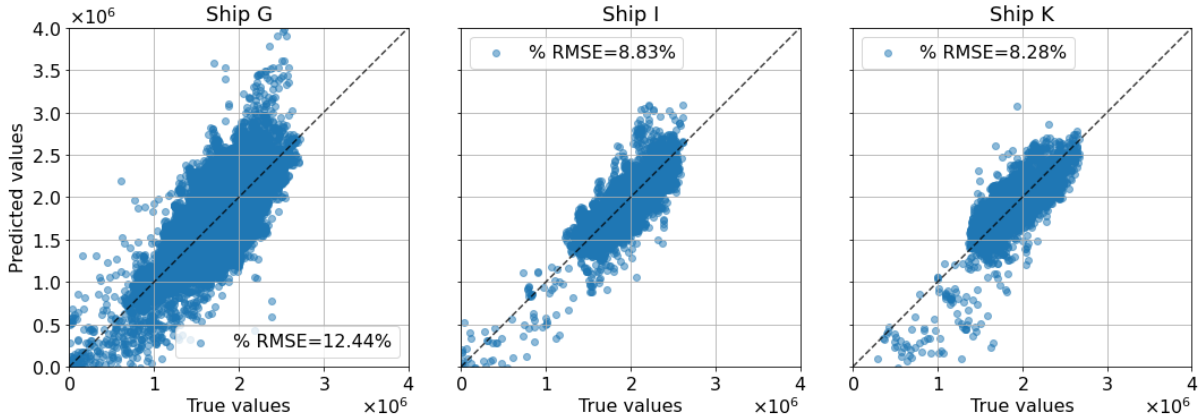

Fig.3: Scatter plots of true and prediction values of the total resistance using the entire dataset

Table II presents the coefficients estimated from regression models for ships G, I, and K before and after applying z-score filtering. Cells marked with "-" indicate variables with high p-values, considered statistically insignificant and unreported. The presence of outliers significantly impacted these coefficients, and their removal through filtering allowed for more accurate coefficient estimation.

Table II: Regression analysis coefficients before and after outlier removal for entire dataset

Coefficients	Ship G		Ship I		Ship K	
	Before filtering	After filtering (Ratio)	Before filtering	After filtering (Ratio)	Before filtering	After filtering (Ratio)
C_{calm}	2.59×10^{-3}	2.56×10^{-3} (98.8%)	2.84×10^{-3}	2.70×10^{-3} (94.9%)	3.16×10^{-3}	3.04×10^{-3} (96.2%)
C_{wind}	1.47×10^{0}	2.55×10^{0} (173.2%)	1.63×10^{0}	2.67×10^{0} (163.2%)	1.82×10^{0}	2.31×10^{0} (126.9%)
$C^{-}_{current}$	1.42×10^{-2}	6.48×10^{-3} (45.6%)	3.59×10^{-2}	2.20×10^{-2} (61.3%)	5.72×10^{-2}	6.81×10^{-2} (119.1%)
$C^{+}_{current}$	4.70×10^{-2}	6.45×10^{-2} (137.1%)	4.69×10^{-2}	1.19×10^{-1} (253.6%)	5.20×10^{-2}	7.77×10^{-2} (149.5%)
$c_{wave,00}$	8.64×10^{-1}	4.02×10^{-1} (46.5%)	3.24×10^{-1}	1.19×10^{0} (366.2%)	5.82×10^{-1}	8.70×10^{-1} (149.5%)
$c_{wave,10}$	-2.25×10^{0}	-7.71×10^{-1} (34.2%)	-7.61×10^{-1}	-2.68×10^{0} (352.0%)	-	-
$c_{wave,01}$	1.68×10^{0}	1.19×10^{0} (70.7%)	1.49×10^{0}	1.12×10^{0} (74.8%)	1.05×10^{0}	7.59×10^{-1} (72.2%)
$c_{wave,11}$	-9.55×10^{-1}	-7.16×10^{-1} (74.9%)	-1.59×10^{0}	-1.21×10^{0} (76.3%)	-1.13×10^{0}	-5.47×10^{-1} (48.2%)
$c_{wave,20}$	1.79×10^{0}	6.46×10^{-1} (36.0%)	2.19×10^{0}	2.99×10^{0} (137.0%)	2.06×10^{0}	-
$c_{wave,02}$	-1.80×10^{-1}	-1.24×10^{-1} (68.9%)	-1.14×10^{-1}	-1.26×10^{-1} (110.0%)	-4.24×10^{-2}	-9.87×10^{-2} (232.6%)

Fig.4 **Fehler! Verweisquelle konnte nicht gefunden werden.**illustrates different resistance components, including the calm water resistance, the added resistance due to wind, waves, and current, for each ship.

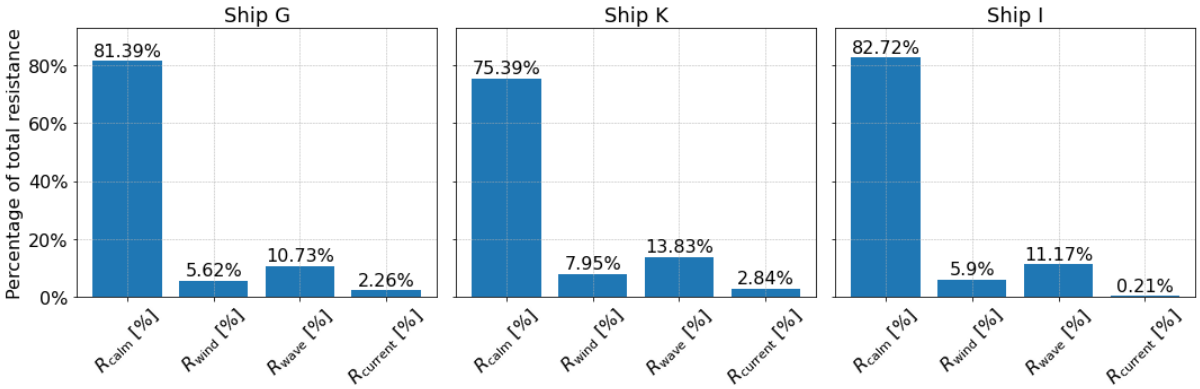

Fig.4: Bar chart on percentage distributions of resistance components for entire dataset

Fig.5 presents the results of added resistance due to wind for three ships, denoted Ship G. The added resistance is expressed as a percentage of the calm water resistance. Data is divided into 15° intervals and represented using boxplots to examine the effect of relative wind direction thoroughly. Additionally, histograms are included below each boxplot to show relative wind direction data distribution. Here, a relative wind direction of 0° indicates head wind, and 180° indicates following wind. Positive values of the added resistance indicate an increase in resistance (wind pushing from the front), while negative values indicate a decrease (wind pushing from behind).

4.2.1. Added resistance due to wind

Fig.6 presents detailed analyses of the added resistance due to wind for Ships G, segmented by relative

wind speed and direction. These figures build on the data presented in Fig.5. by further segmenting the data into different wind speed ranges, thereby providing a more detailed view of the results. The wind speed ranges are divided into five categories: 0-5 m/s, 5-10 m/s, 10-15 m/s, 15-20 m/s, and over 20 m/s.

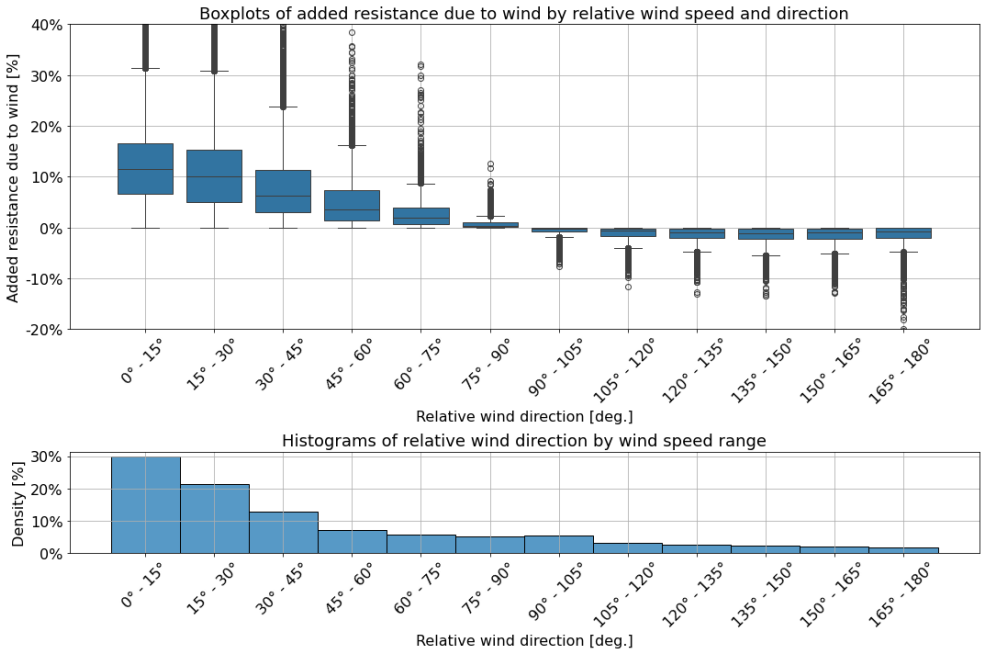

Fig.5: Added resistance due to wind [%] by relative wind direction for Ship G

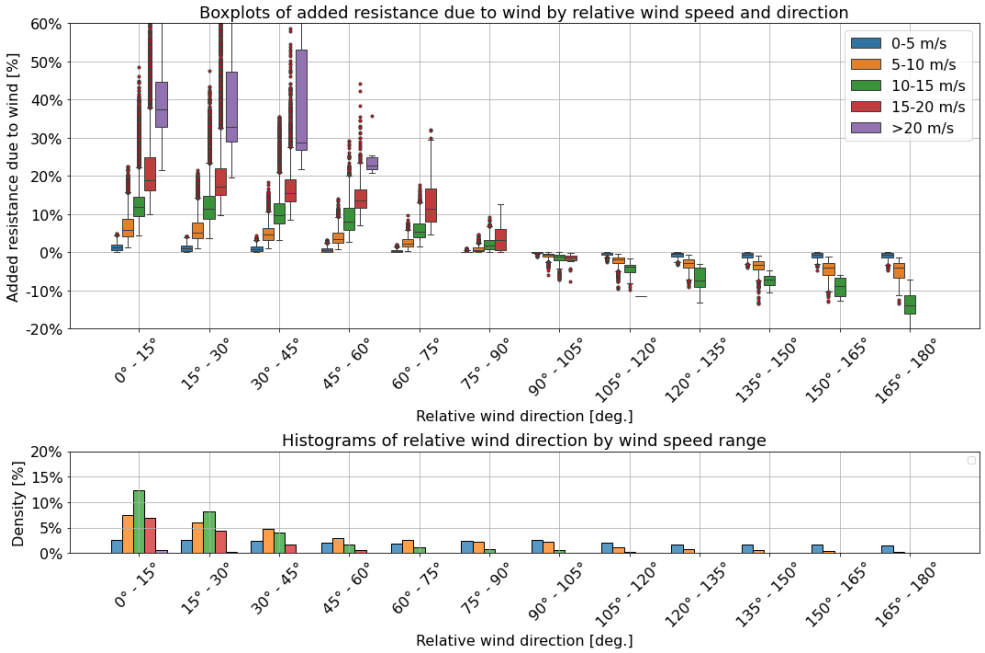

Fig.6: Added resistance due to wind [%] by relative wind speed and direction for Ship G

In the head wind range (0-15º), all three ships exhibit a median added resistance of approximately 15-20%, with maximum values reaching up to 28%. As the relative wind direction approaches 90º (beam wind), the added resistance decreases significantly, centering around 0%, indicating a small impact from the wind. At 180º (following wind), the added resistance becomes slightly negative, around -5%, reflecting a minor reduction in resistance due to wind pushing the ship from behind. The overall trend shows a decrease in added resistance as the relative wind direction moves from head wind to following wind, affirming the regression analysis's validity.

4.2.2. Added Resistance due to Waves

Fig.7 presents the results of added resistance due to waves for Ships G. The added resistance is expressed as a percentage of the calm water resistance. The horizontal axis represents the non-dimensionalized mean wave period, which is the mean wave period divided by the ship's length. The relative mean wave direction is segmented into ranges from 0° to 180° in 30° intervals, and each of these intervals is depicted as a separate subplot. To provide a comprehensive view of data distribution, histograms are included along both the horizontal and vertical axes of the joint plots (bivariate distribution). The scatter plot's data points are represented by hexagonal bins, where the density of the data is indicated by the intensity of the color. Additionally, the plot features an average curve and a 95% confidence interval, highlighting the central trend and indicating the data's variability.

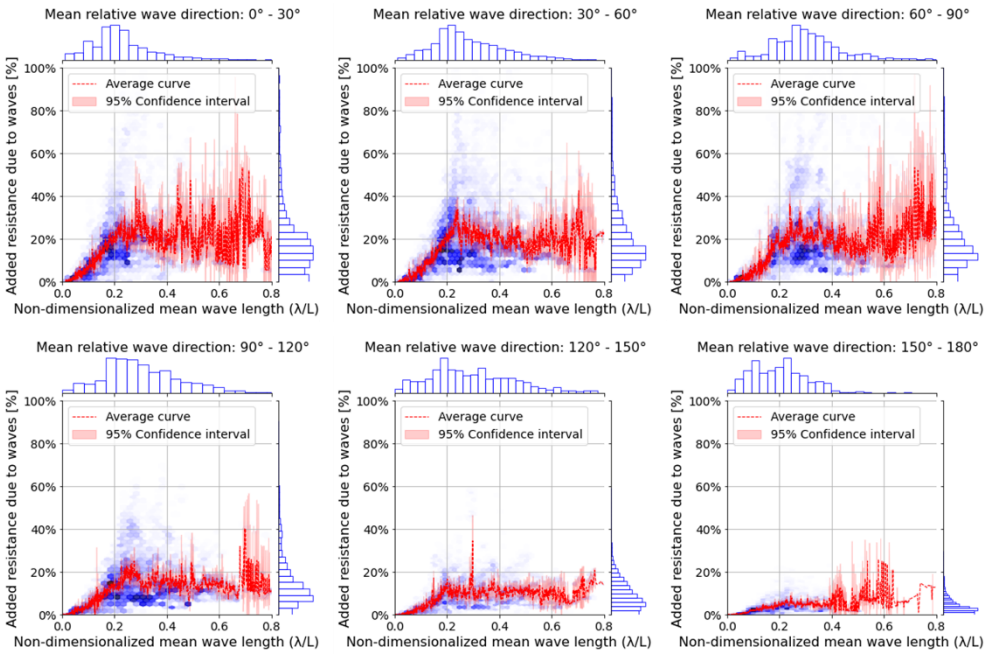

Fig.7: Added resistance due to waves [%] by non-dimensionalized mean wave period and mean relative wave direction ranges for Ship G

Histograms at the top of each subplot present the non-dimensionalized mean wave length data distribution. The overall data ranges from 0 to 0.8, but most are concentrated between approximately 0.2 and 0.4. This range is notable where wave reflection is dominant, indicating that waves striking the hull and reflecting off it disrupt the water surface around the hull due to the energy involved, *Faltinsen (1983), Townsin and Kwon (1983), Wang et al. (2021).*

The results indicate a linear relationship between non-dimensionalized wave length and the added resistance due to waves from 0 to 0.3, suggesting that as the wave length increases, so does the added resistance. Beyond 0.3, this increase seems to plateau. Although the data becomes significantly less dense beyond 0.3, reducing reliability, Ship G, which has data in this range, still does not show a marked increase in added resistance. Comparing these findings with various model test results would be beneficial. However, most previous studies focus on model tests with wave lengths between 0.3 and 2.0. Model tests involving extremely short waves might face physical limitations of wave generators or wave breaking due to excessive wave steepness, potentially preventing accurate tests. Most previous studies present model test or numerical analysis results with intervals larger than 0.3, *Guo et al. (2012), Kashiwagi (2013), Sprenger et al. (2017), Stocker (2016).* This underscores the need for further research and testing for large ships. Given that the target ship in this study has a length of approximately 340 m, model tests to compare the added resistance in extremely short wave conditions for large ships over 300 m in length would be useful.

When examining the impact of mean relative wave direction, the added resistance due to waves

increases not merely because of proximity to 0° (head wave). From 0° to 90°, the increase is relatively uniform, peaking around a 0.3 non-dimensionalized wave length at an average of about 20%. Beyond 90°, as the mean direction shifts towards the stern or rear quarters of the ship, added resistance decreases. However, Ship K does not follow this trend closely, likely due to its sparse and uneven data distribution, necessitating further verification of how data quantity and distribution impact results. Moreover, in contrast to the added resistance due to wind, where following wind provides a pushing effect, waves do not have a pushing effect, emphasizing the differences in how resistance from these elements impacts the ship.

4.2.3. Added Resistance due to Current

Fig.8 is a joint plot graph depicting the added resistance due to current, expressed as a percentage, in relation to relative current speed. This figure illustrates how the resistance experienced by the ship varies with changes in the speed of the current relative to a ship.

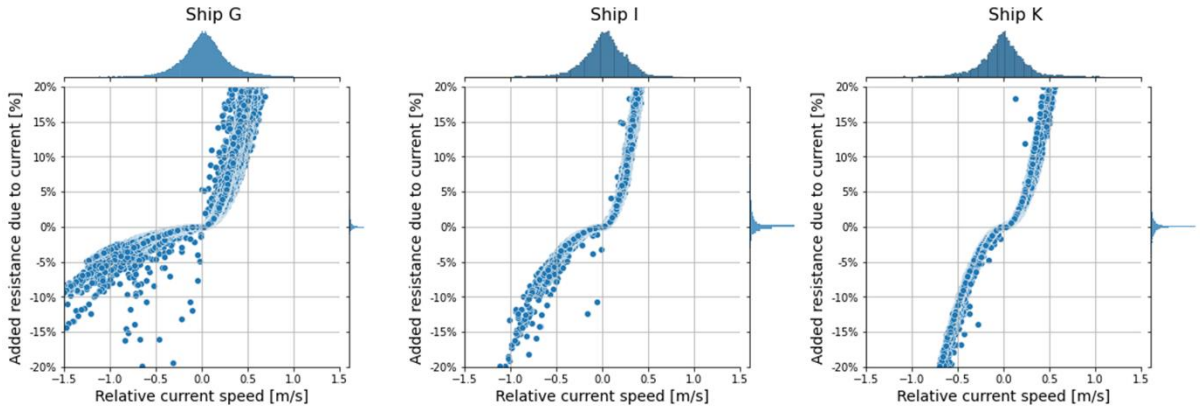

Fig.8: Added resistance due to current [%] by relative current speed

The analysis indicates that when the relative current speed is positive, meaning a head current, even a modest speed of 0.5 can cause an increase in resistance of up to 20%. Conversely, when the relative current speed is negative, indicating a following current, a speed of 0.5 results in a resistance reduction of approximately 5-10%. This left-right asymmetry suggests that the impact of the current pushing against the front of the ship is significantly greater than that of the current pushing from behind, even at the same current speed.

4.2. Regression analysis results using sub-datasets by loading conditions, individual routes, and speed ranges

One crucial observation from the data distribution histograms on the right side of each subplot is that data points exceeding the 2-3% range are rare. This indicates that most resistance increases and decreases are concentrated within the 2-3% range. This means that resistance changes beyond this range are infrequent and likely to occur in specific and localized conditions. This knowledge equips us to understand better and prepare for ship performance in various conditions. The ships in this study primarily operate in the vast open seas, which likely contributes to these findings. Ships operating in regions with very fast currents over short periods might exhibit a different data distribution, with a higher frequency of data points showing significant resistance changes.

Figs.9 and 10 present comparisons of the calm water resistance coefficient by route and speed range with model test results for Ship G under scantling and normal ballast conditions, respectively.

Following the previous segmentation methodology, this analysis divided the data based on loading conditions, individual routes, and speed ranges. Speed ranges are segmented in 2-knot intervals, with the midpoint value representing each segment. For instance, 8-10 knots range data is considered performance at 9 knots. When data is absent due to z-score filtering, those subplots are marked with

"No data." For comparative analysis, model test results and design speed are also included. This ship's operational speed range predominantly falls within 10-15 knots, whereas model tests are conducted in the 11-17 knots range. The design speed is 14.62 knots for the scantling condition and 15.75 knots for the normal ballast condition.

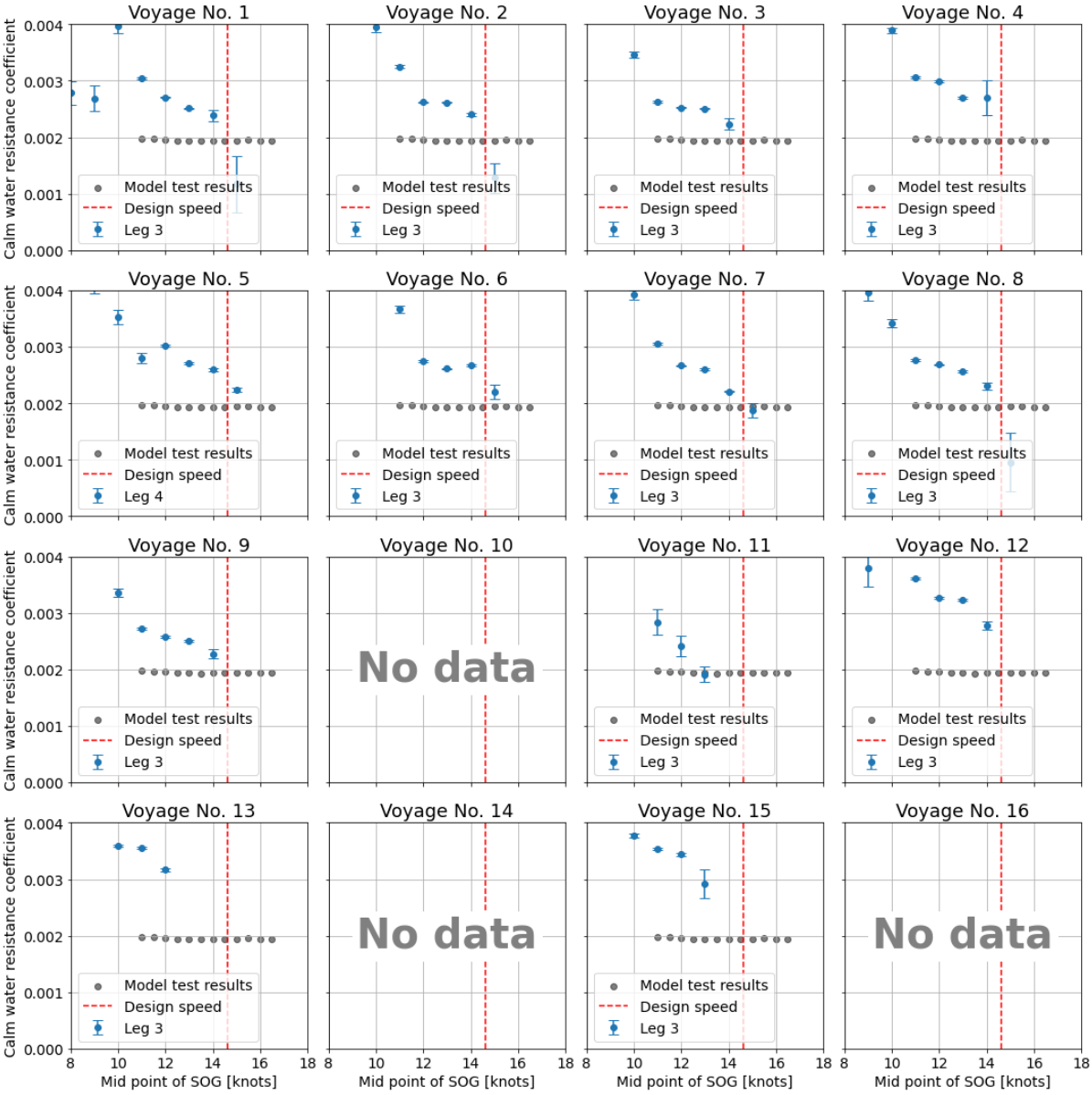

Fig.9: Comparison of the calm water resistance coefficient by route and speed range with model test results for Ship G under scantling condition

Interpreting the results, it can be observed that the calm water resistance coefficients are somewhat similar to model test results or slightly higher near the design speed. However, as the speed decreases to 10 knots, the coefficients derived from regression analysis increasingly exceed model test results, reaching up to 75% higher. This has significant implications for ship design and performance evaluation. It suggests that the shipyard ensures the guaranteed performance at the design speed, as specified in contracts, resulting in better alignment at this speed. Conversely, it indicates that the actual resistance of the ship in the medium speed range (10-14 knots) is higher than the model test results. Interpreting these findings accurately, it becomes clear that there is a pressing need to revise the empirical factors or methods used to extrapolate model test results to account for speed-specific scale effects.

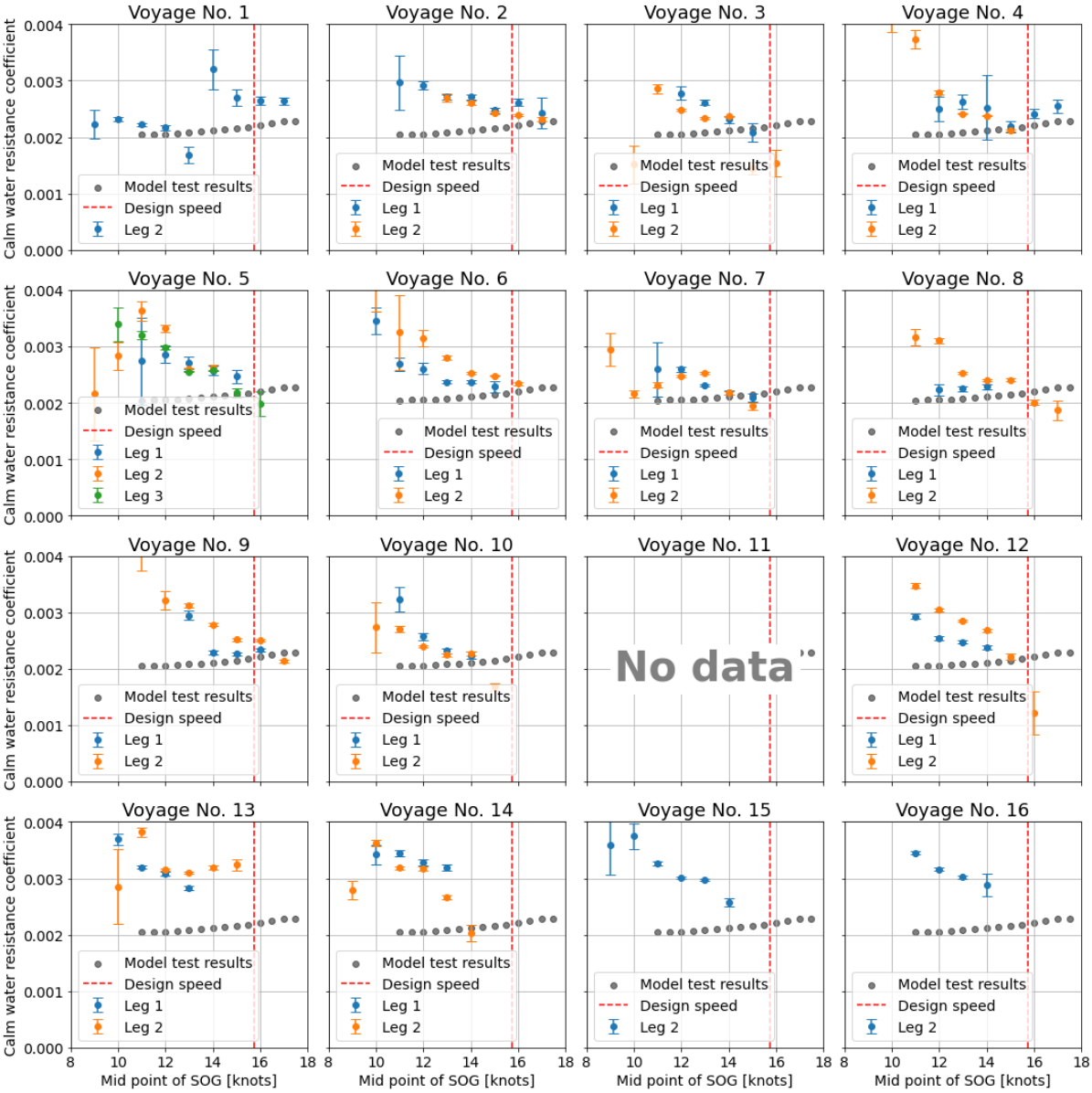

Fig.10: Comparison of the calm water resistance coefficient by route and speed range with model test results for Ship G under normal ballast condition

Fig.11 shows the calm water resistance coefficients obtained through regression for each route and speed on a single graph to observe the overall trend. To ensure a meaningful comparison, it is focused on the speed range of 11 to 15 knots, which overlaps with the model test's speed range and where the data points are predominantly distributed. It is performed for the linear regression within this speed range and include the results in the graph for a comprehensive trend analysis.

The results from Figs.9 and 10 are more clearly and distinctly illustrated in Fig.11. The calm water resistance coefficient data distribution for both loading conditions aligns closely with the model test results near the design speed. However, it is observed that the difference increases as the speed decreases below the design speed. Although further research on a more diverse range of ships is necessary, this finding supports the earlier-mentioned suspicion that the traditional method of estimating ship scale performance through model tests may not be valid across all speed ranges, particularly in the medium-speed range (approximately 10-14 knots) observed in this study.

Figs.12 and 13 show the results for Ship I and Ship G, respectively. In the case of the normal ballast condition, where the data distribution is relatively broad and includes results near the design speed, a

similar trend to Ship G is observed. However, in the scantling condition, where the data distribution is sparse, the results are slightly higher than the model test, even at the design speed. If Ships I and K had a data distribution as extensive as Ship G, they would likely exhibit a similar trend.

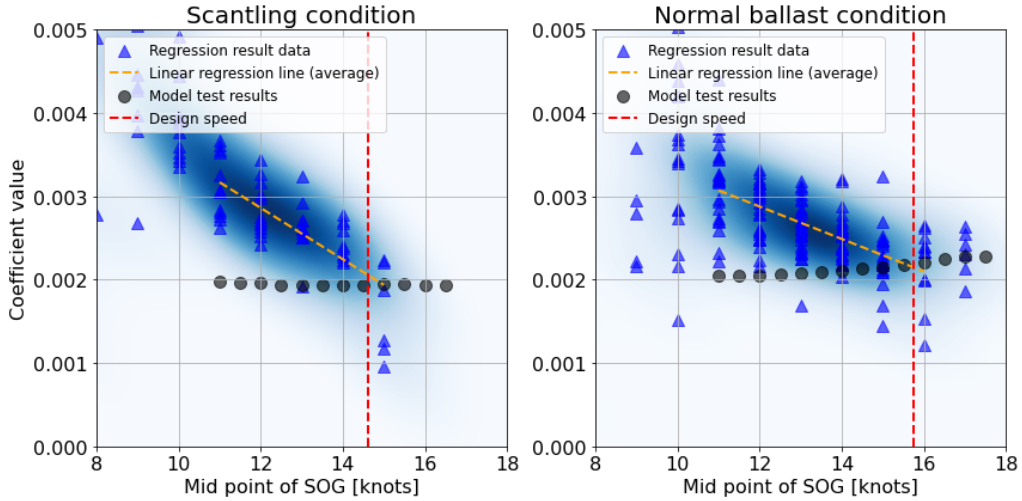

Fig.11: Trend comparison of all calm water resistance coefficients by route and speed range with model test results for Ship G

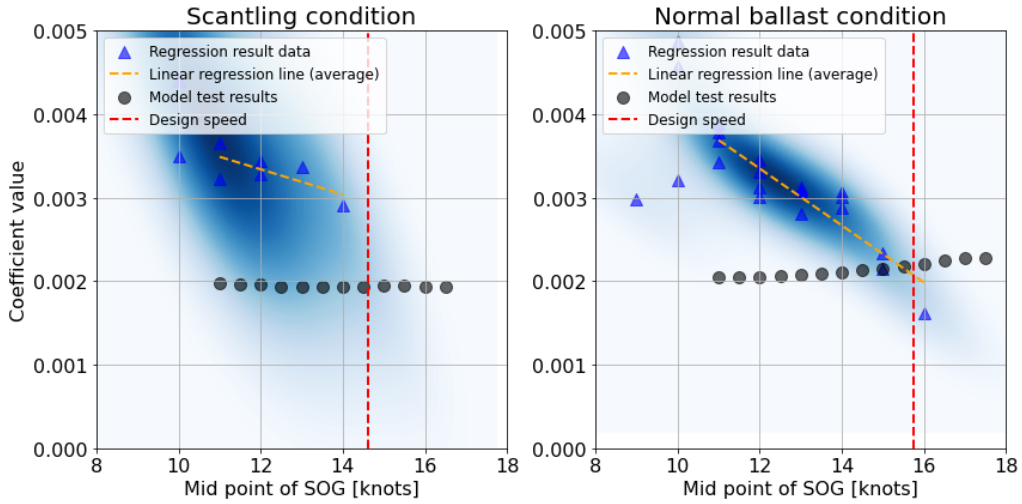

Fig12: Trend comparison of all calm water resistance coefficients by route and speed range with model test results for Ship I

Generally, when analyzing sub-datasets segmented by route and ship speed, the calm water resistance coefficient is expected to reveal a fouling effect, showing a changing trend over time. However, no clear increasing trend is observed. To properly analyze this, records of hull maintenance activities aimed at reducing the fouling effect (i.e.; efforts to restore the hull to its initial state), such as hull cleaning, repainting, and blasting, are necessary, *Adland et al. (2018), Akinfiev et al. (2007), Dev and Saha (2017)*. Unfortunately, such records are not separately available. Upon further investigation, it is found that cleaning is performed 1-2 times every 6-12 months, and there are also instances of repainting and hull blasting in dry dock. This suggests that appropriate hull surface maintenance measures effectively manage the hull fouling condition. Therefore, it is necessary to obtain these records accurately in the future to conduct a quantitative study on the fouling effect.

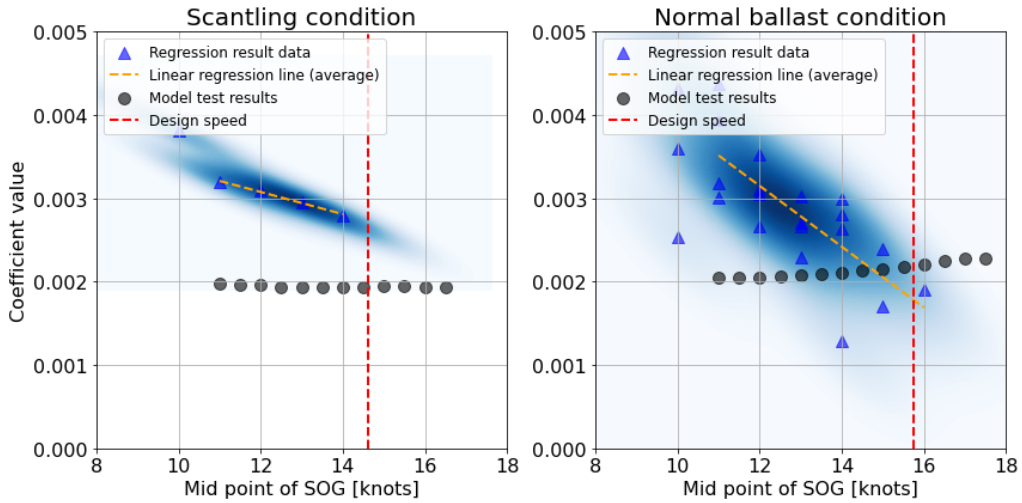

Fig.13: Trend comparison of all calm water resistance coefficients by route and speed range with model test results for Ship K

5. Concluding Remark

This study aimed to develop a comprehensive data-driven model to analyze ship resistance using operational data. By integrating theoretical background with practical data, the research offers a robust framework for understanding the different components of ship resistance. The findings provide valuable insights into improving ship design and operational strategies for more efficient and sustainable maritime operations. The key findings are:

- The results for calm water resistance are statistically reliable, showing a variation within 5% to 10% of the average. However, comparisons with model test results indicate that in-service performance tends to be higher, especially at medium to low speeds. This discrepancy suggests that additional research is necessary to understand and bridge the performance gap between model ships and full-scale ships at these speeds.
- The added resistance due to wind is statistically significant, with variations within 5% to 10% of the average. A new finding reveals that the transverse projected area does not always proportionally affect the added resistance due to wind. This highlights the need for further studies on the wind speed profile at the waterline and the forces acting on different parts of the ship (upper, middle, and lower) to improve the accuracy of wind resistance models under various loading conditions. Additionally, it is observed that head winds have a greater impact on resistance than following winds, even at the same wind speed.
- While the added resistance due to waves is statistically significant, the transfer function coefficients show some inconsistency, with high p-values suggesting that a simpler model structure could be more effective. A key finding is that, for large ships, most wave conditions correspond to very short waves. In these cases, added resistance increases proportionally with the non-dimensionalized wave length.
- The calm water resistance coefficient is anticipated to increase over time due to fouling; however, this trend is not observed. Instead, the analysis is limited to comparing coefficients among different ships. This indicates that the current methodology is insufficient for detecting fouling effects over time. Detailed records of hull maintenance, such as cleaning, repainting, and blasting, are necessary for a more accurate assessment of fouling impacts. Future research should incorporate these maintenance histories to understand better and model the fouling effect on ship resistance.
- Segmenting data by loading conditions, individual routes, and speed ranges improves the accuracy of regression analysis, as indicated by the %RMSE results. However, overly segmenting the dataset can reduce data diversity and significantly decrease the reliability of regression analysis. Ensuring a minimum number of diverse data points for regression is crucial. This

aspect requires continuous research to balance practical applications, model construction, and theoretical comparisons.

Future work will entail:

- Future studies should focus on establishing robust methodologies to assess the minimum number and diversity of data points necessary for successful regression analysis. This will ensure that the models are statistically reliable and can accurately capture the variations in ship resistance under different operational conditions.
- Research is needed to develop methods to effectively incorporate the inherent uncertainties in onboard measurement and weather data. This will enhance the robustness and accuracy of the resistance models, making them more reliable for real-world applications.
- Future work should involve comprehensive comparative studies, model tests, and various numerical methods. These will help validate the resistance models developed from operational data and provide insights into improving them based on empirical and numerical findings.
- Expanding the scope of research to include a broader range of ship types and routes is crucial. This will ensure that the findings are generalizable across different classes of vessels and operational conditions, thereby enhancing the applicability and reliability of the resistance models in diverse maritime contexts.

Acknowledgement
This research was supported by the Research Institute of Marine System Engineering (RIMSE) and the Institute of Engineering Research at Seoul National University. It was also supported by the Korea Institute of Marine Science & Technology Promotion (KIMST), funded by the Ministry of Oceans and Fisheries (2520000243). Additionally, this study is partially based on the key findings of our previous work published in IJNAOE: *Data-driven modeling and regression analysis on ship resistance of in-service performance*.

References

ALDOUS, L.G. (2016), *Ship operational efficiency: performance models and uncertainty analysis*, PhD thesis, University College London

ALDOUS, L.; SMITH, T.; BUCKNALL, R.; THOMPSON, P. (2015), *Uncertainty analysis in ship performance monitoring*, Ocean Eng. 110, pp.29-38

BAI, J.; NG, S. (2005), *Tests for skewness, kurtosis, and normality for time series data*, J. Business & Economic Statistics 23(1), pp.49-60

COLEMAN, T.F.; LI, Y. (1996), *An interior trust region approach for nonlinear minimization subject to bounds*, SIAM J. Optimization 6(2), pp.418-445

FASANO, G.; FRANCESCHINI, A. (1987), *A multidimensional version of the Kolmogorov–Smirnov test*, Monthly Notices of the Royal Astronomical Society 225(1), pp.155-170

FALTINSEN, O.M. (1983), *Bow flow and added resistance of slender ships at high Froude number and low wave lengths*, J. Ship Research 27(3), pp.160-171

GUO, B.J.; STEEN, S.; DENG, G.B. (2012), *Seakeeping prediction of KVLCC2 in head waves with RANS*, Applied Ocean Research 35, pp.56-67

ISO (2002), *ISO 15016:2002 Ships and marine technology-Guidelines for the assessment of speed and power*, Int. Standard Org. Geneva

ISO (2015), *ISO 15016:2015 Ships and marine technology-Guidelines for the assessment of speed and power*, Int. Standard Org. Geneva

ISO (2016), *ISO 19030-1 Ships and marine technology-Measurement of changes in hull and propeller performance*, Int. Standard Org. Geneva

ITTC (2011), *ITTC – Recommended procedures, Fresh Water and Seawater Properties (7.5-02-01-03 Rev. 02)*, Int. Towing Tank Conf.

ITTC, 2017, *ITTC – Recommended Procedures and Guidelines, 1978 ITTC Performance Prediction Method (7.5-02-03-01.4 Rev. 04)*, Int. Towing Tank Conf.

ITTC (2021), *ITTC – Recommended Procedures and Guidelines, Calculation of the Weather Factor for Decrease of Ship Speed in Wind and Waves (7.5-02-07-02.8 Rev.01),* Int. Towing Tank Conf.

KASHIWAGI, M. (2013), *Hydrodynamic study on added resistance using unsteady wave analysis*, J. Ship Research 57(04), pp.220-240

KENNEDY-SHAFFER, L. (2019), *Before p < 0.05 to beyond p < 0.05: using history to contextualize p-values and significance testing*, The American Statistician 73(sup1), pp.82-90

LIU, S.; PAPANIKOLAOU, A. (2019), *Approximation of the added resistance of ships with small draft or in ballast condition by empirical formula*, J. Eng. for the Mar. Environment 233(1), pp.27-40

LIU, S.; PAPANIKOLAOU, A. (2020), *Regression analysis of experimental data for added resistance in waves of arbitrary heading and development of a semi-empirical formula*, Ocean Eng. 206

LIU, S.; SHANG, B.; PAPANIKOLAOU, A.; BOLBOT, V. (2016), *Improved formula for estimating added resistance of ships in engineering applications*, J. Marine Science and Application 15, pp.442-451

MANEEJUK, P.; YAMAKA, W. (2021), *Significance test for linear regression: how to test without P-values?*, J. Applied Statistics 48(5), pp.827-845

MOISEEV, N.A. (2017), *p-Value adjustment to control type I errors in linear regression models*, J. Statistical Computation and Simulation 87(9), 1701-1711

ROUSSEEUW, P.J.; HUBERT, M. (2011), *Robust statistics for outlier detection*, Wiley Inter-disciplinary Reviews (WIREs): Data Mining and Knowledge Discovery 1(1), pp.73-79

SPRENGER, F.; MARON, A.; DELEFORTRIE, G.; VAN ZWIJNSVOORDE, T.; CURA-HOCH-BAUM, A.; LENGWINAT, A.; PAPANIKOLAOU, A. (2017), *Experimental studies on seakeeping and maneuverability of ships in adverse weather conditions*, J. Ship Research 61(3), pp.131-152

STOCKER, M.R. (2016), *Surge free added resistance tests in oblique wave headings for the KRISO container ship model*, Master's thesis, University of Iowa, Iowa City

TOWNSIN, R.L.; KWON, Y.J. (1983), *Approximate formulae for the speed loss due to added resistance in wind and waves*, RINA Supplementary Papers 125, 199

WANG, J.; BIELICKI, S.; KLUWE, F.; ORIHARA, H.; XIN, G.; KUME, K.; OH, S.; LIU, S.; FENG, P. (2021), *Validation study on a new semi-empirical method for the prediction of added resistance in waves of arbitrary heading in analyzing ship speed trial results*, Ocean Eng. 240

Assurance of Performance Claims for Hull Coating that Reduce Biofouling

Ditte Gundermann, Hempel, Lyngby/Denmark, digu@hempel.com
Mads Raun Bertelsen, Hempel, Lyngby/Denmark, madb@hempel.com
Andrea Farkas, Hempel, Zagreb/Croatia, afar@hempel.com
Olav Rognebakke, DNV, Oslo/Norway, olav.rognebakke@dnv.com
Shuai Li, DNV, Oslo/Norway, Shuai.Li@dnv.com

Abstract

It is well known that biofouling on ship hulls significantly increases fuel consumption, leading to higher operational costs and environmental impact. A top performing hull coating is among the lowest hanging fruits for vessel decarbonisation, by efficiently minimizing the risk of fouling to keep operational costs and CO2 emissions at a minimum. At the same time, there is a lot of uncertainty and claims around the performance of different hull coatings, which are not always seen as holding up in the market. This paper presents the collaboration between Hempel and DNV to review and validate the claims made by Hempel regarding the potential fuel savings from using Hempaguard silicone paint. The claimed fuel savings have been validated by DNV in an independent comprehensive evaluation, which could be seen as a first step in getting more rigid transparency from independent sources on different vessel retrofits to reduce fuel consumption. The paper presents the various data and the method used in the validation to assess biofouling prevention and fuel savings. Results demonstrate that Hempel's coating significantly reduces biofouling, leading to notable fuel savings and operational efficiency. In addition, the collaboration highlights the substantial economic and environmental benefits that can be obtained from an independent organisation like DNV engaging in increased transparency of performance claims across available solutions.

1. Introduction

Choosing the right energy efficiency measures is critical to ensure the marine industry remains on the right decarbonization paths as set forth by IMO. A number of operational measures (slow steaming, route planning and trim optimization) and technical upgrades (in terms of energy saving devices, engine modifications, propeller or bow modifications, etc.) are available on the market today, *Barreiro et al. (2022)*, but it remains a key challenge for the shipping industry to choose the strategies that gives the highest return on investment and impact on GHG emissions. Two very important energy efficiency measures are choosing adequate hull coating and optimization of maintenance schedule, which can combined save a lot of energy in shipping industry, *Bouman et al. (2017)*.

Retaining a clean and smooth hull, free of biofouling growth, reduces the frictional resistance, which in turn significantly reduces the vessel fuel consumption compared to a fouled hull. The new generation of silicone-based antifouling coating systems with active antifouling technology such as Actiguard®, has been recognized as one of the most mature technology upgrades that can provide immediate improvement to ship energy efficiency, Fig.1.

For both silicone coatings and other energy saving devices, it is however a well-known pain point that there is limited transparency and industry agreement on the ship specific fuel savings gained by each technology, and fleets around the world are currently pursuing a wide range of different technical upgrades to achieve the same target of GHG emissions. The challenge exists both when deciding between investment in different types of energy saving devices and, if an advanced high-performance coating is preferred, on the choice of coating. This represents an important problem, because traditionally in chartering market, the main beneficiary of the energy savings associated with energy saving technologies is often not the one that has invested in such technologies, *Dirzka and Acciaro (2021)*. Consequently, even if the total cost can be reduced with the installation of certain energy saving technology, in many cases the one responsible for funding might not benefit from it. This has been recognized as an important energy efficiency barrier in shipping industry, *Rehmatulla and Smith (2015)*. A big element of this challenge is the absence of an independent framework or body to evaluate the different solutions available on the market in a uniform way. For suppliers of energy efficiency solutions

such as Hempel, validation by an independent 3rd party is also a helpful way to further understanding of own performance and increase the quality of communicated performance claims.

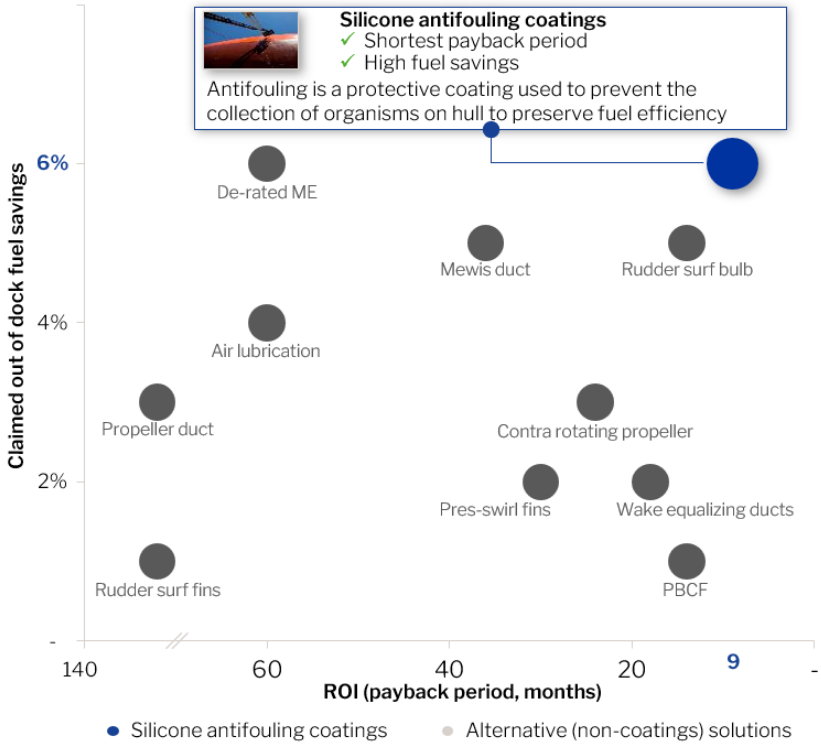

Fig.1: Overview of claimed fuel savings and ROI (Hempel internal compilation)

In 2023, Hempel and DNV engaged in a collaboration to verify the performance of Hempaguard, which is one of the most widespread energy efficiency measures with more than 4000 vessel applications since 2013. In the absence of an industry standard evaluation framework, this paper describes the steps taken in the present validation process including methodology, evidence, challenges, as well as recommended steps forward for an industry wide evaluation framework. The present case does in no way constitute a finalized framework for third-party validation of performance claims, but it highlights the potential benefits for all parties in the shipping industry of increased 3rd party validation, and the importance in furthering data transparency, use of in-service data and an updated verification framework.

2. Claims to be validated

The claims to be validated relate to performance of Hempaguard technology in terms of its direct impact on fuel consumption for a single vessel as well as for a fleet of vessels. The fuel consumption claims on fleet level concern the combined savings of all vessels applied with Hempaguard.

When assessing and quantifying the performance of a vessel or fleet with a certain technology, a number of effects will play a role. For the present claims, three main aspects are important to consider:

- The ability of the hull coating to prevent biofouling over the lifetime of the coating, hereafter referred to as the “antifouling performance”
- The impact of surface properties on the frictional resistance and hence power and fuel consumption of a ship with the coating as applied, i.e. without any fouling on the hull, hereafter referred to as the “out of dock” effect
- The baseline to which the performance and fuel consumption should be compared.
- The specific claims made by Hempel on the above three aspects as well as the assumptions behind the calculation of combined fuel savings for all Hempaguard applications are presented in this section.

2.1. Antifouling performance and out of dock effect

The antifouling performance claim for Hempaguard consists of a value for the maximum "speed loss" that can be expected over a 5-year dry docking cycle. The speed loss is to be measured and defined according to the ISO 19030 standard on performance monitoring, *ISO (2016)*. In short, the speed loss is the difference in the average speed deviation from a reference curve between the first year and the remaining years in the dry-docking period, Fig.2. The claimed maximum speed loss is 1.4% over a 5-year dry docking period for Hempaguard X7.

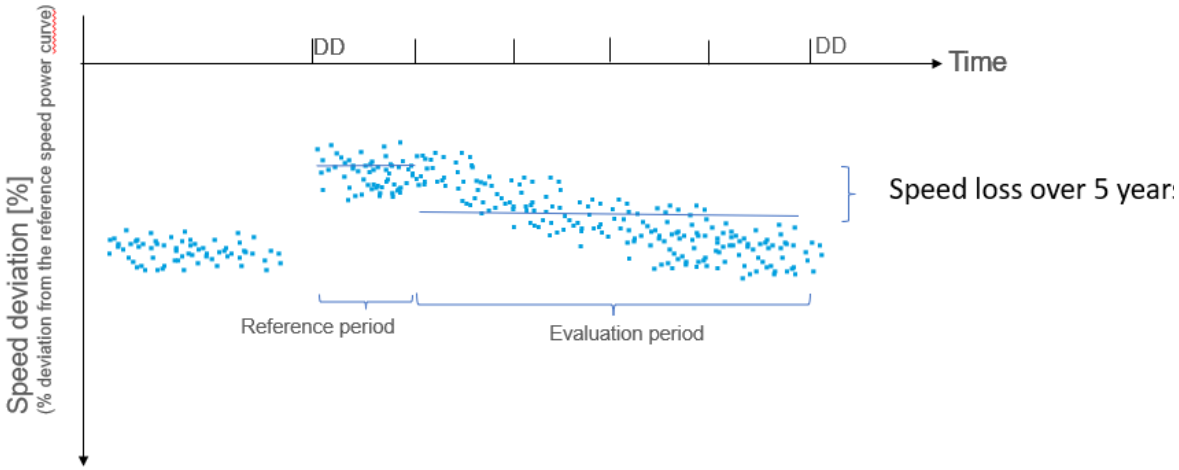

Fig.2: Illustration of definition of "speed loss"

The "out of dock" gain is most often measured in reduced power to obtain a constant average cruising speed. Fig.3 shows Hempel's speed loss and out of dock performance claims for Hempaguard. The out of dock effect claim is 6% in power.

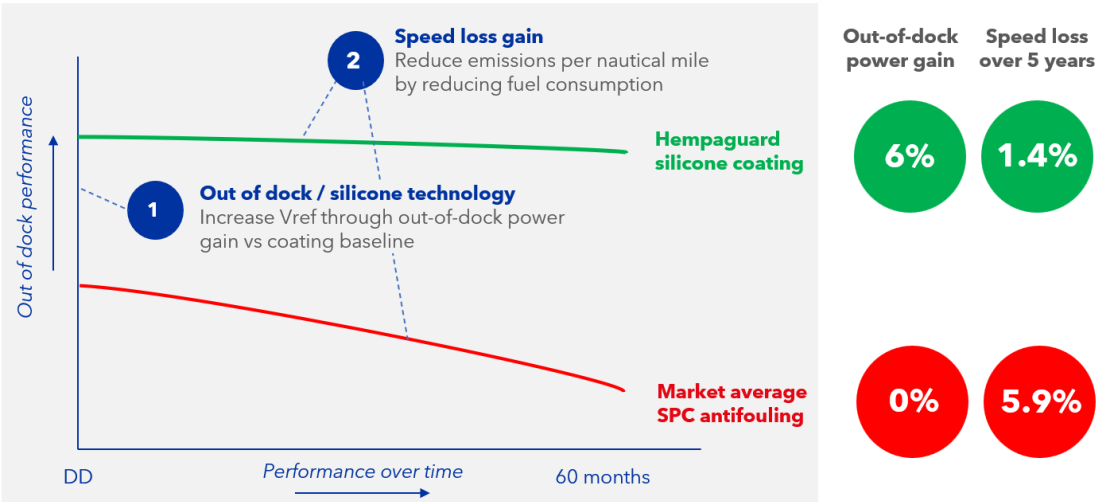

Fig.3: Overview of the claimed Hempaguard performance against chosen baseline

Although both the out of dock effect and the speed loss value for a given vessel will depend on ship hydrodynamic characteristics and operational profile, the values presented in Fig.3 represent fleet averages and these are the values that are being claimed as average values for all vessels.

2.2. Performance baseline

All vessels in the world fleet apply coatings on their underwater surface to protect the steel against corrosion and, in almost all cases, against fouling growth. As the ability of various coatings in preventing fouling over the lifespan of the coating varies a lot, it makes sense to establish a baseline for

comparison of antifouling coatings. It has for several years been the accepted assumption, that a "market average" coating can be expected to have a speed loss of 5.9% over 5 years measured as defined in the ISO 19030 standard on performance monitoring.

The market average speed loss of 5.9% originates mainly from the 2nd IMO GHG study, *IMO (2009)*. This is one of the only sources of "market average" fouling performance available in the industry. The use of average speed loss is a core component of the ISO19030 performance monitoring framework. While the framework is from 2009 and thus at risk of becoming dated, a recent report from the IMO GloFouling Project, *GloFouling (2022)*, reiterates that biofouling has a significant impact on frictional resistance and GHG emissions for the world fleet.

2.3. Fuel consumption claims

The fuel consumption claim regards the total performance advancements obtained from all Hempaguard applications since 2013, measured against the "market average" baseline. The method for arriving at an estimate for these total savings will be described in this section.

First of all, the average expected performance of a given vessel with Hempaguard is assumed to be as described in Section 2.1, Anti fouling performance and out of dock effect, i.e. have a speed loss of 1.4% over 5 years and an out of dock effect of 6% in power relative to a normal antifouling coating. The deterioration of performance is assumed to be linear over the dry-docking period, even though, the reality will look quite different for many cases, with more steady performance in first 3-4 years and a more steep performance deterioration in the last one or one and a half year. On average and for simplicity however, both Hempaguard and market average performance is assumed to be linearly decreasing over time. The value of 5.9% speed loss over 5 years is assumed for the market average coating, while the out of dock effect of a market average coating is assumed to be zero percent. For the conversion of speed loss into added power, a 1:3 ratio is assumed, meaning that a 2% speed loss is equivalent to a 6% power increase and a 6% power gain is equivalent to a 2% speed reduction (note the opposite sign!).

The challenge with estimating the fuel savings on the aggregated fleet level is that not all applied vessels will behave the same. For instance, not all ships will have dry docking periods of exactly 60 months. This was considered by first modelling the claimed performance gains by year after DD for one vessel, and then to correct for the variation in dry docking interval afterwards. Since the performance difference between Hempaguard and a "market average" coating widens over the DD period, an annual performance gain to the baseline was calculated and an adjustment of the share of vessels still sailing during each service year was applied. While some Hempaguard vessels have DD cycles longer than 5 years, the performance gain was disregarded for this analysis. Table I shows the share of vessels still in service by year after DD.

Table I: Share of vessels still in service by in-service year from DD

Year	Share of vessels in-service
1	100%
2	98%
3	95%
4	80%
5	75%

Finally, it is acknowledged that not all vessels applied with any coating or other Energy Saving Device obtain the expected performance benefits. In the example of silicone coatings, events such as ice trading, idle periods beyond the guaranteed idle duration or excessive mechanical damage will impact the performance of the coating negatively. In comparison to the other coatings, the ratio of raised performance complaints is low, pointing that the majority of the vessels are performing as expected, but

it was still decided to have a necessary adjustment factor in the aggregate fleet performance claims. Rather than trying to calculate the exact performance gain, including the cases of non-performance, a 35% “buffer” adjustment was applied to all aggregate performance claims, which was >4 times larger than the ratio of complaints received by Hempel on Hempaguard complaints, Fig.4. This conservative approach is used to avoid overstating the fleet aggregate performance claims.

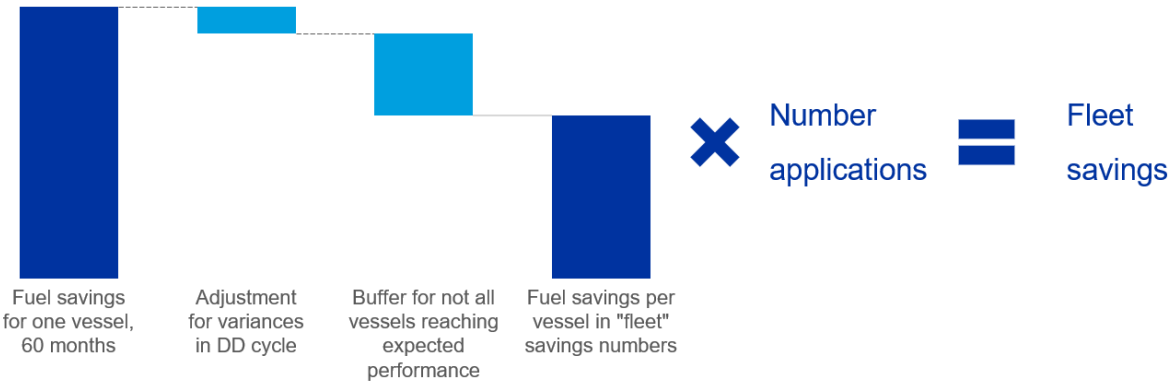

Fig.4: Relationship between performance claims of a single vessel and all historical applications

In addition to the relative savings per vessel, the total fuel consumption saved by all applied vessels is claimed. While the actual fuel consumption for all applied vessels is not available to Hempel, the fuel consumption was modelled using an average activity level of 56% and an average daily consumption of 36 tons/day.

Since the launch of Hempaguard X7 in 2013, Hempel has launched several leading silicone antifouling products. In 2019, Hempaguard MaX / X8 was launched and in 2024, Hempaguard Ultima was launched, both with slightly higher performance claims than Hempaguard X7. Hempaguard X7 does, however, continue to be the product with the most historical applications and most performance evidence available to review. For this reason, all Hempaguard applications were normalized to the Hempaguard X7 performance claims for the study regardless of product, even if the actual performance gains in these cases would be expected to be slightly higher.

3. Method of validation

In absence of an established framework for performance validation, a number of considerations were made prior to reviewing the evidence of silicone coating performance. When working with assurance and validation of claims, it is important to be precise in the use of terminology.

3.1. Verification versus validation and assurance

The current standard for quantification of the effect of fuel saving measures based on in-service measurements is ISO19030:2016, *ISO (2016)*. This was developed to quantify the changes to hull and propeller performance over time. The newbuild or out-of-dock performance of a vessel is typically quantified by following the ISO15016:2015, *ISO (2015),* standard for assessing speed and power performance. Verification may be done against these standards.

Validation is used as a more general term when results are checked against industry accepted methodology, best practices or published results. Validity and accuracy are checked, and the action is to confirm the results to be true or correct.

Assurance is done to build trust and provide confidence. Assurance enhances the credibility and reliability of information for decision-making purposes. It provides a second independent assessment. Confidence in claims may be provided by applying sound engineering judgement when looking at the

evidence and results. Auditing is a common part of assurance, and the assurance process may start with a workshop where the claim is substantiated and a detailed scope for further validation is developed.

3.2. Ideal and possible approaches to working with the in-service evidence

Performance monitoring is done by operators and owners for many reasons, e.g. as a basis for hull and propeller maintenance, optimizing fleet utilization and benchmarking. Many systems exist with a large span of features, accuracy and transparency. There is a lack of standards for performance data, which makes such data costly and difficult to work with.

Performance data has a high commercial value and access is strictly controlled. It is challenging for a supplier of emission reduction technology to convince their clients to share data. It might be easier for an independent 3rd party to get access as part of an assurance process.

In an ideal world, it would be possible to assess the current technical vessel performance in calm water conditions. This would include the deterioration due to hull and propeller fouling. The Vessel Technical Index as presented in *Guo et al. (2021,2024*) proposes a method for continuous quantification of the vessel technical condition. This promises improved accuracy relative to the speed-loss calculation in ISO 19030, but also sets higher requirements to measured quantities and the accuracy of the vessel base-line performance.

The assurance scope of work to support claims related to hull coating performance includes a variety of activities. Independent analysis of raw data is costly but may be required. Another common task is to review analysis scripts and test them on data where validated results exist. If the analysis is supposed to follow e.g. ISO19030, verification against this standard is possible. A powerful and efficient method is to work on a selection of random samples. Sensitivity checks are always useful to understand and quantify the effect of modelling assumptions. The scope could be to perform independent analyses, spot-checks of analyses, review of analysis scripts, require sensitivity checks and more.

Public data and results may be used to benchmark and for plausibility checks. The third-party assurer will normally have knowledge that is directly applicable, but that may not be directly used due to confidentiality.

4. Evidence for claims

4.1. Potential evidence

With the first product launch in 2013 and close to 5000 applications as of January 2025, Hempaguard silicone coatings is one of the most widespread coating solutions on the market. The product is in January 2025 applied on >10% of the hull surface on the global merchant fleet (IMO numbered vessels, DWT > 5000, built year = 1999-2019). This provides a huge potential for validation of the performance through real life evidence, Fig.5, through different data streams:

- In-service vessel performance data
- In-docking pictures and AHR data from the subsequent DD application
- Inspection data from divers or ROVs reports

In addition to data on actual applications, Hempel has a variation of laboratory data on both the surface properties (relating to “out of dock” effect) and antifouling performance (relating to Speed loss claim).

There are several studies in the literature which demonstrate the benefits of silicone coatings - fouling release coatings over the conventional antifouling coatings in terms of out of dock effect, *Weinell et al. (2003)*, *Candries et al. (2003), Holm et al. (2004), Candries and Atlar (2005), Yeginbayeva and Atlar (2018), Unal (2015)*. *Farkas et al. (2021)* demonstrated that the savings in brake power due to the

application of silicone coating in comparison to conventional antifouling coatings are from 5 % to 8.5 % depending on the initial surface condition of hull surface. Thus for laboratory conditions (ideally smooth hull surface – cannot be achieved in practice even for newbuilt condition) the obtained savings for very large crude oil tanker and handymax bulk carrier are around 5 %, for more rougher hull surface condition (closer to first in docking condition) savings are around 7 %, while for high initial hull surface roughness (closer to second or third dry-docking conditions) savings are up to 8.5 %.

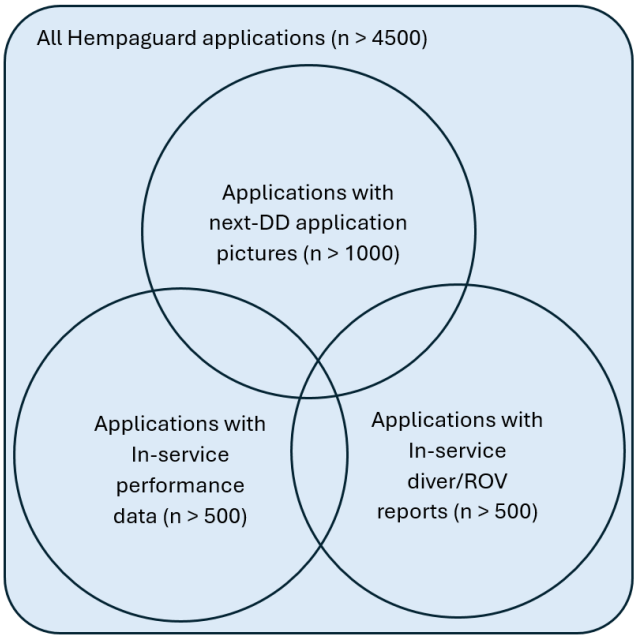

Fig.5: Available real life evidence of silicone coating applications

4.2. Uncertainties and limitations in the evidence data

Having the full set of data: underwater images, in service data and information (AHR data and images) about arriving condition at end of dry-docking period for many vessels of different types and with different trading profiles would be the ideal scenario for truly evaluating performance of a given product. Unfortunately, both data availability and data quality remain limiting factors for Hempel as well as everyone else in the industry.

On the availability side, Hempel has access to in-docking reports on the next DD for the vessels that reapply their next docking with Hempel. While this covers the majority of applications, some vessels have not yet reached the time of the next DD, and some vessels will choose to change the coating system. For in-service performance data and underwater reports, this data is shared with Hempel only by some customers enrolled in performance guarantee schemes or interested in expert advisory during the in-service period. The availability of both performance data and underwater images are hence limited, and the number of vessels with overlapping data in all data streams (represented by intersection in Fig.5) are very limited.

Although each of the data streams individually has a strong potential to provide real life evidence, they also have challenges of their own. Poor quality of in-service data is a significant limiting factor when it comes to performance monitoring. Many shipping companies still rely on noon data, which may not contain all necessary variables and are prone to mistakes and even occasional fraud. The introduction of automatically collected high frequency data on more and more vessels is improving the situation but also introduces other challenges in terms of sensor drift and fallout. The above means that even with available performance data for many vessels, there will be a significant fraction of the data that cannot be considered reliable evidence due to issues with data quality. For both underwater and arrival condition images, data quality can also be an issue in terms of visibility and image quality.

The lack of standardized analysis frameworks is another challenge. In service data is the only of the three sources that can be evaluated via an ISO standard, *ISO (2016)*, but this method is no longer state-of-the-art in hull performance monitoring. Even though, there are lot of concerns regarding the standardized analysis framework which are discussed in *Bertram (2017), Farkas et al. (2025),* and there are lot of modelling advancements which are made and presented at HullPIC conferences, yet there is no update in standard framework for the industry. For both underwater reports and in-docking pictures, no industry standard on reporting, analysis and the link to fuel efficiency exists as of yet, although multiple workgroups are working on this topic. With the lack of industry standards for the analysis methods and interpretation, there is a risk that the results will be inconsistent or biased and the method not transparent.

Potential data bias is important to consider when drawing conclusions from any of the data sets. The occurrence of cleaning is an important example. If the ambition is to evaluate the performance of a certain hull coating without cleaning, then it is essential that the data evaluated is from vessels that have not been cleaned. At the same time, a fouled propeller will also give rise to performance degradation that cannot easily be separated from hull performance degradation. Information about cleanings and polishings are not always shared, which means that some added uncertainty should be considered when drawing conclusions based on performance data.

It is a fact that the results of most performance analysis methods will to some degree be dependent on the operational pattern, and if this changes, this introduces bias in the analysis, which cannot be attributed hull performance.

Combining the results from performance analysis of in-service data with underwater images can in some cases compensate for the bias mentioned. Underwater images can give information about the type and coverage degree of fouling on the hull and propeller and from that, a rough estimate for the performance at the time of inspection can be made. However, the uncertainty on such estimations is large because there is no standardized way of quantifying and reporting fouling and the estimation of the resulting effect of certain fouling on the powering of a vessel is complex and uncertain. Despite the mentioned challenges with underwater images, they can be used to support or discard the results of performance data.

With only a subset of the applications being supported by in-service data and underwater images, there will be a bias in which scenarios of performance shipowners or operators are choosing to share data with Hempel. Some customers prefer to enroll in a proactive monitoring of their Hempaguard applied fleet, which gives an unbiased view of the performance, but some customers share in-service data or underwater images only for vessels with performance uncertainties or questions, which will lead to a bias in the aggregated performance average.

One frequently used indication of the out of dock level of performance is the average hull roughness (AHR), which are often measured across the hull surface after application. It is well known that the surface properties of a hull coating affect the frictional resistance of the vessel. Although a theoretical formula for the effect of various surface properties does not exist, there has been historical attempts to derive an empirical relationship between surface properties and added frictional resistance. In particular, the relationship between average hull roughness (AHR) and added frictional resistance has been in focus. The focus on AHR has made sense historically as it was developed for coatings of certain type, with similar surface characteristics. Within the current ITTC 1978 Performance Prediction Method, *ITTC (2017),* still the Townsin equation is utilized to account for roughness effects on the increase in frictional resistance. However, this relationship lacks physical foundation and fails to consider most surface properties, and they are not necessarily suited for modern coating technologies with different surface properties. An important study which clearly demonstrates the inaccuracy of the Townsin equation is presented in *Song et al. (2024)*. Furthermore, *Andersson et al. (2020)* demonstrated that even for newly coated surfaces there is only moderate correlation between increase in frictional resistance and AHR, with quite large scatter due to variations in surface texture, hydrophobicity, surface elasticity, poor coating application or coating damages. Because of these problems regarding proper

description of roughness penalties using only one roughness parameter, AHR should only be used to indicative rather than deriving actual out of dock effects and properties.

4.3. Used evidence data

Taking into account the mentioned issues with data uncertainty and limitations, a subset of data within each data stream was used for the validation.

This section shows some examples of what and how evidence was evaluated by DNV as part of the Hempaguard performance validation process. Due to customer confidentiality, not all material including identifiable information can be shared. This section is not an attempt to recreate the full extent of in-service evidence evaluated by DNV but to show a few examples. As described in the methodology chapter, the cases are constituting Hempaguard X7 vessels performing as expected.

The data for this validation was delivered by Hempel with a deep-dive validation by DNV done for some select cases. A future "best-practice" verification framework would include the data being available from a neutral 3rd party for a wider portion of the applied fleet as well as with an established framework for evaluating the link between e.g. inspection visuals and vessel performance.

4.3.1. In service performance data

Fig.6 shows two examples of performance data sets shared with DNV. The top plot shows speed deviation over 60 months for an LNG carrier with high frequency auto logged data. The bottom plot shows speed deviation plot over 48 months for a container carrier using noon data.

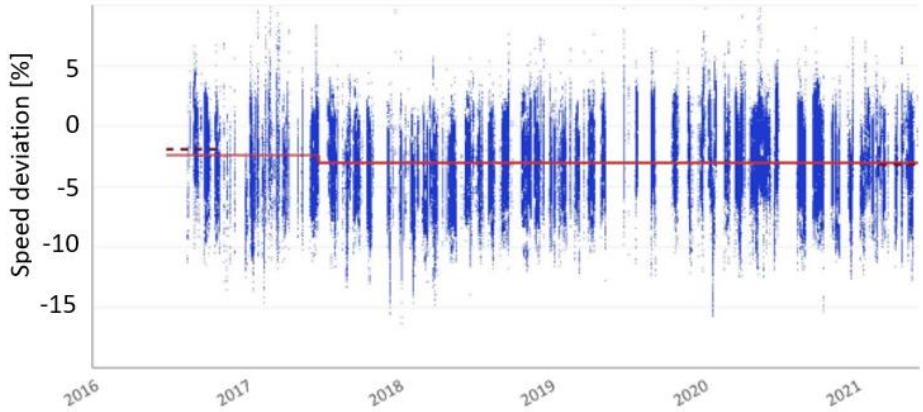

Fig.6a: Example of speed deviation plot for an LNG carrier over 60 months. The speed loss is 1.3%

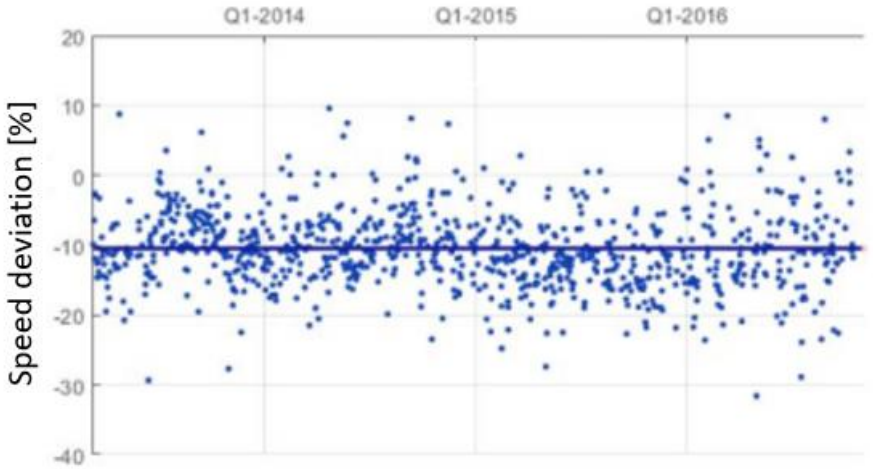

Fig.6b: Example of speed deviation plot for a container carrier over 48 months. The speed loss is close to zero.

4.3.2. In docking pictures

Fig.7 shows examples of indocking photos of two vessels, an MR tanker and a container vessel.

Fig.7a: Arrival condition of MR tanker with Hempaguard X7 and 50 months DD cycle. No hull cleanings, 55% activity 27° C water temp, 12 knots operational speed

Fig.7b: Arrival condition in dock of container carrier after 62 months Hempaguard X7 application. No hull cleanings, 75% activity, 25°C water, 16 knots speed

4.3.3. Hull roughness measurement

Even though AHR is not a unique indicator for the increase in frictional resistance, it represents an important indicator, and data on AHR for many applications can contribute to get an indication on the ability of a given coating to minimize hull roughness and thereby frictional resistance keeping other factors constant.
Fig.8 shows results of AHR values for 100 vessels coated with Hempaguard. 86% of AHR values are below 100 µm; hulls coated with conventional antifouling coatings have an average of 140-160 µm.

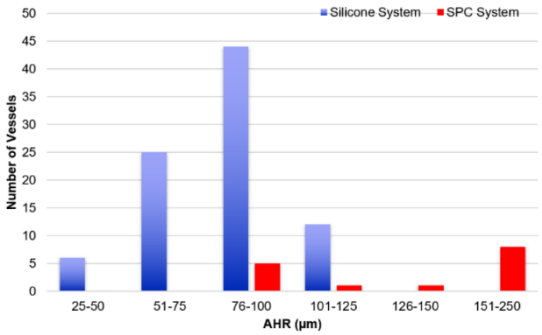

Fig.8: Real-life data from AHR measurements – sample of ~100 vessels including containerships, tankers and bulkers of different sizes

Fig. 9 shows surface scans of two coatings, a silicone and a self-polishing coating, after application and after immersion in sea water for 7 weeks at 12 knots. The images show that while roughness of self-polishing coating has increased after 7 weeks due to leach layer formation, the roughness of the silicone coating stays the same.

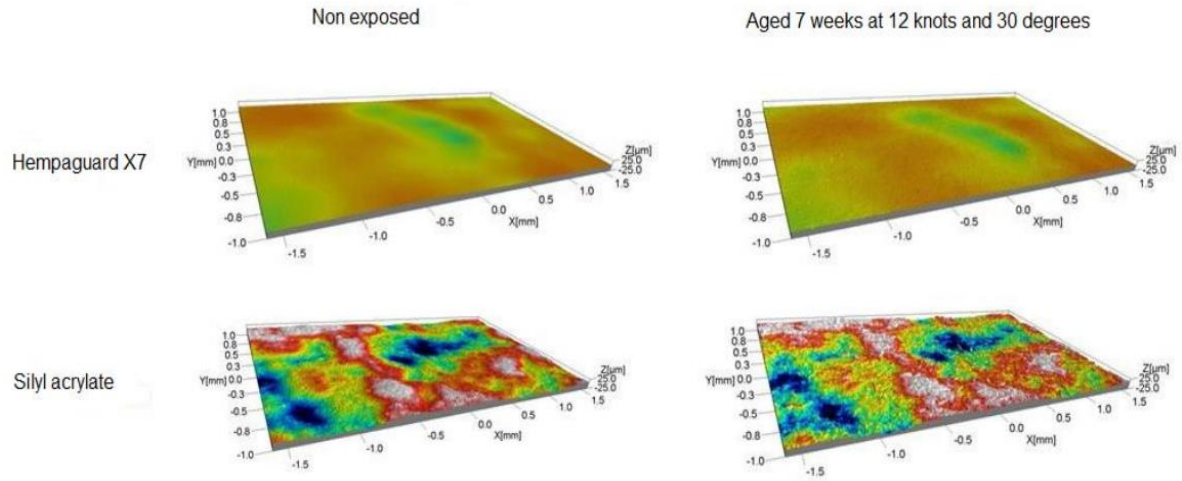

Fig.9: Comparison of surface roughness before and after the exposure to sea water

Hempel carried out a series of research projects in collaboration with TNO, FORCE Technology, and Indian Institute of Technology Madras to establish the differences in frictional resistance between different coating technologies. Several experimental studies are carried out including rotary disk experiments, towing tank tests of flat plates and towing tank tests of ship model. Since various silicone coatings generate the same low surface roughness, a modified version of Hempaguard was used for simplicity reasons in the towing tank tests. Within rotary disk experiments it has been demonstrated that hydrogel-based fouling release coating with biocide will always provide smoother surface in comparison a silyl acrylate based antifouling coating. The difference is more pronounced as the substrate roughness increases. In towing tank tests carried out in Force Technology and Indian Institute of Technology Madras it was also clearly demonstrated that the Hempaguard equivalent coating has lower frictional resistance compared to conventional antifouling paint, where on average initial saving is around 6 %.

DNV reviewed reports from the relevant research projects to build confidence around the out-of-dock reduced resistance claim. Supporting material was found in open literature. It is important to include the measurements from actual dry-dock applications as an assumption of laboratory specimen roughness levels may be overly optimistic.

4.3.4. Inspection data

Fig.10 shows examples of in-water inspection data for two vessels after 37 months and 31 months after application of Hempaguard.

Fig.10a: Underwater inspection of VLCC tanker, 37 months after application with Hempaguard X7. No Hull cleanings, 70% activity, 27°C water temp, 12 knot operational speed

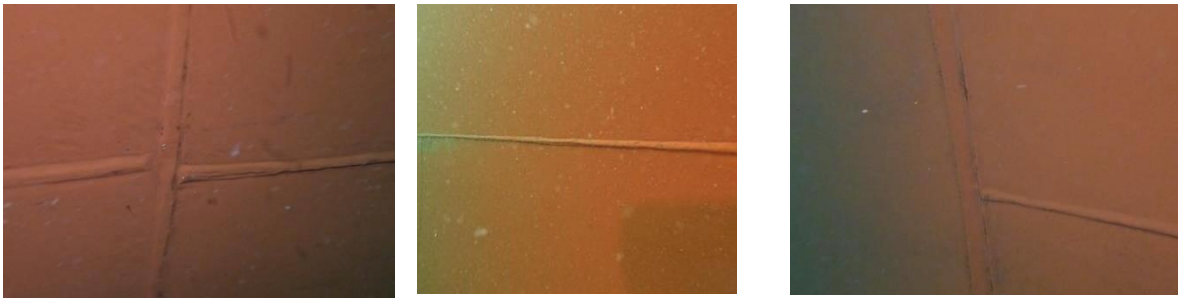

Fig.10b: Underwater inspection of LNG tanker, 31 months after application of Hempaguard X7. No Hull cleanings, 80% activity, 27°C water temp, 15 knot operational speed

4.3.4. Assessment based on combined evidence

The shared evidence was used in combination to document the claims on both antifouling performance and out of dock savings for silicone compared to a market average antifouling. The combined effect of out-of-dock reduced hull friction and an average speed-loss well below the benchmark is basis for a calculated annual CO_2 saving. DNV performed an independent calculation of the total emission of the fleet of vessels with Hempaguard. AIS data for all the vessels were combined with the DNV emission prediction model MASTERv2, see *Guo et al. (2022)* to arrive at the total emissions. The emission prediction model has been thoroughly calibrated to produce accurate emissions on a fleet level. Calibration is done by comparing predictions with an extensive benchmark database of reported and verified annual emissions.

5. Conclusion

5.1. Benefits for the maritime industry

Increased collaboration on validating and evaluating performance of anti-fouling coatings or other energy saving devices is beneficial for both solution suppliers like Hempel and third-party companies like DNV and shipowners/operators.

Shipowners and operators face an endless selection of vessel technical upgrades when allocating their investments into vessel newbuild and retrofit decisions for their vessels. The absence of a verification framework and established validation methods means that it is almost impossible to get educated on every newbuild or retrofit choice available in the market. In addition, it is difficult to assess the validity of performance claims made by suppliers, leading to lower levels of trust between shipowners and suppliers in the market and imperfect capital allocation. It is commonly noted that in a case that all possible energy saving devices are installed on the vessel and they perform as they were marketed, achieved savings would be enormous. An improved validation method of performance claims would benefit shipowners with better capital allocation towards the highest ROI savings for their specific ships and a more efficient path towards decarbonization in shipping.

Suppliers of coatings and other energy saving solutions face a knowledge and transparency gap in the market. In the absence of established performance verification frameworks, a myriad of activities is taking place to convince potential buyers of the solution of the performance, with decentral verification from single cases or fancy marketing brochures. Increased transparency presents both opportunities and challenges for suppliers. If their solutions perform as advertised, they stand to gain significant benefits. However, if the actual performance falls short of expectations, their business may face considerable difficulties. The authors of this article see net benefits in such increased performance transparency, allowing the best performing solutions to grow faster and moving focus from fancy brochures to well documented and trustworthy performance records.

Finally, for third-party companies like DNV, increased transparency is central to these companies' role in driving fleet decarbonization. Being at the forefront of knowledge when it comes to performance

verification is crucial to advise ship owners on their best choice of action and engage with IMO on the possible pace of decarbonization requirements. It is essential that the third-party can deliver increased trust and provide a consistent and fair assurance service. This requires an unbiased and consistent approach, which is greatly facilitated by a standardized framework.

5.2. Recommended next steps to facilitate performance validation

The collaboration between Hempel and DNV has provided useful insights regarding challenges and opportunities for performance validation.

The following presents a wish list to further facilitate validation and quantification of the effect of hull characteristics on vessel performance:

- Accurate out-of-dock vessel performance quantification
    - Improved techniques to test the hull coating properties and resulting effect on the wall shear force, e.g. via the roughness function
    - Measurements in dock after application of the hull coating properties that influence the roughness function
    - Better methods to calculate vessel resistance based on the established roughness function
    - Increased accuracy in sea-trial measurements

- Continuous measurement of in-service vessel performance
    - Standardized measurements (quantities, accuracy, quality, frequency) and analysis
    - Results made available to a trusted third party
    - Accuracy to allow for detection of rapid changes in the performance
    - Supporting data like vessel operational parameters, recorded events like hull and propeller cleaning, pictures from under-water surveys. All data should be in a standardized format

- Standardized baselines for out-of-dock hull coating frictional resistance and in-service performance deterioration

Addressing the second point, DNV has released a recommended practice describing the Vessel Technical Index, see *Guo et al. (2021,2024), Tvete et al. (2022)*. Experience has shown that this index can be used to monitor vessel hull performance with a higher accuracy and temporal resolution than applying ISO 19030. Still, the method requires high-frequency in-service data as well as a reasonably accurate ship model. The effort needed to apply the method will be reduced by further automation and data integration via e.g. the DNV Veracity platform.

References

ANDERSSON, J.; OLIVEIRA, D.R.; YEGINBAYEVA, I.; LEER-ANDERSEN, M.; BENSOW, R.E. (2020), *Review and comparison of methods to model ship hull roughness*, Applied Ocean Research 99

BARREIRO, J.; ZARAGOZA, S.; DIAZ-CASAS, V. (2022), *Review of ship energy efficiency*, Ocean Eng. 257

BERTRAM, V. (2017). *Some Heretic Thoughts on ISO 19030*, 2nd HulllPIC Conf., Ulrichshusen, pp.4-12, data.hullpic.info/hullpic2017_ulrichshusen.pdf

BOUMAN, E.A.; LINDSTAD, E.; RIALLAND, A.I.; STRØMMAN, A.H. (2017), *State-of-the-art technologies, measures, and potential for reducing GHG emissions from shipping–A review*. Transportation Research Part D: Transport and Environment 52, pp.408-421

CANDRIES, M.; ATLAR, M.; MESBAHI, E.; PAZOUKI, K. (2003), *The measurement of the drag characteristics of tin-free self-polishing co-polymers and fouling release coatings using a rotor apparatus*, Biofouling 19(S1), pp.27-36

CANDRIES, M., ATLAR, M. (2005), *Experimental investigation of the turbulent boundary layer of surfaces coated with marine antifoulings*, J. Fluid Engineering 127(2), pp.219-232

DIRZKA, C.; ACCIARO, M. (2021), *Principal-agent problems in decarbonizing container shipping: A panel data analysis*, Transportation Research Part D: Transport and Environment 98

FARKAS, A.; DEGIULI, N.; MARTIĆ, I.; VUJANOVIĆ, M. (2021), *Greenhouse gas emissions reduction potential by using antifouling coatings in a maritime transport industry*, J. Cleaner Production 295

FARKAS, A.; GUNDERMANN, D.; MEHRI, S. (2025). *On the speed and loading condition dependency of the most common performance values*, 10th HullPIC Conf., Mülheim

GLOFOULING (2022), *Analysing the Impact of Marine Biofouling on the Energy Efficiency of Ships and the GHG Abatement Potential of Biofouling Management Measures*, Analysing the Impact of Marine Biofouling on the Energy Efficiency of Ships and the GHG Abatement Potential of Biofouling Management Measures

GUO, B.; LIANG, Q.; TVETE, H.A.; BRINKS, H.; VANEM, E. (2022), *Combined machine learning and physics-based models for estimating fuel consumption of cargo ships*, Ocean Eng. 255

GUO, B.; ROGNEBAKKE, O.; TVETE, H.A.; ADAL, C.; STORHAUG, G.; SCHMIDT, M.; BRUSET, T.; PRYTZ, G. (2021), *Setting the Standard for Evaluation of In-service Technical Ship Performance,* 6th HullPIC Conf., Pontignano, pp.77-94, HullPIC2021_Pontignano.pdf

GUO, B.; TVETE, H.A.; VARTDAL, B.J.; WANG, S. (2024), *Piloting of Vessel Technical Index*, Int. Conf. Offshore Mechanics and Arctic Engineering (OMAE) (Vol. 87820, p. V05AT06A038)

HOLM, E.; SCHULTZ, M.; HASLBECK, E.; TALBOTT, W.; FIELD, A. (2004), *Evaluation of hydrodynamic drag on experimental fouling-release surfaces, using rotating disks,* Biofouling 20(4-5), pp.219-226

IMO (2009), *Second IMO Greenhouse Gas Study 2009,* Int. Mar. Org., London

ISO (2015), *ISO 15016: Ships and marine technology — Guidelines for the assessment of speed and power performance by analysis of speed trial data,* Int. Standard Org., Geneva
ISO (2016), *ISO 19030 - Measurement of changes in hull and propeller performance,* Int. Standard Org., Geneva

ITTC (2017), *ITTC Recommended Procedures and Guidelines 1978 ITTC Performance prediction method*, Int. Towing Tank Conf.

REHMATULLA, N.; SMITH, T. (2015), *Barriers to energy efficient and low carbon shipping,* Ocean Eng. 110, pp.102-112

SONG, S.; CHOI, W.S.; EOM, M.J.; KIM, M.H.; KIM, B.G. (2024), *Townsin's formula vs CFD: Evaluating hull roughness effect in ship resistance*, Ocean Eng. 303

TVETE, H.A.; GUO, B.; AGRELL, C.; FERREIRA, C.; ELDEVIK, S.; SCHMIDT, M.; STORHAUG, G. (2022), *Uncertainty analysis on vessel technical index for technical ship performance*, 15th Int. Symp. on Practical Design of Ships and Other Floating Structures, pp.1107-1123

ÜNAL, U.O. (2015), *Correlation of frictional drag and roughness length scale for transitionally and fully rough turbulent boundary layers*, Ocean Eng. 107, pp.283-298

WEINELL, C.E.; OLSEN, K.N.; CHRISTOFFERSEN, M.W.; KIIL, S. (2003), *Experimental study of drag resistance using a laboratory scale rotary set-up*. Biofouling, 19(S1), pp.45-51

YEGINBAYEVA, I.A.; ATLAR, M. (2018), *An experimental investigation into the surface and hydrodynamic characteristics of marine coatings with mimicked hull roughness ranges*, Biofouling 34(9), pp.1001-1019

Choose Your Words Carefully: The Business Risks and Rewards of Differing 'Warranted Conditions' in Speed-Fuel Warranties

Angela Cabeza Iacobucci, Toqua, Gent/Belgium, angela@toqua.ai
Abhijith Mundanad Narayanan, Toqua, Gent/Belgium, abhijith@toqua.ai
Casimir Morobé, Toqua, Gent/Belgium, casimir@toqua.ai
Cem Musluoglu, Toqua, Gent/Belgium, cem@toqua.ai
David Boxall, Ziethen/Germany, info@waveforce.info

Abstract

Speed-fuel warranties are the cornerstone of commercial agreements in shipping. A vessel's value is directly tied to its speed-fuel performance. Every metric ton it consumes less than the market average should, in theory, result in a higher hire rate. However, comparing a vessel's warranted consumption against a market reference is not simple, due to the wide variety of 'warranted conditions' circulating today. Even worse, many chartering professionals today don't fully appreciate the commercial implications of these 'warranted conditions', leading to costly misjudgments. This paper explores the business risks and rewards of differing 'warranted conditions', while also arguing that more standardized performance warranties and normalization-based performance analysis will accelerate maritime decarbonization.

1. Introduction

Speed-fuel warranties are fundamental to commercial shipping agreements, directly influencing vessel valuations, chartering decisions, and financial risk. However, the lack of standardized 'warranted conditions' has led to widespread ambiguity, creating room for misinterpretation, commercial disputes, and even arbitration battles. Without clear definitions, shipowners and charterers frequently find themselves at odds over what constitutes 'good weather', leading to costly misjudgments in performance and contentious claims. This paper explores the commercial and legal risks associated with inconsistent warranty wording, highlighting real-world financial impacts. More importantly, it argues that a shift toward clearer, standardized performance benchmarks will not only reduce disputes and improve market predictability but also accelerate maritime decarbonization. By rewarding efficiency and eliminating loopholes that mask underperformance, standardization can drive investment into greener, higher-performing vessels, creating a financial incentive for sustainability in global shipping.

2. Different wordings

As the warranted conditions applicable are the result of every unique negotiation, endless variations exist. In this section, we try to cover some of the most frequently occurring variations in practice. We recognize many more variations are possible.

We propose two tables: one focusing on factors affecting the speed-fuel figures and the other on factors determining the percentage of conditions covered under warranty. Some factors appear in both tables, while others are placed in just one for clarity, even if they potentially have an effect on both. The goal is to keep things simple while covering the most important influences.

FACTORS MOSTLY AFFECTING THE SPEED-FUEL NUMBERS		
Factor	**Variation**	**Comment**
Wind	Up to and including Beaufort scale 2	Assuming headwinds and taking the upper limit of Beaufort scale. So the most conservative interpretation.
	Up to and including Beaufort scale 3	
	Up to and including Beaufort scale 4	
	Up to and including Beaufort scale 5	
Waves	Up to and including Douglas Seastate 3 (max. wave height 1.25m)	Distinctions between swell waves and wind waves could also be considered. As well as using 'significant' wave height or not. Left out of scope for this paper.
	Up to and including Douglas Seastate 3 (max. wave height 2.0m)	
Currents	'No adverse currents' → +0.25kn on avg.	As favourable currents still apply, a certain factor of average favourable currents over time needs to be assumed.
	'No adverse currents' → +0.5kn on avg.	
	'Currents factored in' → 0kn	Normalized using hindcast weather data
Fuel Type	VLSFO	Assuming LCV of 41.5 MJ/kg
	MGO	Assuming LCV of 42.6 MJ/kg
Draft	'Laden' interpreted as summer load line	Ballast condition left out of scope for this paper.
	'Laden' interpreted as summer load line -1m	
	'Laden' interpreted as summer load line -2m	
Abouts	-0.5kn speed and +5% consumption	The latter provides more safety margin if warranties are made for over 10kn.
	+-5% on both speed and consumption	
	No abouts	

FACTORS MOSTLY AFFECTING THE COVERAGE (= what % of conditions are considered to be 'within warranty')		
Factor	**Variation**	**Comment**
Period to be considered	Over 24h (no mention of 'continuous')	Different stretches across time can all be aggregated regardless of being continuous or not.
	Continuous period of 24h	'Continuous' periods are evaluated by considering weather averages over 6 hour sub-periods, that should then continuously meet the criteria for 12-24-48 hours respectively.
	Continuous period of 12h	
	Continuous period of 48h	
Wind	Up to and including Beaufort scale 2	
	Up to and including Beaufort scale 3	
	Up to and including Beaufort scale 4	
	Up to and including Beaufort scale 5	
Waves	Up to and including Douglas Seastate 3 (max. wave height 1.25m)	Distinctions between swell waves and wind waves could also be considered. As well as using 'significant' wave height or not. Left out of scope for this paper.
	Up to and including Douglas Seastate 3 (max. wave height 2.0m)	
	'No adverse swell'	Interpreted as all swell waves from -90 to +90 degrees relative to ship heading
Currents	'No adverse currents'	Interpreted as all currents from -90 to +90 degrees relative to ship heading
	'Currents factored in'	
Loading condition	'Even keel'	Violated whenever trim exceeds 1.5m
	No mention of 'even keel'	

3. Impact on speed-fuel figures

In this study, we will quantify the amount the different wordings can have on the speed-fuel numbers. We choose to keep speed at a constant value - corresponding to a speed over ground (SOG) of 12 knots - while selecting various factors to change in our experiment to then observe the fuel consumption

estimation. The factors are the ones presented in the previous section, while the estimations for fuel are obtained using Toqua's Ship Kernels, a proprietary form of physics-informed machine learning applied to vessel performance modeling, Colle and Morobé (2022). Formally, we compute the fuel predictions y using a speed input x with additional parameters θ using model f as $y = f(x; \theta)$.

For this experiment, we selected two different models, one for a Suezmax tanker, and another for a Kamsarmax Bulker. We will mostly be interested in the variations between the different conditions compared to a reference point, which is given by:

- Wind: Up to and including Beaufort scale 4.
- Waves: Up to and including Douglas sea state 3 with a max. wave height of 1.25 m
- Currents: 'No adverse currents' interpreted as '+0.25 kn favourable currents on average'
- Fuel type: VLSFO
- Draft: 'Laden' interpreted as summer load line
- Abouts: -0.5 kn on speed and +5% on consumption

These reference conditions give the following consumption values:

- Tanker, Suezmax: 25.13 mt/day,
- Bulker, Kamsarmax: 28.91 mt/day.

Throughout this exercise, we will look at how the predictions using the different conditions will deviate from these reference values, in percentage, absolute value, and difference in cost (assuming a fuel price equal to $p = \$600/mt$). The reference condition will be taken as the baseline, and one factor will be changed at a time.

The results for different conditions are presented in the table below, where, for each condition, the absolute, percentage, and cost variation is computed as:

$$\Delta = y_{ref} - y_{cond}, \Delta_p = \frac{\Delta}{y_{ref}}, \Delta_c = -\Delta \cdot p,$$

respectively.

The results are presented in the table below. For each factor, different variations are applied, and the resulting delta compared to the reference condition is expressed in three ways. First the % deviation in consumption, secondly the absolute consumption deviation in mt/day, and lastly the daily bunker deviation is expressed in dollars, under the assumption that a better-described vessel will fetch a higher rate in the market equal to its lower cost to operate.

FACTORS MOSTLY AFFECTING THE SPEED-FUEL NUMBERS			
Factor	**Variation**	**Impact Suezmax Tanker** **% | mt/day | $/day**	**Impact Kamsarmax Bulker** **% | mt/day | $/day**
Wind	Up to and including Beaufort scale 2	-2.1% | -0.55 mt/day | +$330/day	-2% | -0.6 mt/day | +$350/day
	Up to and including Beaufort scale 3	-1.6% | -0.41 mt/day | +$240/day	-1.4% | -0.41 mt/day | +$250/day
	Up to and including Beaufort scale 4 (Reference)	0% | 0 mt/day | $0/day (25.13 mt/day | $15.1k/day)	0% | 0 mt/day | $0/day (28.91 mt/day | $17.3k/day)

	Up to and including Beaufort scale 5	+1.6% | +0.40 mt/day | -$240/day	+1.4% | +0.42 mt/day | -$250/day
Waves	Up to and including Douglas Seastate 3 (max. wave height 1.25m)	0% | 0 mt/day | $0/day (25.13 mt/day | $15.1k/day)	0% | 0 mt/day | $0/day (28.91 mt/day | $17.3k/day)
	Up to and including Douglas Seastate 3 (max. wave height 2.0m)	+9.6% | +2.41 mt/day | -$1450/day	+4% | +1.2 mt/day | -$730/day
Currents	'No adverse currents' → +0.5kn on avg.	-5.3% | -1.33 mt/day | +$800/day	-4.7% | -1.36 mt/day | +$820/day
	'No adverse currents' → +0.25kn on avg. (Reference)	0% | 0 mt/day | $0/day (25.13 mt/day | $15.1k/day)	0% | 0 mt/day | $0/day (28.91 mt/day | $17.3k/day)
	'Currents factored in' → 0kn	+5.5% | +1.38 mt/day | -$830/day	+4.9% | +1.41 mt/day | -$840/day
Fuel Type	VLSFO (Reference)	0% | 0 mt/day | $0/day (25.13 mt/day | $15.1k/day)	0% | 0 mt/day | $0/day (28.91 mt/day | $17.3k/day)
	MGO	-2.6% | -0.65 mt/day | +$390/day	-2.6% | -0.75 mt/day | +$450/day
Draft	'Laden' interpreted as summer load line (Reference)	0% | 0 mt/day | $0/day (25.13 mt/day | $15.1k/day)	0% | 0 mt/day | $0/day (28.91 mt/day | $17.3k/day)
	'Laden' interpreted as summer load line -1m	-4.1% | -1.04 mt/day | +$620/day	-3.9% | -1.12 mt/day | +$670/day
	'Laden' interpreted as summer load line -2m	-8% | -2.02 mt/day | +$1210/day	-7.5% | -2.18 mt/day | +$1310/day
Abouts	-0.5kn speed and +5% consumption (Reference)	0% | 0 mt/day | $0/day (25.13 mt/day | $15.1k/day)	0% | 0 mt/day | $0/day (28.91 mt/day | $17.3k/day)
	+-5% on both speed and consumption	-2.1% | -0.53 mt/day | +$320/day	-1.9% | -0.54 mt/day | +$330/day
	No abouts	+16.6% | +4.16 mt/day | -$2500/day	+15.3% | +4.42 mt/day | -$2650/day

These tables give an experimental demonstration how consumption can vary across different warranted conditions, and that this variation can be significant in certain scenarios. If we were to look at two extreme examples, the difference becomes even more apparent. Below, we provide the results when combining the most and least restrictive variations of each factor from our previous experiment. For our tanker example, the variation between these two extremes reaches around 45%. In both cases, the

variation leads to more than $5000/day of difference. This comparison of extreme - yet possible - examples here, combined with the results presented above clearly highlights the huge commercial implications that ambiguity in the wordings of the warranted conditions can lead to.

Comparing the best, worst, and a typical scenario		
Scenario	**Impact Suezmax Tanker** **% | mt/day | $/day**	**Impact Kamsarmax Bulker** **% | mt/day | $/day**
Most restrictive case - **Beaufort scale 2** - **Max. wave height 1.25 m** - **'No adverse currents'** in the '+0.5kn on avg.' sense - **MGO fuel** - **'Laden' interpreted as summer load line -2m** - **+-5% on both speed and consumption**	Absolute values: **20.32 mt/day** | $12.2k/day Relative to reference: -19.2 % | -4.82 mt/day | +$2900/day	Absolute values: **23.78 mt/day** | $14.3k/day Relative to reference -17.7% | -5.13 mt/day | +$3080/day
Reference (average case) - **Beaufort scale 4.** - **Max. wave height of 1.25m** - **'No adverse currents' in the '+0.25kn on avg.' sense** - **VLSFO fuel** - **'Laden' interpreted as summer load line** - **-0.5 knots on speed and +5% on consumption**	**25.13 mt/day** | $15.1k/day	**28.91 mt/day** | $17.3k/day
Least restrictive case - **Beaufort scale 5** - **Max. wave height 2 m** - 'Currents factored in' → 0kn - **VLSFO fuel** - **'Laden' interpreted as summer load line** - **No abouts**	Absolute values: **34.01 mt/day** | $20.4k/day Relative to reference: +35.3% | +8.88 mt/day | -$5330/day	Absolute values: **36.74 mt/day** | $25.6k/day Relative to reference: +27.1% | +7.84 mt/day | -$4700/day

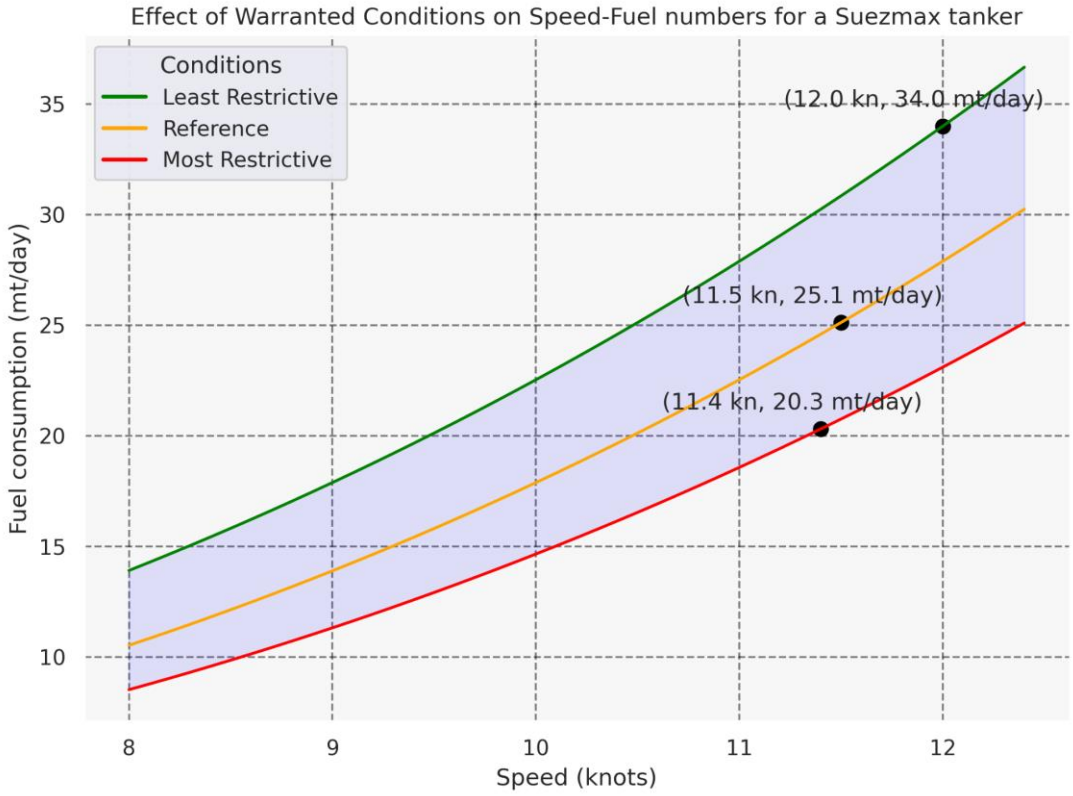

4. Impact on coverage (% within warranted conditions)

In this section, we consider a different experiment, where we focus on the percentage of time where vessels are within the coverage of the warranted conditions, where our goal is again to highlight the difference wording has on this percentage. For this exercise, we again focus on two vessels from the same category as in the previous section, and we assess a full year of data. Note that this is meant to be an example of two vessels, while more robust statistics would require analyzing more vessels over a longer time period.

As before, we consider one reference scenario among the options from the second table presented in Section 2., given as:

- Period to be considered: Continuous period of 24h
- Wind: Up to and including Beaufort scale 4
- Waves: Up to and including Douglas Seastate 3 (max. wave height 1.25m)
- Adverse swell: No exclusion of adverse swell
- Currents: No adverse currents
- Loading condition: No mention of ‘even keel’
- Extrapolation: No extrapolation

Considering these conditions, we obtain:

- Tanker: 23.94% of sailing time covered
- Bulker: 35.02% of sailing time covered

We will also provide an estimate on the worth of a fictional claim, depending on the covered percentage. For this, we assume a fictional scenario with an average overconsumption of 3 mt/day, at a cost of $600 of fuel per mt, over 290 sailing days. Therefore, if 100% of the data is covered, the claim would be worth $522k (= 290 days x 3 mt/day at $600/day). For the above reference conditions and corresponding

coverage, this would give a claim worth $125k for the tanker (since we have a coverage of 23.94%), and $182.8k for the bulker (for 35.02% of coverage), assuming no extrapolation is allowed in the claim.

The table below provides the coverage results for both vessels under different conditions. All results are in absolute values, i.e., not compared to the reference. As in the previous section, the reference condition is taken as the baseline, and we change a single factor at a time.

FACTORS MOSTLY AFFECTING THE COVERAGE (= what % of conditions are considered to be 'within warranty')			
Factor	**Variation**	**Coverage Tanker** **% | $-value of claim**	**Coverage Bulker** **% | $-value of claim**
Period to be considered	Over 24h (no mention of 'continuous')	35.58% | $185.3k	47.63% | $248.6k
	Continuous period of 12h	33.79% | $176.5k	45.48% | $237.4k
	Continuous period of 24h (Reference)	23.94% | $125k	35.02% | $182.8k
	Continuous period of 48h	12.46% | $65.1k	25.62% | $133.8k
Wind	Up to and including Beaufort scale 2	4.51% | $23.5k	8.45% | $44.1k
	Up to and including Beaufort scale 3	14.08% | $73.5k	22.27% | $116.3k
	Up to and including Beaufort scale 4 (Reference)	23.94% | $125k	35.02% | $182.8k
	Up to and including Beaufort scale 5	24.08% | $125.7k	37.97% | $198.2k
Waves	Up to and including Douglas Seastate 3 (max. wave height 1.25m) (Reference)	23.94% | $125k	35.02% | $182.8k
	Up to and including Douglas Seastate 3 (max. wave	37.24% | $194.5k	47.22% | $246.5k

	height 2.0m)		
Adverse Swell	'No adverse swell'	9.50% | $49.6k	18.78% | $98k
	No exclusion of adverse swell (Reference)	23.94% | $125k	35.02% | $182.8k
Currents	'No adverse currents' (Reference)	23.94% | $125k	35.02% | $182.8k
	'Currents factored in'	53.79% | $280.8k	61.98% | $323.5k
Loading condition	'Even keel'	13.48% | $70.4k	18.08% | $94.4k
	No mention of 'even keel' (Reference)	23.94% | $125k	35.02% | $182.8k
Extrapolation	No Extrapolation (Reference)	23.94% | $125k	35.02% | $182.8k
	Extrapolation allowed	100% | $522k	100% | $522k

As expected, more restrictive conditions cover a lesser portion of the total data, however, as before, our goal is to put emphasis on the extent of how different options can have a significant impact on the coverage. We will again look closer at two extreme conditions, where the most restrictive and least restrictive options of each factor have been selected. Note that for the least strict condition, we still consider no extrapolation to look at more interesting examples. The results are provided below.

Comparing the best, worst, and a typical scenario		
Scenario	**Impact Tanker** **% | $**	**Impact Bulker** **% | $**
Most restrictive - **Continuous period of 48h** - **Beaufort scale 2** - **Max. wave height 1.25 m** - **No adverse swell** - **No adverse currents** - **Even keel**	**0%** | $0	**0%** | $0
Reference (average case) - **Continuous period of 24h** - **Beaufort scale 4** - **max. wave height 1.25m** - **No exclusion of adverse**	**23.94%** | $125k	**35.02%** | $182.8k

swell - **No adverse currents** - **No mention of 'even keel'**		
Least restrictive - **No mention of 'continuous'** - **Beaufort scale 5** - **Max. wave height 2 m** - **No exclusion of adverse swell** - **Currents factored in** - **No mention of 'even keel'**	**79.35%** | $414.2k	**88.54%** | $462.2k

The difference between the most and least strict conditions in this example is extremely significant, where we observe that certain coverage scenarios can actually lead to covering no data at all due to how strict they are. This would mean that the claim would not have any worth. While on the other hand, the more 'generous' coverage conditions can lead to more than 80% of coverage, making the claim worth above $400k.

5. Results

5.1. Impact of warranted conditions on speed-fuel figures

The results show that differing wordings of warranted conditions have huge implications. First of all, a speed-fuel figure can mean two completely different things depending on the conditions it is warranted for. For the tanker example, the exact same vessel would be correctly described at 20.3 mt/day in the most restrictive version of 'warranted conditions', while it would also be correctly described at 34.0 mt/day when using the least restrictive version of 'warranted conditions'. A difference of ~12 mt/day or 48% - purely due to what variation of warranted conditions apply. For the bulker, the same applies, where the same vessel can be described at 23.8 mt/day or 36.8 mt/day depending on what warranted conditions are used, good for a total difference of ~13 mt/day or 44%.

5.2. Impact of warranted conditions on coverage of claims

Secondly, different warranted conditions have huge implications on what % of data falls 'within warranty' and for which can be claimed in case of underperformance. For the tanker example, the exact same year of sailing data was analyzed, wherein the least restrictive case 100% of all data would be 'within warranty' and in the most restrictive case 0% would be 'within warranty'. Likewise for the bulker. On average, for the reference conditions representing what occurs frequently in practice, only ~25% of all data remained 'within warranty'. Additional restrictions like 'even keel' or 'no adverse swell' can each in itself reduce coverage by another factor of 4x, often leaving the eventual coverage with extra restrictions to be a single digit %. To the authors, this indicates a broken system that does not protect charterers as it removes almost all the value of the given 'warranty'.

6. Proposed solutions

The authors propose several practical recommendations to establish a more standardized, transparent, and fair framework for defining vessel performance.

6.1. Standardized Wording for Warranted Conditions

To enhance consistency, chartering and legal departments should adopt uniform warranted conditions across all agreements, minimizing unnecessary variations. The focus of negotiations should be on speed-

fuel figures rather than modifying the warranted conditions, as altering them introduces excessive complexity and ambiguity, making interpretation difficult for both parties.

While any level of standardization would be a step forward, the authors recommend the following conditions.

Recommended warranted conditions to foster standardization and fairness:

- Period to be considered: All data above 24 h (so no ‘continuous’)
- Wind: Up to and including Beaufort scale 4
- Waves: Up to and including Douglas Seastate 3 (max. wave height 1.25 m)
- Adverse swell: No exclusion of adverse swell
- Currents: Normalization of currents.
  Fuel type: Fuel type & corresponding LCV used for warranty should be made explicit
- Loading condition: No mention of ‘even keel’. Draft applicable for ‘laden’ and ‘ballast’ should be specifically mentioned in meters.
- Extrapolation: should always be an option

Many of these conditions are already quite common in the industry today. However, we propose two key changes to current practices. First, we suggest removing the word "continuous" from the warranty-covered periods. This adjustment ensures a broader range of data falls under warranty, aligning more closely with its original intent of a warranty. Second, we recommend normalizing for currents. This increases coverage significantly, while also removing the variable aspect of favourable currents, which ensures more clarity and comparability between results.

6.2. Normalization-based approach instead of filter-based approach

Another significant improvement involves rethinking how speed-fuel figures are determined. Current methodologies rely heavily on filtering, treating any data that passes the filters as representative of actual performance. However, when using criteria such as ‘up to and including 4BFT’, a broad spectrum of data gets through the filters, where performance in 1BFT is treated equal to performance at 4BFT, which creates huge fluctuations on what ‘performance’ might mean, depending on what distribution of ‘good weather’ data the vessels coincidentally ran into. A further downside of this is that, to improve accuracy, stricter filtering always needs to be applied, further reducing the amount of data to be considered ‘within warranty’, which is already a key problem.

A more effective alternative is a normalization-based approach, which accounts for secondary conditions rather than discarding large portions of data. Instead of filtering out data, all reasonable data points would be included and adjusted for external factors such as waves, wind, currents, draft, and fuel type. This process ensures a clearer, more accurate assessment of speed-fuel performance without distortions from variable conditions.

Normalization can be achieved using traditional theoretical methods, such as DNV’s VTI, or through advanced data-driven techniques, such as the Ship Kernels used in this paper. Such data-driven techniques, when implemented correctly, have the benefit of covering more conditions, achieving higher accuracy, while also being able to transparently prove and report on the accuracy attained. A verifiable approach like this would build greater trust, a crucial factor for widespread industry adoption.

The key advantage of normalization is its ability to cover over 80% of available data, while creating a fair, accurate, and verifiable analysis of performance, by stripping away the influence of any variations in weather, speed, draft, fuel type, etc. that would otherwise cause inaccuracies and unfairness.

6.3. Improving data quality

For both standardization (6.1) and normalization (6.2) to be successfully implemented, greater confidence in the underlying data is required. A further shift towards more verification by 3rd parties on manually reported data, as well as the inevitable shift towards more widespread adoption of automated high-frequency data collection, are required. Strengthening data reliability is critical to ensuring fair and verifiable performance assessments, ultimately supporting the transition toward maritime decarbonization.

7. Conclusion

The proliferation of varying 'warranted conditions' has completely hollowed out the true meaning of a 'performance warranty'. In many cases, neither party fully comprehends the terms being negotiated. This issue remains overlooked, partly due to its excessive complexity and ambiguity, but also because the individuals negotiating these terms are often not the ones dealing with the consequences of underperformance. The system is broken. The only beneficiaries of this broken system are owners who would like to conceal underperformance. A more standardized and transparent framework to define performance would certainly be advantageous for charterers, but also for owners of well-performing vessels. Charterers would gain more certainty and lower commercial risk, while owners of more efficient vessels could differentiate themselves in the market and rightfully earn a fair dollar premium. This would ensure that greener vessels are rewarded with higher earnings, generating a strong market-driven momentum for maritime decarbonization.

References

COLLE, C.; MOROBÉ, C. (2022), *Saving AI from its own hype: Getting real about the benefits and challenges of machine learning for ship performance modelling aimed at operational optimizations*, 7th HullPIC Conf., Tullamore, pp.198-206, http://data.hullpic.info/HullPIC2022_Tullamore.pdf

GUO, B.; ROGNEBAKKE, O.; TVETE, H. A.; ADAL, C.; STORHAUG, G., SCHMIDT, M.; BRUSET, T.; PRYTZ, G. (2021), *Setting the Standard for Evaluation of In-Service Technical Ship Performance*, 6th HullPIC Conf., Pontignano, pp.77-94, http://data.hullpic.info/HullPIC2021_Pontignano.pdf

ISO (2015), *ISO 15016:2015 - Ships and marine technology — Guidelines for the assessment of speed and power performance by analysis of speed trial data*, Int. Standard Org., Geneva

Index by Authors

11th Hull Performance & Insight Conference (HullPIC)

Pontignano/Italy, 16-18.3.2026

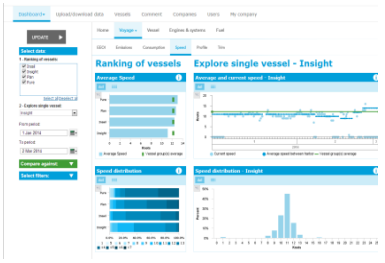


Topics: ISO 19030 and beyond / sensor technology / human factors in reporting / information fusion / big data / sea trials / uncertainty analysis / hydrodynamic models / business models / CII management

Organiser: Volker Bertram (VB conferences)
Morten Sten Johansen (Jotun)

Advisory Committee:

Gerry Docherty	Ardmore Shipping	**Erik Hagestuen**	Danelec	**Richard Marioth**	Idealship
Johnny Eliasson	Chevron Shipping	**Søren V. Hansen**	VesOPS	**Ivana Melillo**	GNV
Inno Gatin	Cloud Towing Tank	**Liz Haslbeck**	NSWC-CD	**Geir Axel Oftedahl**	Breakthrough Factory
Wojciech Gorski	Enamor	**Jan Kelling**	Hasytec	**Beom-Jin Park**	KRISO
Ditte Gundermann	Hempel	**Manolis Levantis**	Jotun	**Sofia Werner**	RISE SSPA
		Carsten Manniche	Navigator Gas		

Venue: The conference will be held in the Certosa di Pontignano.

Format: Papers to the above topics are invited and will be selected by a selection committee.
The proceedings will be made freely available to the general public.

Deadlines:

anytime	Optional “early warning” of interest to submit paper / participate
20.11.2025	First round of abstract selection (1/3 of available slots)
20.12.2025	Second round of abstract selection (remaining slots)
28.02.2026	Payment due for authors
28.02.2026	Final papers due

Admin. Fees: **850 €** – early registration (by 10.1.2026)
950 € – late registration

Fees are subject to German VAT

Sponsors: Jotun, Tutech Innovation (more tbd)

Media Partners: Hansa, The Royal Institution of Naval Architects

Information: volker@vb-conferences.com

Operators: tbd